Solubilisation, fragmentation and precipitation of colloidal particles of cellulose as stabilising agents in foods

Katherine Sarah Lefroy

Submitted in accordance with the requirements for the degree of
Doctor of Philosophy

The University of Leeds
School of Food Science and Nutrition

September, 2022

The candidate confirms that the work submitted is her own, except where work which has formed part of jointly-authored publications has been included. The contribution of the candidate and the other authors to this work has been explicitly indicated below. The candidate confirms that appropriate credit has been given within the thesis where reference has been made to the work of others. Details of the jointly-authored publications and the contributions of the candidate and the other authors to the work are outlined on the pages iv and v.

Further details of the jointly-authored publications and the contributions of the candidate and the other authors to the work are included below:

Chapter 2

Lefroy, K. S., Murray, B. S, and Ries, M. E. (2021). Advances in the use of microgels as emulsion stabilisers and as a strategy for cellulose functionalisation. *Cellulose*, *28*, 647-670.

Chapter 3

Lefroy, K. S., Murray, B. S and Ries, M. E. (2021). Rheological and NMR Studies of Cellulose Dissolution in the Ionic Liquid BmimAc. *Journal of Physical Chemistry B*,*125* (29), 8205-8218.

Chapter 4

Lefroy, K. S., Murray, B. S, Ries, M. E and Curwen T. D. (2021). A natural, cellulose-based microgel for water-in-oil emulsions. *Food Hydrocolloids*, *113*, 106408.

Chapter 5

Lefroy, K. S., Murray, B. S and Ries, M. E. (2022). Relationship between size and cellulose content of cellulose microgels (CMGs) and their water-in-oil emulsifying capacity. *Colloids and Surfaces A: Physicochemical and Engineering Aspects*, *647*, 128926.

Chapter 6

Lefroy, K. S., Murray, B. S and Ries, M. E. (*under review*). The effect of oil on cellulose dissolution in the ionic liquid 1-butyl-3-methyl imidazolium acetate. *ACS Omega*.

Details of authorship contributions:

Katherine S. Lefroy: designed and conducted the experiments, carried out data analysis and interpretation, drafted and edited the manuscripts and replied to comments from reviewers.

Brent S. Murray and Michael E. Ries: provided supervision, discussion of results, feedback and contributed to proofreading and editing of manuscripts, including replying to comments from reviewers.

Thomas D. Curwen: provided industrial supervision, discussion of results, feedback and contributed to the interpretation of results for the manuscript included in **Chapter 3**.

List of accepted conference abstracts:

Poster presentations:

Lefroy, K. S., Murray, B. S, Ries, M. E and Curwen T. D. (2021). A Natural, Cellulose-Based Microgel for Water-in-Oil Emulsions as a Route to Fat and Sugar Replacement in Foods. *Designed Assembly of Colloids at Interfaces – Fundamentals to Applications*. Online.

Lefroy, K. S., Murray, B. S, Ries, M. E and Curwen T. D. (2022). A Natural, Cellulose-Based Microgel for Water-in-Oil Emulsions. *11th International Colloids Conference.* Lisbon, Portugal.

Oral presentations:

Lefroy, K. S., Murray, B. S, Ries, M. E and Curwen T. D. (2020). A Natural, Cellulose-Based Microgel for Water-in-Oil Emulsions as a Route to Fat and Sugar Replacement in Foods. *UK Colloids (Joint Colloids Group)*. Online.

Lefroy, K. S., Murray, B. S, Ries, M. E and Curwen T. D. (2021). A Natural, Cellulose-Based Microgel for Water-in-Oil Emulsions. *EUSMI (European Soft Matter Infrastructure)/SoftComp Annual Meeting*. Online.

Lefroy, K. S., Murray, B. S, Ries, M. E and Curwen T. D. (2021). A Natural, Cellulose-Based Microgel for Water-in-Oil Emulsions. *35th Conference of the European Colloids & Interface Society*. Athens, Greece.

Lefroy, K. S., Murray, B. S, Ries, M. E and Curwen T. D. (2022). Relationship between size and cellulose content of cellulose microgels (CMGs) and their water-in-oil emulsifying capacity. *18th Food Colloids Conference*. Online.

Lefroy, K. S., Murray, B. S, Ries, M. E and Curwen T. D. (2022). Cellulose Microgels (CMGs) From Ionic Liquids: A Novel Approach To A Water-in-oil (w/o) Biocompatible Pickering Emulsifier. *17th Conference of the International Association of Colloid and Interface Scientists*. Brisbane, Australia.

Lefroy, K. S., Murray, B. S, Ries, M. E and Curwen T. D. (2022). A Natural, Cellulose-Based Microgel for Water-in-Oil Emulsions. *SOFI Showcase*. University of Leeds, UK.

Lefroy, K. S., Murray, B. S, Ries, M. E and Curwen T. D. (2022). “Hydrophobic” cellulose microgels: the influence of particle size on water-in-oil emulsion stability. *36th Conference of the European Colloids & Interface Society*. Chania, Greece.

Acknowledgements

Studying for a PhD during a global pandemic has brought about many challenges, but has been enjoyable and possible with the support of those around me.

Firstly, I would like to thank my supervisors for their constant encouragement throughout my project: Brent and Mike, you have always been available to guide and help me, direct my thinking and planning, supervise me and help me to manage the project. I have thoroughly enjoyed working with you and really appreciate all of the time you have put into mine and the project's development. Tom: thank you for your advice and support on the project, as well as your sense of humour! And in particular, for your career guidance: thanks to you and the people I met during my placement at Mondelēz, I have been able to plan my career path and the experience has been invaluable in prompting job applications!

I gratefully acknowledge Soft Matter and Functional Interfaces (SOFI) CDT, EPSRC and Mondelēz International for financial support during my PhD (Grant Ref. No. EP/L015536/1).

Next, thank you to all of my fellow PhD/post doc students and the staff at Leeds University. I can't list everyone who's friendship has meant so much throughout my PhD, but extra special thanks to Olivia, Andrea, Ecaterina, Aygul and Amna for countless lunches and chats; Fran for all the coffees and walks; Sam for your company in the main building and for always being willing to chat about colloids, and Lorenzo, Ben and Liam. Natalie, Neil and Lilla, for your constant willingness to help; Tabitha, Amie and Ian, it's been so enjoyable to teach undergraduates alongside you; Miles, for managing the department and getting us back so quickly after the lockdown. Gita, a special thanks to you for organising many a SIPR, conference booking, expenses claim, and for solving all of my travel problems! I'd also like to add thanks to Dan Baker, Alex Kulak, Andy Hobson, Stuart Micklethwaite, Ruth Hughes and Sally Boxall, for their kind support in other departments.

Many thanks to all of the people from the SOFI CDT: especially to Joanne, Daniel, Lian and Linda, cohort 5 and particularly those in Leeds – Adele, Kalila, Charlotte, Merin and Jordan. Marie, Burhan, Lloyd and Lucas – thank you for all the beers and laughs, I have truly met lifelong friends through the programme.

Finally, I'd like to thank my family for their unconditional love and support. You have always encouraged me and Becca, I hope that I can give you the same support when you start your research this year. Lastly my boyfriend and best friend Sam, thank you for everything. I am very lucky to have you and forever grateful for your support and love throughout the last 4 years.

Abstract

Cellulose is often referred to as the most abundant biopolymer on earth. It has many interesting properties and is dense, zero-calorie and tasteless, thus finding a wealth of applications across the food industry (including bulking, thickening and stabilising products). In light of upcoming legislation affecting products high in fat, salt and sugar (HFSS), there is huge necessity for the UK food industry to reduce calories and reformulate using sustainable, 'clean-label' ingredients. With the recent reassessment of its inherent amphiphilicity along the backbone, native cellulose has the potential to address some of these challenges if it can be suitably functionalised as a water-in-oil (W/O) emulsion stabiliser.

Incorporation of water into confectionary products via an emulsion is a promising strategy for fat reduction, however both the lack of non-synthetic W/O emulsifiers and their low stabilities present issues. In this thesis, novel cellulose microgel particles (CMGs) have been produced based on a dissolution-reprecipitation method, adhering to clean-label restrictions where possible. An ionic liquid (IL) was investigated as a cellulose solvent and the properties of the cellulose-IL solutions were firstly characterised in detail, prompting the design of cellulose materials. CMGs were then fabricated from the solutions and various processing methods were employed, adopting different solvents and mechanical treatments. The best performing emulsifiers were CMGs with oil incorporated into the gel structure ('oily'-CMGs), which were well-dispersed in hydrophobic media and stabilised W/O emulsions for at least 5 months. The cellulose-oil interaction was investigated in more detail, to further understand the origin of CMG-interfacial activity.

In summary, this thesis addresses the need for replacement of synthetic surfactants in food, exploring the properties of native cellulose and its potential to be functionalised without chemical modification. These insights present an interesting opportunity for cellulose-based ingredients to be applied to reduced fat products, considering the upcoming HFSS requirements.

Table of Contents

List of Tables

List of Figures

List of Abbreviations

A-cell	Avicel cellulose
AGU	Anhydrous glucose unit
AmimAc	1-allyl-3-methylimidazolium acetate
AmimCl	1-allyl-3-methylimidazolium chloride
ATR	Attenuated total reflection
BC	Bacterial cellulose
BHD	Bromohexadecane
BMI	Body mass index
BmimAc	1-butyl-3-methyl imidazolium acetate
BmimCl	1-butyl-3-methyl imidazolium chloride
$BmimHSO_4$	1-butyl-3-methylimidazolium hydrogen sulfate
BNC	Bacterial nanocellulose
BPP	Bloembergen, Purcell and Pound
CAD	Coronary artery disease
CAGR	Compound annual growth rate
ChArg	Cholinium arginate
CI	Crystallinity index
CLSM	Confocal laser scanning microscopy
CMC	Carboxymethyl cellulose
CMG	Cellulose microgel
CNC	Cellulose nanocrystals
CNF	Cellulose nanofibers
CNP	Cellulose nanoparticles
CP	Cone-plate
Cryo	Cryogenic
CS_2	Carbon disulfide
CW	Calcofluor White
DES	Deep eutectic solvent

DLS	Dynamic light scattering
DMAc	*N,N*-dimethylacetamide
DMF	Dimethylformamide
DMSO	Dimethyl sulfoxide
DOS	Degree of swelling
DP	Degree of polymerisation
DS	Degree of substitution
EC	Ethyl cellulose
EDG	Electron donating group
EDS/EDX	Energy dispersive x-ray spectroscopy
EFSA	European food safety authority
EmimAc	1-ethyl-3-methyl imidazolium acetate
EmimCl	1-ethyl-3-methyl imidazolium chloride
EP	Emulsion polymerisation
ETD	Everhart-Thornley detector
EWG	Electron withdrawing group
FDA	Food and Drug Administration
FFC	Fast-field cycling
FIB	Focussed ion beam
FID	Free induction decay
FT	Fourier transform
FTIR	Fourier-transform infrared
GRAS	Generally recognised as safe
H-bond	Hydrogen bond
H-CMGs	‘High’-shear cellulose microgels (top-down)
HBA	Hydrogen bond acceptor
HBD	Hydrogen bond donor
HFSS	High in fat, salt and sugar
HIPE	High internal phase emulsion

HmimAc	1-hexyl-3-methyl imidazolium acetate
HMWS	High molecular weight surfactants
HOSO	High oleic acid sunflower oil
HPH	High-pressure homogenisation
HPMC	Hydroxypropyl methylcellulose
IL	Ionic liquid
IR	Infrared
IRE	Internal reflection element
JH	Jet homogeniser
L-CMGs	‘Low’-shear cellulose microgels (top-down)
LF	Liquid fat
LiCl	Lithium Chloride
LMWS	Low molecular weight surfactants
MAA	Methacrylic acid
MC	Methyl cellulose
MCC	Microcrystalline cellulose
MCT	Medium-chain triglyceride
MD	Molecular dynamics
MFC	Microfibrillated cellulose
MIPE	Medium internal phase emulsion
MW	Molecular weight
NaDIA	National diabetes inpatient audit
NaOH	Sodium hydroxide
NCC	Nanocrystalline cellulose
NFC	Nanofibrillated cellulose
NIPAM	*N*-isopropylacrylamide
NMMO	*N*-methylmorpholine-*N*-oxide
NMR	Nuclear magnetic resonance
NMRD	Nuclear magnetic resonance dispersion

O/W	Oil-in-water
O/W/O	Oil-in-water-in-oil
OmimAc	1-octyl-3-methyl imidazolium acetate
PFG	Pulsed-field gradient
PGPR	Polyglycerol polyricinoleate
PNIPAM	*Poly-N*-isopropylacrylamide
PSD	Particle size distribution
PVAm	Polyvinyl amine
RI	Refractive index
SEM	Scanning electron microscopy
SF	Solid fat
SFEP	Surfactant-free emulsion polymerisation
SLS	Static light scattering
SNR	Signal-to-noise ratio
SRM	Solvent releasing method
TFA	Trifluoroacetic acid
TIR	Total internal reflection
TLD	Through the lens detector
TMS	Tetramethylsilane
TSIL	Task-specific ionic liquids
UV	Ultraviolet
V-cell	Vitacel cellulose
VH-CMGs	‘Very high’-shear cellulose microgels (bottom-up)
Vis	Visible
W/O	Water-in-oil
W/O/W	Water-in-oil-in-water
WAXS	Wide angle x-ray scattering
WHO	World Health Organization
XG	Xanthan gum

List of Symbols

$\dot{\gamma}$	Shear rate
$[\eta]$	Intrinsic viscosity
1°	Primary
2°	Secondary
A	Absorbance / Hertz's association parameter
a	Constant (model-independent relationship, FFC NMR)
A_k	Constant (intrinsic viscosity equation)
α	Associated fraction
B	Constant (Huggins equation)
b	Constant (model-independent relationship, FFC NMR)
C	Cross-model time constant
c	Concentration / number density of interacting spins
c^*	Crossover concentration
c_e	Entanglement concentration
D	Self-diffusion coefficient
D_0	Pre-exponential factor (Arrhenius-type equation)
$d3,2$	Surface-weighted mean diameter
$d4,3$	Volume-weighted mean diameter
d_i	Diameter of the particle
d_p	Depth of penetration
E	Young's modulus
E_a	Activation energy
$E_{a,D}$	Activation energy for diffusion
$E_{a,T1}$	Activation energy for rotation
$E_{a,\eta}$	Activation energy for flow
f	Correction factor (microviscosity pre-factor, Stokes-Einstein)

f'	Correction factor (Stokes-Einstein-Debye)
h	Plate gap
$\hbar$	Reduced Planck's constant
H_1	Total volume in the tube (cream height)
H_2	Bottom layer (cream height)
I	Nuclear spin / intensity
J	Coupling constant
J_{trans}	Spectral density function
k	Constant (power-law equation)
k_B	Boltzmann constant
K_H	Huggins constant
L	Path length / elastocapillary length
m	Cross-model rate constant / constant (Huggins equation)
M	Molar mass
M_{GU}	Mass of 'glucose units'
M_{IL}	Mass of ionic liquid
MW	Molecular weight
n	Power-law
N	Number of spins per unit volume / number of OH groups 'per glucose unit'
n_1	Refractive index of medium (1)
n_2	Refractive index of medium (2)
N_A	Avagadro's number
n_H	Number of protons per IL molecule
n_i	Number of droplets
ϕ	Volume fraction / amount (wt %)
q	Scattering vector
R	Universal gas constant / radius
R_1	Spin-lattice relaxation rate

R_2	Spin-spin relaxation rate
r_{eff}	Effective inter-proton distance
r_H	Effective hydrodynamic radius
T	Temperature
T_1	Spin-lattice relaxation time
$T_{1,0}$	Pre-exponential factor (Arrhenius-type equation)
T_2	Spin-spin relaxation time
T_{on}	Onset temperature
γ	Shear strain (force) / gyromagnetic ratio (NMR)
δ	Chemical shift
$\Delta\delta$	Change in chemical shift
ε	Molar adsorption coefficient
η	Viscosity
η_∞	Infinite shear viscosity
η_0	Zero shear viscosity
η_{rel}	Relative viscosity
η_{sol}	Zero shear-rate viscosity of pure solvent
η_{sp}	Specific viscosity
θ	Scattering angle
θ_C	Critical angle
θ_I	Incident angle
θ_R	Angle of refraction
λ	X-ray wavelength
μ_0	Vacuum permittivity
v	Velocity / resonance frequency
v_0	Resonance frequency of reference nucleus
π	Pi
ρ	Density
σ	Shear stress

τ	Correlation time
τ_{rot}	Rotational correlation factor
ω	Larmor frequency (NMR)

Chapter 1
General Introduction

In 2003, 26.3 % of admissions to hospital through the emergency department were linked to circulatory disorders (Elixhauser and Owens, (2006)). Furthermore, approximately one sixth of patients occupying hospital beds in 2020 had diabetes, according to the National Diabetes Inpatient Audit (NaDIA) (Elvin, (2020)). Both cardiovascular complications and type 2 diabetes have been strongly linked to obesity, a disease which is defined as a medical problem involving an excessive amount of body fat (Staff, (2021)) and is usually diagnosed when a patient has a body mass index (BMI) above 30. Obesity is a rapidly rising problem all over the globe and has almost tripled since 1975, with 39 million children under the age of 5 being classified as overweight (BMI of 25-29.9) or obese (BMI of 30 and above) in 2020 (World Health Organization (WHO), (2021)).

Excessive weight gain is, for the most part, avoidable and has been linked to excessive calorie intake. This is often caused by overconsumption of high-fat foods (Li et al., (2007); Norton et al., (2013)) and in particular, solid fat (SF). SFs like cocoa butter and palm oil provide a 'melt-in-your-mouth' sensation and are used extensively in confectionary products to create desirable sensory properties such as creaminess and richness, as well as to improve product consistencies and flavours. In baked goods, SF (or shortening) acts as a leavening agent, helps gluten spread and can aid air incorporation during dough mixing, leading to a finer and softer crumb structure (Pehlivanoglu et al., (2018)). However, SFs are high in saturated and *trans*-fats and the WHO recommends limiting calorie intake through such fats to 10 % and 1 % respectively (World Health Organization (WHO), (2018)), since both are being increasingly linked to chronic health effects (Ascherio et al., (1994); Aro et al., (1997); Valsta et al., (2005); Singh et al., (2017)).

Liquid fats (LFs) on the other hand are generally high in unsaturated fats and may have health benefits, such as significantly lowering cholesterol levels and reducing the risk of coronary artery disease (CAD) (Hu, (2003); Mozaffarian and Willett, (2007); Rogers et al., (2009); Hunter et al., (2010)). As a result, there has been considerable effort to reformulate confectionary products and replace SFs with LFs, including but not limited to: structuring oil (with gums, fibres or other agents), producing oleogels ('gel-in-oil') (Schaink et al., (2007); Tavernier et al., (2017); Lee et al., (2018); Demirkesen and Mert, (2019); Jiang et al., (2019)) and fabricating water-in-oil (W/O) emulsions (Surh et al., (2007);

Bou et al., (2014); Linke and Drusch, (2018); Öztürk-Kerimoğlu et al., (2021); G. Li et al., (2021)).

1.1 Water-in-oil (W/O) emulsions as a strategy for fat reduction

W/O emulsions are an active research area in fat reduction/replacement and have the potential to tackle some of the textural problems associated with structured-oil products. Reducing the volume of the fat/oil phase with stabilised water droplets is a well-known technology in margarines and low-fat spreads, where water and oil phases are held at specific temperatures and emulsified, followed by cooling to induce the desired fat crystallisation (Miskandar et al., (2002)). However, it is a challenge to obtain long-term stabilisation of water droplets, particularly when minimising the amount of SF in the continuous phase and especially when limited to using food-grade stabilisers.

Recently, both consumer interest and food regulations have demanded development of more sustainable, 'clean-label' ingredients (Ozturk and McClements, (2016); Linke and Drusch, (2018)) and this is reflected by a compound annual growth rate (CAGR) of 6.78 % (according to Brandessence Market Research (Brandessence, (2022))). The term 'clean-label,' which is also positioned as 'natural,' 'organic' and/or 'free from additives/preservatives' on a food label, refers to products which contain fewer, simple ingredients which a consumer would generally recognise and accept (Gunst and Roodenburg, (2019)). The growth in the clean-label ingredient market is in part due to consumer concerns and preferences around *E*-numbers/synthetic ingredients (Gunst and Roodenburg, (2019)), which has led to increased interest in novel colloidal stabilisers for W/O emulsions (e.g. Pickering stabilisers and microgel particles) (Murray, (2019b); Sarkar and Dickinson, (2020)). Particle stabilisers have the potential to improve emulsion stabilities compared to traditionally used surfactants, since particles are effectively irreversibly adsorbed once located at the water-oil interface. Greater stability has also been demonstrated using next generation double oil-in-water-in-oil (O/W/O) emulsions, where the internal water phase can be gelled (Surh et al., (2007)).

There are many advantages of using an emulsion approach to fat reduction, including the minimal effect on sensory properties due water-saliva miscibility, the potential for encapsulation of water-soluble bioactive compounds and/or controlled release (Matos et al., (2013); Nadin et al., (2014); Zhu et al., (2019); Tang et al., (2022)) and good distribution of fat and therefore flavour within the

emulsion (Brewer, (2012); Mitsou et al., (2016); Marchetti et al., (2017); Lefroy, Murray, Ries, et al., (2021)). However, many fat-based products still contain chemically-synthesised emulsifiers (e.g. polyglycerol polyricinoleate, (PGPR)) and there are relatively few clean-label stabilisers currently available to food manufacturers.

1.2 Overall Research Aim

The overall aim of this thesis is to develop a novel, biocompatible stabiliser derived from cellulose, which could provide long-lasting stability to W/O emulsions. Suitably stable W/O emulsions could be used as a route for fat reduction in high-calorie confectionary products, as well as margarines/spreads. In light of the Covid-19 pandemic, many consumers are increasingly concerned with the cleanliness of their food labels and are more focussed on eating healthier, natural products (Brandessence, (2022)). Therefore, this work aims to avoid chemical modification of cellulose and employ physical manipulation and functionalisation alone, to produce a novel, clean-label ingredient which is more acceptable for food applications.

Native cellulose has been studied extensively in the literature as an oil-in-water (O/W) stabiliser due to its perceived hydrophilicity (Kalashnikova et al., (2013); Capron and Cathala, (2013); Bai et al., (2018); Lu et al., (2019); Li et al., (2019); Lu et al., (2021)), however it has been overlooked as a W/O stabiliser. Furthermore, it is insoluble in water and oil and must be processed to achieve functionality, but the lack of sustainable processing methods has hindered the implementation of native cellulose in food products. The development of ionic liquids (ILs) in the last 20 years (Swatloski et al., (2002)) has allowed small-scale dissolution of cellulose to be carried out rapidly and effectively, without employing harsh chemical treatments. Fabrication of various cellulosic materials via coagulation from ILs has subsequently been reported (Liu et al., (2015); Sun et al., (2015); Fryczkowska et al., (2018); Peng et al., (2018); Napso et al., (2018); Bazbouz et al., (2019)), however dispute remains about the details of the dissolution and reprecipitation mechanisms. Further clarity and a deeper understanding about the molecular interactions occurring during each stage would be of great value for the specific design of novel cellulose materials, from ILs.

This thesis aims to test novel coagulation routes for enhancing the hydrophobic properties of cellulose, providing further insight into cellulose-IL interactions, and to subsequently demonstrate the ability of native cellulose to function as a stabiliser for W/O systems. ILs dissolve cellulose into to its molecular state, from which the hydrophobic/hydrophilic properties of the

polymer can be controlled (to some extent). The fabrication of cellulose microgels (CMGs) from the cellulose-IL solution is achieved by coagulation/reprecipitation, whilst different mechanical processing methods are applied in order to assess their effect on CMG size and properties. To our knowledge, CMGs have not been fabricated via this exact method before.

1.2.1 Hypothesis

This thesis was built on the premise that cellulose has amphiphilic properties and therefore does not necessarily require covalent modification to function as an effective stabiliser. We hypothesise that introduction of an oil to the IL, before cellulose coagulation, may allow 'coating' of the cellulose hydrophobic planes, whilst the fabrication of a cellulose gel results in 'trapping' of its hydrophobic character. Attempts to harness cellulose hydrophobicity in this way have not, to our knowledge, been conducted experimentally. However, molecular dynamic (MD) simulations have shown that cellulose planes have a different arrangement in water and benzene (Miyamoto et al., (2009)), demonstrating the potential to manipulate the surface properties and hydrophobic/hydrophilic balance.

We hypothesise that dispersal of 'hydrophobic' CMGs in an oil/fat phase may delay cellulose aggregation/network formation, allowing CMGs to arrange at the water-oil interface upon emulsification and function as Pickering stabilisers. Formation of a thick interfacial layer may occur over time by a compression/adsorption mechanism shown schematically in Figure 1.1, where microgels anchored at the interface compress and excess CMGs adsorb and aggregate to them.

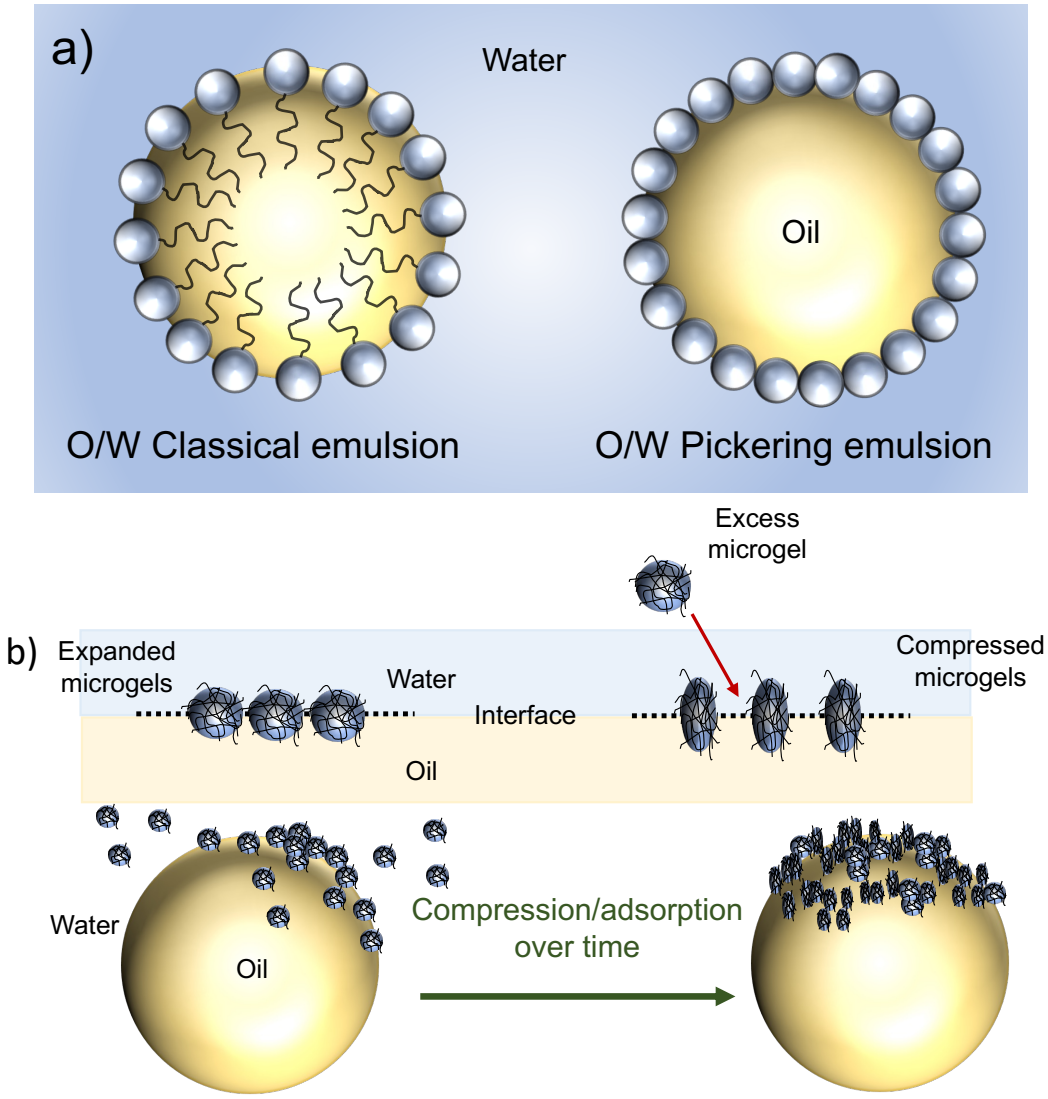

Figure 1.1. a) Schematic showing classical (surfactant) and Pickering stabilised O/W emulsions; b) schematic showing rearrangement and adsorption of excess CMGs over time, from the oil continuous phase to the water-oil interface, as described in (Pinaud et al., (2014)).

1.3 Rationale behind the use of cellulose

In order to understand the properties of cellulose and its potential to function as a W/O stabiliser, the following section includes details about the structure of cellulose and specific properties/applications of micro, nano-, regenerated and coagulated cellulose. Details on modified (derivatised) celluloses are also included, in order to review their physicochemical properties, food applications and need for their replacement in food.

Cellulose is frequently referred to as the most abundant biopolymer (H. Wang et al., (2012); Olsson and Westman, (2013); Onwukamike et al., (2019)) and is the major component of plant cell walls, found in trees, plants and algae. Therefore, it is readily available and constitutes a large proportion of

conventional waste in the form of biomass in agriculture and food (particularly fruit and vegetable peels) as well as textiles (El Seoud et al., (2020)), giving a large incentive for the recycling and reuse of fibrous materials and value added sourcing of raw materials (Rieland and Love, (2020)). Cellulose has indeed been functionalised and used in many industries for decades, including food, agriculture, textiles and pharmaceuticals (Kamel et al., (2008); Rahatekar et al., (2009); Kabir et al., (2018); Mu et al., (2019); He et al., (2021); Wang et al., (2021); Mishra et al., (2022)). However, many industrial pre-treatments involve harsh chemical treatments and/or extreme conditions, leading to environmental concern and limiting the application range of cellulose materials (Halder et al., (2019)). More recently, ILs have shown promise in the area of cellulose processing and further details will be given in section 1.5.

1.3.1 Basic structure of cellulose

About 40-50 % of wood biomass is constituted by cellulose, along with lignin (20-35 %) and hemicelluloses (20-35 %). On a molecular level (Figure 1.2), cellulose consists of β(1-4)-linked anhydrous glucose units (AGUs) which form long, linear chains and wood cellulose is typically made up of 300-1700 units. Different cellulose sources, such as cotton and bacterial cellulose, may have chain lengths between 800-10,000 AGUs (Klemm et al., (2005)).

Cellulose is insoluble in water and many common organic solvents since a large volume of intermolecular interactions form within and between cellulose chains, due to its highly ordered structure. Both hydrogen bonding (H-bonding) interactions between hydroxyl groups and hydrophobic stacking interactions between glucopyranose planes lead to the formation of crystalline structures that form microfibrils, which in turn form macrofibrils (often referred to as cellulose fibres), giving cellulose a complex hierarchical structure. Amorphous regions also exist between crystalline domains, which are commonly removed via acid or mechanical treatments to obtain crystalline cellulose (Costa, Medronho, et al., (2019)) (see section 1.3.2).

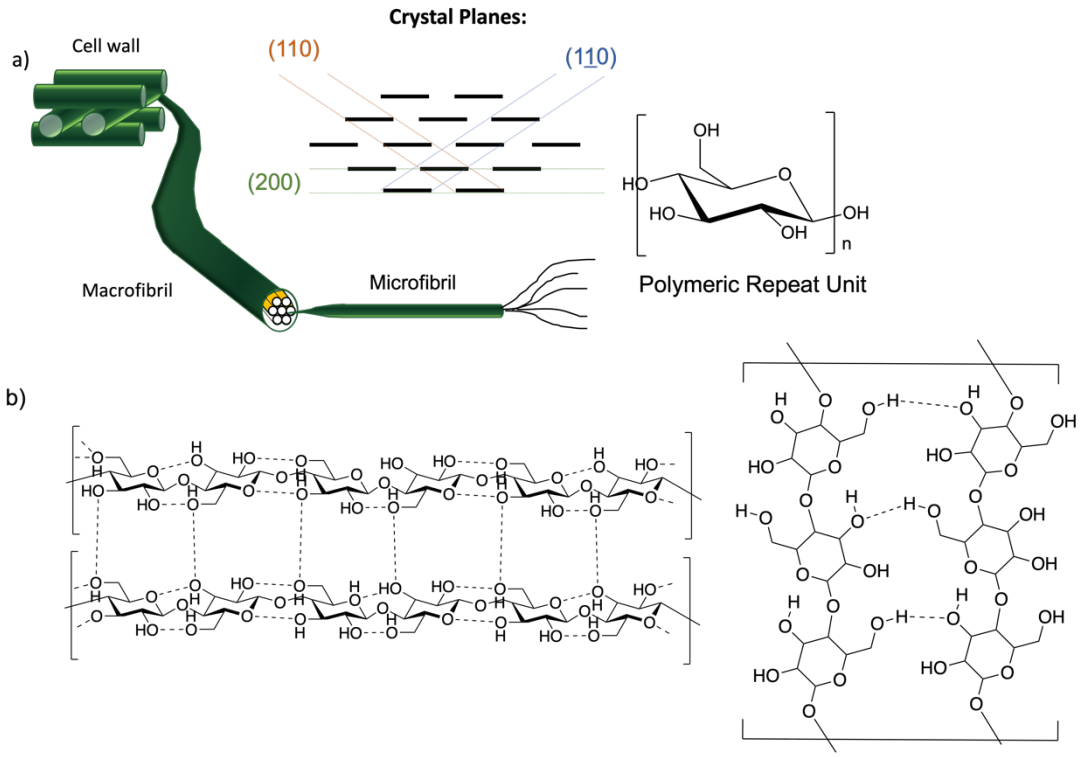

Figure 1.2. a) Hierarchal structure of cellulose, showing macrofibrils, microfibrils and crystalline structure giving rise to the hydrophilic planes ((100), (110)) and the hydrophobic plane (200); b) Chemical structure of cellulose, showing inter- and intramolecular H-boning and hydrophobic interactions (dashed lines) and top-down view (right), reproduced from (Medronho et al., (2015)).

Whilst most research has historically focussed on H-bonding as the reason for cellulose recalcitrance, its structure has been revisited in the last 20 years. Each glucopyranose ring adopts a $^4C_1$ chair conformation in its lowest energy form, resulting in equatorial positioning of the hydroxy groups (the 'hydrophilic' plane) and axial positioning of the H-groups, forming the previously overlooked 'hydrophobic' plane (Klemm et al., (2005)). The presence of both planes give cellulose structural anisotropy and several more recent reports have focussed on the role of the hydrophobic interactions (Lindman et al., (2010); Medronho et al., (2012); Medronho and Lindman, (2014); Medronho et al., (2015)).

1.3.2 Micron-sized and nanocellulose

1.3.2.1 Micron-sized cellulose

Micron-sized cellulose is most commonly used in the form of microcrystalline cellulose (MCC) and is generally obtained via two stages: i) purifying the raw material (pre-treatment) and ii) treating the purified extract to obtain MCC. Controlled degradation of wood and cotton fibres using sulfuric acid was first reported in the late 1940s (Rånby, (1949)) which led to commercialisation of

MCC, first branded as Avicel PH in 1964 (Battista and Smith, (1962); Thoorens et al., (2014)). Like native cellulose, MCC is water insoluble but can be dispersed as colloidal particles that aggregate and form 3D networks, increasing the solution viscosity and/or even forming gels at sufficient concentrations.

Depending on the cellulose source and processing conditions, MCC with a different degree of polymerisation (DP), crystallinity index (CI), particle size and shape can be obtained, which all affect its properties (Nsor-Atindana et al., (2017)). Large molecular weight (MW) MCC tends to have a greater volume of amorphous domains (and thus lower CI), and a greater water-holding capacity (Zeug et al., (2002); Thoorens et al., (2014)). MCC has been used for over 50 years by the pharmaceuticals industry as an excipient, due to its excellent compressibility (Albers et al., (2006)). It is also used to enhance the stabilities of food emulsions, providing opacity as well as desirable textures (e.g. creamy mouthfeel) in sauces, meats and dressings (McClements, (2004)). More details on MCC applications and nutritional benefits is given by Nsor-Atindana in the following reference (Nsor-Atindana et al., (2017)).

1.3.2.2 Nanocellulose

Nano-structured cellulose or nanocellulose, which encompasses cellulose nanofibers/nanofibrillated cellulose (CNFs/NFC), cellulose nanocrystals/nanocrystalline cellulose (CNCs/NCC, or whiskers), microfibrillated cellulose (MFC) or bacterial nanocellulose (BNC), can be obtained through processing of raw materials (e.g. acid hydrolysis of MCC (Bondeson et al., (2006); Bondeson and Oksman, (2007))) to reveal the building blocks of cellulose (Uetani and Kitaoka, (2020)). Like MCC, the type of nanocellulose obtained depends on the source, raw material pre-treatment and the disintegration process (Turbak et al., (1983); Herrick et al., (1983)). Nanosized, uniform fibrils can be obtained using enzymatic or chemical pre-treatments, paired with mechanical homogenisation (Saito et al., (2006); Pääkko et al., (2007)). Chemical treatments rely on the addition of negative charges to the microfibril surface, (e.g. sulfate groups for sulfuric acid), leading to repulsive forces and consequently easier separation of microfibrils (Marchessault et al., (1959); Dong et al., (1996)). The charged surface also effects the adsorption properties of the fibrils and can result in chemical reactions with some additives (Ahola et al., (2008)). A useful review on the properties of CNCs produced via over 30 production methods is provided by Vanderfleet and Cranston (Vanderfleet and Cranston, (2021)).

Nanocellulose has been frequently used as a reinforcement agent in composite materials (Hubbe et al., (2008)), due to its impressive mechanical properties, high thermal stability, low density and biodegradability (Man et al., (2011); Li et al., (2017)). Compared to MCC, nanocelluloses generally have a higher surface area, aspect ratio and crystallinity, making them comparable in mechanical performance to materials like Kevlar and steel (Moon et al., (2011)). Nanocellulose shows great promise for applications in the food industry, for sustainable and edible packaging films (Savadekar et al., (2012); Savadekar et al., (2015); Rahman and Netravali, (2017); Han et al., (2018); Arifin et al., (2022); Papadaki et al., (2022); Aghajani-Memar et al., (2022)) and as a Pickering stabiliser (Kalashnikova et al., (2011); Cherhal et al., (2016); X. Li et al., (2018)) (more details in section 1.4.2.1). Figure 1.3 gives a summary of the different types of nanocellulose and their applications in various industries, illustrating the wealth of their potential.

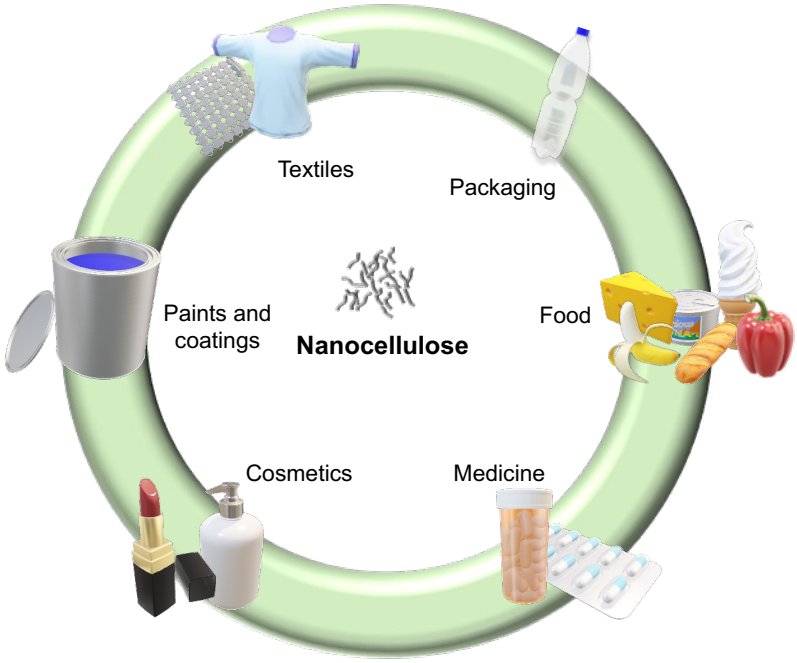

Figure 1.3. Applications and types nanocellulose, across various industries: textiles (e.g. replacing plastic coating); packaging (e.g. increasing shelf-life/spoilage prevention in food); food (e.g. stabiliser and dietary fibre); medicine (e.g. excipient in pharmaceuticals); cosmetics (e.g. replacing synthetic polymers such as polyethylene) and paints and coatings (e.g. binder and reinforcing agent).

1.3.3 Regenerated and coagulated cellulose

The term ‘regenerated cellulose’ is widely applied to cellulose which has been dissolved and reprecipitated from a solution, encompassing all ‘man-made’ cellulosic materials. It is used to describe both cellulose which has been derivatised in order to solubilise it (e.g. the Viscose process), as well as

cellulose which is dissolved and reprecipitated using an anti-solvent (non-solvent) in non-derivatising solvents (e.g. many ILs). However, in this thesis we distinguish between 'regenerated' and 'coagulated/reprecipitated' cellulose, defining the former as cellulose obtained from a derivatising solvent and the latter as cellulose from a non-derivatising solvent (which has undergone physical modification exclusively).

Solvents are defined as 'derivatising' if dissolution involves formation of an intermediate, 'unstable' cellulose species (e.g. ether or ester), and covalent interactions occur (Heinze and Koschella, (2005)). This includes the Viscose procedure which, although developed over a century ago, still dominates the production of regenerated cellulose on a commercial scale (Swatloski et al., (2002)). Cellulose reacts with carbon disulphide (CS_2) to generate cellulose xanthate, which is soluble in sodium hydroxide (NaOH) and forms viscose (as shown in Figure 1.4). Other derivatising solvents include trifluoroacetic acid (TFA) (Geddes, (1956)), *N,N*-dimethylformamide (DMF)/N_2O_4 (Klemm et al., (1997)) and dimethyl sulfoxide (DMSO)/paraformaldehyde (Baker et al., (1978)), which produce cellulose intermediates that are subsequently modified to produce esters, carbamates and ethers. More details on cellulose derivatives and their applications are given in section 1.3.4.

On the other hand, non-derivatising solvents disrupt the inter- and intramolecular H-bonding and hydrophobic interactions to achieve cellulose solubility, without prior chemical modification (Sen et al., (2013)). This includes many ILs (Swatloski et al., (2002)), aqueous alkali solutions (Cai and Zhang, (2005); Budtova and Navard, (2016)), inorganic molten salt hydrates (Fischer et al., (2003)) and organic solvent/inorganic salt mixtures (McCormick et al., (1985); Heinze et al., (2008)), where a precipitating solvent is added to obtain cellulose. Antisolvents commonly used include water, acetone or alcohols, which initiate the reformation of hydrophobic/H-bonding interactions between cellulose chains and generally alter the MW, DP and CI relative to the starting cellulose material (Zhao et al., (2009); Sen et al., (2013)). Cellulose can be coagulated in different forms, including particles (Swatloski et al., (2002); Sescousse et al., (2011); Han et al., (2013); Suzuki et al., (2014); Fan et al., (2018)), gels (Napso et al., (2016); Fan et al., (2017); Idenoue et al., (2019)), fibres (Swatloski et al., (2002); Kosan et al., (2008); Sun et al., (2015); Bazbouz et al., (2019); Yang et al., (2020)) and films (Zhang et al., (2005); Hameed and Guo, (2010); Sadeghifar et al., (2019)), depending on the coagulation process. In all cases, the resultant cellulose is chemically unchanged, although its physical properties can be modified by varying the

anti-solvent type (Fryczkowska et al., (2018); Hedlund, Köhnke, et al., (2019)), coagulation conditions (e.g. with/without mechanical stirring) (Fan et al., (2017); Fan et al., (2018)), order of combining solutions (Zhao et al., (2009)) and initial cellulose concentration (de Oliveira and Glasser, (1996); Duchemin et al., (2009)).

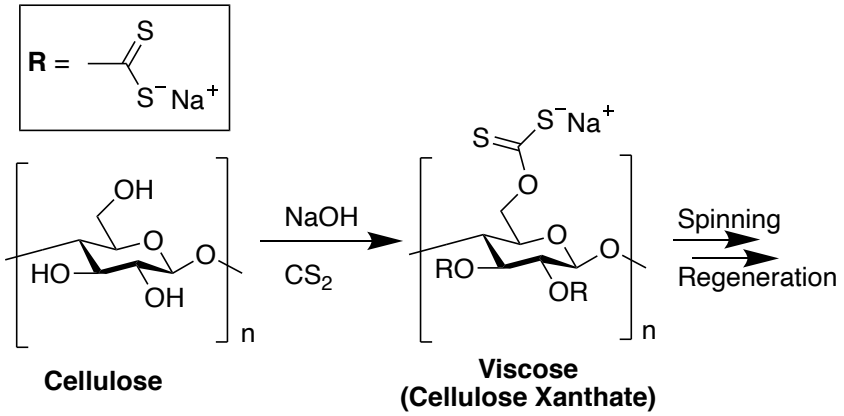

Figure 1.4. The Viscose process: chemical derivatisation of cellulose using CS_2, where cellulose is treated with NaOH and CS_2 to form cellulose xanthate (viscose). Viscose is then forced through a spinneret and regenerated in an acidic solution to form fine strands (Rayon, used in textiles) or cellophane (used in food packaging).

1.3.4 Covalently modified cellulose

As previously discussed in section 1.3.1, native cellulose is insoluble in water (and most common solvents), and is often modified to generate water-soluble cellulose ethers (Figure 1.5). Modification creates novel functionalities (He et al., (2021)) and broadens the use of cellulose across many fields (including paints, printing, cosmetics, pharmaceuticals, textiles and foods) (Marsh and Wood, (1942); Andresen et al., (2006); Medronho and Lindman, (2014); Medronho et al., (2015)). The presence of three free hydroxyl groups on each glucose monomer give cellulose chemical reactivity (Nsor-Atindana et al., (2017)) and covalent modification can take place during dissolution if a derivatising solvent is used (Henniges et al., (2010)), reducing cellulose-cellulose (H-bonding/hydrophobic) interactions (Zhu et al., (2017)).

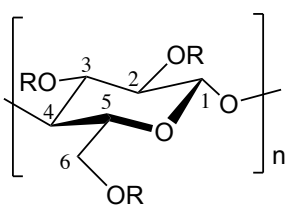

Methylcellulose (MC): R = H or $-CH_3$

Carboxymethylcellulose (CMC): R = H or $-CH_2CO_2H$

Hydroxypropyl methylcellulose (HPMC): R = H, $-CH_3$ or $-(OCH_2CHCH_3)_xOH$

Ethylcellulose (EC): R = H or $-CH_2CH_3$

Figure 1.5. Repeat chemical structure of cellulose derivatives (methylcellulose, carboxymethylcellulose, hydroxypropyl methylcellulose and ethylcellulose).

Carboxymethylcellulose (CMC), often referred to as ‘colloidal cellulose,’ is the most widely used of all the cellulose ethers and makes up over half of their total consumption (Arca et al., (2018)) across the food, textiles, pharmaceutical, personal care and oil sectors (and more). MC has been commercially manufactured since the 1920s (Grover, (1986)) and represents the second most widely used cellulose ether, along with its derivatives (including HPMC) (Arca et al., (2018)). EC is water-insoluble, unlike other common cellulose ethers, and possesses more hydrophobic properties.

Due to the excellent physical properties of cellulose derivatives, they have been used extensively in the food industry as bulking agents, fat replacers, thickeners/binders/gelators, stabilisers and for oil/moisture retention (Burdock, (2007)). Cellulose ethers are commonly added to control the rheological properties of the food matrix and MC was one of the first synthetic polymers used to replace natural gums (Grover, (1986)) (e.g. in sauces, yoghurts, ice creams (Tasneem et al., (2014); Gomes et al., (2020))). Various cellulose derivatives also display excellent surface activity (MC, HMPC, EC) and further details are given in section 1.4.2.3.

Although cellulose derivatives have been approved for use in the food industry for at least 50 years in the US and 25 years in the EU (Table 1.1, (Watson and Johnson, (1965); Burdock, (2007))), some concerns have been raised around cellulose derivatives and their application as food additives. Numerous studies on the toxicology, acute toxicity, metabolism, adsorption and biochemical/pharmacological effects of cellulose ethers conclude that they are safe to consume in low quantities (Bauer and Lehman, (1951); McCollister et al., (1973); Obara et al., (1992); Burdock, (2007); Younes et al., (2018)), however there is growing negative perception around the use of *E*-numbers and increasing consumer demand for food companies to provide clear information on why it is necessary to use such additives in their products (Gunst and Roodenburg, (2019)). Furthermore, modified celluloses are less digested than other polysaccharides (Younes et al., (2018)) and chemical derivatisation may reduce some health benefits, whilst processing methods generally employ toxic reagents and are not environmentally friendly (Karaki et al., (2016)). Greener solutions based on enzymatic (Karaki et al., (2016)) and IL (Gericke et al., (2012)) processing for cellulose derivatisation have evolved, but still encounter bottle-necks to their scale-up such as high cost, solvent recyclability and limitation regarding physical and chemical properties.

Despite this, the CAGR for cellulose derivatives has been forecast to increase by a rate of ca. 5.5 % over the next 5 years (Celotech, (2020); Intelligence,

(2021)), which illustrates the reliance of the food industry on modified cellulose and the increasing need for clean-label alternatives. As a result, there is much recent interest in native cellulose, which may be more consumer acceptable and is perceived as 'eco-friendly' (Perrin et al., (2020)).

Table 1.1. Summary of common cellulose derivatives and their approval for use in food by the FDA[1] and EFSA[2].

Cellulose Derivative Type	FDA[1]	EFSA[2]
MC	GRAS[3], when used with a methoxy content of 27.5-31.5 % and in accordance with good manufacturing practise (FDA)	Approved as an authorised food additive (E461) (EFSA, (2018))
HPMC	Not listed GRAS, but permitted as a direct and indirect food additive for specific uses (FDA)	Approved as an authorised food additive (E464) (EFSA, (2004))
EC	Not listed GRAS, but permitted as a direct food additive in accordance with prescribed conditions (FDA)	Approved as an authorised food additive (E462) (EFSA, (2004))
CMC	GRAS, when used with a maximum substitution of 0.95 carboxy methyl groups per AGU and in accordance with good manufacturing practise (FDA)	Approved as an authorised food additive, including sodium CMC (E466); cross-linked CMC (E468); enzymatically hydrolysed CMC (E469) (EFSA, (2004))

[1]U.S Food and Drug Administration

[2]European Food Safety Authority

[3]Generally recognised as safe

1.4 General overview of food emulsions

1.4.1 Background

Many food products contain emulsions, either wholly or partly, with common examples including mayonnaise, milks, creams, butter and yoghurt. Emulsions are composed of two immiscible liquids, with one liquid dispersed within another, and require stabilisers/emulsifiers in order to provide kinetic

stability and delay phase separation (McClements, (2004)). Food emulsions are traditionally stabilised by low molecular weight surfactants (LMWS) or surface-active polymers, which adsorb at the oil-water/water-oil interface and slow down physical destabilisation processes such as coalescence, creaming, flocculation and Ostwald Ripening (Figure 1.6). Oxidation and hydrolysis can also occur and are examples of chemical instability, which results in a change to the molecules. The length of time (shelf-life) (Bai et al., (2018)) for which an emulsion must remain stable varies depending on the type of food product and therefore it is important to understand the general principles which determine stability, in order to predict behaviour in food products and select suitable stabilisers (McClements, (2004)). In the following section, the use of cellulose-based stabilisers in emulsion food products is briefly reviewed.

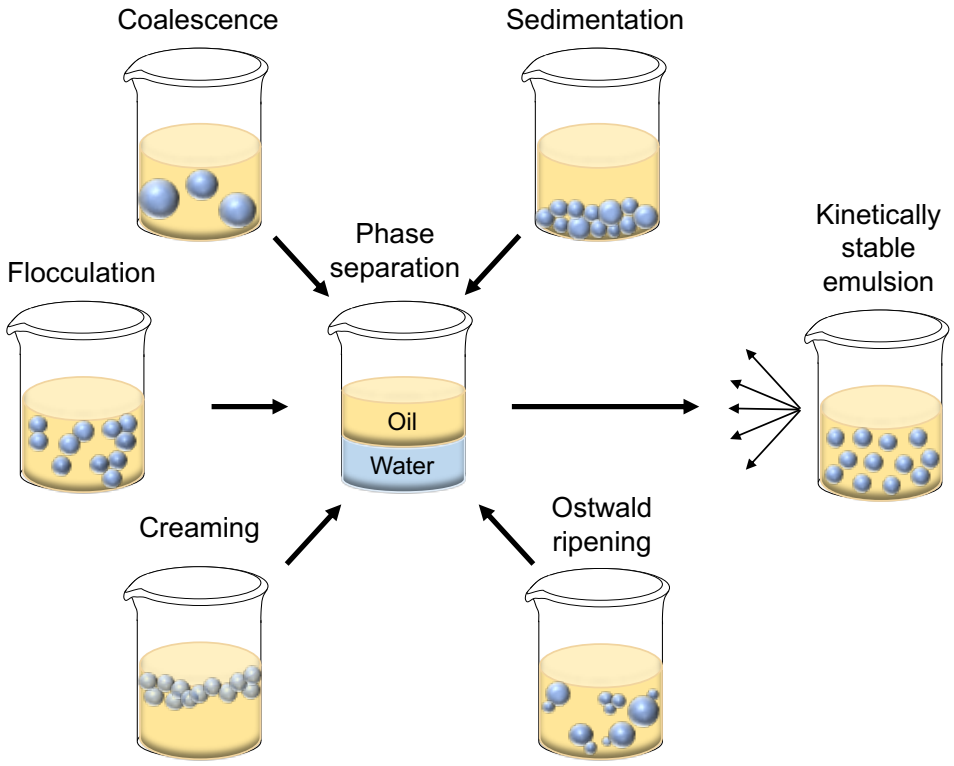

Figure 1.6. Schematic showing the main destabilisation processes in emulsions, where some may occur simultaneously (in this case, a W/O emulsion is depicted).

1.4.2 Cellulose-stabilised emulsions

The aim of this thesis is to determine whether native cellulose can function as an effective W/O emulsion, for food applications. Cellulose-based materials have been used extensively as a stabiliser for emulsions and foams, and various types are briefly reviewed below.

1.4.2.1 Micro- and nanocellulose

MCC has been used as a stabiliser in the food industry for over 40 years (Krawczyk et al., (2009)), whilst more recently nanocellulose has been investigated as a Pickering stabilizer (Kalashnikova et al., (2011)). Both are used for O/W emulsions due to their structural anisotropy, ability to form stabilising particle networks and strong affinity for both the oil and water phase, whilst nanocellulose also possesses charge which can increase stability (Oza and Frank, (1986); Cherhal et al., (2016)). Various types of micro- and nanosized cellulose have been investigated as Pickering stabilisers in food and a comparison of publications on cellulose type is provided in Table 1.2, with CNCs being the most widely researched.

Table 1.2. Searches for various cellulose types and Pickering emulsions, in Food Science Technology from 1900 to 2022 (from Web of Science, July 2022).

Search terms	Number of publications (% within Food Science Technology)
'Nanocellulose,' 'Pickering emulsion'	**164** (18.9 %)
'CNC*,' 'Pickering emulsion'	**151** (9.3 %)
'BC*,' 'Pickering emulsion'	**72** (23.6 %)
'CNF*,' 'Pickering emulsion'	**57** (3.5 %)
'CMC*,' 'Pickering emulsion'	**39** (15.3 %)
'MCC*,' 'Pickering emulsion'	**22** (22.7 %)
'MFC*,' 'Pickering emulsion'	**10** (30 %)

*__CNC__ = cellulose nanocrystals; **BC** = bacterial cellulose; **CNF** = cellulose nanofibers; **CMC** = carboxymethylcellulose; **MCC** = microcrystalline cellulose; **MFC** = microfibrillated cellulose

MCC, MFC, CNF and CNC are highly crystalline forms of cellulose broken down to various sizes, where their preparation involves removing most of the amorphous material (Krawczyk et al., (2009)). The (200)β/(220)α hydrophobic edge and low charge densities (Kalashnikova et al., (2012)) are responsible for the surface activity of micro- and nanocellulose, and this can be varied by changing their properties (e.g. crystalline structure (X. Li et al., (2018)), charge (Cherhal et al., (2016)) and aspect ratio (Kalashnikova et al., (2012); Kalashnikova et al., (2013); Cherhal et al., (2016))). Generally, it is reported that CNCs within the size ranges 100-900 nm length and 13-17 nm width are

able to stabilise emulsions, provided that their charge is sufficiently low (Kalashnikova et al., (2012)).

The flexibility of a cellulose stabiliser, inherently related to its size, has been shown to affect its emulsion properties. Fibre flexibility is advantageous, giving cellulose the ability to adsorb on neighbouring droplets simultaneously (Lu et al., (2019)) and provide strong steric hindrance between droplets (Li et al., (2019); Wang et al., (2020)). Semi-flexible CNFs were found to be the most effective O/W stabilisers when compared to rigid CNCs and more flexible BC (Lu et al., (2021)), which was attributed to the formation of a percolated CNF-network. On the other hand, higher concentrations of CNCs are required with electrostatic repulsion being the dominating stabilisation mechanism, whilst fully flexible, large BC will not form a stable emulsion at any concentration (Lu et al., (2021)).

The remarkable O/W stabilising ability of micro- and nanocellulose is often attributed to a combination of Pickering and network stabilisation mechanisms. Below a critical cellulose concentration, O/W emulsions can be prepared in the limited coalescence regime (since particles are effectively irreversibly adsorbed) (Tasset et al., (2014)) whilst if the concentration of cellulose is sufficiently high, coverage exceeds 100 % and this results in either formation of dense interfacial films (Tasset et al., (2014)) or a cellulose network in the aqueous phase (Olsson et al., (2010); Kalashnikova et al., (2013); Jia et al., (2015); Cherhal et al., (2016); Z. Li et al., (2018); Ni et al., (2020); Q. Li et al., (2021)). The latter usually occurs for more flexible types of cellulose with higher aspect ratios, which can thus achieve extended-chain conformations and entangle (Bai et al., (2018)). At even higher concentrations, nanocellulose forms a gel-like emulsion (Winuprasith and Suphantharika, (2015); Jia et al., (2015); Z. Li et al., (2018)) and this has been reported at concentrations as low as 0.3 wt% (Bai et al., (2018)). Gel-like behaviour is also observed for emulsions with higher oil concentrations, for example medium-internal-phase (Li et al., (2019)) and high-internal-phase emulsions (MIPEs and HIPEs respectively, where HIPES contain >74 % dispersed phase), with CNC concentrations as low as 0.1 wt% (Capron and Cathala, (2013)).

1.4.2.2 Cellulose derivatives

Substitution of the cellulose hydroxyl groups is performed to increase amphiphilicity and various cellulose derivatives display excellent surface activity (MC, HMPC, EC), providing stabilisation to foams and emulsions (Grover, (1986); Gullapalli and Sheth, (1996); Melzer et al., (2003); Arboleya

and Wilde, (2005); Futamura and Kawaguchi, (2012); Karlsson et al., (2015); Zhang et al., (2022)). The interfacial properties can be tuned by varying the degree of substitution (DS) and molar mass (Nasatto et al., (2014)), as well as the processing conditions: for example, homogenised MC shows weaker thickening and stabilising abilities compared to non-homogenised MC (Floury et al., (2003)). EC is the only water-insoluble cellulose ether described and can be used to stabilise W/O emulsions (Melzer et al., (2003)) and gel liquid oils (Zetzl et al., (2012)). Table 1.3 gives a summary of recent applications of cellulose derivatives as emulsion and foam stabilisers, for various food products.

Table 1.3. Summary of various publications on cellulose derivative-based emulsions and foams in the last 10 years, for various food product applications.

Emulsion/foam type	Description of stabiliser	Stability	Reference
O/W	HPMC (1-2 %, 20-60 % oil)	>1 year	(Wollenweber et al., (2000))
O/W	MC (0-1 %), Tween40, Span20 (30 % oil)	>6 months	(Gullapalli and Sheth, (1996))
O/W	HPMC/MC (2 %, 47 % oil)	Tested for fat digestion	(Espert et al., (2017))
O/W	HPMC (40 % oil)	Tested after 3 days	(Futamura and Kawaguchi, (2012))
O/W	MC (2 %, 51 % oil)	Tested for fat digestion	(Espert et al., (2016))
O/W	HPMC/MC (2 %, 51 % oil)	Tested for thermal stability (heated and cooled 20-80-20 °C)	(Sanz et al., (2015))
O/W	EC (10 %), emulsifiers (10 % oil)	Tested for ice cream	(Munk et al., (2018))
W/O	EC (0.5-2 %, % water not mentioned)	Not mentioned	(Melzer et al., (2003))

W/O	EC ‘nanoparticles’ and ‘oleogels’ (0.8-2 %, 40 % water)	>30 days	(Zhang et al., (2022))

1.4.2.3 Cellulose-based oleogels

In the last 10 years, edible oleogels have become of increasing interest as a potential solution to structuring liquid oil and reducing saturated fat, using cellulose stabilisers. Cellulose oleogels are typically fabricated via an emulsion-templated approach, where an O/W emulsion is first produced and subsequently dried and sheared to produce the gel (Patel, Cludts, Bin Sintang, et al., (2014)). Additional thickeners can be added to enhance oleogel properties by providing kinetic stability to the emulsion (Hill et al., (1998); Meng et al., (2018); Jiang et al., (2022)) and altering the textural characteristics of the gel (Patel, Cludts, Sintang, et al., (2014); Jiang et al., (2022)). However, more recently MC (or HPMC) oleogels have been produced without additional thickeners (Espert et al., (2020)) using alternative methods, where a cryogel or aerogel is initially fabricated (oil-adsorbing foam template) (Tanti et al., (2016); Jiang et al., (2021)).

Whilst polymer oleogels based in cellulose derivatives have been applied in the literature to many food products such as chocolate (Patel and Dewettinck, (2015)), cookie fillings (Tanti et al., (2016)) and cakes (Oh and Lee, (2018)), more detailed studies are required to understand their behaviour including response to shear, processing and storage conditions (Demirkesen and Mert, (2020)). Furthermore, the additional processing steps (e.g. emulsion fabrication, freeze-drying, solvent removal) required for oleogelation of cellulose ethers (compared to natural waxes) presents an additional challenge to their scale-up and industrial viability (Patel and Dewettinck, (2016)). Table 1.4 gives an overview of some of the research conducted for oleogels in food products, in the last 10 years.

Table 1.4. Summary of various publications on cellulose-based oleogels in the last 10 years, for various food product applications.

Food Sector	Specific application	Gel ingredients (gelator/structuring agent, thickening agents and oil type)	Reference
Dairy products	Cream cheese	EC, rice bran wax, soybean oil	(Bemer et al., (2016))
	Ice cream	EC, sunflower oil	(Munk et al., (2018))
Meat products	Frankfurters/ground meat products	EC, canola, soybean and flaxseed oils	(Zetzl et al., (2012)), (Zetzl et al., (2014))
	Pork liver pâté	EC, beeswax, olive, linseed and fish oils	(Gómez-Estaca et al., (2019))
Chocolate	Reducing SF	HPMC, sunflower oil	(Patel and Dewettinck, (2015))
	Heat resistant chocolate	EC	(Stortz and Marangoni, (2013)); (Marangoni, (2012))
Bakery products	Partial/full replacement in sandwich cookie fillings	HPMC, MC, canola oil	(Tanti et al., (2016))
	Shortening alternative in muffins	HPMC, sunflower oil	(Oh and Lee, (2018))
	Shortening alternative in cakes	MC, XG[1], sunflower oil	(Patel, Cludts, Bin Sintang, et al., (2014))
	Shortening alternative in bread	EC, soybean oil, palm stearin	(Ye et al., (2019))

[1]XG = xanthan gum

1.4.2.4 Native cellulose

Although cellulose is often modified to improve its surface properties, numerous studies in the last decade have shown that chemically unmodified cellulose can act as a stabiliser/thickener (Kalashnikova et al., (2011); Rein et al., (2012); Jia et al., (2013); Jia et al., (2015); Napso et al., (2016); Zhu et al., (2017); Kasiri and Fathi, (2018); Goi et al., (2019); Szlapak Franco et al., (2020); Ni et al., (2020); Lefroy, Murray, Ries, et al., (2021)). The development of efficient, non-derivatising cellulose solvents, such as ILs (Swatloski et al., (2002)), has provided facile routes for producing novel cellulose materials. Despite this, few reports have demonstrated convincing evidence that cellulose truly adsorbs at the interface, in order to provide long-term emulsion stability. Most studies of native cellulose emulsions (including MCC), describe a network-based stabilisation mechanism, where excess cellulose in the continuous phase aggregates and 'traps' droplets from the discontinuous phase (Oza and Frank, (1986); Jia et al., (2015); Z. Li et al., (2018)).

Cellulose has a tendency to flocculate/aggregate when dispersed in aqueous solution due to its water-insolubility, resulting in the network formation which is commonly observed in O/W emulsions. However, there is far less research into the behaviour of native cellulose dispersed in hydrophobic media and its ability to stabilise W/O emulsions. This thesis contributes to this research gap and aims to revisit the structural features of native cellulose, by investigating physical processing methods for capturing its surface activity. This provides an interesting avenue for novel, Pickering-type cellulose stabilisers.

1.4.3 Microgel-stabilised emulsions

Microgels are discrete particles of approximately micrometre size that are made up of a network, which traps solvent within its structure (Thorne et al., (2011)). They can be produced either by 'bottom-up' or 'top-down' methods, the former of which uses network growth to control the final particle size and the latter of which uses controlled fragmentation of a bulk gel into smaller individual particles (Murray, (2019a)). Further details on microgel synthesis, properties and applications are given in **Chapter 2**.

Emulsions stabilised by microgels are often referred to as 'Mickering' emulsions, reflecting their similarities and differences to 'Pickering' (solid particle-stabilised emulsions). Microgels can adsorb rapidly and effectively irreversibly at the interface whilst being insoluble in both phases individually, analogous to particle stabilisers. However, the softness and compressible nature of microgels make them distinctive from hard particles and they can deform, spread and change shape at an interface. This results in unique

surface properties and in some instances, the ability to stabilise both O/W and W/O emulsions depending on the conditions (Fujii et al., (2006); Brugger et al., (2008)). Microgels may also modify the rheological properties of an emulsion (Murray, (2019a)) and Mickering emulsions have shown impressive resilience to gastric coalescence (Sarkar et al., (2018); Sarkar et al., (2019)), delaying digestion either when microgels are conjugated with particles (Araiza-Calahorra et al., (2020); Yang et al., (2022)) or fused at the interface (Sarkar et al., (2016)).

Microgelation can provide a route to imparting surface activity on polymers displaying poor interfacial properties, such as native cellulose, and thus opens up further opportunity to develop many more emulsion stabilisers with sustainable, cost-effective and biocompatible materials that may be more consumer-acceptable (Murray, (2019a)). Cellulose-based microgels are reviewed in more detail in **Chapter 2.** In this thesis, we have used this principle to capture the surface activity of cellulose by 'trapping' its solution state, within a microgel structure, investigating its potential to function as a W/O stabiliser.

1.5 Rationale behind the use of Ionic Liquids (ILs)

ILs are room temperature liquid salts, unlike organic solvents which are molecular liquids, and are made up of a cation and anion pair (Yang and Pan, (2005)). The ions are relatively bulky and therefore have lower packing densities relative to conventional salts, which means that they can flow at ambient temperatures. ILs have emerged as an alternative to conventional solvents due to their unique and attractive properties, such as low toxicity, low volatility, non-flammability, thermal/chemical stabilities and tuneable properties. Furthermore, they are commonly described as 'environmentally friendly' solvents (Yang and Pan, (2005); Cao et al., (2017); Jiang et al., (2018)) and have the potential to be recycled (as briefly reviewed in section 1.3.1). Whilst they find application across many functions such as biocatalysts (Roberts and Lye, (2002)), lubricants (Qu et al., (2009); Jiang et al., (2018)) and biodiesel production (Yassin et al., (2015)), ILs have also been employed as cellulose solvents in the last 20 years (Swatloski et al., (2002); H. Wang et al., (2012)) and have been utilised to prepare cellulose composite materials (e.g. plastic alternatives) (Swatloski et al., (2002); Hine and Ries, (2020)). This section briefly introduces the properties of ILs and their application in cellulose processing, including their advantages and drawbacks.

1.5.1 Properties of ILs for cellulose processing and recyclability

ILs can be used under relatively mild conditions, exhibit short dissolution times and don't involve the use of toxic chemicals, unlike many other conventional cellulose solvents. They are non-volatile and non-flammable, making them very safe to use at elevated temperatures which are often used to reduce solvent viscosity and improve dissolution efficiency. Furthermore, ILs exhibit far lower degradation potentials compared to alternative non-derivatising cellulose solvents, such as NMMO (Wendler et al., (2012)), due to their high thermal and chemical stabilities. The window between onset temperature (T_{on}) and processing temperature is significantly wide, ensuring a lower risk of exothermic interactions and therefore enhanced process safety at high temperatures (Wendler et al., (2012)). However, the presence of cellulose reduces the thermal stability of ILs, so dissolution is not usually carried out at temperatures exceeding 100 °C (Cao and Mu, (2014); Xue et al., (2018)).

ILs display high cellulose dissolving capacities (ranging from 10-20 wt%) (Rieland and Love, (2020)) and if used under controlled conditions, are generally non-derivatising solvents (Clough et al., (2015); Wang et al., (2016); Zhang et al., (2018)). Thus they have been extensively used for laboratory-scale preparations of various cellulose materials, such as hydrogels (Kadokawa et al., (2008); Li et al., (2009); Johns et al., (2017); Idenoue et al., (2019); Satani et al., (2020); Lefroy, Murray, Ries, et al., (2021)), films (Östlund et al., (2013); Sun et al., (2015)), fibres/rods (Swatloski et al., (2002); Kosan et al., (2008); Cai et al., (2009); Quan et al., (2010)) and particles (Suzuki et al., (2014); Fan et al., (2018)), where cellulose can be easily reprecipitated by adding an anti-solvent. Depending on the method of coagulation and the type of anti-solvent, different cellulose properties (e.g. crystallinity, porosity and densities (Fryczkowska et al., (2018); Hedlund, Köhnke, et al., (2019)) and morphologies (Swatloski et al., (2002); H. Wang et al., (2012); Han et al., (2013); Sun et al., (2015); Bazbouz et al., (2019); Yang et al., (2020))) can be obtained, as discussed in section 1.3.3. Several studies have also used a solvent releasing method (SRM) to obtain very uniform, homogeneous cellulose microspheres/beads from ILs, where the size of cellulose particles is controlled by first forming an IL-in-oil emulsion (Suzuki et al., (2014); Jo et al., (2019)).

As well as being efficient solvents for cellulose, ILs are highly tuneable and versatile. It has been suggested that over 1 million possibilities could be synthesized, owing to their modular nature (Plechkova and Seddon, (2008);

Cao et al., (2017)), and they can be designed for specific purposes by tethering functional groups onto either the cation or anion (or both). For example, task-specific ionic liquids (TSILs) have been fabricated for use in chemical reactions as reagents or catalysts (Yue et al., (2011)).

ILs are commonly referred to as 'green' solvents, owing in part to their alleged recyclability, which not only reduces their environmental impact but also their cost (Kuzmina, (2016)). They have been extracted and reused after cellulose processing using liquid-liquid extraction, distillation, induced phase separation and membrane-based methods (Wasserscheid and Keim, (2000); Gutowski et al., (2003); Han et al., (2005); Deng et al., (2009); Huang et al., (2013); Lynam et al., (2016); Hossain et al., (2019)), however to our knowledge, their recyclability has yet to be applied on a large scale. This is most likely due to difficulty with their separation and recovery from other solvents, which often requires a large amount of energy (Haghighi Mood et al., (2013)) since ILs are extremely hygroscopic and water contamination is an issue (Cao, Chen, Lu, et al., (2013); Cao, Chen and Mu, (2013); Cao et al., (2014)). Despite these challenges, ILs are sufficiently stable and robust even after recycling and several reports have shown that they can be reused at least 5-10 times (Lozano et al., (2012); Auxenfans et al., (2014); Wei et al., (2021)), with little effect on their properties.

1.5.2 Currently understood mechanism of cellulose dissolution

ILs have been increasingly used in cellulose dissolution on a research scale for the last 20 years, as promising, 'green' solvents. However, there is still some debate over the details of the mechanism, with the majority of reports focussing on H-bonding and the ability of the IL to disrupt the inter/intramolecular H-bond network between and within cellulose chains.

Several reports claim that increasing the H-bonding ability of an IL improves its cellulose dissolving capacity (Vitz et al., (2009); Stark et al., (2012); Zhang et al., (2016)), whilst Zhao *et al.* observed the opposite trend (H. Zhao et al., (2008)). It is well known that the type of anion has an effect on the ability of an IL to dissolve cellulose and most studies focus on cellulose-anion interactions, which are predicated to be most significant (Remsing et al., (2006); Remsing et al., (2008); Zhang, Zhang, Wu, et al., (2010)). Imidazolium-based ILs display higher dissolving capabilities when paired with more electronegative halide anions (Holm and Lassi, (2011)), specifically chlorine, which is relatively small in size. This makes it a good H-bond

acceptor with a strong ability to disrupt cellulose-cellulose H-bonding (Rodríguez, (2021)).

On the other hand, the exact role of the cation in cellulose dissolution is less well-understood. Cation-cellulose interactions, which are affected by the properties of the cation, should be considered (Lu et al., (2014)) and the ability of the cation to disrupt hydrophobic cellulose-cellulose interactions may play a role (Lindman et al., (2010); Medronho and Lindman, (2014)). The electronegativity can affect the electrochemical (Xue et al., (2018)) and thermal stability (Z. Chen et al., (2011)) of the IL, as well as the acidity of the protons and the bulkiness (Isik et al., (2014)). An extensive number of computational studies have been conducted in attempt to shed light on the exact mechanism for IL-cellulose dissolution (Gupta and Jiang, (2015)), however many studies up until now have been based on trial and error (Mohd et al., (2017)).

1.6 Rationale behind the use of characterisation techniques

A range of techniques were used to carry out detailed characterisation of the bulk physical properties as well as the microstructures of the cellulose gels, CMG-dispersions and CMG-stabilised emulsions. Theoretical and technical details of the techniques used in this thesis are outlined below.

1.6.1 Static light scattering (SLS)

Static light scattering (SLS) was employed to measure the size of the CMGs in both oil and water dispersions, as well as the size of water droplets in the CMG-stabilised W/O emulsions.

SLS is suitable for measuring particles sizes between ca. 100 nm-1 mm and is based on the Rayleigh theory, where light passes through a solution of material and is scattered depending on the molecular weight of the material. Light is scattered at different angles, depending on the particle size: small particles scatter light at large angles, whilst larger particles scatter light at smaller angles. The scattering pattern can be converted into a size distribution via the ‘Mie theory’, which uses the difference in refractive indices (RIs) of the particles and the dispersion medium to predict the intensity of the scattered light. Mie scattering describes elastic scattering of light from homogeneous, spherical particles which are larger than the wavelength of incident light, and therefore this theory breaks down for non-spherical particles (Lockwood, (2016)).

The basic set up of a SLS experiment is given in Figure 1.7, showing the measurement of the scattered intensity over the duration of a measurement.

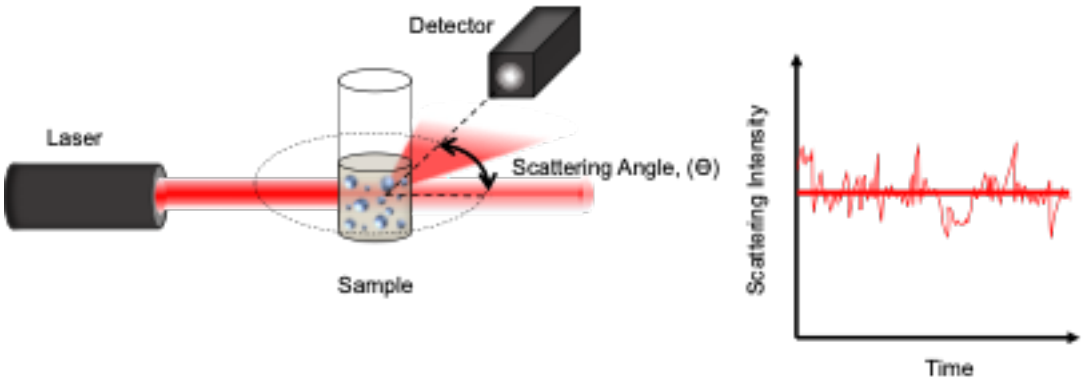

Figure 1.7. Typical setup of a SLS experiment, where a laser passes through a cuvette containing the sample and light is scattered. One or many detectors measures the scattering intensity as a function of the scattering angle.

Size distribution data obtained via SLS is usually presented as a volume-weighted distribution, since the diffraction of light is proportional to the particle volume, but can be converted to a number-weighted distribution. The average particle size diameter is most commonly given as the surface-weighted mean diameter ($d3,2$) and the volume-weighted mean diameter ($d4,3$), as described in Equation 1 and Equation 2:

Equation 1. $$(\boldsymbol{d3,2}) = \frac{\Sigma_i n_i {d_i}^3}{\Sigma_i {n_i}^2}$$

Equation 2. $$(\boldsymbol{d4,3}) = \frac{\Sigma_i n_i {d_i}^4}{\Sigma_i {n_i}^3}$$

Where n_i gives the number of droplets and d_i gives the diameter of the particle.

In this thesis, a Hydro SM small-volume wet dispersion unit (Malvern, Malvern Instruments, UK) was used with sunflower oil as the continuous phase, to analyse the CMG and water droplet size in oil/water dispersions and W/O emulsions, respectively.

1.6.2 Dynamic light scattering (DLS)

In contrast to SLS, where the intensity of the scattering signal is obtained over time and averaged, dynamic light scattering (DLS) analyses the intensity fluctuations of scattered light due to Brownian motion of particles (Dahneke, (1983)). Particles are constantly moving randomly in all directions and colliding with solvent molecules, which results in energy transfer. This energy transfer is more or less constant, but has a greater effect on smaller particles which move at higher speeds. Therefore, fluctuations in the intensity of scattered light are faster for smaller particles, whilst larger particles display

higher amplitudes between their maximum and minimum scattering intensities. The correlation function can be generated from the intensity trace, which is used to determine the translational diffusion coefficient (*D*). The hydrodynamic size (R_H) can then be deduced from *D*, if other parameters which effect particle movement are known, via the Stokes-Einstein (Equation 3):

Equation 3. $$\boldsymbol{D = \frac{k_B T}{6\pi\eta R_H}}$$

Where k_B = Boltzmann constant; *T* = temperature and η = viscosity.

DLS is suitable for measuring particles sizes in the submicron region and the latest instruments can reliably measure down to 1 nm. The upper size limit is based on the onset for sedimentation, since the Stokes-Einstein equation only applies if particle movement is based solely on Brownian motion, whilst the lower size limit is defined by the signal-to-noise ratio (SNR) of the instrument. Particle sizes obtained from DLS refer to the size of smooth, spherical particles and results are obtained as an intensity-based distribution, which can be converted to a volume- or number-weighted distribution. DLS was used in this thesis to analyse the CMG particle size distributions, in aqueous dispersions only.

1.6.3 Microscopy across length scales (stereo; optical including polarised; confocal laser scanning (CLSM); scanning electron (SEM))

Various types of microscopy across different length scales are employed in this thesis, to analyse the microstructures of the CMG-dispersions, emulsions and cellulose gels.

Optical (light) microscopes use visible light to generate magnified images of a specimen and have evolved to allow us to see things more deeply, more specifically and more quickly within a sample. The basic setup of an optical microscopy is given in Figure 1.8.

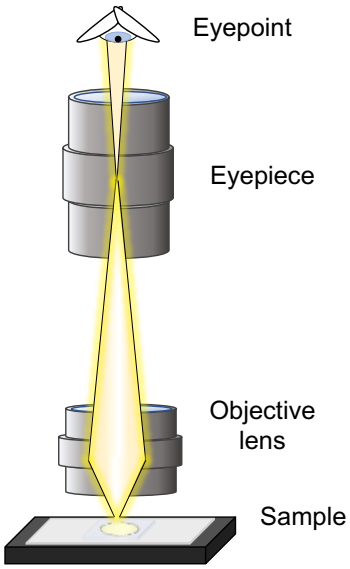

Figure 1.8. Schematic depicting the basic setup for an optical microscope, where the sample is placed on a stage and viewed through an eyepiece. The objective lens focusses light and magnifies the sample.

Conventional optical microscopy is often a primary tool employed in the microstructural characterisation of particle dispersions and emulsions. It uses wide-field illumination, capturing images of the sample below and above the focal plane, and is useful for examining emulsion properties such as a droplet shape and size distribution (Hu et al., (2017)). However, high-powered magnification cannot be achieved at the same time as a large depth of field and it is impossible to focus exclusively on specific sample planes. Usually a large number of images must be captured and several sample slides prepared to generate reliable data (Xiaodong Chen et al., (2011)), whilst a thin sample film is required potentially altering the emulsion structure and making it less suitable for thicker samples (e.g. gels) (Hu et al., (2017)). The resolution of conventional optical microscopes is often limited to around ~250 nm and >450-700 nm in the x/y and z directions, respectively (Galbraith and Galbraith, (2011)).

In order to perform more detailed microstructural characterisation of particles and droplets of the nano- to micrometre size orders, confocal laser scanning microscopy (CLSM) can be employed. CLSM is a type of fluorescent imaging and allows visualisation of specific fluorophores which are tagged or stained within a sample. Unlike conventional optical microscopy techniques based on scattering, reflection or adsorption of light, fluorescent techniques use adsorption of energy by molecules in the form of photons, which are then emitted as fluorescent photons at longer wavelengths (and lower energies) a few nanoseconds later. The (excitation) wavelength of the adsorbed light is

usually shorter than the (emission) wavelength of the emitted light, because some energy is lost in the process (Stokes Shift, Figure 1.9a) (Sanderson et al., (2016)). The basic set-up of a CLSM is given in Figure 1.9b, depicting the key components. Light emitted from the sample is directed through a pinhole which increases the resolution, reduces the amount of out-of-focus photon emission and detects fluorescence which is close to the in-focus plane only. Therefore, images can be captured of a single x-y plane and the in-focus position along the z-plane can be adjusted using a stepping motor, to capture multiple consecutive images and allow 3D image reconstruction.

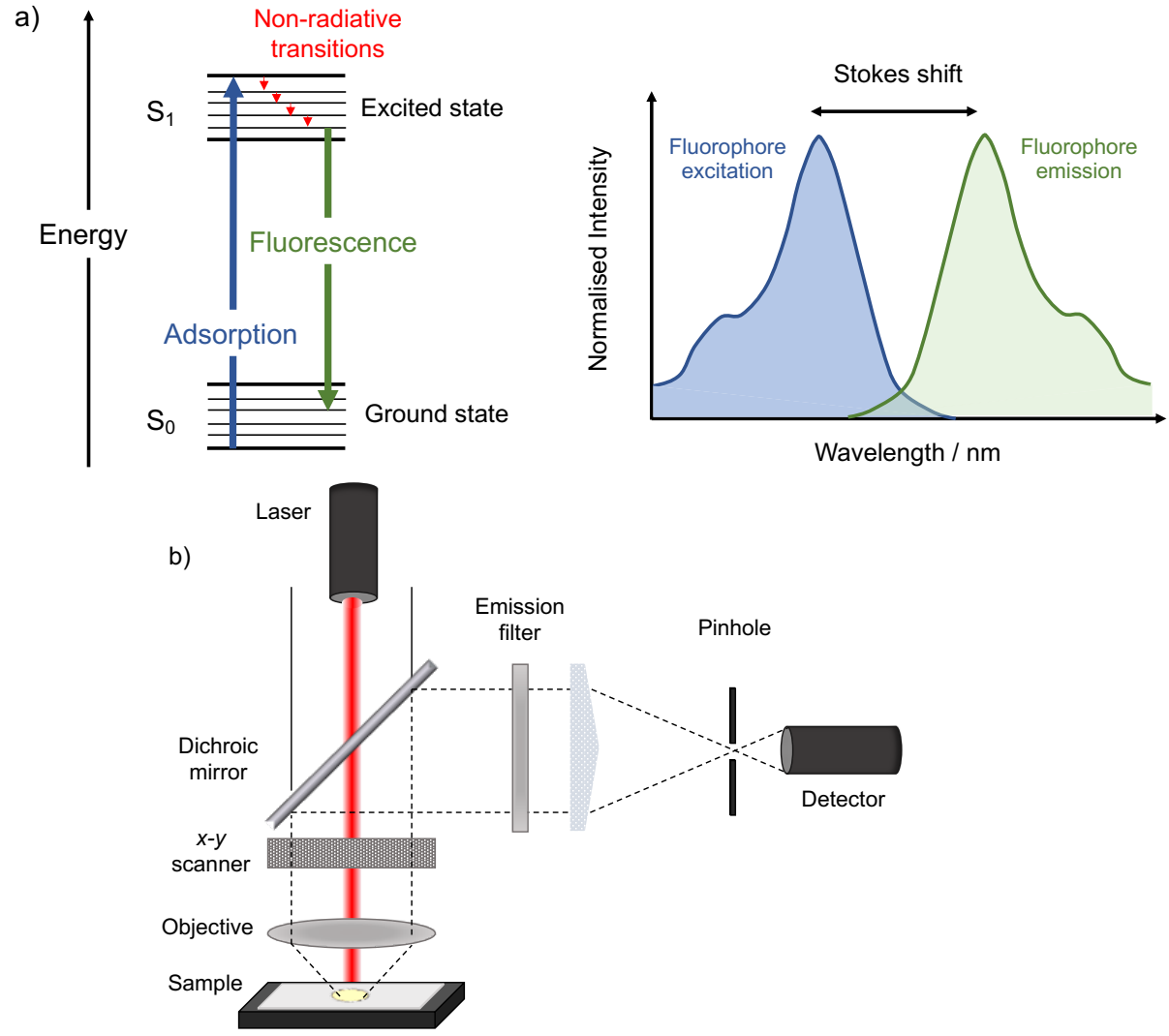

Figure 1.9. a) Jablonski energy diagram depicting Stokes shift, showing the transitions corresponding the adsorption (from ground state to excited state) and fluorescence (from excited state to ground state); b) setup of a CLSM, where a laser beam passes through a light source aperture and is focussed by the objective lens onto a small area of sample. Photons are emitted by fluorophores in the sample and collected to generate an image.

Scanning electron microscopy (SEM) is used to obtain high resolution images sample surfaces and can give detailed information on the surface topography, chemical composition, crystalline structure and electrical behaviour of a specimen. Electrons possess shorter wavelengths compared to visible light, and therefore higher magnification and better resolution can be achieved by using electron radiation imaging. Whilst the maximum achievable magnification of a conventional optical microscope is around 1,000x, it can be up to 1,000,000x for an electron microscope (Vernon-Parry, (2000)).

In a SEM experiment, an electron gun generates an incident beam which passes through two or three electromagnetic condensers and forms a probe that is focussed onto an area of the sample. The electron probe is scanned across the surface and penetrates the sample to a depth of around 1 μm, producing secondary, backscattered and Auger electrons, as well as x-rays and sometimes light (Figure 1.10). Different detectors within the specimen chamber collect different signals to generate images.

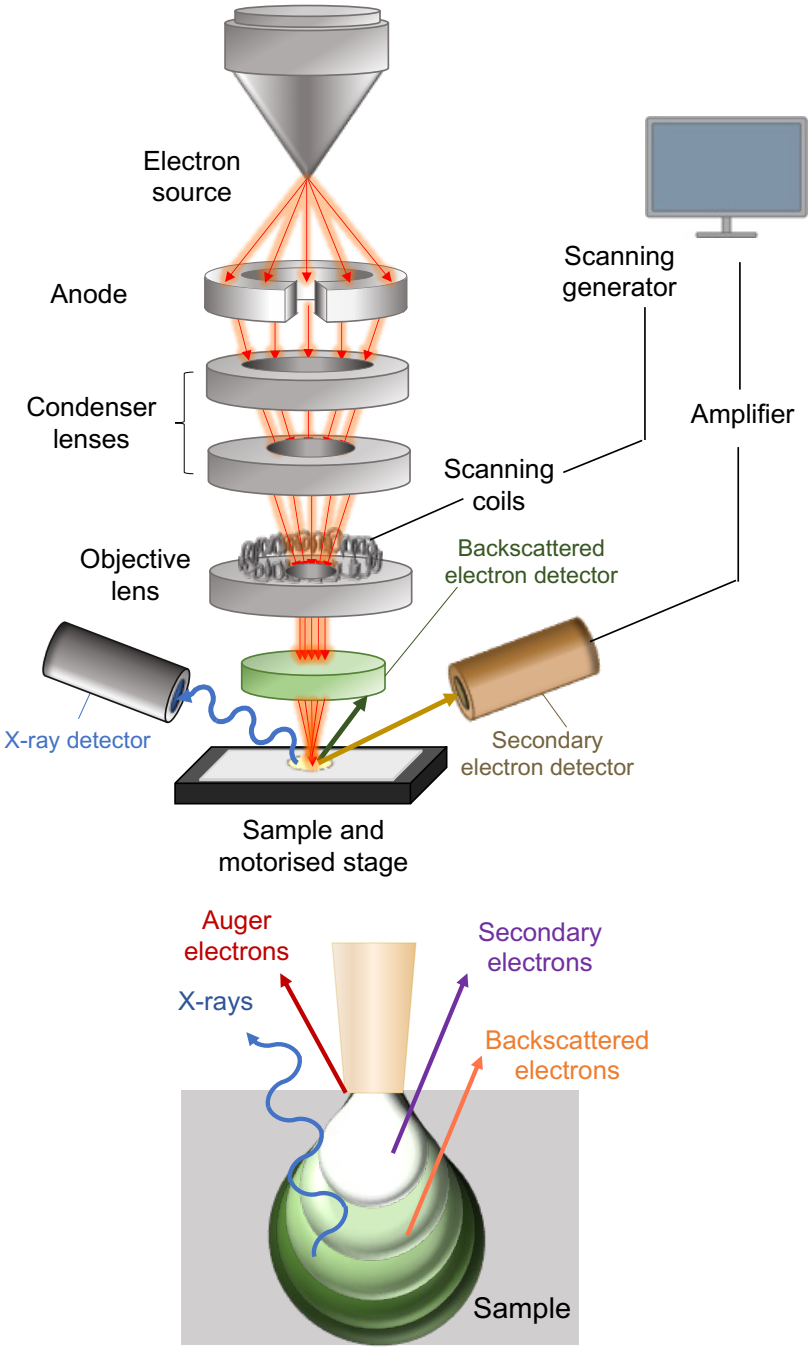

Figure 1.10. Typical setup of an SEM, showing the different types of electrons that are generated. An electron beam is generated by a filament, focussed and scanned across the sample, producing various signals which are collected by various detectors.

Secondary electrons provide the highest resolution images, since they escape from electron orbits further from the nuclei of atoms, and are used to obtain mainly topographic information. Backscattered electrons have higher energies and escape from electron shells close to the nucleus, generating lower resolution images. They are usually used for compositional analysis and can also provide information about the crystal structures. Auger electron imaging is performed more rarely on specific instruments, since a relatively low number of electrons are generated, and can give information about the surface

chemistry. Finally, x-rays can give valuable information on the chemical composition of a sample and most SEM instruments are equipped with energy dispersive x-ray spectroscopy (EDS or EDX), which can allow rapid quantitative analysis.

1.6.4 Rheology

Rheology is used to describe the physical properties of deformation and flow behaviour of matter. It is widely applied in food science to understand how different products can be mixed and processed, as well as giving information about their sensory properties (Day and Golding, (2016)).

All materials, whether solid or liquid, are described by both a viscous (liquid) and elastic (solid) component. This is known as the theory of viscoelasticity and the degree to which a material appears liquid or solid depends on both the rate and the magnitude of deformation (shape change). When an external force is applied, a material either moves or changes shape (or both) in response. The simplest form of this is uniaxial extension, where the force acts only in one direction and this generates a stress (σ) and strain (γ) within the material. σ describes the force required to cause deformation, whilst γ provides a measure of the degree of deformation.

Stress and strain are proportional to each other for small deformations when Hooke's law applies and are linked by the elastic (Young's) modulus (E), which is a constant for a given material and gives information on how easily it can stretch and deform. As the magnitude of deformation is increased beyond the elastic limit, Hooke's law no longer applies and other limits are reached: proportionality limit, yield point, fracture point and ultimate tensile strength (Figure 1.11).

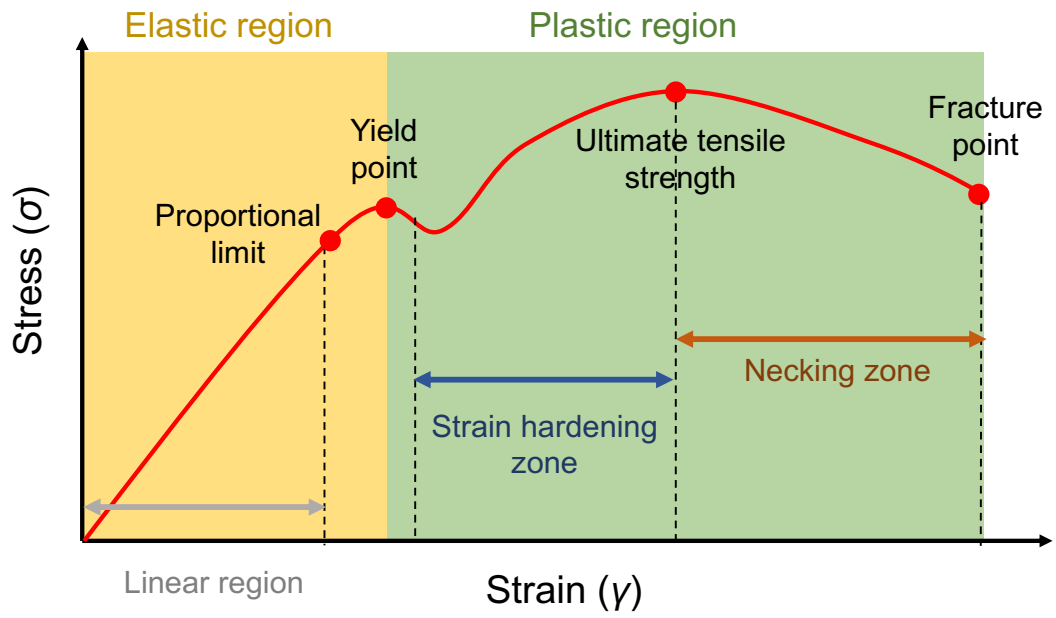

Figure 1.11. Example of a stress-strain curve for structural steel material, indicating the elastic, plastic, strain-hardening and necking zones; proportional limit; yield point; ultimate tensile strength and fracture point.

On a rotational rheometer with a parallel plate system, the shear viscosity can be measured by loading the sample between the two plates and applying a shear stress (force, σ), resulting in deformation of the material under the application of a given force (γ). γ describes the displacement gradient which is generated across the sample and the two-plates model is used to describe flow behaviour, where the lower plate is stationary and the upper plate moves (Figure 1.12). If the gap between the plates is known (h), the shear rate ($\dot{\gamma}$) can be determined by measuring the velocity (v) of the upper plate. $\dot{\gamma}$ is defined as:

Equation 4 $$\dot{\gamma} = d\gamma/dt$$

Where $d\gamma$ = rate of change in strain and dt = rate of change in time.

The shear flow (viscosity, η) of a material depends on the ability of constituent components to move past each other on application of a shear force, which transfers momentum to the fluid. This momentum is then transferred through the fluid layers through component collisions and interactions, reducing the fluid velocity and kinetic energy. η is defined as:

Equation 5 $$\eta = \sigma/\dot{\gamma}$$

Where η (Pa.s) gives a quantitative measure of the internal fluid friction associated with the loss of kinetic energy within the system (Malvern Instruments, (2016)).

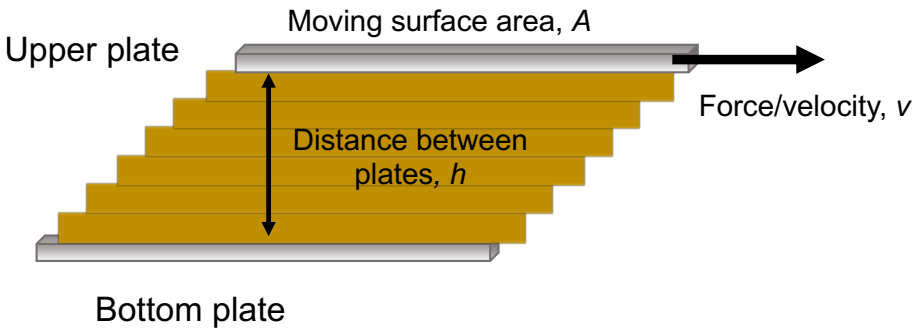

Figure 1.12. Schematic describing the two-plates model, used to define rheological parameters of flow behaviour.

For Newtonian fluids, like pure water and oil, σ and γ are linearly related and therefore η remains the same regardless of $\dot{\gamma}$. However, many dispersions/emulsions display non-Newtonian behaviour and are most commonly shear-thinning, displaying a decrease in η upon increasing shear rate. At low shear, fluids may display Newtonian behaviour and this is termed the zero shear viscosity plateau (η_0). At a given shear stress, the viscosity drops indicating the start of the shear-thinning region and continues to decrease up to a point where the viscosity becomes linear again at very high shear rates, defined as the infinite shear viscosity plateau (η_∞). A schematic is given in Figure 1.13 depicting the possible microstructural arrangements that may occur in a shear-thinning dispersion/emulsion, upon the application of a shear force.

In this thesis, rheological analysis is used to measure the viscosities of cellulose solutions dissolved in the IL 1-butyl-3-methyl imidazolium acetate (BmimAc), as well as CMG-in-oil/water dispersions and W/O emulsions.

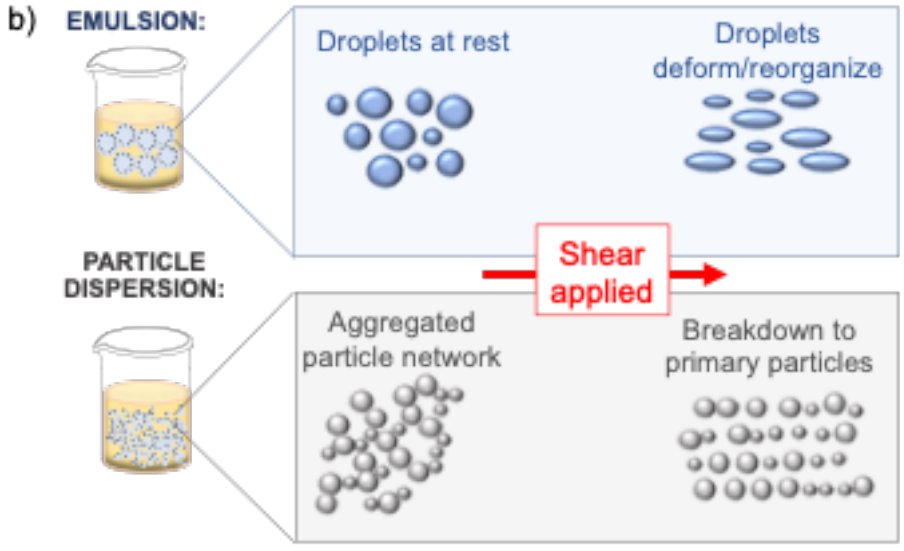

Figure 1.13. Examples of microstructural rearrangements in emulsions/dispersions that lead to shear-thinning behaviour.

1.6.5 ^{1}H Nuclear magnetic resonance (NMR) spectroscopy (high resolution) and fast-field cycling (FFC) NMR

Nuclear magnetic resonance (NMR) spectroscopy is a powerful and versatile technique which can be used for structural determination and to quantitatively analyse mixtures of components (Pesek and Matyska, (1999)). In this thesis, high-field ^{1}H (proton) NMR is used to characterise solutions of cellulose in BmimAc (with and without oil), and to gain information on specific interactions occurring in these solutions. Diffusion ^{1}H NMR and fast-field cycling (FFC) NMR are also employed to gain information on the solution dynamics, proving further insight into microscopic molecular interactions.

Hydrogen atoms possess spin-½ nuclei (I = ½) which act as magnets and are split into two energy levels, in the presence of a magnetic field. At the lower (base) energy level, the spin is aligned with the magnetic field and at the higher (upper) energy level, the spin is opposed to the external field. Transitions between the two energy levels occur at a specific wavelength, corresponding to the radiofrequencies (Figure 1.14). The ^{1}H nucleus is very commonly studied due to its high abundance, presence in all organic molecules and high sensitivity. The latter is a result of the high value for the magnetic moment to angular momentum ratio (gyromagnetic ratio, γ) of protons, which leads to a higher population difference between the upper and lower energy levels. This phenomenon gives a greater signal intensity and therefore ^{1}H signals are easily detected via NMR.

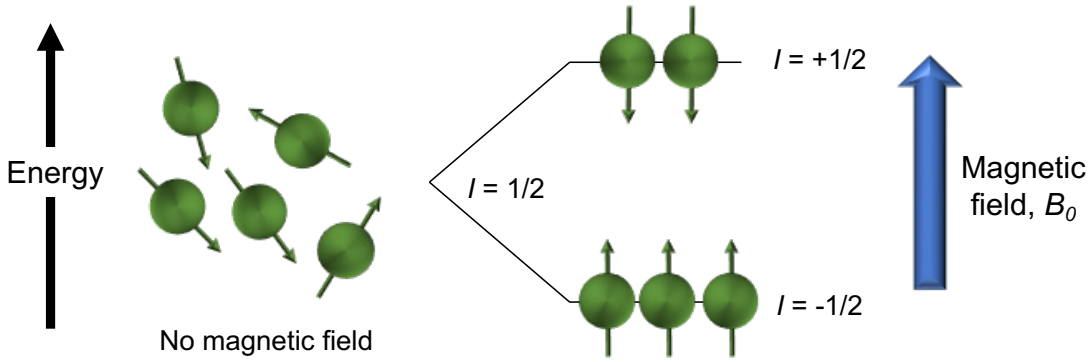

Figure 1.14. Illustration to show the energy level splitting for spin-½ nuclei, upon application of an external field.

The resonant frequency at which the transition between energy levels occurs depends on the chemical environment of the proton. Electrons around the nuclei shield the external magnetic field, reducing the effective field experienced by the nuclei and resulting in different resonance frequencies. Specific proton environments can be assigned to certain functional groups in an NMR spectrum, allowing identification of certain compounds. A reference

compound is usually added (e.g. tetramethylsilane, TMS) and its resonance frequency is set to zero, so that the chemical shift (δ) values of all the other peaks are defined relative to this:

Equation 6 $$\boldsymbol{\delta = (\nu - \nu_0)/\nu_0}$$

Where v = resonant frequency of a given nucleus and v_0 = resonance frequency of the reference nucleus.

Protons which are next to electronegative groups (electron withdrawing groups, EWGs) 'feel' the effect of the external magnetic field to a greater extent because of the reduction in electron density by the EWG. Thus, the effective field experienced is reduced and a smaller field is required for protons to be brought into resonance. On the other hand, protons adjacent to electropositive groups (electron donating groups, EDGs) experience shielding from the external magnetic field due to the increase in electron density by the EDG, and require a higher field. In the former case, this is described as 'de-shielding' and proton signals appear at higher δ values, whilst for the latter case, 'shielding' occurs and proton signals appear at lower δ values. If the sample contains an unknown compound, the NMR spectrum can be used to identify which functional groups are present.

Adjacent spin active nuclei on neighbouring atoms can cause a proton signal to split due to spin-spin coupling, since they also possess a magnetic field (Clark, (2000)). The magnitude of splitting or the coupling constant (J) is independent of the magnetic field, whilst the splitting gives information on the number of neighbouring nuclei which are chemically bonded to the nucleus being observed. The n+1 rule applies for ^{1}H NMR, since the number of 'sub-peaks' is one more than the number of neighbouring protons.

High-field NMR operates at one resonance frequency and uses a very powerful magnet, generating strong magnetic fields that result in large differences between the energy levels of nuclei (and thus higher sensitivities). Excellent spectral resolution can be achieved and peaks as well as splitting patterns can be easily distinguished. It is also possible to accurately calculate the number of protons in a given chemical environment by integrating peaks, enabling quantitative analysis of components.

FFC NMR operates over a range of lower magnetic fields and uses a switchable field to measure relaxation, most commonly of ^{1}H nuclei. As NMR is an inherently insensitive technique, low frequency measurements are complicated by very low SNR and signal intensity decreases almost quadratically with frequency. This is the limiting factor in low-field NMR

(Anoardo et al., (2001)), however FFC NMR can be extended over a wide range of relaxation fields (100 Hz – 40 MHz) (Mikac et al., (2019)) and the frequency dependence of the spin-lattice (R_1) and spin-spin (R_2) relaxation values can be probed, as a dispersion. Fast and slow dynamics can be separated within a solution, for example rapid motion of side chains on a polymer and comparatively slow centre-of-mass motion of polymers. The magnetic field applied over the course of a sequence is split into the polarisation, evolution and detection period, as depicted in Figure 1.15.

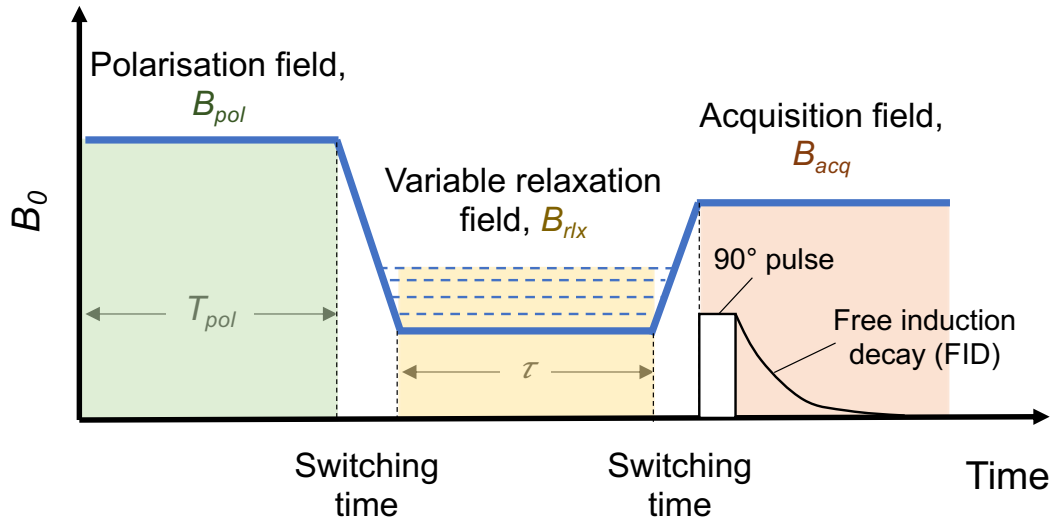

Figure 1.15. Field-cycling sequence, where relaxation of nuclei occurs over the evolution period.

Proton relaxation, which is dominated by dipole-dipole interactions, can be split into two types: i) intramolecular and ii) intermolecular. Intramolecular relaxation occurs as a result of rotational motion, where two interacting nuclei at a given distance *r* both generate local fields that interact with each other. As the molecule rotates, the field experienced by one nucleus from the second nucleus fluctuates and the frequency is proportional to the rate of molecular motion. A correlation time (τ), which represents the time taken for the average molecule to rotate 1 radian, can be extracted (Rössler et al., (2019)).

Intermolecular relaxation occurs because of translational motion, involving movement of a molecule between different environments. This may be due to a chemical, electrical or gravitational gradient, flow, or diffusion, the latter of which is caused by Brownian motion and is entirely random. The translational contribution to dipole-dipole relaxation dominates at low frequencies and can be probed using FFC NMR (Kaszyńska et al., (2017)), by fitting relaxivity values as a function of the measured frequency range. Using an appropriate model, self-diffusion coefficients (*D*) can be obtained and compared to *D* values obtained from pulsed-field gradient (PFG) experiments, conducted at

higher frequencies, in order to check the validity of the fit. Full details of the model and theory employed in this thesis are given in the supporting information for **Chapter 3 (Appendix A).**

1.6.6 Fourier-transform infrared (FTIR) spectroscopy

Infrared (IR) includes radiation with wavelengths between approximately 0.7 – 1000 μm. When IR radiation passes through a sample, some is absorbed and some is transmitted. The absorbed radiation matches the frequencies of vibrational transitions in molecules (which depend on bond strength and atoms in the bond) and therefore functional groups can be identified.

In Fourier Transform IR (FTIR) spectroscopy, all frequencies of light are measured simultaneously. Light from the IR source passes through a beam splitter in the interferometer which generates two optical beams, that are reflected by a fixed or moving mirror. The reflected beams interfere again at the interferometer, where the frequency distribution of IR light constantly changes due to the movement of one mirror. An interferogram is obtained and decoded via FT to give a spectrum of signal intensity as a function of wavenumber, which is sometimes referred to as a 'fingerprint' because it is used to qualify the sample. There are several types of sampling techniques in FTIR spectroscopy: transmission/absorption; attenuated total reflection (ATR); diffuse reflection and specular reflection.

ATR-FTIR uses an internal reflection element (IRE) or a crystal to qualify and quantify solid and liquid samples. IR radiation travels through the IRE to the sample surface and is reflected back, due to the difference between the refractive indices of the crystal and sample. A principle called total internal reflection (TIR) occurs when the following conditions are both met (Anton Paar, https://wiki.anton-paar.com/uk-en/attenuated-total-reflectance-atr/, accessed May 2022):

i) **The IRE is more optically dense than the sample;**
ii) **The incident angle (θ_I) is greater than the critical angle (θ_C);**

Where θ_C describes the angle of incidence at which the refraction angle is 90º (Figure 1.16). This produces an 'evanescent wave,' which passes into the sample and is partially absorbed, giving an attenuated reflection beam. Since the evanescent wave cannot propagate regularly into the sample, it has a high intensity at the point of internal reflection and this decays exponentially. Specific parts of the IR beam will be absorbed depending on the sample's composition and therefore information about bonding and interactions can be obtained.

θ_I and the angle of refraction (θ_R) can be related by Snell's law:

Equation 7. $$n_1 sin\theta_I = n_2 sin\theta_R$$

Where n_1 and n_2 give the refractive indices of the first and second medium respectively.

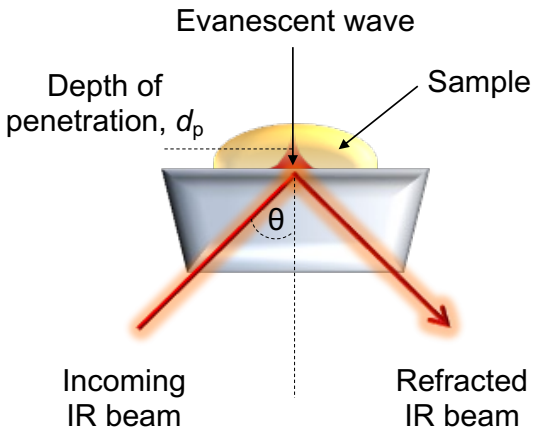

Figure 1.16. Schematic to shown the formation of an evanescent wave as a result of total internal reflection, for a single reflection ATR.

In this thesis, ATR-FTIR spectroscopy is employed to gain information on structural changes occurring upon the dissolution and coagulation of cellulose from BmimAc, such as H-bonding and crystallinity, as well as identification of residual solution components after reprecipitation and drying (Lan et al., (2011)). Comparison of spectra for the original cellulose powder and the reprecipitated material is also performed to determine whether the solvent is derivatising or non-derivatising, by analysing which bands remain intact (Man et al., (2011)).

1.6.7 Ultraviolet-visible (UV-Vis) spectroscopy and spectrofluorometry

An ultraviolet visible (UV-Vis) spectrophotometer uses a light source such as xenon to shine light on a sample at wavelengths within the UV and visible regions. Different sample components (chromophores) adsorb light at differing wavelengths and thus discrete energies, which leads to the promotion of electrons to higher energy levels. Depending on the bonding environment, the energy required to generate an excited state varies.

The basic setup of a UV-Vis spectrophotometer is given in Figure 1.17. A reference or blank sample is firstly measured to generate a 'baseline.' Light passes through the reference/sample, which is usually placed in a quartz cuvette to avoid adsorption of UV light, and some is adsorbed or transmitted. A detector converts the light that passes through into a collectable signal,

which may be presented as absorbance, transmittance or optical density, as a function of wavelength. The wavelength at which the intensity of absorbance is greatest for a given sample is selected for quantitative analysis.

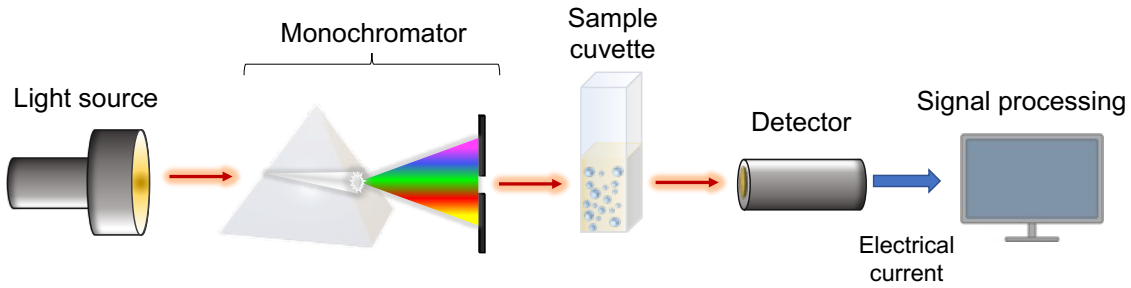

Figure 1.17. Schematic showing the main components of a UV-Vis spectrophotometer, where a beam of light passes through a sample in a cuvette and the intensity of the light which passes through is detected.

If a linear relationship exists between adsorption and concentration for a given component, Beer-Lambert's law (Equation 8) can be used to determine its unknown concentration in a solution. Calibration curves are constructed by preparing reference solutions with known amounts of the component and measuring absorbances, which are plotted as a function of concentration. Generally, it is good practice to limit the absorbance intensity to 1: for a cuvette where the path length (L) = 1 cm, this signifies that 90 % of the incident light is being adsorbed by the sample and therefore only 10 % reaches the detector.

Equation 8. $$A = \varepsilon c L$$

Where A = absorbance; ε = molar adsorption coefficient (L mol^{-1} cm^{-1}) and c = concentration (mol L^{-1}).

In contrast to a spectrophotometer, spectrofluorometers (fluorescence spectrophotometers) are used to analyse transitions from a higher energy level to a ground state which corresponds to the emission of photons. Fluorescent molecules adsorb fluorescent light at specific wavelengths and subsequently emit light at a different, slightly longer wavelength (due to non-radiative decay). Spectrofluorometers are made up of excitation and emission filters, which are used to excite specific fluorophores within a sample and measure emission at a characteristic wavelength, respectively. This allows detection and quantitative analysis of a specific fluorescent component.

In this thesis, UV-Vis spectroscopy is used to quantify the maximum solubility of oil and BmimAc, and oil and cellulose-BmimAc solutions. A spectrofluorometer is used to analyse the excitation and emission wavelength

of Calcofluor White (CW), a fluorescent dye commonly used to stain cellulose, in solutions of both oil and water.

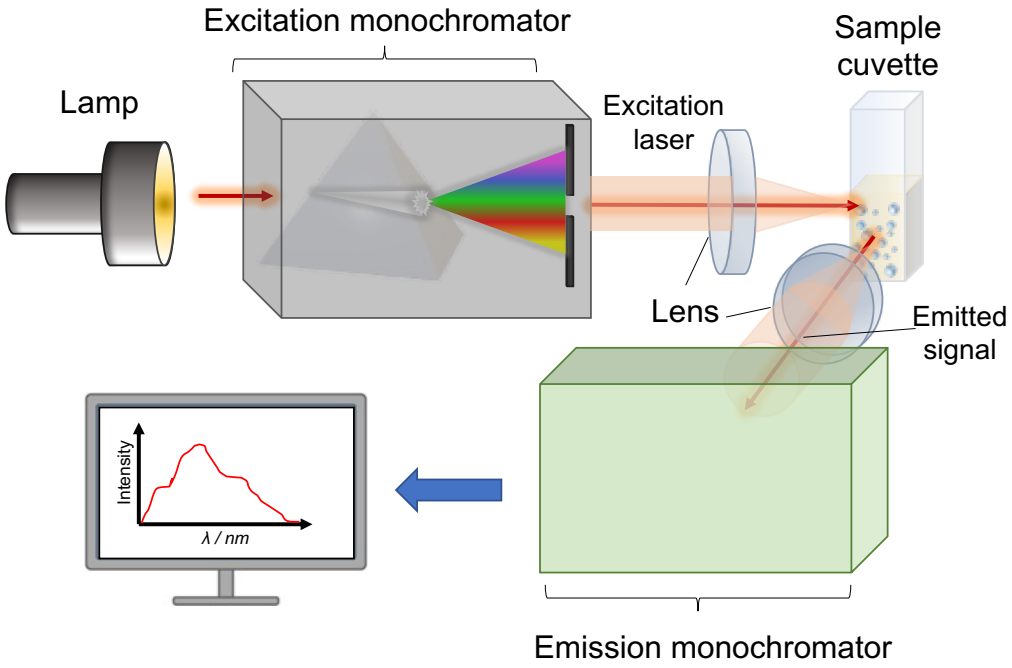

Figure 1.18. Basic setup of a spectrofluorometer, where a high intensity light source excited the sample (in a cuvette) and emission from the sample is collected and analysed.

1.7 Outline of the thesis

This thesis includes a further literature review, detailing cellulose processing methods and focussing on uses of cellulose as a stabiliser. It follows with detailed characterisation of cellulose-BmimAc (IL) solutions, introduction of a method for producing novel, 'oily' CMG stabilisers from ILs, optimisation of the physical processing and finally, study of the solution interactions between cellulose, IL and oil to elucidate interactions in the CMGs. The outline of each chapter in this thesis is shown in Figure 1.19.

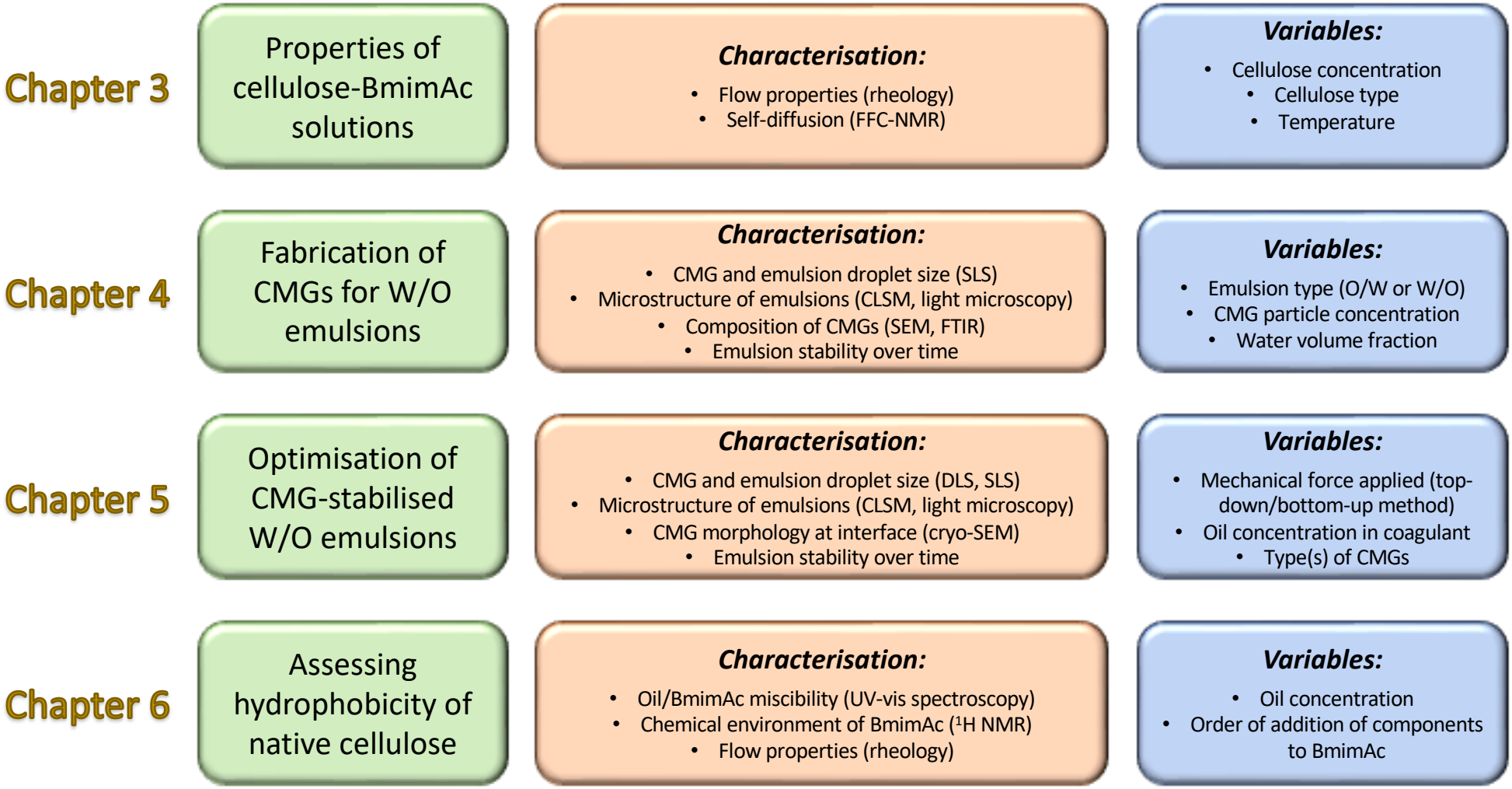

Figure 1.19. Schematic framework of this thesis.

Chapter 2 - *Advances in the use of microgels as emulsion stabilisers and as a strategy for cellulose functionalisation*

This chapter includes a literature review giving detailed information about microgels, how they are synthesised and their ability to act as emulsion stabilisers. It reviews recent advances in understanding about microgel behaviour at interfaces, with a specific focus on cellulose microgels (CMGs) and this includes details of cellulose processing methods. The lack of both physical methods for producing CMGs and research on unmodified cellulose as a W/O stabiliser are highlighted as knowledge gaps, outlining the experimental aims for this thesis. The literature review forming this chapter was published in the peer-reviewed journal, '*Cellulose*.'

Chapter 3 – *Rheological and NMR studies of Cellulose Dissolution in the Ionic Liquid BmimAc*

This chapter includes detailed characterisation of the macroscopic properties of two types of cellulose (Avicel and Vitacel) in the ionic liquid (IL) 1-butyl-3-methyl imidazolium acetate (BmimAc), which is used to dissolve cellulose this thesis. It provides key insight into the bulk properties of the solutions using rheology, defining crossover (c^*) and entanglement (c_e) concentrations as well as the intrinsic viscosities ([η]). Further study on the microscopic properties of Vitacel-BmimAc solutions is reported using NMR. This chapter was published in the peer-reviewed journal, '*Journal of Physical Chemistry B*.'

Chapter 4 – *A natural, cellulose-based microgel for water-in-oil emulsions*

This chapter introduces a novel method for producing 'oily' CMGs from the IL BmimAc, via a dissolution-coagulation route. The addition of oil during the cellulose processing results in fabrication of 'hydrophobic' CMGs which are able to stabilise W/O emulsions, and detailed characterisation of the emulsions is reported including particle sizing, CLSM and FTIR spectroscopy. This chapter was published in the peer-reviewed journal, '*Food Hydrocolloids*.'

Chapter 5 – *Relationship between size and cellulose content of cellulose microgels (CMGs) and their water-in-oil emulsifying capacity*

This chapter includes further insight into CMG properties and optimisation of their preparation method described in **Chapter 4**. An increasing amount of shear force is applied during cellulose coagulation, which results in fabrication of CMGs with a range of sizes. Detailed characterisation is performed, including techniques used in **Chapter 4** as well as cryo-SEM, of

the W/O emulsions. This chapter was published in a special edition of the peer-reviewed journal, '*Colloids and Surfaces A: Physicochemical Aspects*.'

Chapter 6 – *The effect of oil on cellulose dissolution in the ionic liquid 1-butyl-3-methyl imidazolium acetate*

This chapter includes detailed characterisation of oil-cellulose (Vitacel)-BmimAc solutions, using NMR spectroscopy. The order of oil addition has an effect on the interactions which develop between the cellulose, oil and IL. This chapter also compares the properties of cellulose-based solutions to cellobiose-based solutions, providing further insight into the dissolution and coagulation mechanisms of cellulose from IL solutions. This chapter has been submitted to the peer-reviewed journal, '*ACS Omega*' and is currently under review.

Chapter 7 – *General discussion*

This chapter includes a general summary and discussion of the main results presented in this thesis, including conclusions to the highlighted knowledge gaps and ideas for future studies.

1.8 References

Aghajani-Memar, S., Mohammadkazemi, F., Kermanian, H. and Hamedi, S. (2022). Synergistic effect of bacterial cellulose and halloysite nanotubes on the properties of the sodium caseinate-based nanobiocomposites. *Applied Clay Science*. *222*, 106493.

Ahola, S., Österberg, M. and Laine, J. (2008). Cellulose nanofibrils - Adsorption with poly(amideamine) epichlorohydrin studied by QCM-D and application as a paper strength additive. *Cellulose*. *15*(2), 303–314.

Albers, J., Knop, K. and Kleinebudde, P. (2006). Brand-to-brand and batch-to-batch uniformity of microcrystalline cellulose in direct tableting with a pneumohydraulic tablet press. *Pharmazeutische Industrie*. *68*(12), 1420–1428.

Andresen, M., Johansson, L.S., Tanem, B.S. and Stenius, P. (2006). Properties and characterization of hydrophobized microfibrillated cellulose. *Cellulose*. *13*(6), 665–677.

Anoardo, E., Galli, G. and Ferrante, G. (2001). Fast-Field-Cycling NMR: Applications and Instrumentation. *Applied Magnetic Resonance*. *20*(3), 365–404.

Anton Paar. Attenuated total reflectance (ATR). Available from: https://wiki.anton-paar.com/uk-en/attenuated-total-reflectance-atr/.

Araiza-Calahorra, A., Glover, Z.J., Akhtar, M. and Sarkar, A. (2020). Conjugate microgel-stabilized Pickering emulsions: Role in delaying gastric digestion. *Food Hydrocolloids*. *105*, 105794.

Arboleya, J.C. and Wilde, P.J. (2005). Competitive adsorption of proteins

with methylcellulose and hydroxypropyl methylcellulose. *Food Hydrocolloids*. *19*(3), 485–491.

Arca, H.C., Mosquera-Giraldo, L.I., Bi, V., Xu, D., Taylor, L.S. and Edgar, K.J. (2018). Pharmaceutical Applications of Cellulose Ethers and Cellulose Ether Esters. *Biomacromolecules*. *19*(7), 2351–2376.

Arifin, H.R., Djali, M., Nurhadi, B., Hasim, S.A., Hilmi, A. and Puspitasari, A.V. (2022). Improved properties of corn starch-based bio-nanocomposite film with different types of plasticizers reinforced by nanocrystalline cellulose. *International Journal of Food Properties*. *25*(1), 509–521.

Aro, A., Jauhiainen, M., Partanen, R., Salminen, I. and Mutanen, M. (1997). Stearic acid, trans fatty acids, and dairy fat: Effects on serum and lipoprotein lipids, apolipoproteins, lipoprotein(a), and lipid transfer proteins in healthy subjects. *American Journal of Clinical Nutrition*. *65*(5), 1419–1426.

Ascherio, A., Hennekens, C.H., Buring, J.E., Master, C., Stampfer, M.J. and Willett, W.C. (1994). Trans-fatty acids intake and risk of myocardial infarction. *Circulation*. *89*(1), 94–101.

Auxenfans, T., Buchoux, S., Larcher, D., Husson, G., Husson, E. and Sarazin, C. (2014). Enzymatic saccharification and structural properties of industrial wood sawdust: Recycled ionic liquids pretreatments. *Energy Conversion and Management*. *88*, 1094–1103.

Bai, L., Huan, S., Xiang, W. and Rojas, O.J. (2018). Pickering emulsions by combining cellulose nanofibrils and nanocrystals: Phase behavior and depletion stabilization. *Green Chemistry*. *20*(7), 1571–1582.

Baker, T.J., Schroeder, L.R. and Johnson, D.C. (1978). Dissolution of cellulose in polar aprotic solvents via formation of methylol cellulose. *Carbohydrate Research*. *67*, C4–C7.

Battista, O.A. and Smith, P.A. (1962). MICROCRYSTALLINE CELLULOSE. *Industrial and Engineering Chemistry*. *54*(9), 20–29.

Bauer, R.O. and Lehman, A.J. (1951). Chronic toxicity studies on methylcellulose in rats. *Journal of the American Pharmaceutical Association (Scientific ed.)*. *40*(6), 257–260.

Bazbouz, M.B., Taylor, M., Baker, D., Ries, M.E. and Goswami, P. (2019). Dry-jet wet electrospinning of native cellulose microfibers with macroporous structures from ionic liquids. *Journal of Applied Polymer Science*. *136*(10).

Bemer, H.L., Limbaugh, M., Cramer, E.D., Harper, W.J. and Maleky, F. (2016). Vegetable organogels incorporation in cream cheese products. *Food Research International*. *85*, 67–75.

Bondeson, D., Mathew, A. and Oksman, K. (2006). Optimization of the isolation of nanocrystals from microcrystalline cellulose by acid hydrolysis. *Cellulose*. *13*(2), 171–180.

Bondeson, D. and Oksman, K. (2007). Dispersion and characteristics of surfactant modified cellulose whiskers nanocomposites. *Composite*

Interfaces. *14*(7–9), 617–630.

Bou, R., Cofrades, S. and Jiménez-Colmenero, F. (2014). Influence of high pressure and heating treatments on physical parameters of water-in-oil-in-water emulsions. *Innovative Food Science and Emerging Technologies*. *23*, 1–9.

Brandessence (2022). *Clean Label Ingredients Market Size, Share & Trends Analysis Report By Application (Beverage, Bakery & Confectionary, Sauce & Condiment, Dairy & Frozen Dessert, Other Processed Foods), By Type (Natural Color, Natural Flavor, Starch & Sweetener, Natural Pr* [Online]. Available from: https://brandessenceresearch.com/food-and-beverage/clean-label-ingredients-market.

Brewer, M.S. (2012). Reducing the fat content in ground beef without sacrificing quality: A review. *Meat Science*. *91*(4), 385–395.

Brugger, B., Rosen, B.A. and Richtering, W. (2008). Microgels as stimuli-responsive stabilizers for emulsions. *Langmuir*. *24*(21), 12202–12208.

Budtova, T. and Navard, P. (2016). Cellulose in NaOH–water based solvents: a review. *Cellulose*. *23*(1), 5–55.

Burdock, G.A. (2007). Safety assessment of hydroxypropyl methylcellulose as a food ingredient. *Food and Chemical Toxicology*. *45*(12), 2341–2351.

Cai, J. and Zhang, L. (2005). Rapid dissolution of cellulose in LiOH/urea and NaOH/urea aqueous solutions. *Macromolecular Bioscience*. *5*(6), 539–548.

Cai, T., Zhang, H., Guo, Q., Shao, H. and Hu, X. (2009). Structure and Properties of Cellulose Fibers from Ionic Liquids. *Journal of Applied Polymer Science*. *115*, 1047–1053.

Cao, Y., Chen, Y., Lu, L., Xue, Z. and Mu, T. (2013). Water sorption in functionalized ionic liquids: Kinetics and intermolecular interactions. *Industrial and Engineering Chemistry Research*. *52*(5), 2073–2083.

Cao, Y., Chen, Y. and Mu, T. (2013). A new way to tune relative humidity: By saturated ionic liquid aqueous solutions. *New Journal of Chemistry*. *37*(12), 3890–3898.

Cao, Y. and Mu, T. (2014). Comprehensive investigation on the thermal stability of 66 ionic liquids by thermogravimetric analysis. *Industrial and Engineering Chemistry Research*. *53*(20), 8651–8664.

Cao, Y., Sun, X., Chen, Y. and Mu, T. (2014). Water sorption in amino acid ionic liquids: Kinetic, mechanism, and correlations between hygroscopicity and solvatochromic parameters. *ACS Sustainable Chemistry and Engineering*. *2*(2), 138–148.

Cao, Y., Zhang, R., Cheng, T., Guo, J., Xian, M. and Liu, H. (2017). Imidazolium-based ionic liquids for cellulose pretreatment: recent progresses and future perspectives. *Applied Microbiology and Biotechnology*. *101*(2), 521–532.

Capron, I. and Cathala, B. (2013). Surfactant-free high internal phase emulsions stabilized by cellulose nanocrystals. *Biomacromolecules*.

14(2), 291–296.

Celotech (2020). Modified methyl cellulose and market trends. Available from: https://www.celotech.com/about-celotech/modified-methyl-cellulose-and-market-trends.html.

Chen, X., Zheng, B. and Liu, H. (2011). Optical and digital microscopic imaging techniques and applications in pathology. *Analytical Cellular Pathology*. *34*(1–2), 5–18.

Chen, Z., Liu, S., Li, Z., Zhang, Q. and Deng, Y. (2011). Dialkoxy functionalized quaternary ammonium ionic liquids as potential electrolytes and cellulose solvents. *New Journal of Chemistry*. *35*(8), 1596–1606.

Cherhal, F., Cousin, F. and Capron, I. (2016). Structural Description of the Interface of Pickering Emulsions Stabilized by Cellulose Nanocrystals. *Biomacromolecules*. *17*(2), 496–502.

Clark, J. (2000). Nuclear Magnetic Resonance. *Chemguide*. [Online]. Available from: https://www.chemguide.co.uk/analysis/nmrmenu.html#top.

Clough, M.T., Geyer, K., Hunt, P.A., Son, S., Vagt, U. and Welton, T. (2015). Ionic liquids: Not always innocent solvents for cellulose. *Green Chemistry*. *17*(1), 231–243.

Costa, C., Medronho, B., Filipe, A., Mira, I., Lindman, B., Edlund, H. and Norgren, M. (2019). Emulsion formation and stabilization by biomolecules: The leading role of cellulose. *Polymers*. *11*(10), 1–18.

Dahneke, B.E. (1983). *Measurement of suspended particles by quasi-elastic light scattering*. John Wiley & Sons.

Day, L. and Golding, M. (2016). Food Structure, Rheology, and Texture *In*: *Encyclopedia of Food Chemistry* [Online]. Elsevier, 125–129. Available from: https://www.sciencedirect.com/referencework/9780128140451/encyclopedia-of-food-chemistry#book-description.

Demirkesen, I. and Mert, B. (2019). Recent developments of oleogel utilizations in bakery products. *Critical Reviews in Food Science and Nutrition*. *0*(0), 1–20.

Demirkesen, I. and Mert, B. (2020). Recent developments of oleogel utilizations in bakery products. *Critical Reviews in Food Science and Nutrition*. *60*(14), 2460–2479.

Deng, Y., Long, T., Zhang, D., Chen, J. and Gan, S. (2009). Phase Diagram of [Amim]Cl + Salt Aqueous Biphasic Systems and Its Application for [Amim]Cl Recovery. *Journal of Chemical & Engineering Data*. *54*, 2470–2473.

Dong, X.M., Kimura, T., Revol, J.F. and Gray, D.G. (1996). Effects of ionic strength on the isotropic-chiral nematic phase transition of suspensions of cellulose crystallites. *Langmuir*. *12*(8), 2076–2082.

Duchemin, B.J.C., Newman, R.H. and Staiger, M.P. (2009). Structure-property relationship of all-cellulose composites. *Composites Science*

and Technology. *69*(7–8), 1225–1230.

EFSA. *Commission Regulation (EU) No 1129/2011 of 11 November 2011 amending Annex II to Regulation (EC) No 1333/2008 of the European Parliament and of the Council by establishing a Union list of food additives* [Online]. Available from: https://eur-lex.europa.eu/legal-content/EN/TXT/?uri=CELEX:02011R1129-20131121.

EFSA. *Commission Regulation (EU) No 231/2012 of 9 March 2012 laying down specifications for food additives listed in Annexes II and III to Regulation (EC) No 1333/2008 of the European Parliament and of the Council Text with EEA relevance*.

EFSA. *Official Journal of the European Communities, L 61, 18 March 1995*.

EFSA (2004). Opinion of the Scientific Panel on Food Additives, Flavourings, Processing Aids and Materials in Contact with Food (AFC) on a request from the Commission related to Ethyl Cellulose as a food additive. *The EFSA Journal*. *35*, 1–6.

Elixhauser, A. and Owens, P. (2006). Reasons for Being Admitted to the Hospital through the Emergency Department, 2003: Statistical Brief #2. *Healthcare Cost and Utilization Project (HCUP) Statistical Briefs*.

Elvin, E. (2020). The rise in emergency hospital admissions and the impact of this on diabetes patients. *Diabetes UK*. [Online]. Available from: https://www.openaccessgovernment.org/emergency-hospital-admissions-diabetes-patients/83517/.

Espert, M., Borreani, J., Hernando, I., Quiles, A., Salvador, A. and Sanz, T. (2017). Relationship between cellulose chemical substitution, structure and fat digestion in o/w emulsions. *Food Hydrocolloids*. *69*, 76–85.

Espert, M., Salvador, A. and Sanz, T. (2020). Cellulose ether oleogels obtained by emulsion-templated approach without additional thickeners. *Food Hydrocolloids*. *109*, 106085.

Espert, M., Salvador, A. and Sanz, T. (2016). In vitro digestibility of highly concentrated methylcellulose O/W emulsions: Rheological and structural changes. *Food and Function*. *7*(9), 3933–3942.

Fan, Z., Chen, J., Guo, W., Ma, F., Sun, S. and Zhou, Q. (2018). Anti-solvents tuning cellulose nanoparticles through two competitive regeneration routes. *Cellulose*. *25*(8), 4513–4523.

Fan, Z., Chen, J., Guo, W., Ma, F., Sun, S. and Zhou, Q. (2017). Crystallinity of regenerated cellulose from [Bmim]Cl dependent on the hydrogen bond acidity/basicity of anti-solvents. *RSC Advances*. *7*(65), 41004–41010.

FDA. *Ethyl cellulose, FOOD ADDITIVES PERMITTED FOR DIRECT ADDITION TO FOOD FOR HUMAN CONSUMPTION*.

FDA. *Hydroxylpropyl methylcellulose, FOOD ADDITIVES PERMITTED FOR DIRECT ADDITION TO FOOD FOR HUMAN CONSUMPTION*. U.S.

FDA. *Methylcellulose, SUBSTANCES GENERALLY RECOGNIZED AS SAFE* [Online]. US. Available from: https://www.accessdata.fda.gov/scripts/cdrh/cfdocs/cfcfr/CFRSearch.cf

m?fr=182.1480.

FDA. *Sodium carboxymethylcellulose, SUBSTANCES GENERALLY RECOGNIZED AS SAFE* [Online]. US. Available from: https://www.accessdata.fda.gov/scripts/cdrh/cfdocs/cfcfr/cfrsearch.cfm?fr=182.1745

Fischer, S., Leipner, H., Thümmler, K., Brendler, E. and Peters, J. (2003). Inorganic molten salts as solvents for cellulose. *Cellulose*. *10*(3), 227–236.

Floury, J., Desrumaux, A., Axelos, M.A.V. and Legrand, J. (2003). Effect of high pressure homogenisation on methylcellulose as food emulsifier. *Journal of Food Engineering*. *58*(3), 227–238.

Fryczkowska, B., Kowalska, M., Binias, D., Slusarczyk, C., Janicki, J., Sarna, E. and Wyszomirski, M. (2018). Properties and Structure of Cellulosic Membranes Obtained from Solutions in Ionic Liquids Coagulated in Primary Alcohols. *Autex Research Journal*. *18*(3), 232–242.

Fujii, S., Armes, S.P., Binks, B.P. and Murakami, R. (2006). Stimulus-responsive particulate emulsifiers based on lightly cross-linked poly(4-vinylpyridine) - Silica nanocomposite microgels. *Langmuir*. *22*(16), 6818–6825.

Futamura, T. and Kawaguchi, M. (2012). Characterization of paraffin oil emulsions stabilized by hydroxypropyl methylcellulose. *Journal of Colloid and Interface Science*. *367*(1), 55–60.

Galbraith, C.G. and Galbraith, J.A. (2011). Super-resolution microscopy at a glance. *Journal of Cell Science*. *124*(10), 1607–1611.

Geddes, A.L. (1956). Interaction of trifluoroacetic acid with cellulose and related compounds. *Journal of Polymer Science*. *22*(100), 31–39.

Gericke, M., Fardim, P. and Heinze, T. (2012). Ionic liquids - Promising but challenging solvents for homogeneous derivatization of cellulose. *Molecules*. *17*(6), 7458–7502.

Goi, Y., Fujisawa, S., Saito, T., Yamane, K., Kuroda, K. and Isogai, A. (2019). Dual Functions of TEMPO-Oxidized Cellulose Nanofibers in Oil-in-Water Emulsions: A Pickering Emulsifier and a Unique Dispersion Stabilizer. *Langmuir*. *35*(33), 10920–10926.

Gomes, L.R., Simões, C.D. and Silva, C. (2020). Demystifying thickener classes food additives though molecular gastronomy. *International Journal of Gastronomy and Food Science*. *22*, 100262.

Gómez-Estaca, J., Herrero, A.M., Herranz, B., Álvarez, M.D., Jiménez-Colmenero, F. and Cofrades, S. (2019). Characterization of ethyl cellulose and beeswax oleogels and their suitability as fat replacers in healthier lipid pâtés development. *Food Hydrocolloids*. *87*, 960–969.

Grover, J.A. (1986). Methylcellulose (MC) and Hydroxypropylmethylcellulose (HPMC) *In*: *Food Hydrocolloids* [Online]. CRC Press, 34. Available from: https://www.taylorfrancis.com/chapters/edit/10.1201/9780429290459-6/methylcellulose-mc-hydroxypropylmethylcellulose-hpmc-joseph-

grover.

Gullapalli, R.P. and Sheth, B.B. (1996). Effect of methylcellulose on the stability of oil-in-water emulsions. *International Journal of Pharmaceutics*. *140*(1), 97–109.

Gunst, A. Van and Roodenburg, A.J.C. (2019). Consumer Distrust about E-numbers : A Qualitative. *Foods*. *8*(178), 1–14.

Gupta, K.M. and Jiang, J. (2015). Cellulose dissolution and regeneration in ionic liquids: A computational perspective. *Chemical Engineering Science*. *121*, 180–189.

Gutowski, K.E., Broker, G.A., Willauer, H.D., Huddleston, J.G., Swatloski, R.P., Holbrey, J.D. and Rogers, R.D. (2003). Controlling the aqueous miscibility of ionic liquids: Aqueous biphasic systems of water-miscible ionic liquids and water-structuring salts for recycle, metathesis, and separations. *Journal of the American Chemical Society*. *125*(22), 6632–6633.

Haghighi Mood, S., Hossein Golfeshan, A., Tabatabaei, M., Salehi Jouzani, G., Najafi, G.H., Gholami, M. and Ardjmand, M. (2013). Lignocellulosic biomass to bioethanol, a comprehensive review with a focus on pretreatment. *Renewable and Sustainable Energy Reviews*. *27*, 77–93.

Halder, P., Kundu, S., Patel, S., Setiawan, A., Atkin, R., Parthasarthy, R., Paz-Ferreiro, J., Surapaneni, A. and Shah, K. (2019). Progress on the pre-treatment of lignocellulosic biomass employing ionic liquids. *Renewable and Sustainable Energy Reviews*. *105*, 268–292.

Hameed, N. and Guo, Q. (2010). Blend films of natural wool and cellulose prepared from an ionic liquid. *Cellulose*. *17*(4), 803–813.

Han, J., Zhou, C., French, A.D., Han, G. and Wu, Q. (2013). Characterization of cellulose II nanoparticles regenerated from 1-butyl-3-methylimidazolium chloride. *Carbohydrate Polymers*. *94*(2), 773–781.

Han, S., Wong, H.T. and Livingston, A.G. (2005). Application of organic solvent nanofiltration to separation of ionic liquids and products from ionic liquid mediated reactions. *Chemical Engineering Research and Design*. *83*(3 A), 309–316.

Han, Y., Yu, M. and Wang, L. (2018). Physical and antimicrobial properties of sodium alginate/carboxymethyl cellulose films incorporated with cinnamon essential oil. *Food Packaging and Shelf Life*. *15*, 35–42.

He, X., Lu, W., Sun, C., Khalesi, H., Mata, A., Andaleeb, R. and Fang, Y. (2021). Cellulose and cellulose derivatives: Different colloidal states and food-related applications. *Carbohydrate Polymers*. *255*, 117334.

Hedlund, A., Köhnke, T., Hagman, J., Olsson, U. and Theliander, H. (2019). Microstructures of cellulose coagulated in water and alcohols from 1-ethyl-3-methylimidazolium acetate: contrasting coagulation mechanisms. *Cellulose*. *26*(3), 1545–1563.

Heinze, T. and Koschella, A. (2005). Solvents applied in the field of cellulose chemistry: a mini review. *Polímeros: Ciência e Technologia*. *15*(2), 84–90.

Heinze, T., Lincke, T., Fenn, D. and Koschella, A. (2008). Efficient allylation of cellulose in dimethyl sulfoxide/tetrabutylammonium fluoride trihydrate. *Polymer Bulletin*. *61*(1), 1–9.

Henniges, U., Schiehser, S., Rosenau, T. and Potthast, A. (2010). Cellulose solubility: Dissolution and analysis of 'problematic' cellulose pulps in the solvent system DMAc/LiCl. *ACS Symposium Series*. *1033*, 165–177.

Herrick, F.W., Casebier, R.L., Hamilton, J.K. and Sandberg, K.R. (1983). Microfibrillated cellulose: morphology and accessibility. *Journal of Applied Polymer Science: Applied Polymer Symposium*. *37*, 797–813.

Hill, S.E., Mitchell, J.R. and Ledward, D.A. (1998). *Functional Properties of Food Macromolecules* 2nd Editio. (S. E. Hill, D. A. Ledward, & J. R. Mitchell, eds.). New York: Springer New York, NY.

Hine, P.J. and Ries, M.E. (2020). Composite materials.

Holm, J. and Lassi, U. (2011). *Ionic Liquids in the Pretreatment of Lignocellulosic Biomass* [Online] (A. Kokorin, ed.). IntechOpen. Available from: https://www.intechopen.com/books/1373.

Hossain, M.M., Rawal, A. and Aldous, L. (2019). Aprotic vs Protic Ionic Liquids for Lignocellulosic Biomass Pretreatment: Anion Effects, Enzymatic Hydrolysis, Solid-State NMR, Distillation, and Recycle. *ACS Sustainable Chemistry & Engineering*. *7*, 11928–11936.

Hu, F.B. (2003). Plant-based foods and prevention of cardiovascular disease: An overview. *American Journal of Clinical Nutrition*. *78*(3 SUPPL.), 544–551.

Hu, Y.T., Ting, Y., Hu, J.Y. and Hsieh, S.C. (2017). Techniques and methods to study functional characteristics of emulsion systems. *Journal of Food and Drug Analysis*. *25*(1), 16–26.

Huang, K., Wu, R., Cao, Y., Li, H. and Wang, J. (2013). Recycling and reuse of ionic liquid in homogeneous cellulose acetylation. *Chinese Journal of Chemical Engineering*. *21*(5), 577–584.

Hubbe, M.A., Rojas, O.J., Lucia, L.A. and Sain, M. (2008). Cellulosic Nanocomposites: a Review. *BioResources*. *3*(3), 929–980.

Hunter, J.E., Zhang, J., Kris-Etherton, P.M. and Childs, L. (2010). Cardiovascular disease risk of dietary stearic acid compared with trans, other saturated, and unsaturated fatty acids: A systematic review. *American Journal of Clinical Nutrition*. *91*(1), 46–63.

Idenoue, S., Oga, Y., Hashimoto, D., Yamamoto, K. and Kadokawa, J.I. (2019). Preparation of reswellable amorphous porous celluloses through hydrogelation from ionic liquid solutions. *Materials*. *12*(19), 1–8.

Intelligence, M. (2021). *CELLULOSE DERIVATIVES MARKET - GROWTH, TRENDS, COVID-19 IMPACT, AND FORECASTS (2022 - 2027)* [Online]. Available from: https://www.mordorintelligence.com/industry-reports/cellulose-derivatives-market.

Isik, M., Sardon, H. and Mecerreyes, D. (2014). Ionic liquids and cellulose: Dissolution, chemical modification and preparation of new cellulosic materials. *International Journal of Molecular Sciences*. *15*(7), 11922–

11940.

Jia, X., Chen, Y., Shi, C., Ye, Y., Wang, P., Zeng, X. and Wu, T. (2013). Preparation and characterization of cellulose regenerated from phosphoric acid. *Journal of Agricultural and Food Chemistry*. *61*(50), 12405–12414.

Jia, X., Xu, R., Shen, W., Xie, M., Abid, M., Jabbar, S., Wang, P., Zeng, X. and Wu, T. (2015). Stabilizing oil-in-water emulsion with amorphous cellulose. *Food Hydrocolloids*. *43*, 275–282.

Jiang, C., Li, W., Nian, J., Lou, W. and Wang, X. (2018). Tribological evaluation of environmentally friendly ionic liquids derived from renewable biomaterials. *Friction*. *6*(2), 208–218.

Jiang, Q., Du, L., Li, S., Liu, Y. and Meng, Z. (2021). Polysaccharide-stabilized aqueous foams to fabricate highly oil-absorbing cryogels: Application and formation process for preparation of edible oleogels. *Food Hydrocolloids*. *120*, 106901.

Jiang, Q., Li, P., Ji, M., Du, L., Li, S., Liu, Y. and Meng, Z. (2022). Synergetic effects of water-soluble polysaccharides for intensifying performances of oleogels fabricated by oil-absorbing cryogels. *Food Chemistry*. *372*, 131357.

Jiang, Y., Liu, L., Wang, B., Yang, X., Chen, Z., Zhong, Y., Zhang, L., Mao, Z., Xu, H. and Sui, X. (2019). Polysaccharide-based edible emulsion gel stabilized by regenerated cellulose. *Food Hydrocolloids*. *91*, 232–237.

Jo, S., Park, S., Oh, Y., Hong, J., Kim, H.J., Kim, K.J., Oh, K.K. and Lee, S.H. (2019). Development of cellulose Hydrogel Microspheres for Lipase Immobilization. *Biotechnology and Bioprocess Engineering*. *24*(1), 145–154.

Johns, M.A., Bernardes, A., De Azevêdo, E.R., Guimarães, F.E.G., Lowe, J.P., Gale, E.M., Polikarpov, I., Scott, J.L. and Sharma, R.I. (2017). On the subtle tuneability of cellulose hydrogels: Implications for binding of biomolecules demonstrated for CBM 1. *Journal of Materials Chemistry B*. *5*(21), 3879–3887.

Kabir, S.M.F., Sikdar, P.P., Haque, B., Bhuiyan, M.A.R., Ali, A. and Islam, M.N. (2018). Cellulose-based hydrogel materials: chemistry, properties and their prospective applications. *Progress in Biomaterials*. *7*(3), 153–174.

Kadokawa, J. ichi, Murakami, M. aki and Kaneko, Y. (2008). A facile preparation of gel materials from a solution of cellulose in ionic liquid. *Carbohydrate Research*. *343*(4), 769–772.

Kalashnikova, I., Bizot, H., Bertoncini, P., Cathala, B. and Capron, I. (2013). Cellulosic nanorods of various aspect ratios for oil in water Pickering emulsions. *Soft Matter*. *9*(3), 952–959.

Kalashnikova, I., Bizot, H., Cathala, B. and Capron, I. (2012). Modulation of cellulose nanocrystals amphiphilic properties to stabilize oil/water interface. *Biomacromolecules*. *13*(1), 267–275.

Kalashnikova, I., Bizot, H., Cathala, B. and Capron, I. (2011). New pickering

emulsions stabilized by bacterial cellulose nanocrystals. *Langmuir*. *27*(12), 7471–7479.

Kamel, S., Ali, N., Jahangir, K., Shah, S.M. and El-Gendy, A.A. (2008). Pharmaceutical significance of cellulose: A review. *Express Polymer Letters*. *2*(11), 758–778.

Karaki, N., Aljawish, A., Humeau, C., Muniglia, L. and Jasniewski, J. (2016). Enzymatic modification of polysaccharides: Mechanisms, Properties, And potential applications: A review. *Enzyme and Microbial Technology*. *90*, 1–18.

Karlsson, K., Schuster, E., Stading, M. and Rigdahl, M. (2015). Foaming behavior of water-soluble cellulose derivatives: hydroxypropyl methylcellulose and ethyl hydroxyethyl cellulose. *Cellulose*. *22*(4), 2651–2664.

Kasiri, N. and Fathi, M. (2018). Production of cellulose nanocrystals from pistachio shells and their application for stabilizing Pickering emulsions. *International Journal of Biological Macromolecules*. *106*, 1023–1031.

Kaszyńska, J., Rachocki, A., Bielejewski, M. and Tritt-Goc, J. (2017). Influence of cellulose gel matrix on BMIMCl ionic liquid dynamics and conductivity. *Cellulose*. *24*(4), 1641–1655.

Klemm, D., Heinze, T., Philipp, B. and Wagenknecht, W. (1997). New approaches to advanced polymers by selective cellulose functionalization. *Acta Polymer*. *48*, 277–297.

Klemm, D., Heublein, B., Fink, H.P. and Bohn, A. (2005). Cellulose: Fascinating biopolymer and sustainable raw material. *Angewandte Chemie - International Edition*. *44*(22), 3358–3393.

Kosan, B., Michels, C. and Meister, F. (2008). Dissolution and forming of cellulose with ionic liquids. *Cellulose*. *15*(1), 59–66.

Krawczyk, G., Venables, A. and Tuaso, D. (2009). Microcrystalline cellulose *In*: *Handbook of Hydrocolloids*. Cambridge: Woodhead Publishing, 740–758.

Kuzmina, O. (2016). Economical Aspects of Ionic Liquid Application *In*: *Application, Purification, and Recovery of Ionic Liquids*. Elsevier, 249–263.

Lan, W., Liu, C.F., Yue, F.X., Sun, R.C. and Kennedy, J.F. (2011). Ultrasound-assisted dissolution of cellulose in ionic liquid. *Carbohydrate Polymers*. *86*(2), 672–677.

Lee, M.C., Jiang, X., Brenna, J.T. and Abbaspourrad, A. (2018). Oleogel-structured composite for the stabilization of ω3 fatty acids in fish oil. *Food and Function*. *9*(11), 5598–5606.

Lefroy, K.S., Murray, B.S., Ries, M.E. and Curwen, T.D. (2021). A natural, cellulose-based microgel for water-in-oil emulsions. *Food Hydrocolloids*. *113*, 106408.

Li, G., Lee, W.J., Liu, N., Lu, X., Tan, C.P., Lai, O.M., Qiu, C. and Wang, Y. (2021). Stabilization mechanism of water-in-oil emulsions by medium- and long-chain diacylglycerol: Post-crystallization vs. pre-crystallization.

LWT – Food Science and Technology. *146*, 111649.

Li, L., Lin, Z., Yang, X., Wan, Z. and Cui, S. (2009). A novel cellulose hydrogel prepared from its ionic liquid solution. *Chinese Science Bulletin*. *54*(9), 1622–1625.

Li, P., Sirviö, J.A., Haapala, A. and Liimatainen, H. (2017). Cellulose nanofibrils from nonderivatizing urea-based deep eutectic solvent pretreatments. *ACS Applied Materials and Interfaces*. *9*(3), 2846–2855.

Li, Q., Wang, Y., Wu, Y., He, K., Li, Y., Luo, X., Li, B., Wang, C. and Liu, S. (2019). Flexible cellulose nanofibrils as novel pickering stabilizers: The emulsifying property and packing behavior. *Food Hydrocolloids*. *88*, 180–189.

Li, Q., Wu, Y., Shabbir, M., Pei, Y., Liang, H., Li, J., Chen, Y., Li, Y., Li, B., Luo, X. and Liu, S. (2021). Coalescence behavior of eco-friendly Pickering-MIPES and HIPEs stabilized by using bacterial cellulose nanofibrils. *Food Chemistry*. *349*, 129163.

Li, X., Li, J., Gong, J., Kuang, Y., Mo, L. and Song, T. (2018). Cellulose nanocrystals (CNCs) with different crystalline allomorph for oil in water Pickering emulsions. *Carbohydrate Polymers*. *183*, 303–310.

Li, Y., Zhai, F., Yang, X., Schouten, E.G., Hu, X., He, Y., Luan, D. and Ma, G. (2007). Determinants of childhood overweight and obesity in China. *British Journal of Nutrition*. *97*(1), 210–215.

Li, Z., Wu, H., Yang, M., Xu, D., Chen, J., Feng, H., Lu, Y., Zhang, L., Yu, Y. and Kang, W. (2018). Stability mechanism of O/W Pickering emulsions stabilized with regenerated cellulose. *Carbohydrate Polymers*. *181*, 224–233.

Lindman, B., Karlström, G. and Stigsson, L. (2010). On the mechanism of dissolution of cellulose. *Journal of Molecular Liquids*. *156*(1), 76–81.

Linke, C. and Drusch, S. (2018). Pickering emulsions in foods - opportunities and limitations. *Critical Reviews in Food Science and Nutrition*. *58*(12), 1971–1985.

Liu, Z., Sun, X., Hao, M., Huang, C., Xue, Z. and Mu, T. (2015). Preparation and characterization of regenerated cellulose from ionic liquid using different methods. *Carbohydrate Polymers*. *117*, 54–62.

Lockwood, D.J. (2016). Rayleigh and Mie Scattering *In*: *Encyclopedia of Colour Science and Technology* [Online]. Springer New York, NY. Available from: https://link.springer.com/referenceworkentry/10.1007/978-1-4419-8071-7_218.

Lozano, P., Bernal, B., Recio, I. and Belleville, M.P. (2012). A cyclic process for full enzymatic saccharification of pretreated cellulose with full recovery and reuse of the ionic liquid 1-butyl-3- methylimidazolium chloride. *Green Chemistry*. *14*(9), 2631–2637.

Lu, B., Xu, A. and Wang, J. (2014). Cation does matter: How cationic structure affects the dissolution of cellulose in ionic liquids. *Green Chemistry*. *16*(3), 1326–1335.

Lu, Y., Li, J., Ge, L., Xie, W. and Wu, D. (2021). Pickering emulsion stabilized with fibrous nanocelluloses: Insight into fiber flexibility-emulsifying capacity relations. *Carbohydrate Polymers*. *255*, 117483.

Lu, Y., Qian, X., Xie, W., Zhang, W., Huang, J. and Wu, D. (2019). Rheology of the sesame oil-in-water emulsions stabilized by cellulose nanofibers. *Food Hydrocolloids*. *94*, 114–127.

Lynam, J.G., Chow, G.I., Coronella, C.J. and Hiibel, S.R. (2016). Ionic liquid and water separation by membrane distillation. *Chemical Engineering Journal*. *288*, 557–561.

Malvern Instruments (2016). A Basic Introduction to Rheology. *Whitepaper*., 1–20.

Man, Z., Muhammad, N., Sarwono, A., Bustam, M.A., Kumar, M.V. and Rafiq, S. (2011). Preparation of Cellulose Nanocrystals Using an Ionic Liquid. *Journal of Polymers and the Environment*. *19*(3), 726–731.

Marangoni, A.G. (2012). Chocolate compositions containing ethylcellulose. US 2012O183651A1.

Marchessault, R.H., Morehead, F.F. and Walter, N.M. (1959). Liquid Crystal Systems from Fibrillar Polysaccharides. *Nature*. *184*, 632–633.

Marchetti, L., Muzzio, B., Cerrutti, P., Andrés, S.C. and Califano, A.N. (2017). Bacterial nanocellulose as novel additive in low-lipid low-sodium meat sausages. Effect on quality and stability. *Food Structure*. *14*, 52–59.

Marsh, J.T. and Wood, F.C. (1942). *An introduction to the chemistry of cellulose* [Online] 2nd ed. London: Chapman & Hall, Ltd. Available from: https://catalogue.nla.gov.au/Record/2066241.

Matos, M., Timgren, A., Sjöö, M., Dejmek, P. and Rayner, M. (2013). Preparation and encapsulation properties of double Pickering emulsions stabilized by quinoa starch granules. *Colloids and Surfaces A: Physicochemical and Engineering Aspects*. *423*, 147–153.

McClements, D.J. (2004). *Food Emulsions: Principle, Practices, and Techniques* [Online] second ed. Boca Raton: CRC Press. [Accessed 9 September 2019]. Available from: https://www.taylorfrancis.com/books/mono/10.1201/9781420039436/food-emulsions-david-julian-mcclements.

McCollister, S.B., Kociba, R.J. and McCollister, D.D. (1973). Dietary feeding studies of methylcellulose and hydroxypropylmethylcellulose. *Food and Cosmetics Toxicology*. *11*(6), 943–953.

McCormick, C.L., Callais, P.A. and Hutchinson, B.H. (1985). Solution studies of cellulose in lithium chloride and N,N-dimethylacetamide. *Macromolecules*. *18*(12), 2394–2401.

Medronho, B., Duarte, H., Alves, L., Antunes, F., Romano, A. and Lindman, B. (2015). Probing cellulose amphiphilicity. *Nordic Pulp & Paper Research Journal*. *30*(1), 58-66.

Medronho, B. and Lindman, B. (2014). Competing forces during cellulose dissolution: From solvents to mechanisms. *Current Opinion in Colloid*

and Interface Science. *19*(1), 32–40.

Medronho, B., Romano, A., Miguel, M.G., Stigsson, L. and Lindman, B. (2012). Rationalizing cellulose (in)solubility: Reviewing basic physicochemical aspects and role of hydrophobic interactions. *Cellulose*. *19*(3), 581–587.

Melzer, E., Kreuter, J. and Daniels, R. (2003). Ethylcellulose: A new type of emulsion stabilizer. *European Journal of Pharmaceutics and Biopharmaceutics*. *56*(1), 23–27.

Meng, Z., Qi, K., Guo, Y., Wang, Y. and Liu, Y. (2018). Effects of thickening agents on the formation and properties of edible oleogels based on hydroxypropyl methyl cellulose. *Food Chemistry*. *246*, 137–149.

Mikac, U., Sepe, A., Gradišek, A., Kristl, J. and Apih, T. (2019). Dynamics of water and xanthan chains in hydrogels studied by NMR relaxometry and their influence on drug release. *International Journal of Pharmaceutics*. *563*, 373–383.

Mishra, S., Singh, P.K., Pattnaik, R., Kumar, S., Ojha, S.K., Srichandan, H., Parhi, P.K., Jyothi, R.K. and Sarangi, P.K. (2022). Biochemistry, Synthesis, and Applications of Bacterial Cellulose: A Review. *Frontiers in Bioengineering and Biotechnology*. *10*, 1–12.

Miskandar, M.S., Man, Y.B.C., Yusoff, M.S.A. and Rahman, R.A. (2002). Effect of Emulsion Temperature on Physical Properties of Palm Oil-Based Margarine. *Journal of the American Oil Chemists Society*. *79*(12), 1163-1168.

Mitsou, E., Tavantzis, G., Sotiroudis, G., Ladikos, D., Xenakis, A. and Papadimitriou, V. (2016). Food grade water-in-oil microemulsions as replacement of oil phase to help process and stabilization of whipped cream. *Colloids and Surfaces A: Physicochemical and Engineering Aspects*. *510*, 69–76.

Miyamoto, H., Umemura, M., Aoyagi, T., Yamane, C., Ueda, K. and Takahashi, K. (2009). Structural reorganization of molecular sheets derived from cellulose II by molecular dynamics simulations. *Carbohydrate Research*. *344*(9), 1085–1094.

Mohd, N., Draman, S.F.S., Salleh, M.S.N. and Yusof, N.B. (2017). Dissolution of cellulose in ionic liquid: A review. *AIP Conference Proceedings*. *1809*, 020035.

Moon, R.J., Martini, A., Nairn, J., Simonsen, J. and Youngblood, J. (2011). Cellulose nanomaterials review: structure, properties and nanocomposites. *Chem. Soc. Rev*. *40*, 3941–3994.

Mozaffarian, D. and Willett, W.C. (2007). Trans fatty acids and cardiovascular risk: A unique cardiometabolic imprint? *Current Atherosclerosis Reports*. *9*(6), 486–493.

Mu, R., Hong, X., Ni, Y., Li, Y., Pang, J., Wang, Q., Xiao, J. and Zheng, Y. (2019). Recent trends and applications of cellulose nanocrystals in food industry. *Trends in Food Science and Technology*. *93*, 136–144.

Munk, M.B., Munk, D.M.E., Gustavsson, F. and Risbo, J. (2018). Using

Ethylcellulose to Structure Oil Droplets in Ice Cream Made with High Oleic Sunflower Oil. *Journal of Food Science*. *83*(10), 2520–2526.

Murray, B.S. (2019a). Microgels at fluid-fluid interfaces for food and drinks. *Advances in Colloid and Interface Science*. *271*, 101990.

Murray, B.S. (2019b). Pickering emulsions for food and drinks. *Current Opinion in Food Science*. *27*, 57–63.

Nadin, M., Rousseau, D. and Ghosh, S. (2014). Fat crystal-stabilized water-in-oil emulsions as controlled release systems. *LWT - Food Science and Technology*. *56*(2), 248–255.

Perrin, L., Gillet, G., Gressin, L. and Desobry, S. (2020). Interest of Pickering Emulsions for Sustainable Cosmetic Applications. *Polymers. 12*, 2385.

Napso, S., Rein, D.M., Fu, Z., Radulescu, A. and Cohen, Y. (2018). Structural Analysis of Cellulose-Coated Oil-in-Water Emulsions Fabricated from Molecular Solution. *Langmuir*. *34*(30), 8857–8865.

Napso, S., Rein, D.M., Khalfin, R., Kleinerman, O. and Cohen, Y. (2016). Cellulose gel dispersion: From pure hydrogel suspensions to encapsulated oil-in-water emulsions. *Colloids and Surfaces B: Biointerfaces*. *137*, 70–76.

Nasatto, P.L., Pignon, F., Silveira, J.L.M., Duarte, M.E.R., Noseda, M.D. and Rinaudo, M. (2014). Interfacial properties of methylcelluloses: The influence of molar mass. *Polymers*. *6*(12), 2961–2973.

Ni, Y., Li, J. and Fan, L. (2020). Production of nanocellulose with different length from ginkgo seed shells and applications for oil in water Pickering emulsions. *International Journal of Biological Macromolecules*. *149*, 617–626.

Norton, J.E., Fryer, P.J. and Norton, I.T. (2013). *Formulation Engineering of Foods* [Online] (J. E. Norton, P. J. Fryer, & I. T. Norton, eds.). John Wiley & Sons, Ltd. Available from: https://onlinelibrary.wiley.com/doi/book/10.1002/9781118597651.

Nsor-Atindana, J., Chen, M., Goff, H.D., Zhong, F., Sharif, H.R. and Li, Y. (2017). Functionality and nutritional aspects of microcrystalline cellulose in food. *Carbohydrate Polymers*. *172*, 159–174.

Obara, S., Muto, H., Kokubo, H., Ichikawa, N., Kawanabe, M. and Tanaka, O. (1992). STUDIES ON SINGLE-DOSE TOXICITY OF HYDROPHOBICALLY MODIFIED HYDROXYPROPYL METHYLCELLULOSE IN RATS. *The Journal of Toxicological Sciences*. *17*, 13–19.

Oh, I.K. and Lee, S. (2018). Utilization of foam structured hydroxypropyl methylcellulose for oleogels and their application as a solid fat replacer in muffins. *Food Hydrocolloids*. *77*, 796–802.

de Oliveira, W. and Glasser, W.G. (1996). Hydrogels from polysaccharides. I. Cellulose beads for chromatographic support. *Journal of Applied Polymer Science*. *60*(1), 63–73.

Olsson, C. and Westman, G. (2013). Direct Dissolution of Cellulose: Background, Means and Applications *In*: *Cellulose - Fundamental*

Aspects [Online]. IntechOpen, 143–178. Available from: https://doi.org/10.5772/2705.

Olsson, R.T., Azizi Samir, M.A.S., Salazar-Alvarez, G., Belova, L., Ström, V., Berglund, L.A., Ikkala, O., Nogués, J. and Gedde, U.W. (2010). Making flexible magnetic aerogels and stiff magnetic nanopaper using cellulose nanofibrils as templates. *Nature Nanotechnology*. *5*(8), 584–588.

Onwukamike, K.N., Grelier, S., Grau, E., Cramail, H. and Meier, M.A.R. (2019). Critical Review on Sustainable Homogeneous Cellulose Modification: Why Renewability Is Not Enough. *ACS Sustainable Chemistry and Engineering*. *7*(2), 1826–1840.

Östlund, Å., Idström, A., Olsson, C., Larsson, P.T. and Nordstierna, L. (2013). Modification of crystallinity and pore size distribution in coagulated cellulose films. *Cellulose*. *20*(4), 1657–1667.

Oza, K.P. and Frank, S.G. (1986). Microcrystalline cellulose stabilized emulsions. *Journal of Dispersion Science and Technology*. *7*(5), 543–561.

Öztürk-Kerimoğlu, B., Kara, A., Urgu-Öztürk, M. and Serdaroğlu, M. (2021). A new inverse olive oil emulsion plus carrot powder to replace animal fat in model meat batters. *LWT – Food Science and Technology*. *135*, 110044.

Ozturk, B. and McClements, D.J. (2016). Progress in natural emulsifiers for utilization in food emulsions. *Current Opinion in Food Science*. *7*, 1–6.

Pääkko, M., Ankerfors, M., Kosonen, H., Nykänen, A., Ahola, S., Österberg, M., Ruokolainen, J., Laine, J., Larsson, P.T., Ikkala, O. and Lindström, T. (2007). Enzymatic hydrolysis combined with mechanical shearing and high-pressure homogenization for nanoscale cellulose fibrils and strong gels. *Biomacromolecules*. *8*(6), 1934–1941.

Papadaki, A., Manikas, A.C., Papazoglou, E., Kachrimanidou, V., Lappa, I., Galiotis, C., Mandala, I. and Kopsahelis, N. (2022). Whey protein films reinforced with bacterial cellulose nanowhiskers: Improving edible film properties via a circular economy approach. *Food Chemistry*. *385*, 132604.

Patel, A.R., Cludts, N., Sintang, M.D. Bin, Lesaffer, A. and Dewettinck, K. (2014). Edible oleogels based on water soluble food polymers: Preparation, characterization and potential application. *Food and Function*. *5*(11), 2833–2841.

Patel, A.R., Cludts, N., Bin Sintang, M.D., Lewille, B., Lesaffer, A. and Dewettinck, K. (2014). Polysaccharide-based oleogels prepared with an emulsion-templated approach. *ChemPhysChem*. *15*(16), 3435–3439.

Patel, A.R. and Dewettinck, K. (2015). Comparative evaluation of structured oil systems: Shellac oleogel, HPMC oleogel, and HIPE gel. *European Journal of Lipid Science and Technology*. *117*(11), 1772–1781.

Patel, A.R. and Dewettinck, K. (2016). Edible oil structuring: An overview and recent updates. *Food and Function*. *7*(1), 20–29.

Pehlivanoglu, H., Ozulku, G., Yildirim, R.M., Demirci, M., Toker, O.S. and

Sagdic, O. (2018). Investigating the usage of unsaturated fatty acid-rich and low-calorie oleogels as a shortening mimetics in cake. *Journal of Food Processing and Preservation*. *42*(6), 1–11.

Peng, H., Wang, S., Xu, H. and Dai, G. (2018). Preparations, properties, and formation mechanism of novel cellulose hydrogel membrane based on ionic liquid. *Journal of Applied Polymer Science*. *135*(7), 25–28.

Pesek, J.J. and Matyska, M.T. (1999). Spectroscopic characterization of chemically modified oxide surfaces. *Studies in Surface Science and Catalysis*. *120*, 117–142.

Plechkova, N. V. and Seddon, K.R. (2008). Applications of ionic liquids in the chemical industry. *Chemical Society Reviews*. *37*(1), 123–150.

Qu, J., Blau, P.J., Dai, S., Luo, H. and Meyer, H.M. (2009). Ionic Liquids as Novel Lubricants and Additives for Diesel Engine Applications. *Tribology Letters*. *35*(3), 181–189.

Quan, S.L., Kang, S.G. and Chin, I.J. (2010). Characterization of cellulose fibers electrospun using ionic liquid. *Cellulose*. *17*(2), 223–230.

Rahatekar, S.S., Rasheed, A., Jain, R., Zammarano, M., Koziol, K.K., Windle, A.H., Gilman, J.W. and Kumar, S. (2009). Solution spinning of cellulose carbon nanotube composites using room temperature ionic liquids. *Polymer*. *50*(19), 4577–4583.

Rahman, M.M. and Netravali, A.N. (2017). High-performance green nanocomposites using aligned bacterial cellulose and soy protein. *Composites Science and Technology*. *146*, 183–190.

Rånby, B.G. (1949). Aqueous Colloidal Solutions of Cellulose Micelles. *Acta Chemica Scandinavica*. *3*, 649–650.

Rein, D.M., Khalfin, R. and Cohen, Y. (2012). Cellulose as a novel amphiphilic coating for oil-in-water and water-in-oil dispersions. *Journal of Colloid and Interface Science*. *386*(1), 456–463.

Remsing, R.C., Hernandez, G., Swatloski, R.P., Massefski, W.W., Rogers, R.D. and Moyna, G. (2008). Solvation of carbohydrates in N,N'-dialkylimidazolium ionic liquids: A multinuclear NMR spectroscopy study. *Journal of Physical Chemistry B*. *112*(35), 11071–11078.

Remsing, R.C., Swatloski, R.P., Rogers, R.D. and Moyna, G. (2006). Mechanism of cellulose dissolution in the ionic liquid 1-n-butyl-3-methylimidazolium chloride: A 13C and 35/37Cl NMR relaxation study on model systems. *Chemical Communications*. *12*, 1271–1273.

Rieland, J.M. and Love, B.J. (2020). Ionic liquids: A milestone on the pathway to greener recycling of cellulose from biomass. *Resources, Conservation and Recycling*. *155*, 104678.

Roberts, N.J. and Lye, G.J. (2002). Application of Room-Temperature Ionic Liquids in Biocatalysis: Opportunities and Challenges *In*: *Ionic Liquids: Industrial Applications for Green Chemistry*. American Chemical Society, 347–359.

Rodríguez, H. (2021). Ionic liquids in the pretreatment of lignocellulosic biomass. *Acta Innovations*. *38*, 23–36.

Rogers, M.A., Wright, A.J. and Marangoni, A.G. (2009). Oil organogels: The fat of the future? *Soft Matter*. *5*(8), 1594–1596.

Rössler, E.A., Hofmann, M. and Fatkullin, N. (2019). Chapter 8 Application of Field-cycling 1H NMR Relaxometry to the Study of Translational and Rotational Dynamics in Liquids and Polymers *In*: *Field-cycling NMR Relaxometry: Instrumentation: Model Theories and Applications* [Online]. The Royal Society of Chemistry, 181–206. Available from: http://dx.doi.org/10.1039/9781788012966-00181.

Sadeghifar, H., Venditti, R., Pawlak, J.J. and Jur, J. (2019). Cellulose transparent and flexible films prepared from DMAc/LiCl solutions. *BioResources*. *14*(4), 9021–9032.

Saito, T., Nishiyama, Y., Putaux, J.L., Vignon, M. and Isogai, A. (2006). Homogeneous suspensions of individualized microfibrils from TEMPO-catalyzed oxidation of native cellulose. *Biomacromolecules*. *7*(6), 1687–1691.

Sanderson, M.J., Smith, I., Parker, I. and Bootman, M.D. (2016). Fluorescence Microscopy. *Cold Spring Harbor protocols*. *10*, 1–36.

Sanz, T., Falomir, M. and Salvador, A. (2015). Reversible thermal behaviour of vegetable oil cellulose ether emulsions as fat replacers. Influence of glycerol. *Food Hydrocolloids*. *46*, 19–27.

Sarkar, A., Ademuyiwa, V., Stubley, S., Esa, N.H., Goycoolea, F.M., Qin, X., Gonzalez, F. and Olvera, C. (2018). Pickering emulsions co-stabilized by composite protein/ polysaccharide particle-particle interfaces: Impact on in vitro gastric stability. *Food Hydrocolloids*. *84*, 282–291.

Sarkar, A. and Dickinson, E. (2020). Sustainable food-grade Pickering emulsions stabilized by plant-based particles. *Current Opinion in Colloid & Interface Science*. *49*, 69–81.

Sarkar, A., Murray, B., Holmes, M., Ettelaie, R., Abdalla, A. and Yang, X. (2016). In vitro digestion of Pickering emulsions stabilized by soft whey protein microgel particles: Influence of thermal treatment. *Soft Matter*. *12*(15), 3558–3569.

Sarkar, A., Zhang, S., Holmes, M. and Ettelaie, R. (2019). Colloidal aspects of digestion of Pickering emulsions: Experiments and theoretical models of lipid digestion kinetics. *Advances in Colloid and Interface Science*. *263*, 195–211.

Satani, H., Kuwata, M. and Shimizu, A. (2020). Simple and environmentally friendly preparation of cellulose hydrogels using an ionic liquid. *Carbohydrate Research*. *494*, 108054.

Savadekar, N.R., Karande, V.S., Vigneshwaran, N., Bharimalla, A.K. and Mhaske, S.T. (2012). Preparation of nano cellulose fibers and its application in kappa-carrageenan based film. *International Journal of Biological Macromolecules*. *51*(5), 1008–1013.

Savadekar, N.R., Karande, V.S., Vigneshwaran, N., Kadam, P.G. and Mhaske, S.T. (2015). Preparation of cotton linter nanowhiskers by high-pressure homogenization process and its application in thermoplastic starch. *Applied Nanoscience*. *5*, 281–290.

Schaink, H.M., van Malssen, K.F., Morgado-Alves, S., Kalnin, D. and van der Linden, E. (2007). Crystal network for edible oil organogels: Possibilities and limitations of the fatty acid and fatty alcohol systems. *Food Research International*. *40*(9), 1185–1193.

Sen, S., Martin, J.D. and Argyropoulos, D.S. (2013). Review of cellulose non-derivatizing solvent interactions with emphasis on activity in inorganic molten salt hydrates. *ACS Sustainable Chemistry and Engineering*. *1*(8), 858–870.

El Seoud, O.A., Kostag, M., Jedvert, K. and Malek, N.I. (2020). Cellulose Regeneration and Chemical Recycling: Closing the “Cellulose Gap” Using Environmentally Benign Solvents. *Macromolecular Materials and Engineering*. *305*(4), 1–21.

Sescousse, R., Gavillon, R. and Budtova, T. (2011). Wet and dry highly porous cellulose beads from cellulose-NaOH-water solutions: Influence of the preparation conditions on beads shape and encapsulation of inorganic particles. *Journal of Materials Science*. *46*(3), 759–765.

Singh, A., Auzanneau, F.I. and Rogers, M.A. (2017). Advances in edible oleogel technologies – A decade in review. *Food Research International*. *97*, 307–317.

Staff, M.C. (2021). Obesity. *Mayo Clinic*. [Online]. Available from: https://www.mayoclinic.org/diseases-conditions/obesity/symptoms-causes/syc-20375742.

Stark, A., Sellin, M., Ondruschka, B. and Massonne, K. (2012). The effect of hydrogen bond acceptor properties of ionic liquids on their cellulose solubility. *Science China Chemistry*. *55*(8), 1663–1670.

Stortz, T.A. and Marangoni, A.G. (2013). Ethylcellulose solvent substitution method of preparing heat resistant chocolate. *Food Research International*. *51*(2), 797–803.

Sun, L., Chen, J.Y., Jiang, W. and Lynch, V. (2015). Crystalline characteristics of cellulose fiber and film regenerated from ionic liquid solution. *Carbohydrate Polymers*. *118*, 150–155.

Surh, J., Vladisavljević, G.T., Mun, S. and McClements, D.J. (2007). Preparation and characterization of water/oil and water/oil/water emulsions containing biopolymer-gelled water droplets. *Journal of Agricultural and Food Chemistry*. *55*(1), 175–184.

Suzuki, T., Kono, K., Shimomura, K. and Minami, H. (2014). Preparation of cellulose particles using an ionic liquid. *Journal of Colloid and Interface Science*. *418*, 126–131.

Swatloski, R.P., Spear, S.K., Holbrey, J.D. and Rogers, R.D. (2002). Dissolution of cellulose with ionic liquids. *Journal of the American Chemical Society*. *124*(18), 4974–4975.

Szlapak Franco, T., Martínez Rodríguez, D.C., Jiménez Soto, M.F., Jiménez Amezcua, R.M., Urquíza, M.R., Mendizábal Mijares, E. and de Muniz, G.I.B. (2020). Production and technological characteristics of avocado oil emulsions stabilized with cellulose nanofibrils isolated from agroindustrial residues. *Colloids and Surfaces A: Physicochemical and*

Engineering Aspects. *586*, 124263.

Tang, X.Y., Wang, Z.M., Yu, D., Yu, S.J., Meng, H.C., Zhang, T., Chen, H.L., Yang, Z.W., Yang, Q.Y. and Li, L. (2022). Fabrication of ultrastable water-in-oil high internal phase emulsion as versatile delivery vehicle through synergetic stabilization. *Food Hydrocolloids*. *126*, 107455.

Tanti, R., Barbut, S. and Marangoni, A.G. (2016). Hydroxypropyl methylcellulose and methylcellulose structured oil as a replacement for shortening in sandwich cookie creams. *Food Hydrocolloids*. *61*, 329–337.

Tasneem, M., Siddique, F., Ahmad, A. and Farooq, U. (2014). Stabilizers: Indispensable Substances in Dairy Products of High Rheology. *Critical Reviews in Food Science and Nutrition*. *54*(7), 869–879.

Tasset, S., Cathala, B., Bizot, H. and Capron, I. (2014). Versatile cellular foams derived from CNC-stabilized Pickering emulsions. *RSC Advances*. *4*(2), 893–898.

Tavernier, I., Patel, A.R., Van der Meeren, P. and Dewettinck, K. (2017). Emulsion-templated liquid oil structuring with soy protein and soy protein: κ-carrageenan complexes. *Food Hydrocolloids*. *65*, 107–120.

Thoorens, G., Krier, F., Leclercq, B., Carlin, B. and Evrard, B. (2014). Microcrystalline cellulose, a direct compression binder in a quality by design environment - A review. *International Journal of Pharmaceutics*. *473*, 64–72.

Thorne, J.B., Vine, G.J. and Snowden, M.J. (2011). Microgel applications and commercial considerations. *Colloid and Polymer Science*. *289*, 625–646.

Turbak, A.F., Snyder, F.W. and Sandberg, K.R. (1983). Microfibrillated cellulose, a new cellulose product: properties, uses, and commercial potential. *Journal of Applied Polymer Science: Applied Polymer Symposium*. *37*, 815–827.

Uetani, K. and Kitaoka, T. (2020). Nanocellulose: Beyond the ordinary. *BioResources*. *16*(1), 1–4.

Valsta, L.M., Tapanainen, H. and Männistö, S. (2005). Meat fats in nutrition. *Meat Science*. *70*, 525–530.

Vanderfleet, O.M. and Cranston, E.D. (2021). Production routes to tailor the performance of cellulose nanocrystals. *Nature Reviews Materials*. *6*(2), 124–144.

Vernon-Parry, K.D. (2000). Scanning Electron Microscopy : an introduction. *III-Vs Review*. *13*(4), 40–44.

Vitz, J., Erdmenger, T., Haensch, C. and Schubert, U.S. (2009). Extended dissolution studies of cellulose in imidazolium based ionic liquids. *Green Chemistry*. *11*(3), 417–42.

Wang, H., Gurau, G. and Rogers, R.D. (2012). Ionic liquid processing of cellulose. *Chemical Society Reviews*. *41*(4), 1519–1537.

Wang, J., Wang, L., Gardner, D.J., Shaler, S.M. and Cai, Z. (2021). Towards a cellulose-based society: opportunities and challenges. *Cellulose*. *28*,

4511-4543.

Wang, S., Lu, A. and Zhang, L. (2016). Recent advances in regenerated cellulose materials. *Progress in Polymer Science*. *53*, 169–206.

Wang, Y., Xie, W. and Wu, D. (2020). Rheological properties of magnetorheological suspensions stabilized with nanocelluloses. *Carbohydrate Polymers*. *231*, 115776.

Wasserscheid, P. and Keim, W. (2000). Ionic Liquids - New 'Solutions' for Transition Metal Catalysis. *Angewandte Chemie - International Edition. 39*, 3772–3789.

Watson, C.A. and Johnson, J.A. (1965). Studies on the Gelatinization of Starch I. Competition for water by protein and cellulose derivatives. *Journal of Food Science*. *30*(3), 450–456.

Wei, H.L., Wang, Y.T., Hong, Y.Y. and Zhu, M.J. (2021). Pretreatment of rice straw with recycled ionic liquids by phase-separation process for low-cost biorefinery. *Biotechnology and Applied Biochemistry*. *68*(4), 871–880.

Wendler, F., Todi, L.N. and Meister, F. (2012). Thermostability of imidazolium ionic liquids as direct solvents for cellulose. *Thermochimica Acta*. *528*, 76–84.

Winuprasith, T. and Suphantharika, M. (2015). Properties and stability of oil-in-water emulsions stabilized by microfibrillated cellulose from mangosteen rind. *Food Hydrocolloids*. *43*, 690–699.

Wollenweber, C., Makievski, A. V., Miller, R. and Daniels, R. (2000). Adsorption of hydroxypropyl methylcellulose at the liquid/liquid interface and the effect on emulsion stability. *Colloids and Surfaces A: Physicochemical and Engineering Aspects*. *172*, 91–101.

World Health Organization (WHO) (2018). Healthy diets: Fact sheet. *World Health Organisation*. *FACT SHEET*(394), 1–6.

World Health Organization (WHO) (2021). Obesity and overweight. Available from: https://www.who.int/news-room/fact-sheets/detail/obesity-and-overweight.

Xue, Z., Qin, L., Jiang, J., Mu, T. and Gao, G. (2018). Thermal, electrochemical and radiolytic stabilities of ionic liquids. *Physical Chemistry Chemical Physics*. *20*(13), 8382–8402.

Yang, J., Lu, X., Zhang, Y., Xu, J., Yang, Y. and Zhou, Q. (2020). A facile ionic liquid approach to prepare cellulose fiber with good mechanical properties directly from corn stalks. *Green Energy and Environment*. *5*(2), 223–231.

Yang, M., Liu, J., Guo, J., Yang, X., Liu, C., Zhang, M., Li, Y., Zhang, H., Zhang, T. and Du, Z. (2022). Tailoring the physicochemical stability and delivery properties of emulsions stabilized by egg white microgel particles via glycation: Role of interfacial particle network and digestive metabolites. *Food Hydrocolloids*. *131*, 107833.

Yang, Z. and Pan, W. (2005). Ionic liquids: Green solvents for nonaqueous biocatalysis. *Enzyme and Microbial Technology*. *37*(1), 19–28.

Yassin, F.A., El Kady, F.Y., Ahmed, H.S., Mohamed, L.K., Shaban, S.A. and Elfadaly, A.K. (2015). Highly effective ionic liquids for biodiesel production from waste vegetable oils. *Egyptian Journal of Petroleum*. *24*(1), 103–111.

Ye, X., Li, P., Lo, Y.M., Fu, H. and Cao, Y. (2019). Development of Novel Shortenings Structured by Ethylcellulose Oleogels. *Journal of Food Science*. *84*(6), 1456–1464.

Younes, M., Aggett, P., Aguilar, F., Crebelli, R., Di Domenico, A., Dusemund, B., Filipič, M., Jose Frutos, M., Galtier, P., Gott, D., Gundert-Remy, U., Georg Kuhnle, G., Lambré, C., Leblanc, J.C., Lillegaard, I.T., Moldeus, P., Mortensen, A., Oskarsson, A., Stankovic, I., Tobback, P., Waalkens-Berendsen, I., Wright, M., Tard, A., Tasiopoulou, S. and Woutersen, R.A. (2018). Re-evaluation of celluloses E 460(i), E 460(ii), E 461, E 462, E 463, E 464, E 465, E 466, E 468 and E 469 as food additives. *EFSA Journal*. *16*(1), 1–104.

Yue, C., Fang, D., Liu, L. and Yi, T.F. (2011). Synthesis and application of task-specific ionic liquids used as catalysts and/or solvents in organic unit reactions. *Journal of Molecular Liquids*. *163*(3), 99–121.

Zetzl, A.K., Gravelle, A.J., Kurylowicz, M., Dutcher, J., Barbut, S. and Marangoni, A.G. (2014). Microstructure of ethylcellulose oleogels and its relationship to mechanical properties. *Food Structure*. *2*(1–2), 27–40.

Zetzl, A.K., Marangoni, A.G. and Barbut, S. (2012). Mechanical properties of ethylcellulose oleogels and their potential for saturated fat reduction in frankfurters. *Food and Function*. *3*(3), 327–337.

Zeug, A., Zimmermann, J., Röder, B., Gabriela Lagorio, M. and San Román, E. (2002). Microcrystalline cellulose as a carrier for hydrophobic photosensitizers in water. *Photochemical and Photobiological Sciences*. *1*(3), 198–203.

Zhang, H., Wu, J., Zhang, J. and He, J. (2005). 1-allyl-3-methylimidazolium chloride room temperature ionic liquid: A new and powerful nonderivatizing solvent for cellulose. *Macromolecules*. *38*(20), 8272–8277.

Zhang, J., Xu, L., Yu, J., Wu, J., Zhang, X., He, J. and Zhang, J. (2016). Understanding cellulose dissolution: effect of the cation and anion structure of ionic liquids on the solubility of cellulose. *Science China Chemistry*. *59*(11), 1421–1429.

Zhang, J., Zhang, H., Wu, J., Zhang, J., Hea, J and Xiang, J. (2010). NMR spectroscopic studies of cellobiose solvation in EmimAc aimed to understand the dissolution mechanism of cellulose in ionic liquids. *Physical Chemistry Chemical Physics*. *12*(8), 1941–1947.

Zhang, R., Jingjing Y., Liu, N., Gao, Y. and Mao, L. (2022). W/O emulsions featuring ethylcellulose structuring in the water phase, interface and oil phase for multiple delivery. *Carbohydrate Polymers*. *283*, 119158.

Zhang, X., Xiao, N., Wang, H., Liu, C. and Pan, X. (2018). Preparation and characterization of regenerated cellulose film from a solution in lithium bromide molten salt hydrate. *Polymers*. *10,* 614.

Zhao, H., Baker, G.A., Song, Z., Olubajo, O., Crittle, T. and Peters, D. (2008). Designing enzyme-compatible ionic liquids that can dissolve carbohydrates. *Green Chemistry*. *10*(6), 696–70.

Zhao, H., Jones, C.L., Baker, G.A., Xia, S., Olubajo, O. and Person, V.N. (2009). Regenerating cellulose from ionic liquids for an accelerated enzymatic hydrolysis. *Journal of Biotechnology*. *139*(1), 47–54.

Zhu, Q., Pan, Y., Jia, X., Li, J., Zhang, M. and Yin, L. (2019). Review on the Stability Mechanism and Application of Water-in-Oil Emulsions Encapsulating Various Additives. *Comprehensive Reviews in Food Science and Food Safety*. *18*(6), 1660–1675.

Zhu, Y., Luo, X., Wu, X., Li, W., Li, B., Lu, A. and Liu, S. (2017). Cellulose gel dispersions: fascinating green particles for the stabilization of oil/water Pickering emulsion. *Cellulose*. *24*(1), 207–217.

Chapter 2
Advances in the use of microgels as emulsion stabilisers and as a strategy for cellulose functionalisation[1]

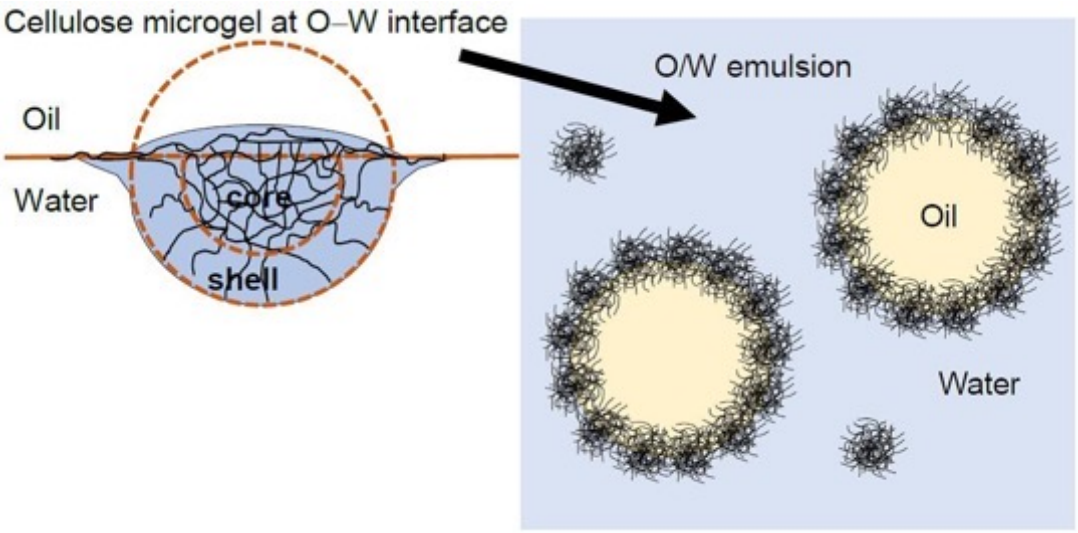

2.1 Abstract

Microgel particles have recently emerged as an alternative route to emulsion stabilisation. Classed as soft colloidal particles, their ability to swell to differing degrees in certain solvents and to rearrange once attached to an interface makes them highly suitable for systems requiring long-term stabilization, such as formulations in the food, agricultural, cosmetic and pharmaceutical industries. Microgels made with biocompatible polymers such as proteins and polysaccharides in particular offer an environmental advantage and currently form a very active area of research.

Cellulose, being a natural, biodegradable polymer, is an attractive ingredient for gels and microgels. However, its use as a functional material is often somewhat hindered by its insolubility in water and most other organic solvents. Furthermore, the surface activity of cellulose has proven difficult to harness and therefore its ability to act as an emulsion stabiliser has been almost exclusively applied to oil-in-water (O/W) emulsions, with very few reports on its water-in-oil (W/O) activity.

This review aims to summarise some of the recent progress made in the microgel field including their ability to act as emulsion stabilisers, with a focus on cellulose microgels (CMGs). A brief overview of cellulose processing is also given, describing the dissolution and reprecipitation routes

[1]Published as: Lefroy, K.S., Murray, B.S. and Ries, M.E. (2021). Advances in the use of microgels as emulsion stabilisers and as a strategy for cellulose functionalisation. *Cellulose*. *28*, 647–670. DOI: 10.1007/s10570-020-03595-8

used to functionalise cellulose without covalent modification and the potential for cellulose particles and CMGs to act as O/W and W/O emulsion stabilisers.

2.2 Microgel particles

Microgel particles (also referred to as “microgels”) are a class of soft colloidal species which are receiving increasing interest in the area of emulsion stabilisation (Dickinson, (2015)). Originally, the term microgel was introduced in 1949, with the word “micro” referring to the gel particle size and “gel” meaning the ability of the particles to swell in organic solvents (Baker, (1949); Pelton and Hoare, (2011)). They are often now referred to as “colloidal dispersions of gel-like particles”, in which each individual microgel exists as a long-lived, kinetically stable particle (Dickinson, (2015)). Microgels are made up of a covalently, or strong physically cross-linked polymer network that must be dispersed in and swollen by the solvent. Their swelling “state” is to an extent governed by the cross-link density, polymer/solvent compatibility and the presence (or not) of electrical charges (Pelton and Hoare, (2011)). In some cases, thermodynamic parameters such as temperature and pH can be used to control their degree of swelling (DOS) and such microgels are often referred to as “intelligent” or “responsive,” since they may shrink and expand in response to an external stimulus (Figure 2.1a) (Schmitt and Ravaine, (2013)). Unlike surfactant micelles and other self-assembling molecular aggregates, they have a static composition. Although they may aggregate to different extents in ‘solution,’ the polymer network remains stable.

Altering the synthetic method and conditions of formation allows one to access to a broad range of gel particles with specific morphologies, sizes and microstructures, depending on the desired application. This is reflected by the huge potential impact of microgels in a wide variety of industries, such as food, (Murray, (2019a)) cosmetics, (Boularas et al., (2018)) medicine, (Agrawal and Agrawal, (2018)) and agriculture (Abd El-Rehim, (2005)).

2.2.1 Microgel synthesis

Three general approaches to microgel synthesis, as defined by Pelton *et al*., are given in Figure 2.1b: i) from monomer; ii) from polymer; iii) from macrogel (Pelton and Hoare, (2011)). It is important to distinguish between the terms “macrogel” and “microgel” at this stage: macrogel refers to a large, cross-linked structure or “a bowl of jelly,” whilst microgels are discrete particles (illustrated in Figure 2.1b) (Thorne et al., (2011)). The former routes (i and ii) are often referred to as “bottom-up” and the latter (iii) as “top-down” approaches (Torres et al., (2016)). Different approaches may be preferred depending on the level of control required during synthesis and the nature of

the polymeric material but, generally, a specific distribution of a functional groups, a narrow microgel size distribution and high colloidal stability are desired (Pelton and Hoare, (2011); Agrawal and Agrawal, (2018)). Some examples of microgel synthesis will be briefly described below, however we refer readers to comprehensive reviews for a more detailed discussion of these aspects (Saunders and Vincent, (1999); Ballauff and Lu, (2007); Burey et al., (2008); Dendukuri and Doyle, (2009); Pich and Richtering, (2010)).

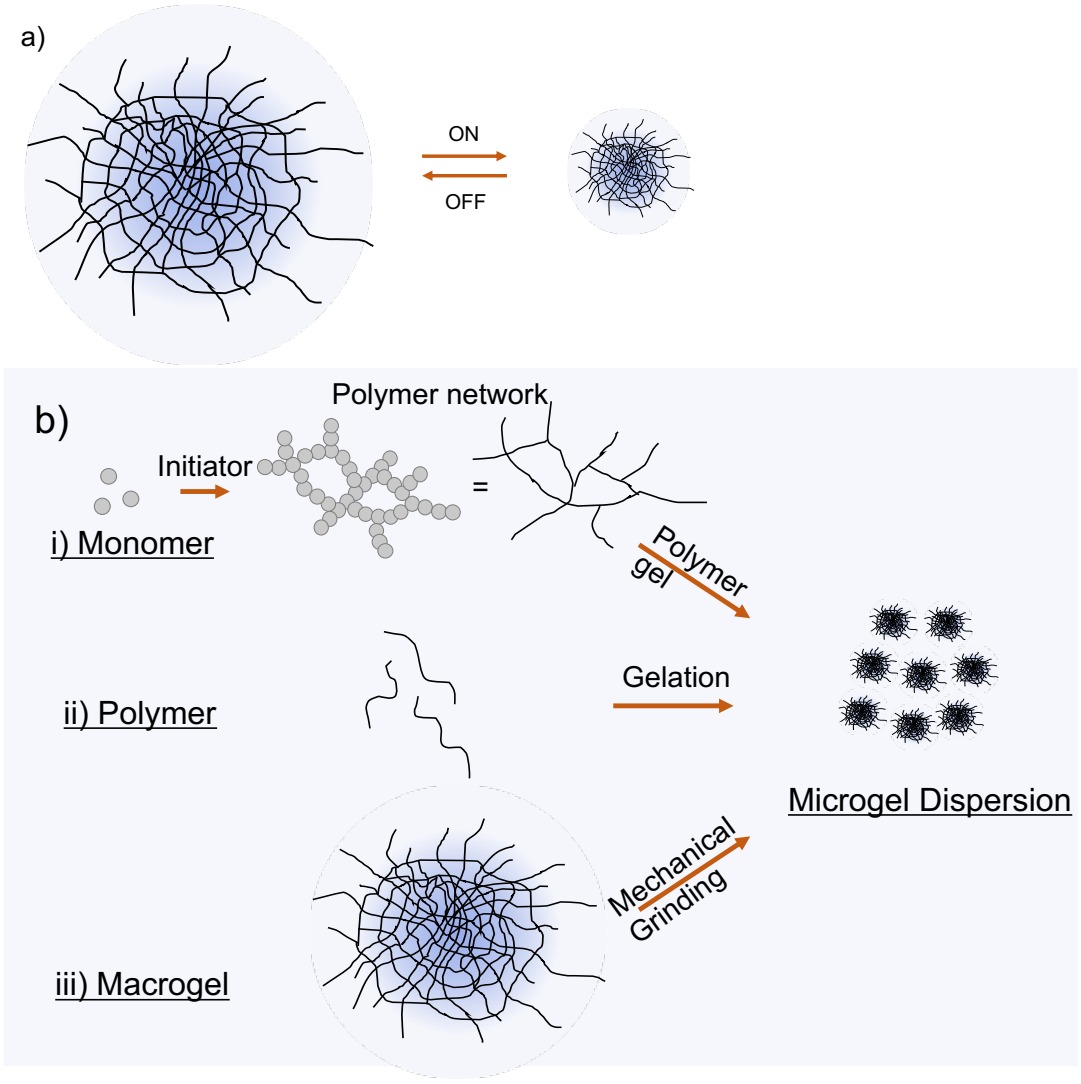

Figure 2.1. a) Illustration of "intelligent" microgels experiencing contraction and swelling in response to an external stimulus (on and off, respectively); b) different methods of microgel synthesis discussed in section 2.2.1: i) from monomer; ii) from polymer; iii) from macrogel.

2.2.1.1 “Bottom up” approaches

Microgel “bottom-up” preparation methods can be further classified into those formed by homogeneous nucleation, emulsification and complex formation (Pelton and Hoare, (2011)), each of which will be briefly discussed below.

2.2.1.2 Homogeneous nucleation, emulsion polymerisation and precipitation polymerisation

Homogeneous nucleation describes the polymerisation of a monomer from a homogenous (or nearly homogeneous) solution, usually employing an initiator or cross-linking agent. Microgel size dispersion can be controlled in many different ways depending on the monomer- and polymer-type, for example by changing the solvent composition, temperature and initiator concentration (Pelton, (2000)). Homogeneous nucleation is further characterised into two forms of emulsion polymerisation, (distinct from the emulsification method described in the sub-section below): conventional emulsion polymerization (EP) and surfactant-free emulsion polymerisation (SFEP). EP uses a surfactant, giving some control over microgel particle size through colloidal stabilisation (McPhee et al., (1993); Zhang et al., (2004)). Generally, a higher concentration of surfactant leads to formation of microgel particles with a lower hydrodynamic radius and lower polydispersity (Saunders et al., (2009); Haider et al., (2014)). SFEP has the advantage of mitigating surfactant contamination and has been used to fabricate temperature sensitive poly-*N*-isopropylacrylamide *poly*-(NIPAM) microgels since the 1980s (Pelton and Chibante, (1986)). Higher reaction temperatures are conventionally employed to produce smaller particle sizes (Dowding et al., (2000)), however generally the preparation of very small particles is complicated by the higher surface area to volume ratio and limited number of charges available (Zhang et al., (2004)). Finally, precipitation polymerisation has been used as a facile route to prepare *poly*-NIPAM (PNIPAM) microgels where the monomer is soluble but the polymer is not (Schmitt and Ravaine, (2013)). Growing polymer chains therefore collapse once a critical length is reached, leading to relatively monodisperse microgel particle sizes (Grinberg et al., (2020)). This type of microgel preparation is referred to as “batch synthesis” and has been reported to yield heterogeneous core-shell microgel structures, since the cross-linking agent is consumed at a faster rate than the NIPAM monomers (Kyrey et al., (2019)). Therefore, the formation of a highly dense core and a loose corona is commonly observed (Gavrilov et al., (2020)).

2.2.1.3 Emulsification

The emulsification strategy involves the formation of a water-in-oil (W/O) emulsion, made up of an oil/brine continuous phase and a monomer or polymer aqueous solution discontinuous phase, often referred to as a "pre-gel." The monomer/polymer located within the droplets are subsequently gelled through a cross-linking or nucleation reaction (Dowding et al., (2000); Ikkai et al., (2005); Burey et al., (2008); MacHado et al., (2012)). Preparation of polysaccharide microgels have been reported using the emulsification technique, using alginate dissolved in the aqueous phase and Ca^{2+} ions injected into the emulsion as bridging/gelling agent (MacHado et al., (2012)). Alternatively, it has been demonstrated that mixing of two aqueous phases containing alginate and calcium ions under highly turbulent conditions produces microgel particles which are ca. 100 nm in size (Pravinata et al., (2016)).

Gelation is most commonly induced by the application of heat or through a low-temperature redox reaction, depending on the type of polymer and monomer (Schosseler et al., (1991); Takata et al., (1999)). On the other hand, photo-polymerisation is mostly used for continuous flow reactors: (Gokmen and Du Prez, (2012)) for example, UV-induced gelation has been coupled with microchannel emulsification to produce microgel particles of low size polydispersity (Ikkai et al., (2005)). Microfluidics have also been applied to alginate microgel particles, where the size of droplets displayed an indirect dependence on the concentration of reagents (aqueous alginate and $CaCl_2$) and flow rate, which in turn affect the time for an alginate-structured solution to form and the time for microgel particles to form, respectively (Amici et al., (2008)).

2.2.1.4 Complex formation

In complex formation, two oppositely charged polyelectrolytes are mixed to form microgel suspensions or coacervate particles (Azarikia et al., (2015)). One of the species must be present in excess to avoid charge neutralisation (Pelton and Hoare, (2011)) as evidenced in the phase diagram of carboxymethyl cellulose (CMC) ± polyvinylamine (PVAm) (anionic and cationic, respectively), where mixtures containing an excess of one polyelectrolyte give stable colloidal complexes whilst a stoichiometric mixture yields a macrogel or macroscopic precipitates (Feng et al., (2007)). Although complexation is a very simple method for microgel preparation, it can be challenging to prepare monodisperse particles. Monodispersity has been improved by first synthesising a microgel based on one polymer, then adding

the second polyelectrolyte later. For example, anionic PNIPAM microgels, whose composition and size dispersion can be carefully controlled, have been subsequently complexed with cationic PVAm to give a stable, colloidal suspension of monodisperse spheres (Wen et al., (2012)). Gelatin-OSA starch hydrogel particles have also been fabricated by simply mixing aqueous solutions and acidifying the mixture to pH 5, where it was shown again that the cation:anion ratio has an effect on particle size and polydispersity. In this instance, adjusting the pH varied the electrostatic interactions between the two polyelectrolytes and therefore provided a means of controlling the strength of complex formation (Wu and McClements, (2015)).

2.2.1.5 "Top-down" approaches

"Top-down" processing to produce microgels simply involves formation of a macrogel followed by mechanical comminution to produce particles of micron size, or less. Generally, this type of approach yields highly polydisperse microgel dispersions with particles of irregular morphologies and as a result, somewhat fewer reports are available in the literature (Pelton and Hoare, (2011)). However, sizes of < 90 nm have been achieved via mechanical shearing of heat-set gels (Sarkar et al., (2016)). Furthermore, the top-down approach may offer some level of control over the microgel particle properties by fine-tuning the macrogel structure, since at least some characteristics of the microgel are expected to be inherited from the initial macrogel, e.g. the *internal* cross-link density in the microgel (Murray, (2019a)). Thus specific "gel recipes" can be designed in order to produce macrogels with a certain desired microscopic structure: for example, more brittle, highly porous heterogenous gels break down more easily to give microgels with a narrower and smaller size distribution compared to gels which are elastic and homogenous (Saavedra Isusi et al., (2019)). Microgel size dispersity is also affected by the concentration (and type) of salt, for gel systems where inorganic ions act the bridging agents (Matsumiya and Murray, (2016)). The effect of pH is particularly important for protein-based microgels, where significant particle aggregation can occur at their isoelectric point (Jiao et al., (2018); Zhang et al., (2020)). Polymer properties such as the distribution of functional groups, molecular weight and branching versus linearity will also have an influence on gel properties (Fraeye et al., (2009)). For example, a decrease in degree of polymerisation (DP) has been correlated with the formation of more brittle gels (Fraeye et al., (2010)) which are more easily broken down to form microgel particles.

The type of (e.g. compressive, tensile or shear) and magnitude of stress applied during top-down processing also affects how a gel breaks down (Saavedra Isusi et al., (2019)). Processing may deform and alter the gel network structure, often leading to a more open structure in the microgel particles (Murray, (2019a)). It has been reported that pectin-based microgels are more easily broken down when conditions favouring extensional forces were employed, for example laminar flow in a rotor-stator device, since the tensile strength of the gels was lower than the compressive strength (Saavedra Isusi et al., (2019)). Smaller microgels are usually produced, up to a limit, by higher energy processing methods: for example, a mixture of blending and high-pressure homogenisation (HPH) was shown to produce smaller soybean-protein-isolate microgel particles compared to blending and ultrasonication or blending alone (Matsumiya and Murray, (2016)). Similarly, peanut-protein-isolate microgel particles prepared using a rotor-stator homogeniser followed by HPH gave an average diameter range of 200-300 nm (Jiao et al., (2018)). However, to our knowledge, few attempts have been made to relate directly the properties manifested in the microgel particles to the initial macrogel from which they were formed.

2.2.2 Cellulose microgels (CMGs)

Gels made up of cellulose can be broken down using mechanical force such as HPH, producing cellulose microgels (CMGs) via a top-down approach (Figure 2.2). As discussed previously (section 2.2.1.5), like other polymer microgels the nature and morphology is highly dependent on the properties of the macrogel, which in turn is affected by the amount of cellulose dissolved and the method and conditions of coagulation (applied shear force, temperature, anti-solvent, etc.) (Li et al., (2009); Fan et al., (2017); Rajeev and Basavaraj, (2019)).

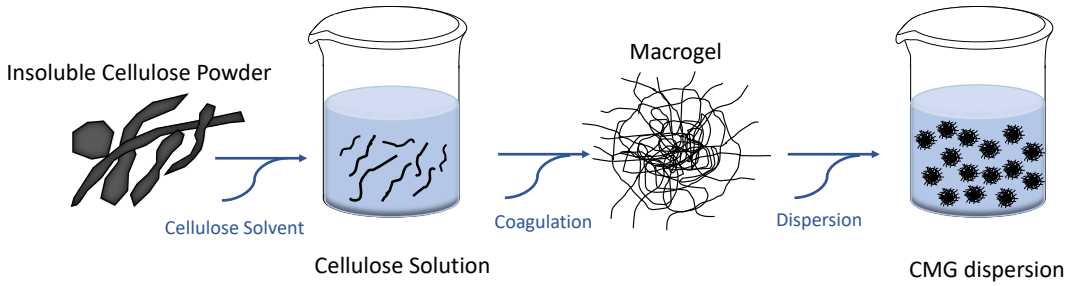

Figure 2.2 Top-down method for producing CMGs: dissolution of insoluble cellulose powder in a solvent, coagulation from the solvent to form a cellulose macrogel, breakdown of the cellulose macrogel into a microgel particle dispersion.

Cellulose-based gels can be fabricated via dissolution of cellulose followed by re-coagulation of the polymer molecules so that they spontaneously form a network structure, or by chemical reactions that form cross-links between polymer molecules. In the former approach, the regions of reassociation of the cellulose molecules via H-bonds form the cross-links, or junction zones of the gel (Kadokawa et al., (2008); Takada and Kadokawa, (2015)) whilst in the latter, active groups on derivatized cellulose interact to from the cross-links (H. Kang et al., (2016)). Many covalently cross-linked cellulose gels have been fabricated for various applications, with derivatization of the cellulose commonly being the first step in their synthesis (Lu et al., (2000); Sannino et al., (2005); Demitri et al., (2008); Butun et al., (2011)). However, we focus herein on reviewing physically cross-linked cellulose gels, in the interest of functionalising cellulose in its natural state, which can be formed via H-bonding, hydrophobic, ionic and host-guest interactions (Shang et al., (2008); H. Kang et al., (2016)).

2.3 Preparation of cellulose particles and cellulose microgel particles

2.3.1 Solubilisation of cellulose

2.3.1.1 Acid hydrolysis

Cellulose is found naturally in wood and cotton fibres, along with lignin and hemicellulose (see Figure 2.3), which are broken down into their components using acid hydrolysis to yield cellulose crystals and monomeric sugars (Rånby, (1949); Zhao et al., (2007)). The treated cellulose retains the same crystalline structure as the original material (Mukherjee et al., (1952)) and various forms of crystalline cellulose can be obtained depending on the source, treatment temperatures and times (Habibi et al., (2010)). Acid hydrolysis is a well-established method for the production of cellulose nanoparticles (CNPs) or cellulose nanocrystals (CNCs), which have impressive mechanical properties (Zhao et al., (2007)), as well as microcrystalline cellulose (MCC), which has now been used for over 50 years in the pharmaceutical industry (Battista and Smith, (1962); Thoorens et al., (2014)). Since acid hydrolysis generally yields fragments of cellulose, it might be argued that this is not true solubilisation; in the following we concentrate on solvent systems that results in ‘true,’ complete, molecular solubilisation.

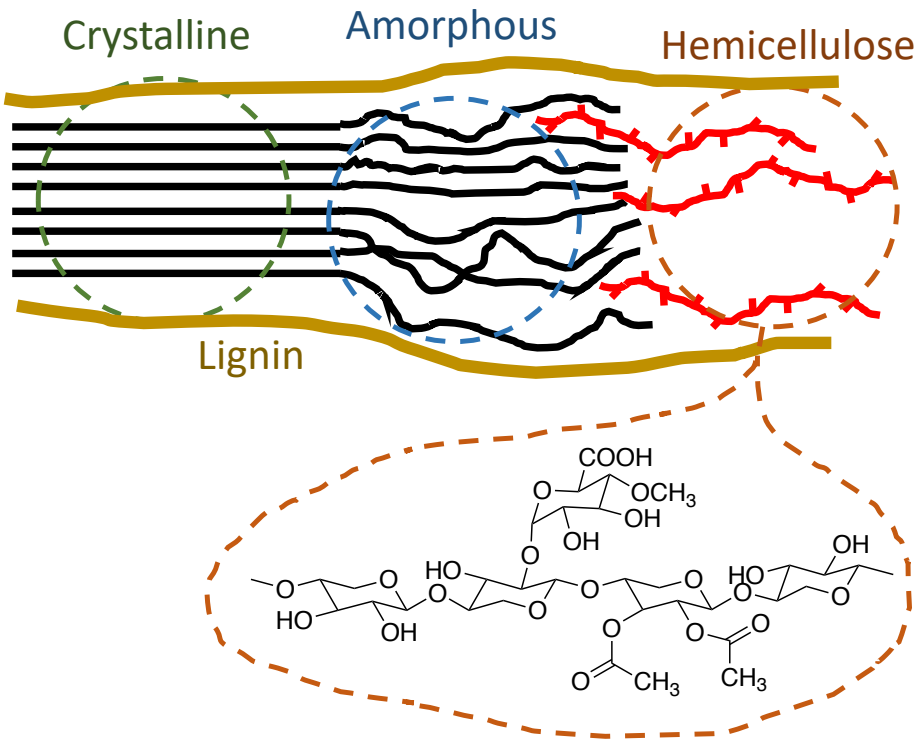

Figure 2.3. Schematic of cellulose feedstock with crystalline and amorphous regions shown, as well as lignin and a type of hemicellulose (chemical structure shown).

2.3.1.2 Cellulose solvents

Crystalline cellulose obtained via acid hydrolysis, however, is still insoluble in water and most other organic solvents and therefore further modification is often required through dissolution in a particular solvent system. A summary of various cellulose solvents and their discoveries is given in the timeline below (Figure 2.4). Aqueous alkali/urea solvent systems have been developed (Zhou and Zhang, (2000); Cai and Zhang, (2005); Qi et al., (2011)), in which the urea is proposed to aid dissolution by interacting with the hydrophobic part of cellulose through its nitrogen atoms (Xiong et al., (2014); Medronho et al., (2015)). Other additives such as thiourea and polyethylene glycol (PEG) have shown success in dissolving cellulose when combined with an alkali and are believed to play a similar role to urea (Cai and Zhang, (2005); Yan and Gao, (2008); Xiong et al., (2014); H. Kang et al., (2016)).

N-Methylmorpholine-*N*-oxide (NMMO) has also been widely used as a non-derivatizing solvent for cellulose since it was first patented in 1969 (Johnson, (1969)). A mixture of NMMO and water is used, (50-60 % and 20-30 % respectively), with the relative optimum amounts depending on the cellulose source (Gagnaire et al., (1980); Rosenau et al., (2001)). Finally, we focus in more detail on ionic liquids (ILs) as cellulose solvents.

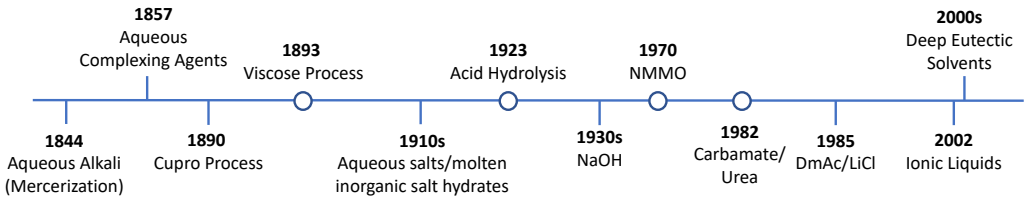

Figure 2.4. Schematic showing the discovery of various solvents for cellulose dissolution, with those used industrially represented by circles. References are given in the following order, from left to right: (Cross et al., (1893); Rinaldi and Schüth, (2009); Liebert, (2010); Olsson and Westman, (2013)).

2.3.1.3 Ionic liquids

"Liquified quaternary ammonium salts" were first patented at the start of the 20th century, providing a route for cellulose dissolution and derivatization (Graenacher, (1934)). However, a molten solution of *N*-alkylpyridinium chloride was used and because the melting point was greater than 100 °C, the process was deemed to be "of little practical value" and no further interest was reported for some time. Almost 70 years later, salts made up of a large, organic cation and a variety of anions now described as ionic liquids (ILs) were shown to be liquid over a wide temperature range (Huddleston et al., (2001)). In 2002, Swatloski *et al.* demonstrated that imidazolium-based ionic liquids (ILs) with melting points < 100 °C were suitable solvents for cellulose (Swatloski et al., (2002)). Since then, a number of ILs have been successfully applied for cellulose dissolution: 1-butyl-3-methylimidazolium chloride (BmimCl), 1-allyl-3-methylimidazolium chloride (AmimCl) and 1-ethyl-3-methylimidazolium acetate (EmimAc) (Zhang et al., (2017)), as well as ammonium-, morpholium- and cholinium-based cations paired with carboxylate (formate, acetate) and chloride anions (Zhang et al., (2005); Ignatyev et al., (2010); Z. Chen et al., (2011); Tang et al., (2012); Meenatchi et al., (2017)). ILs are promising due to their high thermal and chemical stability, ease of handling, non-flammability and low vapour pressure, amongst other things (Zhang et al., (2017)). They are also often described as "green" solvents due to their recyclability and mild operating temperatures.

As with NMMO systems, microwave assistance can be applied during IL-cellulose dissolution which results in highly efficient heating. However, in general, dissolution temperatures of < 120 °C are used in order to prevent thermal degradation of cellulose to increase the quality of the resulting material (Swatloski et al., (2002); Zhu et al., (2006); H. Wang et al., (2012); Olsson and Westman, (2013)). Whilst most conventional ILs have an onset

temperature (T_{on}) of over 170 °C in their pure form (and therefore won't decompose until they reach very high temperatures), the addition of cellulose decreases T_{on} and notably increases the degree of heat release and therefore the potential for cellulose degradation. Consequently, slower dissolution times at lower temperatures may be more suitable for industrial scale up (Wendler et al., (2012)). Milder conditions have also been shown to limit unwanted by-product formation, maintaining the ability of the IL to act as a non-derivatizing solvent (Clough et al., (2015)).

Different conditions, co-solvents and dissolution times have been employed to obtain different cellulose microstructures, as well as the design of so-called "task specific" ILs (TSILs), fabricated for highly specific applications (Gericke et al., (2012)). TSILs have a functional group tethered covalently to the anion or cation (or both), which can be a reagent or a catalyst in a chemical reaction or simply act as part of the reaction medium. A comprehensive review was published in 2011 on the synthesis and role of TSILs in organic reactions (Yue et al., (2011)), which focuses on ILs and their use as non-derivatizing cellulose solvents (Table 2.1).

Table 2.1. Various ionic liquids with acetate or chloride anions and the extent of their cellulose solubility at different temperatures (MCC = Microcrystalline Cellulose; DP = degree of polymerisation). Chemical structures are given below.

Ionic Liquid	Type of Cellulose (DP)	Dissolving Capacity/wt%	Temperature/°C	References
EmimAc[1]	Long fibres, C 6663	10	> 40	(Fryczkowska et al., (2018))
	Avicel PH-101 (180)	15	80	(Lovell et al., (2010))
	MCC (220)	18	80	(Song et al., (2011))
	MCC (220)	15.1	80	(Zhang et al., (2016))
EmimCl[2]	MCC Avicel (<350)	5	90	(Zavrel et al., (2009))
BmimAc[3]	Linter Cellulose	10	100	(Liu et al., (2015))
	MCC (220)	9.5	80	(Zhang et al., (2016))
BmimCl[4]	MCC (ca. 350)	10	100	(Rajeev et al., (2018))
	Dissolving Pulp (ca. 1000)	3	70	(Swatloski et al., (2002))
	Avicel PH-101 (180)	10	80	(Sescousse et al., (2010))
	MCC (220)	<10	80	(Zhang et al., (2016))

	Dissolving Pulp (ca. 1000)	10	100	(Swatloski et al., (2002))
AmimAc[5]	MCC (220)	11.6	80	(Zhang et al., (2016))
AmimCl[6]	MCC (220)	14.5	80	(Zhang et al., (2016))
	Dissolving Pulp (ca. 1000)	14.5	80	(Zhang et al., (2005))
	MCC (ca. 350)	20	100	(Rajeev et al., (2018))
HmimAc[7]	MCC (220)	7.1	80	(Zhang et al., (2016))
	Dissolving Pulp (ca. 1000)	5	100	(Swatloski et al., (2002))
OmimAc[8]	MCC (220)	4.5	80	(Zhang et al., (2016))
	Dissolving Pulp (ca. 1000)	Slightly Soluble	100	(Swatloski et al., (2002))

Cation

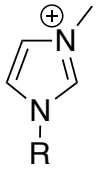

Anion

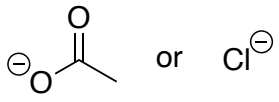

AmimAc: R = $CH_2CH{=}CH_2$
EmimAc: R = CH_2CH_3
BmimAc: R = $CH_2(CH_2)_2CH_3$
HmimAc: R = $CH_2(CH_2)_4CH_3$
OmimAc: R = $CH_2(CH_2)_6CH_3$

[1]1-ethyl-3-methylimidazolium acetate;
[2]1-ethyl-3-methylimidazolium chloride;
[3]1-butyl-3-methylimidazolium acetate;
[4]1-butyl-3-methylimidazolium chloride;
[5]1-allyl-3-methylimidazolium acetate;
[6]1-allyl-3-methylimidazolium chloride;
[7]1-hexyl-3-methylimidazolium acetate;
[8]1-octyl-3-methylimidazolium acetate

2.3.1.4 Deep eutectic solvents (DESs)

A more recently developed class of “advanced ionic liquids” or Deep Eutectic Solvents (DESs) may offer a relatively cheap and more practical route for cellulose dissolution compared to conventional ILs, which are generally much more air-sensitive due to their hygroscopicity (Brinchi et al., (2013); Van Osch et al., (2017); Satlewal et al., (2018); Verma et al., (2019)). DESs were first reported in 2001 (Abbott et al., (2001)) and are comprised of a hydrogen bond donor (HBD) and a halide salt or hydrogen bond acceptor (HBA): for example urea, carboxylic acids, polyols and metal chlorides (Zhang et al., (2017)). The resulting mixtures have a much lower melting temperature compared to their anion and cation components, due to the formation of hydrogen bonding between the two (Van Osch et al., (2017)). Numerous reports of DESs displaying good cellulose dissolving capacity at impressive rates can be found in the literature (Wang et al., (2006); Zhang et al., (2012); Li et al., (2017); Sirviö, (2019); Ling et al., (2019)). Ma *et al.* used a hydrated choline chloride/oxalic acid dihydrate DES to prepare CNCs, reporting that their solvent dissolving capability is further improved by the addition of water. It is also mentioned that such solvents clearly comply with the green chemistry principles and therefore have high potential for scale-up (Ma et al., (2019)). However, currently DESs display inferior cellulose dissolution capacities and rates compared to conventional ILs (Chen et al., (2019)) and further work is required to fully understand their thermal stabilities and toxicities.

2.3.1.5 ILs from renewable feedstocks

Finally, many ILs prepared from renewable feedstocks have been reported (Halder et al., (2019)), further improving their case as “green,” environmentally friendly solvents. ILs made up of cholinium- or choline-based cations, choline being a water-soluble nutrient, have received attention due to their biodegradability and biocompatibility (Abbott et al., (2006); Bisht and Venkatesu, (2017); Depoorter et al., (2019)). Choline-chloride + oxalic acid and choline chloride + urea have both shown to be effective pre-treatments for biomass (Satlewal et al., (2018)), whilst choline butyrate was used to dissolve MCC and produce a cellulose aerogel (Xu et al., (2018)). Furthermore, amino-acids which are cost-effective and natural have been used as IL precursors (Jiang et al., (2018)). A mini-review on amino-acid ILs provides a useful summary on how the structure relates to the properties of ILs fabricated from raw materials (Ossowicz et al., (2019)). Alternative bio-based ILs fabricated from proteins, (Bao et al., (2003)) polysaccharides, (Handy et al., (2003)) lignin, (Socha et al., (2014)) and terpenes (Nageshwar

et al., (2009)) have also been reported, offering the potential for a “closed-loop” biorefinery (Hulsbosch et al., (2016)).

A comprehensive overview of ILs and the temperatures, conditions and dissolution times required to solubilise different concentrations of cellulose has been compiled by Van Osch *et al.*, which also provides a comparison of the particle sizes of the cellulose regenerated from different sources (Van Osch et al., (2017)). Given the impressive cellulose dissolution capacities that have been achieved (up to 25 wt%), the mild conditions required (relative to conventional methods) and the potential for recycling the solvent, ILs offer a convenient route for cellulose processing and whole biomass treatment (Hossain et al., (2019)). However, it must be highlighted that plenty of understanding is still required regarding their recyclability on an industrial scale and any potential toxicity.

2.3.2 Cellulose reprecipitation

2.3.2.1 Cellulose particles

Once cellulose has been dissolved, it is generally reprecipitated, or coagulated, by addition of an “anti-solvent”, which competes with the cellulose for bonding to the solvent and initiates phase separation. This method of regeneration can be used for the NaOH-based aqueous systems (Qi et al., (2011)), NMMO (Ilyin et al., (2018)) and ILs/DESs described above (Hedlund, Köhnke, et al., (2019); Sirviö, (2019)), but in this review we focus herein on cellulose processed from ILs.

A good anti-solvent forms stronger H-bonds with the IL than cellulose, resulting in the reaggregation of cellulose chains via H-bonds. The use of different anti-solvents during the regeneration of cellulose from ILs allows access to a wide range of morphologies (Brinchi et al., (2013)). Most commonly water, ethanol or acetone are added as anti-solvent, each yielding cellulose with differing levels of crystalline structure. The concentration of cellulose in solution and the physical conditions of coagulation also affect the properties of the precipitated cellulose. It has been widely observed that the use of water as a coagulant produces cellulose II (from feedstocks high in cellulose I, e.g. MCC), whilst addition of alcohols leads to a larger decrease in crystallinity and an increase in amorphous cellulose (Xu et al., (2008); Lan et al., (2011); Östlund et al., (2013); Sun et al., (2015); Zhang et al., (2018)). For example, cellulose dissolved in EmimAc was regenerated separately in water and ethanol, giving degrees of crystallinity of 43.33% and 13.45% respectively (Tan et al., (2019)), whilst similar observations were made for CNPs regenerated in water, methanol, ethanol and *n*-propanol (43.9 %, 26.9 %, 20.3

% and 12.5 % respectively) (Fan et al., (2018)). In all of these examples, the coagulated material consisted of cellulose particles.

Different flow conditions (e.g. extrusion, stirring) during coagulation have also been employed and introduce an additional level of tunability. Thus if water is added to a stirred solution of MCC dissolved in 1-butyl-3-methylimidazolium hydrogen sulfate ($BmimHSO_4$) and the mixture then sonicated, washed and centrifuged, highly crystalline nanocellulose crystals (NCC) can be obtained (Man et al., (2011)). Cellulose films with an impressive tensile strength of 138 MPa have been fabricated by Zhang *et al.* using AmimCl or EmimAc with regeneration in water (Zhang et al., (2005)), whilst rods and fibres can be prepared via direct extrusion into water (Swatloski et al., (2002)). Cellulose membranes have also been produced by pouring cellulose/EmimAc solutions onto a glass plate followed by immersion in a coagulation bath of water/alcohol at room temperature (Fryczkowska et al., (2018)).

2.3.2.2 Cellulose gels

Cellulose gels can also be fabricated from cellulose solutions using anti-solvents through the reformation of hydrophobic interactions and H-bonds (Isobe et al., (2012)), if the coagulation medium is not stirred during regeneration. As with cellulose particles, the type of medium dictates the properties of the gel obtained, such as “thickness”, transparency and tensile strength (Saito et al., (2003)). However, the regeneration mechanism differs to that of cellulose particles and therefore varying the coagulation conditions will have a different effect on the gel properties. For example, cellulose gels and CNPs regenerated using the same four anti-solvents displayed the opposite trend in crystallinity. As described above (Fan et al., (2018)), the crystallinity of the CNPs decreases as the polarity of the anti-solvent decreases, however crystallinity decreased in the following order for cellulose gels: *n*-propanol > ethanol > methanol > water (Fan et al., (2017)). Such a different result is believed to be governed by the diffusion coefficient (D) of the various anti-solvents molecules. Regeneration in water without stirring results in the water molecules, that have the highest D ($27.39 \pm 1.68 \times 10^{-6}$ cm^2 s^{-1}), precipitating the cellulose at a much faster rate than *n*-propanol ($D = 2.03 \pm 0.47 \times 10^{-6}$ cm^2 s^{-1}), which therefore “fixes” the cellulose chains before they can realign to form crystalline structures. On the other hand, regeneration with high enough stirring generates cellulose particles in which the anti-solvent H-bonding properties dictate the crystallinity of the regenerated cellulose. Thus two competitive mechanisms occurring during regeneration can take place (Fan et al., (2018)). It is also important to mention that cellulose gels will only

form when the concentration of dissolved cellulose is sufficiently high, in order for the reprecipitating material to be able to form a network structure.

In general, cellulose gels fabricated via the dissolution-regeneration route are aqueous-based, made up of cellulose networks trapping large amounts of water in the pores and are therefore usually termed cellulose hydrogels. The coagulation step usually involves water as the anti-solvent or some other water-compatible polar solvent such as an alcohol, the latter of which is generally sequentially exchanged for water in the final gel washing step, in order to ensure complete removal of the original cellulose solvent (Östlund et al., (2013)). The type of anti-solvent and/or anti-solvent sequence affects both the gel porosity and crystallinity (Östlund et al., (2013)). Cellulose concentration and the cellulose DP also have an effect on the strength of the coagulated hydrogel (de Oliveira and Glasser, (1996)), whilst the amount of anti-solvent used in the coagulation bath can be varied to alter the hydrogel properties (Östlund et al., (2009)). A summary of cellulose hydrogels and their formation from a wide variety of solvents can be found in several reviews (Sannino et al., (2009); Chang and Zhang, (2011); Kabir et al., (2018); Fu et al., (2019)).

In order for CMGs to be produced via a top-down approach, the cellulose gel must be brittle enough to be broken down into small particle sizes, however the cellulose concentration must be sufficiently high to form a gel during regeneration. Therefore, controlling the gel cross-link density is important, whilst the coagulation medium and conditions can also be altered in order to produce a gel most suitable for breaking down to a CMG-dispersion. It is important to understand the form of the cellulose in its dissolved state in order to manipulate the properties of the cellulose gel in its precipitated state.

2.4 Microgels as stabilisers for emulsions

2.4.1 Emulsion systems

Conventionally, low molecular weight surfactants (LMWS) and high molecular weight surfactants (HMWS), such as proteins, have been used as stabilisers of emulsions. The stabiliser lowers the interfacial tension and provides a steric and also electrostatic (if the stabiliser is charged) colloidal stability to the system, preventing coalescence and thereby separation of the two liquids (Costa, Medronho, et al., (2019)). LMWS generally consist of a hydrophilic “head” and a hydrophobic “tail,” classified by their hydrophilic-lipophilic balance, or HLB value, which indicates the type of emulsion that the stabiliser will preferentially form (O/W or W/O, for high and low values, respectively) (Bastida-Rodríguez, (2013)). Proteins, as biopolymeric HMWS possessing

much more complex structures, cannot be classified in this way, but can provide excellent stabilisation of O/W emulsions. Over the last 20 years, the use of solid particles, or “Pickering” particles as emulsion stabilisers has received great interest. Pickering stabilisation has been studied for at least 100 years and occurs naturally in many types of emulsion. More recently, however, particle stabilisation has received much renewed interest (Hunter et al., (2008); Rousseau, (2013); Murray, (2019b)).

Even more recently, microgels have emerged as a separate class of stabiliser, as an alternative to LMWS, HMWS or solid particles. Microgels can help form highly stable emulsions due to the formation of thick, long-lasting viscoelastic layers at the interface (Schmitt and Ravaine, (2013); Dickinson, (2015)). In comparison to LMWS, HMWS and particles, microgel interfacial behaviour is somewhat more complicated to predict, since the stabiliser combines the properties of both a polymer and particle (Dickinson, (2015)). Microgels can undergo structural rearrangement at the interface but are also considered to be irreversibly adsorbed, due to the high binding energy per particle. Characterised as “soft” colloidal particles, microgels can deform when adsorbed to an interface, changing their size and shape depending on their surrounding environment. Microgel emulsion systems are sometimes referred to as “Mickering emulsions,” reflecting their similarities and differences to Pickering emulsions (Gong et al., (2014)).

2.4.2 Size, morphology and packing of microgels interfaces

Most microgels display interesting interfacial properties, regardless of whether they are amphiphilic in nature (Plamper and Richtering, (2017)). Emulsifying activity can be imparted via weakly surface-active polymers through microgel formation and/or “trapping” of certain structures through gelation. For example, in proteins a trapped, unfolded state may result in increased exposure of hydrophobic/hydrophilic groups and a higher surface activity (Ishii et al., (2018); Murray, (2019a); Zembyla et al., (2020)). Microgels change morphology upon adsorption from bulk solution to an interface (Geisel et al., (2015)) and can stretch out in order to reduce the interfacial energy. FreSCa cryo-SEM images revealed that PNIPAM-based microgels flatten and almost double in size when adsorbed at the interface, compared to in bulk water (Geisel et al., (2012)). Furthermore, in the absence of strong interfacial effects, microgels may adopt asymmetric shapes due to the difference in microgel-solubility in the two liquid phases, swelling and collapsing for respective high and low affinities (Rey et al., (2020)). This is sometimes referred to as a

“double-lens” configuration, due to the different curvatures in water and oil (Figure 2.5a) (Tay and Bresme, (2006); Geisel et al., (2012)).

Microgel properties such as size and cross-link density influence how they behave at an interface. For example, it was shown that small microgels may pack tightly and uniformly in a homogenous manner, whilst larger microgels may pack more sparsely giving a combination of dense cores and thin shells at the interface. Heterogeneous surface-packing can lead to a more rigid oil-water interface in emulsions, encouraging bridging flocculation (Figure 2.5b) (Schmitt and Ravaine, (2013); Destribats, Eyharts, et al., (2014)). Cross-link density affects the swelling capacity and deformability of a microgel, or in other words how “soft” it is (Rey et al., (2020)). In general, microgels in a bulk suspension can be described by a “core-shell” model with a dense cross-linked interior and a soft exterior of dangling chains, and therefore do not have a uniform cross-link density throughout their microstructures. For core-shell microgels, a “fried-egg” morphology has been observed at the interface (Pinaud et al., (2014)) describing the highly deformed corona (outer region) which flattens and spreads over the interface and the less deformable core (inner region), which is comparatively rigid (Rey et al., (2020)).

The equilibrium size and shape that microgels adopt at an oil-water interface is consequently related to the balance of solvation between the two liquid phases, microgel interfacial activity and microgel elasticity (Geisel et al., (2012)). The ratio between the radius (R) and the elastocapillary length (L) of the microgel particles can be a useful prediction for the degree of deformation that will occur at an interface, where the lower the value of R/L, the greater the extent of deformation. In other words, for small microgels (low R) with less cross-links, deformability is high and particles may even be considered as a liquid at the interface whilst when R is large relative to L, the particles can be considered as effectively rigid and may adopt more spherical shapes, similar to microgels in bulk solutions (Rey et al., (2020)). It is also important to note that other factors such as pH and temperature may affect the form that microgels adopt at an interface, depending on the nature of the polymer (Destribats, Rouvet, et al., (2014)).

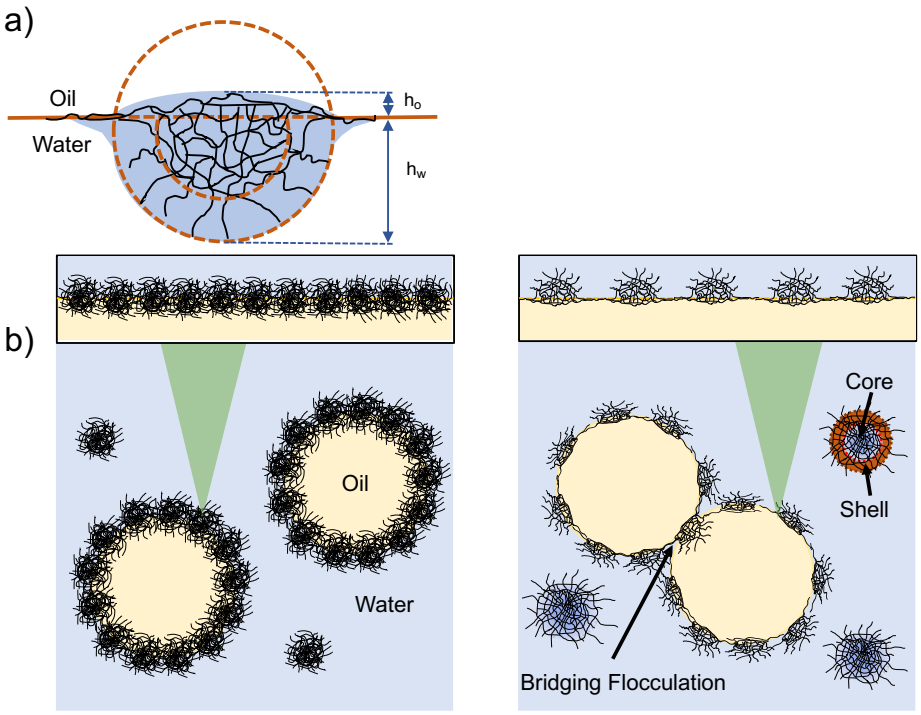

Figure 2.5. a) Illustration of a microgel particle at an oil-water interface, showing different curvatures and degrees of swelling in each liquid phase (so-called "double lens" configuration). h_o and h_w give the height protrusions in oil and water, respectively; b) microgel-stabilised oil droplets in water with 'stiff' microgels giving a homogenous protecting layer (left) and core-shell microgels giving a heterogeneous protecting layer and exhibiting bridging flocculation (right).

2.4.3 Stability of microgel-stabilized emulsions

The ability of microgels to spread, interpenetrate and/or cross-link at the interface, plus their relatively large thickness at the interface, leads to the formation of very stable emulsions. The polymers within the gel network have been shown to stretch and rearrange over time, increasing the area of the interface that the microgel covers, reducing the interfacial tension (energy) (Geisel et al., (2014)). S. Chattopadhyay *et al.* showed that physically-crossed nanogels could even form ultrathin films when adsorbed at solid interfaces, due to "unfolding" which may be a result of stresses induced on adsorption (Chattopadhyay et al., (2016)). Furthermore, highly deformable microgels may spontaneously absorb and simultaneously compress at the interface if an excess of microgel is present in the continuous phase, increasing the surface coverage over time (Pinaud et al., (2014)). Full coverage of the interface, however, is not always necessary, as seen for Pickering emulsions: if a rigid network is formed at the interface, a sufficiently high steric barrier will prevent droplet coalescence for long time periods (Destribats, Rouvet, et al., (2014)).

2.4.4 Aqueous versus non-aqueous microgels

Most of the literature on microgel particles as emulsion stabilisers focusses on aqueous microgels, which are largely composed of water (Murray, (2019a)) and therefore have a higher affinity for the more hydrophilic phase at an oil-water interface. Aqueous microgels tend to swell in the water phase and partially collapse in the oil phase, yielding a contact angle which favours O/W emulsion-type stabilization (Geisel et al., (2012); Rey et al., (2020)). Some microgels have been shown to stabilise W/O emulsions where the oil is more polar, for example 1-undecanol (Tsuji and Kawaguchi, (2008)) and fatty alcohols (Destribats et al., (2011)), whilst hydrophobic particles have been incorporated into microgels in order to increase their affinity for the hydrophobic phase (Watanabe et al., (2019)). Non-aqueous microgels which swell in organic solvents have also been fabricated, either by freeze-drying, rotary evaporation or washing at the end of microgel synthesis followed by transfer into organic solvents, or by directly carrying out the polymerisation in a non-aqueous solvent (Bonham et al., (2014)).

2.4.5 Controlling emulsion type

Predicting the type of emulsion that will form with a particular microgel stabiliser is more complicated compared to surfactant and solid particle systems. Microgels can be described as having an adjustable surface activity and as a result cannot be defined by a distinct contact angle (Murray, (2019a)). In cases where severe deformation occurs at an interface, there is discussion of two effective contact angles developing: one in the water phase and one in the oil phase (Geisel et al., (2012)). However, there is no sharp boundary between the solvent trapped in the microgel network and the surrounding solvent, since exchange between the two environments alters the microgel size and shape (Plamper and Richtering, (2017)). The size, shape, deformability and therefore the behaviour of microgels at an interface must be controlled at the earlier stages of synthesis. Hydrophobic nanoparticles have been incorporated into synthetic microgels in order to control the emulsion type: W/O for high amounts, O/W for low amounts (Watanabe et al., (2019)).

It has been reported, however, that the water/oil ratio, microgel concentration and applied shear rate can all have an effect on the emulsion type and stability for PNIPAM-*co*-methacrylic acid (MAA) microgel stabilisers. Lower shear rates favoured the formation of O/W emulsions, since a higher amount of energy is required to split water into droplets and form W/O emulsions. Higher microgel concentrations also increased the viscosity and prevented dispersion of the water phase, however W/O emulsions were formed if sufficiently high

energy emulsification was employed in order to overcome viscosity effects, by generating a strong shear flow (Brugger et al., (2008)). Both W/O and O/W emulsions could be formed using poly-(4-vinylpyridine)-silica nanocomposite microgels, with the polarity of the oil phase and the particle purity determining the emulsions type (Fujii et al., (2006)).

In summary, further work is required to fully understand the interfacial properties and behaviour of microgels, however promising studies suggest that they may be suitable for both W/O and O/W emulsification and therefore possess a tuneable surface-activity (Brugger et al., (2008)). It has been shown that the same microgel particles can act as stabilisers for both W/O and O/W systems, for which the emulsion type is controlled through water-oil ratio, emulsification conditions and microgel concentration (Fujii et al., (2006); Brugger et al., (2008)). The ability to control the stability and type of emulsion formed is important in many processes such as oil extraction and recovery, heterogeneous and multiphase catalysis (Wang and Wang, (2016)), food processing and drug delivery (Xie et al., (2012); Xie et al., (2020)), and therefore using a single, “multi-purpose” stabiliser to fabricate emulsions with switchable behaviour could be hugely advantageous in many fields.

2.5 Regenerated cellulose as an emulsion stabiliser

Cellulose is being increasingly considered for its amphiphilic properties and potential oil-water surface activity (Lindman et al., (2010)), with structural studies revealing that cellulose possesses hydrophobic character due to the presence of C-H groups in axial positions, whilst the glucose ring with O-H groups positioned in the equatorial plane are clearly hydrophilic (Figure 2.6a and b, respectively) (Kalashnikova et al., (2012); Rein et al., (2012)). However, these surfaces are often hidden in native cellulose due to its highly repeating polymer conformation, which allows close packing of individual chains and the development of many inter- and intra-molecular hydrogen bonds (H-bonds), as well as hydrophobic and Van der Waals interactions (Wang et al., (2016)). As a result, cellulose clumps and sediments in both water and oil, as well as in many other common solvents, making it unsuitable as a stabiliser. In order to expose the amphiphilic character of cellulose and harness its surface activity, hydrogen bonds and hydrophobic interactions must be prevented from re-forming during reprecipitation. This may be achieved by changing the morphology and characteristics of cellulose particles through regeneration or more specifically, by forming a cellulose gel. Both cellulose particle-stabilisers and CMG-stabilisers are reviewed in the following section.

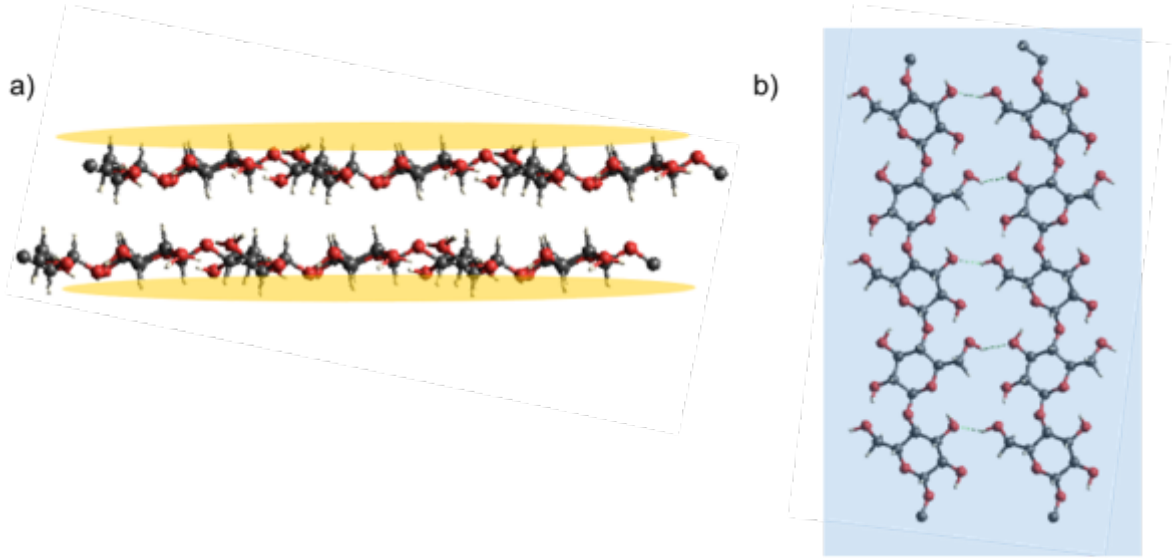

Figure 2.6. Crystal structures of Cellulose II showing a) the "hydrophobic plane," made up of the axial C-H bonds; b) the hydrophilic surface, made up of equatorial hydroxyl groups. Oxygen, carbon and hydrogen atoms shown in red, grey and white, respectively.

2.5.1 Cellulose particles in emulsion stabilisation

Cellulose particles obtained from dissolution-regeneration methods can have both crystalline and amorphous character, depending on the source and coagulation conditions, and both types have been used to stabilise emulsions (Costa, Medronho, et al., (2019)). Jia *et al.* reported that highly amorphous cellulose particles (with up to 87% recovery of the original cellulose biomass) were obtained when coagulated from a phosphoric acid solution coagulated in water followed by centrifugation (Jia et al., (2013)). The regenerated amorphous cellulose displayed much better O/W emulsion stabilising capacity compared to the original MCC, via a combination of Pickering and network stabilization (Jia et al., (2015)). Interestingly, the cellulose suspensions in water were stable over a range of pH values, suggesting that the stability of amorphous cellulose in aqueous media is not due to electrostatic stabilisation. Similarly, it was shown that *in-situ* regeneration of cellulose from a phosphoric acid solution with dispersed oil droplets led to the formation of highly stable O/W emulsions, whilst non-regenerated cellulose still in its dissolved state was less effective (Costa, Mira, et al., (2019)).

CNCs have also been extensively employed as Pickering stabilisers for O/W emulsions (Kalashnikova et al., (2011); Kalashnikova et al., (2012); X. Li et al., (2018); Mackie et al., (2019); Bertsch et al., (2019)). Charged groups are formed on cellulose chains when it is hydrolysed using sulfuric or phosphoric acid, giving the resultant CNCs high colloidal stability (Cherhal et al., (2016)).

It was shown that sulfated (charged) CNCs assembled in a monolayer at the oil-water interface, whilst de-sulfated (neutral) CNCs formed a thicker, but more porous layer due to the deposition of aggregates on the surface (Cherhal et al., (2016)). MCC particles have also been successfully employed as O/W stabilisers and are reported to form thick layers around oil droplets (Oza and Frank, (1986); Oza and Frank, (1989)). Increasing the concentration of stabiliser leads to the formation of MCC particle networks in the aqueous phase, which increases the viscosity and "traps" the dispersed phase, enhancing stability (Kargar et al., (2012)).

Cellulose particles are better wetted by water than by oil and therefore have been less investigated as W/O emulsion stabilisers (Rein et al., (2012)). This may be due to the fact that the hydrophobic surfaces of cellulose are the first to interact during coagulation: it has been shown that the glucopyranoside rings stack firstly through hydrophobic interactions and that this initial interaction has a large influence on the final structure of the regenerated material (Miyamoto et al., (2009); El Seoud et al., (2019)). In these cases, both the solvent and the coagulant were aqueous and therefore it is unfavourable for the hydrophobic glucopyranoside ring planes to be exposed to the polar media (Isobe et al., (2012)). Preventing the reformation of hydrophobic interactions during coagulation and favouring the exposure of the hydrophobic (200) edge (Cellulose Iβ) (French, (2014)) may be possible using a less-polar coagulant or through cellulose gelation, in order to make the coagulated cellulose more suitable as a W/O stabiliser. Added surfactants and other amphiphilic molecules have also been found to reduce the reformation of hydrophobic interactions during aggregation (Medronho et al., (2015)).

2.5.2 Cellulose microgels in emulsion stabilisation

As previously mentioned, (section Cellulose Gels), generally highly polar anti-solvents are employed in cellulose gelation from a solution, generating a cellulose hydrogel. Therefore, the obtained CMGs are typically hydrophilic and swollen in water. If the microgel is at all surface active, this will therefore favour its stabilisation of O/W emulsions. Cellulose hydrogels coagulated from aqueous-NaOH solutions displayed good O/W emulsifying ability when broken down, with the amount of oil effecting the size of emulsion droplets as well as aggregated-droplet size (Alfassi et al., (2019)). A cellulose hydrogel formed via coagulation from EmimAc was also used to form O/W emulsions, which displayed excellent stability with no flocculation or coalescence occurring within a year (Rein et al., (2012)). The cellulose is described to be acting as a coating or "encapsulating cellulose shell," as opposed to a CMG

Mickering-type stabiliser. Cellulose/IL solutions were shown to form stable O/W emulsions stabilised by CMGs, however the IL was included within the emulsion to allow stabilization with a higher concentration of cellulose. Removal of the IL led to much larger size distributions for microgel aqueous dispersions at lower cellulose concentrations (Napso et al., (2016)).

W/O emulsions have apparently been stabilised by amorphous cellulose gels regenerated via two different approaches: i) by formation of a cellulose hydrogel on addition of water to a cellulose/IL solution; ii) by addition of oil and water directly into the cellulose/IL solution followed by dialysis, to completely remove the IL (Rein et al., (2012)). Using the second approach, it was reasoned that regeneration of cellulose in the presence of a water-oil interface would affect the conformation of the polymer molecules and therefore the way in which they would reassemble. Whist the influence of a water-oil interface during cellulose regeneration has been investigated for O/W emulsions (Costa, Mira, et al., (2019)), it appears this aspect has yet to be addressed for W/O emulsions. Rein *et al.* also suggested that any W/O emulsions formed were much less stable than the equivalent O/W emulsions (Rein et al., (2012)), so that much further work remains to optimise the conditions for W/O emulsion stabilisation. However, recent success in fabricating “hydrophobic” cellulose has been reported including CMG-emulsifiers for oil-based systems (Lefroy, Murray, Ries, et al., (2021)) as well as an interesting method for cellulose oleogelation, in which aqueous cellulose fibre dispersions were initially formed through shear-activation and then shear-mixed with either palm or olive oil (Phoon and Henry, (2020)). The resulting “jammed” W/O emulsion was then freeze-dried to form an oleogel, which contained a close-packed oil/cellulose continuous phase. This study provides a helpful reminder of the amphiphilic properties that cellulose chains possess and the potential for the hydrophobic surface to be exfoliated (Table 2.2).

Table 2.2. Summary of reports on cellulose materials used to stabilise emulsions, with type of cellulose, average droplet size and stabilities compared (CNC = cellulose nanocrystal; CNF = cellulose nanofibril; MFC = microfibrillated cellulose).

Emulsion Type	Description of emulsifier	Droplet Size/μm	Stability	Reference
O/W	CNCs	Ca. 4[a]	Several months	(Kalashnikova et al., (2011))
O/W	CNCs	Ca. 4[a]	Not reported	(Cherhal et al., (2016))
O/W	CNCs	0.5-2	15 days	(Esparza et al., (2020))
O/W	CNCs/CNFs	ca. 2.2[a]	7 months	(Bai et al., (2018))
O/W	Nanocellulose Particles	5-25	At least 3 months	(Ni et al., (2020))
O/W	Nanocellulose Particles	ca. 1-10	At least 24h	(Buffiere et al., (2017))
O/W	Cellulose Nanofibers	10[b]	At least 2 days	(Li et al., (2020))
O/W	MFC	1-11[a]	80 days	(Winuprasith and Suphantharika, (2015))
O/W	Cellulose Particles (amorphous)	20-40[a]	Up to 3 months	(Jia et al., (2015))
O/W	Cellulose "film"	2.6-4.9[c]	Over 1 year	(Costa, Mira, et al., (2019))
O/W	Regenerated Cellulose Particles	10-30[d]	At least 24h	(Z. Li et al., (2018))

O/W	Milled Cellulose Particles	40-60	At least 1 month	(Lu et al., (2018))
O/W	Cellulose Hydrogel Dispersion	0.400-4[e]	Not reported	(Alfassi et al., (2019))
O/W	Cellulose Hydrogel Dispersion	0.2-20	Up to 1 year	(Rein et al., (2012))
O/W	Cellulose Hydrogel Dispersion	ca. 20	More than 3 months	(Napso et al., (2016))
O/W	Cellulose Gel Dispersion	5-30	More than 60 days	(Zhu et al., (2017))
O/W	Cellulose Gel	0.4-3	Up to several months	(Napso et al., (2018))
W/O	Cellulose Hydrogel Dispersion	Not reported	Several months	(Rein et al., (2012))

[a]d(*3,2*)

[b]d(*4,3*)

[c]d(*0.5*)

[d]d(*50*)

[e]average

2.6 Final remarks

The emergence of microgel particles as colloidal stabilisers has led to exciting possibilities in the areas of food, cosmetics, pharmaceuticals and more. Different preparation methods, conditions and polymers have been used to produce microgels with a range of interesting properties, including so-called “intelligent” microgels, which respond to a stimulus and display switchable behaviour. However, most of the literature to date concerns synthetic polymer microgels with covalent cross-links, whilst microgels based on natural materials, such as biopolymers, with physical cross-links are still rather novel. Furthermore, there remains much to be understood in terms of the interfacial behaviour of microgels, including their morphology, DOS and structural changes over time at an interface.

Microgelation of cellulose has more recently been investigated as a method of harnessing its amphiphilicity and improving its dispersibility in water and oil, therefore making it a suitable emulsion stabiliser. CMGs are obtained via a top-down approach, through breaking down cellulose-based gels obtained via a dissolution-regeneration method. Most efforts thus far have concentrated on the ability of CMGs to stabilise O/W emulsions, with little focus on the fabrication of non-aqueous CMGs for W/O emulsions. However, we highlight the versatility of the dissolution-reprecipitation approach and the potential for tuning the CMG properties through this regeneration method. We conclude by emphasising the fact that simple, “green” methods can be employed to fabricate CMGs and this opens up new possibilities for the functionalisation of cellulose.

2.7 References

Abbott, A.P., Bell, T.J., Handa, S. and Stoddart, B. (2006). Cationic functionalisation of cellulose using a choline based ionic liquid analogue. *Green Chemistry*. *8*(9), 784–786.

Abbott, A.P., Capper, G., Davies, D.L., Munro, H.L., Rasheed, R.K. and Tambyrajah, V. (2001). Preparation of novel, moisture-stable, lewis-acidic ionic liquids containing quaternary ammonium salts with functional side chains. *Chemical Communications*. 2010–2011.

Abd El-Rehim, H.A. (2005). Swelling of radiation crosslinked acrylamide-based microgels and their potential applications. *Radiation Physics and Chemistry*. *74*(2), 111–117.

Agrawal, G. and Agrawal, R. (2018). Functional Microgels: Recent Advances in Their Biomedical Applications. *Small*. *14*(39), 1–18.

Alfassi, G., Rein, D.M. and Cohen, Y. (2019). Cellulose emulsions and their hydrolysis. *Journal of Chemical Technology and Biotechnology*. *94*(1), 178–184.

Amici, E., Tetradis-Meris, G., de Torres, C.P. and Jousse, F. (2008). Alginate gelation in microfluidic channels. *Food Hydrocolloids*. *22*(1), 97–104.

Azarikia, F., Wu, B. cheng, Abbasi, S. and McClements, D.J. (2015). Stabilization of biopolymer microgels formed by electrostatic complexation: Influence of enzyme (laccase) cross-linking on pH, thermal, and mechanical stability. *Food Research International*. *78*, 18–26.

Bai, L., Huan, S., Xiang, W. and Rojas, O.J. (2018). Pickering emulsions by combining cellulose nanofibrils and nanocrystals: Phase behavior and depletion stabilization. *Green Chemistry*. *20*(7), 1571–1582.

Baker, W.O. (1949). Microgel, A New Macromolecule. *Industrial & Engineering Chemistry*. *41*(3), 511–520.

Ballauff, M. and Lu, Y. (2007). 'Smart' nanoparticles: Preparation, characterization and applications. *Polymer*. *48*(7), 1815–1823.

Bao, W., Wang, Z. and Li, Y. (2003). Synthesis of chiral ionic liquids from natural amino acids. *Journal of Organic Chemistry*. *68*(2), 591–593.

Bastida-Rodríguez, J. (2013). The Food Additive Polyglycerol Polyricinoleate (E-476): Structure, Applications, and Production Methods. *ISRN Chemical Engineering*. *2013*, 1–21.

Battista, O.A. and Smith, P.A. (1962). MICROCRYSTALLINE CELLULOSE. *Industrial and Engineering Chemistry*. *54*(9), 20–29.

Bertsch, P., Arcari, M., Geue, T., Mezzenga, R., Nyström, G. and Fischer, P. (2019). Designing Cellulose Nanofibrils for Stabilization of Fluid Interfaces. *Biomacromolecules*. *20*(12), 4574–4580.

Bisht, M. and Venkatesu, P. (2017). Influence of cholinium-based ionic liquids on the structural stability and activity of α-chymotrypsin. *New Journal of Chemistry*. *41*(22), 13902–13911.

Bonham, J.A., Faers, M.A. and Van Duijneveldt, J.S. (2014). Non-aqueous microgel particles: Synthesis, properties and applications. *Soft Matter*. *10*(47), 9384–9398.

Boularas, M., Radji, S., Gombart, E., Tranchant, J.F., Alard, V. and Billon, L. (2018). Functional film by trigger-free self-assembly of adhesive soft microgels at skin temperature. *Materials and Design*. *147*, 19–27.

Brinchi, L., Cotana, F., Fortunati, E. and Kenny, J.M. (2013). Production of nanocrystalline cellulose from lignocellulosic biomass: Technology and applications. *Carbohydrate Polymers*. *94*(1), 154–169.

Brugger, B., Rosen, B.A. and Richtering, W. (2008). Microgels as stimuli-responsive stabilizers for emulsions. *Langmuir*. *24*(21), 12202–12208.

Buffiere, J., Balogh-Michels, Z., Borrega, M., Geiger, T., Zimmermann, T. and Sixta, H. (2017). The chemical-free production of nanocelluloses from microcrystalline cellulose and their use as Pickering emulsion stabilizer. *Carbohydrate Polymers*. *178*, 48–56.

Burey, P., Bhandari, B.R., Howes, T. and Gidley, M.J. (2008). Hydrocolloid gel particles: Formation, characterization, and application. *Critical*

Reviews in Food Science and Nutrition. *48*(5), 361–377.

Butun, S., Ince, F.G., Erdugan, H. and Sahiner, N. (2011). One-step fabrication of biocompatible carboxymethyl cellulose polymeric particles for drug delivery systems. *Carbohydrate Polymers*. *86*(2), 636–643.

Cai, J. and Zhang, L. (2005). Rapid dissolution of cellulose in LiOH/urea and NaOH/urea aqueous solutions. *Macromolecular Bioscience*. *5*(6), 539–548.

Chang, C. and Zhang, L. (2011). Cellulose-based hydrogels: Present status and application prospects. *Carbohydrate Polymers*. *84*(1), 40–53.

Chattopadhyay, S., Heine, E., Mourran, A., Richtering, W., Keul, H. and Möller, M. (2016). Waterborne physically crosslinked antimicrobial nanogels. *Polymer Chemistry*. *7*(2), 364–369.

Chen, Y.L., Zhang, X., You, T.T. and Xu, F. (2019). Deep eutectic solvents (DESs) for cellulose dissolution: a mini-review. *Cellulose*. *26*(1), 205–213.

Chen, Z., Liu, S., Li, Z., Zhang, Q. and Deng, Y. (2011). Dialkoxy functionalized quaternary ammonium ionic liquids as potential electrolytes and cellulose solvents. *New Journal of Chemistry*. *35*(8), 1596–1606.

Cherhal, F., Cousin, F. and Capron, I. (2016). Structural Description of the Interface of Pickering Emulsions Stabilized by Cellulose Nanocrystals. *Biomacromolecules*. *17*(2), 496–502.

Clough, M.T., Geyer, K., Hunt, P.A., Son, S., Vagt, U. and Welton, T. (2015). Ionic liquids: Not always innocent solvents for cellulose. *Green Chemistry*. *17*(1), 231–243.

Costa, C., Medronho, B., Filipe, A., Mira, I., Lindman, B., Edlund, H. and Norgren, M. (2019). Emulsion formation and stabilization by biomolecules: The leading role of cellulose. *Polymers*. *11*(10), 1–18.

Costa, C., Mira, I., Benjamins, J.W., Lindman, B., Edlund, H. and Norgren, M. (2019). Interfacial activity and emulsion stabilization of dissolved cellulose. *Journal of Molecular Liquids*. *292*, 111325.

Cross, C.F., Bevan, E.T. and Beadle, C. (1893). Thiokohlensäureester der Cellulose. *Journal of Chemical Information and Modeling*. *26*(1), 1090–1097.

Demitri, C., Del Sole, R., Scalera, F., Sannino, A., Vasapollo, G., Maffezzoli, A., Ambrosio, L. and Nicolais, L. (2008). Novel Superabsorbent Cellulose-Based Hydrogels Crosslinked with Citric Acid. *Journal of Applied Polymer Science*. *110*, 2453–2460.

Dendukuri, D. and Doyle, P.S. (2009). The synthesis and assembly of polymeric microparticles using microfluidics. *Advanced Materials*. *21*(41), 4071–4086.

Depoorter, J., Mourlevat, A., Sudre, G., Morfin, I., Prasad, K., Serghei, A., Bernard, J., Fleury, E. and Charlot, A. (2019). Fully Biosourced Materials from Combination of Choline Chloride-Based Deep Eutectic Solvents and Guar Gum. *ACS Sustainable Chemistry and Engineering*.

7(19), 16747–16756.

Destribats, M., Eyharts, M., Lapeyre, V., Sellier, E., Varga, I., Ravaine, V. and Schmitt, V. (2014). Impact of pNIPAM microgel size on its ability to stabilize pickering emulsions. *Langmuir*. *30*(7), 1768–1777.

Destribats, M., Lapeyre, V., Sellier, E., Leal-Calderon, F., Schmitt, V. and Ravaine, V. (2011). Water-in-oil emulsions stabilized by water-dispersible poly(N- isopropylacrylamide) microgels: Understanding anti-Finkle behavior. *Langmuir*. *27*(23), 14096–14107.

Destribats, M., Rouvet, M., Gehin-Delval, C., Schmitt, C. and Binks, B.P. (2014). Emulsions stabilised by whey protein microgel particles: Towards food-grade Pickering emulsions. *Soft Matter*. *10*(36), 6941–6954.

Dickinson, E. (2015). Microgels - An alternative colloidal ingredient for stabilization of food emulsions. *Trends in Food Science and Technology*. *43*(2), 178–188.

Dowding, P.J., Vincent, B. and Williams, E. (2000). Preparation and swelling properties of poly(NIPAM) 'minigel' particles prepared by inverse suspension polymerization. *Journal of Colloid and Interface Science*. *221*(2), 268–272.

Esparza, Y., Ngo, T.D. and Boluk, Y. (2020). Preparation of powdered oil particles by spray drying of cellulose nanocrystals stabilized Pickering hempseed oil emulsions. *Colloids and Surfaces A: Physicochemical and Engineering Aspects*. *598*, 124823.

Fan, Z., Chen, J., Guo, W., Ma, F., Sun, S. and Zhou, Q. (2018). Anti-solvents tuning cellulose nanoparticles through two competitive regeneration routes. *Cellulose*. *25*(8), 4513–4523.

Fan, Z., Chen, J., Guo, W., Ma, F., Sun, S. and Zhou, Q. (2017). Crystallinity of regenerated cellulose from [Bmim]Cl dependent on the hydrogen bond acidity/basicity of anti-solvents. *RSC Advances*. *7*(65), 41004–41010.

Feng, X., Pelton, R., Leduc, M. and Champ, S. (2007). Colloidal complexes from poly(vinyl amine) and carboxymethyl cellulose mixtures. *Langmuir*. *23*(6), 2970–2976.

Fraeye, I., Colle, I., Vandevenne, E., Duvetter, T., Van Buggenhout, S., Moldenaers, P., Van Loey, A. and Hendrickx, M. (2010). Influence of pectin structure on texture of pectin-calcium gels. *Innovative Food Science and Emerging Technologies*. *11*(2), 401–409.

Fraeye, I., Doungla, E., Duvetter, T., Moldenaers, P., Van Loey, A. and Hendrickx, M. (2009). Influence of intrinsic and extrinsic factors on rheology of pectin-calcium gels. *Food Hydrocolloids*. *23*, 2069–2077.

French, A.D. (2014). Idealized powder diffraction patterns for cellulose polymorphs. *Cellulose*. *21*(2), 885–896.

Fryczkowska, B., Kowalska, M., Binias, D., Slusarczyk, C., Janicki, J., Sarna, E. and Wyszomirski, M. (2018). Properties and Structure of Cellulosic Membranes Obtained from Solutions in Ionic Liquids

Coagulated in Primary Alcohols. *Autex Research Journal*. *18*(3), 232–242.

Fu, L.H., Qi, C., Ma, M.G. and Wan, P. (2019). Multifunctional cellulose-based hydrogels for biomedical applications. *Journal of Materials Chemistry B*. *7*(10), 1541–1562.

Fujii, S., Armes, S.P., Binks, B.P. and Murakami, R. (2006). Stimulus-responsive particulate emulsifiers based on lightly cross-linked poly(4-vinylpyridine) - Silica nanocomposite microgels. *Langmuir*. *22*(16), 6818–6825.

Gagnaire, D., Mancier, D. and Vincendon, M. (1980). Cellulose organic solutions: A nuclear magnetic resonance investigation. *Journal of Polymer Science: Polymer Chemistry Edition*. *18*(1), 13–25.

Gavrilov, A.A., Rudyak, V.Y. and Chertovich, A. V. (2020). Computer simulation of the core-shell microgels synthesis via precipitation polymerization. *Journal of Colloid and Interface Science*. *574*, 393–398.

Geisel, K., Henzler, K., Guttmann, P. and Richtering, W. (2015). New insight into microgel-stabilized emulsions using transmission X-ray microscopy: Nonuniform deformation and arrangement of microgels at liquid interfaces. *Langmuir*. *31*(1), 83–89.

Geisel, K., Isa, L. and Richtering, W. (2012). Unraveling the 3D localization and deformation of responsive microgels at oil/water interfaces: A step forward in understanding soft emulsion stabilizers. *Langmuir*. *28*(45), 15770–15776.

Geisel, K., Richtering, W. and Isa, L. (2014). Highly ordered 2D microgel arrays: Compression versus self-assembly. *Soft Matter*. *10*(40), 7968–7976.

Gericke, M., Fardim, P. and Heinze, T. (2012). Ionic liquids - Promising but challenging solvents for homogeneous derivatization of cellulose. *Molecules*. *17*(6), 7458–7502.

Gokmen, M.T. and Du Prez, F.E. (2012). Porous polymer particles - A comprehensive guide to synthesis, characterization, functionalization and applications. *Progress in Polymer Science*. *37*, 365–405.

Gong, X., Hua, L., Wei, J. and Ngai, T. (2014). Tuning the particle-surface interactions in aqueous solutions by soft microgel particles. *Langmuir*. *30*(44), 13182–13190.

Graenacher, C. (1934). Cellulose Solution. US 1943176A.

Grinberg, V.Y., Burova, T. V., Grinberg, N. V., Buyanovskaya, A.G., Khokhlov, A.R., Kozhunova, E.Y., Vyshivannaya, O. V. and Nasimova, I.R. (2020). Functionalized thermoresponsive microgels based on N-isopropylacrylamide: Energetics and mechanism of phase transitions. *European Polymer Journal*. *133*, 109722.

Habibi, Y., Lucia, L.A. and Rojas, O.J. (2010). Cellulose nanocrystals: Chemistry, self-assembly, and applications. *Chemical Reviews*. *110*(6), 3479–3500.

Haider, I., Siddiq, M., Shah, S.M. and Ur Rehman, S. (2014). Synthesis and

characterization of multi-responsive poly (NIPAm-co-AAc) microgels. *IOP Conference Series: Materials Science and Engineering*. *60*(1), 012046.

Halder, P., Kundu, S., Patel, S., Setiawan, A., Atkin, R., Parthasarthy, R., Paz-Ferreiro, J., Surapaneni, A. and Shah, K. (2019). Progress on the pre-treatment of lignocellulosic biomass employing ionic liquids. *Renewable and Sustainable Energy Reviews*. *105*, 268–292.

Handy, S.T., Okello, M. and Dickenson, G. (2003). Solvents from biorenewable sources: Ionic liquids based on fructose. *Organic Letters*. *5*(14), 2513–2515.

Hedlund, A., Köhnke, T., Hagman, J., Olsson, U. and Theliander, H. (2019). Microstructures of cellulose coagulated in water and alcohols from 1-ethyl-3-methylimidazolium acetate: contrasting coagulation mechanisms. *Cellulose*. *26*(3), 1545–1563.

Hossain, M.M., Rawal, A. and Aldous, L. (2019). Aprotic vs Protic Ionic Liquids for Lignocellulosic Biomass Pretreatment: Anion Effects, Enzymatic Hydrolysis, Solid-State NMR, Distillation, and Recycle. *ACS Sustainable Chemistry & Engineering*. *7*, 11928–11936.

Huddleston, J.G., Visser, A.E., Reichert, W.M., Willauer, H.D., Broker, G.A. and Rogers, R.D. (2001). Characterization and comparison of hydrophilic and hydrophobic room temperature ionic liquids incorporating the imidazolium cation. *Green Chemistry*. *3*(4), 156–164.

Hulsbosch, J., De Vos, D.E., Binnemans, K. and Ameloot, R. (2016). Biobased Ionic Liquids: Solvents for a Green Processing Industry? *ACS Sustainable Chemistry and Engineering*. *4*(6), 2917–2931.

Hunter, T.N., Pugh, R.J., Franks, G. V. and Jameson, G.J. (2008). The role of particles in stabilising foams and emulsions. *Advances in Colloid and Interface Science*. *137*(2), 57–81.

Ignatyev, I.A., Mertens, P.G.N., Van Doorslaer, C., Binnemans, K. and De Vos, D.E. (2010). Cellulose conversion into alkylglycosides in the ionic liquid 1-butyl-3-methylimidazolium chloride. *Green Chemistry*. *12*(10), 1790–1795.

Ikkai, F., Iwamoto, S., Adachi, E. and Nakajima, M. (2005). New method of producing mono-sized polymer gel particles using microchannel emulsification and UV irradiation. *Colloid and Polymer Science*. *283*(10), 1149–1153.

Ilyin, S.O., Makarova, V. V., Anokhina, T.S., Ignatenko, V.Y., Brantseva, T. V., Volkov, A. V. and Antonov, S. V. (2018). Diffusion and phase separation at the morphology formation of cellulose membranes by regeneration from N-methylmorpholine N-oxide solutions. *Cellulose*. *25*(4), 2515–2530.

Ishii, T., Matsumiya, K., Aoshima, M. and Matsumura, Y. (2018). Microgelation imparts emulsifying ability to surface-inactive polysaccharides—bottom-up vs top-down approaches. *npj Science of Food*. *2*(15), 1–12.

Isobe, N., Kimura, S., Wada, M. and Kuga, S. (2012). Mechanism of

cellulose gelation from aqueous alkali-urea solution. *Carbohydrate Polymers*. *89*(4), 1298–1300.

Jia, X., Chen, Y., Shi, C., Ye, Y., Wang, P., Zeng, X. and Wu, T. (2013). Preparation and characterization of cellulose regenerated from phosphoric acid. *Journal of Agricultural and Food Chemistry*. *61*(50), 12405–12414.

Jia, X., Xu, R., Shen, W., Xie, M., Abid, M., Jabbar, S., Wang, P., Zeng, X. and Wu, T. (2015). Stabilizing oil-in-water emulsion with amorphous cellulose. *Food Hydrocolloids*. *43*, 275–282.

Jiang, C., Li, W., Nian, J., Lou, W. and Wang, X. (2018). Tribological evaluation of environmentally friendly ionic liquids derived from renewable biomaterials. *Friction*. *6*(2), 208–218.

Jiao, B., Shi, A., Wang, Q. and Binks, B.P. (2018). High-Internal-Phase Pickering Emulsions Stabilized Solely by Peanut-Protein-Isolate Microgel Particles with Multiple Potential Applications. *Angewandte Chemie - International Edition*. *57*(30), 9274–9278.

Johnson, D.L. (1969). United States Patent Office. *Journal of the American Society for Naval Engineers*. *39*(4), 620–622.

Kabir, S.M.F., Sikdar, P.P., Haque, B., Bhuiyan, M.A.R., Ali, A. and Islam, M.N. (2018). Cellulose-based hydrogel materials: chemistry, properties and their prospective applications. *Progress in Biomaterials*. *7*(3), 153–174.

Kadokawa, J. ichi, Murakami, M. aki and Kaneko, Y. (2008). A facile preparation of gel materials from a solution of cellulose in ionic liquid. *Carbohydrate Research*. *343*(4), 769–772.

Kalashnikova, I., Bizot, H., Cathala, B. and Capron, I. (2012). Modulation of cellulose nanocrystals amphiphilic properties to stabilize oil/water interface. *Biomacromolecules*. *13*(1), 267–275.

Kalashnikova, I., Bizot, H., Cathala, B. and Capron, I. (2011). New pickering emulsions stabilized by bacterial cellulose nanocrystals. *Langmuir*. *27*(12), 7471–7479.

Kang, H., Liu, R. and Huang, Y. (2016). Cellulose-Based Gels. *Macromolecular Chemistry and Physics*. *217*(12), 1322–1334.

Kargar, M., Fayazmanesh, K., Alavi, M., Spyropoulos, F. and Norton, I.T. (2012). Investigation into the potential ability of Pickering emulsions (food-grade particles) to enhance the oxidative stability of oil-in-water emulsions. *Journal of Colloid and Interface Science*. *366*(1), 209–215.

Kyrey, T., Witte, J., Feoktystov, A., Pipich, V., Wu, B., Pasini, S., Radulescu, A., Witt, M.U., Kruteva, M., Von Klitzing, R., Wellert, S. and Holderer, O. (2019). Inner structure and dynamics of microgels with low and medium crosslinker content prepared: Via surfactant-free precipitation polymerization and continuous monomer feeding approach. *Soft Matter*. *15*(32), 6536–6546.

Lan, W., Liu, C.F., Yue, F.X., Sun, R.C. and Kennedy, J.F. (2011). Ultrasound-assisted dissolution of cellulose in ionic liquid. *Carbohydrate*

Polymers. *86*(2), 672–677.

Lefroy, K.S., Murray, B.S., Ries, M.E. and Curwen, T.D. (2021). A natural, cellulose-based microgel for water-in-oil emulsions. *Food Hydrocolloids*. *113*, 106408.

Li, L., Lin, Z., Yang, X., Wan, Z. and Cui, S. (2009). A novel cellulose hydrogel prepared from its ionic liquid solution. *Chinese Science Bulletin*. *54*(9), 1622–1625.

Li, P., Sirviö, J.A., Haapala, A. and Liimatainen, H. (2017). Cellulose nanofibrils from nonderivatizing urea-based deep eutectic solvent pretreatments. *ACS Applied Materials and Interfaces*. *9*(3), 2846–2855.

Li, X., Li, J., Gong, J., Kuang, Y., Mo, L. and Song, T. (2018). Cellulose nanocrystals (CNCs) with different crystalline allomorph for oil in water Pickering emulsions. *Carbohydrate Polymers*. *183*, 303–310.

Li, X., Li, J., Kuang, Y., Guo, S., Mo, L. and Ni, Y. (2020). Stabilization of Pickering emulsions with cellulose nanofibers derived from oil palm fruit bunch. *Cellulose*. *27*, 839–851.

Li, Z., Wu, H., Yang, M., Xu, D., Chen, J., Feng, H., Lu, Y., Zhang, L., Yu, Y. and Kang, W. (2018). Stability mechanism of O/W Pickering emulsions stabilized with regenerated cellulose. *Carbohydrate Polymers*. *181*, 224–233.

Liebert, T. (2010). Cellulose Solvents – Remarkable History, Bright Future *In*: *Cellulose Solvents: For Analysis, Shaping and Chemical Modification*. American Chemical Society, 3–54.

Lindman, B., Karlström, G. and Stigsson, L. (2010). On the mechanism of dissolution of cellulose. *Journal of Molecular Liquids*. *156*(1), 76–81.

Ling, Z., Edwards, J.V., Guo, Z., Prevost, N.T., Nam, S., Wu, Q., French, A.D. and Xu, F. (2019). Structural variations of cotton cellulose nanocrystals from deep eutectic solvent treatment: micro and nano scale. *Cellulose*. *26*(2), 861–876.

Liu, Z., Sun, X., Hao, M., Huang, C., Xue, Z. and Mu, T. (2015). Preparation and characterization of regenerated cellulose from ionic liquid using different methods. *Carbohydrate Polymers*. *117*, 54–62.

Lovell, C.S., Walker, A., Damion, R.A., Radhi, A., Tanner, S.F., Budtova, T. and Ries, M.E. (2010). Influence of cellulose on ion diffusivity in 1-ethyl-3-methyl-imidazolium acetate cellulose solutions. *Biomacromolecules*. *11*, 2927–2935.

Lu, X., Hu, Z. and Gao, J. (2000). Synthesis and light scattering study of hydroxypropyl cellulose microgels. *Macromolecules*. *33*, 8698–8702.

Lu, X., Zhang, H., Li, Y. and Huang, Q. (2018). Fabrication of milled cellulose particles-stabilized Pickering emulsions. *Food Hydrocolloids*. *77*, 427–435.

Ma, Y., Xia, Q., Liu, Yongzhuang, Chen, W., Liu, S., Wang, Q., Liu, Yixing, Li, J. and Yu, H. (2019). Production of Nanocellulose Using Hydrated Deep Eutectic Solvent Combined with Ultrasonic Treatment. *ACS Omega*. *4*, 8539–8547.

MacHado, A.H.E., Lundberg, D., Ribeiro, A.J., Veiga, F.J., Lindman, B., Miguel, M.G. and Olsson, U. (2012). Preparation of calcium alginate nanoparticles using water-in-oil (W/O) nanoemulsions. *Langmuir*. *28*(9), 4131–4141.

Mackie, A., Gourcy, S., Rigby, N., Moffat, J., Capron, I. and Bajka, B. (2019). The fate of cellulose nanocrystal stabilised emulsions after simulated gastrointestinal digestion and exposure to intestinal mucosa. *Nanoscale*. *11*(6), 2991–2998.

Man, Z., Muhammad, N., Sarwono, A., Bustam, M.A., Kumar, M.V. and Rafiq, S. (2011). Preparation of Cellulose Nanocrystals Using an Ionic Liquid. *Journal of Polymers and the Environment*. *19*(3), 726–731.

Matsumiya, K. and Murray, B.S. (2016). Soybean protein isolate gel particles as foaming and emulsifying agents. *Food Hydrocolloids*. *60*, 206–215.

McPhee, W., Tam, K.C. and Pelton, R. (1993). Poly(N-isopropylacrylamide) latices prepared with sodium dodecyl sulfate. *Journal of Colloid And Interface Science*. *156*(1), 24–30.

Medronho, B., Duarte, H., Alves, L., Antunes, F., Romano, A. and Lindman, B. (2015). Probing cellulose amphiphilicity. *Nordic Pulp & Paper Research Journal*. *30*(1), 58-66.

Meenatchi, B., Renuga, V. and Manikandan, A. (2017). Cellulose dissolution and regeneration using various imidazolium based protic ionic liquids. *Journal of Molecular Liquids*. *238*, 582–588.

Miyamoto, H., Umemura, M., Aoyagi, T., Yamane, C., Ueda, K. and Takahashi, K. (2009). Structural reorganization of molecular sheets derived from cellulose II by molecular dynamics simulations. *Carbohydrate Research*. *344*(9), 1085–1094.

Mukherjee, S.M., Sikorski, J. and Woods, H.J. (1952). Electron-microscopy of Degraded Cellulose Fibres. *Journal of the Textile Institute Transactions*. *43*(11), T563–T564.

Murray, B.S. (2019a). Microgels at fluid-fluid interfaces for food and drinks. *Advances in Colloid and Interface Science*. *271*, 101990.

Murray, B.S. (2019b). Pickering emulsions for food and drinks. *Current Opinion in Food Science*. *27*, 57–63.

Nageshwar, D., Rao, D.M. and Acharyulu, P.V.R. (2009). Terpenes to ionic liquids: Synthesis and characterization of citronellal-based chiral ionic liquids. *Synthetic Communications*. *39*(18), 3357–3368.

Napso, S., Rein, D.M., Fu, Z., Radulescu, A. and Cohen, Y. (2018). Structural Analysis of Cellulose-Coated Oil-in-Water Emulsions Fabricated from Molecular Solution. *Langmuir*. *34*(30), 8857–8865.

Napso, S., Rein, D.M., Khalfin, R., Kleinerman, O. and Cohen, Y. (2016). Cellulose gel dispersion: From pure hydrogel suspensions to encapsulated oil-in-water emulsions. *Colloids and Surfaces B: Biointerfaces*. *137*, 70–76.

Ni, Y., Li, J. and Fan, L. (2020). Production of nanocellulose with different length from ginkgo seed shells and applications for oil in water Pickering

emulsions. *International Journal of Biological Macromolecules*. *149*, 617–626.

de Oliveira, W. and Glasser, W.G. (1996). Hydrogels from polysaccharides. I. Cellulose beads for chromatographic support. *Journal of Applied Polymer Science*. *60*(1), 63–73.

Olsson, C. and Westman, G. (2013). Direct Dissolution of Cellulose: Background, Means and Applications *In*: *Cellulose - Fundamental Aspects* [Online]. IntechOpen, 143–178. Available from: https://doi.org/10.5772/2705.

Van Osch, D.J.G.P., Kollau, L.J.B.M., Van Den Bruinhorst, A., Asikainen, S., Rocha, M.A.A. and Kroon, M.C. (2017). Ionic liquids and deep eutectic solvents for lignocellulosic biomass fractionation. *Physical Chemistry Chemical Physics*. *19*(4), 2636–2665.

Ossowicz, P., Klebeko, J., Roman, B., Janus, E. and Rozwadowski, Z. (2019). The relationship between the structure and properties of amino acid ionic liquids. *Molecules*. *24*(18), 3252.

Östlund, Å., Idström, A., Olsson, C., Larsson, P.T. and Nordstierna, L. (2013). Modification of crystallinity and pore size distribution in coagulated cellulose films. *Cellulose*. *20*(4), 1657–1667.

Östlund, Å., Lundberg, D., Nordstierna, L., Holmberg, K. and Nydén, M. (2009). Dissolution and gelation of cellulose in TBAF/DMSO solutions: The roles of fluoride ions and water. *Biomacromolecules*. *10*(9), 2401–2407.

Oza, K.P. and Frank, S.G. (1986). Microcrystalline cellulose stabilized emulsions. *Journal of Dispersion Science and Technology*. *7*(5), 543–561.

Oza, K.P. and Frank, S.G. (1989). Multiple emulsions stabilized by colloidal microcrystalline cellulose. *Journal of Dispersion Science and Technology*. *10*(2), 163–185.

Pelton, R. (2000). Temperature-sensitive aqueous microgels. *Advances in Colloid and Interface Science*. *85*, 1–33.

Pelton, R. and Hoare, T. (2011). Microgels and Their Synthesis: An Introduction *In*: *Microgel Suspensions: Fundamentals and Applications* [Online]. Weinheim: Wiley-VCH, 1–32. Available from: https://doi.org/10.1002/9783527632992.ch1.

Pelton, R.H. and Chibante, P. (1986). Preparation of aqueous latices with N-isopropylacrylamide. *Colloids and Surfaces*. *20*(3), 247–256.

Phoon, P.Y. and Henry, C.J. (2020). Fibre-based oleogels: effect of the structure of insoluble fibre on its physical properties. *Food and Function*. *11*(2), 1349–1361.

Pich, A. and Richtering, W. (2010). Microgels by Precipitation Polymerization: Synthesis, Characterization, and Functionalization *In*: *Chemical Design of Responsive Microgels*. Berlin, Heidelberg: Springer Berlin Heidelberg, 1–37.

Pinaud, F., Geisel, K., Massé, P., Catargi, B., Isa, L., Richtering, W.,

Ravaine, V. and Schmitt, V. (2014). Adsorption of microgels at an oil-water interface: Correlation between packing and 2D elasticity. *Soft Matter*. *10*(36), 6963–6974.

Plamper, F.A. and Richtering, W. (2017). Functional Microgels and Microgel Systems. *Accounts of Chemical Research*. *50*(2), 131–140.

Pravinata, L., Akhtar, M., Bentley, P.J., Mahatnirunkul, T. and Murray, B.S. (2016). Preparation of alginate microgels in a simple one step process via the Leeds Jet Homogenizer. *Food Hydrocolloids*. *61*, 77–84.

Qi, H., Yang, Q., Zhang, L., Liebert, T. and Heinze, T. (2011). The dissolution of cellulose in NaOH-based aqueous system by two-step process. *Cellulose*. *18*(2), 237–245.

Rajeev, A. and Basavaraj, M.G. (2019). Colloidal Particle-Induced Microstructural Transition in Cellulose/Ionic Liquid/Water Mixtures. *Langmuir*. *35*(38), 12428–12438.

Rajeev, A., Deshpande, A.P. and Basavaraj, M.G. (2018). Rheology and microstructure of concentrated microcrystalline cellulose (MCC)/1-allyl-3-methylimidazolium chloride (AmimCl)/water mixtures. *Soft Matter*. *14*(37), 7615–7624.

Rånby, B.G. (1949). Aqueous Colloidal Solutions of Cellulose Micelles. *Acta Chemica Scandinavica*. *3*, 649–650.

Rein, D.M., Khalfin, R. and Cohen, Y. (2012). Cellulose as a novel amphiphilic coating for oil-in-water and water-in-oil dispersions. *Journal of Colloid and Interface Science*. *386*(1), 456–463.

Rey, M., Fernandez-Rodriguez, M.A., Karg, M., Isa, L. and Vogel, N. (2020). Poly- N-isopropylacrylamide Nanogels and Microgels at Fluid Interfaces. *Accounts of Chemical Research. 53*(2), 414-424.

Rinaldi, R. and Schüth, F. (2009). Acid hydrolysis of cellulose as the entry point into biorefinery schemes. *ChemSusChem*. *2*(12), 1096–1107.

Rosenau, T., Potthast, A., Sixta, H. and Kosma, P. (2001). The chemistry of side reactions and byproduct formation in the system NMMO/cellulose (Lyocell process). *Progress in Polymer Science*. *26*, 1763–1837.

Rousseau, D. (2013). Trends in structuring edible emulsions with Pickering fat crystals. *Current Opinion in Colloid and Interface Science*. *18*(4), 283–291.

Saavedra Isusi, G.I., Karbstein, H.P. and van der Schaaf, U.S. (2019). Microgel particle formation: Influence of mechanical properties of pectin-based gels on microgel particle size distribution. *Food Hydrocolloids*. *94*, 105–113.

Saito, H., Sakurai, A., Sakakibara, M. and Saga, H. (2003). Preparation and properties of transparent cellulose hydrogels. *Journal of Applied Polymer Science*. *90*(11), 3020–3025.

Sannino, A., Demitri, C. and Madaghiele, M. (2009). Biodegradable cellulose-based hydrogels: Design and applications. *Materials*. *2*(2), 353–373.

Sannino, A., Pappadà, S., Madaghiele, M., Maffezzoli, A., Ambrosio, L. and

Nicolais, L. (2005). Crosslinking of cellulose derivatives and hyaluronic acid with water-soluble carbodiimide. *Polymer*. *46*(25), 11206–11212.

Sarkar, A., Murray, B., Holmes, M., Ettelaie, R., Abdalla, A. and Yang, X. (2016). In vitro digestion of Pickering emulsions stabilized by soft whey protein microgel particles: Influence of thermal treatment. *Soft Matter*. *12*(15), 3558–3569.

Satlewal, A., Agrawal, R., Bhagia, S., Sangoro, J. and Ragauskas, A.J. (2018). Natural deep eutectic solvents for lignocellulosic biomass pretreatment: Recent developments, challenges and novel opportunities. *Biotechnology Advances*. *36*(8), 2032–2050.

Saunders, B.R., Laajam, N., Daly, E., Teow, S., Hu, X. and Stepto, R. (2009). Microgels: From responsive polymer colloids to biomaterials. *Advances in Colloid and Interface Science*. *147–148*, 251–262.

Saunders, B.R. and Vincent, B. (1999). Microgel particles as model colloids: Theory, properties and applications. *Advances in Colloid and Interface Science*. *80*(1), 1–25.

Schmitt, V. and Ravaine, V. (2013). Surface compaction versus stretching in Pickering emulsions stabilised by microgels. *Current Opinion in Colloid and Interface Science*. *18*(6), 532–541.

Schosseler, F., Ilmain, F. and Candau, S.J. (1991). Structure and Properties of Partially Neutralized Poly(acrylic acid) Gels. *Macromolecules*. *24*(1), 225–234.

El Seoud, O.A., Kostag, M., Jedvert, K. and Malek, N.I. (2019). Cellulose in ionic liquids and alkaline solutions: Advances in the mechanisms of biopolymer dissolution and regeneration. *Polymers*. *11*(12), 1–28.

Sescousse, R., Le, K.A., Ries, M.E. and Budtova, T. (2010). Viscosity of cellulose-imidazolium-based ionic liquid solutions. *Journal of Physical Chemistry B*. *114*(21), 7222–7228.

Shang, J., Shao, Z. and Chen, X. (2008). Electrical behavior of a natural polyelectrolyte hydrogel: Chitosan/carboxymethylcellulose hydrogel. *Biomacromolecules*. *9*(4), 1208–1213.

Sirviö, J.A. (2019). Fabrication of regenerated cellulose nanoparticles by mechanical disintegration of cellulose after dissolution and regeneration from a deep eutectic solvent. *Journal of Materials Chemistry A*. *7*(2), 755–763.

Socha, A.M., Parthasarathi, R., Shi, J., Pattathil, S., Whyte, D., Bergeron, M., George, A., Tran, K., Stavila, V., Venkatachalam, S., Hahn, M.G., Simmons, B.A. and Singh, S. (2014). Efficient biomass pretreatment using ionic liquids derived from lignin and hemicellulose. *Proceedings of the National Academy of Sciences of the United States of America*. *111*(35), 3587–3595.

Song, H., Niu, Y., Wang, Z. and Zhang, J. (2011). Liquid crystalline phase and gel-sol transitions for concentrated microcrystalline cellulose (MCC)/1-ethyl-3-methylimidazolium acetate (EMIMAc) solutions. *Biomacromolecules*. *12*(4), 1087–1096.

Sun, L., Chen, J.Y., Jiang, W. and Lynch, V. (2015). Crystalline characteristics of cellulose fiber and film regenerated from ionic liquid solution. *Carbohydrate Polymers*. *118*, 150–155.

Swatloski, R.P., Spear, S.K., Holbrey, J.D. and Rogers, R.D. (2002). Dissolution of cellulose with ionic liquids. *Journal of the American Chemical Society*. *124*(18), 4974–4975.

Takada, A. and Kadokawa, J.I. (2015). Fabrication and characterization of polysaccharide ion gels with ionic liquids and their further conversion into value-added sustainable materials. *Biomolecules*. *5*(1), 244–262.

Takata, S.I., Norisuye, T. and Shibayama, M. (1999). Preparation temperature dependence and effects of hydrolysis on static inhomogeneities of poly(acrylamide) gels. *Macromolecules*. *32*(12), 3989–3993.

Tan, X., Chen, L., Li, X. and Xie, F. (2019). Effect of anti-solvents on the characteristics of regenerated cellulose from 1-ethyl-3-methylimidazolium acetate ionic liquid. *International Journal of Biological Macromolecules*. *124*, 314–320.

Tang, S., Baker, G.A., Ravula, S., Jones, J.E. and Zhao, H. (2012). PEG-functionalized ionic liquids for cellulose dissolution and saccharification. *Green Chemistry*. *14*(10), 2922–2932.

Tay, K.A. and Bresme, F. (2006). Wetting properties of passivated metal nanocrystals at liquid-vapor interfaces: A computer simulation study. *Journal of the American Chemical Society*. *128*(43), 14166–14175.

Thoorens, G., Krier, F., Leclercq, B., Carlin, B. and Evrard, B. (2014). Microcrystalline cellulose, a direct compression binder in a quality by design environment - A review. *International Journal of Pharmaceutics*. *473*, 64–72.

Thorne, J.B., Vine, G.J. and Snowden, M.J. (2011). Microgel applications and commercial considerations. *Colloid and Polymer Science*. *289*, 625–646.

Torres, O., Murray, B. and Sarkar, A. (2016). Emulsion microgel particles: Novel encapsulation strategy for lipophilic molecules. *Trends in Food Science and Technology*. *55*, 98–108.

Tsuji, S. and Kawaguchi, H. (2008). Thermosensitive pickering emulsion stabilized by poly(N- isopropylacrylamide)-carrying particles. *Langmuir*. *24*(7), 3300–3305.

Verma, C., Mishra, A., Chauhan, S., Verma, P., Srivastava, V., Quraishi, M.A. and Ebenso, E.E. (2019). Dissolution of cellulose in ionic liquids and their mixed cosolvents: A review. *Sustainable Chemistry and Pharmacy*. *13*, 100162.

Wang, H., Gurau, G. and Rogers, R.D. (2012). Ionic liquid processing of cellulose. *Chemical Society Reviews*. *41*(4), 1519–1537.

Wang, S., Cheng, Q., Rials, T.G. and Lee, S.H. (2006). Cellulose microfibril/nanofibril and its nanocompsites. *Proceedings of the 8th Pacific Rim Bio-based Composites Symposium*., 20–23.

Wang, S., Lu, A. and Zhang, L. (2016). Recent advances in regenerated cellulose materials. *Progress in Polymer Science*. *53*, 169–206.

Wang, Z. and Wang, Y. (2016). Tuning Amphiphilicity of Particles for Controllable Pickering Emulsion. *Materials*. *9*(11), 903.

Watanabe, T., Takizawa, M., Jiang, H., Ngai, T. and Suzuki, D. (2019). Hydrophobized nanocomposite hydrogel microspheres as particulate stabilizers for water-in-oil emulsions. *Chemical Communications*. *55*(43), 5990–5993.

Wen, Q., Vincelli, A.M. and Pelton, R. (2012). Cationic polyvinylamine binding to anionic microgels yields kinetically controlled structures. *Journal of Colloid and Interface Science*. *369*(1), 223–230.

Wendler, F., Todi, L.N. and Meister, F. (2012). Thermostability of imidazolium ionic liquids as direct solvents for cellulose. *Thermochimica Acta*. *528*, 76–84.

Winuprasith, T. and Suphantharika, M. (2015). Properties and stability of oil-in-water emulsions stabilized by microfibrillated cellulose from mangosteen rind. *Food Hydrocolloids*. *43*, 690–699.

Wu, B. cheng and McClements, D.J. (2015). Microgels formed by electrostatic complexation of gelatin and OSA starch: Potential fat or starch mimetics. *Food Hydrocolloids*. *47*, 87–93.

Xie, H., She, Z.G., Wang, S., Sharma, G. and Smith, J.W. (2012). One-step fabrication of polymeric Janus nanoparticles for drug delivery. *Langmuir*. *28*(9), 4459–4463.

Xie, S., Xie, S., Chen, S., Chen, S., Zhu, Q., Zhu, Q., Li, X., Li, X., Wang, D., Wang, D., Shen, S., Shen, S., Jin, M., Jin, M., Zhou, G., Zhou, G., Zhu, Y., Shui, L., Shui, L. and Shui, L. (2020). Janus Nanoparticles with Tunable Amphiphilicity for Stabilizing Pickering-Emulsion Droplets via Assembly Behavior at Oil-Water Interfaces. *ACS Applied Materials and Interfaces*. *12*(23), 26374–26383.

Xiong, B., Zhao, P., Hu, K., Zhang, L. and Cheng, G. (2014). Dissolution of cellulose in aqueous NaOH/urea solution: Role of urea. *Cellulose*. *21*(3), 1183–1192.

Xu, A.R., Wang, J.J. and Guo, X. (2018). Fabrication of Cellulose Aerogels Using a Green/Clean Procedure. *Journal of Macromolecular Science, Part B: Physics*. *57*(1), 1–7.

Xu, S., Zhang, J., He, A., Li, J., Zhang, H. and Han, C.C. (2008). Electrospinning of native cellulose from nonvolatile solvent system. *Polymer*. *49*(12), 2911–2917.

Yan, L. and Gao, Z. (2008). Dissolving of cellulose in PEG/NaOH aqueous solution. *Cellulose*. *15*(6), 789–796.

Yue, C., Fang, D., Liu, L. and Yi, T.F. (2011). Synthesis and application of task-specific ionic liquids used as catalysts and/or solvents in organic unit reactions. *Journal of Molecular Liquids*. *163*(3), 99–121.

Zavrel, M., Bross, D., Funke, M., Büchs, J. and Spiess, A.C. (2009). High-throughput screening for ionic liquids dissolving (ligno-)cellulose.

Bioresource Technology. *100*(9), 2580–2587.

Zembyla, M., Lazidis, A., Murray, B.S. and Sarkar, A. (2020). Stability of water-in-oil emulsions co-stabilized by polyphenol crystal-protein complexes as a function of shear rate and temperature. *Journal of Food Engineering*. *281*, 109991.

Zhang, H., Wu, J., Zhang, J. and He, J. (2005). 1-allyl-3-methylimidazolium chloride room temperature ionic liquid: A new and powerful nonderivatizing solvent for cellulose. *Macromolecules*. *38*(20), 8272–8277.

Zhang, J., Wu, J., Yu, J., Zhang, X., He, J. and Zhang, J. (2017). Application of ionic liquids for dissolving cellulose and fabricating cellulose-based materials: State of the art and future trends. *Materials Chemistry Frontiers*. *1*(7), 1273–1290.

Zhang, J., Xu, L., Yu, J., Wu, J., Zhang, X., He, J. and Zhang, J. (2016). Understanding cellulose dissolution: effect of the cation and anion structure of ionic liquids on the solubility of cellulose. *Science China Chemistry*. *59*(11), 1421–1429.

Zhang, Q., Benoit, M., Dea Oliveiraa Vigier, K., Barrault, J. and Jérŏme, F. (2012). Green and inexpensive choline-derived solvents for cellulose decrystallization. *Chemistry - A European Journal*. *18*(4), 1043–1046.

Zhang, S., Holmes, M., Ettelaie, R. and Sarkar, A. (2020). Pea protein microgel particles as Pickering stabilisers of oil-in-water emulsions: Responsiveness to pH and ionic strength. *Food Hydrocolloids*. *102*, 105583.

Zhang, X., Xiao, N., Wang, H., Liu, C. and Pan, X. (2018). Preparation and characterization of regenerated cellulose film from a solution in lithium bromide molten salt hydrate. *Polymers*. *10*, 614.

Zhang, Y., Zha, L.S. and Fu, S.K. (2004). Kinetic Analysis of Poly(N-Isopropylacrylamide-co-dimethylaminoethyl methacrylate) Microgel Latex Formation. *Journal of Applied Polymer Science*. *92*(2), 839–846.

Zhao, H., Kwak, J.H., Conrad Zhang, Z., Brown, H.M., Arey, B.W. and Holladay, J.E. (2007). Studying cellulose fiber structure by SEM, XRD, NMR and acid hydrolysis. *Carbohydrate Polymers*. *68*(2), 235–241.

Zhou, J. and Zhang, L. (2000). Solubility of cellulose in NaOH Urea.pdf. . *32*(10), 866–870.

Zhu, S., Wu, Y., Chen, Q., Yu, Z., Wang, C., Jin, S., Ding, Y. and Wu, G. (2006). Dissolution of cellulose with ionic liquids and its application: A mini-review. *Green Chemistry*. *8*(4), 325–327.

Zhu, Y., Luo, X., Wu, X., Li, W., Li, B., Lu, A. and Liu, S. (2017). Cellulose gel dispersions: fascinating green particles for the stabilization of oil/water Pickering emulsion. *Cellulose*. *24*(1), 207–217.

Chapter 3
Rheological and NMR Studies of Cellulose Dissolution in the Ionic Liquid BmimAc[2]

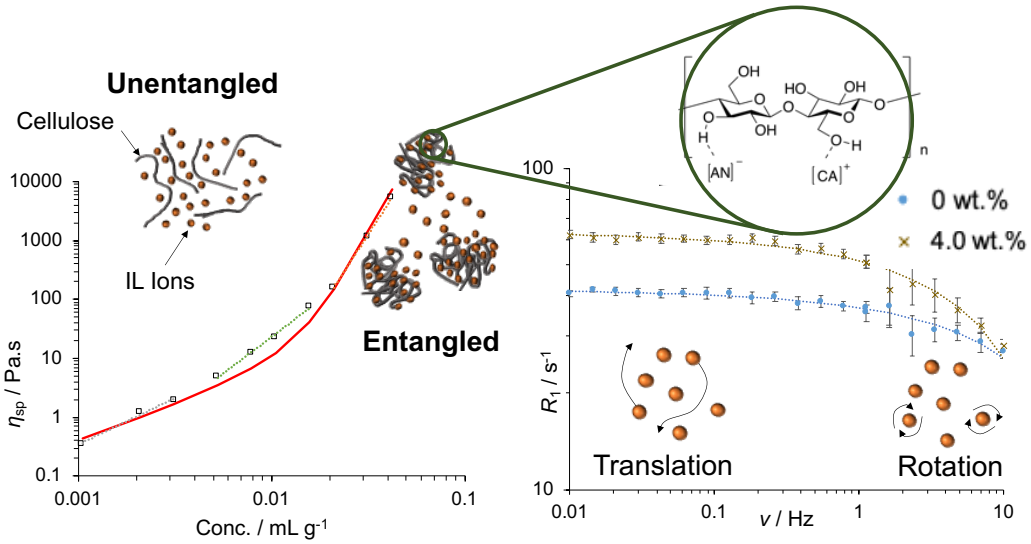

3.1 Abstract

Solutions of two types of cellulose in the ionic liquid 1-butyl-3-methyl-imidazolium acetate (BmimAc) have been analyzed using rheology and fast-field cycling nuclear magnetic resonance (NMR) spectroscopy, in order to analyze the macroscopic (bulk) and microscopic environments, respectively. The degree of polymerization (*DP*) was observed to have a significant effect on both the overlap (c^*) and entanglement (c_e) concentrations and the intrinsic viscosity ([η]). For microcrystalline cellulose (MCC)/BmimAc solutions, [η] = 116 mL g^{-1}, which is comparable to that of MCC/1-ethyl-3-methyl-imidazolium acetate (EmimAc) solutions, while [η] = 350 mL g^{-1} for the commercial cellulose (higher *DP*). Self-diffusion coefficients (*D*) obtained via the model-independent approach were found to decrease with cellulose concentration and increase with temperature, which can in part be explained by the changes in viscosity; however, ion interactions on a local level are also important. Both Stokes-Einstein and Stokes-Einstein-Debye analyses were carried out to directly compare rheological and relaxometry analyses. It was found that polymer entanglements affect the microscopic environment to a much lesser extent than for the macroscopic environment. Finally, the temperature dependencies of η, *D* and relaxation time (T_1) could be well described by Arrhenius relationships, and thus, activation energies (E_a) for

[2]Published as: Lefroy, K.S., Murray, B.S. and Ries, M.E. (2021). Rheological and NMR Studies of Cellulose Dissolution in the Ionic Liquid BmimAc. *Journal of Physical Chemistry B*. *125*(29), 8205–8218. DOI: 10.1021/acs.jpcb.1c02848

temperature and cellulose concentration have different effects on short- and long-range interactions.

3.2 Introduction

Ionic liquids (ILs) are made up of a cationic and anionic species and can be defined as low-melting point salts; Walden defined ILs as salts with a melting point below 100 °C (Walden, (1914); Takada and Kadokawa, (2015)). ILs are non-volatile and potentially recyclable and can be designed for specific processes by altering the cation and anion structures (Xu et al., (2008)). Recently, a new class of cholinium- and amino acid-based ILs has emerged, fulfilling the need for ILs to be biodegradable, non-toxic, and safe for producing biocompatible compounds (Chua et al., (2019)).

ILs have had an enormous impact in the area of cellulose processing, owing in part to their ability to break the strong network of hydrogen bonds that forms between polymer chains (Lindman et al., (2010)). Mild conditions, relatively easy recovery of cellulose, and potential recyclability of the solvent make ILs superior to many other reported cellulose solvents, such as *N*-methylmorpholine *N*-oxide, which often require high energy inputs and are thermally unstable (Tan et al., (2016); Lefroy, Murray and Ries, (2021)). However, high viscosity(Pinkert et al., (2009)) and cost of ILs has led to practical issues with their scale-up and has restricted their use in industrial cellulose processing (Tang et al., (2012)). Dissolving small amounts of cellulose in an IL can result in a large viscosity increase, which hinders further solubilization (El Seoud et al., (2007)) and complicates IL-cellulose handling on a large scale. Furthermore, their ability to dissolve cellulose decreases as the amount of water within the system increases (Marks et al., (2019)), since water causes cellulose to coagulate (Hauru et al., (2012); Verma et al., (2019)). Almost all ILs are hygroscopic, and as a result, small-scale cellulose dissolution is generally carried out within a sealed system or a glovebox, in order to reduce water vapor uptake from the atmosphere. Dissolution may alternatively require vacuum distillation throughout the process in order to remove water (Wendler et al., (2012)).

Understanding the viscosity-concentration-temperature behavior of cellulose-IL solutions is not only important for the design of processing strategies (Haward et al., (2012)) but also gives insight into the properties of materials obtained via IL-cellulose processing (Sescousse et al., (2010)). Factors which determine the viscosity and flow properties of the polymer solutions will also affect the morphology of the cellulose material obtained (Lu et al., (2015)). For example, it has been shown that cellulose gels coagulated from lower

concentration solutions (< ca. 7 wt%) are relatively heterogeneous, while more concentrated cellulose-IL solutions (> ca. 9 wt%) yield homogeneous cellulose gels (Napso et al., (2016)). Dilute solution viscometry can be employed to gain valuable information about the size and conformation of the macromolecule in solution and the entanglement state (Kulicke and Kniewske, (1984)), properties that may be manifested in the coagulated cellulose material. Generally, low concentration polymer solutions are divided into two regimes, dilute and semi-dilute, in which the viscoelastic behavior differs (Colby, (2010)). An overlap concentration (c^*) is defined when moving between these two regimes, corresponding to the concentration at which polymer chains start to overlap (Lu et al., (2013)). Furthermore, if the polymer molecular weight and critical concentration are sufficiently high, chains may entangle and slow down the dynamics, observed by a second critical concentration, the entanglement concentration (c_e) (Lopez et al., (2020)). Since the molecular weight of native cellulose is expected to exceed 500,000 Da (Kraemer and Lansing, (1935)), all three regimes have been observed for cellulose-IL solutions (Haward et al., (2012)). Less overlap is generally required to cause entanglements in polysaccharide solutions compared to synthetic polymers, observed by relatively low values of $c_e[\eta] \simeq$3-5 for the former compared to $c_e[\eta] \simeq$10 for the latter, which is in part explained by the inflexibility of polysaccharide chains (Horinaka et al., (2018); Lopez et al., (2020)). Cellulose derivatives also display similar behavior, whilst charged cellulose polymers can even “hyper-entangle” at higher concentrations,(Lopez et al., (2020)) if attractive interactions are present between chains.

Rheological experiments generally characterize the bulk or macroscopic properties of a polymer solution, which are determined by how much volume the solute occupies in the dilute regime (Ries et al., (2018)). On the other hand, it is useful to analyze cellulose-IL solutions on a molecular or microscopic level in order to gain further insight into specific solvent-solute interactions. Nuclear Magnetic Resonance (NMR) spectroscopy has been successfully applied to the study of cellulose-IL interactions during dissolution (Remsing et al., (2006); Zhang, Zhang, Wu, et al., (2010); Xu et al., (2010); Zhang et al., (2016)), through determination of self-diffusion coefficients (D) (Youngs et al., (2011); Radhi et al., (2015); Gentile and Olsson, (2016)). Conventionally, pulsed-field gradient (PFG) NMR experiments at high frequencies are used to determine D; however, relaxometry has also been applied to the study of translational diffusion (Kruk et al., (2012); Rachocki and Tritt-Goc, (2014); Ordikhani Seyedlar et al., (2015)). In fast-field cycling (FFC) NMR relaxometry, the dependence of relaxation time (T_1) is studied as a

function of frequency giving a dispersion (NMRD) profile, from which *D* can be determined. T_1 is the result of the intra- and intermolecular interactions, therefore probing the rotational and diffusional motion in solutions, respectively. FFC NMR has previously been used to study the translational dynamics of ILs in polymer systems, where the molecular dynamics of spin nuclei of less-abundant molecules can be probed (Kruk et al., (2014); Rachocki et al., (2015); Kaszyńska et al., (2017)).

Low-field relaxometry experiments at single frequencies have also been used to compare the effects of cellulose, cellobiose, and glucose on the mobility of 1-ethyl-3-methylimidazolium acetate (EmimAc) ions, through measuring T_1 and T_2 relaxation times (Ries et al., (2018)). Interestingly, it was reported that cellulose solutions gave the longest T_1 times but the highest viscosities, indicating the highest level of mobility on a molecular scale and the lowest on a macroscopic scale. The authors highlight that the factors affecting the macroscopic and microscopic properties of cellulose/EmimAc solutions are different, and therefore, it is useful to investigate both when considering the dissolution of cellulose.

The solution properties of various types of commercial cellulose powder have been analyzed in EmimAc (Sescousse et al., (2010); Haward et al., (2012); Tan et al., (2016); Green et al., (2017)), 1-butyl-3-methylimidazolium chloride (BmimCl), (Sescousse et al., (2010); Green et al., (2017)) and 1-allyl-3-methylimidazolium chloride (AmimCl); (Kuang et al., (2008)) however, to the best of our knowledge, rheological and relaxometry experiments have not been performed with 1-butyl-3-methylimidazolium acetate (BmimAc). BmimAc and EmimAc have displayed similar cellulose dissolving capacities (Kosan et al., (2008); Vitz et al., (2009)), whilst alkyl chain length is reported to have no influence over the onset temperature (T_{on}), and therefore, both ILs are similar in terms of their safety with respect to industrial processing (Wendler et al., (2012)). However, BmimAc is slightly cheaper than EmimAc and therefore may be a more affordable approach to IL processing of cellulose. In this work, the bulk properties of low-concentration cellulose/BmimAc solutions (0-4 wt%) were analyzed using steady-state flow rheology, and we determine the zero-shear-rate viscosities (η_0), crossover and entanglement concentrations (c^* and c_e), and intrinsic viscosity ([η]). Two types of cellulose, Vitacel L 00 powder (*V*-cell) and Avicel Microcrystalline Cellulose PH-101 (*A*-cell), were investigated in order to compare the effect of cellulose molecular weight on solvent properties and to provide a comparison to other cellulose-ILs in literature. FFC NMR relaxometry was then used in order to obtain *D* values for the solvent at

different cellulose concentrations, while relaxation times (T_1) obtained at a single frequency (10 MHz) are reported and analyzed. Finally, macroscopic and microscopic properties of the solutions were compared using Stokes-Einstein and Stokes-Einstein-Debye equations, correlating the rheological and relaxometry analyses. The solutions were studied over a temperature range using each method, and a classic Arrhenius approach was used to calculate the activation energies and compare the three different processes being probed: flow, diffusional, and rotational motion ($E_{a,\eta}$, $E_{a,D}$ and $E_{a,T1}$ respectively).

Detailed studies of cellulose dissolution in BmimAc will not only provide a comparison between different ILs but also give further insights into the interactions between cellulose and itself and cellulose and the solvent ions. This information will be valuable in understanding the process of cellulose dissolution in ILs and therefore aid the design of more suitable cellulose solvents for larger-scale processing.

3.3 Methods

3.3.1 Materials

Vitacel powdered cellulose L 00 (JRS, supplied by Mondelēz International) [degree of polymerization (*DP*) ≈ 730-830, as estimated below] and Avicel PH-101 microcrystalline cellulose (MCC) (Sigma-Aldrich, DP ≈ 180)(Ries et al., (2018)) were both used to investigate the effect of *DP* on the viscosity of cellulose in IL solutions. The Vitacel cellulose and the Avicel cellulose are abbreviated to '*V*-cell' and '*A*-cell,' respectively. Whilst the *DP* of *V*-cell is estimated, other known properties such as fiber size are listed in **Appendix A** (Table A 1). The IL 1-butyl-3-methyl-imidazolium acetate (BmimAc) (≥98 % purity, Sigma-Aldrich) was used to dissolve the *A*-cell and *V*-cell.

3.3.2 Preparation of Cellulose-IL Solutions

A-cell or *V*-cell powders were first dried in a vacuum oven at 60 °C for at least 24 h, in order to remove any moisture. A total of 0 to 4 wt% of the cellulose was then dissolved in BmimAc in a sealed vial with slow stirring (70 °C, 400 rpm) using a magnetic stirrer bar, in order to minimize the incorporation of air bubbles. Concentrations greater than 4 wt% *V*-cell were not investigated since the resultant solutions were highly viscous and inhomogeneous and required long stirring times at higher temperatures, which may lead to cellulose degradation (Hermanutz et al., (2008); Haward et al., (2012)). Dissolution was said to be complete when the solution was clear and no particles were visible. Samples were then stored in a desiccator until required, to prevent uptake of any water vapor from the atmosphere by BmimAc.

3.3.3 Rheology

Steady-state viscosity measurements of 0 to 4 wt% cellulose/BmimAc solutions were measured using an Anton Paar Rheometer, equipped with a water bath temperature control system and a Peltier hood. A 50 mm-diameter circular cone-plate geometry was used, with an angle of 2 °. Viscosity measurements were conducted in the range 0.01-1000 s^{-1} at a constant temperature (25-70 °C), and flow curves were obtained. Each sample was heated to the desired measurement temperature for 1 min and then pre-sheared for 1 min at 1 s^{-1}, to ensure adequate heating throughout. Measurements were repeated three times, and an average viscosity value was deduced.

3.3.4 ^{1}H NMR (High-Field) Quantitative NMR

^{1}H NMR spectra for cellulose-BmimAc solutions (0-4 wt%) were recorded on a wide-bore Avance II NMR spectrometer (Bruker Biospin) operating at a proton resonance frequency of 400 MHz (25 °C). An average water content of 0.44 ±0.24 wt% was determined for all *V*-cell/BmimAc solutions except for 3 and 4 wt%, which were highly viscous, due to the increased time taken to fill the NMR tube and therefore longer exposure of the IL to air. Therefore, data for these two solutions should be treated with caution, since water contamination is likely to affect the accuracy of the results.

3.3.5 FFC NMR Relaxometry

FFC NMR was conducted on a Stelar SMARtracer FFC NMR Relaxometer (Stelar s.r.l., Mede, PV, Italy), generating ^{1}H NMRD dispersion profiles. Glass tubes of 5 mm diameter (WilmadR, Sigma-Aldrich) were filled with ca. 2.5 mL of sample and sealed. Samples were analyzed at constant temperatures (25-70 °C), with 10 min thermal equilibration time allowed after each temperature was reached. Temperature was controlled via a variable temperature controller with an accuracy of 0.1 K. 4 scans were recorded for each, and an average value of these is reported. T_1 values were calculated using a single-exponential function, since magnetization decay was monoexponential over the range of frequencies measured, for all samples. During each measurement, a polarization field of 7 MHz was initially applied for a period of approximately 5 times the T_1 value estimated at this frequency. The magnetization was then switched to the measurement relaxation field (0.01-10 MHz). A single ^{1}H 90 ° pulse at 7 MHz was then applied and the free induction decay (FID) recorded. A non-polarized FFC sequence was applied for all samples over the frequency range measured. A field-switching time of

0.003 ms, a dead time of 15-20 μs, and a recycle delay of 5 times T_1 were used.

NMRD profiles were fitted to the well-known model-independent approach, as first described by Kruk *et al.* (Kruk et al., (2012)), in order to obtain *D* values for each cellulose concentration over a range of temperatures. Full details of the relaxometry theory, equations, and method can be found in **Appendix A**.

3.4 Results and Discussion

3.4.1 Rheological Properties of *A*-Cell/BmimAc

Initially, the flow curves for *A*-cell in BmimAc (0-4 wt%) were analyzed in order to compare the solvent properties of BmimAc to those of EmimAc and other acetate-based ILs. Figure A 1a gives viscosity (η) plotted as a function of shear rate ($\dot{\gamma}$) for 0-4 wt% *A*-cell at 25 °C. Flow curves were fitted to the well-known Cross model, (Cross, (1965)) as given by:

Equation 3.1.
$$\eta_{(\dot{\gamma})} = \eta_{(\infty)} + \frac{\eta_{(0)} - \eta_{(\infty)}}{1 + (C\dot{\gamma})^m}$$

where $\eta_{(0)}$ = zero-shear rate viscosity; $\eta_{(\infty)}$ = infinite-shear rate viscosity; *C* = Cross time constant, and *m* = (Cross) rate constant. Both *C* and *m* give information on the shear-thinning region: 1/*C* gives the critical shear rate, which is a good indication of the onset of shear thinning, while *m* gives the degree of the dependence of viscosity on shear (within the shear thinning region). It should be noted that for all of the cellulose-BmimAc solutions, no positive inflexion was observed in the data towards the higher shear rates, and therefore, it was assumed that $\eta_{(\infty)}$ was approximately the value of the pure solvent when fitting the data. Furthermore, only the extrapolated zero-shear rate viscosities were considered for further analysis, and therefore, $\eta_{(0)}$ will be referred to as simply the viscosity, η.

Viscosity decreases as the concentration of cellulose decreases, as expected for a classical polymer solution. Shear thinning is observed due to alignment of polymer molecules with the shear direction, (Lu et al., (2015)) and this behavior becomes more pronounced with increasing cellulose concentration, as reported elsewhere for cellulose dissolved in ILs (Kuang et al., (2008); Sescousse et al., (2010); Xun Chen et al., (2011); Haward et al., (2012)). This is reflected by the onset of shear-thinning, 1/*C*, which is given in Table 3.1.

Table 3.1. Values for η, m, and $1/C$ for *A*-cell/BmimAc solutions (0-4 wt%) at 25 °C, obtained by fitting data to the Cross model.

concentration of *A*-cell/wt%	η/Pa.s	m	C/s	$1/C$/s^{-1}
0	0.390	0.891	0.001	1260
0.1	0.446	0.316	0.001	1000
0.2	0.468	0.794	0.001	891
0.3	0.575	0.794	0.00115	871
0.5	0.640	0.794	0.00120	832
0.75	0.946	0.794	0.00126	794
1.0	1.19	0.794	0.00129	776
1.5	1.89	0.794	0.00158	631
2.0	2.90	0.891	0.00178	562
3.0	5.33	0.977	0.00182	550
4.0	9.46	0.977	0.00344	291

For the pure IL and low concentrations of *A*-cell/BmimAc (<1.0 wt%) viscosity was largely independent of the shear rate (Newtonian behavior); however, a low-shear rate and shear thinning regime was sometimes observed ($\dot{\gamma} \approx 0.01$-$0.1$ s^{-1}, Figure A 2). Low shear rate and shear thinning have been reported for *A*-cell in EmimAc (Tan et al., (2016)) and cellulose dissolved in AmimCl (Kuang et al., (2008)) and may be explained by IL molecular interactions; it is proposed that in pure solvent, IL molecules undergo hydrogen bonding with each other and form clusters (left schematic, Figure 3.1), which can in turn form a dynamic network that begins to gradually break down as the shear rate increases. This behavior is observed despite the introduction of a pre-shear (1 s^{-1}), suggesting that these weak cluster networks are dynamic and reform rapidly. Specific hydrogen bond-type interactions have been similarly reported for other halide-based ILs, (Q. Wang et al., (2012); Cha et al., (2014)) whilst cluster formation in pure ILs has been extensively reported (Chen et al., (2014)). At low wt% cellulose (0.1-1 wt%), this dynamic network of IL molecules is only partially disrupted by the presence of polysaccharide chains, and IL aggregates are still present (middle schematic, Figure 3.1). It is also speculated that cellulose molecules and IL molecules may form dynamic clusters, further contributing to the shear thinning behavior (Kuang et al.,

(2008)). Low shear rate shear-thinning behavior begins to disappear as the wt% cellulose increases, due to significant disruption of the physical IL network and solvation of cellulose chains by the $Bmim^+$ cation and Ac^- anion (right schematic, Figure 3.1).

In order to the compare the solvent properties of BmimAc to those of EmimAc, η values extrapolated from flow curves of *A*-cell/BmimAc are listed with literature values for *A*-cell/EmimAc solutions (Tan et al., (2016)) in Table 3.2. At concentrations of 0.5 and 1.0 wt%, *A*-cell/EmimAc was reported to have η values of approximately 1.05 and 2.28 times larger compared to those of the pure solvent (Tan et al., (2016)), whilst *A*-cell/BmimAc has η values of approximately 1.32 and 2.45 times larger, for the same concentrations. Therefore, the effect of cellulose on the solvent viscosity appears to be relatively similar for the two types of IL. This will be further investigated through comparing the overlap concentrations and the intrinsic viscosities of *A*-cell in BmimAc and EmimAc.

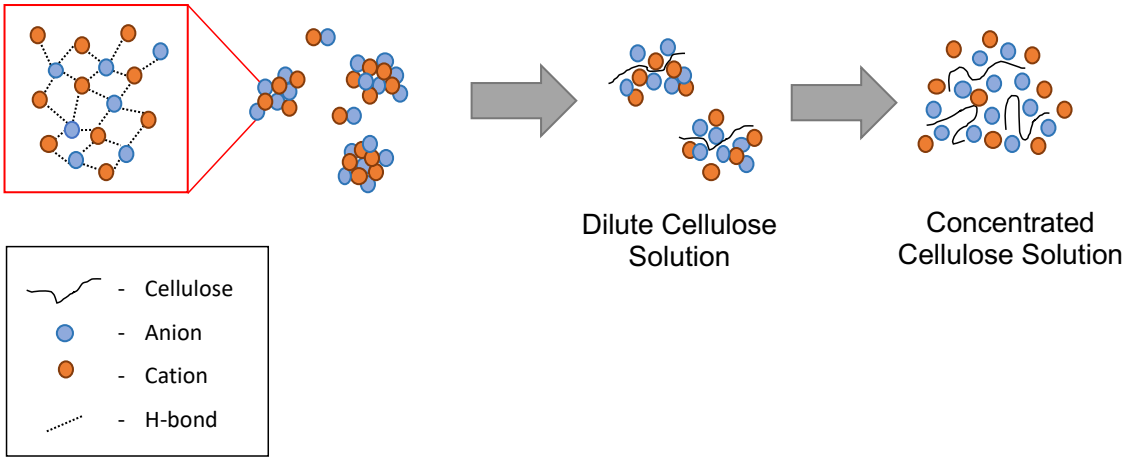

Figure 3.1. From left to right: schematic to show formation of H-bonded ion clusters in pure ILs; formation of cellulose-IL clusters at low cellulose concentrations; and breakdown of clusters at higher cellulose concentrations.

Table 3.2. *A*-cell in EmimAc and BmimAc (25 °C), η values compared, with the viscosity increase relative to the pure solvent ($\eta_{(c)}/\eta_{(0)}$) given in brackets ($\eta_{(0)}$ = viscosity in the pure solvent).

Concentration/wt%	η in EmimAc/Pa.s	η in BmimAc/Pa.s
0	0.162 (Fendt et al., (2011))	0.485 (Fendt et al., (2011))
0.5	0.169 (Tan et al., (2016)) (1.05 times)	0.640 (1.32 times)
1	0.369 (Tan et al., (2016)) (2.28 times)	1.19 (2.45 times)

3.4.2 Dilute and Semi-dilute Regimes

The concentration dependence of the zero-shear rate viscosity at 25 °C is given in Figure 3.2a for *A*-cell/BmimAc solutions. A linear region was observed for concentrations up to ca. 1 wt% for *A*-cell/BmimAc solutions with an exponent of 1.5 for conc. > 1 wt%. The former appears as a curved line, and the latter appears as a straight line in Figure 3.2a, since the data are plotted on a logarithmic scale. This is lower than exponents of 3.08(Tan et al., (2016)) and 2.4(Haward et al., (2012)) reported for MCC in EmimAc at 25 °C, which may be due to the lack of data points at higher cellulose concentrations in this instance (i.e., not > 4 wt%).

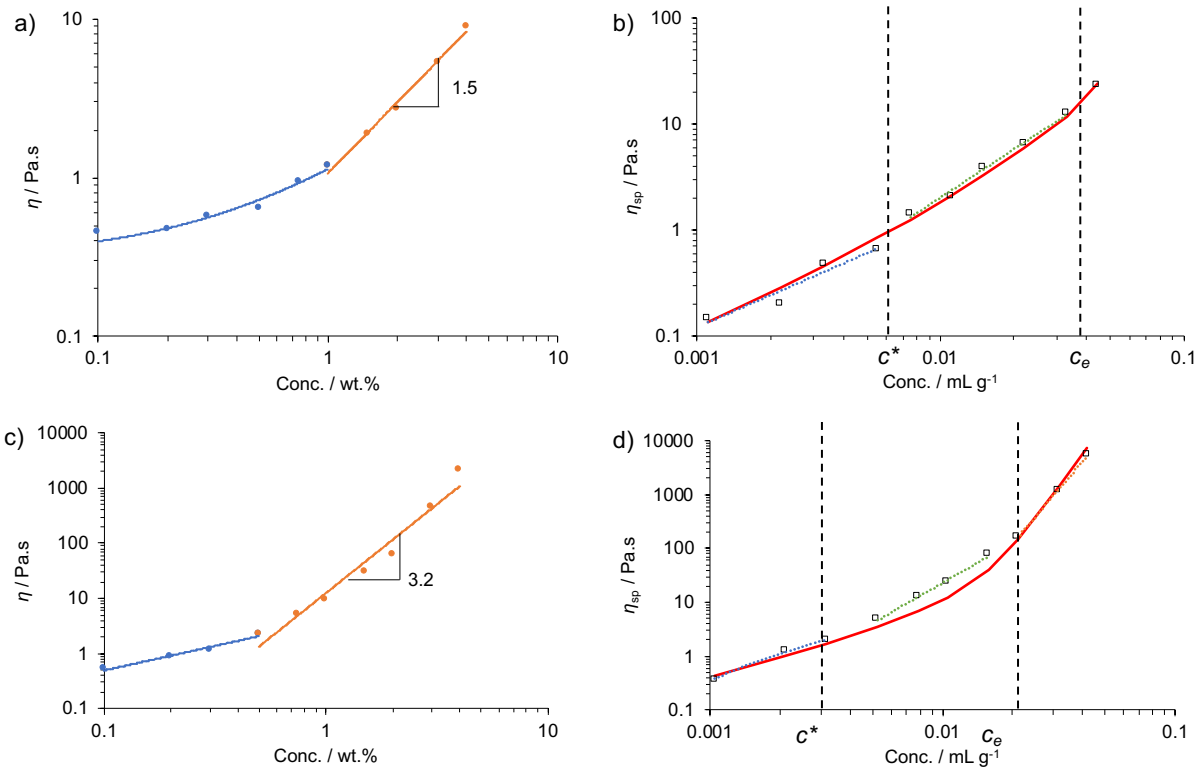

Figure 3.2. η as a function of *A*-cell (a) and *V*-cell (c) concentration in BmimAc (25 °C), showing the linear region (blue) and the exponential region (orange); specific viscosity (η_{sp}) as a function of *A*-cell (b) and *V*-cell (d) concentration in BmimAc (25 °C), showing the estimated overlap (c^*) and entanglement (c_e) concentrations. The red line gives the best fit to Equation 3.4; the blue, green, and orange dashed lines give the dilute, semi-dilute unentangled, and semi-dilute entangled regions, respectively.

The specific viscosity (η_{sp}) was used, so as to normalize out the effects of the pure solvent viscosity, (Lu et al., (2013)) to predict c^* and c_e at 25 °C for *A*-cell in BmimAc (Figure 3.2b). Concentration was converted from wt% into mL g^{-1},

assuming that the density of BmimAc remains constant over the concentration range (ρ = 1.05 g mL^{-1}).

Three regions can generally be identified corresponding to the dilute, semi-dilute unentangled, and semi-dilute entangled regimes. Each region can be described by a power-law dependency:

Equation 3.2. $$\eta_{sp} = kc^n$$

where *k* is a constant and *n* gives the power law for each region. The scaling prediction for neutral polymers in solvent estimates power law dependencies of 1, 2, and 14/3 (θ-solvents) and 1, 1.3, and 3.9 (good solvents), for the dilute, semi-dilute unentangled, and semi-dilute entangled regions, respectively (Lu et al., (2015)). Since a linear dependence in the dilute regime is predicted for both types of solvent, the first term of the equation was fixed as *n* = 1, whilst the other two *n* values, corresponding to the two semi-dilute regimes, were fitted to experimental data. At 25 °C, just two exponents could be determined over the concentration range 0-4 wt%, since 4.0 wt% appeared to be the only concentration at which *A*-cell/BmimAc fell within the semi-dilute entangled regime (i.e., above c_e). Power laws of *n* = 1 and 1.9 were obtained, corresponding to the dilute and semi-dilute unentangled regimes (Figure 3.2b). These values are close to the scaling predictions for a θ-solvent, which has been reported previously for cellulose in EmimAc (Gericke et al., (2009); Haward et al., (2012)).

c^* was estimated for *A*-cell/BmimAc solutions by extrapolating fits for the semi-dilute unentangled regime to η_{sp} = 1 (Behra et al., (2019)). c_e values were defined as a change in gradient from η_{sp} versus *c* plots, observed by the eye (Figure 3.2b). It is worth noting that the cellulose source is expected to be relatively polydisperse, and therefore, transitions between the different regimes are more likely to be defined by a concentration range rather than by a specific value (Behra et al., (2019)). c^* and c_e at 25 °C were found to be 0.77 and 3.4 wt% respectively, which is in agreement with the approximation $c_e \approx$ 3 to 5 x c^* (Kuang et al., (2008); Xun Chen et al., (2011); Lu et al., (2013); Lu et al., (2015)). The value of c^* for *A*-cell in BmimAc is slightly lower than previously reported values for *A*-cell in EmimAc (Sescousse et al., (2010); Tan et al., (2016)), suggesting that the polymer chains may overlap at a lower concentration in BmimAc relative to EmimAc.

3.4.3 Intrinsic Viscosity

The intrinsic viscosity ([η]) gives information about the size of a polymer in a solution and thermodynamic quality of the solvent. [η] is a measure of the

hydrodynamic volume of polymer coils; 1/[η] gives an approximate value for c^* and can be compared to the values obtained from the power law fits (Lue et al., (2011)). Traditionally, a capillary Ubbelohde viscometer is used for the determination of [η], where solution and solvent flow times are measured, and the relative viscosity (η_{rel}) is analyzed as a function of concentration. However, this approach is problematic for IL solutions due to the high viscosity and hygroscopicity of the solvent.

A method outlined by Kulicke *et al.* is preferred in this instance, taking viscosity values over a large concentration range and relating η_{sp} and [η] in the following manner (Kulicke and Kniewske, (1984); Sescousse et al., (2010)):

Equation 3.3. $$\boldsymbol{\eta_{sp} = \sum_{k=1}^{n} A_k (c[\eta])^k}$$

where A_k is a constant and c is cellulose concentration.

The Huggins equation gives a truncated version of this when all parameters have exponents higher than 2, as described in by Kulicke and Kniewske, (Kulicke and Kniewske, (1984)) and is defined as follows:

Equation 3.4. $$\boldsymbol{\eta_{sp} = c[\eta] + K_H (c[\eta])^2 + B(c[\eta])^m}$$

Here, K_H is the Huggins constant and B and m are constants. The Huggins constant has not yet been found for BmimAc, to the best of our knowledge. As a first approximation, K_H was taken to be 0.5, since the exponent α in the Mark-Kuhn equation was $0.4 < \alpha < 0.6$ for EmimAc (between 0 and 100 °C), and similarly, it has been shown that EmimAc is close to a θ-solvent for cellulose at room temperature (Haward et al., (2012)).

A plot of log(η_{sp}) versus log(c[η]) for *A*-cell/BmimAc solutions at 25 °C was used to deduce values for B, [η], and m, approximated by the best fit of Equation 3.4 to the experimental data (Figure A 3). An estimation of [η] was initially made by calculating η_{sp}/c and ln(η_{rel})/c, in order to assess the accuracy of the obtained [η] value from the equation and hence the quality of the fit (Ren et al., (2003)).

At 25 °C, [η] = 116 mL g^{-1} for *A*-cell/BmimAc solutions, while B and m were within the range 0.021 – 6.4 x 10^{-5} and 4.5 – 7, respectively, which is very close to values previously reported for *A*-cell/EmimAc ([η] = 112 mL g^{-1} (Tan et al., (2016)) and [η] = ca. 100 to 110 mL g^{-1} (Sescousse et al., (2010)). This suggests that both the thermodynamic quality of the solvent and the hydrodynamic volume of the dissolved cellulose molecules are almost identical in BmimAc and EmimAc and that therefore, the anion has a greater influence on cellulose dissolution compared to the cation. This is in agreement with recent work by Brehm *et al.,* who reported that the cellulose-anion

interactions are significantly stronger than cellulose-cation interactions in ILs, and hence, the former contribute much more significantly to the total potential energy of cellulose dissolution (Brehm et al., (2020)). Thus, ILs with common anions are expected to display very similar macroscopic solution properties, when cellulose is dissolved.

Using the assumption $c^* = 1/[\eta]$ and the abovementioned value for $[\eta]$ gives $c^* = 8.62 \times 10^{-3}$ g mL^{-1} (equivalent to 0.82 wt%) for *A*-cell/BmimAc, which is in good agreement with the value of 0.77 wt% found in the section given above (3.4.2).

3.4.4 Rheological Properties of *V*-Cell/BmimAc

The macroscopic properties of a different kind of cellulose (*V*-cell) in BmimAc were also studied and compared to those of *A*-cell. We have recently published work on *V*-cell/BmimAc solutions and their coagulation to produce cellulose microgels (Lefroy, Murray, Ries, et al., (2021)), which have a wealth of potential applications in the food, cosmetic and medical industries. Therefore, this study of the *V*-cell/BmimAc solution properties was motivated by the need to understand the state of the dissolved cellulose before subsequent microgel fabrication.

Figure 3.3 and Figure A 1b give the flow curves for *V*-cell/BmimAc solutions (0-4 wt%) and the low-shear rate and shear thinning behavior described in Figure 3.1 is given in **Appendix A**, for dilute solutions (Figure A 4). In contrast to *A*-cell/BmimAc, low-shear rate and shear thinning was observed up to concentrations of ca. 0.3 wt% *V*-cell/BmimAc, with 0 and 0.2 wt% displaying the most significant shear thinning between $\dot{\gamma}$ = 0.001 and 0.01 s^{-1}. This suggests that BmimAc “clusters” were broken up with smaller amounts of dissolved *V*-cell compared to *A*-cell and that two “stages” of cluster formation may occur at 0 and 0.3 wt%, (see section 3.4.5.2 given below). Furthermore, *V*-cell/BmimAc solutions were found to be much more viscous with η values of up to approximately 220 times larger (c = 4.0 wt%), compared to *A*-cell/BmimAc. Both of these observations suggest that *V*-cell has a much larger *DP* compared to *A*-cell, and therefore, the larger polymer chains have a greater influence on the IL viscosity at much lower concentrations. The *DP* of *V*-cell will be estimated in the following section, using the intrinsic viscosity.

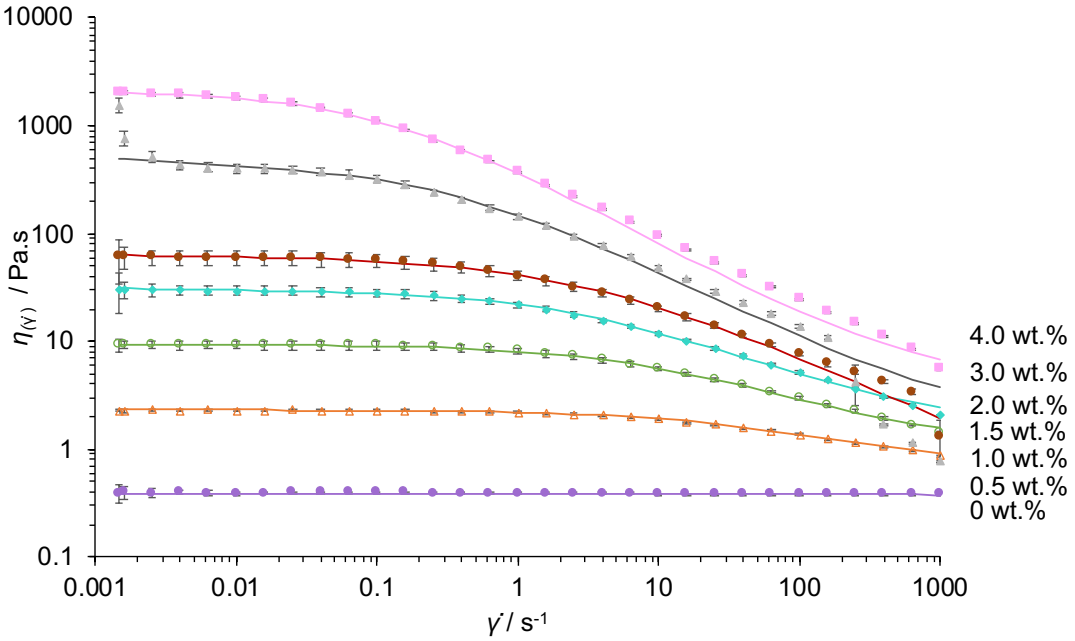

Figure 3.3. Flow curves for 0-4 wt% *V*-cell/BmimAc, showing the logarithmic plot of viscosity v shear rate at 25 °C. (Purple closed circle = 0 wt%; orange open triangle = 0.5 wt%; green open circle = 1.0 wt%; cyan closed diamond = 1.5 wt%; red closed circle = 2.0 wt%; grey closed triangle = 3.0 wt%; and pink closed square = 4.0 wt%). Fits to the Cross-model (Equation 3.1) are given by the solid lines in the corresponding colours. Error bars are all shown, but some may be hidden by the symbol.

The concentration dependences of η and η_{sp} are given in Figure 3.2c and d, respectively, and once again, the data are shown on a logarithmic scale. An exponent of over twice the value of *A*-cell was observed for the non-linear region, and all 3 regimes (dilute, semi-dilute unentangled, and semi-dilute entangled) seemed to be present over the concentration range studied. The power laws (fitted to Equation 3.2) for the three regions were 1, 2.2, and 4.4, which are again close to the scaling predictions for *θ*-solvents outlined in the section 3.4.2. c^* was estimated to be 0.20 wt% at 25 °C, which is over three times smaller than c^* for *A*-cell/BmimAc, suggesting that *V*-cell chains begin to overlap at much lower concentrations and again indicating a significantly larger *DP*. c_e was estimated at 2.0 wt%, which is not within the prediction $c_e \approx 3 - 5c^*$, confirming that less overlap is required to cause entanglement. This might in part be explained again by the chain inflexibility of polysaccharides, which is evidently more significant for cellulose with a larger *DP* (Horinaka et al., (2018); Lopez et al., (2020)).

Considering the abovementioned observations, it follows that $[\eta]$ should be larger for *V*-cell/BmimAc compared to *A*-cell/BmimAc solutions, at a given temperature. As expected, a value of $[\eta]$ = 350 mL g^{-1} was obtained for *V*-cell

at 25 °C, which is approximately three times larger than *A*-cell (obtained by fitting to Equation 3.4, Figure A 5). 1/[η] gives an estimated value of c^* = 0.27 wt%, which is remarkably close to the value predicted above (by extrapolation to η_{sp} = 1). The *DP* of *V*-cell was estimated from [η] using the simple relationship below (Xun Chen et al., (2011)):

Equation 3.5. $$[\eta] \approx 0.42DP$$

giving a value of *DP* ≈ 833, and therefore, *M* ≈ 135,000 for *V*-cell. This *DP* is over 4.5 times larger than the *DP* of *A*-cell (*DP* = 180) (Ries et al., (2018)), and therefore, the higher viscosities observed for *V*-cell/BmimAc solutions are clearly due to the significantly larger polymer chain size.

Table 3.3 gives a comparison between different types of cellulose in different ILs and their intrinsic viscosities. Interestingly, while *A*-cell gave an almost identical value of [η] in both EmimAc and BmimAc, *V*-cell gives a value of almost two times as large in BmimAc when compared to cellulose pulp in EmimAc, which is expected to have a similar *DP* (as predicted by Equation 3.5). This suggests that there may be more significant differences observable between EmimAc and BmimAc when cellulose with a larger *DP* is dissolved. While cellulose-anion interactions are expected to be more important than cellulose-cation interactions in ILs (Brehm et al., (2020)), possibly the contribution of the cation may become more significant in BmimAc compared to EmimAc. [η] is more comparable between *V*-cell/BmimAc and α-cellulose/BmimCl solutions, which have the same cation, suggesting that cellulose-cation interactions may be more important for dissolution of larger *DP* cellulose. Further studies of the same cellulose type with a larger *DP* in BmimAc and EmimAc separately are required to make a more direct comparison between the two solvents.

Table 3.3. Intrinsic viscosity values for cellulose-IL systems with varying *DP*s.

Type of Cellulose (*DP*)	Solvent	[η]/mL g^{-1}	Reference
Vitacel L 00 '*V*-cell' (ca. 730-830)	BmimAc	350	-
Avicel MCC '*A*-cell' (180)	BmimAc	116	-
Avicel MCC (180)	EmimAc	Ca. 110	(Sescousse et al., (2010))
MCC (235)	EmimAc	112	(Tan et al., (2016))
Cellulose pulp (860)	EmimAc	188	(Haward et al., (2012))
Cellulose (850)	EmimCl/DMSO	236	(Lu et al., (2015))
Dissolving Pulp Cellulose (650)	AmimCl	288.2	(Kuang et al., (2008))
α-Cellulose (C8002, ca. 850)	BmimCl	357	(Xun Chen et al., (2011))

3.4.5 Effect of Temperature on Macroscopic Properties of V-Cell/BmimAc and Activation Energies

The effect of temperature (T) on the rheological properties of *V*-cell/BmimAc solutions was investigated at various concentrations. Figure 3.4 gives ln(η) as a function of 1/T for *V*-cell/BmimAc solutions (0-4 wt%), showing that the viscosity decreases as temperature increases (as expected for classical polymer solutions). Data for some of the dilute solutions have been omitted to make the figure clear, and the full dataset can be found in **Appendix A** (Figure A 6).

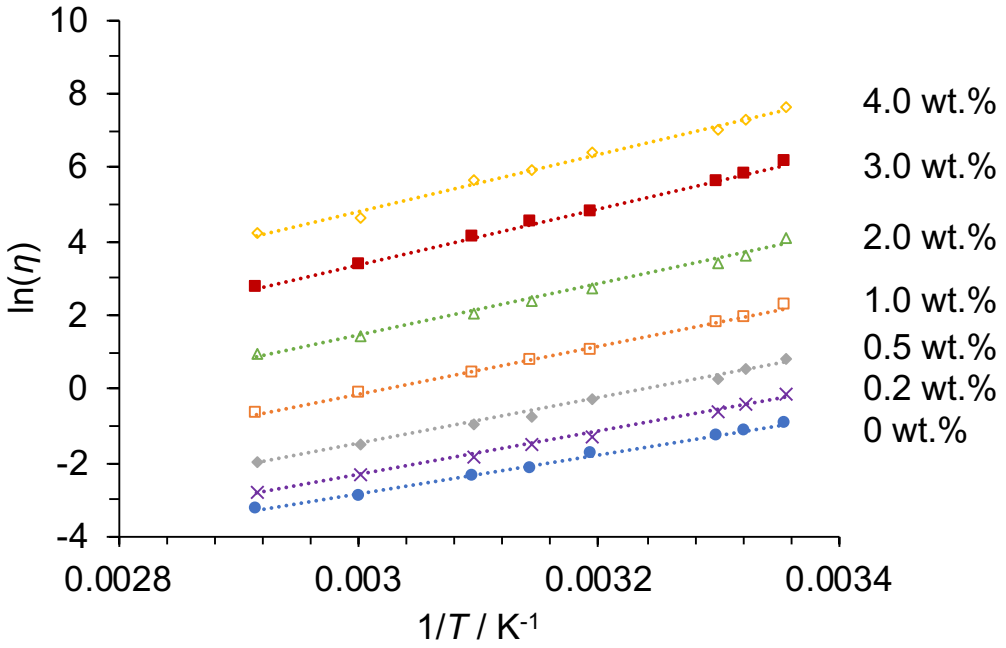

Figure 3.4. ln(η) as a function of 1/T (25 to 70 °C) for 0-4 wt% *V*-cell in BmimAc, obtained from the Cross model (blue closed circle = 0 wt%; purple cross = 0.2 wt%; grey closed diamond = 0.5 wt%; orange open square = 1.0 wt%; green open triangle = 2.0 wt%; red closed square = 3.0 wt%; yellow open diamond = 4.0 wt%). The straight lines give the Arrhenius analysis (Equation 3.6).

The viscosity-temperature dependence for *V*-cell/BmimAc solutions was further analyzed using the following Arrhenius-type equation (Gericke et al., (2009)):

Equation 3.6.

$$ln\eta = ln\eta_0 + \frac{E_{a,\eta}}{RT}$$

where η_0 represents the pre-exponential factor, $E_{a,\eta}$ is the activation energy for flow to occur, and R is the universal gas constant. $E_{a,\eta}$ can be deduced from the slope of ln(η) versus inverse temperature, if the dependence is linear.

Arrhenius plots for various concentrations of *V*-cell/BmimAc are given in Figure 3.4, with linear fitting of each set of experimental data to deduce $E_{a,\eta}$. Activation energies over the concentration range 0-4 wt% and R^2 values corresponding to each linear fit are supplied in **Appendix A** (Table A 3). An increase in $E_{a,\eta}$ with *V*-cell concentration is observed, as depicted in Figure 3.5, which is due to an increase in the barrier for viscous flow in the bulk solution. $E_{a,\eta}$ therefore gives a macroscopic parameter, which increases as the volume of cellulose-IL interactions increases. Surprisingly, a dip in the value of $E_{a,\eta}$ is observed at 2.0 wt% (Table A 3), around the estimated value of $c_{e,}$ which is most likely due to a poor fit to Equation 3.6 for the preceding data point (1.5 wt% *V*-cell/BmimAc). The relationship between ln(η) and inverse temperature for MCC-EmimAc solutions has been approximated by a

concave dependence elsewhere (Gericke et al., (2009)). However, $E_{a,\eta}$ is observed to increase with cellulose concentration within the error margins calculated, and in this instance, the Arrhenius approach was considered to give adequate accuracy.

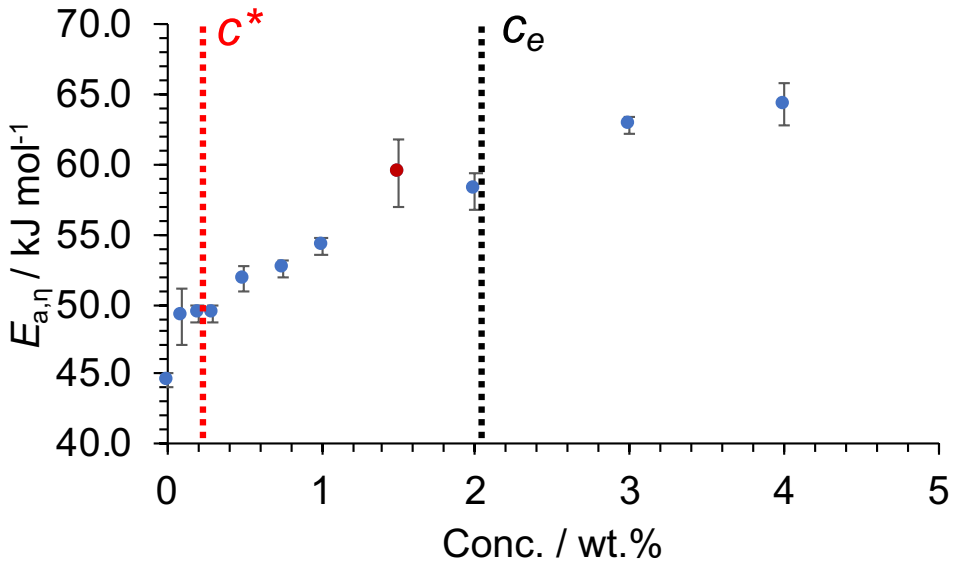

Figure 3.5. Plot of activation energies ($E_{a,\eta}$) for flow, as deduced from Equation 3.6, for *V*-cell dissolved in BmimAc at various concentrations of cellulose (conc. = 0-4.0 wt%). Estimated values of c^* and c_e at 25 °C are shown in red and black, respectively, and $E_{a,\eta}$ for conc. = 1.5 wt% is represented in red, to signify a linear fit to Equation 3.6 with $R^2 < 0.99$. Error bars were calculated based on the fit to Equation 3.6, and therefore, the uncertainty in determining the gradient and subsequently $E_{a,\eta}$ from the data. % errors are listed in Table A 3.

It was observed that the onset of shear thinning occurs at higher shear rates as the temperature is increased, as illustrated by a plot of $1/C$ (from Equation 3.1) versus T (Figure A 7). c^* and c_e were found to increase with T (**Appendix A**, Table A 2 and Figure A 8), while the exponent value in the non-linear region decreased correspondingly, suggesting that as the temperature increases, polymer chains overlap at a higher concentration. To confirm this, $[\eta]$ was found to decrease with T (Figure 3.6, obtained from η_{sp} vs concentration plots at 25-70 °C, Figure A 9), and therefore, a decrease in solvent thermodynamic quality and polymer chain size is observed, which has been previously reported for various cellulose-IL solutions (Gericke et al., (2009); Sescousse et al., (2010)).

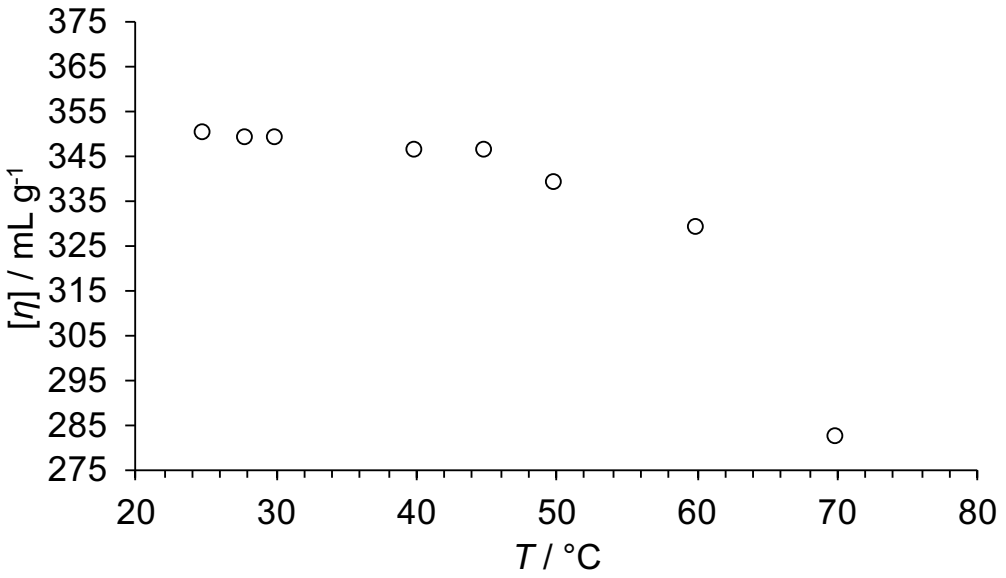

Figure 3.6. Intrinsic viscosity ([η]) as a function of temperature for *V*-cell dissolved in BmimAc.

3.4.5.1 FFC NMR Studies of *V*-Cell/BmimAc Solutions

While rheological analysis offers insights into bulk properties of solutions, self-diffusion coefficients (*D*) obtained from NMR can be used to probe interactions on a local level. Therefore, using the two techniques, one can compare the macroscopic and microscopic environment experienced by solvent molecules. Since molecular tumbling is expected to correlate with viscosity, FFC NMR was selected as a technique in this instance to provide a comparison to the rheological analysis. Only *V*-cell/BmimAc solutions were analyzed via FFC-NMR since c^* and c_e were within the concentration range (0-4 wt%) unlike for *A*-cell, which requires higher concentrations to be within the semi-dilute entanglement regime (see analysis discussed above). Therefore, the effect of entanglements on the macroscopic and microscopic properties of *V*-cell/BmimAc could be compared. The water content of each sample was determined using quantitative NMR and is given in **Appendix A** (Table A 4). All of the *V*-cell/BmimAc solutions had an average water content of 0.44 ± 0.24 wt%, except for the higher concentrations (3 and 4 wt%). Therefore, these data have been included but have been highlighted (in red) in the subsequent plots (Figure 3.8b and Figure 3.10b) to signify that water may be significantly affecting the NMR signal.

Using the model-independent approach as first described by Kruk *et al.* (Kruk et al., (2012)), *D* values can be obtained from the NMR dispersion (NMRD) curves characterized within the low-frequency range (0-10 MHz). The measured relaxation rate (R_1) gives a sum of the intra- and intermolecular contributions to relaxation (Equation A 1). At sufficiently low frequencies, the

translational contribution to R_1 is dominant, and therefore, D can be determined in a model-independent way (Kruk et al., (2012)):

Equation 3.7. $$\boldsymbol{R_1(\omega) = a - b\sqrt{\nu}}$$

Where *a* and *b* are constants, given by the following equations:

Equation 3.8. $$\boldsymbol{a = R_1(0)}$$

Equation 3.9. $$\boldsymbol{b = N\left(\frac{\mu_0}{4\pi}\gamma^2\hbar\right)^2\left(\frac{\sqrt{2}+8}{30}\right)\left(\frac{\pi}{D}\right)^{3/2}}$$

Full details of the theory can be found in the literature(Kruk et al., (2012)) and are also provided in **Appendix A**.

D values were determined for 0 to 4 wt% V-cell/BmimAc solutions using this approach over a range of temperatures, by fitting to Equation A 2 (Figure A 10) (Kruk et al., (2014)). *D* values gave good agreement with literature values for cellulose/EmimAc systems in terms of the order of magnitude as well as the trend seen with increasing cellulose concentration (Figure A 11) (Lovell et al., (2010)). Therefore, this was deemed an accurate method for determining the translational motion of solvent molecules, BmimAc, with low concentrations of cellulose.

Ion size, shape, and the strength of ion interactions all effect ion diffusivities (Y. Zhao et al., (2008)). Figure 3.7 gives the dependence of *D* on temperature, in a range of cellulose concentrations. As expected, for all *V*-cell/BmimAc solutions, *D* decreases accordingly with decreasing temperature, corresponding to slower translational motion. At lower temperatures, *D* also mostly decreases with increasing *V*-cell concentration, as generally observed for solvent molecules diffusing in polymer solutions (Lovell et al., (2010)). This can be explained in part by the corresponding power law increase in viscosity as a function of concentration, which drastically inhibits the diffusion of solvent molecules through the solution. As the temperature decreases, a wider range of values are obtained for *D,* and the effect of cellulose concentration on ion diffusivities becomes more enhanced. Therefore, the addition of cellulose appears to alter the ion diffusivities more significantly at lower temperatures, and interactions occurring on a local level should also be considered. Some further discussion of hydrodynamic interactions and their influence on ion diffusion can be found in the literature (Lovell et al., (2010)).

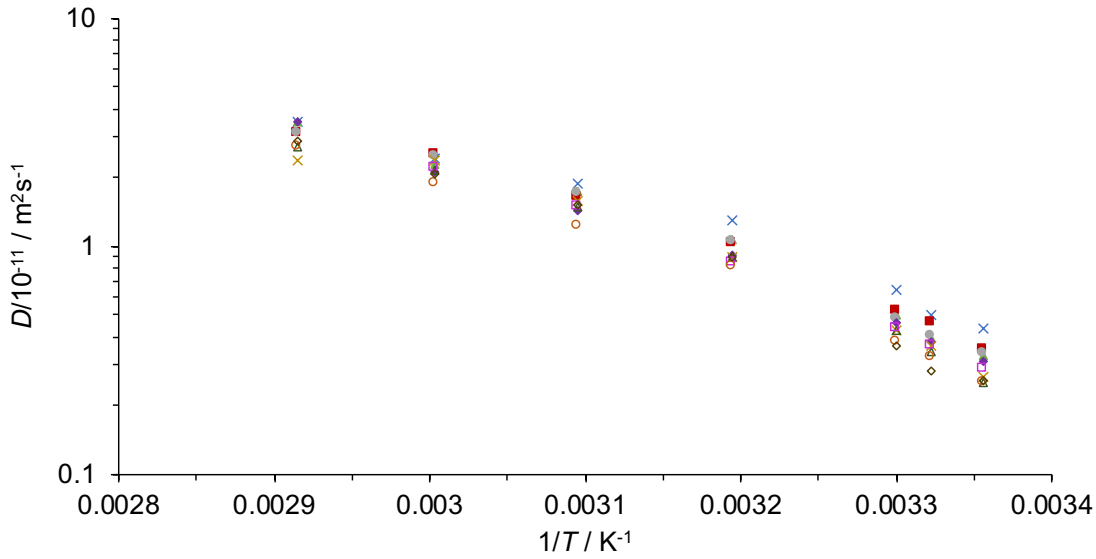

Figure 3.7. Logarithmic plot of self-diffusion coefficients (*D*) as a functional of the reciprocal temperature, for V-cell/BmimAc solutions: 0 wt% (cross, blue); 0.1 wt% (closed triangle, light green); 0.2 wt% (closed square, red); 0.3 wt% (closed circle, light grey); 0.5 wt% (closed diamond, purple); 0.75 wt% (cross, dark yellow); 1.0 wt% (open triangle, dark green); 2.0 wt% (open square, pink); 3.0 wt% (open square, orange); and 4.0 wt% (open diamond, brown).

3.4.5.2 Stokes-Einstein Analysis of *V*-Cell/BmimAc Solutions

Rheology and NMR experiments were compared using the Stokes-Einstein relationship, which correlates diffusivity and fluidity ($1/\eta$) as follows (Radhi et al., (2015)):

Equation 3.10. $$D = \frac{k_B T}{6\pi f \eta r_H}$$

Where f is a correction factor (sometimes referred to as the microviscosity pre-factor) and r_H is the effective hydrodynamic radius of a molecule. Other variations of Equation 3.10 may alternatively use a constant, c, which is linked to the correction factor as $c = 6f$ (Mclaughlin, (1959); Tokuda et al., (2004)). For large molecules diffusing into smaller molecules, the hydrodynamic assumptions made by the Stokes-Einstein equation are valid, and therefore, $f = 1$ (Powell et al., (1941)). However, many small molecules show deviations from this value, and Equation 3.10 may underpredict the value of r_H (Antony et al., (2005)), as in the case of pure solvent where the diffusing molecule is the same size as the surrounding molecules. For ILs, the presence of strong intermolecular H-bonding networks and “dynamic heterogeneities” further invalidates the Stokes-Einstein relationship (Köddermann et al., (2008)). The latter describes the presence of spatial regions, which have significantly different relaxation times compared to the average relaxation time of the

system, as studied for the IL 1-ethyl-3-methylimidazolium nitrate via molecular dynamics (Del Pópolo and Voth, (2004)), where the formation of highly mobile ion clusters and short-lived cation-anion pairs is predicted.

An estimation of r_H can be determined from the following equation (Radhi et al., (2015)):

Equation 3.11. $$r_H = \frac{1}{2}\left(\frac{M}{\rho N_A}\right)^{\frac{1}{3}}$$

Where M = molar mass; ρ = density; and N_A = Avogadro's number. Values of r_H = 3.01 and 2.26 Å for the $[Bmim]^+$ cation and $[OAc]^-$ anion, respectively, which are close to previously published values of 3.3 (Tokuda et al., (2004)) and 2.24 Å (Green et al., (2017)). Since self-diffusion coefficients were obtained via fitting of the FFC NMR data, the individual motion of the cation and anion cannot be distinguished. Therefore, D describes the average motion across the ions, and an average value of r_H = 2.64 Å was used.

Figure 3.8a gives the relationship between D obtained from FFC NMR and T/η obtained from rheological experiments for 0 to 4 wt% *V*-cell/BmimAc solutions, with straight-line fits given by the dashed lines. A linear dependence in the ln-ln plot is observed with a gradient of ca. 0.9 for pure BmimAc, confirming the validity of the Stokes-Einstein relationship; however, the gradient decreases as the concentration of cellulose increases. Therefore, the macroscopic and microscopic properties are affected to differing extents by cellulose concentration. The macroscopic viscosity increases dramatically as the concentration of cellulose increases, which is in agreement with the behavior of MCC/EmimAc solutions; (Ries et al., (2018)) however, the microviscosity is much less affected. Such observations can be explained by the effect of entanglements, which have a significant impact on the macroscopic viscosity but almost no effect on the microviscosity and therefore D. This can be seen by an increase in the spacing of lines above c^* (conc. ≈ 0.2 wt%) and again above c_e (conc. ≈ 2.0 wt%). For large polymers such as cellulose, large-scale effects such as these are observable using rheology but do not have an effect at the smaller length scales, and therefore, the local microviscosity as determined using NMR.

The correction factor (f) was determined from the gradient of the linear plots of D versus T/ η, and f is plotted as a function of cellulose concentration in Figure 3.8b. A value of f = ca. 1 was obtained for the pure solvent and low-concentration cellulose solutions, suggesting that the Stokes-Einstein relationship is correctly relating the macroscopic to the microscopic environments (Hall et al., (2012)). However, as cellulose is added, f decreases

in value as the Stokes-Einstein relationship starts to break down; the macroscopic viscosity is increasing much more rapidly than the microscopic viscosity. This is because the addition of cellulose causes overlap, entanglements, and large-scale structures, which dramatically increase the macroscopic viscosity. The value of *f* drops most significantly between 0 and 0.1 wt%, which is in agreement with observations from the rheological analysis, (where low-frequency shear thinning behavior and therefore cluster formation was observed for the pure solution).

H-bonding has also been reported to increase the observed *f* value (Hall et al., (2012)). Various studies have shown that a pre-factor of $f = 2/3$ is suitable for a variety of molecular liquids(Mclaughlin, (1959); Cussler, (1984); Tokuda et al., (2004)), and this value has been applied to Stokes-Einstein analysis of EmimAc (Hall et al., (2012); Green et al., (2017)). However, we report that a value of $f = 1$ may be more suitable for pure BmimAc, which may have a higher degree of cluster formation compared to EmimAc.

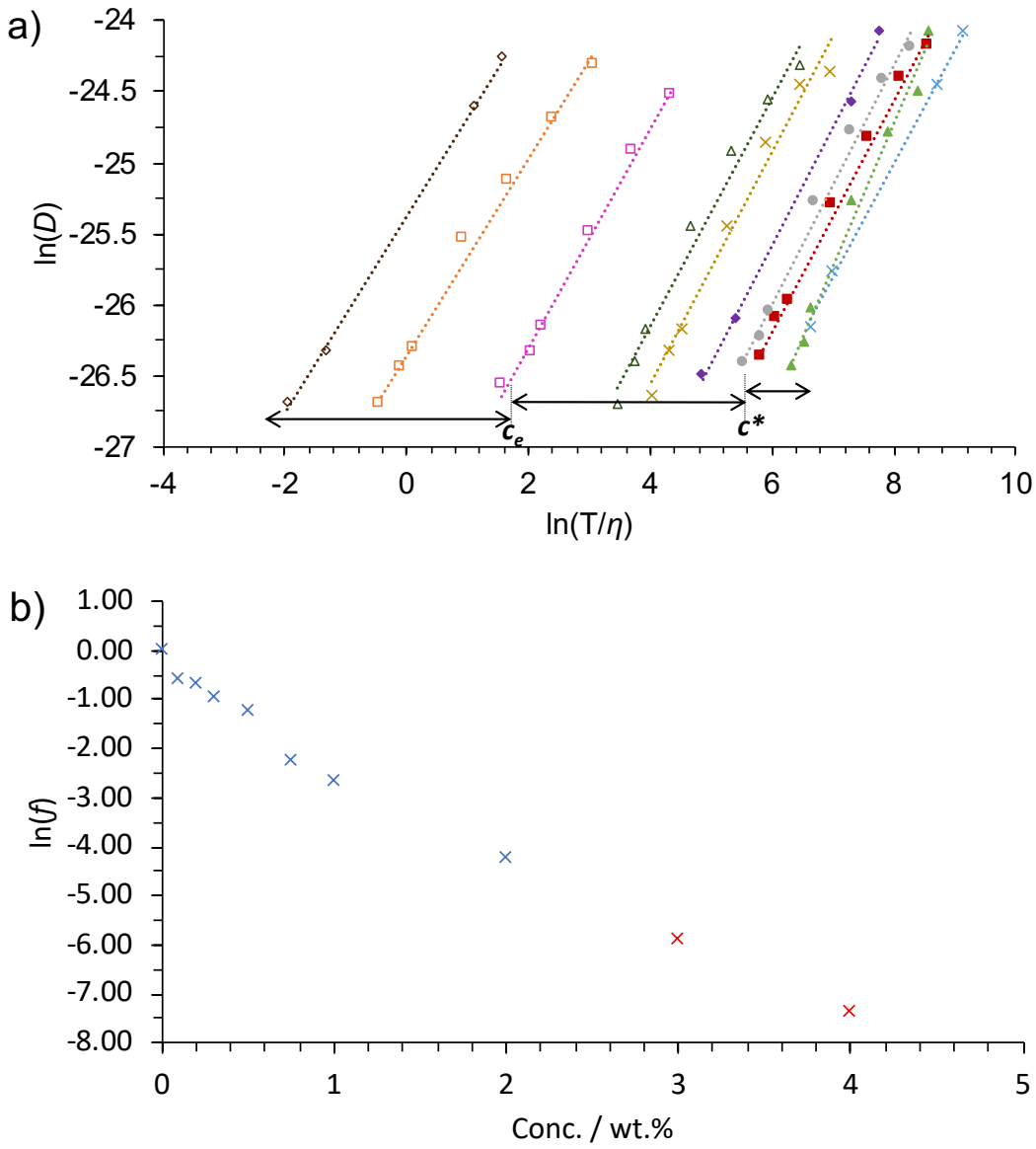

Figure 3.8. a) Relationship between ln(*D*) and ln(*T/η*), as determined by FFC NMR and rheology, respectively: 0 wt% (cross, blue); 0.1 wt% (closed triangle, light green); 0.2 wt% (closed square, red); 0.3 wt% (closed circle, light grey); 0.5 wt% (closed diamond, purple); 0.75 wt% (cross, dark yellow); 1.0 wt% (open triangle, dark green); 2.0 wt% (open square, pink); 3.0 wt% (open square, orange); and 4.0 wt% (open diamond, brown). The dashed lines give linear fits, as in Equation 3.10, and the dilute (green), semi-dilute unentangled (blue), and semi-dilute entangled (yellow) regions have been highlighted along with *c and c_e; b) Correction factor *(f)* shown as a function of cellulose concentration, as determined from Equation 3.10. Data for 3.0 and 4.0 wt% *V*-cell/BmimAc are shown in red, due to the higher water content in samples.**

3.4.5.3 FFC NMR Relaxometry at a Single Frequency (*v* = 10 MHz)

Further comparison of the macroscopic and microscopic environments can be made using relaxation times (T_1) at a single frequency. T_1 was analyzed at 10

MHz (low-field relaxometry) for each concentration of *V*-cell/BmimAc, over a range of temperatures. At 10 MHz, the NMR relaxation is dominated by rotational motion, giving complimentary information to the translational motion analyzed above (Ries et al., (2018)).

The logarithmic plot of T_1 as a function of inverse temperature is given in Figure 3.9. Analogous to *D,* T_1 decreases with decreasing temperature as molecular motion is slowed, and consequently, proton relaxation occurs more rapidly. Generally, T_1 was found to decrease with an increase in cellulose concentration, which can be once again explained by a decrease in molecular motion with an increase in polymer-solvent interactions (Figure A 12). This is in agreement with previous studies of T_1 as a function of *A*-cell concentration in EmimAc, (Ries et al., (2018)) where it was reported that T_1 is dependent on the number of OH groups on the cellulose "available" to bind to the IL molecules. However, the effect of *V*-cell concentration on T_1 was less pronounced than the effect on *D.* This is possibly due to the fact that relaxation is expected to be primarily governed by molecular tumbling at this frequency, while *D* describes the effect of translational motion of molecules. Translational motion may be more significantly affected by concentration compared to tumbling, as a higher energy barrier for translational motion is required compared to rotational motion, and therefore, the increase in solvent-cellulose interactions will have a greater effect on the former. Furthermore, T_1 values for *V*-cell/BmimAc solutions were approximately three times smaller than relaxation times reported for *A*-cell/EmimAc (Ries et al., (2018)). This corresponds to the difference in solvent viscosities, where $\eta_{BmimAc} \approx 3 \times \eta_{EmimAc}$ (Table 3.2), since $1/T_1$ is proportional to viscosity when rotational motion dominates the NMR relaxation mechanism (Equation 3.12 and Equation 3.13).

Further valuable information on binding equilibria in cellulose-IL solutions may be gained from the intermolecular relaxation rate and the self-diffusion coefficient, by determination of the Hertz's association parameter (*A*), ($A = (1/T_{1,inter}).D/c$, where *c* is the number density of interacting spins) (Holz and Patil, (1991)). The concentration dependence of the *A*-parameter can be studied and used to describe the effect of dilution on solvent-solvent interactions in binary liquid mixtures (Müller and Hertz, (1996)). However, it is essential that the total relaxation rate is divided into $1/T_{1,inter}$ and $1/T_{1,intra}$, for which the most reliable method is isotopic dilution (Holz and Patil, (1991)).

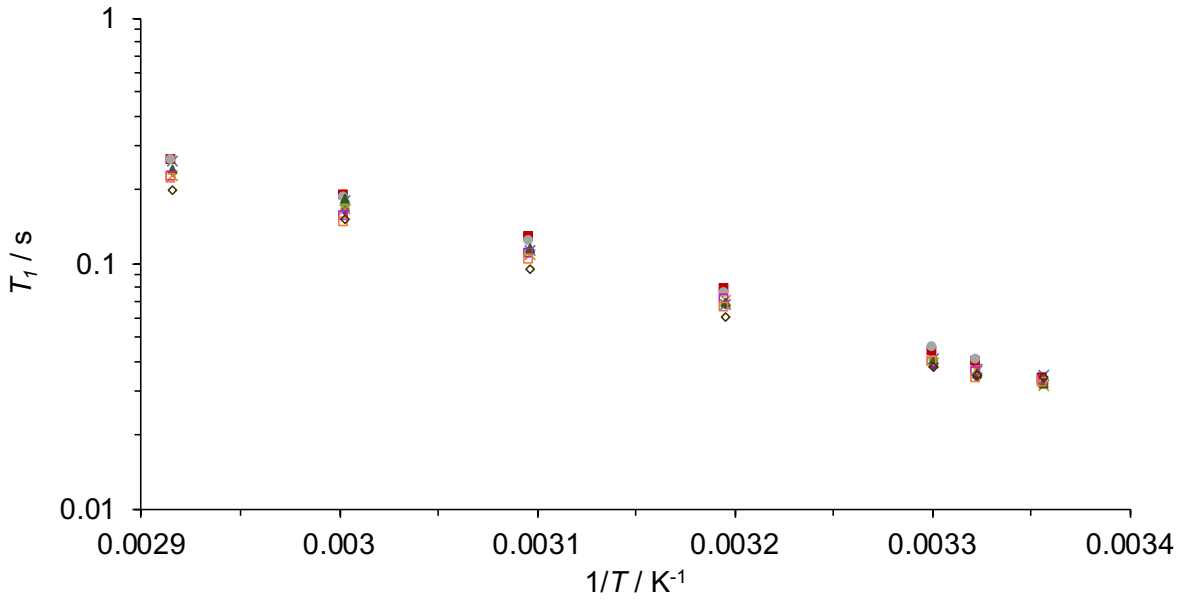

Figure 3.9. Logarithmic plot of relaxation time (T_1) as a function of the reciprocal temperature for *V*-cell/BmimAc solutions: 0 wt% (cross, blue); 0.1 wt% (closed triangle, light green); 0.2 wt% (closed square, red); 0.3 wt% (closed circle, light grey); 0.5 wt% (closed diamond, purple); 0.75 wt% (cross, dark yellow); 1.0 wt% (open triangle, dark green); 2.0 wt% (open square, pink); 3.0 wt% (open square, orange); and 4.0 wt% (open diamond, brown).

3.4.5.4 Stokes-Einstein-Debye Analysis of *V*-Cell/BmimAc Solutions

The Stokes-Einstein equation can be extended to compare the rotational correlation time, τ_{rot}, of a diffusing particle in a viscous medium, as described by Green *et al.* (Green et al., (2017)), using the Stokes-Einstein-Debye equation:

Equation 3.12.
$$\tau_{rot} = \frac{4}{3}\pi r_H^3 f' \frac{\eta}{k_B T}$$

where τ_{rot} gives the rotational correlation time and f' is a correction factor, similar to the term given in Equation 3.10. Equation 3.12 can then be combined with the work of Bloembergen, Purcell, and Pound (BPP) to relate the molecular rotational correlation time and the NMR relaxation times (T_1), in the high-temperature limit:

Equation 3.13.
$$\frac{1}{T_1} = \frac{1}{T_2} = 5K\tau_{rot}$$

where K, for spin ½ nuclei, is described as follows:

Equation 3.14.
$$K = \frac{3}{10}\gamma^4\hbar^2\left(\frac{\mu_0}{4\pi}\right)^2\frac{1}{r_{eff}^6}$$

where γ is the gyromagnetic ratio for protons, $\hbar$ is reduced Planck's constant, μ_0 is the permeability of free space, and r_{eff} is an effective inter proton distance.

The two protons are assumed to be at a fixed distance and interacting via their magnetic dipolar fields. In this case, it is also assumed that $T_1 = T_2$ or, in other words, that rotational motion dominated the NMR relaxation. This is a reasonable assumption when working at a resonance frequency of 10 MHz and within the high-temperature limit but may breakdown at frequencies below this (Hall et al., (2012)).

Combining Equation 3.12 and Equation 3.13 gives the following relationship between T_1 and the viscosity (Hall et al., (2012)):

Equation 3.15.

$$\frac{1}{T_1} = \left(\frac{20\pi}{3} K r_H{}^3 f'\right)\frac{\eta}{k_B T}$$

A value for *f'* can be determined for each concentration of *V*-cell/BmimAc from the gradient of Stokes-Einstein-Debye plots ($1/T_1$ vs. η/T). As reported previously, an average value of r_H = 2.64 Å was used, and an estimation of r_{eff} = 2.59 x 10^{-10} m was made (taking the molecular weight of BmimAc as 198.26 g mol^{-1}, the density as 1.055 g cm^{-3}, and the number of protons per molecule as 18 and assuming that protons are on a cubic lattice).

Figure 3.10a gives values of T_1 measured at a frequency of 10 MHz plotted as a function of T/η for 0-4 wt% *V*-cell/BmimAc, with straight-line fits given by the dashed lines. Once again, a linear dependence (as displayed in Figure 3.10a) was observed, and the cellulose concentration evidently has a greater effect on the macroscopic than the microscopic properties, indicated by an increase in the gradient of T_1 against T/η, with cellulose concentration. Therefore, the Stokes-Einstein-Debye relationship also breaks down as the polymer concentration increases.

Figure 3.10b shows ln(*f'*) as a function of cellulose concentration, obtained from the gradient of straight-line fits from Equation 3.15. As with the diffusion, *f'* tends towards zero on an increase in cellulose concentration, revealing a far stronger dependence of macroscopic viscosity on cellulose concentration to that of the microviscosity. Since we are expecting to probe tumbling of ions at 10 MHz, it can be said that the rotational motion has a very similar dependence on concentration as the translational motion probed in the section given above, using the NMR dispersion curve. It is difficult to locate both c^* and c_e from Figure 3.10b, again indicating that the effect of entanglements is greatly reduced at the microscopic level.

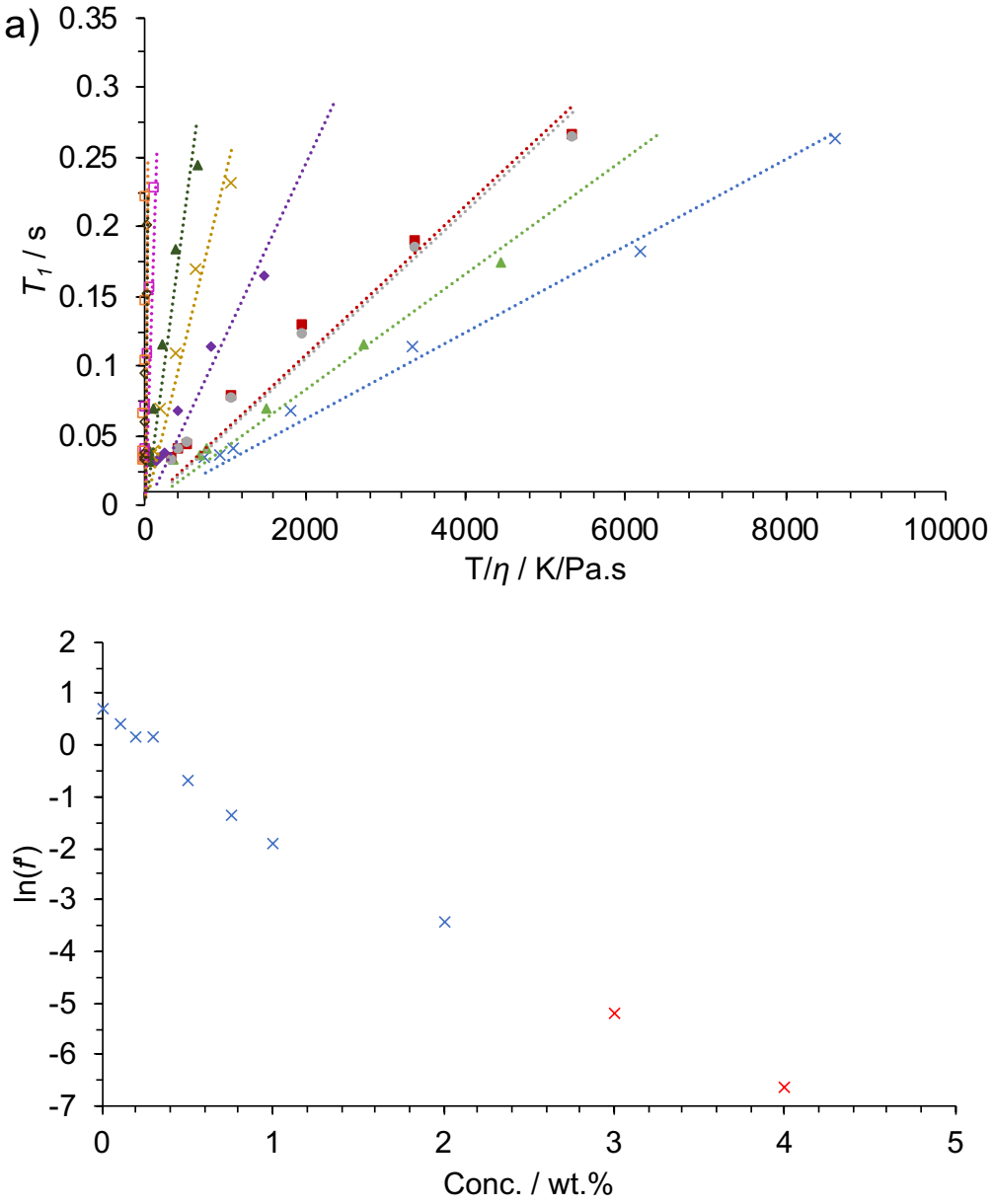

Figure 3.10. a) Spin-lattice relaxation time (T_1) as a function of temperature over zero-shear rate viscosity (T/η_0) as determined by low-field NMR (10 MHz) and rheology, respectively: 0 wt% (cross, blue); 0.1 wt% (closed triangle, light green); 0.2 wt% (closed square, red); 0.3 wt% (closed circle, light grey); 0.5 wt% (closed diamond, purple); 0.75 wt% (cross, dark yellow); 1.0 wt% (open triangle, dark green); 2.0 wt% (open square, pink); 3.0 wt% (open square, orange); and 4.0 wt% (open diamond, brown). The dashed lines give linear fits, as in Equation 3.15; b) correction factor (*f'*) shown as a function of cellulose concentration, as determined from Equation 3.15. Data for 3.0 and 4.0 wt% *V*-cell/BmimAc are shown in red, due to the higher water content in samples. The remarkable similarity between Figure 3.10b and Figure 3.8b indicates that the same microviscosity is determining both the translational and rotational motions of the ions.

3.4.5.5 Comparing the Activation Energies

Finally, in order to compare the results from self-diffusion, relaxometry, and rheological analysis, activation energies were calculated using the following Arrhenius-type equations:

Equation 3.16. $$\boldsymbol{lnD = lnD_0 - \frac{E_{a,D}}{RT}}$$

Equation 3.17. $$\boldsymbol{lnT_1 = lnT_{1,0} - \frac{E_{a,T_1}}{RT}}$$

where D_0 and $T_{1,0}$ represent pre-exponential factors and $E_{a,D}$ and $E_{a,T1}$ represent the activation energies of diffusion and rotation, respectively. As with $E_{a,\eta}$, the gradient from linear fits of ln$D$ or lnT_1 versus inverse temperature was used to determine the activation energies for each process. $E_{a,D}$ and $E_{a,T1}$ were both within the range of 30 to 40 kJ mol^{-1}, which is about 10 kJ mol^{-1} lower than activation energies reported for MCC/EmimAc solutions (Lovell et al., (2010)). E_a values from viscosity, self-diffusion, and relaxation are compared in Figure 3.11, where it is clear that $E_{a,\eta}$ displays by far the greatest cellulose concentration dependence. This is in agreement with the Stokes-Einstein analysis, where the microviscosity was found to be less affected by concentration compared to the macroscopic viscosity. $E_{a,D}$ (self-diffusion) and $E_{a,\eta}$ (viscosity) values obtained for pure BmimAc differed by ca. 10 kJ mol^{-1}, whereas they were reported to be the same for pure EmimAc (Lovell et al., (2010)), which could again be attributed to more significant cluster formation in BmimAc (Figure 3.1).

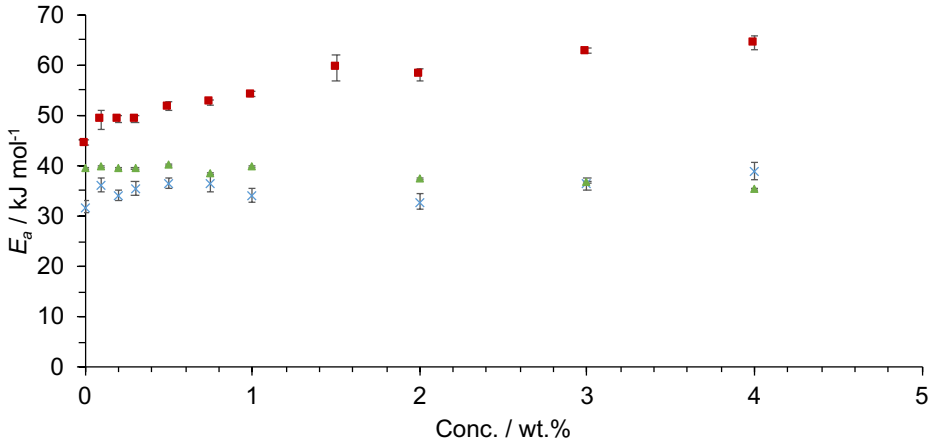

Figure 3.11. Activation energies for flow ($E_{a,\eta}$), translational ($E_{a,D}$), and rotational ($E_{a,T1}$) motion as determined from the viscosities (rheology), self-diffusion coefficients (FFC NMR), and relaxation times (low-field NMR, 10 MHz), respectively, as a function of cellulose concentration: $E_{a,\eta}$ = red square; $E_{a,D}$ = blue cross; and $E_{a,T1}$ = green triangle. Error bars were calculated based on the fit to Equation 3.6, Equation 3.16, and Equation 3.17, therefore giving the uncertainty in determining the gradient and subsequently $E_{a,\eta}$, $E_{a,D}$, and $E_{a,T1}$ respectively.

3.5 Conclusions

Cellulose/BmimAc solutions with two different types of cellulose have been studied using rheology, where cellulose *DP* was found to have an effect on the macroscopic solution properties, c^*, c_e, and $[\eta]$. The commercial cellulose *V*-cell (estimated $DP \simeq 730\text{-}830$) began to entangle at a much lower concentration compared to *A*-cell ($DP = 180$). Furthermore, $[\eta]$ of *V*-cell was approximately three times the value of *A*-cell, consistent with the larger *DP* and indicating a larger effective size of the polymer in solution. Interestingly, *A*-cell/BmimAc solutions displayed a very similar $[\eta]$ value to that of *A*-cell/EmimAc solutions (Sescousse et al., (2010)); however *V*-cell gave a much lower $[\eta]$ value when compared to cellulose of a similar *DP* in EmimAc (Haward et al., (2012)). This suggests that the IL cation has an effect on the dissolution of the cellulose and therefore may affect the macroscopic properties of the cellulose solutions.

The microscopic properties of *V*-cell/BmimAc solutions were then studied using FFC NMR and low-field relaxometry. Both D and T_1 were found to decrease with increasing cellulose concentration, corresponding to both the increase observed in viscosity and an increase in the number of interactions between the solvent molecules and cellulose. Both of these factors result in a decrease in ion mobility as more polymer is added to the solution. Rheology and NMR could be directly compared using Stokes-Einstein and Stokes-Einstein-Debye analyses, where it was found that cellulose concentration has a much greater effect on the macroscopic viscosity compared to that on the microviscosity. This can be attributed to polymer entanglements, which affect much less significantly the microviscosity of cellulose/BmimAc solutions and therefore the short-range interactions, in agreement with work previously published on *A*-cell/EmimAc solutions (Ries et al., (2018)). Finally, an Arrhenius approach was used to obtain E_a values from rheological, FFC NMR, and low-field relaxometry analysis, corresponding to the respective energy barriers for flow, diffusional, and rotational motion. Consistent with the failure of the Stokes-Einstein relationship at higher cellulose concentrations, $E_{a,\eta}$ was found to be greater than both $E_{a,D}$ and $E_{a,T1}$ at all cellulose concentrations and displayed by far the greatest concentration dependence. This indicates that the energy barrier for flow (a bulk solution property) is affected much more significantly by polymer concentration than the energy barriers for rotation and diffusion (microscopic solution properties). This study provides further insights into the interactions occurring on a macroscopic and local level in cellulose-IL solutions, which is crucial to understand the properties of cellulose materials coagulated from cellulose-IL solutions.

3.6 References

Antony, J.H., Dölle, A., Mertens, D., Wasserscheid, P., Carper, W.R. and Wahlbeck, P.G. (2005). 13C NMR relaxation rates in the ionic liquid 1-methyl-3-nonylimidazolium hxafluorophosphate. *Journal of Physical Chemistry A*. *109*(30), 6676–6682.

Behra, J.S., Mattsson, J., Cayre, O.J., Robles, E.S.J., Tang, H. and Hunter, T.N. (2019). Characterization of Sodium Carboxymethyl Cellulose Aqueous Solutions to Support Complex Product Formulation: A Rheology and Light Scattering Study. *ACS Applied Polymer Materials*. *1*(3), 344–358.

Brehm, M., Radicke, J., Pulst, M., Shaabani, F., Sebastiani, D. and Kressler, J. (2020). Dissolving cellulose in 1,2,3-triazolium-and imidazolium-based ionic liquids with aromatic anions. *Molecules*. *25*(15), 1–20.

Cha, S., Ao, M., Sung, W., Moon, B., Ahlström, B., Johansson, P., Ouchi, Y. and Kim, D. (2014). Structures of ionic liquid-water mixtures investigated by IR and NMR spectroscopy. *Physical Chemistry Chemical Physics*. *16*(20), 9591–9601.

Chen, S., Zhang, S., Liu, X., Wang, J., Wang, J., Dong, K., Sun, J. and Xu, B. (2014). Ionic liquid clusters: Structure, formation mechanism, and effect on the behavior of ionic liquids. *Physical Chemistry Chemical Physics*. *16*(13), 5893–5906.

Chen, X., Zhang, Y., Wang, H., Wang, S.-W., Liang, S. and Colby, R.H. (2011). Solution rheology of cellulose in 1-butyl-3-methyl imidazolium chloride. *Journal of Rheology*. *55*(3), 485–494.

Chua, E.T., Brunner, M., Atkin, R., Eltanahy, E., Thomas-Hall, S.R. and Schenk, P.M. (2019). The Ionic Liquid Cholinium Arginate Is an Efficient Solvent for Extracting High-Value Nannochloropsis sp. Lipids. *ACS Sustainable Chemistry and Engineering*. *7*(2), 2538–2544.

Colby, R.H. (2010). Structure and linear viscoelasticity of flexible polymer solutions: Comparison of polyelectrolyte and neutral polymer solutions. *Rheologica Acta*. *49*(5), 425–442.

Cross, M.M. (1965). Rheology of non-Newtonian fluids: A new flow equation for pseudoplastic systems. *Journal of Colloid Science*. *20*(5), 417–437.

Cussler, E.L. (1984). *Diffusion: Mass Transfer in Fluid Systems* First Edit. New York: Cambridge University Press, .

Fendt, S., Padmanabhan, S., Blanch, H.W. and Prausnitz, J.M. (2011). Viscosities of acetate or chloride-based ionic liquids and some of their mixtures with water or other common solvents. *Journal of Chemical and Engineering Data*. *56*(1), 31–34.

Freed, J.H. (1978). Dynamic effects of pair correlation functions on spin relaxation by translational diffusion in liquids. II. Finite jumps and independent T 1 processes. *The Journal of Chemical Physics*. *68*(9), 4034–4037.

Gentile, L. and Olsson, U. (2016). Cellulose–solvent interactions from self-diffusion NMR. *Cellulose*. *23*(4), 2753–2758.

Gericke, M., Schlufter, K., Liebert, T., Heinze, T. and Budtova, T. (2009). Rheological properties of cellulose/ionic liquid solutions: From dilute to concentrated states. *Biomacromolecules*. *10*(5), 1188–1194.

Green, S.M., Ries, M.E., Moffat, J. and Budtova, T. (2017). NMR and Rheological Study of Anion Size Influence on the Properties of Two Imidazolium-based Ionic Liquids. *Scientific Reports*. *7*(1), 1–12.

Hall, C.A., Le, K.A., Rudaz, C., Radhi, A., Lovell, C.S., Damion, R.A., Budtova, T. and Ries, M.E. (2012). Macroscopic and microscopic study of 1-Ethyl-3-methyl-imidazolium acetate-water mixtures. *Journal of Physical Chemistry B*. *116*(42), 12810–12818.

Hauru, L.K.J., Hummel, M., King, A.W.T., Kilpeläinen, I. and Sixta, H. (2012). Role of solvent parameters in the regeneration of cellulose from ionic liquid solutions. *Biomacromolecules*. *13*(9), 2896–2905.

Haward, S.J., Sharma, V., Butts, C.P., McKinley, G.H. and Rahatekar, S.S. (2012). Shear and extensional rheology of cellulose/ionic liquid solutions. *Biomacromolecules*. *13*(5), 1688–1699.

Hermanutz, F., Gähr, F., Uerdingen, E., Meister, F. and Kosan, B. (2008). New developments in dissolving and processing of cellulose in ionic liquids. *Macromolecular Symposia*. *262*(1), 23–27.

Holz, M. and Patil, K.J. (1991). Cation-Cation Association of Tetramethylammonium Ions in Aqueous Mixed Electrolyte Solutions. *Berichte der Bunsengesellschaft für Physikalische Chemie*. *95*(2), 107–113.

Horinaka, J. ichi, Chen, K. and Takigawa, T. (2018). Entanglement properties of carboxymethyl cellulose and related polysaccharides. *Rheologica Acta*. *57*(1), 51–56.

Kaszyńska, J., Rachocki, A., Bielejewski, M. and Tritt-Goc, J. (2017). Influence of cellulose gel matrix on BMIMCl ionic liquid dynamics and conductivity. *Cellulose*. *24*(4), 1641–1655.

Köddermann, T., Ludwig, R. and Paschek, D. (2008). On the validity of Stokes-Einstein and Stokes-Einstein-Debye relations in ionic liquids and ionic-liquid mixtures. *ChemPhysChem*. *9*(13), 1851–1858.

Kosan, B., Michels, C. and Meister, F. (2008). Dissolution and forming of cellulose with ionic liquids. *Cellulose*. *15*(1), 59–66.

Kraemer, E.O. and Lansing, W.D. (1935). The molecular weights of cellulose and cellulose derivatives. *Journal of Physical Chemistry*. *39*(1), 153–168.

Kruk, D., Meier, R., Rachocki, A., Korpała, A., Singh, R.K. and Rössler, E.A. (2014). Determining diffusion coefficients of ionic liquids by means of field cycling nuclear magnetic resonance relaxometry. *Journal of Chemical Physics*. *140*(24), 244509.

Kruk, D., Meier, R. and Rössler, E.A. (2012). Nuclear magnetic resonance relaxometry as a method of measuring translational diffusion coefficients in liquids. *Physical Review E - Statistical, Nonlinear, and Soft Matter Physics*. *85*(2), 1–5.

Kuang, Q.L., Zhao, J.C., Niu, Y.H., Zhang, J. and Wang, Z.G. (2008). Celluloses in an ionic liquid: The rheological properties of the solutions spanning the dilute and semidilute regimes. *Journal of Physical Chemistry B*. *112*(33), 10234–10240.

Kulicke, W.-M. and Kniewske, R. (1984). The viscosity dependence on concentration, molecular weight and shear rate of xanthan solutions. *Rheologica Acta*. *23*, 75–83.

Lefroy, K.S., Murray, B.S. and Ries, M.E. (2021). Advances in the use of microgels as emulsion stabilisers and as a strategy for cellulose functionalisation. *Cellulose*. *28*, 647–670.

Lefroy, K.S., Murray, B.S., Ries, M.E. and Curwen, T.D. (2021). A natural, cellulose-based microgel for water-in-oil emulsions. *Food Hydrocolloids*. *113*, 106408.

Lindman, B., Karlström, G. and Stigsson, L. (2010). On the mechanism of dissolution of cellulose. *Journal of Molecular Liquids*. *156*(1), 76–81.

Lopez, C.G., Voleske, L. and Richtering, W. (2020). Scaling laws of entangled polysaccharides. *Carbohydrate Polymers*. *234*, 115886.

Lovell, C.S., Walker, A., Damion, R.A., Radhi, A., Tanner, S.F., Budtova, T. and Ries, M.E. (2010). Influence of cellulose on ion diffusivity in 1-ethyl-3-methyl-imidazolium acetate cellulose solutions. *Biomacromolecules*. *11*, 2927–2935.

Lu, F., Song, J., Cheng, B.W., Ji, X.J. and Wang, L.J. (2013). Viscoelasticity and rheology in the regimes from dilute to concentrated in cellulose 1-ethyl-3-methylimidazolium acetate solutions. *Cellulose*. *20*(3), 1343–1352.

Lu, F., Wang, L., Zhang, C., Cheng, B., Liu, R. and Huang, Y. (2015). Influence of temperature on the solution rheology of cellulose in 1-ethyl-3-methylimidazolium chloride/dimethyl sulfoxide. *Cellulose*. *22*(5), 3077–3087.

Lue, A., Liu, Y., Zhang, L. and Potthas, A. (2011). Light scattering study on the dynamic behaviour of cellulose inclusion complex in LiOH/urea aqueous solution. *Polymer*. *52*, 3857–3864.

Marks, C., Mitsos, A. and Viell, J. (2019). Change of C(2)-Hydrogen–Deuterium Exchange in Mixtures of EMIMAc. *Journal of Solution Chemistry*. *48*(8–9), 1188–1205.

Mclaughlin, E. (1959). Viscosity and self-diffusion. *Transactions of the Faraday Society*. *55*, 28–38.

Müller, K.J. and Hertz, H.G. (1996). A parameter as an indicator for water-water association in solutions of strong electrolytes. *Journal of Physical Chemistry*. *100*(4), 1256–1265.

Napso, S., Rein, D.M., Khalfin, R., Kleinerman, O. and Cohen, Y. (2016). Cellulose gel dispersion: From pure hydrogel suspensions to encapsulated oil-in-water emulsions. *Colloids and Surfaces B: Biointerfaces*. *137*, 70–76.

Ordikhani Seyedlar, A., Stapf, S. and Mattea, C. (2015). Dynamics of the

ionic liquid 1-butyl-3-methylimidazolium bis(trifluoromethylsulphonyl)imide studied by nuclear magnetic resonance dispersion and diffusion. *Physical Chemistry Chemical Physics*. *17*(3), 1653–1659.

Pinkert, A., Marsh, K.N., Pang, S. and Staiger, M.P. (2009). Ionic liquids and their interaction with cellulose. *Chemical Reviews*. *109*(12), 6712–6728.

Del Pópolo, M.G. and Voth, G.A. (2004). On the structure and dynamics of ionic liquids. *Journal of Physical Chemistry B*. *108*(5), 1744–1752.

Powell, R.E., Roseveare, W.E. and Eyring, H. (1941). Diffusion, Thermal Conductivity, and Viscous Flow of Liquids. *Industrial & Engineering Chemistry*. *33*(4), 430–435.

Rachocki, A., Andrzejewska, E., Dembna, A. and Tritt-Goc, J. (2015). Translational dynamics of ionic liquid imidazolium cations at solid/liquid interface in gel polymer electrolyte. *European Polymer Journal*. *71*, 210–220.

Rachocki, A. and Tritt-Goc, J. (2014). Novel application of NMR relaxometry in studies of diffusion in virgin rape oil. *Food Chemistry*. *152*, 94–99.

Radhi, A., Le, K.A., Ries, M.E. and Budtova, T. (2015). Macroscopic and microscopic study of 1-ethyl-3-methyl-imidazolium acetate-DMSO mixtures. *Journal of Physical Chemistry B*. *119*(4), 1633–1640.

Remsing, R.C., Swatloski, R.P., Rogers, R.D. and Moyna, G. (2006). Mechanism of cellulose dissolution in the ionic liquid 1-n-butyl-3-methylimidazolium chloride: A 13C and 35/37Cl NMR relaxation study on model systems. *Chemical Communications*. *12*, 1271–1273.

Ren, Y., Ellis, P.R., Ross-Murphy, S.B., Wang, Q. and Wood, P.J. (2003). Dilute and semi-dilute solution properties of (1 → 3), (1 → 4)-β-D-glucan, the endosperm cell wall polysaccharide of oats (Avena sativa L.). *Carbohydrate Polymers*. *53*(4), 401–408.

Ries, M.E., Radhi, A., Green, S.M., Moffat, J. and Budtova, T. (2018). Microscopic and Macroscopic Properties of Carbohydrate Solutions in the Ionic Liquid 1-Ethyl-3-methyl-imidazolium Acetate. *Journal of Physical Chemistry B*. *122*(37), 8763–8771.

El Seoud, O.A., Koschella, A., Fidale, L.C., Dorn, S. and Heinze, T. (2007). Applications of ionic liquids in carbohydrate chemistry: A window of opportunities. *Biomacromolecules*. *8*(9), 2629–2647.

Sescousse, R., Le, K.A., Ries, M.E. and Budtova, T. (2010). Viscosity of cellulose-imidazolium-based ionic liquid solutions. *Journal of Physical Chemistry B*. *114*(21), 7222–7228.

Takada, A. and Kadokawa, J.I. (2015). Fabrication and characterization of polysaccharide ion gels with ionic liquids and their further conversion into value-added sustainable materials. *Biomolecules*. *5*(1), 244–262.

Tan, X., Li, X., Chen, L. and Xie, F. (2016). Solubility of starch and microcrystalline cellulose in 1-ethyl-3-methylimidazolium acetate ionic liquid and solution rheological properties. *Physical Chemistry Chemical Physics*. *18*(39), 27584–27593.

Tang, S., Baker, G.A., Ravula, S., Jones, J.E. and Zhao, H. (2012). PEG-functionalized ionic liquids for cellulose dissolution and saccharification. *Green Chemistry*. *14*(10), 2922–2932.

Tokuda, H., Hayamizu, K., Ishii, K., Susan, M.A.B.H. and Watanabe, M. (2004). Physicochemical properties and structures of room temperature ionic liquids. 1. Variation of anionic species. *Journal of Physical Chemistry B*. *108*(42), 16593–16600.

Verma, C., Mishra, A., Chauhan, S., Verma, P., Srivastava, V., Quraishi, M.A. and Ebenso, E.E. (2019). Dissolution of cellulose in ionic liquids and their mixed cosolvents: A review. *Sustainable Chemistry and Pharmacy*. *13*, 100162.

Vitz, J., Erdmenger, T., Haensch, C. and Schubert, U.S. (2009). Extended dissolution studies of cellulose in imidazolium based ionic liquids. *Green Chemistry*. *11*(3), 417–42.

Walden, P. (1914). Molecular magnitude and electrical conductivity of some fused salts. *Bulletin de l'Academie Imperiale des Sciences de St. Petersbourg*. *8*(6), 405–422.

Wang, Q., Yang, Y., Chen, X. and Shao, Z. (2012). Investigation of rheological properties and conformation of silk fibroin in the solution of AmimCl. *Biomacromolecules*. *13*(6), 1875–1881.

Wendler, F., Todi, L.N. and Meister, F. (2012). Thermostability of imidazolium ionic liquids as direct solvents for cellulose. *Thermochimica Acta*. *528*, 76–84.

Xu, A., Wang, J. and Wang, H. (2010). Effects of anionic structure and lithium salts addition on the dissolution of cellulose in 1-butyl-3-methylimidazolium-based ionic liquid solvent systems. *Green Chemistry*. *12*(2), 268–27.

Xu, S., Zhang, J., He, A., Li, J., Zhang, H. and Han, C.C. (2008). Electrospinning of native cellulose from nonvolatile solvent system. *Polymer*. *49*(12), 2911–2917.

Youngs, T.G.A., Holbrey, J.D., Mullan, C.L., Norman, S.E., Lagunas, M.C., D'Agostino, C., Mantle, M.D., Gladden, L.F., Bowron, D.T. and Hardacre, C. (2011). Neutron diffraction, NMR and molecular dynamics study of glucose dissolved in the ionic liquid 1-ethyl-3-methylimidazolium acetate. *Chemical Science*. *2*(8), 1594–1605.

Zhang, J., Xu, L., Yu, J., Wu, J., Zhang, X., He, J. and Zhang, J. (2016). Understanding cellulose dissolution: effect of the cation and anion structure of ionic liquids on the solubility of cellulose. *Science China Chemistry*. *59*(11), 1421–1429.

Zhang, J., Zhang, H., Wu, J., Zhang, J., He, J. and Xiang, J. (2010). NMR spectroscopic studies of cellobiose solvation in EmimAc aimed to understand the dissolution mechanism of cellulose in ionic liquids. *Physical Chemistry Chemical Physics*. *12*, 1941–1947.

Zhao, Y., Gao, S., Wang, J. and Tang, J. (2008). Aggregation of ionic liquids [Cnmim]Br (n = 4, 6, 8, 10, 12) in D2O: A NMR study. *Journal of Physical Chemistry B*. *112*(7), 2031–2039.

Chapter 4
A natural, cellulose-based microgel for water-in-oil emulsions[3]

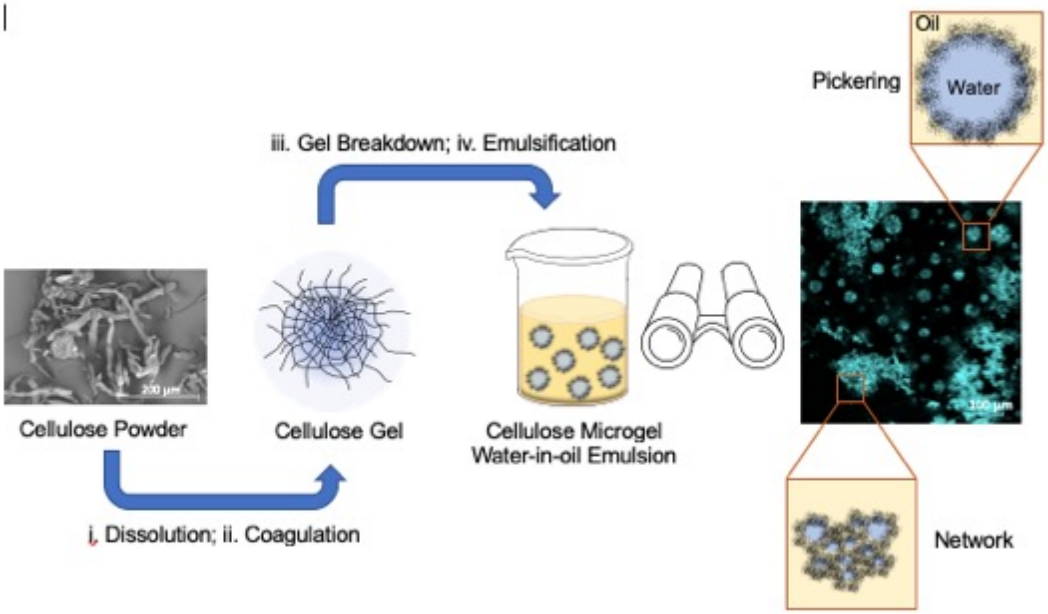

4.1 Abstract

Non-derivatised cellulose is generally assumed to have poor surface activity and therefore be unsuitable as a water in oil (W/O) emulsifier. In this work, a “natural” cellulose microgel (CMG) is fabricated via a top-down approach and used to stabilise W/O emulsions, without employing chemical modification. The cellulose is coagulated from an ionic liquid through a solvent-exchange process, in the presence and absence of added sunflower oil, in order to tune the cellulose morphology and properties. Detailed characterization of the nature of these microgels and the effect of the solvent change sequence on their emulsifying properties was investigated. In the presence of oil, Fourier transform infrared (FTIR) spectroscopy confirmed the retention of oil in the coagulum during regeneration and the resultant CMGs were more easily dispersed in oil than water, suggesting the fabrication of a “hydrophobic” microgel. Confocal microscopy confirmed the adsorption of CMGs to the water-oil interface and W/O emulsions of up to 20 vol% water displayed good stability over at least 1 month. This study therefore describes a “novel” route to W/O stabilisation using a natural emulsifier, which could be then used as a method of reducing fat and sugar in food products.

---

[3]Published as: Lefroy, K.S., Murray, B.S., Ries, M.E. and Curwen, T.D. (2021). A natural, cellulose-based microgel for water-in-oil emulsions. *Food Hydrocolloids*. *113*, 106408. DOI: 10.1016/j.foodhyd.2020.106408

4.2 Introduction

The dramatic rise in obesity levels over the last few decades has been linked to the increased availability of high-energy foods, as well as genetic susceptibility and reduced physical activity (Kopelman, (2000)). Reducing the calories in food products is not only demanded by consumers but is also an effective method for lessening the impact of obesity and related health problems (Borreani et al., (2020)). The World Health Organization (WHO) recommends reformulation of foods in order to reduce *trans*-fat, fat and free-sugar content, with the goal of eventually eliminating *trans*-fats completely (Rogers et al., (2009)).

High-calorie confectionary products such as creams, fillings and spreads are “rich” in texture and taste and highly desired by consumers for the feelings of luxury and indulgency they impart, but reducing the fat content without affecting product quality is a huge challenge (Borreani et al., (2020)). Within the food industry, water is an attractive replacement for fat and sugar. Forming a water-in-oil (W/O) emulsion and thus reducing the overall fat content, as opposed to using a bulking agent, allows the ‘smoothness’ and ‘creaminess’ of products to be maintained (Mitsou et al., (2016); Marchetti et al., (2017)). Furthermore, it has been shown that perceived ‘creaminess’ is directly correlated to emulsion viscosity and therefore controlling bulk rheological properties of a system allows manipulation of its sensory attributes, regardless of droplet size and water-volume fraction (Dickinson, (2011)).

W/O emulsions are already used extensively in the food, pharmaceutical, agricultural and cosmetic industries in order to deliver and protect functional compounds, modify sensory properties and improve shelf-life, amongst other things (McClements, (2004); Neethirajan et al., (2011); Albert et al., (2019); Martinez et al., (2019); Azmi et al., (2019)). The usual way of preparation is to disperse a hydrophobic emulsifier in the oil phase, followed by addition of water under mechanical agitation to yield an emulsion of stabilised water droplets.

Since for W/O emulsions the emulsifier must be dispersible in the continuous oil phase, generally non-ionic, (i.e. uncharged) low hydrophilic-lipophilic balance (HLB) surfactants are utilized, so that steric stabilization might be thought to be the dominant mechanism (Bastida-Rodríguez, (2013)). However, charges and dipoles may still be present at the interface, that result in significant long-range electrostatic repulsion between droplets across the low dielectric constant oil phase. This is still likely with particulate stabilizers, i.e. Pickering emulsions, where hydrophobic particles may still carry a range

of ionizable groups or adsorbed or trapped ionic species. Particles ranging in size from a few 10s of nm to several μm have proved effective as Pickering emulsifiers. Unlike surfactants, true Pickering stabilizers are insoluble in both oil and water, and are characterised by their wettability or contact angle (Wang and Wang, (2016); Murray, (2019b)). Particles have numerous advantages over more traditional surfactants used in foods, for example the superior stability against coalescence they impart at much lower concentrations, due to their extremely high affinity for the interface (high energy of desorption) and the large steric barrier they give due to their size (Ghosh and Rousseau, (2011); Dickinson, (2012)). Ideally Pickering stabilizers of W/O emulsions should be 1 μm or less, in order to stabilize droplets that are small enough to avoid flocculation, coalescence and/or rapid sedimentation. Microgels, or microgel particles have been shown to be very effective emulsion stabilizers, acting similarly to classic Pickering stabilizers (Murray, (2019a); Murray, (2019b)).

Particles may play a very important role in future W/O formulations in foods (and other consumer products) because there is a considerable lack of acceptable W/O surfactants available to food manufacturers. To our knowledge, all of those currently approved have a limit on their usage (Murray, (2019b)). For example, polyglycerol polyricinoleate (PGPR) has a maximum level of 4g/kg in dressings, spreadable fats and similar spreadable products, and of 5g/kg in chocolate in Europe (Bastida-Rodríguez, (2013)). Whilst PGPR is considered to have no toxicity and carcinogenicity at these levels, it has been removed from certain chocolate brands due to consumer demand (Wilson and Smith, (1998); Mortensen et al., (2017)) (Fox Business, https://www.foxbusiness.com/features/hersheys-remake-of-the-great-american-chocolate-bar, accessed March 2020). Furthermore, PGPR is conventionally produced via a four-stage chemical process, requiring long reaction times and high operating temperatures (Bastida-Rodríguez, (2013)). The demand for alternative natural emulsifiers which involve simple, non-chemical routes to production is increasing, with emphasis on providing ‘clean-label’ foodstuffs (Ozturk and McClements, (2016)). The use of particles in food products is therefore particularly attractive due to the lower amount of emulsifier required, the fact that they are not produced via chemical synthesis and also that they may provide reduced irritancy to the skin and membranes, since they do not have a typical ‘detergent-like’ structure (Arditty et al., (2003)).

Much recent attention has been turned to the functionalisation of cellulose in its native form without chemical modification. Commonly found in plant cell walls, cellulose is well known for its highly robust structure which arises from a large volume of physical contacts between polysaccharide chains. Both inter- and intramolecular H-bonds form between the glucopyranose rings, reinforcing the highly repetitive crystalline structure. Within the food industry, native cellulose has also begun to emerge as a potential Pickering stabiliser, thickener and reinforcing agent for packaging, for example (Huang et al., (2020)). From an ingredient perspective, cellulose is colourless, odourless and tasteless as well as an important dietary fibre. Incorporation of 'natural' cellulose into a food matrix therefore has the potential to not only significantly reduce the calorie-content, but to also improve its nutritional make-up (Gómez and Martinez, (2018)).

Large scale cellulose solubilisation is traditionally achieved using the Viscose process, which has numerous disadvantages such as complex reaction conditions, slow reaction times and harmful side products (Zhang et al., (2017); Paunonen et al., (2019)). Such methods result in grafting of groups onto the cellulose chains during dissolution, producing so-called derivatised cellulose. This charges the surface of the cellulose and affects its swelling properties as well as its ability to act as an emulsifier, since electrostatic repulsion between particles leads to a higher barrier for interfacial adsorption (Stana-Kleinschek et al., (2002); Bertsch et al., (2019)). Alternative non-derivatising solvent systems such as NaOH/aqueous solutions (Qi et al., (2011)), *N,N*-dimethylacetamide (DMAc)/lithium chloride (LiCl)(Sadeghifar et al., (2019)) and ionic liquids (ILs) (Zhang et al., (2017)) have been developed on a small scale, with the aim of producing non-grafted regenerated cellulose in an environmentally friendly manner (Cai and Zhang, (2005)). In this particular work, we focus on ILs as cellulose solvents.

Numerous ILs have been reported to dissolve large amounts of cellulose without chemical modification, under mild conditions and with possible recovery and reuse of the solvent afterwards (Verma et al., (2019)). Amongst these, two of the most common solvents employed are 1-ethyl-3-methylimidazolium acetate (EmimAc) and 1-butyl-3-methylimidazolium acetate (BmimAc). More recently, ILs have been prepared from renewable raw materials and may provide even easier handling, as well as being readily bio-degradable and comparatively lower in cost (Ossowicz et al., (2019)). For example, amino-acid ILs based on cholinium have shown impressive rates of

dissolution under mild conditions, even in the presence of significant amounts of water (Chua et al., (2019)).

Once dissolved in an IL, cellulose can be recovered by adding a so-called ‘coagulant’ or ‘anti-solvent,’ such as water, ethanol or *n*-propanol, which is miscible with the IL but not with cellulose (Tan et al., (2019)). Varying the coagulation conditions, as well as type and amount of anti-solvent, yields cellulose in different forms and allows manipulation of its properties (Gupta et al., (2013); Fan et al., (2018); Tan et al., (2019)). Thorough washing of the regenerated cellulose also completely removes any IL, permitting recovery of the IL and anti-solvents and ensuring that the resultant cellulose is pure and safe for consumption.

In theory, any anti-solvent which is miscible in the IL but that does not dissolve cellulose could be used as a coagulant, but thorough washing with water as a final stage is generally the most convenient way to ensure complete removal of IL, since it seems to be the most effective solvent in breaking cellulose-anion H-bonds (Gupta et al., (2013)). The use of a less polar, slow-diffusing anti-solvent coagulant delays the regeneration process, allowing the gel network to form more gradually through a ‘softer’ precipitation (Fink et al., (2001)). Furthermore, ‘coating’ the hydrophobic planes with a non-polar molecule before regeneration could block hydrophobic interactions between cellulose chains, to a certain degree. A combination of these two approaches, firstly ‘coating’ and protecting hydrophobic regions in cellulose and secondly delaying reprecipitation, may increase the hydrophobicity of the regenerated cellulose. Formation of a porous gel network could not only “lock-in” such hydrophobic character, but may also allow interpenetration of phases at an interface, hereby improving its ability to function as an emulsifier (Murray, (2019b)).

In this work, BmimAc was selected as the IL for dissolution of up to 4 wt% cellulose and the bulk macrogels generated by anti-solvent exchange were mechanically broken down to microgel particles as emulsion stabilizers, a so-called “top-down” approach (Murray, (2019a)). To increase the hydrophobicity of the microgels an edible oil was also introduced during the anti-solvent exchange. These novel cellulose microgels were effective W/O emulsifiers – emulsions of up to 20 vol% water were stable for at least 1 month without the addition of any other surface-active agents. This work therefore provides a potentially inexpensive, and possibly “clean-label” route to fat replacement in foods, using renewable resource materials and simple, convenient methodology.

4.3 Materials and Method

4.3.1 Materials

1-Butyl-3-methyl imidazolium (BmimAc) (≥95% purity), ethanol (absolute, 99.8%), Calcofluor White (1 g/L), Nile red and sodium azide were obtained from Sigma Aldrich. 1-Butanol (Acros Organics, 99.5%) was obtained from Fisher Scientific. Cellulose powder (Vitacel L 600-20 and L 00) and High Oleic acid Sunflower Oil (HOSO, density = 0.92 g mL^{-1}) were supplied by Mondelēz International.

4.3.2 Preparation of "non-oily" macrogel

Vitacel cellulose powder (L 600-20 and L 00) was dissolved in BmimAc (1-4 wt%) under stirring at 75ºC, until complete dissolution (2-5 h). The heated cellulose-IL solution was added dropwise through a syringe to water (2:1 v/v water/cellulose-BmimAc), with each drop forming a spherical precipitate (macrogel). The gel-water mixture was stored overnight at room temperature. Water was replaced 3 times every 4-10 h, with filtering of the macrogel in between each solvent-change (nylon membrane filter, 0.45 µm, 45 mm). During the final filtration step, the macrogel was broken down with a spatula and washed repeatedly with deionised water to ensure complete BmimAc removal. (For example, 2 to 3 washing steps are generally able to reduce the BmimAc levels to < 1 ppm, as detected by UV/Vis adsorption – data not shown).

4.3.3 Preparation of "oily" macrogel

Cellulose powder was dissolved in BmimAc as outlined in 4.2.2. HOSO was added directly to the heated solution (2:1 v/v HOSO/cellulose-BmimAc) and stirred using a high-speed blender (Ultra Turrax T 25, IKA, Germany) at room temperature at 25,000 rpm, until complete disappearance of the phase boundary (ca. 5 mins). The HOSO-cellulose-BmimAc mixture was added dropwise through a syringe to 1-butanol (4:1 v/v 1-butanol/HOSO-cellulose-BmimAc), with each drop forming a spherical precipitate (macrogel), as on addition to water in 4.2.2. The gel-solvent mixture was stored overnight at room temperature. Solvent exchange and regeneration of the macrogel was conducted in the following order, using the same volumes of anti-solvent as initially added: 1-butanol, 2 x ethanol; 2 x water, with immersion in each solvent for 4-10 h. The obtained cellulose macrogel was filtered under gravity between each solvent change (nylon membrane filter, 0.45 µm, 45 mm). During the final filtration step, the macrogel was broken down and washed with deionised water, as outlined in 4.2.2.

4.3.4 Preparation of cellulose microgel (CMG) dispersions in water or oil

The non-oily and oily cellulose macrogels were dispersed in water or HOSO respectively, giving non-oily cellulose microgels (CMGs) and oily cellulose microgels (oil-CMGs). Initially, the macrogel was dispersed in the desired medium under high-speed Ultra Turrax stirring (24,000 rpm, 5 min). The dispersions were then passed through a high-pressure homogeniser (Jet Homogeniser, University of Leeds) (Burgaud et al., (1990)) at 300 bar with 3 passes, in order to obtain a finer CMG dispersion, then diluted to give various concentrations of CMG in water or HOSO (0.15 – 2.0 wt%).

4.3.5 Preparation of oil-in-water (O/W) emulsions

Non-oily microgels (CMGs) were briefly tested to see if they had any ability to stabilize O/W emulsions (10 vol%), prepared by adding pure HOSO dropwise to the CMG in water dispersions obtained via 4.2.2 and 4.2.4. Emulsification was carried out for a total of 5 min under high-speed Ultra Turrax stirring, as follows: agitation of the water phase (1 min), addition of the HOSO (2 min) and stirring of the formed emulsion (2 min, all at 25,000 rpm, room temperature). The resulting emulsion was passed through the Jet Homogeniser (300 bar, 3-5 passes) and subjected to a final period of high-speed Ultra Turrax stirring (25,000 rpm, 1 min) to ensure that the two phases were fully emulsified. Sodium azide was added to all of the emulsions to prevent degradation during storage (0.05 wt%).

4.3.6 Preparation of water-in-oil (W/O) emulsions

W/O emulsions (5 to 20 vol% water) were prepared from the dispersions of oil-CMG in HOSO or oil-CMG dispersed in water. For the former, deionised water was added dropwise to the oil-CMG dispersion in HOSO; for the latter the oil-CMG in water dispersions were added dropwise to pure HOSO. In both cases, emulsification was carried out in a total of 5 min under high-speed Ultra Turrax stirring, as follows: agitation of the oil phase (1 min), addition of the deionised water/oil-CMG-water dispersion (2 min) and stirring of the formed emulsion (2 min, all at 25,000 rpm, room temperature). The resulting emulsion was passed through the Jet Homogeniser (300 bar 3-5 passes) and subjected to a final period of high-speed Ultra Turrax stirring (25,000 rpm, 1 min), as in 4.2.5. Sodium azide was added to all of the emulsions to prevent degradation during storage (0.05 wt%).

All emulsions in 4.2.5 and 4.2.6 are described in wt% cellulose relative to the amount of water in the system and emulsions were prepared in terms of their volume ratio, rather than weight ratio. For example, a 10 vol% W/O emulsion

stabilised by “0.2 wt% cellulose” would contain 0.2 g cellulose, 10 g (= 10 mL) of water and 83 g (= 90 mL) of HOSO since the density of HOSO = 0.92 g mL^{-1}.

4.3.7 Characterization of dispersions and emulsions

The particle size distribution (PSD) of the CMG dispersions and emulsions were characterized via a Malvern Mastersizer 3000. The refractive indices of water, cellulose and HOSO were taken as 1.33, 1.47 and 1.46 respectively, and PSDs were calculated based on the Mie theory. Five measurements were taken for each sample and the average of these reported. The mean distribution of particle sizes are displayed in terms of the surface-weighted mean diameter ($d3,2$), as described:

Equation 4.1.
$$(\boldsymbol{d3,2}) = \frac{\Sigma_i n_i {d_i}^3}{\Sigma_i n_i {d_i}^2}$$

and the volume-weighted mean diameter ($d4,3$), as described:

Equation 4.2.
$$(\boldsymbol{d4,3}) = \frac{\Sigma_i n_i {d_i}^4}{\Sigma_i n_i {d_i}^3}$$

where n_i gives the number of droplets; d_i gives the diameter of the particle.

4.3.8 Attenuated total reflection fourier transform infrared (ATR-FTIR) spectroscopy

An Agilent 4500 series FTIR spectrometer equipped with a single reflection attenuated total reflectance (ATR) accessory was used to analyse the changes in the cellulose during its regeneration and the final composition of regenerated macrogels. Each spectrum was recorded over the wavenumber range 500-3500 cm^{-1} with 1640 scans, and the background was re-recorded every four measurements. Samples were placed on the ATR crystal and uniformly spread over the measurement area with an overhead press. Each measurement was conducted three times and an average of these is reported for each sample. The crystal was cleaned between each sample with distilled water and ethanol.

4.3.9 Wide-angle X-ray scattering (WAXS)

Wide Angle X-ray scattering (WAXS) was conducted on a SAXSpace instrument (Anton Paar GmbH, Graz, Austria) equipped with a sealed-tube Cu-anode operating at 40 kV and 50 mA. Cellulose powder was measured in a thin glass capillary tube, whilst regenerated cellulose macrogels were freeze-dried and then pressed between scattering paper into a capillary cell, to a pellet of approximately 1 mm thickness. In all cases, the background was subtracted using the SAXSQuant software and the scattering intensity at q = 0 was set to unity, to obtain the scattered intensity, $I(q)$:

Equation 4.3. $$q = \frac{4\pi}{\lambda} sin\frac{\theta}{2}$$

Where θ = scattering angle and λ = 0.154 nm (X-ray wavelength). Deconvolution of intensity plot was carried out using peak fitting on OriginPro 9.0.

All ATR-FTIR and WAXS analysis was carried out at room temperature.

4.3.10 Scanning Electron Microscopy (SEM)

Scanning Electron Microscopy (SEM) of the cellulose macrogels was carried out using a FEI NanoSEM Nova 450 operating at 3 kV, with a working distance of 5 mm and an Everhart-Thornley detector (ETD). All gels were freeze-dried either straight after water washing or after washing three times with hexane, in order to remove excess oil from the regeneration. Freeze-dried samples were then mounted on an SEM stub with adhesive copper tape and sputter-coated (Cressington 208 HR) with a 2 nm iridium conductive layer.

4.3.11 Optical microscopy and confocal laser scanning microscopy (CLSM)

The microstructure of both CMG dispersions and W/O emulsions were imaged using a light microscope (Nikon, SMZ-2T, Japan) equipped with a digital camera (Leica MC120 HD). Images were processed using the image analysis software ImageJ.

Confocal laser scanning microscopy (CLSM) was carried out using a Zeiss LSM700 inverted microscope (Germany) with a 20 x/0.5 objective lens. Approximately 80 µL of sample was added to a welled slide and a coverslip was placed on top (0.16-0.19 mm thickness), ensuring that no air bubbles were trapped between the sample and coverslip. Calcofluor White was used to stain cellulose, which was added to the sample before confocal analysis (1 g/L, 10% v/v stain:dispersion/emulsion). Nile red (0.4 mg mL^{-1} in DMSO) was added to W/O emulsions in order to stain the oil phase and analyse the shape of the water droplets (1% v/v stain:emulsion). For Calcofluor White, an excitation wavelength of 405 nm was used and emission between 415-470 nm measured. For Nile red, an excitation wavelength of 488 nm was used and emission between 550 and 640 nm measured. Images were processed using the image analysis software Zen.

4.3.12 Creaming stability measurements

3 mL of each emulsion was taken immediately after preparation and stored in a thin tube with a sealed lid, at room temperature. Cream volume ratio was calculated by measuring the height of the emulsion and the height of the cream using a calliper, over a period of time, where:

Equation 4.4. $$\frac{H_2}{H_1} \times 100 = Cream\ Volume\ ratio$$

where H_1 = total volume in the tube and H_2 = bottom layer (water).

4.4 Results and discussion

4.4.1 Emulsions stabilised by "non-oily" CMGs (CMGs)

Although the principal objective was to achieve W/O emulsion stabilization, the more simple procedure of not introducing oil was tested first to see if the CMGs had any significant surface activity at all, by testing their ability to stabilize O/W emulsions. Figure 4.1 gives the size distribution data over time for a 0.5 wt% CMG-stabilised 10 vol% O/W emulsion. A relatively monodisperse PSD was observed for all O/W emulsions stabilised by 0.3-1.0 wt% CMGs. Droplet sizes did not appear to change over time and emulsions remained fairly stable to creaming (data not shown). However, for concentrations below and above this range, flocculated droplets and some much larger droplets were visible (Figure B 1). Furthermore, a relatively large cream layer formed rapidly (within 5 min) after emulsification at CMG concentrations greater than 0.3 wt%, suggesting that the excess CMG does not remain well-dispersed in the continuous phase. As seen in the confocal image (Figure 4.1b), although cellulose is clearly visible at the O/W interface, surface coverage of the oil droplets is fairly sparse. Thus, the regenerated cellulose as CMGs appeared to display some useful hydrophobic properties and therefore surface activity, capable of stabilizing O/W emulsions but to a limited extent. The O/W emulsions seemed to be poorly dispersed and showed tendency to aggregate in the aqueous phase with time, particularly at higher CMG concentrations. This frustrated attempts to prepare stable O/W emulsions with either smaller oil droplets or high volume fractions of oil droplets. In addition, attempts to prepare W/O emulsions with CMGs were fruitless (data not shown): at the ratios of oil to water used (section 4.2.6) no stable water droplets in oil were observed. For these reasons the oil-CMG route was then largely pursued, to try and enhance the hydrophobicity of the microgel particles, for W/O emulsion stabilization.

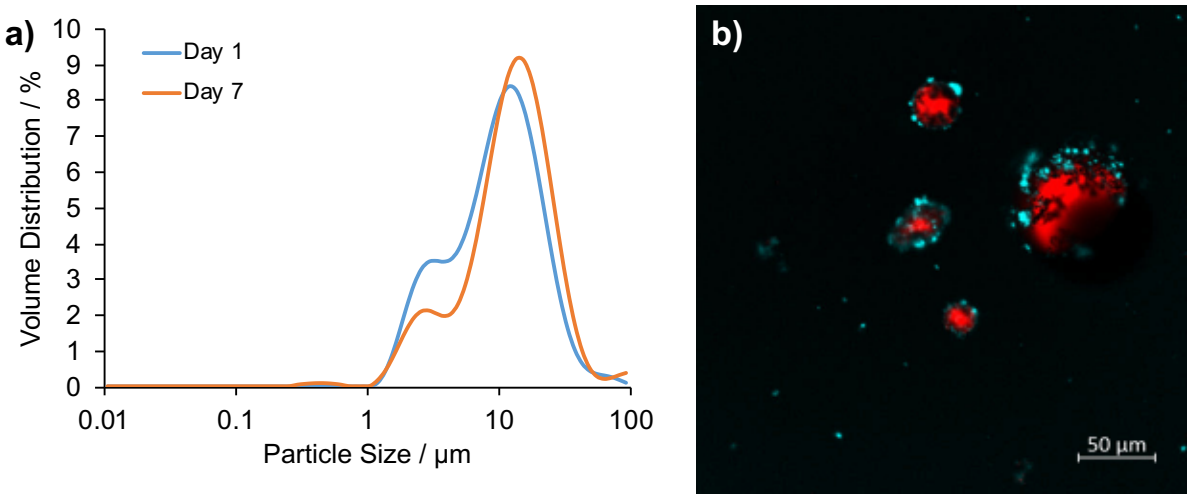

Figure 4.1. a) PSD for 10 vol% O/W emulsion stabilised by 0.5 wt% CMG; b) confocal image of 10 vol% O/W emulsion stabilised by 1.0 wt% CMG. Scale bar = 50 µm.

4.4.2 Composition and structure of regenerated "oily" cellulose macrogels

To fabricate a CMG-based emulsifier suitable for W/O emulsions, oil was introduced into the regeneration process (as outlined in 4.2.3). Figure 4.2 gives the FTIR spectra for the powdered cellulose before any treatment, pure HOSO and regenerated macrogel. Since very similar peaks appear in both the cellulose powder and gel, it can be said that no chemical modification of cellulose has occurred during dissolution and regeneration (Xu et al., (2016); Tan et al., (2019)). However, variation in the crystal structure is apparent due to the shifting of the band at 1433 cm^{-1} in the cellulose powder, which corresponds to CH_2 scissoring, to a lower wavenumber (1425 cm^{-1}) for the gel. The intensity of the peak at 1430 cm^{-1} is often used to quantify the amount of cellulose I, or indeed the crystallinity of the cellulose, which in this case reduces upon regeneration. The shift in wavenumber indicates conversion from cellulose I to a different type of crystalline cellulose and/or amorphous cellulose (Xu et al., (2016); Fryczkowska et al., (2018)). A band at ca. 900 cm^{-1} is seen in both the powdered cellulose and the gel, which can be assigned to C-O stretching in amorphous cellulose. The characteristic broad band corresponding to O-H vibrations in hydrogen bonding is observed between 3000 and 3700 cm^{-1}, with the peak bands at 3335 and 3372 cm^{-1} for cellulose powder and gel, respectively. An increase in wavenumber upon regeneration has been reported elsewhere: this shift signifies the cleavage of H-bonds between cellulose during dissolution, followed by reformation and re-structuring upon re-precipitation (Fryczkowska et al., (2018)). C-*O*-C stretching bands (both the glucopyranose ring and glycosidic bridges) are observed in the region 1160-1060 cm^{-1}. A decrease in the intensity of bands

in this region is observed for the gel, most likely due to reduced order in the regenerated cellulose. Minor differences in the shape of bands are also observed, for example a shoulder is seen at 1099 cm^{-1} in the gel. This indicates a difference in macromolecular structure and, more specifically, changes to the conformation of glucopyranose rings relative to adjacent cellulose chains. Therefore, a change in cellulose inter- and intramolecular H-bonding is clearly seen upon regeneration and therefore a different cellulose structure almost certainly exists in the gel.

Additional peaks at 1747, 2857 and 2924 cm^{-1} are seen in the regenerated gel spectrum due to the presence of HOSO (C=O asymmetric; CH_3 and CH_2 stretching, (Rohman and Che Man, (2012)). Peaks at 1457 and 1378 cm^{-1} in the spectrum for pure HOSO, (corresponding to CH_2 and CH_3 bending respectively), are also identified in the gel. The absence of peaks at 1384 and 1558 cm^{-1} confirms the complete removal of BmimAc during the regeneration and washing (Figure B 2). An additional intense, broad peak at 1653 cm^{-1} appears, which is likely to correspond to the bending mode of water bound to cellulose (Oh et al., (2005)). These observations confirm the presence of both HOSO and water in the regenerated gel, but the absence of IL.

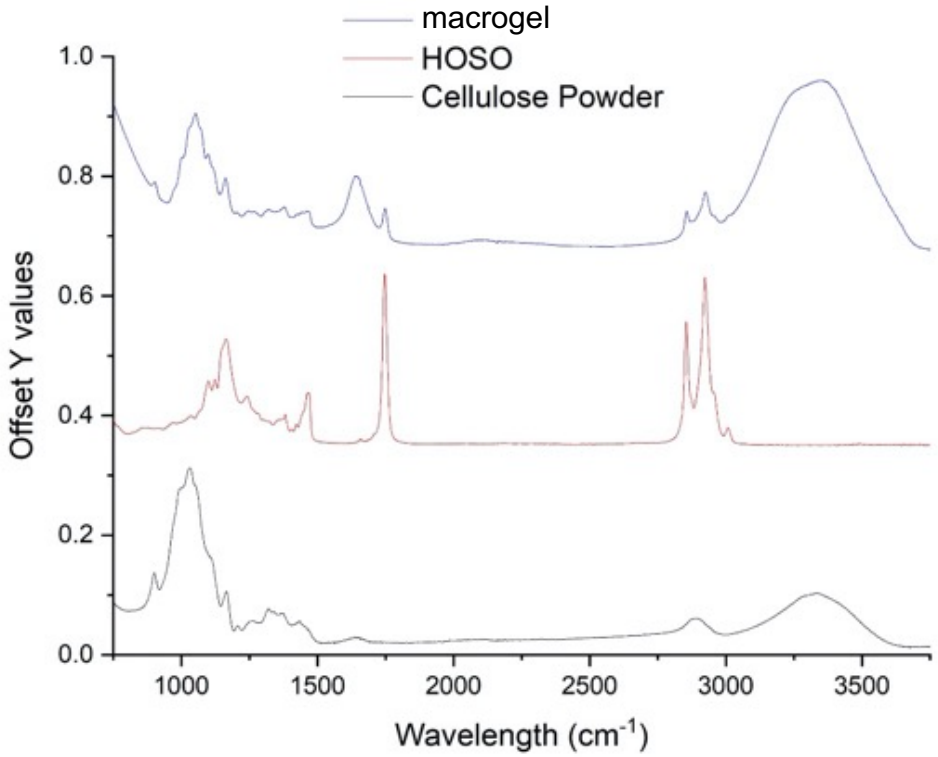

Figure 4.2. ATR-FTIR spectra for cellulose powder (black); HOSO (red) and regenerated gel (blue) plotted with Y offset values versus wavelength, where Y represents intensity of absorbance (a.u.).

The crystal structure of the cellulose powder and regenerated macrogel were analysed using WAXS (Figure 4.3). Peaks corresponding to the $(1\bar{1}0)$, (110) and (200) planes of cellulose I are known to appear at q ≈ 10, 11 and 15 nm^{-1} respectively, (2θ ≈ 14º, 15º and 21º). The intensity data for the cellulose powder was deconvoluted over this range, giving q ≈ 9.5, 11.4 and 15.9 nm^{-1} (2θ ≈ 14º, 16º and 22º) along with a broad amorphous peak and an additional peak at q ≈ 14.3 nm^{-1} (2θ ≈ 20º) (Figure 4.3a) (Sun et al., (2015); Fryczkowska et al., (2018); Hedlund, Köhnke, et al., (2019)). This may be due to the presence of a small amount of cellulose II, formed during previous processing: either scattering from the (110) plane (q ≈ 14.1 nm^{-1}) or a small reflection from the (012) plane (q ≈ 14.5 nm^{-1}). However, it is more likely that peak broadening is observed simply as a result of limited crystallite size and in this instance it can be assumed that the cellulose powder is predominantly cellulose I (Hedlund, Köhnke, et al., (2019)).

It is well reported that conversion from cellulose I to more thermodynamically stable cellulose II and/or amorphous cellulose occurs during dissolution in an IL and subsequent regeneration (Cai and Zhang, (2005); Yan and Gao, (2008); Y. Li et al., (2018)). In particular, the use of both 1-butanol and water as coagulants has been investigated, with both anti-solvents resulting in a reduction to crystallinity in regenerated cellulose (Fryczkowska et al., (2018)). In this instance, Figure 4.3b shows the absence of long-range order in the WAXS spectrum for the gel, due to the broadening of peaks into one ‘amorphous hump.’ During regeneration, fewer regular networks of cellulose intra- and intermolecular H-bonds are able to reform and the re-packing of polysaccharide chains into a crystalline form is clearly disrupted. The intensity data was not deconvoluted to the $(1\bar{1}0)$, (110) and (021) planes of cellulose II (q ≈ 12.6, 20.3 and 21.2 nm^{-1} respectively), since the scattering was too broad. It can be assumed that the regenerated cellulose is mostly amorphous and any crystallinity present is of short-range order.

Figure 4.4 shows representative SEM images for the cellulose macrogels before and after hexane washing (a and b respectively). It is assumed that HOSO appears as black and cellulose as grey, in which case it is evident that a significant amount of HOSO may remain in contact with the cellulose (although the majority is removed). This provides some evidence for an interaction between cellulose and HOSO during coagulation, as also seen via FTIR. Such interaction could also account for the absence of regenerated crystalline cellulose (cellulose II) in the WAXS spectrum (Figure 4.3b), since the presence of HOSO may disrupt the re-packing of cellulose chains into

repeating structures with long range order. Possibly the HOSO interacts with a more hydrophobic cellulose plane exfoliated during the dissolution in BmimAc, resulting in it not being completely removed during regeneration and washing. It is also expected that H-bonding between the ester carbonyl groups in the HOSO and the hydroxyl cellulose groups (C=O···H) is present, reinforcing the hydrophobic interaction (Ghosh et al., (2011)). HOSO bound to cellulose would inhibit any regular reformation of intra- and intermolecular cellulose-cellulose H-bonds, as well as hydrophobic contacts between chains, during coagulation. Of course, the SEM is not able to confirm any specific location of such interactions at the magnification employed.

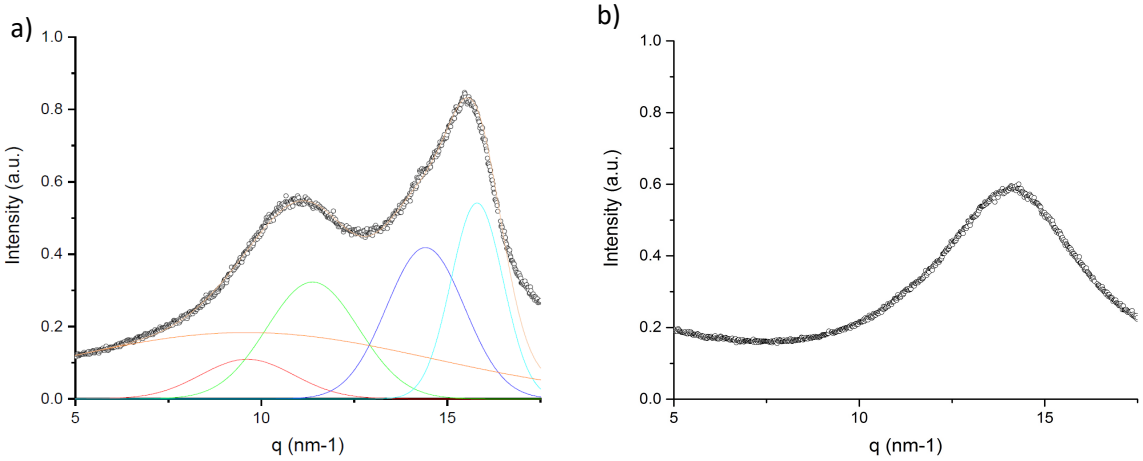

Figure 4.3. WAXS spectra for a) Vitacel cellulose powder; b) regenerated macrogel. Cellulose powder has been fitted to Cellulose I crystal planes ($1\bar{1}0$), (110), (200) and amorphous cellulose (red, green, light blue and orange peaks respectively).

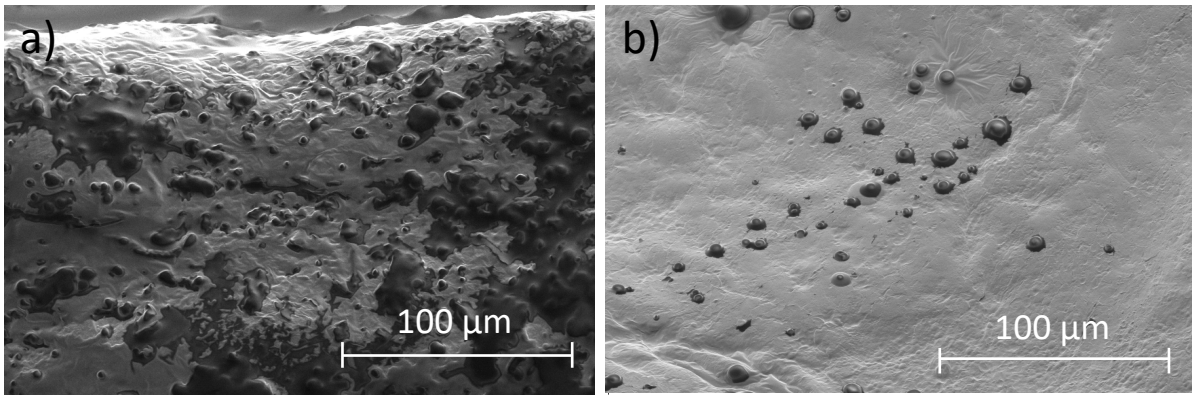

Figure 4.4. SEM images of freeze-dried macrogel a) before and b) after washing in hexane. Oil droplets are seen bound to the cellulose surface in black, scale bar = 100 µm.

4.4.3 Dispersion of Oil-CMGs in water and in oil

In characterizing the behaviour of any new particulate emulsion stabilizer (i.e., Pickering emulsifier) it is important to demonstrate the extent to which the particles are fully dispersed in the continuous phase, otherwise the particles are likely only to provide network stabilization via their aggregation in the bulk phase. Therefore, the regenerated oily macrogel was dispersed as far as possible in both water and HOSO separately, (Figure 4.5a and b respectively). Over the range of measured cellulose concentrations (0.01-1.0 wt%), oil-CMGs showed a smaller mean particle size in the oil dispersions ("oil-CMG-HOSO dispersions") compared to the water dispersions ("oil-CMG-water dispersions"), suggesting that the regenerated cellulose is more easy to disperse in oil and therefore more hydrophobic in character. Large aggregates were formed in water at all concentrations, which did not break down upon further homogenisation. A mono- or bimodal distribution of particle sizes was seen for almost all oil-CMG-HOSO disperisions, whilst a bi- or trimodal distribution was seen for oil-CMG-water dispersions (Figure B 3). During dispersion, formation of the interface will be fast compared to the rate of any microgel particle absorption (Matsumiya and Murray, (2016)) and it can be assumed that the gel character of the macrogel and CMGs is similar (Murray, (2019a)). The macrogels thus retain a much larger amount of water compared to HOSO during regeneration.

Oily cellulose macrogels were freeze-dried, in order to remove water and to try and determine an approximate percentage composition (see Table 4.1). The remaining weight of the dried macrogel could not be entirely accounted for by cellulose alone, considering the amount initially dissolved in the IL. Therefore, a small amount HOSO is expected to be present in the oil-CMGs, as well as traces of IL (assuming that both HOSO and BmimAc are not removed during freeze-drying). This was observed using SEM (Figure B 4).

A significant amount of aggregated cellulose is also visible at the W/O interface, as confirmed via confocal microscopy (Figure 4.5a). Some microgel particles remain as individual networks without attachment to water droplets, accounting for the smaller of the two peaks seen for the particle size dispersions (1-4 μm) (Sarkar et al., (2016)). In oil-CMG-water dispersions, aggregation occurs and a cellulose network forms, in order to minimise contact of the hydrophobic regions with water. Two or three peaks are seen in the particle size dispersion (Figure 4.5b), corresponding to individual CMGs (1-4 μm); aggregated CMGs (10-30 μm) and aggregated cellulose networks (>100 μm).

In summary, the oily macrogel was easier to break down and disperse in oil, as expected for a suitable W/O emulsifier. However, at concentrations above ca. 1.0 wt%, oil-CMGs were poorly dispersed in both water and HOSO: a large volume-weighted particle size is seen for all dispersions above this concentration (Figure B 5).

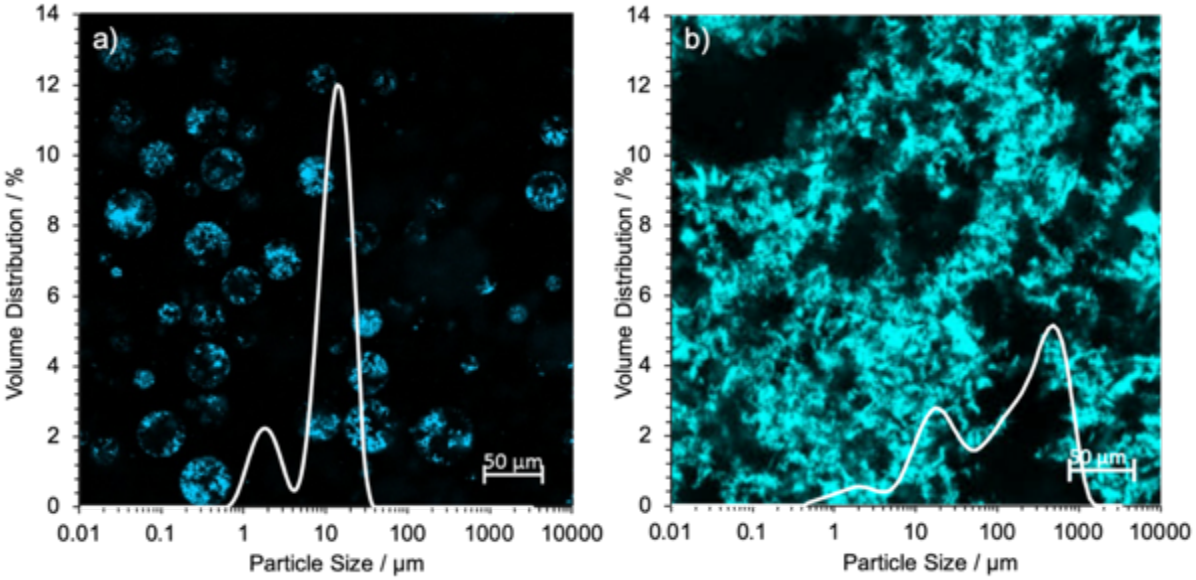

Average Size/µm	a) 0.4 wt% HOSO	b) 0.4 wt% water
(*d*3,2)	5.98	16.8
(*d*4,3)	12.4	255

Figure 4.5. Confocal images of 0.4 wt% oil-CMGs dispersed in a) HOSO; b) water seperately, with particle size data overlaid (volume distribution vs. particle size). Mean particle sizes are given in the table below. Scale bar = 50 µm.

Table 4.1. Weights of oily cellulose macrogels before and after freeze-drying. The percentage amounts of water and oil/BmimAc were calculated assuming that only water is removed during freeze-drying.

Weight before drying/mg	Weight after drying/mg	Amount of water/%	Amount of cellulose in BmimAc/%	Amount of HOSO/BmimAc/%
69.0	11.7	83.0	4.00	13.0
143	19.6	86.3	2.00	11.7

4.4.4 Water-in-oil emulsions

W/O emulsions formed from both oil-CMG-HOSO and oil-CMG-water dispersions had a surprisingly similar appearance as shown by the

representative images in Figure 4.6 (and extra images in Fig. A6), considering the significant difference in the appearance and behaviour of these two dispersions as discussed in section 4.3.2 above. For comparison, W/O emulsions formed from CMGs without the addition of oil during regeneration gave relatively poor interfacial coverage and separated out within a few days, most likely due to more problematic dispersion of the macrogel (data not shown).

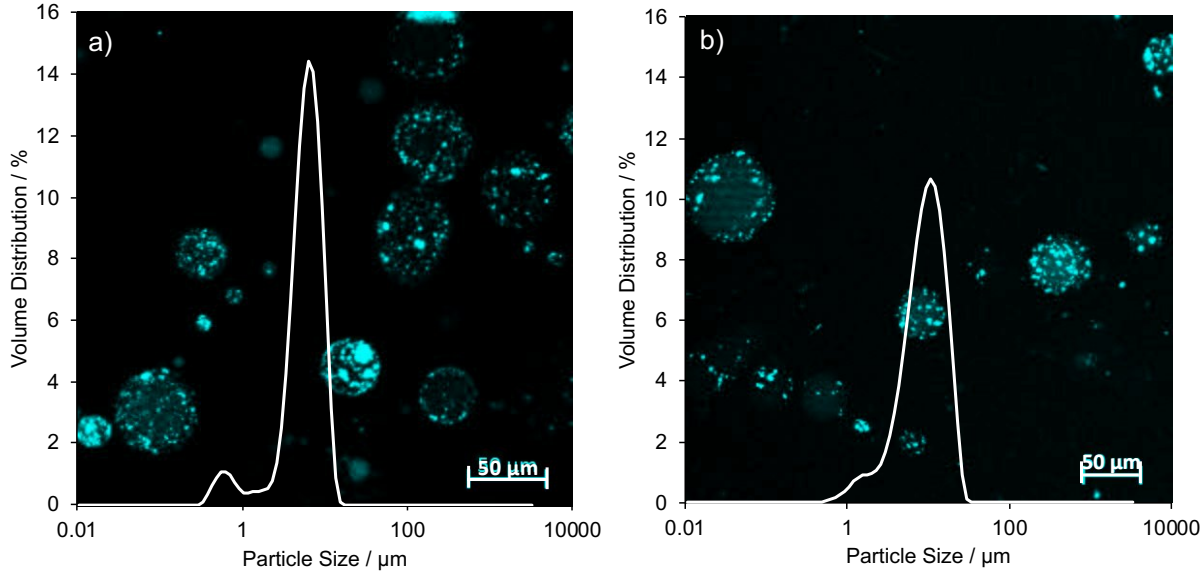

Average Size/µm	0.1 wt% HOSO (W/O)	0.1 wt% water (W/O)
(*d*3,2)	3.74	3.90
(*d*4,3)	6.10	6.28

Figure 4.6. Confocal images of 10 vol% W/O emulsions formed from 0.1 wt% oil-CMG-HOSO a) oil-CMG-HOSO oil dispersion; b) CMG-water dispersion, with particle size data overlaid (volume distribution vs. particle size). Mean particle sizes are given in the table below. Scale bar = 50 µm.

In addition, the PSDs of the emulsions were also approximately the same, regardless of the dispersion route. This was observed for W/O emulsions made from oil-CMG-water and oil-CMG-HOSO dispersions over a range of concentrations (Figure B 7). At the lowest CMG concentrations (ca. 0.05 wt%) some droplet flocculation was observed, whilst at the highest CMG concentrations (>5 wt%), droplet size increased (Figure B 7a-c). The average particle size was generally marginally smaller for W/O emulsions formed from the oil-CMG-HOSO dispersions, possibly owing to the initial smaller size of CMGs in the dispersions. These results confirm a) the amphiphilic nature of the oil-CMGs; b) the 'limiting factor' for droplet size, as discussed below.

Figure 4.7 shows a schematic that possibly describes the dispersion and emulsification stages, discussed as follows. The PSD reduces upon emulsification and the resultant increased area of the water-oil interface. For oil-CMG-HOSO dispersions, the addition of extra water during the formation of the final W/O emulsions breaks down aggregates of cellulose at the water-oil interface, since there is a larger boundary area available to which CMGs can absorb. Therefore, the average CMG particle size reduces and smaller water droplets can be stabilised (Figure 4.6a). Droplets are further broken down by more passes through the homogeniser, owing to higher energy input and resultant increase in disruption (due to turbulence and cavitation) (Long et al., (2012)). The CMGs eventually form a more uniform layer around the final W/O droplets and a relatively monodisperse droplet size is recorded (see Figure 4.6a). A similar situation arises when oil-CMG-water dispersions are homogenised with extra added oil, since the extent of the available W/O interface becomes identical. Homogenisation helps to break up cellulose networks and fast absorption of CMGs to the water-oil interface prevents CMG re-aggregation (e.g., Figure 4.6b). Consequently, the appearance and the PSD of the final W/O emulsions are very similar. Very few free (i.e., non-adsorbed) CMGs are observable in the emulsions, confirming their amphiphilicity.

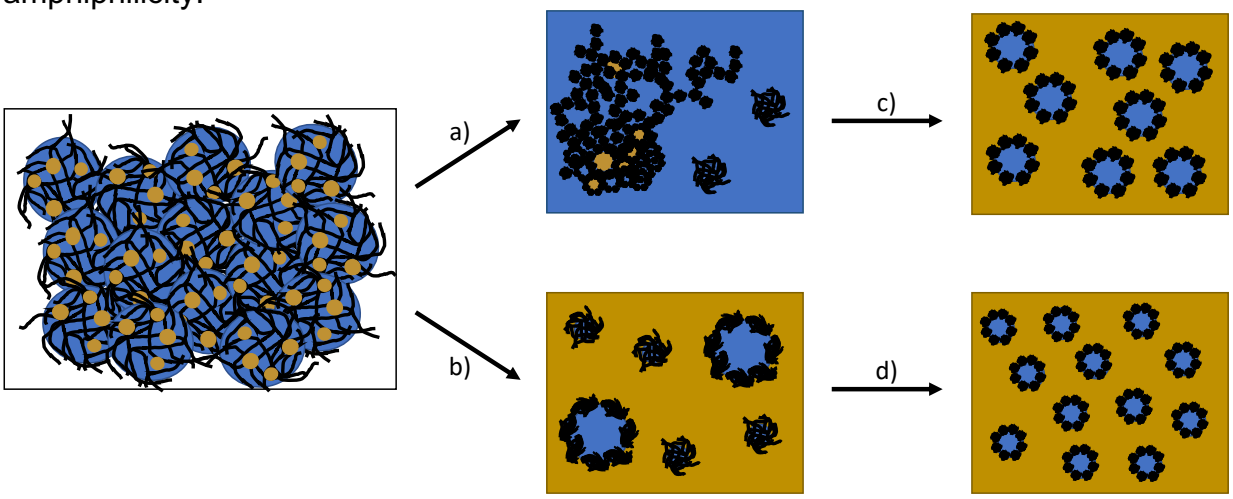

Figure 4.7. Schematic showing dispersion and emulsification of oil-CMGs, from left to right: initial cellulose macrogel; a) oil-CMG-water dispersion; b) oil-CMG-oil dispersion; c and d) emulsification to form oil-CMG-stabilised W/O emulsion (from oil-CMG-water and oil-CMG-HOSO dispersions, respectively). Water is shown in blue, oil in yellow and cellulose in black.

It would appear that the emulsification method is the limiting factor for droplet size distribution - since droplet size is fairly uniform, regardless of the dispersion route (see confocal images, Figure 4.6 and Figure B 6). In this case, the oil, water and CMG amounts are consistent and therefore the

emulsions formed are almost identical. Increasing the water content to 20 vol% gave similar droplets sizes to 10 vol% water emulsions, with droplets remaining uniform in size across a range of cellulose concentrations (Figure B 8). This suggests that for concentrations within the range 0.05-0.25 wt% CMG, the CMG emulsifier is present in excess and the droplet size depends primarily on the homogenisation conditions (McClements, (2004)).

4.4.5 W/O emulsion stability tests

The stability of the W/O emulsions formed via both routes was monitored by measuring the cream volume ratio. PSD measurements, light and confocal microscopy as a function of storage time. W/O emulsions from both oil-CMG-HOSO and oil-CMG-water dispersions exhibited similar creaming behaviour. Figure 4.8 gives the change in cream volume over a period of 37 days, with images shown in the inset, for 20 vol% W/O emulsions from oil-CMG-water dispersions. Four concentrations are given: 0.04, 0.14, 0.2 and 0.4 wt% cellulose. The cream volume ratio did not reach the internal phase volume percentage (20 vol%) for emulsions made with 0.14 and 0.2 wt% oil-CMG, demonstrating that some water remained in the emulsion over the period of time measured. No phase inversion occurred over the 37-day period and a stable emulsion fraction was observed from day 17, for 0.14 wt% cellulose. Oil-CMG-stabilised water droplets were still clearly visible in the emulsions after 7 days via light and confocal microscopy (Figure B 9), with no significant change in droplet size. The increase in cream volume ratio over the period of observation is most likely due to larger water droplets sedimenting out. This was confirmed by size measurements: emulsions were sampled from the top emulsion layer only and average PSDs shifted to smaller values over time. Larger droplets appear to settle out over time and smaller droplets remain well-stabilised in the emulsion (Figure B 10). When the emulsion was shaken and sampled after storage, a large mean droplet size was recorded, due to the re-incorporation of the lower layer and therefore larger droplets (Figure B 11). Through further homogenisation steps, it may be possible to increase the uniformity of the droplet size distribution and improve the overall stability of the emulsion, preventing noticeable sedimentation.

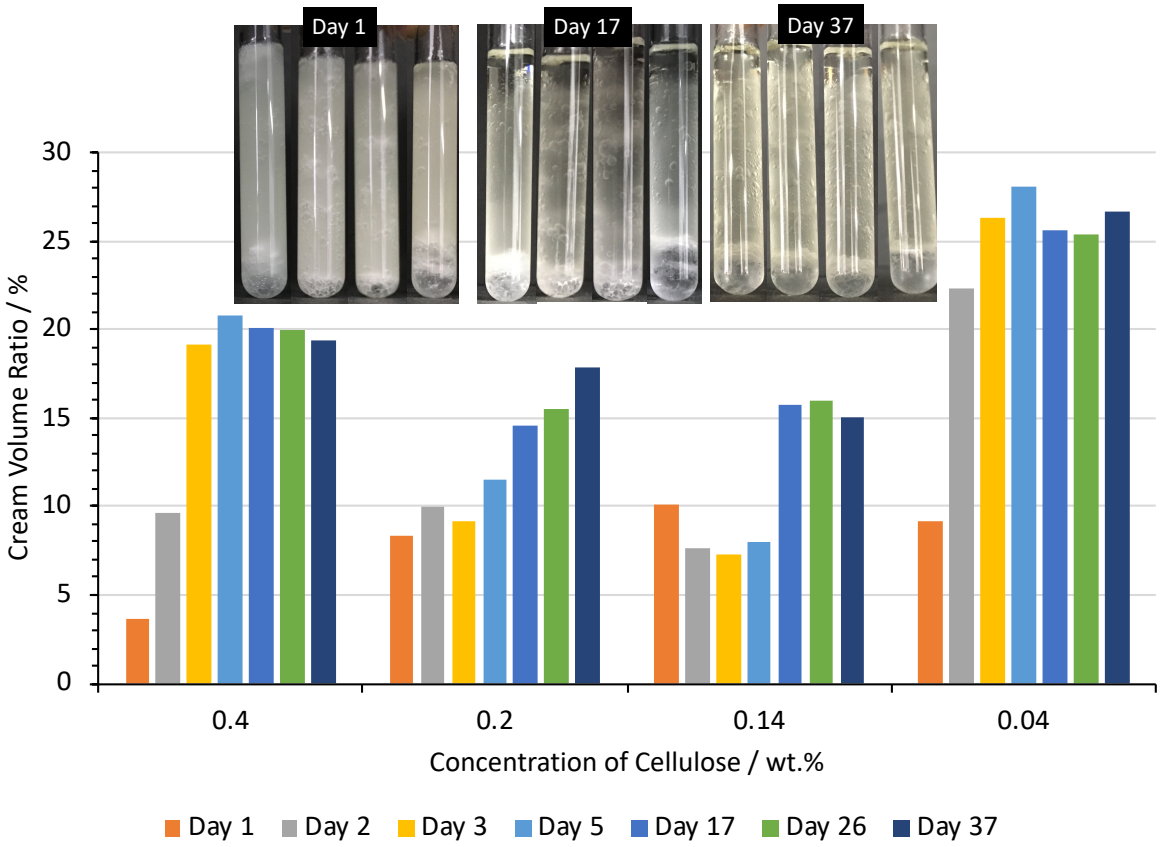

Figure 4.8. Cream Volume Ratio heights over 37 days for 20 vol% W/O emulsions formed from 0.4, 0.2, 0.14 and 0.04 wt% oil-CMG-HOSO dispersions. Inset: pictures of emulsions from left to right on day 1, day 17 and day 37 (from left to right: 0.4, 0.2, 0.14 and 0.04 wt%).

Evidently, a delicate balance between CMG and internal phase amount is required to produce W/O emulsions of good stability. From the cream volume ratio data, a concentration of ca. 0.2 wt% cellulose seems to be the optimum. Sufficient oil-CMG must be added in order to cover the water-oil interface and provide good coverage, however addition of excess oil-CMG leads to seemingly irreversible aggregation of cellulose in the continuous oil phase. This was evidenced in the confocal images (Figure 4.9). Good cellulose coverage is visible for an emulsion of 0.2 wt% cellulose, with Pickering-type stabilization via oil-CMGs and non-spherical droplets. However, an aggregated network of flocculated oil-CMGs is visible in the continuous phase at 0.4 wt% cellulose, stabilizing larger water droplets.

Such behaviour was confirmed by particle size measurements, where changes over time were quantified by $d3,2$ values of the emulsions, at various concentrations of oil-CMG (Figure 4.10). The highest emulsion stability was observed for 0.2 to 0.25 wt% cellulose, which gave the smallest initial droplet sizes and values remaining within a 2 μm range during 1 week of storage. For concentrations <0.25 wt% cellulose, the initial particle size was relatively large

due to insufficient droplet coverage but decreased over time, most probably due to sedimentation of larger droplets, (as discussed above). For concentrations >0.25 wt%, the initial droplet size increased again relative to 0.25 wt%, possibly due to the presence of excess, flocculated oil-CMGs in the oil phase. However, over time particle size became comparable to those of 0.2 to 0.25 wt% cellulose emulsions, with no significant sedimentation observable. Confocal images show that at higher concentrations, oil-CMGs adsorb to the interface over time, leading to better coverage of water droplets and higher stability (Figure B 12). Therefore, although higher concentrations of cellulose may lead to an initially larger particle size, rearrangement of oil-CMGs at the interface allows space for excess CMG in the oil phase to spontaneously adsorb to the interface. “De-flocculation” may occur, due to the rearrangement of the polymer chains within the oil-CMGs, resulting in a particle size reduction. This behaviour has also been reported for poly(*N*-isopropylacrylamide) (pNIPAM) polymer microgels (Pinaud et al., (2014)).

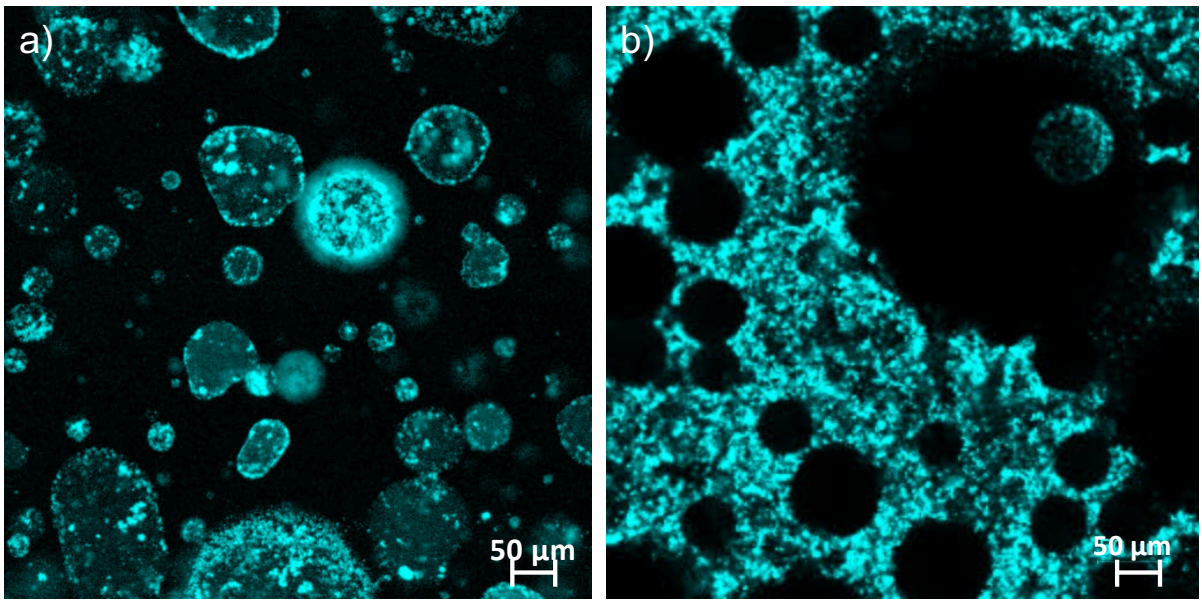

Figure 4.9. Confocal images of 20 vol% W/O emulsions stabilised by a) 0.2 wt% oil-CMG; b) 0.4 wt% oil-CMG. Scale bar = 50 µm.

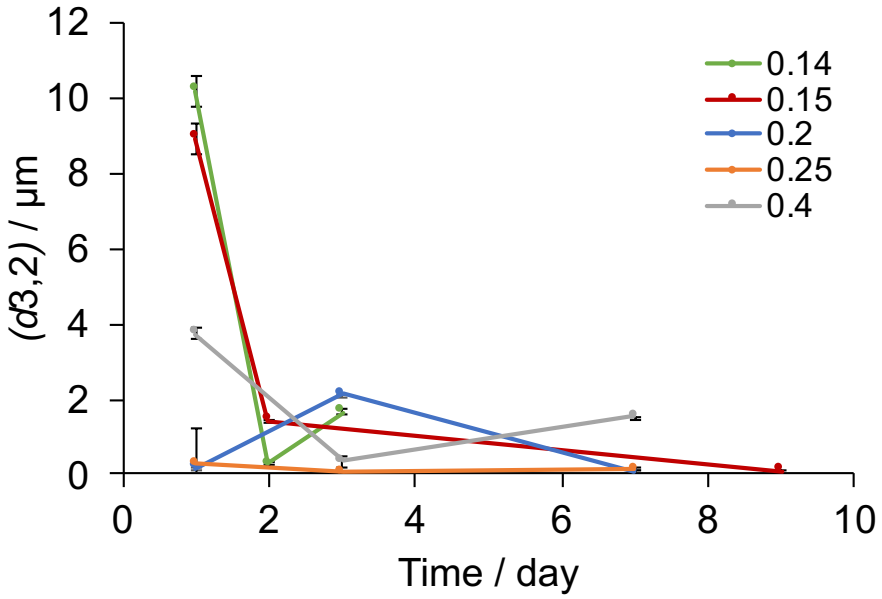

Figure 4.10. Changes in the particle size of W/O emulsions over time, with 0.14, 0.15, 0.2, 0.25 and 0.4 wt% oil-CMG-emulsifier (green, red, blue, orange and grey respectively). Particle size is given as the surface-weighted mean diameter (*d*3,2).

It is also important to consider the amount of cellulose present during regeneration, i.e. the amount of cellulose dissolved initially in the IL, which also affects the size and packing of the cellulose networks in the CMGs. A denser gel network is expected to form at higher wt% cellulose in the IL, potentially increasing the adsorption and retention of oil during the regeneration process. However, higher network density may lead to reduced macrogel break down, yielding a greater average CMG particle size and therefore a larger overall droplet size in the final emulsion. Furthermore, it has been reported that microgels with lower cross-link densities display faster adsorption rates to the interface and higher compressibility. A more elastic interface is expected to give higher stability (Pinaud et al., (2014)). The effect of CMG network density on emulsion stability is currently being investigated, alongside studies employing NMR and FTIR in order to further understand the mechanism of CMG-regeneration. Such investigations aim to probe the interactions between cellulose and oil, as well as their individual interactions with 1-butanol and IL during the regeneration.

4.5 Conclusions

A natural, unmodified cellulose emulsifier has been prepared, by fabricating a “hydrophobic” microgel using a facile regeneration method from an IL. An edible oil was introduced to the cellulose after dissolution, which appeared to remain bound in some way to the cellulose throughout the coagulation process, as confirmed using FTIR, SEM and WAXS. It is suggested that an

“oily” or hydrophobic surface is exposed, allowing the cellulose to act as a W/O emulsifier after breakdown to form microgel particles in a dispersion. The oily macrogel was much easier to disperse in oil and a better W/O emulsifier – W/O emulsions containing 0.2 wt% cellulose and at least 20 vol% water being stable for at least 4 weeks. At higher concentrations, an increase in CMG present in the continuous phase resulted in formation of flocculated microgel regions. Regeneration from higher wt% cellulose/IL solutions is thought to increase the density of the cellulose gel network, possibly leading to a higher retention of oil and resulting in even better CMG-W/O surface activity, whilst also affecting their swelling properties at the interface (Pinaud et al., (2014)).

Thus, the current study proposes a novel approach to forming a hydrophobic cellulose-based emulsifier without employing chemical modification, that meets the demand for a natural, renewable W/O emulsifier. This could be of great value to the food industry as a method of reducing fat as well as finding applications in agricultural, cosmetic and medical areas. Further work on the understanding of the interactions between cellulose and the oil in both the microgels and the emulsions is required to optimise the W/O emulsion formulations. Shelf-stability of the CMGs as ingredients could also be addressed by considering their dried and swollen states.

4.6 References

Albert, C., Beladjine, M., Tsapis, N., Fattal, E., Agnely, F. and Huang, N. (2019). Pickering emulsions: Preparation processes, key parameters governing their properties and potential for pharmaceutical applications. *Journal of Controlled Release*. *309*, 302–332.

Arditty, S., Whitby, C.P., Binks, B.P., Schmitt, V. and Leal-Calderon, F. (2003). Some general features of limited coalescence in solid-stabilized emulsions. *European Physical Journal E*. *11*(3), 273–281.

Azmi, N.A.N., Elgharbawy, A.A.M., Motlagh, S.R., Samsudin, N. and Salleh, H.M. (2019). Nanoemulsions: Factory for food, pharmaceutical and cosmetics. *Processes*. *7*, 617.

Bastida-Rodríguez, J. (2013). The Food Additive Polyglycerol Polyricinoleate (E-476): Structure, Applications, and Production Methods. *ISRN Chemical Engineering*. *2013*, 1–21.

Bertsch, P., Arcari, M., Geue, T., Mezzenga, R., Nyström, G. and Fischer, P. (2019). Designing Cellulose Nanofibrils for Stabilization of Fluid Interfaces. *Biomacromolecules*. *20*(12), 4574–4580.

Borreani, J., Hernando, I. and Quiles, A. (2020). Cream replacement by hydrocolloid-stabilized emulsions to reduce fat digestion in panna cottas. *LWT – Food Science and Technology*. *119*, 108896.

Burgaud, I., Dickinson, E. and Nelson, P. V. (1990). An improved high-

pressure homogenizer for making fine emulsions on a small scale. *International Journal of Food Science & Technology*. *25*(1), 39–46.

Cai, J. and Zhang, L. (2005). Rapid dissolution of cellulose in LiOH/urea and NaOH/urea aqueous solutions. *Macromolecular Bioscience*. *5*(6), 539–548.

Chua, E.T., Brunner, M., Atkin, R., Eltanahy, E., Thomas-Hall, S.R. and Schenk, P.M. (2019). The Ionic Liquid Cholinium Arginate Is an Efficient Solvent for Extracting High-Value Nannochloropsis sp. Lipids. *ACS Sustainable Chemistry and Engineering*. *7*(2), 2538–2544.

Dickinson, E. (2011). Double Emulsions Stabilized by Food Biopolymers. *Food Biophysics*. *6*(1), 1–11.

Dickinson, E. (2012). Use of nanoparticles and microparticles in the formation and stabilization of food emulsions. *Trends in Food Science and Technology*. *24*(1), 4–12.

Fan, Z., Chen, J., Guo, W., Ma, F., Sun, S. and Zhou, Q. (2018). Anti-solvents tuning cellulose nanoparticles through two competitive regeneration routes. *Cellulose*. *25*(8), 4513–4523.

Fink, H.P., Weigel, P., Purz, H.J. and Ganster, J. (2001). Structure formation of regenerated cellulose materials from NMMO-solutions. *Progress in Polymer Science. 26*, 1473–1524.

Fryczkowska, B., Kowalska, M., Binias, D., Slusarczyk, C., Janicki, J., Sarna, E. and Wyszomirski, M. (2018). Properties and Structure of Cellulosic Membranes Obtained from Solutions in Ionic Liquids Coagulated in Primary Alcohols. *Autex Research Journal*. *18*(3), 232–242.

Ghosh, S. and Rousseau, D. (2011). Fat crystals and water-in-oil emulsion stability. *Current Opinion in Colloid and Interface Science*. *16*(5), 421–431.

Ghosh, S., Tran, T. and Rousseau, D. (2011). Comparison of pickering and network stabilization in water-in-oil emulsions. *Langmuir*. *27*(11), 6589–6597.

Gómez, M. and Martinez, M.M. (2018). Fruit and vegetable by-products as novel ingredients to improve the nutritional quality of baked goods. *Critical Reviews in Food Science and Nutrition*. *58*(13), 2119–2135.

Gupta, K.M., Hu, Z. and Jiang, J. (2013). Cellulose regeneration from a cellulose/ionic liquid mixture: The role of anti-solvents. *RSC Advances*. *3*(31), 12794–12801.

Hedlund, A., Köhnke, T., Hagman, J., Olsson, U. and Theliander, H. (2019). Microstructures of cellulose coagulated in water and alcohols from 1-ethyl-3-methylimidazolium acetate: contrasting coagulation mechanisms. *Cellulose*. *26*(3), 1545–1563.

Huang, S., Liu, X., Chang, C. and Wang, Y. (2020). Recent developments and prospective food-related applications of cellulose nanocrystals: a review. *Cellulose*. *27*(6), 2991–3011.

Kopelman, P.G. (2000). Obesity as a medical problem. *Nature*. *404*(6778),

635–643.

Li, Y., Wang, J., Liu, X. and Zhang, S. (2018). Towards a molecular understanding of cellulose dissolution in ionic liquids: Anion/cation effect, synergistic mechanism and physicochemical aspects. *Chemical Science*. *9*, 4027–4043.

Long, Z., Zhao, M., Zhao, Q., Yang, B. and Liu, L. (2012). Effect of homogenisation and storage time on surface and rheology properties of whipping cream. *Food Chemistry*. *131*(3), 748–753.

Marchetti, L., Muzzio, B., Cerrutti, P., Andrés, S.C. and Califano, A.N. (2017). Bacterial nanocellulose as novel additive in low-lipid low-sodium meat sausages. Effect on quality and stability. *Food Structure*. *14*, 52–59.

Martinez, R.M., Rosado, C., Velasco, M.V.R., Lannes, S.C.S. and Baby, A.R. (2019). Main features and applications of organogels in cosmetics. *International Journal of Cosmetic Science*. *41*(2), 109–117.

Matsumiya, K. and Murray, B.S. (2016). Soybean protein isolate gel particles as foaming and emulsifying agents. *Food Hydrocolloids*. *60*, 206–215.

McClements, D.J. (2004). *Food Emulsions: Principle, Practices, and Techniques* [Online] second ed. Boca Raton: CRC Press. [Accessed 9 September 2019]. Available from: https://www.taylorfrancis.com/books/mono/10.1201/9781420039436/food-emulsions-david-julian-mcclements.

Mitsou, E., Tavantzis, G., Sotiroudis, G., Ladikos, D., Xenakis, A. and Papadimitriou, V. (2016). Food grade water-in-oil microemulsions as replacement of oil phase to help process and stabilization of whipped cream. *Colloids and Surfaces A: Physicochemical and Engineering Aspects*. *510*, 69–76.

Mortensen, A., Aguilar, F., Crebelli, R., Di Domenico, A., Dusemund, B., Frutos, M.J., Galtier, P., Gott, D., Gundert-Remy, U., Leblanc, J., Lindtner, O., Moldeus, P., Mosesso, P., Parent-Massin, D., Oskarsson, A., Stankovic, I., Waalkens-Berendsen, I., Woutersen, R.A., Wright, M., Younes, M., Boon, P., Chrysafidis, D., Gürtler, R., Tobback, P., Rincon, A.M., Tard, A. and Lambré, C. (2017). Re-evaluation of polyglycerol polyricinoleate (E 476) as a food additive. *EFSA Journal*. *15*(3), 4743.

Murray, B.S. (2019a). Microgels at fluid-fluid interfaces for food and drinks. *Advances in Colloid and Interface Science*. *271*, 101990.

Murray, B.S. (2019b). Pickering emulsions for food and drinks. *Current Opinion in Food Science*. *27*, 57–63.

Neethirajan, S., Kobayashi, I., Nakajima, M., Wu, D., Nandagopal, S. and Lin, F. (2011). Microfluidics for food, agriculture and biosystems industries. *Lab on a Chip*. *11*(9), 1574–1586.

Oh, S.Y., Yoo, D. Il, Shin, Y. and Seo, G. (2005). FTIR analysis of cellulose treated with sodium hydroxide and carbon dioxide. *Carbohydrate Research*. *340*(3), 417–428.

Ossowicz, P., Klebeko, J., Roman, B., Janus, E. and Rozwadowski, Z.

(2019). The relationship between the structure and properties of amino acid ionic liquids. *Molecules*. *24*(18), 3252.

Ozturk, B. and McClements, D.J. (2016). Progress in natural emulsifiers for utilization in food emulsions. *Current Opinion in Food Science*. *7*, 1–6.

Paunonen, S., Kamppuri, T., Katajainen, L., Hohenthal, C., Heikkilä, P. and Harlin, A. (2019). Environmental impact of cellulose carbamate fibers from chemically recycled cotton. *Journal of Cleaner Production*. *222*, 871–881.

Pinaud, F., Geisel, K., Massé, P., Catargi, B., Isa, L., Richtering, W., Ravaine, V. and Schmitt, V. (2014). Adsorption of microgels at an oil-water interface: Correlation between packing and 2D elasticity. *Soft Matter*. *10*(36), 6963–6974.

Qi, H., Yang, Q., Zhang, L., Liebert, T. and Heinze, T. (2011). The dissolution of cellulose in NaOH-based aqueous system by two-step process. *Cellulose*. *18*(2), 237–245.

Rogers, M.A., Wright, A.J. and Marangoni, A.G. (2009). Oil organogels: The fat of the future? *Soft Matter*. *5*(8), 1594–1596.

Rohman, A. and Che Man, Y.B. (2012). Quantification and classification of corn and sunflower oils as adulterants in olive oil using chemometrics and FTIR spectra. *The Scientific World Journal*. *2012,* 1-6.

Sadeghifar, H., Venditti, R., Pawlak, J.J. and Jur, J. (2019). Cellulose transparent and flexible films prepared from DMAc/LiCl solutions. *BioResources*. *14*(4), 9021–9032.

Sarkar, A., Murray, B., Holmes, M., Ettelaie, R., Abdalla, A. and Yang, X. (2016). In vitro digestion of Pickering emulsions stabilized by soft whey protein microgel particles: Influence of thermal treatment. *Soft Matter*. *12*(15), 3558–3569.

Stana-Kleinschek, K., Ribitsch, V., Kreze, T. and Fras, L. (2002). Determination of the adsorption character of cellulose fibres using surface tension and surface charge. *Materials Research Innovations*. *6*(1), 13–18.

Sun, L., Chen, J.Y., Jiang, W. and Lynch, V. (2015). Crystalline characteristics of cellulose fiber and film regenerated from ionic liquid solution. *Carbohydrate Polymers*. *118*, 150–155.

Tan, X., Chen, L., Li, X. and Xie, F. (2019). Effect of anti-solvents on the characteristics of regenerated cellulose from 1-ethyl-3-methylimidazolium acetate ionic liquid. *International Journal of Biological Macromolecules*. *124*, 314–320.

Verma, C., Mishra, A., Chauhan, S., Verma, P., Srivastava, V., Quraishi, M.A. and Ebenso, E.E. (2019). Dissolution of cellulose in ionic liquids and their mixed cosolvents: A review. *Sustainable Chemistry and Pharmacy*. *13*, 100162.

Wang, Z. and Wang, Y. (2016). Tuning Amphiphilicity of Particles for Controllable Pickering Emulsion. *Materials*. *9*(11), 903.

Wilson, R. and Smith, M. (1998). Human studies on polyglycerol

polyricinoleate (PGPR). *Food and Chemical Toxicology*. *36*(9–10), 743–745.

Xu, A.R., Guo, X. and Ma, J. (2016). Properties of Cellulose Regenerated from Powerful 1-Butyl-3-methylimidazolium Acetate/Dimethyl Sulfoxide Solvent. *Journal of Macromolecular Science, Part B: Physics*. *55*(6), 559–565.

Yan, L. and Gao, Z. (2008). Dissolving of cellulose in PEG/NaOH aqueous solution. *Cellulose*. *15*(6), 789–796.

Zhang, J., Wu, J., Yu, J., Zhang, X., He, J. and Zhang, J. (2017). Application of ionic liquids for dissolving cellulose and fabricating cellulose-based materials: State of the art and future trends. *Materials Chemistry Frontiers*. *1*(7), 1273–1290.

Chapter 5
Relationship between size and cellulose content of cellulose microgels (CMGs) and their water-in-oil emulsifying capacity[4]

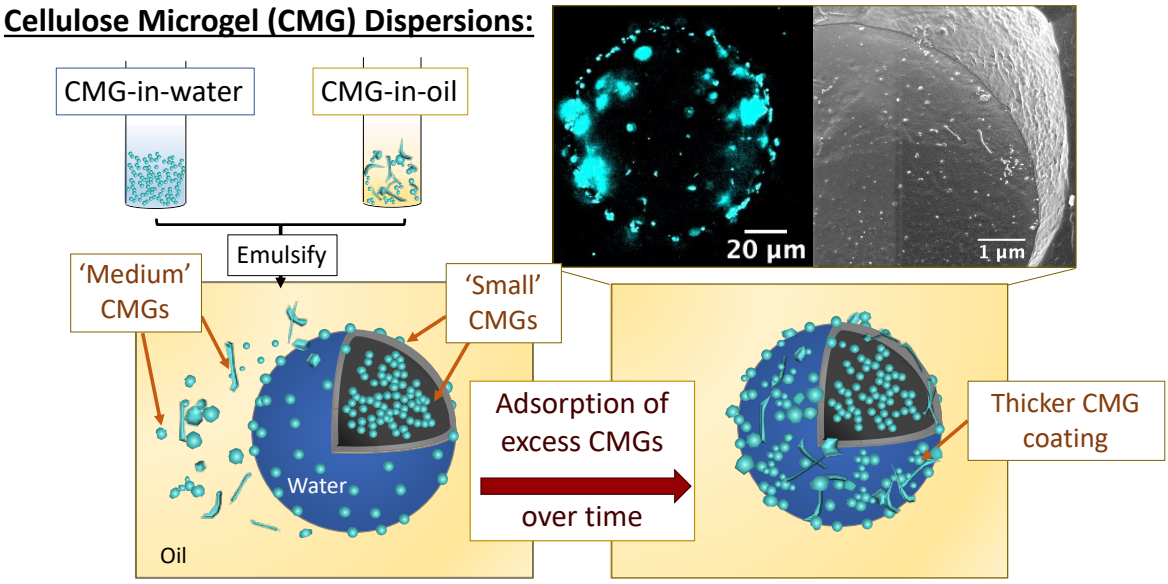

5.1 Abstract

Soluble polysaccharides have been used extensively as gelling/thickening agents in emulsions, but they generally display weak surface activity. Insoluble polysaccharides such as cellulose can be converted to thickening agents and even emulsifiers, but generally only after considerable chemical modification. Here we use the ionic liquid (IL) 1-butyl-3-methyl imidazolium acetate (BmimAc) to dissolve and reprecipitate cellulose in the presence of oil, i.e., a *physical* process, to tune the cellulose properties. ILs have previously been used in this way to form hydrophobic ('oily') cellulose microgels (CMGs), potentially capable of stabilizing water-in-oil (W/O) emulsions. However, these previous CMGs were made via a 'top-down' method and were relatively large and polydisperse, giving limited stability to the W/O emulsions formed. Here we demonstrate how the CMG size can be drastically reduced via a 'bottom-up' approach and employing high-pressure homogenization (HPH), thus achieving sub-micron CMG particle sizes. This has previously been impossible with other reported IL-cellulose coagulation methods and the corresponding W/O emulsions were more stable. In addition, confocal and cryo-scanning electron microscopy (SEM) revealed

[4]Published as: Lefroy, K.S., Murray, B.S. and Ries, M.E. (2022). Relationship between size and cellulose content of cellulose microgels (CMGs) and their water-in-oil emulsifying capacity. *Colloids and Surfaces A: Physicochemical and Engineering Aspects*. *647*, 128926. DOI: 10.1016/j.colsurfa.2022.128926

that the surface coverage of these CMGs on droplets increased over time, which led to the formation of even thicker interfacial layers and further enhanced emulsion stability (at least 2 months). We also demonstrate unequivocally that the stability of the W/O emulsions is indeed due to the CMGs adsorbing via the Pickering mechanism, rather than forming a stabilizing cellulosic network in the continuous phase, thus providing a novel route to 'green' Pickering emulsions.

5.2 Introduction

Emulsions are colloidal dispersions of two immiscible liquids with different compositions, which are mixed in the presence of a stabilizer/emulsifier. Most commonly, in their simplest form, an emulsion is either made up of a water-continuous phase and an oil-discontinuous phase (oil-in-water, O/W) or vice versa (water-in-oil, W/O). Both types are used widely across many fields (McClements, (2004); Schramm, (2005); Albert et al., (2019)) and can be fabricated for different purposes, for example in the delivery of water-insoluble drugs (Cannon and Long, (2008)), in personal care for non-greasy formulations (Ali et al., (2015)) and in food for fat reduction (Mitsou et al., (2016); Marchetti et al., (2017)).

Biopolymers such as polysaccharides and plant-proteins can act as emulsion stabilizers, by lowering the interfacial tension and/or changing the bulk viscosity of the system (Bouyer et al., (2012); Zhu et al., (2017); Tavernier et al., (2017); Amagliani and Schmitt, (2017)). Depending on the biopolymer type, they can also provide electrostatic and steric stability to droplets, preventing destabilizing processes such as flocculation and coalescence. On the other hand, there are no natural biopolymers that are soluble in oil and therefore suitable as W/O emulsion stabilizers. Demand for suitable biopolymers to replace conventional synthetic surfactants has been rapidly increasing in the food, pharmaceutical and cosmetic industries, due to environmental factors (Sarkar and Dickinson, (2020)) and toxicity issues (Liwarska-Bizukojc et al., (2005)), as well as a shift towards more sustainable, plant-based diets (Pimentel and Pimentel, (2003)). Pickering stabilizers based on materials from natural resources also offer enhanced emulsion stability (Pang et al., (2018)).

Cellulose, frequently described as the most abundant natural polymer (H. Kang et al., (2016)), is a highly attractive candidate for replacing synthetic surfactants since it is biocompatible, chemically inactive and physiologically inert (Habibi et al., (2010)). Typically, cellulose displays a low contact angle with water (Yamane et al., (2006); Andresen and Stenius, (2007)) and is

considered to preferentially stabilize water-continuous emulsions (Jia et al., (2015); Winuprasith and Suphantharika, (2015); Napso et al., (2016); Napso et al., (2018); Z. Li et al., (2018)). As a result, there are many reports of coagulated cellulose being investigated as an O/W stabilizer (Jia et al., (2015); Winuprasith and Suphantharika, (2015); Napso et al., (2016); Napso et al., (2018); Z. Li et al., (2018)) and comparatively few on W/O systems. Rein *et al.* were able to produce W/O emulsions which displayed stability for 2 weeks, but had greater success with stabilizing O/W emulsions (Rein et al., (2012)). Pang *et al.* were able to produce high internal phase Pickering Emulsions (HIPEs) with up to 89% water as the internal phase (Pang et al., (2018)), whilst Andresen *et al.* produced W/O emulsions with cellulose which were remarkably stable to coalescence (Andresen and Stenius, (2007)). However in both cases, the cellulose was chemically modified, which may raise biocompatibility issues.

The discovery that ionic liquids (ILs) could be used to dissolve cellulose under mild conditions has provided a facile route for cellulose functionalization (Swatloski et al., (2002)), with the non-toxicity and potential biodegradability of ILs making them attractive ‘green’ solvents (Asakawa et al., (2016); Satlewal et al., (2018)). As a result, an extensive number of reports have been published on dissolution and reprecipitation of cellulose under different conditions, to form novel cellulose stabilizers (Durmaz and Zeynep Çulfaz-Emecen, (2018); Druel et al., (2018); Zeng et al., (2020); Omura et al., (2020)). However, it is indeed a challenge to achieve monodisperse, regularly shaped cellulose particles using a coagulation method and sizes below 10 μm are rarely achieved. Millimeter-sized cellulose beads have been produced by employing vigorous stirring to the coagulation medium (Park et al., (2015); Kim et al., (2017)) whilst up to 1 micron-sized particles may be achieved via a sol-gel transition and reprecipitating the cellulose from an IL-in-oil emulsion (Jo et al., (2019)). In the latter case, increasing the stirring speed by just 500 rpm resulted in a decrease in the diameter of cellulose microspheres by at least half. Whilst we ourselves were able to produce cellulose microgels (CMGs) of down to 5 μm using a ‘top-down’ method (Lefroy, Murray, Ries, et al., (2021)), the CMG-dispersions were still relatively polydisperse and the presence of larger particles meant that consequently average droplet sizes in the W/O emulsions generally exceeded 50 μm (Wiley, (1954)). A possible strategy for reducing the size of CMGs (and thus improving the stability of the emulsions) is to disrupt or delay the reformation of inter- and intramolecular H-bonds during coagulation, allowing formation of smaller particles (Lefroy, Murray and Ries, (2021)). Agitation of the coagulating solution also leads to a

significant difference in crystallinity of the reprecipitated cellulose (Fan et al., (2017); Fan et al., (2018)), which may make it easier to disperse and may improve the cellulose surface properties.

In this work, we have fabricated highly stable W/O emulsions with CMG stabilizers of different size ranges, produced via cellulose coagulation from an IL. Different forces were employed during reprecipitation to control the CMG size and are described as dropwise ('low shear', L) and high-speed mixing ('high shear,' H). High-pressure homogenization (HPH), ('very high shear,' VH) was also used as a 'bottom-up' approach for producing microgels, producing a very fine dispersion of CMGs in water with particles sizes of ca. 10 nm. Particle sizing and optical microscopy were used to compare droplet sizes in the W/O emulsions stabilized by CMGs produced via the 3 methods, whilst confocal microscopy and cryo-scanning electron microscopy (SEM) provided information about surface coverage and were used to compare the morphologies of CMGs adsorbed at the interface. The mechanism of CMG stabilization was also investigated using rheological analysis, by measuring the change in bulk viscosities of emulsions over time. For each type of CMG, only physical processing methods were employed and therefore they are expected to behave in the same way as insoluble fiber during human digestion, making them suitable for food applications (as well as in other industries).

5.3 Materials and methods

5.3.1 Materials

1-Butyl-3-methyl imidazolium acetate (BmimAc) (≥95% purity), ethanol (absolute, 99.8%) and Calcofluor White (1 g/L) were obtained from Sigma Aldrich. 1-Butanol (Acros Organics, 99.5%) was obtained from Fisher Scientific. Cellulose powder (Vitacel L 00, full details and a wide angle x-ray scattering (WAXS) spectrum are provided in **Appendix C**, Table C 1 and Figure C 1 respectively) and high oleic sunflower oil (HOSO, d = 0.92 g mL^{-1}) were supplied by Mondelēz International. Medium-chain triglyceride oil (MCT-oil) Miglyol 812 with a density of 0.945 g mL^{-1} at 20 °C was obtained from Cremer Oleo GmbH & Co, (Germany).

5.3.2 CMG fabrication with low shear (L)

The first set of CMGs was fabricated by a method reported previously (Lefroy, Murray, Ries, et al., (2021)). Briefly, cellulose powder (3 wt%) was dissolved completely in BmimAc so that a clear solution was obtained (75 °C, 3-5 h). We previously determined that a concentration of 3 wt% cellulose is within the semi-dilute entangled regime and therefore sufficient for a cellulose macrogel

to form (Lefroy, Murray and Ries, (2021)). HOSO or MCT-oil was then added directly to the heated solution (0.25-200 wt% oil with respect to total BmimAc volume) and mixed at high-speed with an UltraTurrax (24,000 rpm, ca. 2 min), in order to 'coat' the molecularly dissolved cellulose. Both types of oil were selected since they display similar properties to food-grade oils, for example sunflower oil, but have had most impurities removed. Less 'polar' oils were also investigated, for example tetradecane, but failed to produce CMGs with the desired stabilizing properties. For mixtures with <1 wt% oil, a clear solution was obtained whilst mixtures with oil contents > 1 wt% became turbid and separated fairly rapidly (but not before they were added to the coagulation medium). Therefore, a range of oil concentrations were investigated to understand the effect of oil amount on the size and stabilizing ability of CMGs. The cellulose-BmimAc-oil mixture was then added dropwise via a syringe to anti-solvent (1-butanol, 4:1 v/v 1-butanol/oil-cellulose-BmimAc) and stored overnight at room temperature, to produce an 'oily,' hydrophobic cellulose macrogel. Solvent exchange was then conducted as follows using the same volume of anti-solvent for each solvent change: 1-butanol; 2 x ethanol; 2 x water, with immersion in each solvent for 4-10 h. A cellulose macrogel was obtained via filtration under gravity at each stage of the solvent exchange (nylon membrane filter, 0.25 µm, 45 mm) and washed with water during the final filtration stage, to ensure complete removal of BmimAc. Oil was visible in the filtrate when a higher concentration was added (>1 wt%), indicating that the majority of the oil was not retained within the cellulose gel when an excess amount was used.

5.3.3 CMG fabrication via high-speed mixing (H)

The second set of CMGs was fabricated under high-speed mixing (H) during coagulation, using a high-speed blender (Ultra Turrax T 25, IKA, Germany). Cellulose was dissolved in BmimAc and mixed with oil, (as described in 2.2). The cellulose-BmimAc-oil mixtures were then added dropwise via a syringe to the anti-solvent (1-butanol, 4:1 v/v 1-butanol/oil-cellulose-BmimAc) *whilst shearing* (24,000 rpm, 5 min). This was so as to disrupt the structure of the cellulose as it is precipitated when coming into contact with the anti-solvent. The solution was then filtered under gravity (as described in 5.3.2) to collect cellulose gel particles, which were redispersed in ethanol two times (24,000 rpm, 5 min), with filtering in between, and finally redispersed in water two times (24,000 rpm, 5 min) and filtered, to complete the solvent exchange process. During the final filtration stage, the cellulose gel particles were washed with portions of water (ca. 10 mL) to ensure complete removal of BmimAc. In some cases where a very fine dispersion of microgel particles was obtained (oil

content < 1 wt%), the sample was centrifuged (4,000 rpm, 15 min) to collect the CMG particles and the resulting gel pellet was washed a further 2 times with water (4,000 rpm, 15 min).

The oily cellulose hydrogels obtained in 5.3.2 and 5.3.3 (L and H) were broken down via homogenization in oil (Ultra Turrax, 24,000 rpm, 2 min) to give CMG-in-oil dispersions of varying cellulose concentrations (1-5 wv%), where the content of cellulose is given as the weight of CMG with respect to the total oil volume. Whilst the CMGs themselves are made up of predominantly cellulose and water (and hence we refer to them as 'microgels'), they were dispersible in oil due to their hydrophobic character, imparted by the presence of oil during coagulation.

5.3.4 CMG fabrication using very high shear (VH)

The third method used was to coagulate cellulose from BmimAc under high pressure homogenization (HPH or 'very high' shear, VH), using a jet homogenizer (JH) as a 'microreactor' (Burgaud et al., (1990)). A similar approach has been reported previously for the preparation of alginate microgels, where the features of the JH are described in detail (Pravinata et al., (2016)). Briefly, one chamber was filled with cellulose dissolve in BmimAc (3 wt%) mixed with oil (0.25-200 wt%, total volume of mixture = 7.5 mL, prepared in the same way as in 2.2), whilst a second chamber was filled with anti-solvent (water, total volume = 15 mL). The ratios of cellulose, BmimAc, oil and water for the VH-CMGs are given in Table 5.1. Two pistons force the solutions out of the chambers and through a narrow hole, inducing mixing of the two solutions under highly turbulent conditions. A suspension of very fine particles (CMGs) can then be collected in a beaker. Pressures of 300-500 bar were used to force the two solutions through the JH. The collected CMG-in-water dispersion was then passed through the JH a further two times (at the same pressures) in order to break down any CMG aggregates and produce a finer CMG suspension (< 1 μm).

Table 5.1. Total amounts (g) of cellulose, BmimAc, oil and water added to the JH, for fabrication of VH-CMGs. Respective densities of BmimAc, oil and water were taken as 1.05, 0.95 and 1.00 g mL^{-1}.

Sample Name	Cellulose/g	BmimAc/g	Oil/g	Water/g
VH-200	0.075	2.63	4.75	15.0
VH-1	0.22	7.80	0.07	15.0
VH-0.25	0.22	7.86	0.02	15.0

CMG-in-water dispersions (containing IL, CMGs, water and oil) were then dialyzed against pure distilled water for ca. 48h (at room temperature), until the conductivity of the water was < 10 μS (that is to say, complete removal of the ionic liquid)(Napso et al., (2016); Islam and Lyon, (2020)). The CMG-in-water dispersion was concentrated on a rotary evaporator (120 rpm, 55 °C) until the volume was less than half the initial volume and subsequently was dried in an oven (80 °C, 6h), to measure the dry weight of the cellulose. The cellulose content of emulsions is given as their dry weight with respect to the oil phase: for example, for a 10:90 W/O emulsion prepared with a 1 wt% cellulose dispersion (dry weight), the cellulose content is given as 0.9 wt%. Table 5.2 gives abbreviations for the samples using the following format: type of agitation-amount of oil. For example, CMGs produced via high-speed mixing with 0.25 wt% oil are denoted as "*H-0.25".* A schematic outlining how each type of CMG stabilizer was fabricated (L-, H- and VH-CMGs) is given in Figure 5.1, for clarity.

Table 5.2. Sample names for CMGs produced via various coagulation routes.

Sample Name	Method of CMG-production	Amount of Oil/wt%
L-0.25	Dropwise addition with low shear (syringe)	0.25
L-1	Dropwise addition with low shear (syringe)	1
L-200	Dropwise addition with low shear (syringe)	200
H-0.25	High-speed mixing (Ultra Turrax)	0.25
H-1	High-speed mixing (Ultra Turrax)	1
H-200	High-speed mixing (Ultra Turrax)	200
VH-0.25	Jet Homogenizer (300-500 bar)	0.25
VH-1	Jet Homogenizer (300-500 bar)	1
VH-200	Jet Homogenizer (300-500 bar)	200

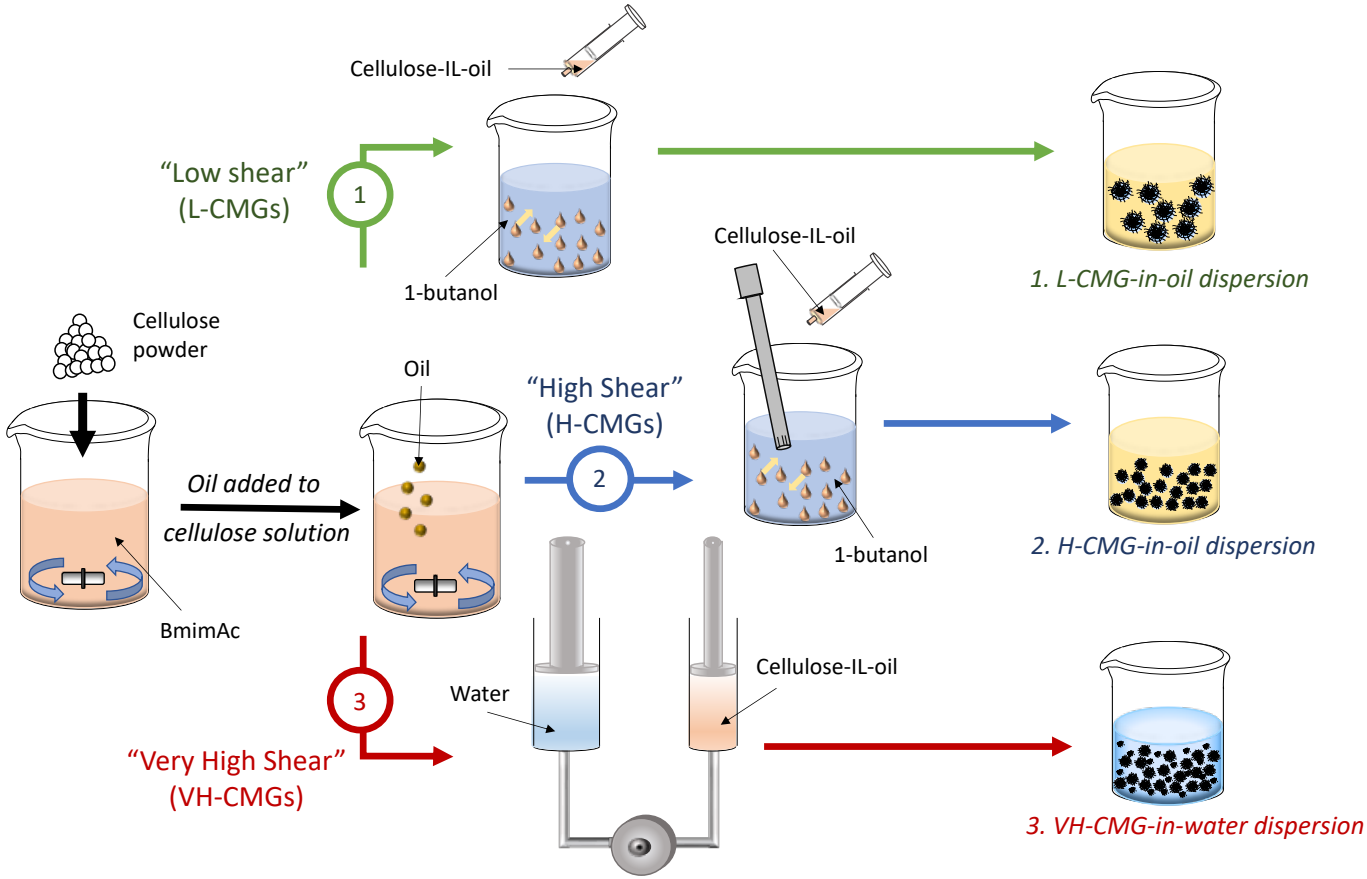

Figure 5.1. Schematic to show methods for producing different CMG stabilizers: 1. 'L-CMGs,' produced by adding cellulose-IL-oil solution dropwise to 1-butanol; 2. 'H-CMGs,' produced by adding cellulose-IL-oil solution dropwise under shear to 1-butanol and 3. 'VH-CMGs,' produced by passing cellulose-IL-oil solution and water through a high-pressure jet homogenizer.

5.3.5 W/O emulsions stabilized by CMGs

10 and 20 vol% water-in-oil (W/O) emulsions were formed by adding the required amount of pure water/CMG-in-water dispersion dropwise to pure oil/CMG-in-oil dispersion, under shearing (Ultra Turrax, 24,000 rpm, 2 min). For the L-/H-CMGs (produced via a 'top-down' method), pure water was added to the CMG-in-oil dispersions, whilst for the VH-CMGs (produced via a 'bottom-up' method), CMG-in-water dispersions were added to pure oil. A combination of CMG-types was also explored, where a water dispersion of VH-CMGs was added dropwise to an oil dispersion of H-CMGs. 2 mL of the emulsion was then taken and stored in a glass vial to analyze stability and sedimentation over time.

5.4 Characterization

5.4.1 Optical microscopy

CMG-in-water, CMG-in-oil dispersions and W/O emulsions were analyzed using a light microscope (Nikon, SMZ-2T, Japan), equipped with a digital camera (Leica MC120 HD) and 10x/20x lenses. A drop of each dispersion was placed on a welled slide and covered with a coverslip (0.17 mm thickness). Images were processed using the image analysis software ImageJ.

5.4.2 Confocal laser scanning microscopy (CLSM)

The microstructure of W/O emulsions was analyzed via confocal laser scanning microscopy (CLSM) using a Zeiss LSM880 inverted microscope (Germany) with a 20x and 40x objective lens. Approximately 290 µL of sample was added to a welled slide and a coverslip was placed on top (0.17 mm thickness), ensuring that no air bubbles were trapped between the sample and coverslip. Calcofluor White was used to stain cellulose, which was added to the sample before confocal analysis (0.1 w/v%, 10 % v/v stain:dispersion/emulsion). Nile Red (0.4 mg mL^{-1} in DMSO) was added to W/O emulsions in order to stain the oil phase and analyze the shape of the water droplets (1 % v/v stain:emulsion). For Calcofluor White, an excitation wavelength of 405 nm was used and emission between 415 and 470 nm measured (unless otherwise stated). For Nile Red, an excitation wavelength of 488 nm was used and emission between 420 and 520 nm measured. Images were processed using the image analysis software Zen or ImageJ.

5.4.3 Particle size measurements

Particle size distributions (PSDs) and ζ-potentials of CMG-in-water dispersions were measured using dynamic light scattering (DLS) via a

Zetasizer Nano ZS. The dispersions were diluted before measuring: briefly, approximately two drops of sample added to a 3 mL cuvette of deionized water. Static light scattering (SLS) was performed on a Malvern Mastersizer 3000 to measure the PSD of CMG-in-oil dispersions and W/O emulsions. In all cases, the dispersions and emulsions were added dropwise to a small volume dispersion unit filled with sunflower oil and equipped with a mixer (until the laser obscuration was around 2-4%), and were therefore diluted at least 10-fold before the measurement. The refractive indices of water, MCT-oil, HOSO and cellulose were taken as 1.33, 1.45, 1.46 and 1.47 respectively and PSDs were calculated based on the Mie theory. Five measurements were taken for each sample and the average of these reported. The mean distribution of particle sizes is displayed in terms of the surface-weighted mean diameter (*d*3,2), as described:

Equation 5.1.
$$(\boldsymbol{d3,2}) = \frac{\boldsymbol{\Sigma_i n_i {d_i}^3}}{\boldsymbol{\Sigma_i n_i {d_i}^2}}$$

and the volume-weighted mean diameter (*d*4,3), as described:

Equation 5.2.
$$(\boldsymbol{d4,3}) = \frac{\boldsymbol{\Sigma_i n_i {d_i}^4}}{\boldsymbol{\Sigma_i n_i {d_i}^3}}$$

where n_i gives the number of droplets; d_i gives the diameter of the particle.

5.4.4 Rheological analysis

Rheological measurements were conducted using an Anton Paar MCR 302 (Anton Paar GmbH, Graz, Austria) rheometer and a 50 mm-diameter cone-plate geometry (CP50), with a fixed gap of 0.208 mm and an angle of 2 °. Viscosity measurements were performed on freshly prepared W/O emulsions and also after 2-, 7- and 14-days storage at a fixed temperature (25 °C), within a frequency range 0.001/0.01 to 1000 s^{-1}. Each sample was heated to the required temperature and allowed to equilibrate for 3 min before the measurements were performed. A Peltier hood system was used for additional temperature control. All raw data was analyzed using the RheoCompass software.

5.4.5 Cryogenic scanning electron microscopy (cryo-SEM)

CMG-in-oil dispersions and W/O emulsions were filled in two freezing rivets and rapidly frozen in slushed nitrogen. Frozen samples were then transferred under vacuum via a cryo shuttle into a Quorum PP3010 cryo preparation chamber, which was kept under high vacuum and at -140 °C. Each sample was fractured with a cooled knife and then sublimed for approximately 3 min at -90 °C, and sputter-coated with a thin layer of Iridium. Finally, they were transferred to a Thermo scientific Helios G4 CX DualBeam (focussed ion

beam scanning electron microscope; FIB-SEM), operating at 2 kV and 0.1 nA . The FIB-SEM was fitted with a cold stage (-140 °C) and cold finger (-175 °C) to reduce ice contamination and a Through the Lens (TLD) detector was used.

5.5 Results and discussion

5.5.1 L- and H-in-oil dispersions

Firstly, CMGs fabricated with low shear (L) were analyzed, which involved breaking the cellulose macrogels down into CMG-in-oil dispersions ('top-down' method). Optical micrographs and PSDs of L-in-oil dispersions at various concentrations are given in **Appendix C** (Figure C 2). As the concentration of CMG ([CMG]) in the dispersion increases, the average size generally increased: $d3,2$ values of 9.73±0.99, 10.2±1.1 and 52.4±1.9 μm were obtained for 2, 4 and 6 wv% L-in-oil dispersions, respectively. Furthermore, CMG-flocculation was visible using optical microscopy when [CMG] exceeded 5 wv% (Figure C 2c), which was reflected by a sharp increase in $d4,3$ (29.7±4.4 and 71.7±3.0 μm for 4 and 6 wv% [CMG] respectively). However, the particles were weakly aggregated since they could be broken up by dilution and therefore could be redispersed upon emulsification via homogenization. It was also observed that the sizes of L-CMGs appeared quite different in the confocal and optical micrographs (Figure 5.2b and Figure C 2). Whilst flocculation is less visible in the former case, it is likely that the Calcofluor White signal from the larger CMGs dominates and therefore smaller CMGs are less visible in the confocal image, compared to the optical image. This will be expanded on later in 5.5.7.

High-speed mixing (H) during coagulation was also adopted to try to reduce the CMG particle size and therefore the W/O droplet size that they stabilize. Figure 5.2a shows the PSDs of L- and H-in-oil CMG dispersions, to provide a comparison between the two coagulation routes. Clearly the introduction of agitation during coagulation had an effect on the CMG particle sizes, with the average size being approximately 10 times smaller for the H-CMGs compared to the L-CMGs at the equivalent concentrations. This was confirmed by CLSM (Figure 5.2b), where it appeared that smaller and more homogeneous particles could be produced by introducing high shear. It should be noted in the micrograph (Figure 5.2b) that the staining agent appears to be inhomogeneously distributed, which we attribute to the inhomogeneous structure of the cellulose macrogels (Figure C 2d) and therefore the CMGs. In both cases, the amount of oil added during coagulation appeared to have no clear effect on the particle sizes of the L- and H-CMGs (data not shown) and therefore we can directly compare CMGs with various quantities of oil.

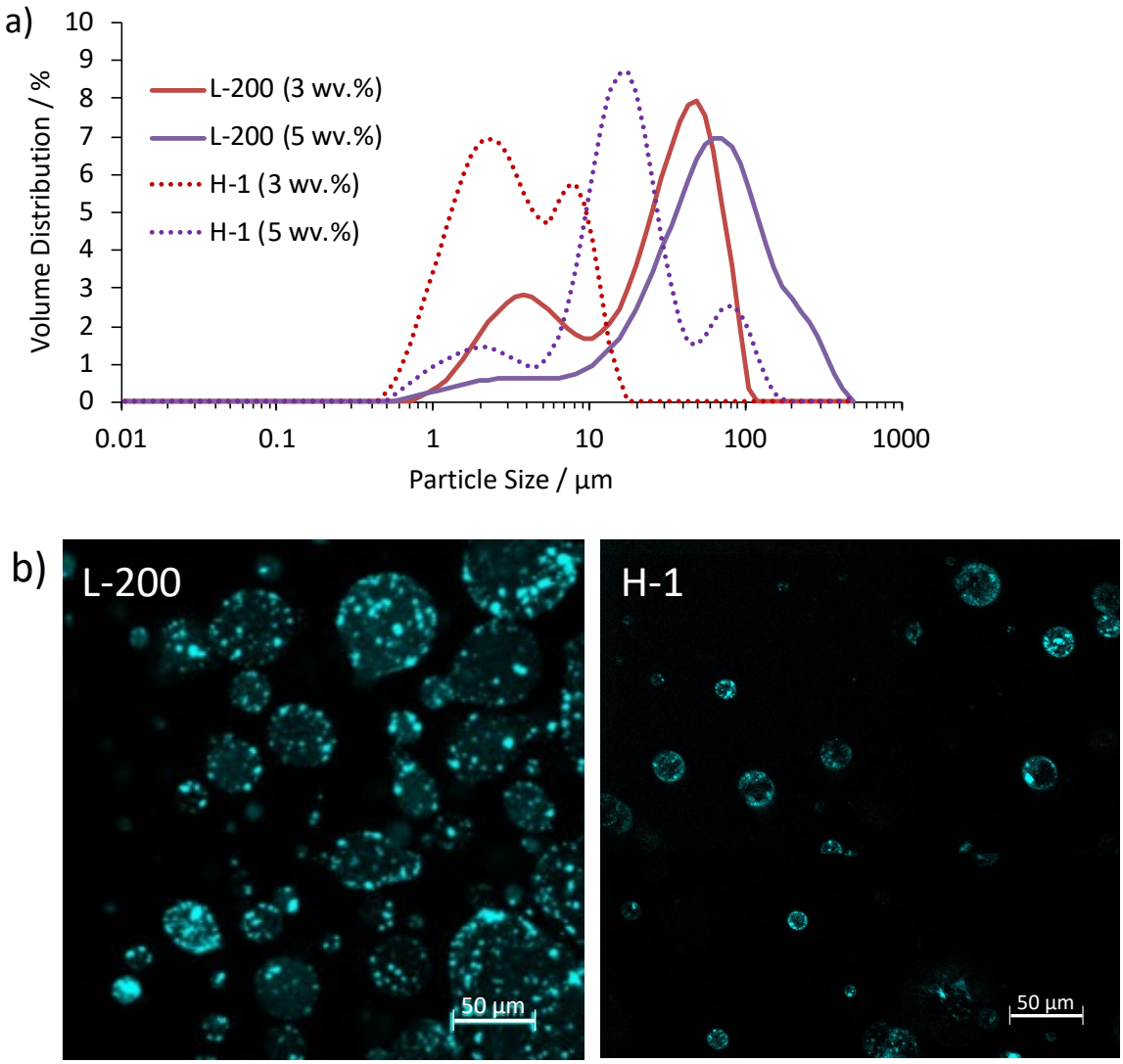

Figure 5.2. a) PSDs of CMG-in-oil dispersions (3 wv% = red and 5 wv% = purple; L = solid lines and H = dashed lines) from L-200 and H-1; b) confocal micrographs of CMG-in-oil dispersions (3 wv%). Scale bar = 50 µm, shown at the bottom right in white.

5.5.2 Particle size of W/O emulsions stabilized by L- and H-CMGs

Various concentrations of L- and H-in-oil CMG dispersions ([CMG] = 1-5 wv% of oil volume) were used to fabricate W/O emulsions, to assess the effect of [CMG] on emulsion stability. An oil-continuous emulsion was produced for all concentrations of CMG, as determined by the drop test method.

Figure 5.3a and b give the optical micrographs and PSDs respectively of W/O emulsions with various L-200 concentrations. From the micrographs, it appears that the droplet size of the emulsions decreases slightly and becomes more uniform as the concentration of L-200 increases, with the 4 and 5 wv% CMG-stabilized emulsions giving the most homogeneous appearance. However, the droplet size does not appear to change significantly between

[CMG] = 2-5 wv% according to the PSDs, suggesting that a ‘threshold’ concentration is reached at 2 wv% CMG and additional CMGs at higher concentrations do not affect droplet size but may increase surface coverage. In addition, some very small particles are visible in the optical micrographs and a corresponding peak appears in the PSD at ca. 1 μm, indicating the presence of small CMGs which do not initially adsorb to the water-oil interface. This will be discussed further in section 5.5.7. The average size from the PSDs does not appear to correlate with the size of droplets visible under the microscope, probably due to the presence of flocculated structures that were not broken down in the Mastersizer measurements due to insufficient stirring speeds (<2000 rpm). The size distribution for the 1 wv% emulsion was significantly broader, in agreement with the larger, non-spherical droplets visible in the micrograph (Figure 5.3a, shown by red arrows). This indicates some droplet coalescence is occurring and a minimum [CMG] of 2 wv% is required for stability.

The degree of interfacial coverage of water droplets by CMGs was demonstrated via CLSM (Figure 5.4). At low [CMG] (1 wv%), there appeared insufficient CMG covering the droplet interface, hence explaining why destabilization processes such as coalescence and flocculation would be expected to occur (Dickinson, (2009)). This was confirmed by a rapid increase in sediment height upon formation of the emulsion, plus after 2 weeks storage, the emulsion layer was almost completely clear (Figure C 3). At [CMG] > 1 wv%, a stable emulsion could be formed with sufficient CMG droplet coverage to delay coalescence, again indicating a ‘threshold’ concentration of 2 wv%. Furthermore, the emulsion layer was still turbid after 3 weeks, however it is unclear from the confocal micrographs in Figure 5.4 whether interfacial coverage increased in the ‘fresh’ emulsions from 3-5 wv% CMG. Thus it cannot be confirmed if ‘excess’ CMGs are initially located in the continuous phase or adsorbing at the interface to form multilayers.

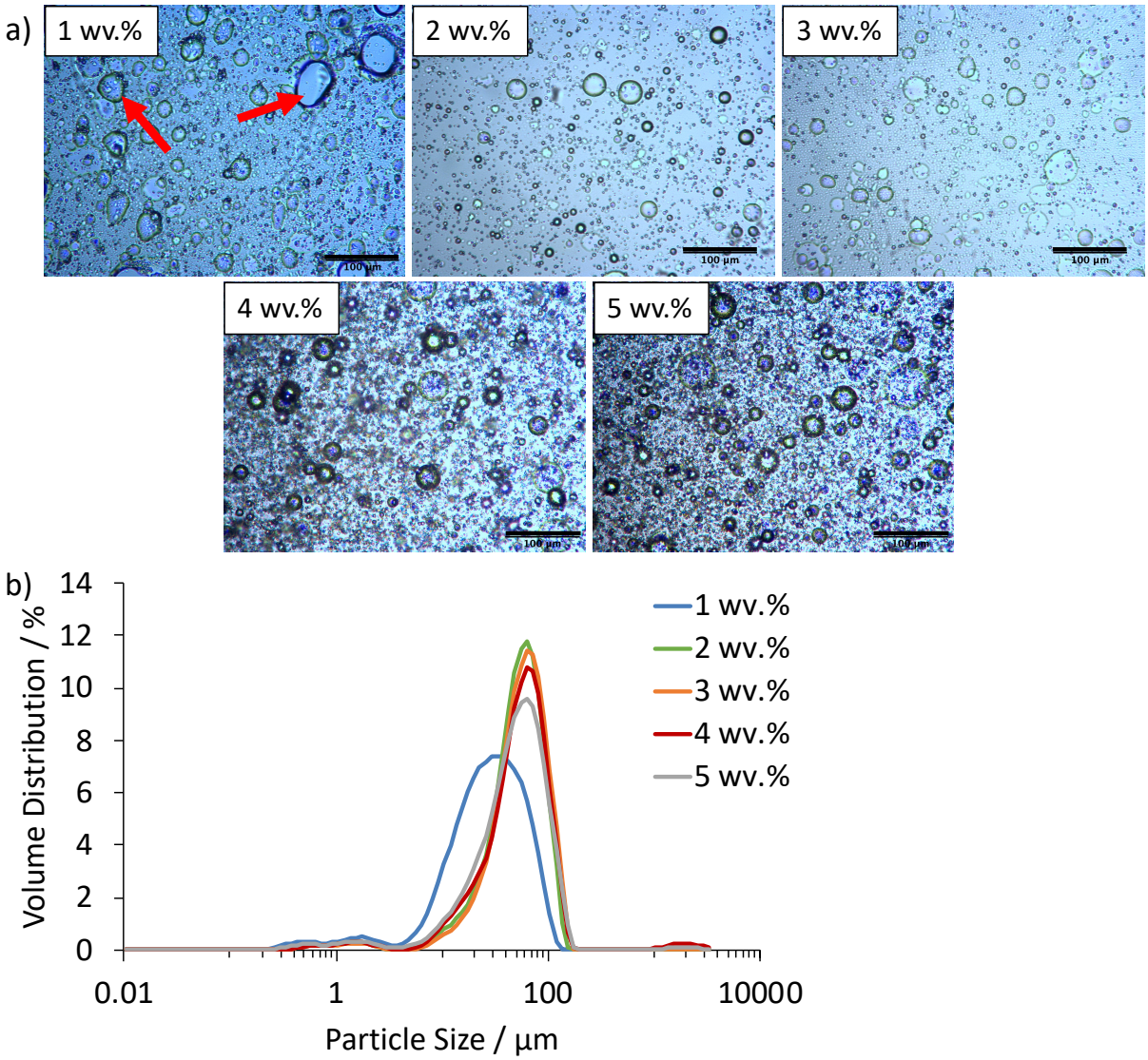

Figure 5.3. a) Optical micrographs (scale bar = 100 µm, shown at the bottom right in black). The red arrows indicate coalescence; b) PSDs of 20:80 W/O emulsions stabilized by L-200 (1 wv% = blue; 2 wv% = green; 3 wv% = orange; 4 wv%= red and 5 wv% = grey).

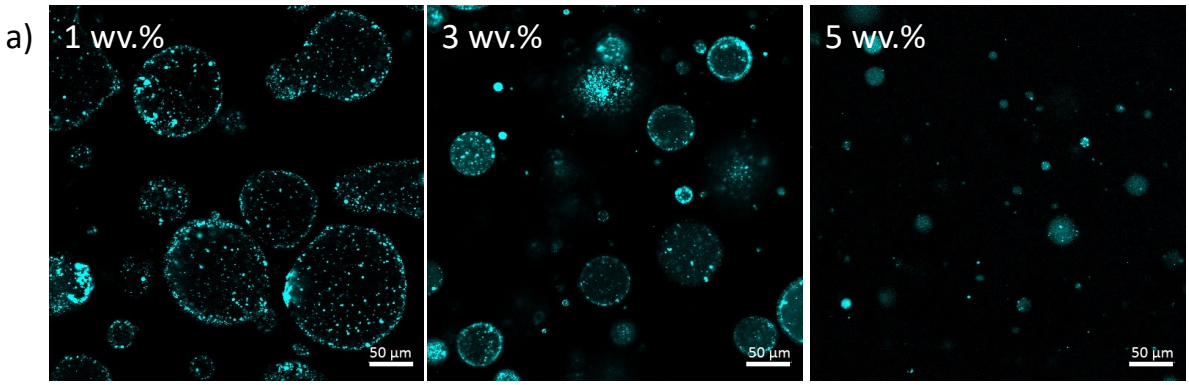

Figure 5.4. Confocal micrographs of 20:80 emulsions stabilized by L-200 (1, 3 and 5 wv%, from left to right). Scale bar = 50 µm, shown at the bottom right in white.

W/O emulsions stabilized by H-CMGs were fabricated in the same way as the L-CMGs, to compare the effect of CMG particle size on emulsion stabilizing ability. Confocal images for emulsions stabilized by H-1 and L-200 are given in Figure 5.5a and b, comparing the appearance of the emulsions. Although once again the PSDs were not significantly different between the H-1 and L-200-stabilized emulsions (data not shown), the droplet sizes appeared much smaller in the confocal micrographs for the former. Furthermore, the *d*3,2 value of the H-CMG emulsions remained stable over time and smaller droplets were visible after 1 week storage, whilst the average droplet size for L-CMG emulsions appeared to steadily increase and reached almost double the initial *d*3,2 value after 2 weeks (Figure 5.5c). Therefore, introducing high-speed mixing during cellulose coagulation not only reduced the CMG size but also improved the emulsion system in terms of smaller and more stable water droplets. The ability to form smaller droplets minimized gravity creaming/sedimentation effects and therefore improved emulsion stability (Dickinson, (1988)).

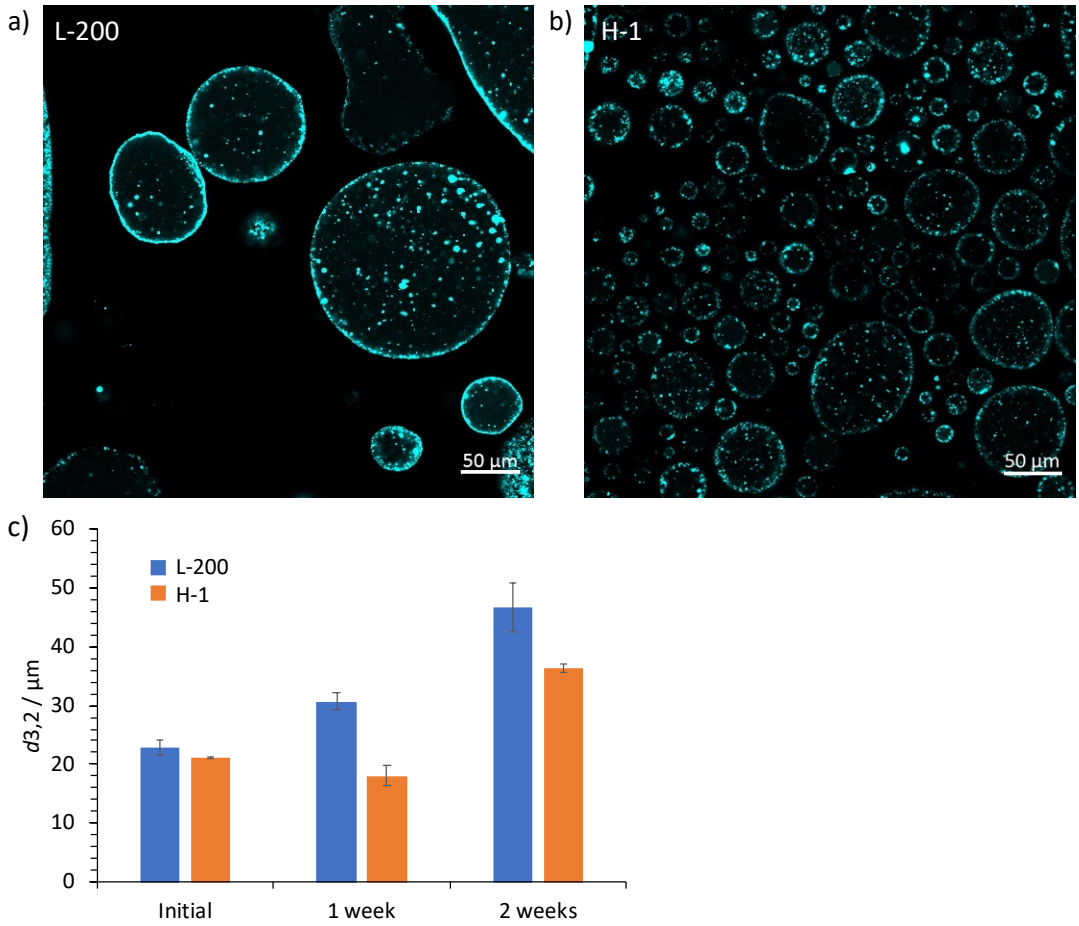

Figure 5.5. Confocal images of 20:80 emulsions stabilized by a) L-200 and b) H-1. Scale bar = 50 µm, shown at the bottom right in white; c) average droplet sizes (*d*3,2) over time of 20:80 emulsions stabilized by L-200 (blue) and H-1 (orange). Error bars give the uncertainties in the measurements.

Droplet sizes and surface coverage of W/O emulsions stabilized by H-CMGs above the ‘threshold’ concentration (3 and 5 wv%) were also compared (Figure C 4). Again, the PSDs were almost identical and little difference in coverage could be observed using CLSM.

5.5.3 VH-in-water dispersions

Finally, a third route for cellulose coagulation was investigated using HPH, in attempt to reduce the particle size even further by ensuring mixing of the cellulose-BmimAc-oil mixture and the anti-solvent under highly turbulent shear conditions. In contrast to the previous methods, water alone was used as anti-solvent for this coagulation route (rather than 1-butanol followed by a solvent exchange, as described for L-CMGs and H-CMGs in 5.3.2 and 5.3.3). This was because particles produced under HPH were too fine to be collected via filtration and therefore the use of HPH describes a ‘bottom-up’ approach to microgelation, as opposed to fabrication of a larger macrogel and subsequent break-down (‘top-down’). To form W/O emulsions from the VH-CMGs, CMG-in-water dispersions were added dropwise to pure oil, therefore limiting the maximum CMG concentration according to the amount of water in the emulsion (20 vol%).

Figure 5.6a and b give the appearance and PSDs respectively of various VH-in-water dispersions. (Some samples of VH-in-water dispersions were dried to determine the amount (wt%) of cellulose + oil, as outlined in 5.3.4). Generally, VH-CMGs were at least an order of magnitude smaller in size than the L- and H-CMGs, and the PSDs were much narrower. This was expected because the JH results in very high fluid velocities and highly turbulent conditions, inducing cavitation and restricting the growth of nascent microgel particles and thus producing much more fine and monodisperse dispersions (Pravinata et al., (2016)). However, when the dispersions were concentrated the CMGs began to aggregate, and in those containing the highest [CMG] 2 peaks were observed in the PSD (Figure 5.6b, [CMG] = 1.217 wt%). Furthermore, aggregation of particles was confirmed via optical microscopy at much lower concentrations for CMG-in-water compared to the CMG-in-oil dispersions (L- and H-CMGs described in 5.5.1), plus large length-scale cellulose networks became visible. Despite this, aggregates appeared to be made up of homogeneous CMG particles with regular morphologies and were loosely bound, and therefore easily broken up by re-dilution of the CMG-in-water dispersions.

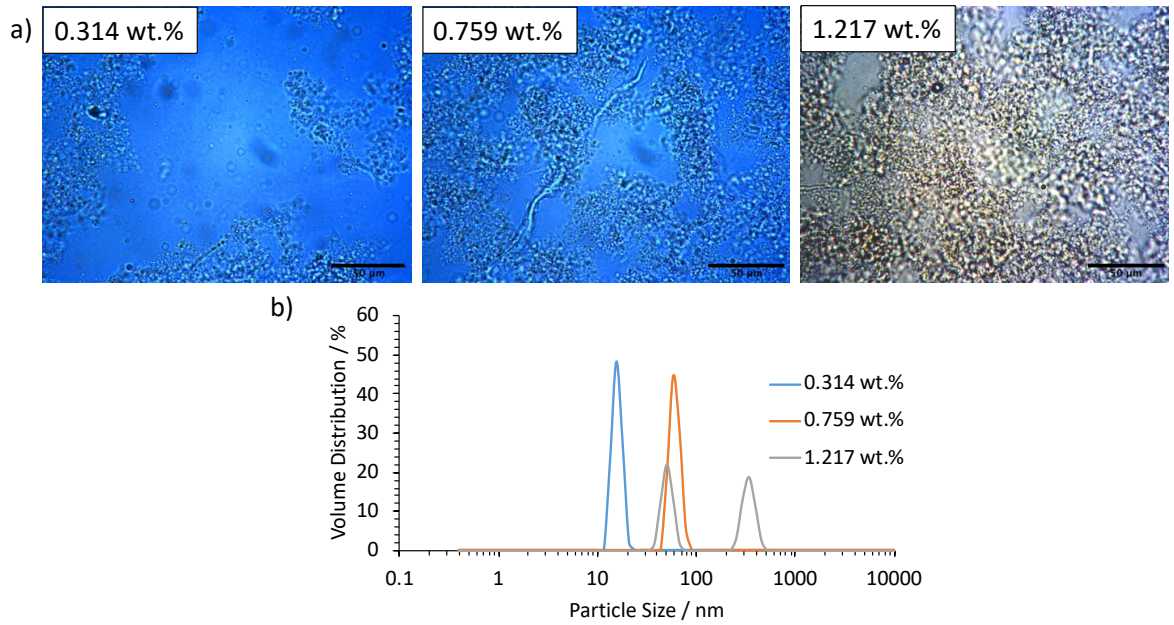

Figure 5.6. a) Optical micrographs and b) PSDs of VH-0.25-in-water dispersions at various concentrations (0.314 wt% = blue; 0.759 wt% = orange and 1.217 wt% = grey). Scale bar = 50 µm, shown at bottom right in black.

5.5.4 Particle size of W/O emulsions stabilized by VH-CMGs

Various concentrations of VH-in-water dispersions were used to explore whether cellulose aggregation influences the W/O stabilizing ability of the CMGs. Figure C 5a and b give the optical micrographs and PSDs of 'fresh' W/O emulsions with 0.278 and 0.836 wt% VH-1 respectively. A slightly narrower PSD was measured for the emulsion with the higher [CMG] (0.836 wt%), but no significant difference in the appearance of the emulsions was observed. Droplet sizes were initially reduced compared to W/O emulsions stabilized by L- and H-CMGs, which is probably due to the higher emulsion efficiency of the smaller, more homogeneous VH-CMGs and their faster diffusion to the interface (Capron et al., (2017); Medronho et al., (2018); Dai et al., (2020)). However, since smaller particles generally require greater surface coverage for stabilization of droplets compared to larger, more irregularly-shaped particles (Costa, Medronho, et al., (2021)), the concentrations of VH-CMGs in the W/O emulsions were insufficient to prevent destabilization processes over time. PSDs of the emulsions were measured 3 h later (data not shown) and in both cases, bimodal PSDs were obtained for both 0.278 and 0.836 wt%-stabilized emulsions with a comparatively large second peak. The *d*4,3 values increased dramatically over 3 h (75.1 ± 9.2-251 ± 19.5 µm and 25.2 ± 1.2-336 ± 36.5 µm for 0.278 and 0.836 wt%-emulsions, respectively), indicating the presence of larger structures in the emulsions. Upon storage for 1 week, large droplets were visible under the microscope

(Figure C 5c and d) and the PSD shifted significantly to larger sizes, indicating further increase in droplet sizes and/or possible further aggregation. The bottom water layer of the emulsions was turbid after 1 week (not shown), indicating that particularly large cellulose aggregates had sedimented out, therefore probably leaving a very low concentration of CMG in the emulsion layer.

Thus, although the smallest and narrowest PSDs were achieved for the VH-CMGs using a 'bottom-up' approach, the use of the JH meant that a very fine gel particle water dispersion was obtained and therefore the stabilizer had to be introduced in the discontinuous phase (water), as opposed to the continuous phase (oil). It did not seem possible or desirable to increase this concentration further (via evaporation or centrifugation), because this just led to increased viscosity of the aqueous phase and CMG aggregates. Consequently, a lower [CMG] as stabilizer was introduced in the system compared to the two previous, 'top-down' methods and although the VH-CMGs were smaller, apparently the interfacial coverage was not high enough to prevent some W/O emulsion destabilization (Albert et al., (2019)).

5.5.5 O/W emulsions stabilized by VH-CMGs

It was considered that the properties of the VH-CMGs are expected to be different to the L-/H-CMGs, due to both the type of coagulant and the method of coagulation.

Firstly, only water was used for the VH-CMGs (5.3.4), whilst 1-butanol (followed by ethanol and water) were used for the L- and H-CMGs (5.3.2 and 5.3.3). Changing the anti-solvent is known to affect the properties of the reprecipitated cellulose material (Fink et al., (2001); Ilyin et al., (2018); Hedlund, Theliander, et al., (2019)): since water has a much higher affinity for both cellulose and BmimAc (compared to 1-butanol), it mixes evenly throughout the solution and supplies intermediate hydrogen bonds during coagulation, leading to more crystalline cellulose (Hedlund, Köhnke, et al., (2019)). On the other hand, 1-butanol is expected to diffuse into the coagulating solution at a slower rate and a more amorphous material is obtained (Fink et al., (2001)). Secondly, cellulose was coagulated under highly turbulent conditions for the VH-CMGs via a 'bottom-up' approach. This is expected to further facilitate rapid mixing of the anti-solvent and IL solution (which is already assisted by the use of a faster diffusing anti-solvent), and results in a 'hard' coagulation (Fink et al., (2001)). Therefore, less oil may be entrapped within the gel structure, making the VH-CMGs less suitable as W/O

stabilizers and less ‘hydrophobic’ compared to the L-/H-CMGs, which are obtained via a ‘softer’ coagulation route.

To understand more about the surface properties of VH-CMGs, attempts were made to fabricate O/W emulsions with VH-1. This was to compare their suitability as oil-continuous versus water-continuous stabilizers. Optical micrographs of the emulsions on day 1 along with average droplet size (*d*4,3) values, over a period of 2 weeks, are given in **Appendix C** (Figure C 6). The O/W droplets were much more flocculated (than W/O emulsions) and this was reflected by significantly larger *d*4,3 values. Furthermore, the O/W emulsions possessed high viscosities (Figure C 7a), suggesting that a reinforcing cellulose network was formed in the continuous aqueous phase, as described in the literature (Oza and Frank, (1986); Jia et al., (2015); Z. Li et al., (2018); Ni et al., (2020)). The viscosity flow curves were almost identical for emulsions after 2 weeks storage and the formation of a flocculated network could be confirmed using confocal microscopy (Figure C 7b and c). The CMGs aggregated significantly in the water-continuous phase and formed thick layers between the oil droplets, contributing somewhat to the stabilization against creaming and coalescence. Size distributions, micrographs and images of W/O and O/W emulsions (20 vol% discontinuous phase) with equivalent VH-1 concentrations (0.243 wt% with respect to the continuous phase) are given in Figure 5.7. Comparing the two emulsion types, it is evident that much smaller W/O droplets could be produced whilst the O/W oil droplets were much more flocculated. Furthermore, some of the larger CMGs are visible within the large oil droplets for the O/W emulsions, which could in fact be described as a double emulsion (water-in-oil-in-water). Thus the VH-CMGs, as prepared via this alternative ‘bottom-up’ route, are still more suitable as hydrophobic particulate stabilizers of W/O emulsions, but challenges remain in creating a sufficiently high concentration of these CMGs in the oil phase before emulsification of the water phase.

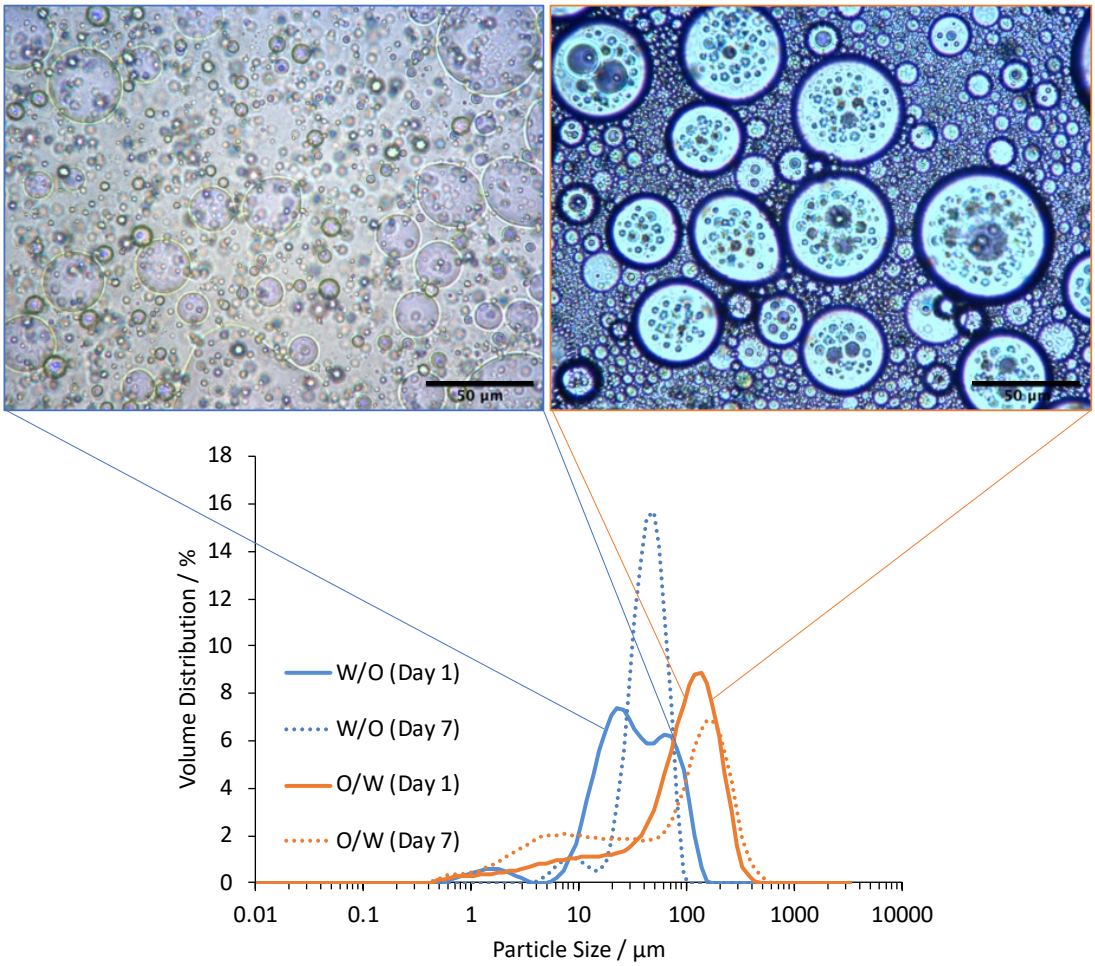

Figure 5.7. PSDs of W/O (blue) and O/W (orange) emulsions stabilized by 0.234 wt% VH-1, analyzed over time (day 1 = filled line, day 7 = dashed line); inset gives optical micrographs of freshly prepared W/O (blue border) and O/W (orange border) emulsions. Scale bar = 50 µm, shown at bottom right in black.

5.5.6 Particle size of W/O emulsions stabilized by a combination of H- and VH-CMGs

Out of the three coagulation routes, emulsions stabilized by H-CMGs displayed the best droplet size stability over time. However, the minimum size of droplets that could be achieved was still limited by the size of the CMG particles in the oil phase. Storage instability becomes a greater problem in systems with larger droplets, since droplet coalescence and therefore phase separation can be more likely (Bai et al., (2018)). Consequently, it was decided to test both H-CMGs and VH-CMGs together, in order to combine the advantages of higher emulsion stability for the former and the creation of smaller, submicron CMGs and droplets for the latter. Confocal micrographs with PSDs overlaid for 20:80 W/O emulsions with H-1 only, VH-1 only and a combination of the two are given below (Figure 5.8a, b and c respectively).

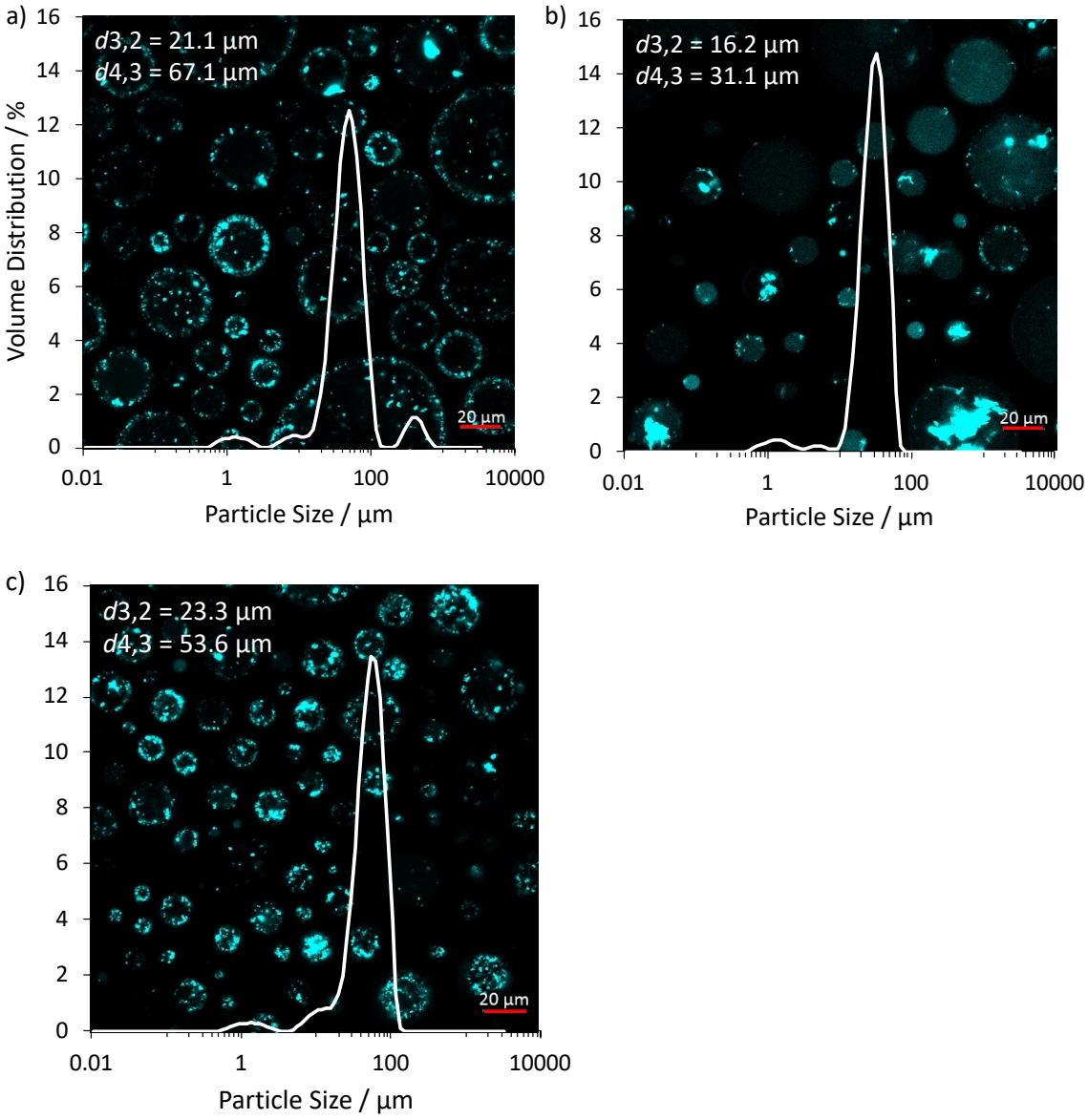

Figure 5.8. Confocal micrographs with PSDs overlaid for 20:80 emulsions stabilised by a) H-1 (3 wv%); b) VH-1 (0.557 wt%) and c) both H-1 and VH-1 (3 wv% and 0.557 wt%, respectively). Scale bar = 20 µm, shown at bottom right in red, *d*3,2 and *d*4,3 values (µm) are given in the upper left corner.

From Figure 5.8, it appears that the use of H-1 (a) and VH-1 (b) alone leads to a relatively thin coverage of water droplets, compared to when both types of CMG are used together (c). In the absence of VH-CMGs, only a few, larger droplets were visible after 2 weeks (Figure C 8a) and a large amount of water sedimented out (Figure C 8b). However when a combination of CMGs was used, thicker layers of cellulose were visible at the droplet interface and the average particle size remained stable for at least 14 days (Figure C 8a). More water remained within the emulsion layer (Figure C 8b) and a large number of small droplets were still visible after 2 months (Figure C 8c), indicating enhanced stability.

Using two types of CMG therefore appears to be the best approach to produce stable, W/O emulsions. Whilst the 'medium' sized particles (H-1) allow sufficient concentration of cellulose to be added to the emulsion, the 'smaller' particles (VH-1) diffuse more rapidly to the interface and produce finer dispersions of droplets. Both confocal imaging and cryo-SEM revealed the formation of a thick layer of cellulose (Figure 5.9a and b (blue arrow) respectively), with a relatively homogeneous droplet size distribution, explaining the high stability. VH-CMGs displayed a highly regular morphology (Figure 5.9b, red arrows) which may allow them to pack more densely at the interface and produce smaller water droplets upon initial emulsification. On the other hand, the larger, heterogeneous H-CMGs require a lower surface coverage and may protrude into the oil phase, providing enhanced steric stability (Capron et al., (2017)). Therefore, this approach takes advantage of cellulose-cellulose attractive interactions, with effectively two types of uncharged CMGs being introduced.

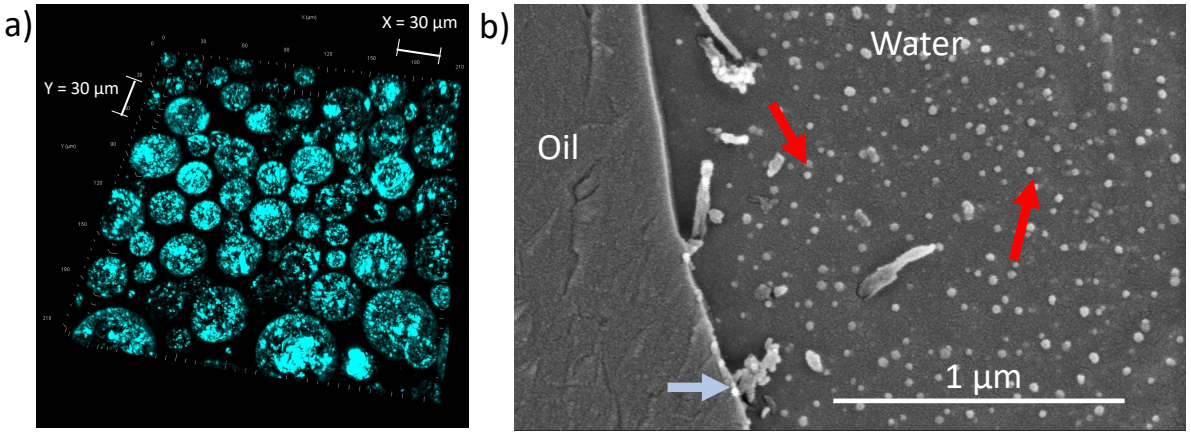

Figure 5.9. a) Confocal image of 3D stack of 20:80 W/O emulsion stabilized by H-1 (3 wv%) and VH-1 (0.557 wt%). Scale bar = 30 µm (X and Y axis), depth of 30 µm (Z axis); b) cryo-SEM of 20:80 W/O emulsion stabilized by H-200 (5 wv%) and VH-0.25 (0.267 wt%). Red arrows indicate regular morphology of VH-CMGs; blue arrow indicates thick cellulose layer at the water/oil interface. Scale bar = 1 µm, shown at bottom right in white.

5.5.7 Presence of excess CMGs in W/O emulsions stabilized with CMGs

In order to try and gain more information about CMG surface coverage, attempts were made to try and distinguish the 'free,' non-adsorbed CMGs from the CMGs which adsorb to the W/O interface, by generating a PSD for the water droplets alone. Briefly, a set fraction of the CMG-in-oil PSD, (determined from the volume of CMGs dispersed in the oil phase), was subtracted from the W/O volume distribution data (full details can be found in **Appendix C**, below Figure C 8). In this case we are assuming that the refractive index of the CMGs

is roughly the same as water, which should be a valid assumption since the major component of the CMGs is water. Figure C 9 gives an example of PSDs for W/O emulsions stabilized by 2 wv% (a) and 5 wv% (b) L-200, before and after subtraction of the excess CMGs. In general, this subtraction had the effect of marginally reducing the volume distributions at the lower size classes and therefore slightly shifting the average droplet size to higher values. However, the difference between the two was very minor across a range of concentrations and was unable to explain the difference observed between the PSDs and the confocal images.

Some success visualizing the surface coverage in detail was achieved through cryo-SEM. Whilst although evidently not conclusive or quantitative, it confirmed the presence of particles at the droplet interface. In Figure C 10a-c, the droplet surface is clearly rough due to the adsorption of CMGs and a ‘coating’ of cellulose fibers is visible.

Non-adsorbed CMGs in the continuous oil phase were also difficult to visualize both by CLSM and cryo-SEM, since they were not effectively stained by the Calcofluor White solution and details in the oil phase were difficult to see (respectively). The former may be due to the fact that the dye was introduced in an aqueous medium and/or because the Calcofluor fluorescence is completely quenched in the oil phase. As a result, any excess CMGs in the oil phase are not visible via confocal microscopy, unlike in the optical images, which therefore appear quite different – it being impossible in the latter to distinguish water droplets from larger CMGs. Brightfield images were overlaid with confocal micrographs in order to visualize the smaller CMGs, since the Calcofluor White signal from the larger CMGs tended to dominate (Figure C 11a). This also allowed visualization of excess CMGs in the oil phase. Furthermore, excitation and emission experiments of CMG-in-oil and CMG-in-water dispersions both stained by Calcofluor White were conducted, to determine whether different emission filters may be used to selectively detect the CMGs in oil (**Appendix C**, Figure C 11c and d). From these experiments, higher emission wavelengths (i.e. 450-550 nm) were investigated during imaging, and Figure C 11b gives a H-0.25-in-oil dispersion with the adjusted emission filters. This approach was somewhat successful and allowed us to confirm the presence of smaller CMGs in the oil phase, which were completely absent when the standard emission wavelengths were used.

The number-weighted PSDs were also considered and compared to the original volume-weighted PSDs generated by the Mastersizer, since number-average tends to be more influenced by the smaller particles. Figure 5.10

gives the confocal micrograph of a 3 wv% CMG-in-oil dispersion (H-0.25) with the brightfield image overlaid, and the corresponding number-weighted and volume-weighted PSDs. As predicted, particle size diameters were much smaller when the number-weighted distributions were considered and a narrower distribution was seen, indicating that probably the majority of the CMG particles in the oil dispersions are within the 1-10 µm range. However, some larger particles and water droplets are present, which fluoresce more strongly and are therefore more visible in the confocal micrographs, causing the volume-weighted PSD to be much higher. Therefore, we conclude that the volume-weighted PSD is representing the stained, larger water droplets (> ca. 10 µm) and that the number-weighted PSD is representing the smaller, individual CMG particles (< 10 µm), visible in the brightfield image. Droplet size analysis conducted using ImageJ agreed with these observations and can be found in **Appendix C**, (above Figure C 11).

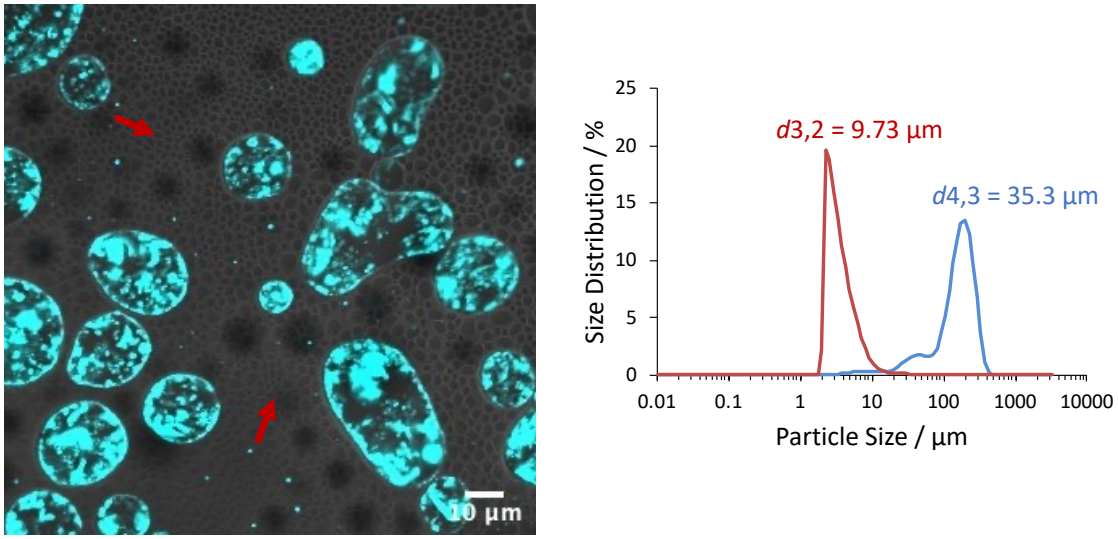

Figure 5.10. Confocal micrograph with brightfield image overlaid for a 3 wv% H-0.25 CMG-in-oil dispersion, with the red arrows indicating the individual CMG particles. The number-weighted and volume-weighted PSDs are given on the right in red and blue, respectively. Scale bar = 10 µm, shown at bottom right in white.

5.5.8 Rheological analysis of W/O emulsions Stabilized by L- and H-CMGs

To try and gain better understanding of the behavior of excess CMGs in the bulk oil and their possible contribution to emulsion stability, viscosity measurements of the 20:80 W/O emulsions were performed. Since the PSDs of W/O emulsions with various [CMG] appeared to be fairly consistent (Figure 5.3b), it was inferred that differences in viscosities should be mainly influenced by changes in the rheological properties of the systems, rather than the droplet size distributions (Medronho et al., (2018)).

The flow curves of 20:80 emulsions stabilized by 1-5 wv% L-200 are given in Figure 5.11a. All emulsions initially displayed shear thinning behavior, which may be attributed to some flocculation in the oil phase (Zembyla et al., (2020)), and a slight increase in viscosity was observed as [CMG] increased (similar to trends in reports for O/W emulsions stabilized by regenerated cellulose (McClements, (2004); Shen et al., (2016))). This may be due to excess CMGs present in the oil phase at higher concentrations, which would be expected to increase the overall viscosity of the emulsion (Costa, Rosa, et al., (2021)). Subsequently, a decrease in viscosity of at least 10-fold was observed after 1 day storage for most W/O emulsions (Figure 5.11b) and very little further change was observed over 1 week storage (Figure 5.11c). At first sight, this observation might be taken as an indication of insufficiently stabilized droplets in the fresh emulsions (Brugger et al., (2008)), however confocal micrographs taken over a period of 1 month revealed a relatively stable droplet size, with cellulose still visible at the interface after 30 days and no evidence of bridging flocculation (Figure 5.11d). Furthermore, a relatively stable sediment height was recorded, eliminating the possibility of significant water separation occurring.

A reduction in viscosity after 1 day may alternatively be due to adsorption of excess CMGs from the continuous phase to the W/O interface. It has previously been reported that when an excess of microgel particles is present in the continuous phase, microgels at the interface may compress and allow excess microgel to adsorb (Pinaud et al., (2014)). This phenomenon occurs when microgels at the interface adopt more flattened structures and spontaneous compression and adsorption of microgels occurs, as opposed to when a densely packed interfacial layer forms initially (Schmitt and Ravaine, (2013)). Over time, this leads to a more complete droplet coverage and consequently a highly stable emulsion. At [CMG] above the ‘threshold’ value required for a stable emulsion (>2 wv%), it is possible that initially excess CMGs are a) dispersing in the continuous phase, or b) forming multilayers at the interface. The former seems more likely, due to the rise in bulk viscosity measured upon increase in [CMG], whilst for the latter, little difference in surface coverage was observed between the ‘fresh’ emulsions (Figure 5.4). However, upon storage an increase in cellulose coverage at the droplet interface was in fact visible using confocal microscopy (Figure C 12). Thick interfacial layers appeared around water droplets whilst little change in droplet size was observed, indicating that excess CMGs may be absorbing from the continuous phase and surface coverage may be increasing. Since the interface initially appears ‘unsaturated,’ with a small concentration of CMGs

sufficient to provide stabilization (2 wv%), there is sufficient space for excess CMGs to adsorb without the need for significant compression of readily adsorbed microgels (which may be less likely for stiffer particles, which are expected to undergo smaller deformations) (Geisel et al., (2012)) and/or the formation of multilayers. Furthermore, unlike other charged particles more commonly used as Pickering stabilizers (Albert et al., (2019)), the CMGs do not electrostatically repel each other and therefore can pack densely at the interface. Therefore, stability of W/O emulsions appears to be a combination of initially Pickering absorption of smaller CMGs particles, followed by the formation of a thicker interfacial layer with larger CMG particles from the continuous phase, leading to enhanced steric stabilization. This is strikingly different to reports for O/W emulsions, where a cellulose network forms in the water phase over time and leads to a dramatic rise in viscosity, providing an ‘indirect’ stabilizing effect and delay in droplet coalescence partly due to entrapment (Oza and Frank, (1986); Z. Li et al., (2018)).

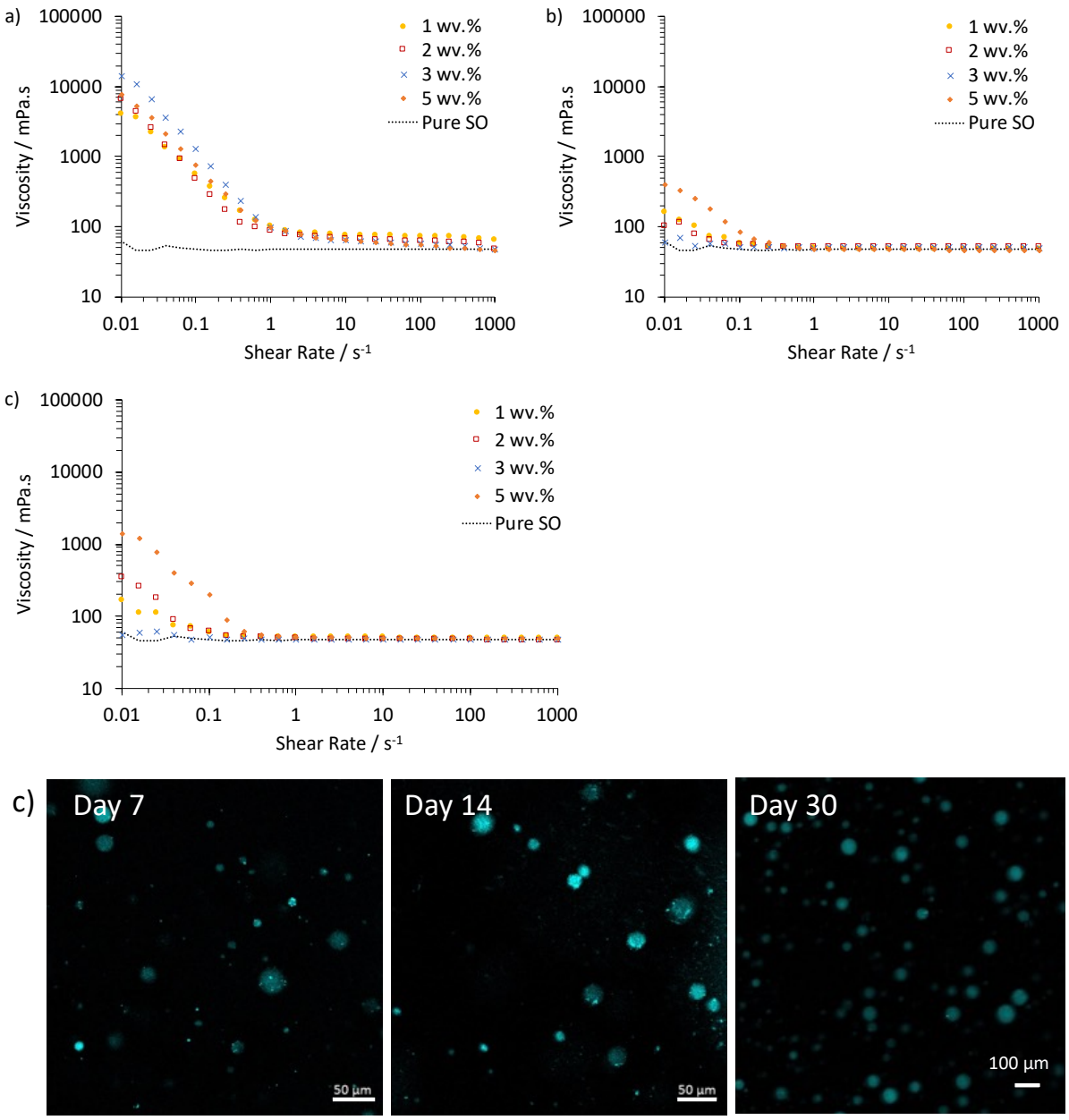

Figure 5.11. Flow curves for 20:80 W/O emulsions stabilized by L-200 (1 wv% = yellow closed circle; 2 wv% = red open square; 3 wv% = blue cross and 5 wv% = orange closed diamond), with pure sunflower oil (dashed black line). Error bars are smaller than the symbols and are therefore not displayed; a) day 1; b) day 2; c) day 7; d) confocal micrographs of 20:80 emulsion stabilized by 5 wv% CMG-L-200. Scale bars = 50, 50 and 100 µm from left to right, shown at bottom right in white.

5.5.9 Dilution of W/O emulsions to confirm 'Pickering' mechanism

Finally, W/O emulsions were diluted with oil and analyzed after 6 days storage, in order to confirm the absence of cellulose networks. Figure 5.12a gives the flow curves for the original and 10x diluted emulsions, stabilized by H-200 CMGs (5 wv%) and VH-0.25 (0.237 wt%). The viscosity of the emulsion

hardly appeared to change upon dilution, both at this concentration (Figure 5.12a) and at a lower concentration (Figure C 13), providing further evidence for a Pickering-type mechanism of stabilization. In addition, the flow curves were almost identical to that of the pure oil (above $\dot{\gamma}$ = 0.1 s^{-1}) after 1 day storage, indicating the absence of aggregated CMGs in the continuous phase and again supporting the phenomenon that larger CMGs may absorb over time. This was further evidenced by CLSM (Figure 5.12b and c), which clearly revealed CMGs at the interface after 6 days and that coverage did not appear to change upon dilution.

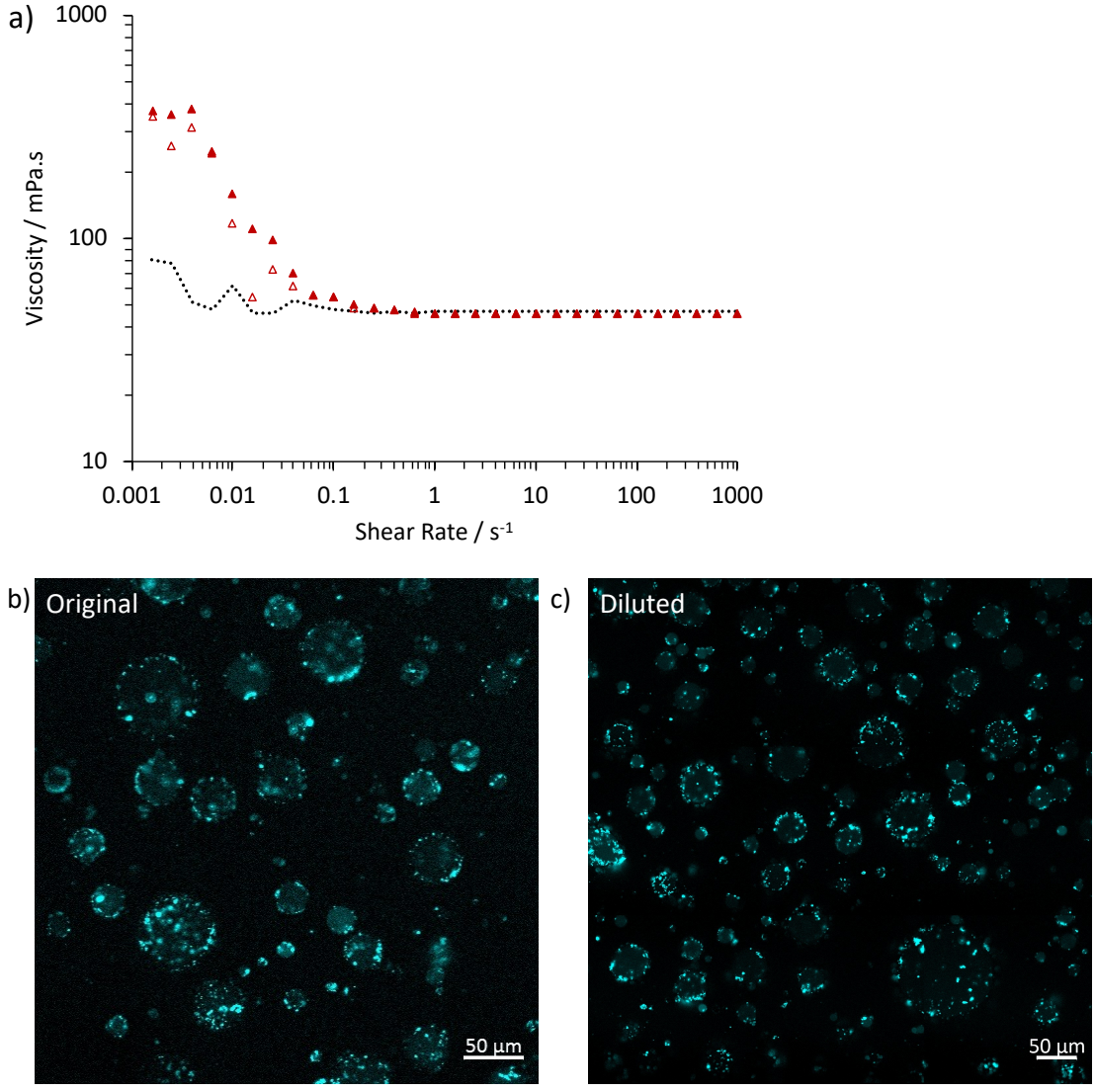

Figure 5.12. a) Flow curves for 20:80 W/O emulsions (day 6), stabilized by 5 wv% H-200 and 0.267 wt% VH-0.25 (closed red triangle = original emulsion; open red triangle = 10x diluted emulsion), with pure sunflower oil (dashed black line). Error bars are all the same size/smaller than the symbols and are therefore not displayed; confocal images of the emulsions on day 6: b) original; c) 10x diluted. Scale bar = 50 µm, shown at bottom right in white.

5.6 Conclusion

In this work, ‘top-down’ and ‘bottom-up’ methods have been used and compared to fabricate ‘hydrophobic’ cellulose stabilizers, via dissolution and coagulation from an IL. It was found that CMG particle size can be reduced by introducing agitation during coagulation, since it is probable that higher shear disrupts the reformation of inter- and intramolecular H-bonds between cellulose chains (to a certain extent). Smaller CMGs could be produced, which dispersed better in the oil-continuous phase and were able to stabilize smaller droplets in the W/O emulsions for a longer period of time. A combination of VH-CMGs (‘small’ particles) and H-CMGs (‘medium’ particles) was found to be the most effective approach, with emulsions displaying high stability for at least 2 months. Confocal microscopy and cryo-SEM revealed thick, interfacial layers in W/O emulsions after storage and viscosity measurements revealed that the stabilization of water is most likely due to interfacial absorption of the CMGs, with no evidence of a cellulose network. Therefore, we propose a mechanism based on a combination of Pickering stabilization followed by subsequent adsorption of excess CMGs to the interface over time. Further investigation into the effect of oil content on the CMG properties and their ability to stabilize oil continuous systems is currently being carried out. However, this work demonstrates that the properties of CMGs can be optimized for W/O emulsions using physical modification only, and therefore has huge potential for application in the food (Ozturk and McClements, (2016)), pharmaceutical (Bouyer et al., (2012)) and cosmetic (Schramm, (2005)) industries, among others.

5.7 References

Albert, C., Beladjine, M., Tsapis, N., Fattal, E., Agnely, F. and Huang, N. (2019). Pickering emulsions: Preparation processes, key parameters governing their properties and potential for pharmaceutical applications. *Journal of Controlled Release*. *309*, 302–332.

Ali, A., Yilmaz, E. and Sjöö, M. (2015). A Novel Technology for Personal Care Emulsions. *Sofwjournal*. *141*, 2–7.

Amagliani, L. and Schmitt, C. (2017). Globular plant protein aggregates for stabilization of food foams and emulsions. *Trends in Food Science and Technology*. *67*, 248–259.

Andresen, M. and Stenius, P. (2007). Water-in-oil emulsions stabilized by hydrophobized microfibrillated cellulose. *Journal of Dispersion Science and Technology*. *28*(6), 837–844.

Asakawa, A., Oka, T., Sasaki, C., Asada, C. and Nakamura, Y. (2016). Cholinium ionic liquid/cosolvent pretreatment for enhancing enzymatic saccharification of sugarcane bagasse. *Industrial Crops and Products*. *86*, 113–119.

Bai, L., Huan, S., Xiang, W. and Rojas, O.J. (2018). Pickering emulsions by combining cellulose nanofibrils and nanocrystals: Phase behavior and depletion stabilization. *Green Chemistry*. *20*(7), 1571–1582.

Bouyer, E., Mekhloufi, G., Rosilio, V., Grossiord, J.L. and Agnely, F. (2012). Proteins, polysaccharides, and their complexes used as stabilizers for emulsions: Alternatives to synthetic surfactants in the pharmaceutical field? *International Journal of Pharmaceutics*. *436*, 359–378.

Brugger, B., Rosen, B.A. and Richtering, W. (2008). Microgels as stimuli-responsive stabilizers for emulsions. *Langmuir*. *24*(21), 12202–12208.

Burgaud, I., Dickinson, E. and Nelson, P. V. (1990). An improved high-pressure homogenizer for making fine emulsions on a small scale. *International Journal of Food Science & Technology*. *25*(1), 39–46.

Cannon, J.B. and Long, M.A. (2008). Emulsions, Microemulsions, and Lipid-Based Drug Delivery Systems for Drug Solubilization and Delivery—Part II: Oral Applications *In*: *Water-Insoluble Drug Formulation*. Boca Raton: CRC Press, 227–254.

Capron, I., Rojas, O.J. and Bordes, R. (2017). Behavior of nanocelluloses at interfaces. *Current Opinion in Colloid and Interface Science*. *29*, 83–95.

Costa, C., Medronho, B., Lindman, B., Edlund, H. and Norgren, M. (2021). Cellulose as a Natural Emulsifier: From Nanocelluloses to Macromolecules *In: Cellulose Science and Derivatives* [Online]. IntechOpen, 1-16. Available from: https://doi.org/10.5772/intechopen.99139.

Costa, C., Rosa, P., Filipe, A., Medronho, B., Romano, A., Liberman, L., Talmon, Y. and Norgren, M. (2021). Cellulose-stabilized oil-in-water emulsions: Structural features, microrheology, and stability. *Carbohydrate Polymers*. *252*, 117092.

Dai, H., Wu, J., Zhang, H., Chen, Y., Ma, L., Huang, H., Huang, Y. and Zhang, Y. (2020). Recent advances on cellulose nanocrystals for Pickering emulsions: Development and challenge. *Trends in Food Science and Technology*. *102*(2), 16–29.

Dickinson, E. (2009). Hydrocolloids as emulsifiers and emulsion stabilizers. *Food hydrocolloids*. *23*(6), 1473–1482.

Dickinson, E. (1988). The structure and stability of emulsions *In*: *Food Structure - Its Creation and Evaluation*. Cambridge: Woodhead Publishing, 41–57.

Druel, L., Niemeyer, P., Milow, B. and Budtova, T. (2018). Rheology of cellulose-[DBNH][CO2Et] solutions and shaping into aerogel beads. *Green Chemistry*. *20*(17), 3993–4002.

Durmaz, E.N. and Zeynep Çulfaz-Emecen, P. (2018). Cellulose-based membranes via phase inversion using [EMIM]OAc-DMSO mixtures as solvent. *Chemical Engineering Science*. *178*, 93–103.

Fan, Z., Chen, J., Guo, W., Ma, F., Sun, S. and Zhou, Q. (2018). Anti-solvents tuning cellulose nanoparticles through two competitive regeneration routes. *Cellulose*. *25*(8), 4513–4523.

Fan, Z., Chen, J., Guo, W., Ma, F., Sun, S. and Zhou, Q. (2017). Crystallinity of regenerated cellulose from [Bmim]Cl dependent on the hydrogen bond acidity/basicity of anti-solvents. *RSC Advances*. *7*(65), 41004–41010.

Fink, H.P., Weigel, P., Purz, H.J. and Ganster, J. (2001). Structure formation of regenerated cellulose materials from NMMO-solutions. *Progress in Polymer Science*. *26*, 1473–1524.

Geisel, K., Isa, L. and Richtering, W. (2012). Unraveling the 3D localization and deformation of responsive microgels at oil/water interfaces: A step forward in understanding soft emulsion stabilizers. *Langmuir*. *28*(45), 15770–15776.

Habibi, Y., Lucia, L.A. and Rojas, O.J. (2010). Cellulose nanocrystals: Chemistry, self-assembly, and applications. *Chemical Reviews*. *110*(6), 3479–3500.

Hedlund, A., Köhnke, T., Hagman, J., Olsson, U. and Theliander, H. (2019). Microstructures of cellulose coagulated in water and alcohols from 1-ethyl-3-methylimidazolium acetate: contrasting coagulation mechanisms. *Cellulose*. *26*(3), 1545–1563.

Hedlund, A., Theliander, H. and Köhnke, T. (2019). Mass transport during coagulation of cellulose-ionic liquid solutions in different non-solvents. *Cellulose*. *26*(16), 8525–8541.

Ilyin, S.O., Makarova, V. V., Anokhina, T.S., Ignatenko, V.Y., Brantseva, T. V., Volkov, A. V. and Antonov, S. V. (2018). Diffusion and phase separation at the morphology formation of cellulose membranes by regeneration from N-methylmorpholine N-oxide solutions. *Cellulose*. *25*(4), 2515–2530.

Islam, M.R. and Lyon, L.A. (2020). Deswelling studies of pH and temperature-sensitive ultra-low cross-linked microgels with cross-linked cores. *Colloid and Polymer Science*. *298*, 395–405.

Jia, X., Xu, R., Shen, W., Xie, M., Abid, M., Jabbar, S., Wang, P., Zeng, X. and Wu, T. (2015). Stabilizing oil-in-water emulsion with amorphous cellulose. *Food Hydrocolloids*. *43*, 275–282.

Jo, S., Park, S., Oh, Y., Hong, J., Kim, H.J., Kim, K.J., Oh, K.K. and Lee, S.H. (2019). Development of cellulose Hydrogel Microspheres for Lipase Immobilization. *Biotechnology and Bioprocess Engineering*. *24*(1), 145–154.

Kang, H., Liu, R. and Huang, Y. (2016). Cellulose-Based Gels. *Macromolecular Chemistry and Physics*. *217*(12), 1322–1334.

Kim, H.J., Jin, J.N., Kan, E., Kim, K.J. and Lee, S.H. (2017). Bacterial cellulose-chitosan composite hydrogel beads for enzyme immobilization. *Biotechnology and Bioprocess Engineering*. *22*(1), 89–94.

Lefroy, K.S., Murray, B.S. and Ries, M.E. (2021). Advances in the use of microgels as emulsion stabilisers and as a strategy for cellulose functionalisation. *Cellulose*. *28*, 647–670.

Lefroy, K.S., Murray, B.S. and Ries, M.E. (2021). Rheological and NMR Studies of Cellulose Dissolution in the Ionic Liquid BmimAc. *Journal of Physical Chemistry B*. *125*(29), 8205–8218.

Lefroy, K.S., Murray, B.S., Ries, M.E. and Curwen, T.D. (2021). A natural, cellulose-based microgel for water-in-oil emulsions. *Food Hydrocolloids*. *113*, 106408.

Li, Z., Wu, H., Yang, M., Xu, D., Chen, J., Feng, H., Lu, Y., Zhang, L., Yu, Y. and Kang, W. (2018). Stability mechanism of O/W Pickering emulsions stabilized with regenerated cellulose. *Carbohydrate Polymers*. *181*, 224–233.

Liwarska-Bizukojc, E., Miksch, K., Malachowska-Jutsz, A. and Kalka, J. (2005). Acute toxicity and genotoxicity of five selected anionic and nonionic surfactants. *Chemosphere*. *58*(9), 1249–1253.

Marchetti, L., Muzzio, B., Cerrutti, P., Andrés, S.C. and Califano, A.N. (2017). Bacterial nanocellulose as novel additive in low-lipid low-sodium meat sausages. Effect on quality and stability. *Food Structure*. *14*, 52–59.

McClements, D.J. (2004). *Food Emulsions: Principle, Practices, and Techniques* [Online] second ed. Boca Raton: CRC Press. [Accessed 9 September 2019]. Available from: https://www.taylorfrancis.com/books/mono/10.1201/9781420039436/food-emulsions-david-julian-mcclements.

Medronho, B., Filipe, A., Costa, C., Romano, A., Lindman, B., Edlund, H. and Norgren, M. (2018). Microrheology of novel cellulose stabilized oil-in-water emulsions. *Journal of Colloid and Interface Science*. *531*, 225–232.

Mitsou, E., Tavantzis, G., Sotiroudis, G., Ladikos, D., Xenakis, A. and Papadimitriou, V. (2016). Food grade water-in-oil microemulsions as replacement of oil phase to help process and stabilization of whipped cream. *Colloids and Surfaces A: Physicochemical and Engineering Aspects*. *510*, 69–76.

Napso, S., Rein, D.M., Fu, Z., Radulescu, A. and Cohen, Y. (2018). Structural Analysis of Cellulose-Coated Oil-in-Water Emulsions Fabricated from Molecular Solution. *Langmuir*. *34*(30), 8857–8865.

Napso, S., Rein, D.M., Khalfin, R., Kleinerman, O. and Cohen, Y. (2016). Cellulose gel dispersion: From pure hydrogel suspensions to encapsulated oil-in-water emulsions. *Colloids and Surfaces B: Biointerfaces*. *137*, 70–76.

Ni, Y., Li, J. and Fan, L. (2020). Production of nanocellulose with different length from ginkgo seed shells and applications for oil in water Pickering emulsions. *International Journal of Biological Macromolecules*. *149*, 617–626.

Omura, T., Suzuki, T. and Minami, H. (2020). Preparation of cellulose particles with a hollow structure. *Langmuir*. *36*(46), 14076–14082.

Oza, K.P. and Frank, S.G. (1986). Microcrystalline cellulose stabilized emulsions. *Journal of Dispersion Science and Technology*. *7*(5), 543–

561.

Ozturk, B. and McClements, D.J. (2016). Progress in natural emulsifiers for utilization in food emulsions. *Current Opinion in Food Science*. *7*, 1–6.

Pang, B., Liu, H., Liu, P., Peng, X. and Zhang, K. (2018). Water-in-oil Pickering emulsions stabilized by stearoylated microcrystalline cellulose. *Journal of Colloid and Interface Science*. *513*, 629–637.

Park, S., Kim, S.H., Kim, J.H., Yu, H., Kim, H.J., Yang, Y.H., Kim, H., Kim, Y.H., Ha, S.H. and Lee, S.H. (2015). Application of cellulose/lignin hydrogel beads as novel supports for immobilizing lipase. *Journal of Molecular Catalysis B: Enzymatic*. *119*, 33–39.

Pimentel, D. and Pimentel, M. (2003). Sustainability of meat-based and plant-based diets and the environment. *American Journal of Clinical Nutrition*. *78*(3), 660–663.

Pinaud, F., Geisel, K., Massé, P., Catargi, B., Isa, L., Richtering, W., Ravaine, V. and Schmitt, V. (2014). Adsorption of microgels at an oil-water interface: Correlation between packing and 2D elasticity. *Soft Matter*. *10*(36), 6963–6974.

Pravinata, L., Akhtar, M., Bentley, P.J., Mahatnirunkul, T. and Murray, B.S. (2016). Preparation of alginate microgels in a simple one step process via the Leeds Jet Homogenizer. *Food Hydrocolloids*. *61*, 77–84.

Rein, D.M., Khalfin, R. and Cohen, Y. (2012). Cellulose as a novel amphiphilic coating for oil-in-water and water-in-oil dispersions. *Journal of Colloid and Interface Science*. *386*(1), 456–463.

Sarkar, A. and Dickinson, E. (2020). Sustainable food-grade Pickering emulsions stabilized by plant-based particles. *Current Opinion in Colloid & Interface Science*. *49*, 69–81.

Satlewal, A., Agrawal, R., Bhagia, S., Sangoro, J. and Ragauskas, A.J. (2018). Natural deep eutectic solvents for lignocellulosic biomass pretreatment: Recent developments, challenges and novel opportunities. *Biotechnology Advances*. *36*(8), 2032–2050.

Schmitt, V. and Ravaine, V. (2013). Surface compaction versus stretching in Pickering emulsions stabilised by microgels. *Current Opinion in Colloid and Interface Science*. *18*(6), 532–541.

Schramm, L.L. (2005). Personal Care Product Applications *In*: *Emulsions, Foams, and Suspensions: Fundamentals and Applications*. Weinheim, Germany: Wiley-VCH Verlag GmbH & Co. KGaA, 337–346.

Shen, W., Guo, L., Wu, T., Zhang, W. and Abid, M. (2016). Stabilizing beverage emulsions by regenerated celluloses. *LWT - Food Science and Technology*. *72*, 292–301.

Sugiyama, J., Vuong, R. and Chanzy, H. (1991). Electron Diffraction Study on the Two Crystalline Phases Occurring in Native Cellulose from an Algal Cell Wall. *Macromolecules*. *24*(14), 4168–4175.

Swatloski, R.P., Spear, S.K., Holbrey, J.D. and Rogers, R.D. (2002). Dissolution of cellulose with ionic liquids. *Journal of the American Chemical Society*. *124*(18), 4974–4975.

Tavernier, I., Patel, A.R., Van der Meeren, P. and Dewettinck, K. (2017). Emulsion-templated liquid oil structuring with soy protein and soy protein: κ-carrageenan complexes. *Food Hydrocolloids*. *65*, 107–120.

Wiley, R.M. (1954). Limited coalescence of oil droplets in coarse oil-in-water emulsions. *Journal of Colloid Science*. *9*(5), 427–437.

Winuprasith, T. and Suphantharika, M. (2015). Properties and stability of oil-in-water emulsions stabilized by microfibrillated cellulose from mangosteen rind. *Food Hydrocolloids*. *43*, 690–699.

Yamane, C., Aoyagi, T., Ago, M., Sato, K., Okajima, K. and Takahashi, T. (2006). Two different surface properties of regenerated cellulose due to structural anisotropy. *Polymer Journal*. *38*(8), 819–826.

Zembyla, M., Lazidis, A., Murray, B.S. and Sarkar, A. (2020). Stability of water-in-oil emulsions co-stabilized by polyphenol crystal-protein complexes as a function of shear rate and temperature. *Journal of Food Engineering*. *281*, 109991.

Zeng, B., Wang, X. and Byrne, N. (2020). Cellulose beads derived fromwaste textiles for drug delivery. *Polymers*. *12*, 1621.

Zhu, Y., Luo, X., Wu, X., Li, W., Li, B., Lu, A. and Liu, S. (2017). Cellulose gel dispersions: fascinating green particles for the stabilization of oil/water Pickering emulsion. *Cellulose*. *24*(1), 207–217.

Chapter 6
The effect of oil on cellulose dissolution in the ionic liquid 1-butyl-3-methyl imidazolium acetate[5]

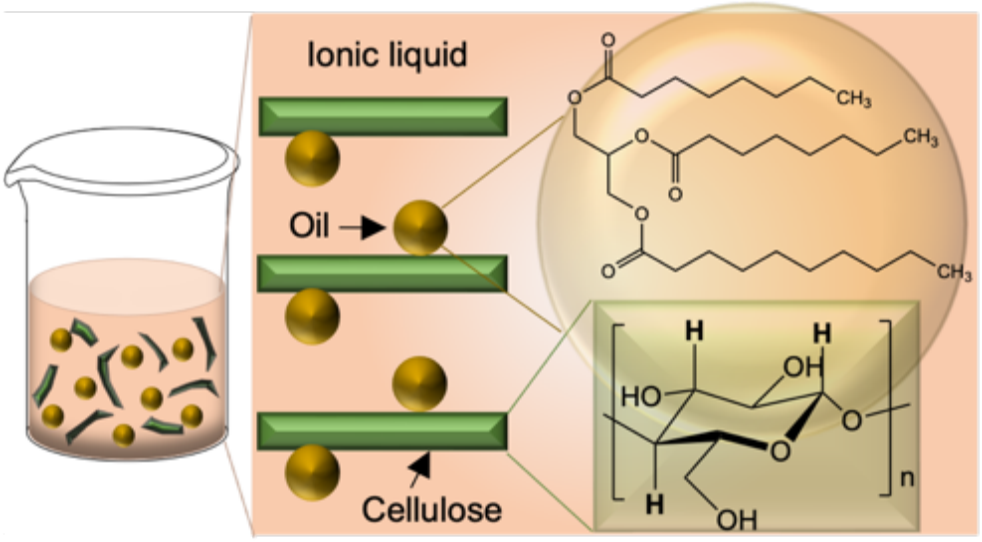

6.1 Abstract

Whilst ionic liquids (ILs) are well known to be excellent solvents for cellulose, the exact mechanism of dissolution has been a much-disputed topic in recent years and is still not completely clear. In this work, we add to current understanding and highlight the importance of hydrophobic interactions, through studying cellulose dissolution in mixtures of 1-butyl-3-methyl imidazolium acetate (BmimAc) and medium-chain triglyceride (MCT) oil. We demonstrate that the order in which constituents are mixed together plays a key role, through nuclear magnetic resonance (NMR) spectroscopic analysis. When small quantities of MCT-oil (0.25-1 wt%) were introduced to BmimAc before cellulose, the effect on BmimAc chemical shift values was much more significant compared to when the cellulose was dissolved first, followed by oil addition. Rheological analysis also showed small differences in the viscosities of oil-cellulose-BmimAc solution viscosities, depending on the order that the constituents were added. On the other hand, no such order effect on the NMR results was observed when cellulose was replaced with cellobiose, suggesting that this observation is unique to the macromolecule. We propose that a cellulose-oil interaction develops, but only when the cellulose structure has a sufficient degree of order and not when the cellulose is molecularly dispersed, since the hydrophobic cellulose plane is no longer intact. In all cases, cellulose-BmimAc-oil solutions were

[5]Published as: Lefroy, K.S., Murray, B.S. and Ries, M.E. (2022). The effect of oil on cellulose dissolution in the ionic liquid 1-butyl-3-imidazolium acetate. *Submitted to ACS Omega.*

stable for at least 4 months. To our knowledge, this is the first work that investigates the effect of oil addition on the dissolving capacity of BmimAc and highlights the need for further re-evaluation of accepted mechanisms for cellulose dissolution in ILs.

6.2 Introduction

Ionic liquids (ILs) have provided a major breakthrough in the dissolution, modification and general functionalisation of biomass and its components, including cellulose, providing a non-toxic and potentially 'greener' pathway to making useful materials (Isik et al., (2014); Halder et al., (2019)). Since their 'rediscovery' (Graenacher, (1934)) in 2002 by Swatloski *et al.* (Swatloski et al., (2002)), ILs have been used extensively in research to dissolve cellulose for different purposes, for example for packaging, novel materials, composites and food ingredients (Isik et al., (2014); Yang et al., (2020); Lefroy, Murray, Ries, et al., (2021); Xu and Cho, (2022)). Imidazolium-based ILs are commonly favoured since they are usually liquid at room-temperature, relatively hydrophilic (Le et al., (2014)) and thus have high cellulose dissolving capabilities (Verma et al., (2019)), (up to 25-27 wt% in some cases) (Swatloski et al., (2002); Lovell et al., (2010); Le et al., (2014)). The mechanism of cellulose dissolution in imidazolium-based ILs should be understood to design more efficient, biodegradable and 'greener' ILs (H. Wang et al., (2012); Lu et al., (2014)), however the role of hydrophilic and hydrophobic interactions is still heavily debated.

The majority of cellulose-IL dissolution studies highlight the importance of the interaction between the anion and the cellulose hydroxyl groups (Swatloski et al., (2002); Remsing et al., (2006); Zhang, Zhang, Wu, et al., (2010)) and it is often cited that inter- and intramolecular H-bonds between cellulose chains must be broken to achieve dissolution (Xiong et al., (2014); X. Kang et al., (2016)). However, the role of the cation is more disputed and the significance of hydrophobic interactions is often not addressed (Lindman et al., (2010); Medronho and Lindman, (2014)). On one hand, it is argued that the cation also participates in H-bonding to the cellulose and therefore very bulky cations cannot penetrate and reach the hydroxyl groups (Feng and Chen, (2008); Kosan et al., (2008)), making the IL less effective for cellulose dissolution. Equally, Lu *et al.* focussed on H-bonding, claiming that the structure of the cation is important and the strength of the anion-cation H-bond must also be taken into account (Lu et al., (2014)). On the other hand, it has been proposed that the cation neutralises the negatively-charged H-bonded anion-cellulose complex, which leads to increased steric repulsion in the complex and the

development of a hydrophobic interaction between the comparatively bulky cation and the hydrophobic regions on cellulose chains (Rabideau et al., (2013); El Seoud et al., (2019)). Furthermore, molecular dynamics (MD) simulations have revealed that hydrophobic interactions are responsible for close contact between the cation and cellulose, exposing a stacking interaction between imidazolium cations and the cellulose pyranose rings (Liu et al., (2010); Mostofian et al., (2014)).

Due to the amphiphilic nature of cellulose molecules, it is necessary to consider both the role of hydrophilic and hydrophobic interactions (Medronho and Lindman, (2015)) when designing ILs for cellulose dissolution. An effective solvent should have both polar and nonpolar regions (Medronho et al., (2015)), however ILs employed in cellulose dissolution are usually water miscible and often described only as hydrophilic (Gericke et al., (2011)), a property controlled by the anion (Huddleston et al., (2001)). Since cellulose is insoluble in water, it is evident that the dissolving ability of ILs for cellulose cannot be solely based on H-bonding and, upon closer inspection of the cation, the best candidates in fact display strong structural asymmetry (Olsson and Westman, (2013)). The amphiphilic nature of the cation influences its hydrophobicity and therefore may play a role in facilitating cellulose dissolution (Lindman et al., (2010)).

Some of the major drawbacks associated with cellulose-IL processing on a large-scale are the relatively high cost and viscosity of ILs (Gericke et al., (2012); Van Osch et al., (2017); Lopes et al., (2017); Halder et al., (2019); Rieland and Love, (2020); Kasprzak and Galiński, (2021)), the latter of which can become very high when significant amounts of cellulose are dissolved (Gericke et al., (2009)). Furthermore, the presence of small impurities such as halides and imidazole (from the preparation of the IL) (Yang and Pan, (2005); Verma et al., (2019)) may also have some effect and even lead to hydrolysis of cellulose and other side reactions (Ebner et al., (2008); Rinaldi et al., (2010); Zhao et al., (2012)), whilst the presence of water can completely disrupt the H-bond network of cation-anion pairs and dramatically alter cellulose dissolving ability (Hall et al., (2012); Radhi et al., (2015); Marekha et al., (2015); Nazari et al., (2017); Rajeev et al., (2018); Marks et al., (2019)). Water contamination has been shown to trigger phase separation (Rieland and Love, (2020)) and can affect cellulose dissolution at concentrations as low as 1 wt% (Swatloski et al., (2002)), which is particularly problematic in imidazolium-based ILs due to their highly hygroscopic nature (Radhi et al., (2015)). However, Fendt *et al.* suggested that if water is present in very small

quantities, it may reduce the viscosity of some ILs and act as a cosolvent, thus improving cellulose dissolution (Fendt et al., (2011)).

More significant lowering of viscosities have been reported with polar aprotic cosolvents, such as dimethyl sulfoxide (DMSO) or dimethyl formamide (DMF), which can be added in greater quantities than water to ILs either before or after cellulose dissolution (Rinaldi, (2011); Parthasarathi et al., (2015); Gale et al., (2016)). Efficient cosolvents can reduce the volume fraction of IL required, lowering the processing cost, and may even enhance IL properties by increasing the cellulose dissolution speed and dissolving capacity (Rinaldi, (2011); Xu et al., (2013); Y. Li et al., (2018); Kasprzak et al., (2019)). Therefore, binary cosolvent/IL mixtures have received much attention in recent years due to their more promising potential for industrial use compared to pure ILs. If the cosolvent is added before dissolution, it is sometimes described as a 'pre-swelling' stage during which the cosolvent can begin to penetrate between cellulose layers and disrupt the highly-ordered structure (Kuzmina et al., (2014)). Furthermore, pre-treatment of biomass with cosolvents can remove lignin and hemicelluloses (which can act as a barrier to cellulose dissolution), increasing the cellulose surface area and further facilitating dissolution in the IL (Asakawa et al., (2016)). In general, solvents which are weak hydrogen bond donors (HBDs) and have high values for polarity, basicity and dipolarity/polarizability are miscible with hydrophilic ILs and therefore considered efficient cosolvents (Gericke et al., (2011)), whilst solvents displaying good HBD ability can have the opposite effect (Gericke et al., (2011)). Most studies therefore focus exclusively on polar cosolvents, whilst less attention is given to nonpolar cosolvents.

Understanding the effect of both polar and nonpolar species on ILs is of fundamental importance, since different impurities may be present in their applications as lubricants (Qu et al., (2009)), biocatalysts (Roberts and Lye, (2002)), electrolytes (Qiu et al., (2013)) and coolants (Kalb, (2020)). In terms of cellulose dissolution, species of different polarities may equally affect the process due to the amphiphilic character of the solvent and the solute. Broadly speaking, the most efficient ILs for cellulose dissolution possess cations with dipolar character (often achieved by a heterocyclic aromatic ring) and anions which are non-bulky and weakly hydrophobic (in order to provide several H-bond acceptor sites) (Pinkert et al., (2010)). It has previously been demonstrated that miscibility between an IL and cosolvent is largely determined by the ratio of alkyl chain lengths for a protic IL and a non-polar additive (Jiang et al., (2014)), whilst certain ILs may support amphiphilic self-

assembly (Greaves and Drummond, (2015)). However, aprotic ILs capable of dissolving cellulose generally have a very limited miscibility with hydrophobic reagents and cellulose derivatives, and therefore adding a small quantity of non-polar cosolvent may allow one to tune the IL properties and potentially provide a route for the preparation of more hydrophobic cellulose materials (Gericke et al., (2011)). This could have advantages in the functionalisation of cellulose from ILs, allowing further manipulation of cellulose properties. Whilst some detailed studies on nonpolar cosolvent/IL binary mixtures have been conducted, to our knowledge, these have been restricted to ILs with rather hydrophobic anions (e.g. Tf_2N^- and PF_6^-) which are not suitable solvents for cellulose (Mellein et al., (2007); Fortunato et al., (2010)).

In this work, we have used a combination of ultraviolet-visible (UV-Vis) and nuclear magnetic resonance (NMR) spectroscopies to investigate the interactions present in cellulose, 1-butyl-3-methyl imidazolium acetate (BmimAc) and medium-chain triglyceride (MCT)-oil mixtures. We present experiments analysing the effects that low concentrations of nonpolar solvent have on cellulose dissolution in ILs. A relatively ‘polar’ oil was selected with some hydrophilic character, in order to maximise the possibility of interaction between the amphiphilic cellulose/BmimAc and the oil. Oil-BmimAc solutions with/without cellulose were analysed, that indicated preferential interaction between the cellulose and the oil as opposed to the oil and the BmimAc, providing further strong evidence for the structural anisotropy of cellulose. However, we also show that amphiphilicity changes depending on the state of the cellulose in solution and its degree of order. This provides, to our knowledge, the first experimental study of its kind investigating the effect of nonpolar solvents in cellulose-IL dissolution. Most notably, the order in which the cellulose and oil were added to the BmimAc was found to have a significant effect on the resultant properties of the solution both microscopically and macroscopically.

6.3 Materials and methods

1-Butyl-3-methyl imidazolium acetate (BmimAc) (≥95% purity was obtained from Sigma Aldrich and cellulose powder (Vitacel L 00) was supplied by Mondelēz International. Full details of the cellulose powder including the degree of polymerization are provided in **Appendix D** (Table D 1). Cellobiose powder was obtained from BioServ UK limited. Medium-chain triglyceride oil (MCT-oil) Miglyol 812 (Caprylic/Capric Triglyceride (Nielsen and Kropke, (2004))) with a density of 0.945 g mL-1 at 20 °C was obtained from Cremer Oleo GmbH & Co, (Germany).

6.3.1 UV-Visible spectroscopy

UV-Visible (Vis) absorbance spectra were recorded on a Specord 210 Plus spectrophotometer (Analytik Jena) with a slit width of 1 nm at T = 298 K. All samples were pipetted into quartz cuvettes (ca. 3 mL) with a path length of 1 cm. The absorbance was scanned over a range of wavelengths (180-800 nm).

6.3.2 ^{1}H NMR (high-field) spectroscopy

^{1}H NMR spectra were recorded on a Bruker Avance II NMR spectrometer, operating at a ^{1}H resonance frequency of 400 MHz. All measurements were recorded at a temperature of 298 K. Each sample was pipetted into 5 mm NMR tubes and a capillary loaded with DMSO-d_6 was added as a reference, so as to avoid any contact between DMSO-d_6 and the samples. Each spectrum was calibrated to the ^{1}H external reference of the residual proton in DMSO-d_6, at 2.5 ppm (Lepre et al., (2016)). All samples were prepared in a glovebox (Braun) to minimise water contamination. All samples have significantly less than 0.5 wt% water.

6.3.3 Rheological measurements

Steady-state shear viscosity measurements of cellulose-BmimAc-oil mixtures were conducted on an Anton Paar MCR 302 (Anton Paar GmbH, Graz, Austria) rheometer, using a circular cone-plate geometry with a diameter of 50 mm and angle of 2 °. The temperature was fixed at a constant 25 °C throughout all of the measurements, controlled by a water bath temperature control unit and a Peltier hood. A pre-shear at 1 s^{-1} was included for 3 minutes, allowing adequate heating throughout the sample, before the viscosity was measured between 0.01-1000 s^{-1}. All measurements were repeated 3 times.

6.3.4 Optical microscopy

Cellulose-BmimAc-oil mixtures were analyzed using a light microscope (Nikon, SMZ-2T, Japan), equipped with a digital camera (Leica MC120 HD) and 10x/20x lenses. A drop of solution was placed on a welled slide and covered with a coverslip (0.17 mm thickness). Images were processed using the image analysis software ImageJ.

6.4 Results and discussion

6.4.1 Determining the miscibility of BmimAc and oil, with and without cellulose (UV-vis)

The miscibility of pure BmimAc and oil was analysed and compared to cellulose-BmimAc solutions and oil, using UV-vis and ^{1}H NMR. As previously described in the introduction, the structural asymmetry of ILs is key to their cellulose dissolving capabilities, since cellulose itself has structural anisotropy (Medronho and Lindman, (2015)). The cationic structural asymmetry also lowers the IL viscosity, making it a more effective cellulose solvent (Remsing et al., (2006)). Figure 6.1 gives the chemical structures of some common ILs used for dissolving cellulose, each consisting of a bulky cation, and MCT-oil. It is reasoned that there is potential for some hydrophobic association between the amphiphilic cation and nonpolar molecules, and therefore a relatively polar oil was selected in order to maximise the chance of IL-oil interaction and miscibility. Furthermore, we have previously reported that oils with higher polarities were most successful in producing 'oily' cellulose stabilisers for water-in-oil (W/O) emulsions, most likely because of their ability to form some kind of hydrophilic interaction with cellulose during coagulation (Lefroy, Murray, Ries, et al., (2021)). Other less-polar oils, for example tetradecane, were not able to produce stable W/O emulsions and the majority of oil appeared to be washed away during coagulation, rather than interacting with cellulose.

Firstly, in order to determine the maximum solubility of oil in BmimAc both with and without cellulose, solutions were prepared with very small amounts of MCT-oil either without cellulose, or with cellulose dissolved initially before the addition of the oil. Solutions were analysed using UV-vis spectroscopy, first by scanning the absorbance wavelengths (λ) and then selecting a set wavelength of 390 nm. Although this was not a 'maximum' absorbance peak (which is expected to be approximately 290 nm for ILs with a $(Bmim)^{+}$ cation (Yassin et al., (2015))), the absorbance was very noisy at lower wavelengths most probably due to instrument limitations. Whilst the reference sample (pure BmimAc) has lower transmission at this wavelength, differences between solutions which appeared optically identical could be observed (Orelma et al., (2020)). Full absorbance spectra for BmimAc-oil solutions with an oil concentration ([oil]) of 0.25 wt% and with a cellulose concentration ([cellulose]) of 0, 0.2 and 2 wt% cellulose can be found in Figure D 1. Figure 6.2 (orange circles) gives the absorbance spectra at a single wavelength (λ = 390 nm) for 0, 0.2 and 2 wt% cellulose in BmimAc-oil solutions, for which the absorbance was measured over a range of [oil] = 0-1 wt%. All solutions became very turbid

after [oil] ≃ 0.5 wt% (both with and without cellulose, image below Figure 6.2), making the measurements less reliable due to scattering of the beam. Therefore, this was determined to be the approximate limit of 'solubility' and [oil] > 0.5 wt% were not measured using this technique. Data points for the 2 wt% cellulose-BmimAc solution at [oil] > 0.3 wt% are also omitted, due to their high viscosity and thus complications with introducing them to the cuvette.

Ionic liquids (ILs):

Cations:

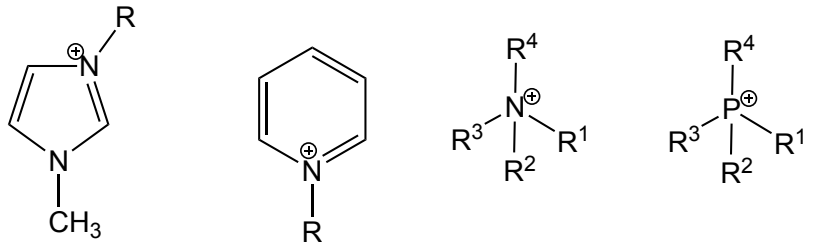

Anions: $CH_3CO_2^{\ominus}$; $Cl^{\ominus}$; $PF_6^{\ominus}$; $NO_3^{\ominus}$

Miglyol 812 MCT-Oil:

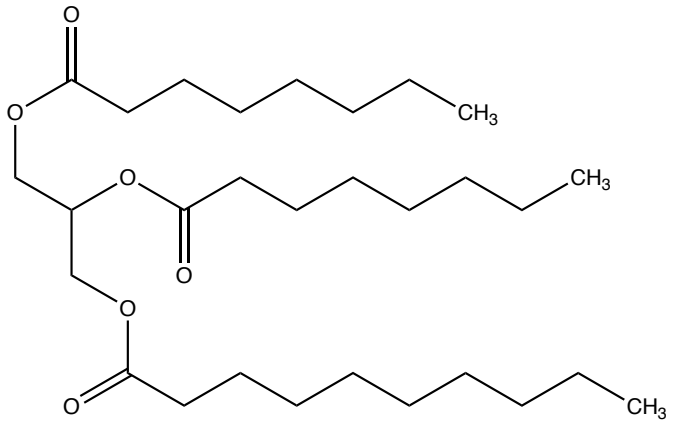

Figure 6.1. Chemical structures of the cations and anions of some common ILs used for dissolving cellulose, and MCT-oil (capric/caprylic triglyceride).

At low concentrations of oil for all solutions, the absorbance increased steadily with increasing [oil]. A sharper increase in absorbance was then observe for [oil] > ca. 0.12 wt%, particularly for the cellulose-free solution, where it rose from 0.505 to 1.37 between [oil] = 0.2 and 0.5 wt%, respectively. This indicates that the MCT-oil may be dispersing rather than dissolving at concentrations exceeding 0.25 wt% and therefore only a very small amount of oil is truly miscible with the pure IL. Interestingly, when just 0.2 wt% cellulose was

dissolved in the solution the increase in absorbance was less drastic, rising from 0.503 to 0.905 between [oil] = 0.2 and 0.5 wt% (respectively), suggesting that cellulose may have an influence on the miscibility of the IL and oil. Unfortunately, data for the solution with the highest cellulose concentration ([cellulose] = 2 wt%) with [oil] > 0.25 wt% was not reproducible, due to the high viscosity of the solution and issues with filling the cuvette. This data has therefore been omitted from Figure 6.2. However, the absorbance at [oil] = 0.25 wt% was indeed the lowest for the 2 wt% cellulose solution, again indicating that the presence of cellulose may influence oil solubility in BmimAc.

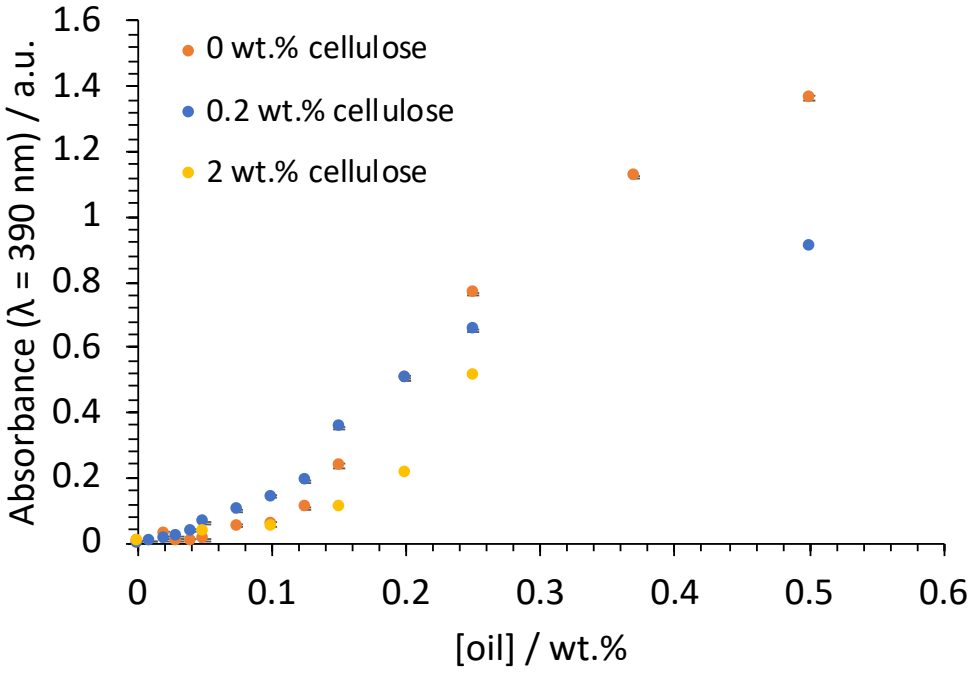

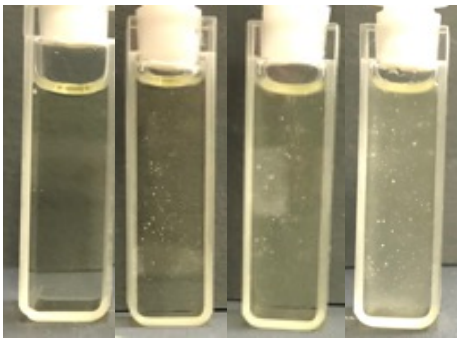

Figure 6.2. Absorbance at λ = 390 nm for BmimAc/MCT-oil mixtures as a function of oil concentration ([oil]), without cellulose (orange circle); with 0.2 wt% L 00 cellulose (blue circle) and with 2 wt% Avicel cellulose (yellow circle). Error bars are shown but some may be hidden by the symbol. Image below shows the appearance of 0.2 wt% cellulose in BmimAc-MCT oil solutions with 0, 0.05, 0.2 and 0.5 wt% oil (from left to right).

6.4.2 ^{1}H NMR

6.4.2.1 Pure BmimAc-oil and BmimAc-cellulose solutions

Mixtures of oil and BmimAc were prepared for high-field ^{1}H NMR, to investigate in more detail any interactions that might be occurring. From the UV-vis analysis, we expect the maximum 'solubility' of oil in BmimAc to be at [oil] $\simeq$ 0.25 wt% and therefore we tested relatively low oil concentrations between 0-1 wt%, above which the oil appears to only temporarily be dispersing in the BmimAc. Full assignment of the ^{1}H NMR spectrum for MCT-oil (Miglyol 812, made up of caprylic/capric triglyceride (Nielsen and Kropke, (2004))) can be found in **Appendix D** (Figure D 2). Since the amounts of oil added were very small, it was almost impossible to detect the corresponding peaks using NMR and therefore the chemical shift change ($\Delta\delta$) of the BmimAc peaks was analysed as a function of oil concentration, where δ of the pure IL peaks are used as a reference (for more details, see below Figure D 2, **Appendix D**). Figure 6.3a gives the spectrum of 'oil-free' (pure) BmimAc with full peak assignments, corresponding to the different proton environments (H1-H9). Through analysing $\Delta\delta$ as a function of the concentration of a component, one is able analyse the effect on specific interactions between the $(Bmim)^{+}$ cation and/or the $(OAc)^{-}$ anion, thus indirectly gaining information about component-IL interactions. This approach has been previously utilised for understanding cellulose dissolution in ILs (Zhang, Zhang, Wu, et al., (2010); Lovell et al., (2010); Zhang et al., (2016)) and here we apply the same principles to the addition of oil. It should be noted that an external reference DMSO-d_6 was added to the NMR tube via a capillary (to ensure accuracy in determining minor peak shifts), since the presence of DMSO may also affect the BmimAc proton environments (see section 6.3 for full details).

Figure 6.3b gives $\Delta\delta$ for BmimAc protons, as determined by ^{1}H NMR, as a function of oil concentration (0-1 wt%). Only very minor changes were observed for BmimAc protons upon the addition of oil ($\Delta\delta$ < 0.01 ppm) and no further changes occurred as [oil] increased, suggesting that any interaction appears to be 'saturated' above [oil] = 0.25 wt%, (in agreement with the UV-vis analysis). Interactions between BmimAc and oil are expected to be of a hydrophobic nature and therefore would involve the aliphatic protons on the butyl chain of the cation (H9, H8, H4) and the CH_3 group on the acetate anion (H7). However, changes in chemical environments for all protons were very minor upon the introduction of oil and it appears that no strong interaction is present.

On the other hand, it is frequently reported that when cellulose dissolution occurs in imidazolium-based ILs a significant change in chemical environment is observed for H2, H3 and in particular, H1 (the most acidic proton), which forms a H-bond with the anion (Zhang, Zhang, Wu, et al., (2010); Lovell et al., (2010); Zhang et al., (2016)). H-bond interactions are generally much stronger than hydrophobic interactions and are estimated to be around 5 kcal/mol/pairing for the former, (e.g. cellulose-cellulose), compared to 2 kcal/mol/residue for the latter (Medronho et al., (2015)). Figure 6.3c gives Δδ for BmimAc protons as a function of cellulose concentration ([cellulose]), for comparison to oil. Once again, cellulose spectral bands were also not observed in the NMR spectra due to the relatively low concentrations studied and therefore the small population of protons associated with the polymer (Lovell et al., (2010)), as well as the low mobility of cellulose molecules. However, a much greater Δδ is observed for the BmimAc peaks upon addition of cellulose, which is widely understood to be a result of displacement of $(Bmim)^+$ cations by cellulose hydroxyl groups, which form stronger H-bonds with $(OAc)^-$ anions (Lovell et al., (2010)). Consequently, weakening of the cation-anion H-bond occurs as indicated by an increase in electron density around the aromatic protons, (H1 in particular), leading to upfield movement of δ (as indicated by a negative Δδ, Figure 6.3c). This has also been described as breakdown of IL-clusters and ultimately ion pairs, which exist in the pure BmimAc solution but are disrupted when small amounts of cellulose are added (0.1-1 wt%) (Lefroy, Murray and Ries, (2021)). Unlike cellulose, oil appears to lack any significant interaction with the IL and there is negligible change to cation-anion H-bonding, suggesting that oil has a minimal effect on IL-clusters. Therefore, it was speculated that at these concentrations, oil will have little or no effect on the ability of the BmimAc to dissolve cellulose (Zhang et al., (2016)), unlike more polar solvents such as water (Swatloski et al., (2002); Hall et al., (2012); Radhi et al., (2015); Marekha et al., (2015); Marks et al., (2019)).

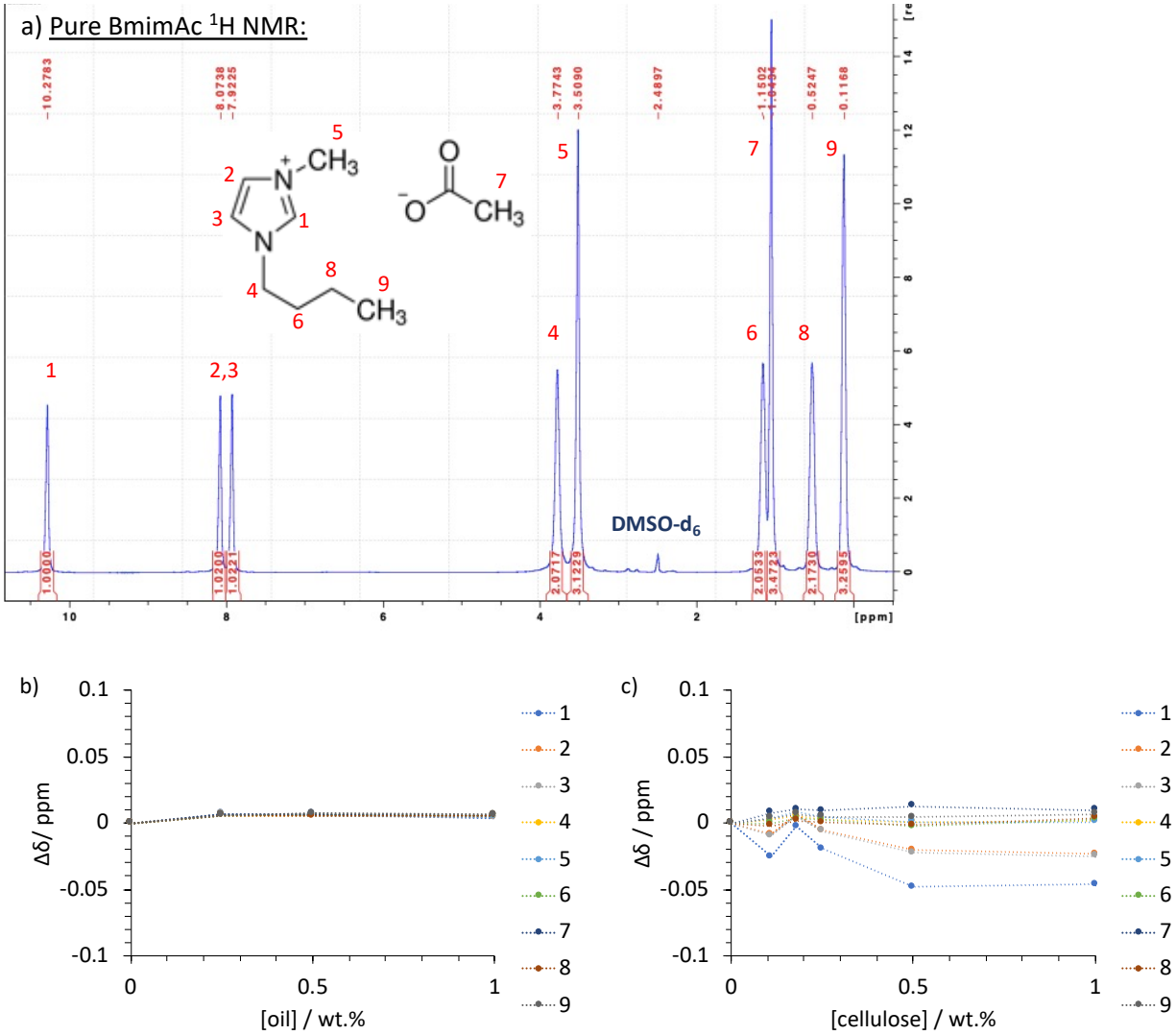

Figure 6.3. a) High-field ^{1}H NMR spectrum (400 MHz) of pure BmimAc (no oil), with peak assignments given in red for protons labelled 1-9. DMSO-d_6 was used as a reference (δ = 2.5 ppm); b) change in chemical shift values (Δδ) of protons 1-9 (BmimAc), as a function of oil concentration ([oil]); c) change in chemical shift values (Δδ) of protons 1-9 (BmimAc), as a function of cellulose concentration ([cellulose]).

6.4.3 Microscopic properties of BmimAc-oil-cellulose mixtures

In order to understand how the presence of oil may affect the cellulose dissolving capacity of ILs, mixtures of all 3 components were prepared by two methods, either A) by dissolving cellulose in BmimAc and subsequently adding the oil; or B) by mixing the oil with BmimAc first, then adding cellulose (as shown by the schematic in Figure 6.4a). Figure 6.4b and c give a comparison of Δδ for BmimAc protons in mixtures prepared by method A and method B, respectively. In both cases, oil was added after (method A) or before (method B) complete dissolution of 2 wt% cellulose (as indicated by the optically clear solutions). δ for each resonance in an 'oil-free' 2 wt%

cellulose-BmimAc solution was used as a starting reference value (for more details, see below Figure D 2, **Appendix D**) and thus Δδ represents the ppm change upon the addition of oil (Ries et al., (2014)).

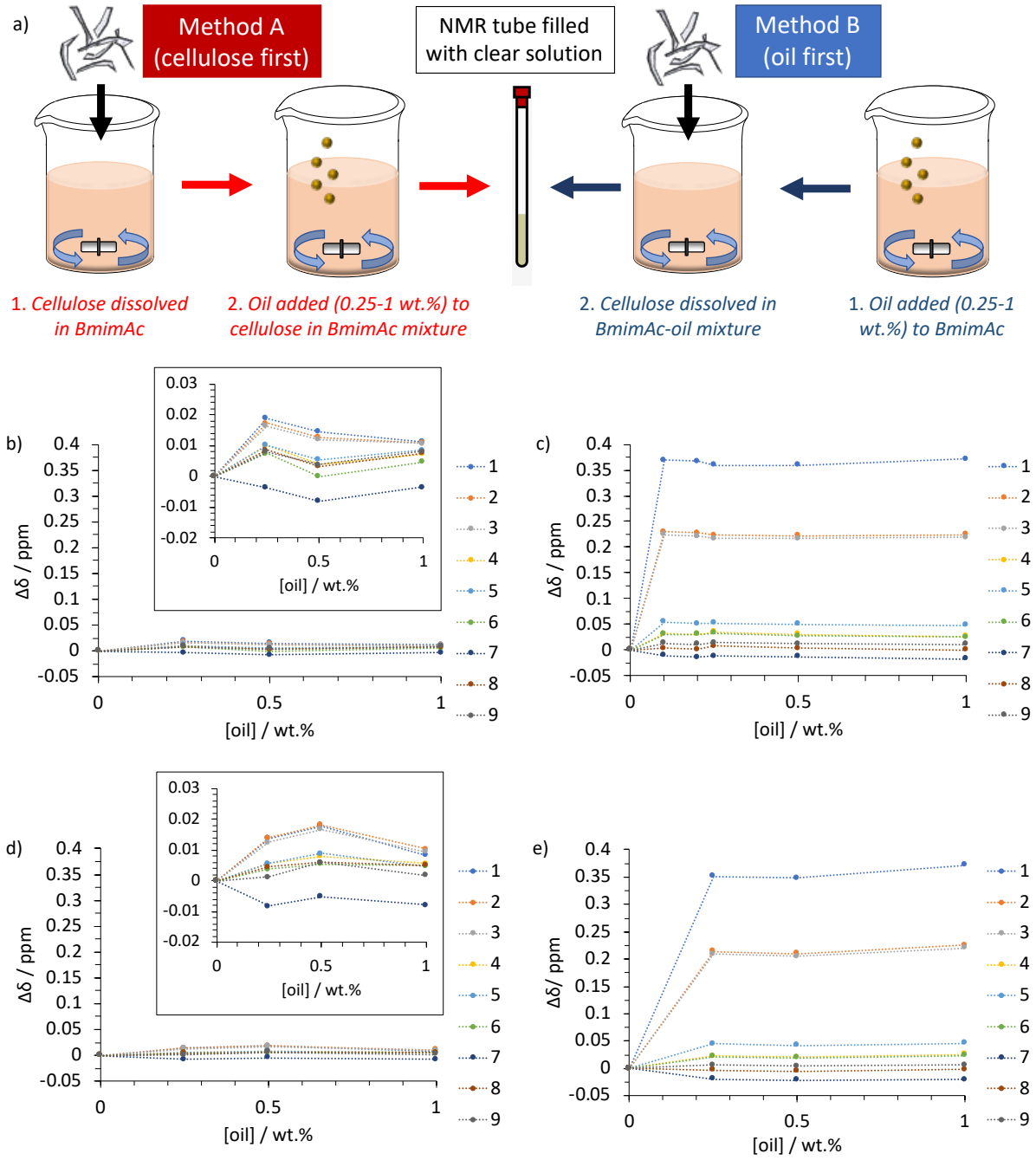

Figure 6.4. a) Schematic to show methods for preparation of BmimAc-cellulose-oil mixtures, where oil was added either after (method A) or before (method B) complete cellulose dissolution; change in chemical shift values (Δδ) of protons 1-9 (BmimAc), as a function of oil concentration ([oil]), where b) cellulose was dissolved before the addition of oil (method A) (inset gives a larger scale version); c) cellulose was dissolved after the addition of oil (method B); d) and e) give Δδ after 4 months storage, for solutions prepared via method A and B respectively. In all cases, [cellulose] = 2 wt%.

From Figure 6.4b and particularly c, it is evident that the presence of cellulose affects Δδ for the BmimAc protons with the addition of oil. When the oil was added after cellulose dissolution (method A, inset Figure 6.4b) the differences were relatively small but slightly more significant compared to BmimAc-oil mixtures in the absence of cellulose (Figure 6.3b), but when solutions were prepared by adding oil to BmimAc before cellulose dissolution (method B, Figure 6.4c), Δδ was at least 10x times higher for the acidic proton H1, (compared to method A). Resonances shifted downfield (increased in δ) with the addition of oil, which surprisingly is the opposite of what happens when cellulose is dissolved in BmimAc (Lefroy, Murray and Ries, (2021)) (where resonances shift upfield, Figure 6.3c). This downfield shift indicates a decrease in electron density around the aromatic protons and therefore strengthening of the cation-anion H-bond, since the aromatic protons (H1, H2 and H3) are much more affected by the addition of oil compared to the rest of the IL protons. Rather than oil interacting very weakly with the hydrophobic regions of the cation (as predicted in the absence of cellulose), we propose that it is now interacting preferentially with the hydrophobic plane of cellulose which weakens the cellulose-anion bond. The schematic in Figure 6.5a illustrates the amphiphilic character of cellulose and the potential IL-cellulose and oil-cellulose interactions present in the cellulose-BmimAc-oil mixtures. The polarity of the oil will also certainly have an effect on the strength of both hydrophilic and hydrophobic interactions and whether or not they even occur (as discussed previously), however we were unable to verify this with lower polarity oils due their inability to solubilise in BmimAc. An oil with a very low polarity index may be ‘too hydrophobic’ (non-polar) for any interaction with cellulose, in which case the cellulose-IL interaction would dominate.

The strengthening effect of the BmimAc H-bond was significantly greater when oil was added before the cellulose (method B, Figure 6.4c) and we propose the following explanation: when cellulose is added via method B, the small amount of oil has already been solubilised as droplets in the IL and forms a kinetically stable system, due to the high viscosity of the BmimAc. Cellulose is distributed throughout the solution and forms interactions with the oil droplets, orienting its hydrophobic planes towards the oil phase. This cellulose-oil interaction is favourable since cellulose has greater hydrophobic surface area compared to $Bmim^{+}$, which arises from the highly ordered axial orientation of C-H groups along cellulose chains and creates structural anisotropy (Medronho and Lindman, (2015)) (Figure 6.5a). Any weak cation-oil interactions are replaced with stronger cellulose-oil interactions, whilst the majority of the cellulose (dispersed in the BmimAc) begins to dissolve. When

oil is added after cellulose dissolution, the cellulose has already been molecularly dissolved and therefore the solution viscosity is much greater compared to pure BmimAc (Lefroy, Murray and Ries, (2021)). Therefore, the oil cannot be distributed as uniformly as in the absence of cellulose and the volume of cellulose-oil interactions are reduced. The more thermodynamically stable state is preferred, where cellulose-IL interactions are maximised. As a result, the IL peaks are much less affected when the oil is added to a solution of cellulose already in its molecularly dispersed state (Figure 6.4b), compared to a more ordered state (Figure 6.4c).

Notably, the δ values for the IL protons remarkably become comparable to δ values in the pure IL when oil is added to the cellulose in BmimAc solution (method B, Figure 6.4c), suggesting that the chemical proton environments are similar to pure BmimAc (Figure D 3). Despite the presence of the predicted cellulose-oil interaction, complete dissolution of cellulose still occurred in the oil-BmimAc solution when oil was added first (method B). This is most likely because such a small quantity of oil was added (<1 wt% compared to the IL) which has little or no effect on the dissolving capability of the BmimAc, and because the oil displays almost no interaction with the IL (as we suggest from the above results). Furthermore, it has been reported that hydroxyl groups on the cellulose interact more strongly with ILs compared to backbone protons (i.e. the hydrophobic planes) (Kuroda et al., (2014)) since the hydrophilic surface areas of cellulose are greater and in this case, the predicted oil-cellulose interaction does not involve hydroxyl groups and does not inhibit hydrophilic interactions between cellulose and the IL.

In order to understand whether solutions prepared via methods A and B are in an equilibrium state or we are observing a short time effect which results in differences, the NMR samples prepared via methods A and B were remeasured after storage for 1 month (Figure D 4a and b) and 4 months (Figure 6.4d and 4e). Almost no change was observed for the solutions prepared via method A (Figure 6.4b and d), suggesting that no further oil-cellulose interactions developed within this time period and no cellulose precipitation occurred, the latter of which would cause the H-bond to restrengthen. The oil, however, remained dispersed within the mixture and no separation occurred. We attribute this to the high viscosity of the cellulose-BmimAc medium and the low concentration of oil, resulting in solubilisation of oil in the IL with long term kinetic stability. Whilst molecular cellulose does possess structural anisotropy and has been shown to arrange itself at the oil-IL interface over time (Napso et al., (2018); Costa, Mira, et al., (2019)), this

doesn't appear to occur in for solutions prepared via method A most likely due to the small volume of oil (and thus less opportunity for cellulose-oil interaction) and the high viscosity of the cellulose-IL solution. Therefore, the $(Bmim)^+$ probably remained stacked within the cellulose planes and again, we suggest that the lack of significant cellulose-oil interaction is due to the molecular dispersion of cellulose in solution, which takes place before the oil is added (method A). Figure 6.4b and 4d also indicate that very little change was also observed microscopically for the solutions prepared via method B, when the oil was added before cellulose dissolution. Δδ was still more significant compared to method A after 4 months and the downfield shift in the resonances for the aromatic protons H1, H2 and H3 remained the highest. Therefore, we conclude that the cellulose-oil interaction previously described was still present and the system remains kinetically stable for this time period. $(Bmim)^+$ cations and/or other cellulose molecules do not disrupt the existing cellulose-oil interactions, which is likely due to preferential exposure of the hydrophobic regions in cellulose to the oil resulting in a significantly favorable interaction that aids long term stability. In both cases, the solutions remained optically clear and therefore no cellulose precipitation was observed.

We propose that the oil is acting as a kind of cosolvent (as shown in the schematic, Figure 6.5b), and either 'loosens' the cellulose structure (by initially 'coating' the cellulose hydrophobic planes) before breakdown of IL clusters and penetration of IL molecules (Figure 6.5b, i) or helps to break up cation-anion pairs, freeing the anion and aiding dissolution (Figure 6.5b, ii). For the latter, a similar mechanism has been described for cellulose dissolution in DMSO-BmimAc mixtures where an increase in DMSO concentration led to a decrease in the viscosity, resulting in higher cellulose solubility (Ren et al., (2021)). However, when we prepared solutions with lower (<0.25 wt%) and higher (>1 wt%) oil concentrations, no correlation was observed between Δδ and oil concentration (Figure D 5a), suggesting that the role of the oil is rather different to the role of DMSO (and other aprotic cosolvents). We hypothesize that oil penetrates between the hydrophobic cellulose planes whilst the anion interacts with cellulose hydroxyl groups in the equatorial planes (represented by R-OH groups) through H-bonding, 'freeing' the $(Bmim)^+$ ions and followed by complete dissolution (Figure 6.5b, ii). Although the cellulose still appeared to be fully dissolved at higher oil concentrations (since no precipitation was observed), droplets of oil were visible under the microscope at [oil] = 2 wt% (Figure D 5b) which probably led to the observed turbidity, and again suggests that there is little/no interaction between the oil and the BmimAc.

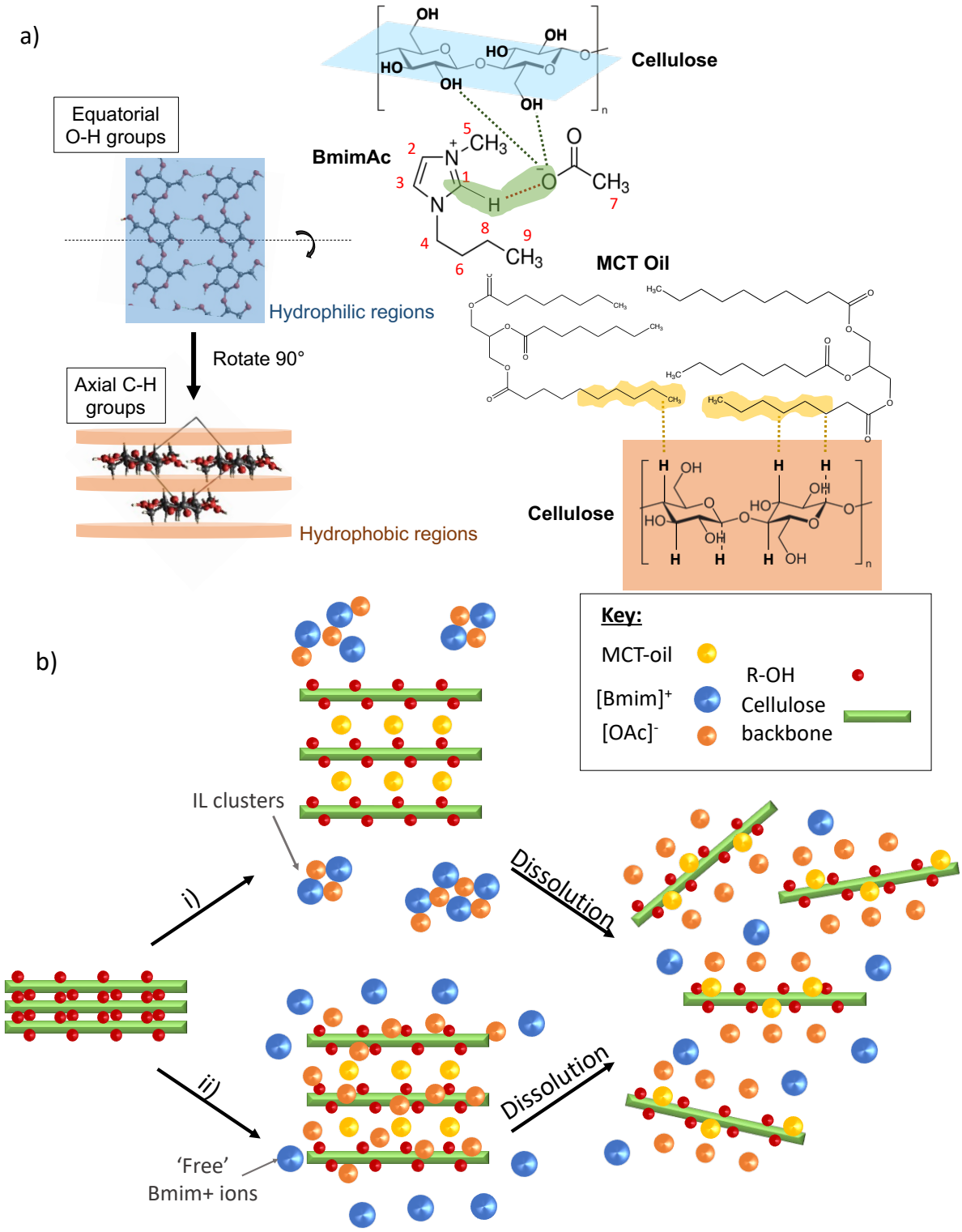

Figure 6.5. a) Schematic showing hydrophobic/hydrophilic regions of cellulose (as described in (Medronho et al., (2015))) and the suggested interactions; b) schematic to show the two proposed possibilities for the dissolution mechanism of cellulose in BmimAc mixtures, with a cosolvent (oil).

6.4.4 Bulk rheology of BmimAc-oil-cellulose mixtures

The bulk properties of BmimAc-oil-cellulose solutions were investigated in attempt to gain further understanding of how the cosolvent (oil), BmimAc ions and cellulose interact. Rheological analysis was chosen because the viscosity is very sensitive to changes in the degree of dissolution and the aggregation of the cellulose, and therefore has the potential to reveal differences in solutions prepared via methods A and B as well as solutions with very minor differences in oil concentration. By eye, the solutions appear identical, however as outlined in section 6.4.3, microscopic differences are clearly observed when oil is added after or before cellulose to BmimAc. Figure 6.6a and b give the flow curves for 2 wt% cellulose-BmimAc solutions with 0-1 wt% oil, prepared via methods A and B (respectively).

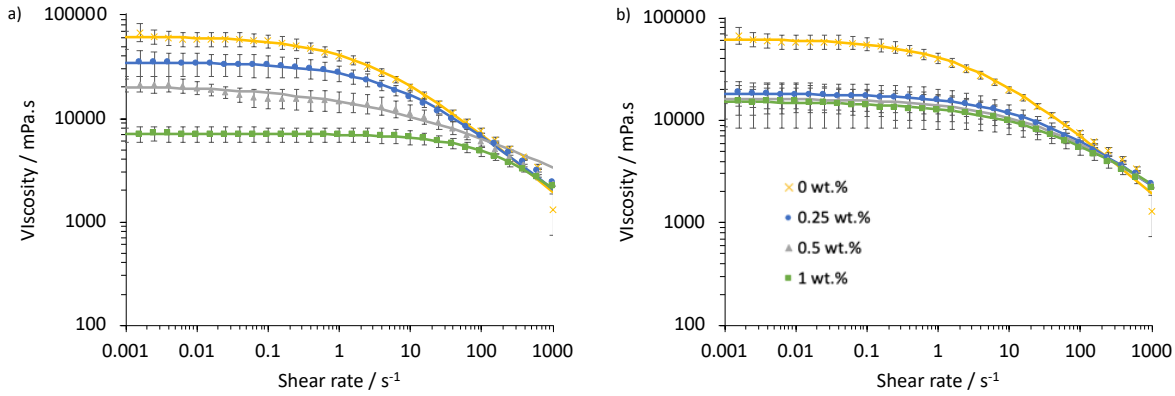

Figure 6.6. Flow curves at 25 °C for 2 wt% cellulose-BmimAc solutions with 0-1 wt% MCT-oil added, where oil was added a) after cellulose dissolution (method A); b) before cellulose dissolution (method B). [oil] = 0 wt% (yellow cross); 0.25 wt% (blue circle); 0.5 wt% (grey triangle) and 1 wt% (green square), legend shown on the bottom left of graph (b). Solid lines show fits to the Cross-model equation (below Figure D 6).

The viscosities of all solutions decreased upon the addition of oil, relative to the 'oil-free' 2 wt% cellulose-BmimAc solution. In all cases, the mixtures showed shear-thinning behaviour which is typical of cellulose-IL solutions (Lu et al., (2015)). When oil was added after cellulose dissolution (method A, Figure 6.6a), the viscosity significantly decreased as the concentration of oil added increased and when [oil] = 1 wt%, the viscosity was 10 times lower compared to the 'oil-free' solution. This is in agreement with the UV-vis and microscopy results and indicates that oil is simply dispersing in the IL-mixture above [oil] = ca. 0.25 wt%. On the other hand, when the oil was added before the cellulose (Figure 6.6b) the viscosity initially decreased again by a larger magnitude but then showed a much less significant decrease upon higher oil addition. These observations again indicate that the order of oil addition has

an effect on the interactions occurring in cellulose-BmimAc-oil mixtures and that oil may affect the mechanism of cellulose dissolution.

The zero-shear rate viscosities (η_0) were obtained by fitting the viscosity curves to the cross-model, given in **Appendix D** (below Figure D 6 and relative viscosity ($\eta_{rel} = \eta_0 / \eta_{sol}$, where η_{sol} is the zero-shear rate viscosity of pure BmimAc) was calculated. Figure D 6 gives a plot of η_{rel} as a function of oil concentration, for the solutions prepared via methods A and B. A clear difference is observed between the two, despite the fact that the formulations of cellulose, oil and BmimAc are identical and again it is clear that the order of addition has an effect on the interactions. For mixtures prepared via method A, η_{rel} decreased with increasing oil concentration whilst for method B, η_{rel} was independent of [oil] (over this concentration range). This again indicates that when the oil is added before cellulose, it disperses in the BmimAc and then 'sticks' to cellulose once it is introduced, thus increasing the amount of oil hardly affects the relative viscosity. On the other hand, the oil is poorly dispersing in the dissolved cellulose-BmimAc solutions (method A) and therefore viscosity decreases as a function of oil concentration.

6.4.5 Mechanism of cellulose dissolution in BmimAc, in the presence of oil

It has been widely reported that dissolution of cellulose in BmimAc (in the absence of oil) is driven by H-bonding, with most mechanistic studies focussing on the hydrophilic interactions (Swatloski et al., (2002); Remsing et al., (2006); Zhang, Zhang, Wu, et al., (2010)). Whilst comparatively fewer reports pay attention to the hydrophobic interactions (Lindman et al., (2010); Medronho and Lindman, (2014)), it has been proposed that the cation interacts with hydrophobic regions on the cellulose chains as a result of solvating the negatively-charged anion-cellulose complex (Rabideau et al., (2013); El Seoud et al., (2019)). Theoretical MD simulations have also indicated a cation-cellulose hydrophobic association, where the $(Bmim)^+$ cation can stack between cellulose pyranose rings and it was suggested that this compensates for the loss of interaction between the cellulose hydrophobic planes (Liu et al., (2010); Mostofian et al., (2014)). Regardless of the type of interaction discussed and its importance, it is generally understood that hydrophilic and hydrophobic contacts between the IL and cellulose develop simultaneously rather than through a step-wise mechanism (El Seoud et al., (2019)) and thus ILs must breakdown both types of interaction in cellulose to achieve full dissolution (Medronho and Lindman, (2015)). In contrast, studying the reverse process of dissolution (precipitation) has revealed that coagulation

of cellulose from solution does in fact proceed via a step-wise mechanism. Isobe *et al.* used time-resolved synchrotron X-ray scattering to study precipitation of cellulose from aqueous alkali-urea (Isobe et al., (2012)) and found that the initial process is driven by hydrophobic interactions. It was speculated that firstly stacking of the glucopyranoside rings occurred to form monomolecular sheets, which were subsequently lined up by H-bonding and formed cellulose crystallites. Several simulation studies have reported similar results, suggesting that H-bonds begin to form between molecular sheets after initial formation of the primary cellulose structure through van der Waals forces, driven by hydrophobic association (Cousins and Brown, (1995); Miyamoto et al., (2009); Maurer et al., (2013)).

Considering the mechanisms for both dissolution (including in the presence of cosolvents, Figure 6.5b) and coagulation, we propose two possible roles for the oil during dissolution of cellulose in BmimAc depending on the order of its addition (method A or B, illustrated in Figure 6.7a and b respectively). If cellulose is dissolved first (method A), disruption of its crystalline structure occurs with the development of both hydrophilic and hydrophobic associations between BmimAc and cellulose. Although hydrophobic interactions between the cation and the hydrophobic regions of cellulose are expected to be weak (Liu et al., (2010); Lindman et al., (2010); Medronho and Lindman, (2014); El Seoud et al., (2019)), when the oil is subsequently introduced it can barely displace the cation. Furthermore, the cellulose is already molecularly dispersed and no longer possesses long range order, resulting in shorter chain lengths (Costa, Mira, et al., (2019)) and a smaller axial hydrophobic surface area available for oil interaction (Figure 6.7a). However, when the cosolvent (oil) is introduced before cellulose (method B), it disperses in the BmimAc with little or no interaction and doesn't make the cations or anions any less available for cellulose. Upon introduction of the cellulose, the oil may 'coat' its intact axial hydrophobic planes and penetrate between the glucopyranose rings by a stacking interaction. Since the amount of oil is small relative to the amount of IL, the $(OAc)^-$ anions can still sufficiently disrupt inter/intramolecular cellulose-cellulose interactions and form hydrogen bonds with the equatorial hydroxyl groups, resulting in complete dissolution (Figure 6.7b). The apparent 're-strengthening' of the cation-anion H-bond observed (Figure 6.4c) is due to the higher volume of 'cellulose-free' $(Bmim)^+$ ions, liberated by the presence of cosolvent (oil) molecules between cellulose chains which 'compete' with the $(Bmim)^+$ cations for hydrophobic association to cellulose.

As well as considering the state of the cellulose at the time of oil addition and its effect on the oil-cellulose interaction, the number of components present at one time in the solution may also be a key factor. Kuzmina *et al.* reported that when formic acid (FA) was introduced as a cosolvent before cellulose dissolution, a 'competition effect' was observed where the FA and BmimAc competed for interaction with the cellulose (Kuzmina et al., (2014)). Although the FA caused an upfield shift of the $(Bmim)^+$ protons (unlike the downfield shift observed in this case with oil), the same principle can be applied. For method B (Figure 6.7b), cellulose is introduced to the oil and BmimAc at the same time whilst for method A (Figure 6.7a), cellulose-IL interactions have already developed before the oil is introduced. Therefore, we propose that the oil must replace the $(Bmim)^+$ ions in the glucopyranose stacks (Mostofian et al., (2014)) for any cellulose-oil interaction to occur in method A, as opposed to oil and $(Bmim)^+$ 'competing' for cellulose interaction during dissolution (method B), and consequently, the cellulose-oil interaction and the observed $\Delta\delta$ is greater in the latter case.

Compared to other cosolvents commonly employed in cellulose dissolution in ILs (e.g. DMSO), MCT-oil is a relatively 'polar' oil with 3 carbonyl groups (making it a weak HBD). Therefore, the oil displays a lower miscibility with BmimAc and can only be added in very small quantities since above ca. 1 wt%, oil is only temporarily dispersing in the IL. Microscopic studies of dissolution in BmimAc with various cosolvents showed that when cellulose is preswollen in 5 wt% DMSO, $\Delta\delta$ was effectively 0 indicating that the cosolvent had little effect on cation-anion bonding (Kuzmina et al., (2014)). Despite this, DMSO influenced cellulose dissolution and the authors attributed this to an initial 'loosening' of the cellulose structure by the DMSO (similar to what we describe in Figure 6.7b), which was then replaced by the main IL solvent most probably entirely, judging by the negligible change in δ of the BmimAc. In our case, we suggest that the oil remains associated with cellulose in the presence of BmimAc, since neither the cation nor anion cannot 'outcompete' the oil for hydrophobic association with cellulose. This explains the positive $\Delta\delta$ (downfield shift) and the strengthening of the cation-anion H-bond that we describe, which is a result of the oil firstly loosening the cellulose structure and then remaining stacked within the hydrophobic planes, whilst a smaller volume of $(Bmim)^+$ ions are locked within the cellulose structure and thus are free for cation-anion H-bonding.

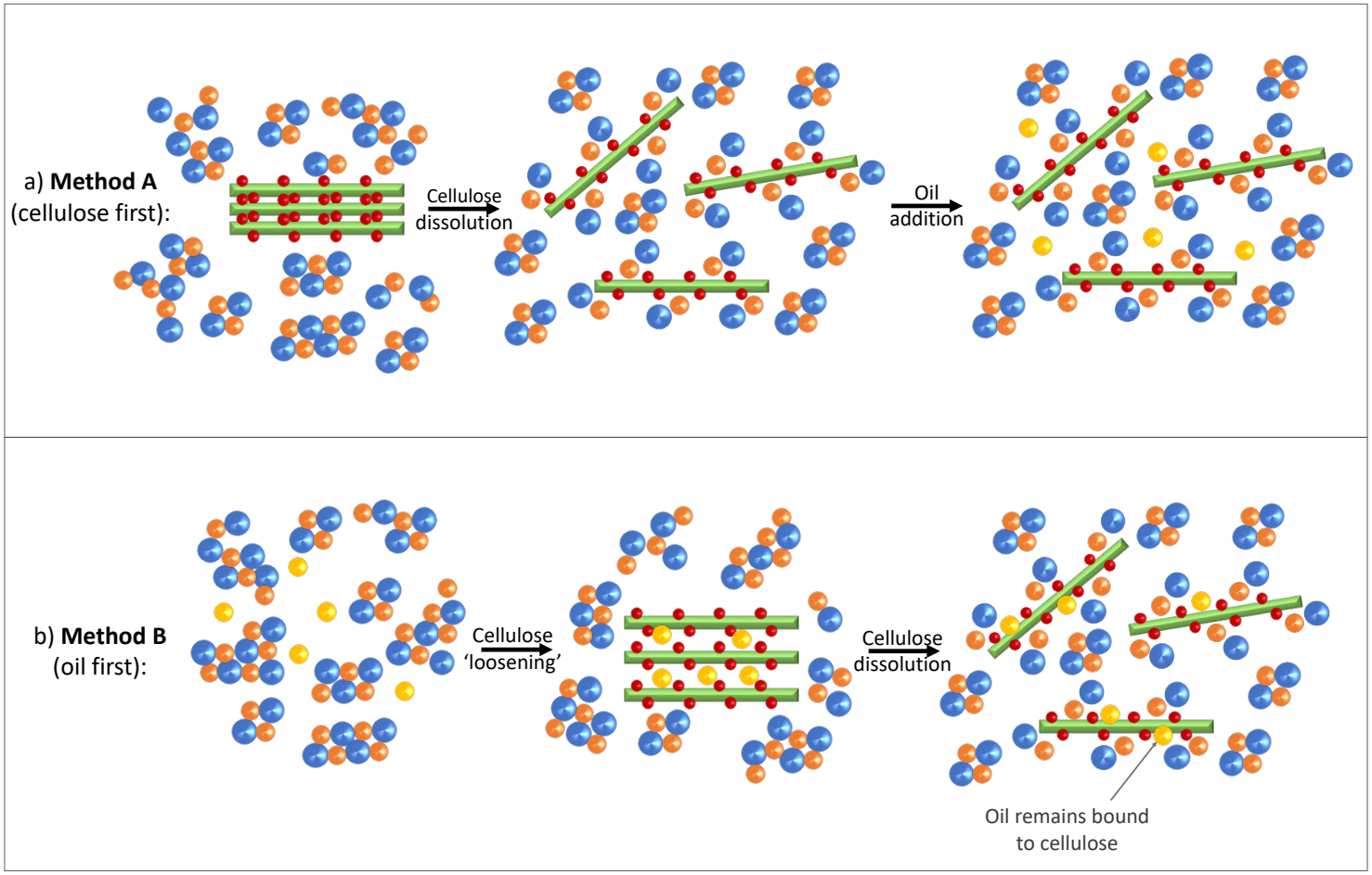

Figure 6.7. Schematic to show cellulose dissolution in the presence of oil, a) when cellulose is added first and dissolution occurs, cosolvent (oil) is added oil after (method A) and oil is dispersed; b) when cosolvent (oil) is added to BmimAc first followed by cellulose (method B), resulting in an oil-cellulose interaction and oil is retained on the cellulose. In both cases, a kinetically stable state is generated. Each component is represented in the same way as Figure 6.5b.

It should also be mentioned that the perceived ‘re-strengthening’ of the cation-anion H-bond could be explained by partial disruption of weakly bound IL clusters by the oil, which would increase the number of cation-anion ion pairs and thus increase the strength of the H-bond interaction (Zheng et al., (2013)). However, we rule out this explanation firstly because the concentration of oil added is too low to have a significant effect, and secondly because one would expect the same Δδ regardless of the order of oil addition, whilst Figure 6.4b and c clearly display a significant different between methods A and B. In addition, we expect any oil-IL interactions to be much weaker than H-bond interactions in IL molecules clusters.

6.4.6 BmimAc-oil-cellobiose mixtures

To further investigate the importance of the cellulose state for the development of cellulose-oil interactions, experiments were carried out using an alternative carbohydrate cellobiose as a cellulose model (Zhang, Zhang, Wu, et al., (2010)). Cellobiose, like cellulose, has the same β-1,4-glycosidic linkage between two glucopyranose units (Figure 6.8a) but does not have the same repeating (polymeric) structure (Figure 6.8b) and therefore the viscosity of cellobiose-BmimAc solutions can be between one and three times lower compared to cellulose-BmimAc solutions (Ries et al., (2018)). This is advantageous because larger concentrations of cellobiose can be dissolved and analysed, which in our case may enhance the cellobiose-oil interactions (and Δδ). It is also commonly used as a cellulose model for simulation studies, due to the limit of computational power (Cao et al., (2016)).

Cellobiose-BmimAc solutions were prepared with 0-1 wt% MCT-oil via method B (oil added before), either with 2 wt% cellobiose for comparison to the cellulose-BmimAc solutions, or with a higher concentration of 15 wt% cellobiose, to maximize the possibility of detecting any oil-cellobiose interaction. In both cases, δ for each resonance in an ‘oil-free’ cellobiose-BmimAc (either 2 or 15 wt%) solution was used as a starting reference value (for more details, see below Figure D 2, **Appendix D**). Table 6.1 gives a comparison between Δδ for the BmimAc protons as a function of [oil], for 2 wt% cellulose/cellobiose-BmimAc solutions.

a) Cellobiose: **b) Cellulose:**

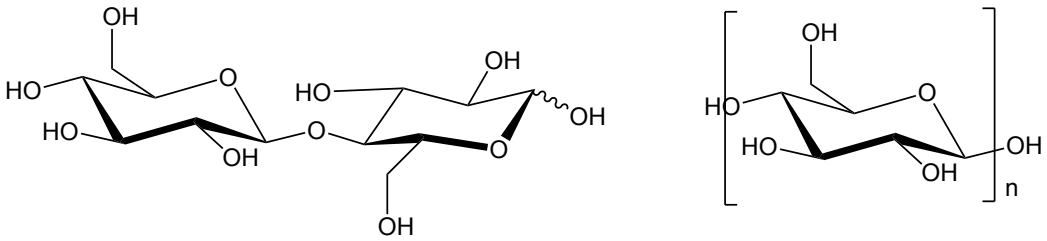

Figure 6.8. Chemical structures of a) cellobiose and b) polymeric repeat unit of cellulose.

Table 6.1. Comparison of the changes to chemical shift (Δδ) for H1 of BmimAc in 2 wt% cellulose/cellobiose-BmimAc-oil solutions, prepared by adding oil before the cellulose/cellobiose (method B). For 0 wt% oil solutions, Δδ is calculated with pure BmimAc as a reference and for 0.25-1 wt% oil solutions, Δδ is calculated with the corresponding 2 wt% cellulose/cellobiose-BmimAc solution as a reference.

Concentration of oil/wt%	Δδ 2 wt% cellulose/ppm	Δδ 2 wt% cellobiose/ppm
0	-0.4142	-0.0364
0.25	0.3594 (ca. ~12x)*	-0.0305
0.5	0.3596 (ca. ~13x)*	-0.0277
1	0.3709 (ca. ~47x)*	-0.0079

*relative to the reference value

Almost no effect was observed for any of the BmimAc protons in cellobiose-BmimAc solutions with the addition of oil (Δδ < 0.01), at both the higher (15 wt%, Figure D 7a) and lower (2 wt%, Figure D 7b) concentrations of cellobiose analyzed. This suggests that oil doesn't play a role in cellobiose dissolution whatsoever, unlike for cellulose, and this difference is clearly displayed in Table 6.1 where Δδ for the most acidic proton (H1) is compared. We argue that this highlights the importance of the long-range order in the cellulose structure and the presence of the hydrophobic planes (Miyamoto et al., (2014)), which are necessary for a significant cellulose-oil interaction and are not present in cellobiose. These results also confirm that the more significant Δδ observed for cellulose-BmimAc-oil solutions prepared by method B (Figure 6.4c) must be due to a hydrophobic interaction rather than hydrophilic, since cellobiose is still capable of forming H-bonds with components in solution. In fact, cellobiose is expected to have a greater capacity for H-bonding compared to cellulose due to the greater number of hydroxyl groups per glucose unit (*N*). A previous study comparing cellulose, cellobiose and glucose (*N* = 3, 4 and 5 respectively) in ILs has shown that the associated

fraction (a) is an important parameter to consider when comparing carbohydrates (Ries et al., (2018)), where α is defined as follows:

Equation 5.2. $$\alpha = N\, x\, \frac{M_{IL}}{M_{GU}} x\, \frac{\phi}{100-\phi}$$

Where N = number of OH groups 'per glucose unit,' (4 for cellobiose and 3 for cellulose); M_{IL} = mass of the IL; M_{GU} = mass of 'glucose units,' (171 and 162 g mol^{-1} for cellobiose and cellulose respectively) and ϕ = wt% of the carbohydrate. Therefore, a gives representative value for the fraction of IL molecules involved in dissolving 'units of glucose,' and thus allows comparison between the carbohydrates. For 2 wt% cellulose and cellobiose solutions, a = 0.075 and 0.095 respectively, whilst for 15 wt% cellobiose solutions, a = 0.818 suggesting potential for a larger volume of hydrophilic cellobiose-IL associations compared to cellulose-IL. This was particularly evident for the 15 wt% cellobiose-IL solutions, where broadening of the peaks was observed ^{1}H NMR spectra (Figure D 8) most probably due to exchange of the cellobiose hydroxy protons with the acidic protons in the $(Bmim)^+$ (Zhang, Zhang, Wu, et al., (2010)), whilst Δδ values displayed in Figure D 7a provide no evidence for a hydrophobic cellobiose-oil interaction. This strongly suggests that the mechanism of cellobiose dissolution in BmimAc involves hydrophilic interactions alone rather than both hydrophilic and hydrophobic as in the case of cellulose, and that the highly orientated repeat structure of cellulose is responsible for its hydrophobicity. Again, it appears that the cellulose structure must be intact for significant oil-cellulose interaction to occur (method B, see section 6.4.5).

6.5 Conclusions

In this work, we highlight the importance of hydrophobic interactions in cellulose dissolution in ILs, which evidently must be disrupted between cellulose molecules in order to achieve complete dissolution. Full dissolution of cellulose was achieved by BmimAc in the presence of MCT-oil, when it was added to the IL both before and after the cellulose. However, we report that the order of oil addition has an effect on the interactions in the solutions and we observed a significant increase in Δδ (downfield shift) for BmimAc-cellulose peaks when MCT-oil was added before cellulose. A more significant decrease in viscosity was also observed with increasing oil concentration when oil was added after cellulose, as opposed to before. We rationalise these differences by considering the solution state of cellulose: when the oil is introduced first, a hydrophobic interaction develops between the intact hydrophobic plane of cellulose and the oil. However, when the cellulose is introduced first, it is molecularly dispersed when the oil is added and there is

no significant interaction. The same effect was not observed for cellobiose (in BmimAc-oil solutions), which is commonly used as a model for cellulose dissolution studies, suggesting that the structural anisotropy of cellulose is important. We also highlight that this indicates differences between the mechanisms of cellulose and cellobiose dissolution in ILs.

Furthermore, the cellulose-oil interaction we describe is similar to a 'pre-swelling' stage described for other cosolvents in ILs, (for example DMSO) and we propose that the oil can act as a type of cosolvent, penetrating between the cellulose glucopyranose rings and interacting with the axial hydrophobic planes of cellulose. Over time, the cellulose-oil interaction remains and is not 'outcompeted' by BmimAc-cellulose or cellulose-cellulose interactions, resulting in a stable system and thus a potential route for trapping oil within the cellulose structure (upon coagulation). This work provides further insight into the mechanism of cellulose dissolution in ILs, the importance of hydrophobic interactions and the effect of non-polar cosolvents, which is important in the design of novel ILs for efficient cellulose dissolution.

6.6 References

Asakawa, A., Oka, T., Sasaki, C., Asada, C. and Nakamura, Y. (2016). Cholinium ionic liquid/cosolvent pretreatment for enhancing enzymatic saccharification of sugarcane bagasse. *Industrial Crops and Products*. *86*, 113–119.

Cao, B., Du, J., Du, D., Sun, H., Zhu, X. and Fu, H. (2016). Cellobiose as a model system to reveal cellulose dissolution mechanism in acetate-based ionic liquids: Density functional theory study substantiated by NMR spectra. *Carbohydrate Polymers*. *149*, 348–356.

Costa, C., Mira, I., Benjamins, J.W., Lindman, B., Edlund, H. and Norgren, M. (2019). Interfacial activity and emulsion stabilization of dissolved cellulose. *Journal of Molecular Liquids*. *292*, 111325.

Cousins, S.K. and Brown, R.M. (1995). Cellulose I microfibril assembly: computational molecular mechanics energy analysis favours bonding by van der Waals forces as the initial step in crystallization. *Polymer*. *36*(20), 3885–3888.

Ebner, G., Schiehser, S., Potthast, A. and Rosenau, T. (2008). Side reaction of cellulose with common 1-alkyl-3-methylimidazolium-based ionic liquids. *Tetrahedron Letters*. *49*(51), 7322–7324.

Fendt, S., Padmanabhan, S., Blanch, H.W. and Prausnitz, J.M. (2011). Viscosities of acetate or chloride-based ionic liquids and some of their mixtures with water or other common solvents. *Journal of Chemical and Engineering Data*. *56*(1), 31–34.

Feng, L. and Chen, Z. lan (2008). Research progress on dissolution and functional modification of cellulose in ionic liquids. *Journal of Molecular Liquids*. *142*, 1–5.

Fortunato, G.G., Mancini, P.M., Bravo, M.V. and Adam, C.G. (2010). New solvents designed on the basis of the molecular-microscopic properties of binary mixtures of the type (protic molecular solvent + 1-butyl-3-methylimidazolium-based ionic liquid). *Journal of Physical Chemistry B*. *114*(36), 11804–11819.

Gale, E., Wirawan, R.H., Silveira, R.L., Pereira, C.S., Johns, M.A., Skaf, M.S. and Scott, J.L. (2016). Directed discovery of greener cosolvents: New cosolvents for use in ionic liquid based organic electrolyte solutions for cellulose dissolution. *ACS Sustainable Chemistry and Engineering*. *4*(11), 6200–6207.

Gericke, M., Fardim, P. and Heinze, T. (2012). Ionic liquids - Promising but challenging solvents for homogeneous derivatization of cellulose. *Molecules*. *17*(6), 7458–7502.

Gericke, M., Liebert, T., Seoud, O.A.E. and Heinze, T. (2011). Tailored media for homogeneous cellulose chemistry: Ionic liquid/co-solvent mixtures. *Macromolecular Materials and Engineering*. *296*(6), 483–493.

Gericke, M., Schlufter, K., Liebert, T., Heinze, T. and Budtova, T. (2009). Rheological properties of cellulose/ionic liquid solutions: From dilute to concentrated states. *Biomacromolecules*. *10*(5), 1188–1194.

Graenacher, C. (1934). Cellulose Solution. US 1943176A.

Greaves, T.L. and Drummond, C.J. (2015). Protic Ionic Liquids: Evolving Structure-Property Relationships and Expanding Applications. *Chemical Reviews*. *115*(20), 11379–11448.

Halder, P., Kundu, S., Patel, S., Setiawan, A., Atkin, R., Parthasarthy, R., Paz-Ferreiro, J., Surapaneni, A. and Shah, K. (2019). Progress on the pre-treatment of lignocellulosic biomass employing ionic liquids. *Renewable and Sustainable Energy Reviews*. *105*, 268–292.

Hall, C.A., Le, K.A., Rudaz, C., Radhi, A., Lovell, C.S., Damion, R.A., Budtova, T. and Ries, M.E. (2012). Macroscopic and microscopic study of 1-Ethyl-3-methyl-imidazolium acetate-water mixtures. *Journal of Physical Chemistry B*. *116*(42), 12810–12818.

Huddleston, J.G., Visser, A.E., Reichert, W.M., Willauer, H.D., Broker, G.A. and Rogers, R.D. (2001). Characterization and comparison of hydrophilic and hydrophobic room temperature ionic liquids incorporating the imidazolium cation. *Green Chemistry*. *3*(4), 156–164.

Isik, M., Sardon, H. and Mecerreyes, D. (2014). Ionic liquids and cellulose: Dissolution, chemical modification and preparation of new cellulosic materials. *International Journal of Molecular Sciences*. *15*(7), 11922–11940.

Isobe, N., Kimura, S., Wada, M. and Kuga, S. (2012). Mechanism of cellulose gelation from aqueous alkali-urea solution. *Carbohydrate Polymers*. *89*(4), 1298–1300.

Jiang, H.J., Fitzgerald, P.A., Dolan, A., Atkin, R. and Warr, G.G. (2014). Amphiphilic self-assembly of alkanols in protic ionic liquids. *Journal of Physical Chemistry B*. *118*(33), 9983–9990.

Kalb, R.S. (2020). Toward Industrialization of Ionic Liquids *In*: *Commercial Applications of Ionic Liquids* [Online]. Cham: Springer International Publishing, 261–282. Available from: https://doi.org/10.1007/978-3-030-35245-5_11.

Kang, X., Kuga, S., Wang, L., Wu, M. and Huang, Y. (2016). Dissociation of intra / inter-molecular hydrogen bonds of cellulose molecules in the dissolution process : a mini review. *Journal of Bioresources and Bioproducts. 1*(1), 58–63.

Kasprzak, D. and Galiński, M. (2021). DMSO as an auxiliary solvent in the fabrication of homogeneous chitin-based films obtaining from an ionic liquid process. *European Polymer Journal*. *158*, 110681.

Kasprzak, D., Krystkowiak, E., Stępniak, I. and Galiński, M. (2019). Dissolution of cellulose in novel carboxylate-based ionic liquids and dimethyl sulfoxide mixed solvents. *European Polymer Journal*. *113*, 89–97.

Kosan, B., Michels, C. and Meister, F. (2008). Dissolution and forming of cellulose with ionic liquids. *Cellulose*. *15*(1), 59–66.

Kuroda, K., Kunimura, H., Fukaya, Y. and Ohno, H. (2014). 1H NMR analysis of cellulose dissolved in non-deuterated ionic liquids. *Cellulose*. *21*(4), 2199–2206.

Kuzmina, O., Jankowski, S., Fabiańska, A., Sashina, E. and Wawro, D. (2014). Preswelling of Cellulose Pulp for Dissolution in Ionic Liquid. *Cellulose Chemistry and Technology*. *48*, 45–51.

Le, K.A., Rudaz, C. and Budtova, T. (2014). Phase diagram, solubility limit and hydrodynamic properties of cellulose in binary solvents with ionic liquid. *Carbohydrate Polymers*. *105*(1), 237–243.

Lefroy, K.S., Murray, B.S. and Ries, M.E. (2021). Rheological and NMR Studies of Cellulose Dissolution in the Ionic Liquid BmimAc. *Journal of Physical Chemistry B*. *125*(29), 8205–8218.

Lefroy, K.S., Murray, B.S., Ries, M.E. and Curwen, T.D. (2021). A natural, cellulose-based microgel for water-in-oil emulsions. *Food Hydrocolloids*. *113*, 106408.

Lepre, L.F., Szala-Bilnik, J., Padua, A.A.H., Traïkia, M., Ando, R.A. and Costa Gomes, M.F. (2016). Tailoring the properties of acetate-based ionic liquids using the tricyanomethanide anion. *Physical Chemistry Chemical Physics*. *18*(33), 23285–23295.

Li, Y., Wang, J., Liu, X. and Zhang, S. (2018). Towards a molecular understanding of cellulose dissolution in ionic liquids: Anion/cation effect, synergistic mechanism and physicochemical aspects. *Chemical Science*. *9*, 4027–4043.

Lindman, B., Karlström, G. and Stigsson, L. (2010). On the mechanism of dissolution of cellulose. *Journal of Molecular Liquids*. *156*(1), 76–81.

Liu, H., Sale, K.L., Holmes, B.M., Simmons, B.A. and Singh, S. (2010). Understanding the interactions of cellulose with ionic liquids: a molecular dynamics study. *Journal of Physical Chemistry B*. *114*(12),

4293–4301.

Lopes, J., Bermejo, M., Martín, Á. and Cocero, M. (2017). Ionic Liquid as Reaction Media for the Production of Cellulose-Derived Polymers from Cellulosic Biomass. *ChemEngineering*. *1*, 1–28.

Lovell, C.S., Walker, A., Damion, R.A., Radhi, A., Tanner, S.F., Budtova, T. and Ries, M.E. (2010). Influence of cellulose on ion diffusivity in 1-ethyl-3-methyl-imidazolium acetate cellulose solutions. *Biomacromolecules*. *11*, 2927–2935.

Lu, B., Xu, A. and Wang, J. (2014). Cation does matter: How cationic structure affects the dissolution of cellulose in ionic liquids. *Green Chemistry*. *16*(3), 1326–1335.

Lu, F., Wang, L., Zhang, C., Cheng, B., Liu, R. and Huang, Y. (2015). Influence of temperature on the solution rheology of cellulose in 1-ethyl-3-methylimidazolium chloride/dimethyl sulfoxide. *Cellulose*. *22*(5), 3077–3087.

Marekha, B.A., Bria, M., Moreau, M., De Waele, I., Miannay, F.A., Smortsova, Y., Takamuku, T., Kalugin, O.N., Kiselev, M. and Idrissi, A. (2015). Intermolecular interactions in mixtures of 1-n-butyl-3-methylimidazolium acetate and water: Insights from IR, Raman, NMR spectroscopy and quantum chemistry calculations. *Journal of Molecular Liquids*. *210*, 227–237.

Marks, C., Mitsos, A. and Viell, J. (2019). Change of C(2)-Hydrogen–Deuterium Exchange in Mixtures of EMIMAc. *Journal of Solution Chemistry*. *48*(8–9), 1188–1205.

Maurer, R.J., Sax, A.F. and Ribitsch, V. (2013). Moleular simulation of surface reorganization and wetting in crystalline cellulose I and II. *Cellulose*. *20*(1), 25–42.

Medronho, B., Duarte, H., Alves, L., Antunes, F., Romano, A. and Lindman, B. (2015). Probing cellulose amphiphilicity. *Nordic Pulp & Paper Research Journal*. *30*(1), 58-66.

Medronho, B. and Lindman, B. (2015). Brief overview on cellulose dissolution/regeneration interactions and mechanisms. *Advances in Colloid and Interface Science*. *222*, 502–508.

Medronho, B. and Lindman, B. (2014). Competing forces during cellulose dissolution: From solvents to mechanisms. *Current Opinion in Colloid and Interface Science*. *19*(1), 32–40.

Mellein, B.R., Aki, S.N.V.K., Ladewski, R.L. and Brennecke, J.F. (2007). Solvatochromic studies of ionic liquid/organic mixtures. *Journal of Physical Chemistry B*. *111*(1), 131–138.

Miyamoto, H., Schnupf, U. and Brady, J.W. (2014). Water structuring over the hydrophobic surface of cellulose. *Journal of Agricultural and Food Chemistry*. *62*(46), 11017–11023.

Miyamoto, H., Umemura, M., Aoyagi, T., Yamane, C., Ueda, K. and Takahashi, K. (2009). Structural reorganization of molecular sheets derived from cellulose II by molecular dynamics simulations.

Carbohydrate Research. *344*(9), 1085–1094.

Mostofian, B., Smith, J.C. and Cheng, X. (2014). Simulation of a cellulose fiber in ionic liquid suggests a synergistic approach to dissolution. *Cellulose*. *21*(2), 983–997.

Napso, S., Rein, D.M., Fu, Z., Radulescu, A. and Cohen, Y. (2018). Structural Analysis of Cellulose-Coated Oil-in-Water Emulsions Fabricated from Molecular Solution. *Langmuir*. *34*(30), 8857–8865.

Nazari, B., Utomo, N.W. and Colby, R.H. (2017). The Effect of Water on Rheology of Native Cellulose/Ionic Liquids Solutions. *Biomacromolecules*. *18*(9), 2849–2857.

Nielsen, J. and Kropke, R. (2004). Cosmetic or dermatological formulations containing glycerin. US 20040258654.

Olsson, C. and Westman, G. (2013). Direct Dissolution of Cellulose: Background, Means and Applications *In*: *Cellulose - Fundamental Aspects* [Online]. IntechOpen, 143–178. Available from: https://doi.org/10.5772/2705.

Orelma, H., Hokkanen, A., Leppänen, I., Kammiovirta, K., Kapulainen, M. and Harlin, A. (2020). Optical cellulose fiber made from regenerated cellulose and cellulose acetate for water sensor applications. *Cellulose*. *27*(3), 1543–1553.

Van Osch, D.J.G.P., Kollau, L.J.B.M., Van Den Bruinhorst, A., Asikainen, S., Rocha, M.A.A. and Kroon, M.C. (2017). Ionic liquids and deep eutectic solvents for lignocellulosic biomass fractionation. *Physical Chemistry Chemical Physics*. *19*(4), 2636–2665.

Parthasarathi, R., Balamurugan, K., Shi, J., Subramanian, V., Simmons, B.A. and Singh, S. (2015). Theoretical Insights into the Role of Water in the Dissolution of Cellulose Using IL/Water Mixed Solvent Systems. *Journal of Physical Chemistry B*. *119*(45), 14339–14349.

Pinkert, A., Marsh, K.N. and Pang, S. (2010). Reflections on the solubility of cellulose. *Industrial and Engineering Chemistry Research*. *49*(22), 11121–11130.

Qiu, B., Lin, B. and Yan, F. (2013). Ionic liquid/poly(ionic liquid)-based electrolytes for energy devices. *Polymer International*. *62*(3), 335–337.

Qu, J., Blau, P.J., Dai, S., Luo, H. and Meyer, H.M. (2009). Ionic Liquids as Novel Lubricants and Additives for Diesel Engine Applications. *Tribology Letters*. *35*(3), 181–189.

Rabideau, B.D., Agarwal, A. and Ismail, A.E. (2013). Observed mechanism for the breakup of small bundles of cellulose Iα and Iβ in ionic liquids from molecular dynamics simulations. *Journal of Physical Chemistry B*. *117*(13), 3469–3479.

Radhi, A., Le, K.A., Ries, M.E. and Budtova, T. (2015). Macroscopic and microscopic study of 1-ethyl-3-methyl-imidazolium acetate-DMSO mixtures. *Journal of Physical Chemistry B*. *119*(4), 1633–1640.

Rajeev, A., Deshpande, A.P. and Basavaraj, M.G. (2018). Rheology and microstructure of concentrated microcrystalline cellulose (MCC)/1-allyl-

3-methylimidazolium chloride (AmimCl)/water mixtures. *Soft Matter*. *14*(37), 7615–7624.

Remsing, R.C., Swatloski, R.P., Rogers, R.D. and Moyna, G. (2006). Mechanism of cellulose dissolution in the ionic liquid 1-n-butyl-3-methylimidazolium chloride: A 13C and 35/37Cl NMR relaxation study on model systems. *Chemical Communications*. *12*, 1271–1273.

Ren, F., Wang, J., Yu, J., Zhong, C., Xie, F. and Wang, S. (2021). Dissolution of Cellulose in Ionic Liquid-DMSO Mixtures: Roles of DMSO/IL Ratio and the Cation Alkyl Chain Length. *ACS Omega*. *6*(41), 27225–27232.

Rieland, J.M. and Love, B.J. (2020). Ionic liquids: A milestone on the pathway to greener recycling of cellulose from biomass. *Resources, Conservation and Recycling*. *155*, 104678.

Ries, M.E., Radhi, A., Green, S.M., Moffat, J. and Budtova, T. (2018). Microscopic and Macroscopic Properties of Carbohydrate Solutions in the Ionic Liquid 1-Ethyl-3-methyl-imidazolium Acetate. *Journal of Physical Chemistry B*. *122*(37), 8763–8771.

Ries, M.E., Radhi, A., Keating, A.S., Parker, O. and Budtova, T. (2014). Diffusion of 1-ethyl-3-methyl-imidazolium acetate in glucose, cellobiose, and cellulose solutions. *Biomacromolecules*. *15*(2), 609–617.

Rinaldi, R. (2011). Instantaneous dissolution of cellulose in organic electrolyte solutions. *Chemical Communications*. *47*(1), 511–513.

Rinaldi, R., Meine, N., vom Stein, J., Palkovits, R. and Schüth, F. (2010). Which controls the depolymerization of cellulose in ionic liquids: The solid acid catalyst or cellulose? *ChemSusChem*. *3*(2), 266–276.

Roberts, N.J. and Lye, G.J. (2002). Application of Room-Temperature Ionic Liquids in Biocatalysis: Opportunities and Challenges *In*: *Ionic Liquids: Industrial Applications for Green Chemistry*. American Chemical Society, 347–359.

El Seoud, O.A., Kostag, M., Jedvert, K. and Malek, N.I. (2019). Cellulose in ionic liquids and alkaline solutions: Advances in the mechanisms of biopolymer dissolution and regeneration. *Polymers*. *11*(12), 1–28.

Swatloski, R.P., Spear, S.K., Holbrey, J.D. and Rogers, R.D. (2002). Dissolution of cellulose with ionic liquids. *Journal of the American Chemical Society*. *124*(18), 4974–4975.

Verma, C., Mishra, A., Chauhan, S., Verma, P., Srivastava, V., Quraishi, M.A. and Ebenso, E.E. (2019). Dissolution of cellulose in ionic liquids and their mixed cosolvents: A review. *Sustainable Chemistry and Pharmacy*. *13*, 100162.

Wang, H., Gurau, G. and Rogers, R.D. (2012). Ionic liquid processing of cellulose. *Chemical Society Reviews*. *41*(4), 1519–1537.

Xiong, B., Zhao, P., Hu, K., Zhang, L. and Cheng, G. (2014). Dissolution of cellulose in aqueous NaOH/urea solution: Role of urea. *Cellulose*. *21*(3), 1183–1192.

Xu, A., Zhang, Y., Zhao, Y. and Wang, J. (2013). Cellulose dissolution at

ambient temperature: Role of preferential solvation of cations of ionic liquids by a cosolvent. *Carbohydrate Polymers*. *92*(1), 540–544.

Xu, F. and Cho, B.U. (2022). Preparation of porous regenerated cellulose microstructures via emulsion-coagulation technique. *Cellulose*. *29*(3), 1527–1542.

Yan, X., Alcouffe, P., Sudre, G., David, L., Bernard, J. and Ganachaud, F. (2017). Modular construction of single-component polymer nanocapsules through a one-step surfactant-free microemulsion templated synthesis. *Chemical Communications*. *53*(8), 1401–1404.

Yang, J., Lu, X., Zhang, Y., Xu, J., Yang, Y. and Zhou, Q. (2020). A facile ionic liquid approach to prepare cellulose fiber with good mechanical properties directly from corn stalks. *Green Energy and Environment*. *5*(2), 223–231.

Yang, Z. and Pan, W. (2005). Ionic liquids: Green solvents for nonaqueous biocatalysis. *Enzyme and Microbial Technology*. *37*(1), 19–28.

Yassin, F.A., El Kady, F.Y., Ahmed, H.S., Mohamed, L.K., Shaban, S.A. and Elfadaly, A.K. (2015). Highly effective ionic liquids for biodiesel production from waste vegetable oils. *Egyptian Journal of Petroleum*. *24*(1), 103–111.

Zhang, J., Xu, L., Yu, J., Wu, J., Zhang, X., He, J. and Zhang, Jun (2016). Understanding cellulose dissolution: effect of the cation and anion structure of ionic liquids on the solubility of cellulose. *Science China Chemistry*. *59*(11), 1421–1429.

Zhang, J., Zhang, H., Wu, J., Zhang, J., Hea, J. and Xiang, J. (2010). NMR spectroscopic studies of cellobiose solvation in EmimAc aimed to understand the dissolution mechanism of cellulose in ionic liquids. *Physical Chemistry Chemical Physics*. *12*(8), 1941–1947.

Zhang, J., Zhang, H., Wu, J., Zhang, J., He, J. and Xiang, J. (2010). NMR spectroscopic studies of cellobiose solvation in EmimAc aimed to understand the dissolution mechanism of cellulose in ionic liquids. *Physical Chemistry Chemical Physics*. *12*, 1941–1947.

Zhao, H., Brown, H.M., Holladay, J.E. and Zhang, Z.C. (2012). Prominent roles of impurities in ionic liquid for catalytic conversion of carbohydrates. *Topics in Catalysis*. *55*, 33–37.

Zheng, Y.Z., Wang, N.N., Luo, J.J., Zhou, Y. and Yu, Z.W. (2013). Hydrogen-bonding interactions between [BMIM][BF4] and acetonitrile. *Physical Chemistry Chemical Physics*. *15*(41), 18055–18064.

Chapter 7
General Discussion

7.1 Introduction

Considering the lack of 'clean-label' emulsifiers for water-in-oil (W/O) emulsions and the increasing need for fat reduction strategies, in light of incoming regulations on products high in fat, salt and sugar (HFSS), it was of interest to study the functional properties of native cellulose and its potential to be used as a stabiliser. Cellulose is the most abundant biopolymer and is readily found in many natural and waste sources. However, it is rarely used in its native form due to its recalcitrance and is often chemical modified, to achieve specific functionalities. We have reviewed in detail the properties of cellulose in **Chapter 2** and provided an overview of microgels, outlining their potential as an innovative concept for food systems. Microgels already form a highly active area in food and beverage research and may provide lubrication in products, mimic fat and stabilise emulsions. Microgelation can also be used as a strategy to impart novel properties on well-studied food-grade compounds, such as cellulose, and this has led to the fabrication of many types of polymeric microgels (Sarkar et al., (2016); Andablo-Reyes et al., (2019); Zembyla et al., (2020); Zhang et al., (2020); Stubley et al., (2021)). However, to our knowledge, *physically modified* cellulose microgels (CMGs) had not previously been fabricated and studied for food systems.

The overarching aim of this thesis was to investigate the functionality of native cellulose and develop an effective W/O stabiliser, which could potentially replace synthetic surfactants such as polyglycerol polyricinoleate (PGPR). W/O emulsions provide a promising route to reducing fat and therefore calories in food products. In order to fulfil clean-label requirements, processing of the cellulose was limited to physical modifications only and a non-derivatising cellulose solvent was used.

ILs have received a huge amount of interest in the last 20 years and are convenient and potentially 'green' solvents for cellulose. However, the properties of cellulose-IL systems depends on the type of both components and the mechanism for dissolution is still not well understood. We first compared a commercial cellulose to microcrystalline cellulose (MCC), in the IL 1-butyl 3-imidazolium acetate (BmimAc) (Figure 7.1, **Chapter 3**), and characterised the cellulose-BmimAc systems in detail. We defined the cross-over and entanglement concentrations (c^* and c_e respectively), the intrinsic viscosities ([η]) and compared bulk properties to the microscopic properties, using the Stokes-Einstein relationship. This allowed detailed understanding of

our cellulose-BmimAc system and prompted the design of cellulose gels, coagulated from these solutions (Figure 7.1, **Chapter 4**). Our novel method for producing CMGs is presented in **Chapter 4**, via dissolution and coagulation and without employing chemical modification. CMGs were used to stabilise W/O and O/W emulsions, but were found to be more suitable for oil-continuous systems. Oil was added to the coagulation medium to increase the 'hydrophobicity' of the CMGs, whilst varying parameters such as stabiliser concentration and water volume changed the emulsion properties (Figure 7.1). W/O emulsions and CMGs were further characterised and optimised in **Chapter 5**, where we demonstrated that a range of CMG sizes could be achieved by employing varying levels of mechanical force during coagulation. Highly stable W/O emulsions were produced by using a combination of CMG sizes and excess CMGs dispersed in the oil could adsorb to the interface over time (Figure 7.1, **Chapter 5**). We further investigated the origin of cellulose 'hydrophobicity' in **Chapter 6** (Figure 7.1) and suggested that a cellulose-oil interaction develops in the BmimAc solution. The order of oil/cellulose addition to the coagulant mixture was found to be key in determining the volume of cellulose-oil interactions, as probed via NMR.

In this thesis, we have therefore introduced a novel method for producing a W/O stabiliser based on cellulose, which has the potential to meet clean-label requirements. We have exploited the functional properties of cellulose using physical modification strategies alone and demonstrate that our system has the potential to be used in fat reduction, for confectionary products such as chocolate/biscuit fillings and creams.

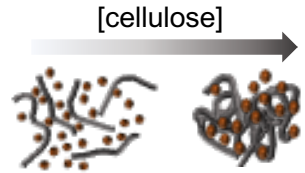

Chapter 3

Properties of cellulose-BmimAc solutions

Variables:
- Cellulose concentration
- Cellulose type
- Temperature

Results:
- Larger DP cellulose entangles at lower concentrations
- Entanglements effect bulk properties more than microscopic properties

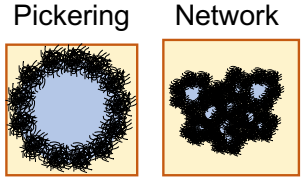

Chapter 4

Fabrication of CMGs for W/O emulsions

Variables:
- Emulsion type (O/W or W/O)
- CMG concentration
- Water emulsion volume

Results:
- CMGs adsorb to the interface in W/O emulsions
- Pickering-type stabilisation
- High [CMG] leads to cellulose network

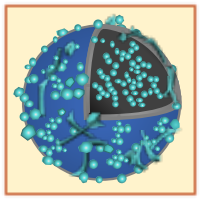

Chapter 5

Optimisation of CMG-stabilised W/O emulsions

Variables:
- Shear force during coagulation
- Top-down/bottom-up method
- Oil concentration in coagulant

Results:
- Higher shear results in smaller CMGs, which produce smaller W/O droplets
- High W/O emulsion stability with combination of CMGs
- Excess CMGs adsorb to form interfacial layer

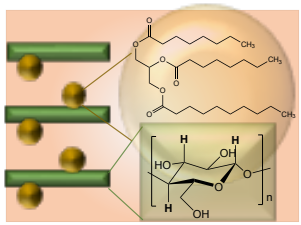

Chapter 6

Assessing hydrophobicity of native cellulose

Variables:
- Oil concentration
- Order of addition of components to BmimAc

Results:
- Oil and BmimAc have limited miscibility
- Cellulose-oil interaction develops when oil is added first
- State of cellulose effects strength of interaction

Figure 7.1. Schematic framework of this thesis.

7.2 Summary of the main results

7.2.1 Solution properties of cellulose in 1-butyl-3-methyl imidazolium acetate (BmimAc)

The solution properties of cellulose (Avicel and Vitacel) dissolved in BmimAc were characterised in **Chapter 3** and Table 7.1 compares c^* and c_e, as well as their $[\eta]$ and deduced degrees of polymerisation (DP). Vitacel (*V-cell*) solutions had higher viscosities compared to the equivalent Avicel (*A-cell*) solutions, which is attributed to the higher DP and thus lower chain flexibility of the former (Horinaka et al., (2018); Lopez et al., (2020)). Overlap and entanglement of polymer chains occurs at a lower concentration of *V-cell* which results in a more rapid viscosity increase with concentration. Good agreement is observed between c^* values for *A-cell*/BmimAc and *A-cell*/1-ethyl 3-imidazolium acetate (EmimAc) solutions from literature (Sescousse et al., (2010); Tan et al., (2016)) (Table 7.1), suggesting that the IL cation chain length doesn't have a significant influence on entanglements.

Table 7.1. c^*, c_e, $([\eta])$ and DP of Avicel and Vitacel celluloses, dissolved in BmimAc.

	Avicel *(A-cell)* (BmimAc, Chapter 3)	**Avicel *(A-cell)* (EmimAc (Sescousse et al., (2010); Tan et al., (2016)))**	**Vitacel (*V-cell)* (BmimAc, Chapter 3)**
c^*/wt%	0.77-0.82	0.8, 0.8-0.9	0.2
c_e/wt%	3.4	-	2
$[\eta]$ (25 °C)/mL g^{-1}	116	112, 100-110	350
DP	180	235, 180	Ca. 730-830

Unlike *A-cell*, cellulose with a larger DP (e.g. *V-cell*) appears to display different properties in BmimAc and EmimAc, with the values of $[\eta]$ (and therefore c^* and c_e) being significantly different. It is concluded in **Chapter 3** that this may be due to more significant cation-cellulose interactions, when the DP of cellulose is greater. This is further evidenced by comparing the difference in chemical shift (Δδ) values for BmimAc protons with *V-cell* (**Chapter 3**) and EmimAc protons with *A-cell* (Lovell et al., (2010)), where a greater Δδ was observed at lower concentrations of *V*-cell (Figure 7.2).

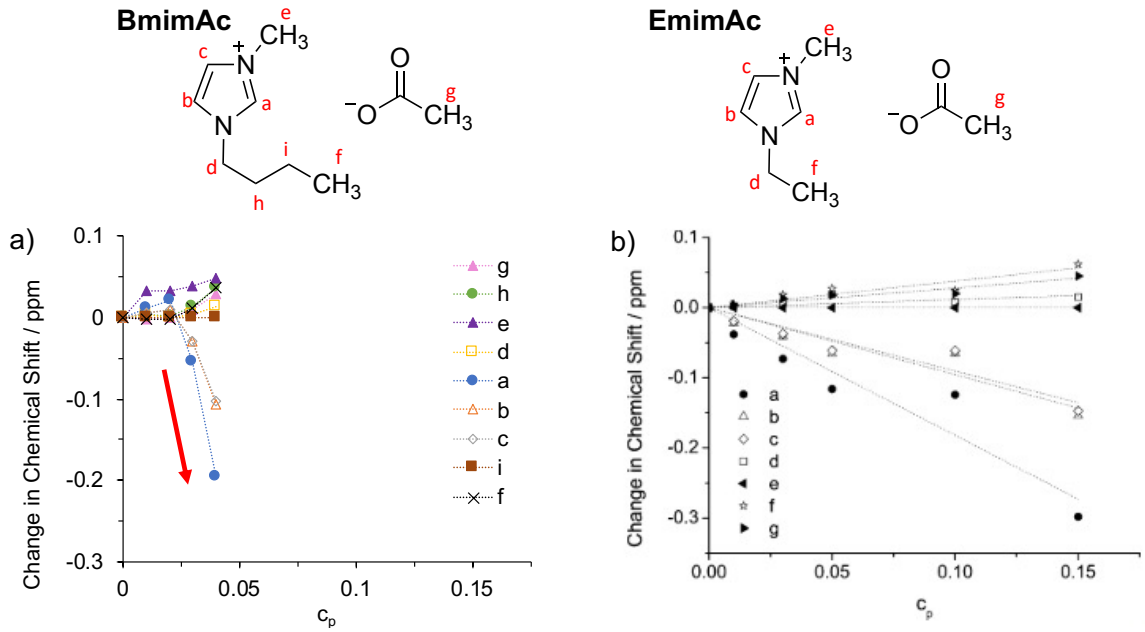

Figure 7.2. Change in chemical shift (*Δδ*) for a) *V-cell* in BmimAc and b) *A-cell* in EmimAc (Lovell et al., (2010)), as function of cellulose concentration. The steep decrease *Δδ* for *V-cell* is highlighted by the red arrow, showing the effect of DP; chemical structures of BmimAc and EmimAc are given above; c_p = mass fraction of cellulose.

V-cell was provided by Mondelēz International, which is a commercial cellulose investigated for use in confectionary products. Therefore, performing detailed characterisation is of interest to understand and predict its behaviour in novel food systems. Studying *V*-cell-BmimAc solution properties and defining c^* and c_e gave information on the type of cellulose material that can be obtained via coagulation (Sescousse et al., (2010)). Above c_e, a cellulose gel can be obtained (at [*V-cell*] > 2 wt%) where significant polymer entanglements are present. Entanglements lead to a sufficiently high density of intermolecular interactions, resulting in the formation of a self-supporting gel upon precipitation. Varying the concentration of cellulose within this semi-dilute entangled regime (**Chapter 3**) allows tuning of the gel properties, such as density, porosity and strength (as evidenced by the SEM in Figure 7.3).

Microscopic studies of the cellulose-BmimAc solutions using NMR were compared to bulk properties obtained from rheology, using the Stokes-Einstein relationship (**Chapter 3**). It was concluded that polymer entanglements greatly influence viscosity, but have less effect on the diffusion of IL molecules and thus the microviscosity. These findings are consistent with work previously published on carbohydrate properties (including *A-cell*) in EmimAc, where on a microscopic level, the intermolecular interactions between cellulose hydroxy groups and solvent govern the properties, whilst

on a macroscopic level, the volume of solvent taken up by the cellulose is the dominant factor (Ries et al., (2018)).

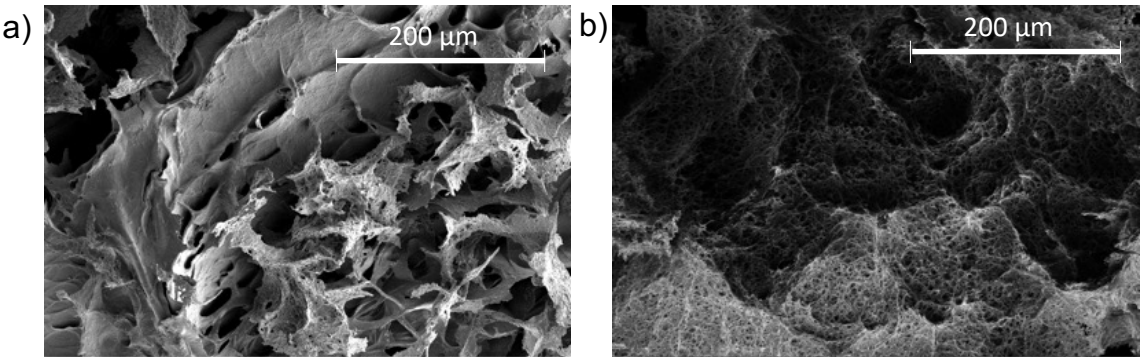

Figure 7.3. SEM image of freeze-dried cellulose gels, with *V-cell* concentrations of a) 2 wt% and b) 4 wt%.

Further information on the mechanism of cellulose dissolution in BmimAc is revealed in **Chapter 6**, where the effect of oil on cellulose-BmimAc interactions is studied. Full dissolution in ILs can disrupt the crystalline structure of cellulose (Zhang et al., (2005); Lindman et al., (2010)) and result in molecular cellulose which is still believed to have amphiphilic character (Costa, Mira, et al., (2019)). When a relatively polar oil was added *before* the cellulose structure has been disrupted, we predict in **Chapter 6** that a cellulose-oil interaction develops and remains even after the cellulose is dissolved. The importance of breaking both hydrophobic and hydrophilic interactions to achieve full dissolution is highlighted by emphasising that efficient cellulose solvents tend to be asymmetric, whilst parallels are drawn between the behaviour of oil and other co-solvents, such as DMSO.

7.2.2 Interfacial properties of cellulose

The evidence for both hydrophobic and hydrophilic interactions in cellulose given in **Chapter 6** (from solution studies) complements the results in **Chapter 4** and **Chapter 5,** where coagulated cellulose displays a strong ability to act as a Pickering stabiliser for W/O emulsions. The origin of cellulose amphiphilicity is still unclear from literature and the following discussion adds to this knowledge, highlighting the contributions of the work in this thesis to the field.

7.2.2.1 Crystalline and amorphous cellulose

Extensive research has revealed the ability of nano/microcelluloses (e.g. CNCs, MCC) to locate at the O/W interface (Oza and Frank, (1986); Kalashnikova et al., (2013); Capron and Cathala, (2013); Bai et al., (2018); X. Li et al., (2018)), often attributing this to the hydrophilic/hydrophobic surfaces on the crystalline particles. Microscopic techniques have been employed to

confirm the location of cellulose at the interface, (analogous to the results presented in **Chapter 4** and **Chapter 5**), for example by staining the cellulose with Calcofluor White and visualising it using confocal/fluorescence microscopy (Kalashnikova et al., (2011); Shen et al., (2016); Bai et al., (2018); Du Le et al., (2020)). Larger-sized microfibrillated and microcrystalline cellulose (MFC and MCC respectively) have similarly been used as O/W stabilisers (Oza and Frank, (1986); Oza and Frank, (1989); Sanchez-Salvador et al., (2019)), and both Pickering/network stabilisation mechanisms are discussed (Oza and Frank, (1989); Ougiya et al., (1997); Winuprasith and Suphantharika, (2013)). The formation of a reinforcing network in the water phase around oil droplets can lead to very high stabilities (Nsor-Atindana et al., (2017); Sanchez-Salvador et al., (2019)), although it is less clear if cellulose amphiphilicity originates from orientation provided by the crystalline structure. The literature around the surface properties of native cellulosic materials is still somewhat confusing and it is clear that the origin of its amphiphilicity is far from well-understood.

Dissolution and coagulation of cellulose can allow allomorphic modification under certain conditions (Habibi et al., (2010); Goldberg et al., (2015)), including conversion of native cellulose I to cellulose II and/or amorphous cellulose. In **Chapter 4**, we introduced a route for producing CMGs, which effectively stabilised W/O emulsions for at least 4 weeks (Lefroy, Murray, Ries, et al., (2021)). The CMGs were fabricated from cellulose powder (*V-cell*) which contained the cellulose II allomorph (as indicated by the WAXS spectrum, Figure 7.4a), but lost almost some of its crystalline structure when dissolved and coagulated into gels (Figure 7.4c). The reformation of any long-range order was further prevented by the addition of oil to the coagulation medium, which resulted in a completely amorphous structure (Figure 7.4d). However, these ‘oily’ CMGs provided the best stabilising performance for W/O systems (**Chapter 4**) and thus we have provided further evidence that the ability of cellulose to act as a stabiliser is not solely dependent on its crystalline order.

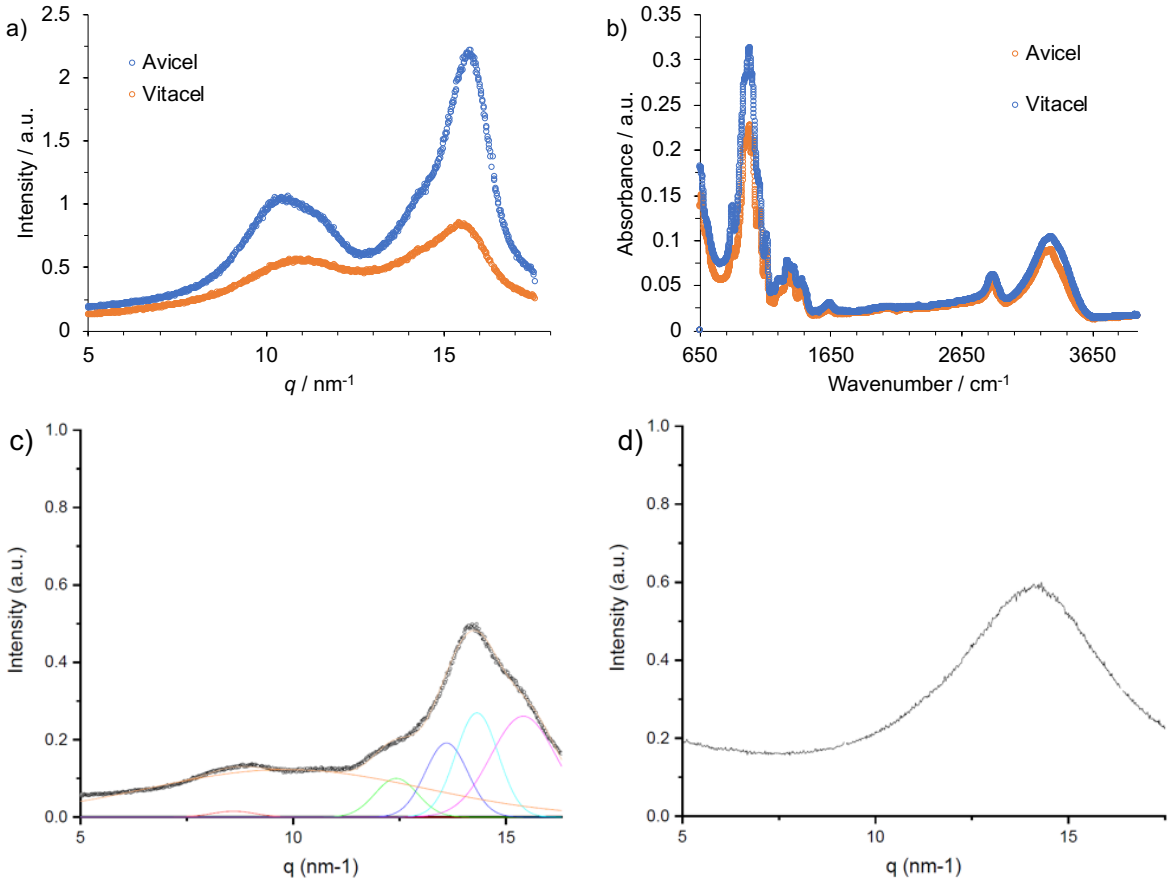

Figure 7.4. WAXS and FTIR spectra (a and b respectively) for Avicel (*A-cell)* and Vitacel (*V-cell)* cellulose. WAXS spectra for coagulated cellulose without (c) and with (d) oil are also given, where peaks have been fitted to the crystalline peaks of cellulose II in c (Han et al., (2013); French, (2014)).

Reports on stabilising ability of amorphous cellulose and its application in food are somewhat lacking. Both chemical and mechanical treatments of biomass usually employ conditions that remove the amorphous domains and recover the crystalline regions of cellulose (native cellulose I), requiring high-energy input and yielding low amounts of cellulose material (Habibi et al., (2010); Klemm et al., (2011)). Crystalline cellulose (for example CNCs) can display high O/W interfacial activity, often attributed to the accessibility of the hydrophobic plane (Kalashnikova et al., (2012)). At the 'elementary brick level,' 3 surface types are believed to be responsible for surface properties of cellulose I (for the *α*/*β* allomorphs): i) the hydrophilic (100)*α*/(1-10)*β* planes; ii) the hydrophobic (220)*α*/(200)*β* plane and iii) hydrophilic (110)*α*/(010)*β* surfaces (Figure 7.5). The hydrophilic plane (i) possesses by far the greatest surface area and thus majorly influences the wetting properties. The comparatively less exposed hydrophobic plane (ii) is located in the corner regions and the crystal structure results in its orientation towards the oil phase, as described in literature (Cherhal et al., (2016); Miyamoto et al., (2017)).

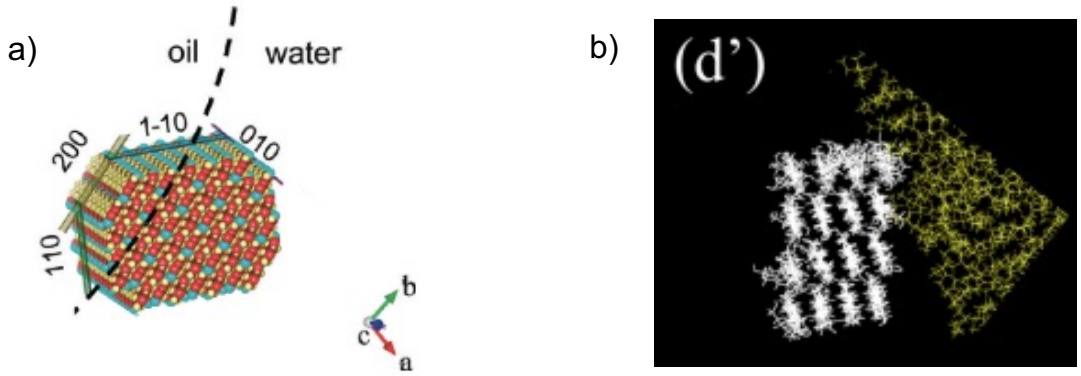

Figure 7.5. a) Schematic showing the orientation of the 3 types of cellulose planes in I*α* and I*β* nanocrystals, reproduced from (Kalashnikova et al., (2012)); b) snapshot of MD simulation showing tilted orientation of cellulose mini-crystal (white) to the oil droplet (yellow), reproduced from (Miyamoto et al., (2017)).

Tuning the type of crystalline allomorph and thus the crystallinity, H-bonding network and the *d*-spacings within cellulose affects the hydrophobic/hydrophilic balance and therefore the ability of CNCs to act as Pickering stabilisers (Kalashnikova et al., (2012); Gong et al., (2018); X. Li et al., (2018); Dai et al., (2020)). CNC morphology is also affected by the type of crystalline allomorph: (Jin et al., (2016)) modification from cellulose I to cellulose II can lead to more rod-like or spherical morphologies, compared to the typical needle-like morphology of CNCs obtained from plant cell walls (Gong et al., (2022)). A combination of both cellulose I and II allomorphs in CNCs may result in the formation of more stable emulsions, compared to when a single cellulose allomorph is present (Kalashnikova et al., (2013); Cherhal et al., (2016)).

Unlike crystalline cellulose, amorphous cellulose can be prepared and recovered in high-yields using more cost-effective methods. Rein *et al.* prepared amorphous cellulose hydrogels from an IL for both O/W and W/O emulsions (Rein et al., (2012)), whilst Jia *et al.* used phosphoric acid to prepare 'regenerated' amorphous cellulose capable of stabilising O/W emulsions which were stable for months (Jia et al., (2015)). Similarly, citrus oil O/W emulsions have been prepared using regenerated cellulose, where convincing evidence for adsorption of cellulose at the interface was provided using CLSM and SEM (Shen et al., (2016)). In **Chapter 4** and **Chapter 5** we similarly demonstrate that cellulose displays amphiphilic character even in disordered states and, rather than describing the hydrophobic character of cellulose to be *a result* of its crystalline structure, we believe that it is more appropriate to describe the *crystalline structure* to be a result of the hydrophobic interactions between polymer chains.

7.2.2.2 Molecular cellulose

In **Chapter 6**, we suggest that an oil-cellulose interaction can develop during dissolution in an IL and provide some discussion on the origin of the interaction. In BmimAc, cellulose is believed to be 'molecularly dispersed' and its conformation may be affected by the presence of oil, which can influence the orientation of the hydrophobic regions. Several previous studies have investigated the ability of molecular cellulose to act as an emulsion stabiliser (Medronho et al., (2015); Lindman et al., (2017); Costa, Mira, et al., (2019)) and *in-situ* emulsification of oil in a dissolved cellulose solution has been performed (Rein et al., (2012); Jia et al., (2013); Jia et al., (2015)). When cellulose is coagulated in the presence of an O/W interface, a 'coating' is predicted to form around oil droplets as dissolved cellulose assembles at the oil droplet surface (Rein et al., (2012)).

Combing the results from this thesis with observations in literature, we confirm that the origin of cellulose hydrophobicity should not be exclusively attributed to its crystalline structure. Whilst molecular dynamic (MD) simulations have revealed that the conformations of molecular cellulose and cellulose mini-crystals at an O/W interface are very similar, molecular cellulose was found to have a greater torsion-angle freedom of movement and slightly different orientational distributions of its hydroxymethyl side chains (Miyamoto et al., (2017)). The cellulose backbone itself is structurally asymmetric, with a primary (1°) hydroxyl group in the C6 position on one side and secondary (2°) hydroxyl groups in the C2 and C3 positions located on the opposite side (Figure 7.6a). 2° hydroxyl groups are less hydrophilic (compared to 1°) and form weaker H-bonds with solvent molecules (e.g. water), giving them a greater tendency to form hydrophobic associations (Glasser et al., (2012)). Furthermore, each AGU is made up of glucopyranose rings with 5 x C atoms and 1 x O atom, making it inherently hydrophobic.

Cellobiose on the other hand, which is often used as a model for cellulose, is made up of 2 AGU units with *trans*-configurations and has a higher degree of symmetry, significantly weakening the hydrophobic interaction (Figure 7.6b). It also has many more possible shapes (including a range of linkage geometries where H-bonds between substituents on adjacent rings can stabilise a *cis* conformation), and thus, cellobiose is less restricted than cellulose which possesses a cooperative length of hydrophobic units that restrict movement (Tanford, (1973); French, (2017)). We highlight the differences between cellulose and cellobiose in **Chapter 6** by showing that no oil-cellobiose interaction can develop in solution and that cellobiose is not

sufficiently hydrophobic. However cellulose, even in its molecular (dissolved) state, was able to interact with oil and therefore use of cellobiose as a model system for cellulose should be avoided, due to these fundamental structure-function differences.

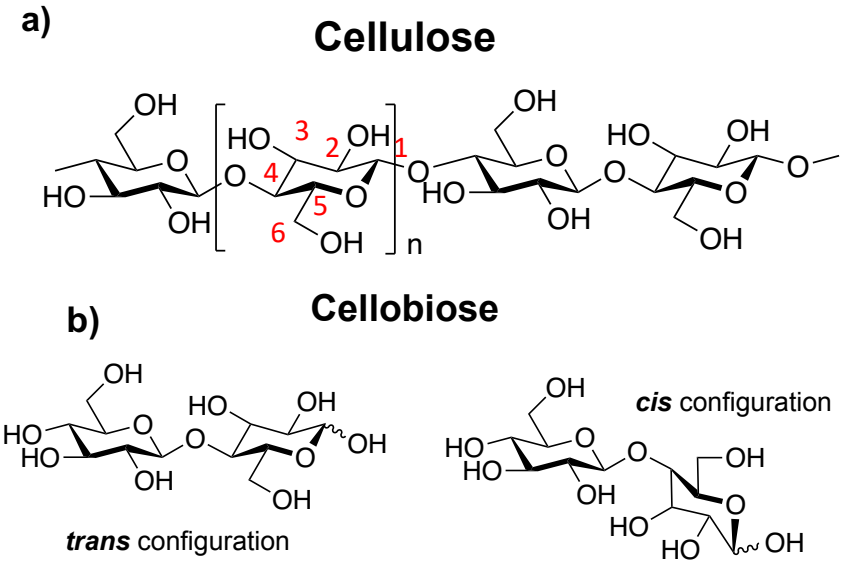

Figure 7.6. Chemical structure of cellulose (a) and cellobiose (b), illustrating the higher level of structural asymmetry present in cellulose.

7.2.2.3 Tuning wettability by adding oil

In **Chapter 4**, we investigated a similar approach to (Rein et al., (2012)) with the aim of fabricating a more 'hydrophobic' cellulose, by adding oil to dissolved cellulose in IL before performing solvent exchange. Some oil appeared to be trapped within the coagulated cellulose (as observed via SEM and FTIR) and this improved oil-dispersibility compared to 'non-oily' CMGs, which produced less stable W/O emulsions. We hypothesised that the presence of the oil during coagulation exposes the hydrophobic regions of cellulose to a greater extent, compared to in the absence of oil, and demonstrated the possibility of modifying surface wettability by physical processing.

In **Chapter 5**, the ratio of oil/IL was varied (0.0025-2:1, 0.25-200 wt% oil) to assess the effect on CMG properties. Changing the amount of oil in the coagulation medium had some effect on CMG-size. Generally, for 'top-down' CMGs dispersed in oil ('low-shear' *L*-CMGs and 'high-shear' *H*-CMG*s*), the microgel size decreased as the amount of oil in the coagulation medium increased (Figure 7.7a). However, the W/O emulsions produced by CMGs with various oil contents displayed very similar sizes for water droplets (and thus similar stabilities), indicating that CMG stabilising ability (wettability) was not dependent on the amount of oil added. For 'bottom-up' CMGs ('very high-shear' *VH*-CMGs), the opposite trend was observed and the particle size of

CMG-in-water dispersions increased with increasing amount of oil, with larger oil droplets visible in the micrographs (Figure 7.7b and c respectively). However, the water droplet size increased for W/O emulsions with a decrease in oil content, suggesting that the more 'oily' *VH*-CMGs were better W/O stabilisers.

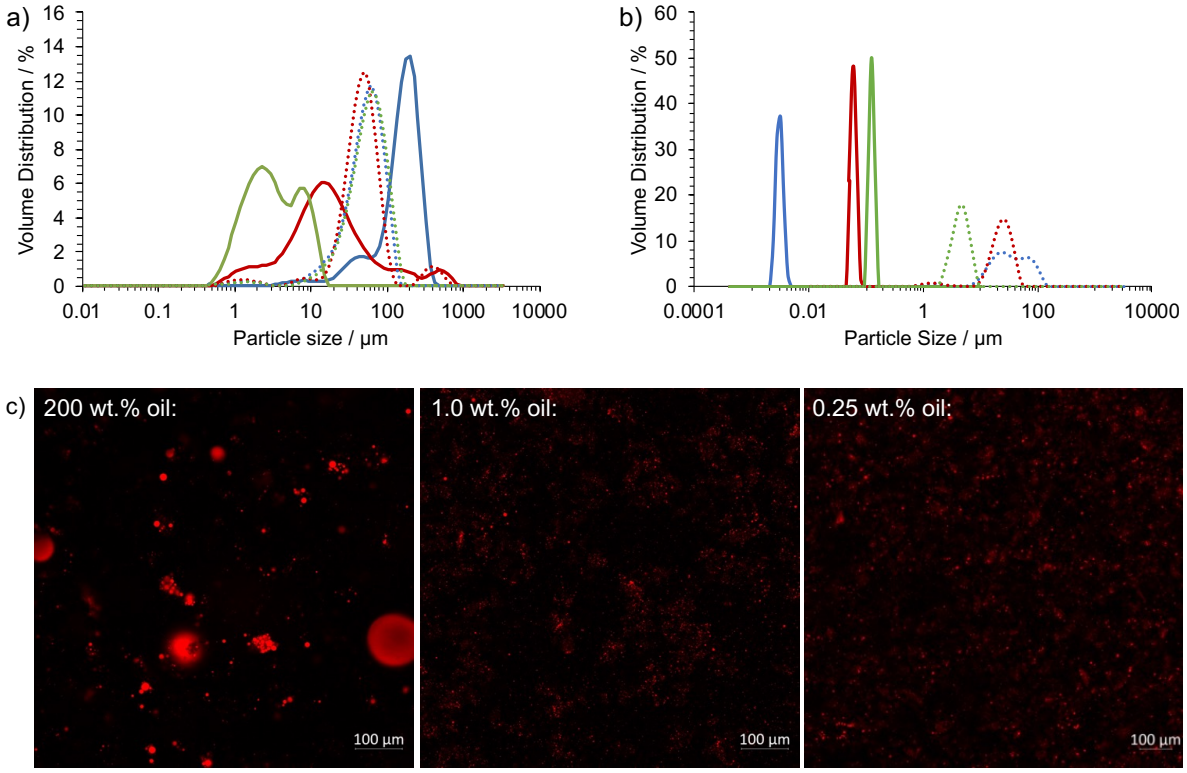

Figure 7.7. PSDs of *H*-CMG-in-oil dispersions (a) and *VH*-CMG-in-water dispersions (b), with varying amounts of oil added during coagulation (0.25 = blue; 1 = red and 200 wt% = green); corresponding 20:80 W/O emulsions (dashed lines); c) confocal micrographs of *VH*-CMG-in-water dispersions (0.25, 1 and 200 wt% oil, left to right), where the oil has been stained by Nile red.

Considering these observations from both 'top-down' and 'bottom-up' CMGs, it follows that an increasing amount of oil in the coagulation medium results in more oil 'sticking' to the cellulose surface and/or preventing re-aggregation of hydrophobic chains during coagulation, resulting in the observed amorphous structure (Figure 7.4d). More 'oily' CMGs disperse better in oil (smaller sized CMGs) but form larger particles in water, due to the higher amount of oil (and the creation of larger oil droplets, (Figure 7.7c).

We attempted to quantify the amount of oil in the CMGs using energy dispersive x-ray (EDX) analysis, by adding bromohexadecane (BHD) to the cellulose-IL solution (to generate contrast between the continuous phase oil and cellulose/water). However, EDX failed to detect any bromine suggesting that either:

i) **only a very small amount of oil is present in the dispersed CMGs;**
ii) **that the majority of 'trapped' oil is dispersed into the continuous phase upon emulsification, rather than being confined in the microgels.**

However, our results from **Chapter 6** indicate that the interaction between cellulose and oil is relatively strong, since the IL cannot eventually 'outcompete' the oil, whilst oil was still visible on the cellulose surface of macrogels, even after washing with hexane (Figure 7.8). It is possible that BHD displayed a weaker interaction with the cellulose compared to MCT-oil/sunflower oil and therefore less oil 'stuck' to the cellulose during coagulation, but the CMGs coagulated with BHD still showed comparable W/O stabilising ability. It is also worth noting that a self-supporting cellulose gel is still obtained, even in the presence of excess MCT-/sunflower oil, suggesting that sufficient cellulose-cellulose interactions can develop and are not inhibited by the oil.

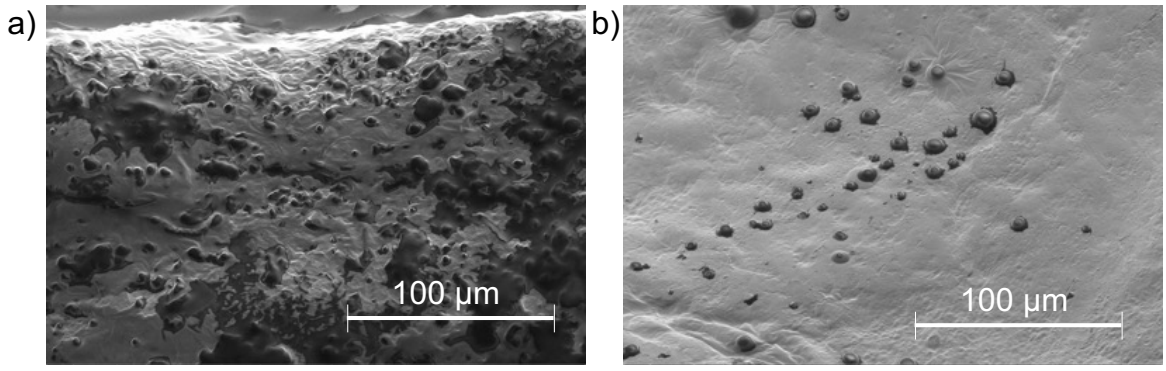

Figure 7.8. SEM images of the 'skin'/outer layer of freeze-dried cellulose macrogels coagulated from BmimAc/oil (1:2), with [cellulose] = 4 wt% either before (a) or after (b) washing with hexane. Scale bar = 100 µm.

Based on the observations in **Chapter 3** of cellulose-BmimAc solutions, we expect the cellulose gel to be formed of a random entangled network of cellulose molecules (polymeric gel) with oil sticking to regions of the hydrophobic surfaces. The cellulose gel is mainly amorphous (Figure 7.4d), and it appears that the oil is less homogeneously distributed within the gel, as the amount of oil increases (Figure 7.7c). Small, regular droplets are visible at the lower oil concentrations (0.25 and 1 wt%, right and middle micrographs respectively) and larger 'pools' of oil are visible when it is added in excess (200 wt%, left micrograph).

It has previously been suggested that the polarity of the environment almost certainly dictates the 'sheet structure' that forms between cellulose molecules (Miyamoto et al., (2009)). We conclude, therefore, that the remarkable stabilising ability of CMGs is most likely due to the effect of the presence of

the oil on cellulose conformations *during coagulation* and the resultant sheet structures in the amorphous gel, as opposed to the presence of trapped surface oil. It appears that the majority of oil is mixed with the continuous phase upon dispersal of the gel in oil and emulsification, whilst a small concentration of oil may remain ‘stuck’ or bound to the hydrophobic regions of cellulose. CMGs are clearly visible at the W/O interface, regardless of the amount of oil added during coagulation.

Combining all of the understanding developed in this thesis from a wide range of experimental techniques, on both the molecular and bulk properties of coagulated ‘oily’ CMGs, Figure 7.9 summarises the role of oil in each stage from the coagulation of cellulose to the stabilisation of W/O emulsions.

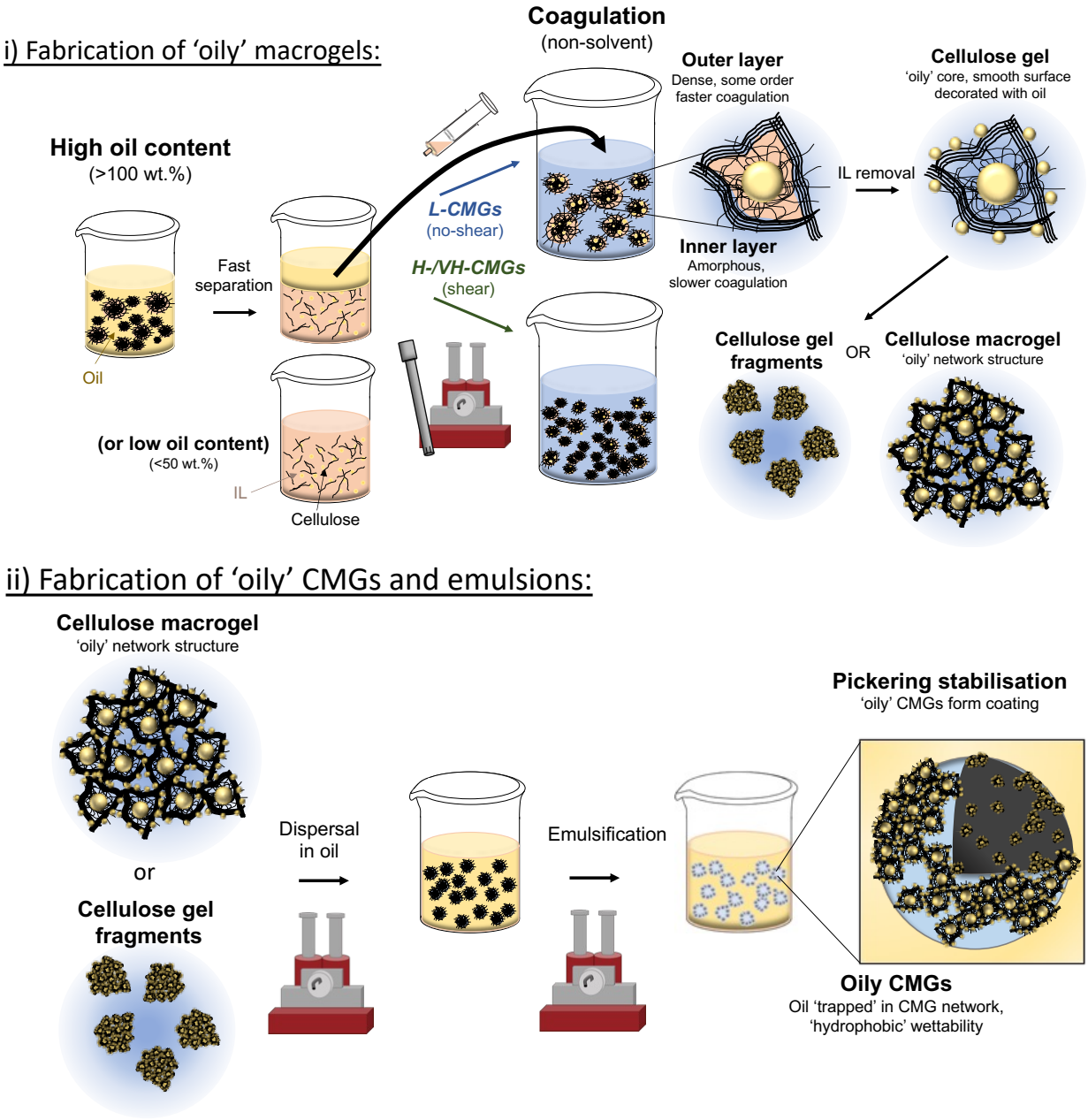

Figure 7.9. Schematic predicting the role of oil throughout the fabrication of CMGs and W/O stabilised emulsions.

7.2.2.4 Tuning wettability by solvent exchange

A novel 'solvent exchange' method was employed to produce the CMGs in **Chapter 4** and **Chapter 5**, where the polarity of the anti-solvent is slowly increased. Previous studies have shown that the type of anti-solvent used in coagulation will affect cellulose properties (such as crystallinity, porosity, morphology and wettability (Fan et al., (2018); Fryczkowska et al., (2018); Hedlund, Köhnke, et al., (2019)), whilst MD simulations have revealed that surface properties are different in water and benzene (Miyamoto et al., (2009)). Non-polar solvents will not generally cause cellulose to precipitate from ILs, since the anti-solvent must be miscible with the IL medium (Fink et al., (2001)). However, 'less polar' alcohols such as 1-octanol and 1-hexanol

can induce precipitation (Fryczkowska et al., (2018)). In **Chapter 4** and **Chapter 5,** 1-butanol is used as the initial anti-solvent followed by solvent exchange to ethanol and then water. 1-butanol was initially employed to deliver a 'softer' coagulation and recover cellulose from solution less suddenly (Fink et al., (2001)), which results in a decrease in chain orientation and lower crystallinity (Fan et al., (2018)). Once the structure of cellulose sheets is established, the 1-butanol (and any excess dissolved oil) is then removed by ethanol and finally water washing, ensuring complete removal of both the IL and alcohols.

The morphologies changed drastically for cellulose macrogels coagulated from various anti-solvents (as in **Chapter 4**, Figure 7.10), confirming that the coagulation route could be varied to produce different types of cellulose material. It is also possible to change the properties after initial coagulation to a certain extent, and modification of cellulose wettability has been achieved by washing with cyclohexane, liquid ammonia or hot glycerine (Yamane et al., (2006)). Hedlund *et al.* reported that post-washing of 2-propanol-coagulated cellulose with water induced arrangement of small crystallites (Hedlund, Köhnke, et al., (2019)). When water alone was used as a coagulant, longer crystallites could form.

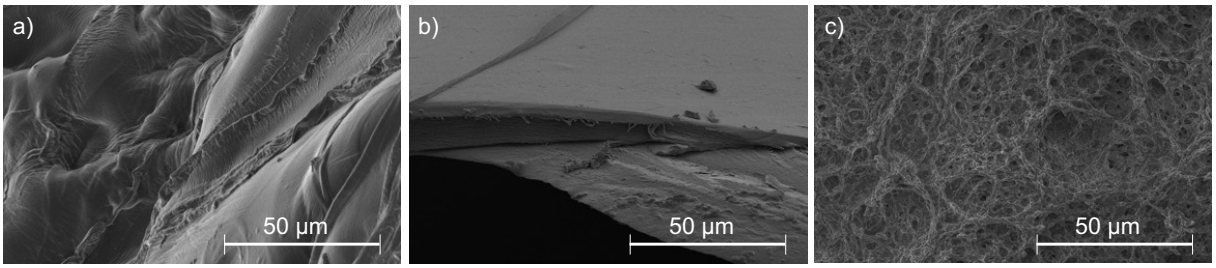

Figure 7.10. SEM images of freeze-dried cellulose macrogels coagulated in a) water; b) ethanol and c) 1-butanol.

Similarly, we compared the properties of cellulose gels obtained via several different solvent exchange coagulations, using combinations 1-butanol, ethanol and water (Table 7.2, Figure 7.11). The size of CMG-in-oil dispersions was similar regardless of the coagulation sequence, apart from CMGs where only water was used (WWW). Furthermore, macrogels coagulated with 1-butanol (BEW and BWW) showed greater stabilising abilities compared to macrogels coagulated without 1-butanol (EEW and EWW). Figure 7.11 compares macrogels prepared via the BEW and BWW routes (i.e. with and without ethanol). The diameter of the turbid 'core' region was greater when ethanol was used in the coagulation sequence (BEW, red arrow) which we predict corresponds to an amorphous cellulose structure (as shown in the SEM image below). On the other hand, when ethanol wasn't used more

ordered sheet structures were visible (yellow arrow). Since water diffuses more rapidly than ethanol which in turn diffuses more rapidly than 1-butanol, it induces the 'hardest' coagulation. Therefore, it expected that more crystalline structures are generated when more water washing stages are employed during coagulation (compared to ethanol and 1-butanol) (Gupta et al., (2013)). However, it is impossible to completely reverse the orientation once any precipitation is induced and the cellulose solvent is removed. Therefore, the first anti-solvent that comes in to contact with the cellulose solution is dominant in determining the material properties. It is difficult to comment on the specific effects of the various solvents, however our results correlate with similar experiments of cellulose 'post-treatments' in the literature (Yamane et al., (2006); Hedlund, Köhnke, et al., (2019)).

Table 7.2. Cellulose macrogels coagulation from BmimAc (3 wt% cellulose), via various solvent exchange coagulation routes.

Sample ID	1st solvent	2nd solvent	3rd solvent	Average size of CMGs in oil (d3,2)/μm
BEW	1-butanol	ethanol	water	4.28
BWW	1-butanol	water	water	1.19
EEW	ethanol	ethanol	water	4.75
EWW	ethanol	water	water	5.43
WWW	water	water	water	32.1

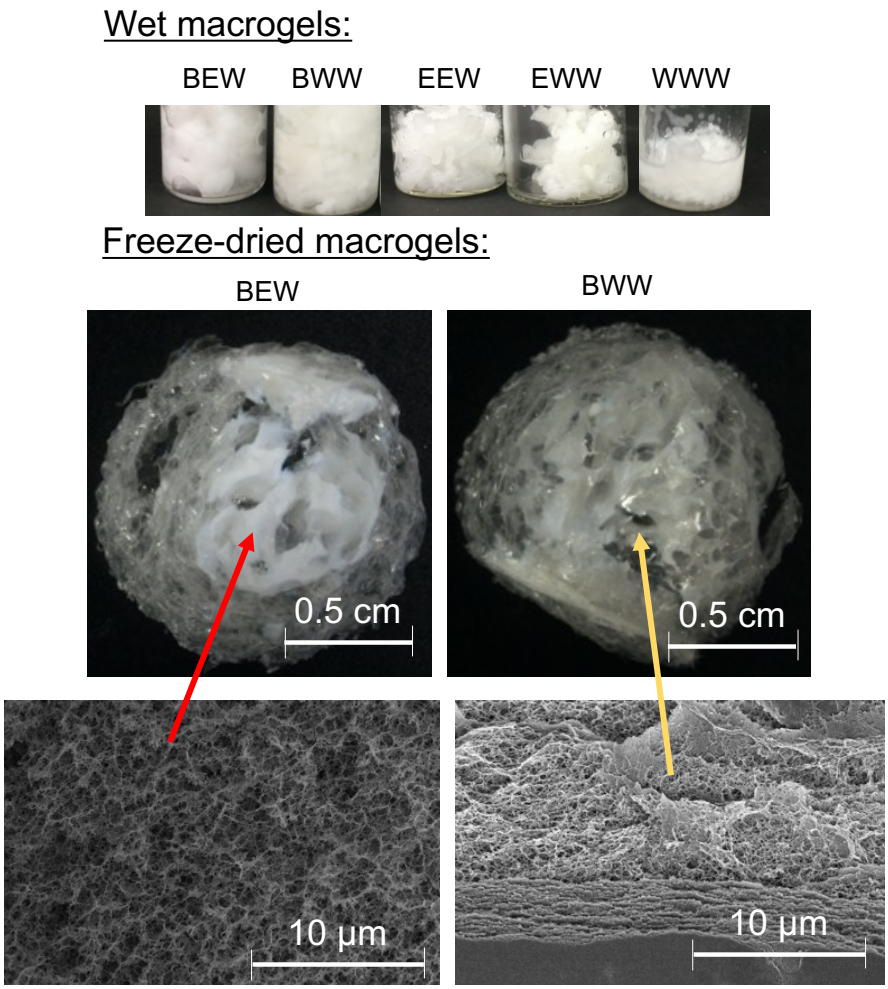

Figure 7.11. Images of cellulose macrogels coagulated via various solvent exchange routes (as detailed in Table 7.2, top image) and stereomicroscope images of freeze-dried macrogels (bottom image), with SEM images of the core structures.

7.3 Concluding remarks and recommendations for future studies

The work presented in this thesis adds to understanding of the relationship between cellulose structure and function, specifically evaluating its interfacial properties and the origins of its structural asymmetry. We have also introduced a method for producing a novel W/O stabiliser, using ILs. We recommend the following areas of research to further realise the potential of the CMGs in food systems and for fat reduction applications, which could also apply to similar oil-based systems in cosmetics, biomedicine and agriculture:

7.3.1.1 Cellulose-BmimAc/oil solutions properties

- Detailed characterisation of *V*-cell/BmimAc solutions was conducted using rheological and NMR analysis. It would be of interest to characterise similar systems with different cellulose types, for example with varying DPs, to see if this behaviour can be replicated with less pure/refined forms of cellulose.

- It is important to conduct similar studies using cheaper, food-grade ILs (or other cellulose solvents), which may be more scalable and suitable for use in the food industry.
- Further understanding on the effect of non-polar additives in ILs on cellulose dissolution is needed. Whilst most known effective solvents for cellulose are predominantly hydrophilic and therefore incompatible with non-polar solvents, the increasing design and development of cheaper and more task-specific ILs will undoubtedly lead to a wider range of IL types. Other oil-types should also be investigated.

7.3.1.2 CMGs in food matrices

- We have demonstrated that CMGs can stabilise W/O emulsions for at least 6 months, through Pickering-type stabilisation. However, future studies are required to understand how CMG interfacial behaviour may be affected by other additives, such as sugar, salt and flavour compounds, and thus their applicability to real food systems. For example, sugar dissolves in water and would provide a slight viscosity increase to the discontinuous phase for W/O emulsions. Different sugar types, such as glucose and sucrose, may interact with the polymer chains of cellulose. Furthermore, sugar syrups with a range of viscosities could be investigated, to tune the emulsion properties and stabilities.
- It is of interest to replace the oil phase with a solid fat phase, such as palm oil, to demonstrate the function of CMGs in confectionary-based systems. This may increase the stability and thus shelf-life of the emulsions, whilst it would allow understanding of the type of products to which CMGs could be applied.
- W/O emulsions offer the possibility to encapsulate water-soluble compounds, such as antioxidants, in the water-emulsion droplets. Such additives may be used as a strategy to control water activity and increase shelf-life.

7.3.1.3 ‘Hydrophobic’ cellulose

- Whilst conformations of molecular cellulose have been investigated in ‘water-rich’ systems using MD (Miyamoto et al., (2009)), there are no studies of the equivalent ‘oil-rich’ systems, to our knowledge. Such investigations would be very useful in elucidating further the conformations of cellulose during coagulation predicted in this work. Furthermore, they would prompt the development and design of more hydrophobic cellulose from dissolution-coagulation methods.
- Few reports thus far have focussed on the application of cellulose in oil-based systems. Through the work in this thesis, we have demonstrated that cellulose can be physically modified and made suitable for oil-/fat-continuous systems. Future studies should aim to exploit the hydrophobicity of cellulose further, for example by physically adsorbing hydrophobic substituents to the cellulose backbone and further tuning the properties.
- In theory, ‘hydrophobic’ cellulose could be prepared by first dissolving cellulose in a non-polar solvent and then coagulating in a non-polar medium, which would result in H-bonding molecular sheets forming between hydrophilic planes and exposure of the hydrophobic planes

(Yamane et al., (2006)). However, experimentally this is (to our knowledge) impossible to achieve, since only highly polar solvents are able to dissolve cellulose and break cellulose-cellulose H-bonds. The development of more non-polar ILs and the investigation of mixed systems (like the one described in **Chapter 6**) is certainly of interest. Furthermore, it may be possible to exchange the solvent in a cellulose gel in order to alter the wettability, as described by Yamane *et al.* (Yamane et al., (2006)). Protein oleogels have been fabricated by a solvent exchange procedure, similar to what we are envisaging, where protein hydrogels are initially formed and water is gradually replaced with oil, transitioning through an intermediate solvent which is both oil and water miscible (e.g. ethanol, acetone) (De Vries et al., (2015)). We began to demonstrate that a similar method can be applied to fabricate cellulose 'oleogels', by first coagulating a hydrogel from an IL and subsequently exchanging water for oil, via ethanol (Figure 7.12). Since the structure of the 1-butanol-coagulated cellulose is very porous (Figure 7.11) and this can be tuned by varying the concentration of cellulose dissolved in the IL, penetration of oil is possible provided that the oil can diffuse into the gel structure. Whilst we have not fully characterised the cellulose 'oleogels' in this thesis, this is undoubtably an interesting avenue for future work.

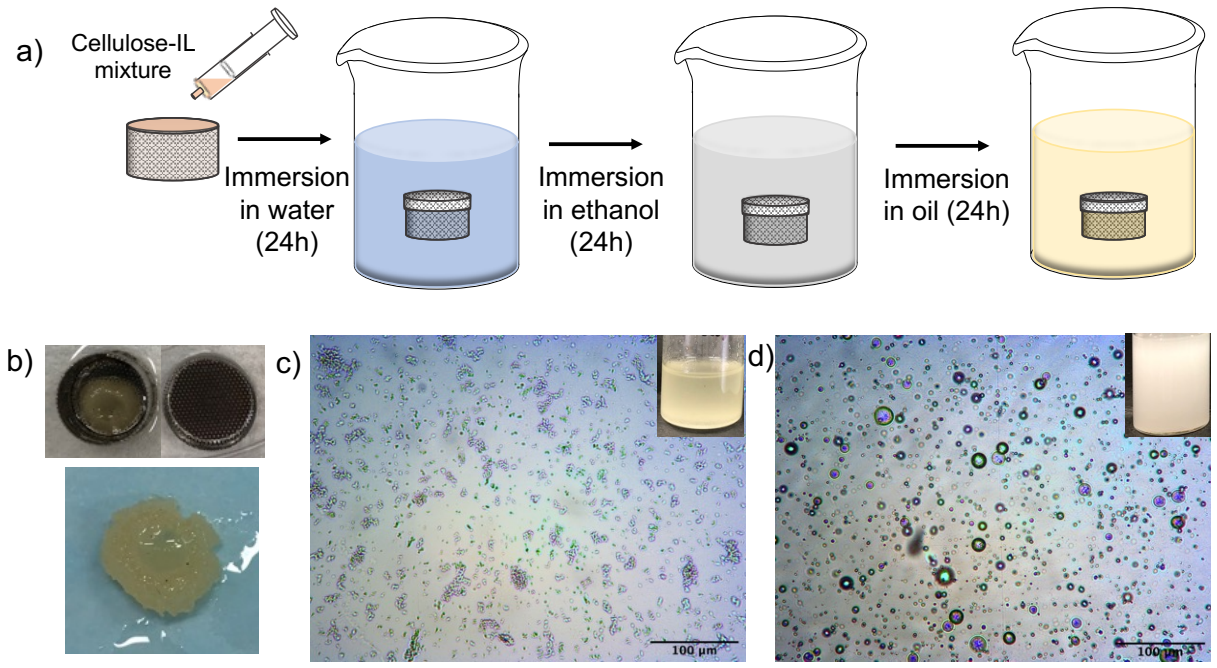

Figure 7.12. a) method for produced cellulose 'oleogel;' b) Appearance of cellulose 'oleogel' produced via a solvent exchange procedure (similar to the method described in (De Vries et al., (2015))); optical micrographs of 3 wv% oil dispersions of c) the oleogel and d) *H*-200 CMGs, with images of the oil dispersion provide in the top right corner. Scale bars = 100 µm.

7.4 References

Andablo-Reyes, E., Yerani, D., Fu, M., Liamas, E., Connell, S., Torres, O. and Sarkar, A. (2019). Microgels as viscosity modifiers influence lubrication performance of continuum. *Soft Matter*. *15*(47), 9614–9624.

Bai, L., Huan, S., Xiang, W. and Rojas, O.J. (2018). Pickering emulsions by combining cellulose nanofibrils and nanocrystals: Phase behavior and depletion stabilization. *Green Chemistry*. *20*(7), 1571–1582.

Capron, I. and Cathala, B. (2013). Surfactant-free high internal phase emulsions stabilized by cellulose nanocrystals. *Biomacromolecules*. *14*(2), 291–296.

Cherhal, F., Cousin, F. and Capron, I. (2016). Structural Description of the Interface of Pickering Emulsions Stabilized by Cellulose Nanocrystals. *Biomacromolecules*. *17*(2), 496–502.

Costa, C., Mira, I., Benjamins, J.W., Lindman, B., Edlund, H. and Norgren, M. (2019). Interfacial activity and emulsion stabilization of dissolved cellulose. *Journal of Molecular Liquids*. *292*, 111325.

Dai, H., Wu, J., Zhang, H., Chen, Y., Ma, L., Huang, H., Huang, Y. and Zhang, Y. (2020). Recent advances on cellulose nanocrystals for Pickering emulsions: Development and challenge. *Trends in Food Science and Technology*. *102*(2), 16–29.

Fan, Z., Chen, J., Guo, W., Ma, F., Sun, S. and Zhou, Q. (2018). Anti-solvents tuning cellulose nanoparticles through two competitive regeneration routes. *Cellulose*. *25*(8), 4513–4523.

Fink, H.P., Weigel, P., Purz, H.J. and Ganster, J. (2001). Structure formation of regenerated cellulose materials from NMMO-solutions. *Progress in Polymer Science*. *26*, 1473–1524.

French, A.D. (2017). Glucose, not cellobiose, is the repeating unit of cellulose and why that is important. *Cellulose*. *24*(11), 4605–4609.

French, A.D. (2014). Idealized powder diffraction patterns for cellulose polymorphs. *Cellulose*. *21*(2), 885–896.

Fryczkowska, B., Kowalska, M., Binias, D., Slusarczyk, C., Janicki, J., Sarna, E. and Wyszomirski, M. (2018). Properties and Structure of Cellulosic Membranes Obtained from Solutions in Ionic Liquids Coagulated in Primary Alcohols. *Autex Research Journal*. *18*(3), 232–242.

Glasser, W.G., Atalla, R.H., Blackwell, J., Brown, M.M., Burchard, W., French, A.D., Klemm, D.O. and Nishiyama, Y. (2012). About the structure of cellulose: Debating the Lindman hypothesis. *Cellulose*. *19*(3), 589–598.

Goldberg, R.N., Schliesser, J., Mittal, A., Decker, S.R., Santos, A.F.L.O.M., Freitas, V.L.S., Urbas, A., Lang, B.E., Heiss, C., Ribeiro Da Silva, M.D.M.C., Woodfield, B.F., Katahira, R., Wang, W. and Johnson, D.K. (2015). A thermodynamic investigation of the cellulose allomorphs: Cellulose(am), cellulose Iβ(cr), cellulose II(cr), and cellulose III(cr). *Journal of Chemical Thermodynamics*. *81*, 184–226.

Gong, J., Kuang, Y., Zhang, X., Luan, P., Xiang, P., Liu, K., Mo, L., Xu, J., Li, J. and Wan, J. (2022). Efficient Shaping of Cellulose Nanocrystals Based on Allomorphic Modification: Understanding the Correlation between Morphology and Allomorphs. *Biomacromolecules*. *23*(3), 687–698.

Gong, J., Mo, L. and Li, J. (2018). A comparative study on the preparation and characterization of cellulose nanocrystals with various polymorphs. *Carbohydrate Polymers*. *195*, 18–28.

Gupta, K.M., Hu, Z. and Jiang, J. (2013). Cellulose regeneration from a cellulose/ionic liquid mixture: The role of anti-solvents. *RSC Advances*. *3*(31), 12794–12801.

Habibi, Y., Lucia, L.A. and Rojas, O.J. (2010). Cellulose nanocrystals: Chemistry, self-assembly, and applications. *Chemical Reviews*. *110*(6), 3479–3500.

Han, J., Zhou, C., French, A.D., Han, G. and Wu, Q. (2013). Characterization of cellulose II nanoparticles regenerated from 1-butyl-3-methylimidazolium chloride. *Carbohydrate Polymers*. *94*(2), 773–781.

Hedlund, A., Köhnke, T., Hagman, J., Olsson, U. and Theliander, H. (2019). Microstructures of cellulose coagulated in water and alcohols from 1-ethyl-3-methylimidazolium acetate: contrasting coagulation mechanisms. *Cellulose*. *26*(3), 1545–1563.

Horinaka, J. ichi, Chen, K. and Takigawa, T. (2018). Entanglement properties of carboxymethyl cellulose and related polysaccharides. *Rheologica Acta*. *57*(1), 51–56.

Jia, X., Chen, Y., Shi, C., Ye, Y., Wang, P., Zeng, X. and Wu, T. (2013). Preparation and characterization of cellulose regenerated from phosphoric acid. *Journal of Agricultural and Food Chemistry*. *61*(50), 12405–12414.

Jia, X., Xu, R., Shen, W., Xie, M., Abid, M., Jabbar, S., Wang, P., Zeng, X. and Wu, T. (2015). Stabilizing oil-in-water emulsion with amorphous cellulose. *Food Hydrocolloids*. *43*, 275–282.

Jin, E., Guo, J., Yang, F., Zhu, Y., Song, J., Jin, Y. and Rojas, O.J. (2016). On the polymorphic and morphological changes of cellulose nanocrystals (CNC-I) upon mercerization and conversion to CNC-II. *Carbohydrate Polymers*. *143*, 327–335.

Kalashnikova, I., Bizot, H., Bertoncini, P., Cathala, B. and Capron, I. (2013). Cellulosic nanorods of various aspect ratios for oil in water Pickering emulsions. *Soft Matter*. *9*(3), 952–959.

Kalashnikova, I., Bizot, H., Cathala, B. and Capron, I. (2012). Modulation of cellulose nanocrystals amphiphilic properties to stabilize oil/water interface. *Biomacromolecules*. *13*(1), 267–275.

Kalashnikova, I., Bizot, H., Cathala, B. and Capron, I. (2011). New pickering emulsions stabilized by bacterial cellulose nanocrystals. *Langmuir*. *27*(12), 7471–7479.

Klemm, D., Kramer, F., Moritz, S., Lindström, T., Ankerfors, M., Gray, D. and

Dorris, A. (2011). Nanocelluloses: A new family of nature-based materials. *Angewandte Chemie - International Edition*. *50*(24), 5438–5466.

Du Le, H., Loveday, S.M., Singh, H. and Sarkar, A. (2020). Pickering emulsions stabilised by hydrophobically modified cellulose nanocrystals: Responsiveness to pH and ionic strength. *Food Hydrocolloids*. *99*, 105344.

Lefroy, K.S., Murray, B.S., Ries, M.E. and Curwen, T.D. (2021). A natural, cellulose-based microgel for water-in-oil emulsions. *Food Hydrocolloids*. *113*, 106408.

Li, X., Li, J., Gong, J., Kuang, Y., Mo, L. and Song, T. (2018). Cellulose nanocrystals (CNCs) with different crystalline allomorph for oil in water Pickering emulsions. *Carbohydrate Polymers*. *183*, 303–310.

Lindman, B., Karlström, G. and Stigsson, L. (2010). On the mechanism of dissolution of cellulose. *Journal of Molecular Liquids*. *156*(1), 76–81.

Lindman, B., Medronho, B., Alves, L., Costa, C., Edlund, H. and Norgren, M. (2017). The relevance of structural features of cellulose and its interactions to dissolution, regeneration, gelation and plasticization phenomena. *Physical Chemistry Chemical Physics*. *19*(35), 23704–23718.

Lopez, C.G., Voleske, L. and Richtering, W. (2020). Scaling laws of entangled polysaccharides. *Carbohydrate Polymers*. *234*, 115886.

Lovell, C.S., Walker, A., Damion, R.A., Radhi, A., Tanner, S.F., Budtova, T. and Ries, M.E. (2010). Influence of cellulose on ion diffusivity in 1-ethyl-3-methyl-imidazolium acetate cellulose solutions. *Biomacromolecules*. *11*, 2927–2935.

Medronho, B., Duarte, H., Alves, L., Antunes, F., Romano, A. and Lindman, B. (2015). Probing cellulose amphiphilicity. *Nordic Pulp & Paper Research Journal*. *30*(1), 58-66.

Miyamoto, H., Rein, D.M., Ueda, K., Yamane, C. and Cohen, Y. (2017). Molecular dynamics simulation of cellulose-coated oil-in-water emulsions. *Cellulose*. *24*(7), 2699–2711.

Miyamoto, H., Umemura, M., Aoyagi, T., Yamane, C., Ueda, K. and Takahashi, K. (2009). Structural reorganization of molecular sheets derived from cellulose II by molecular dynamics simulations. *Carbohydrate Research*. *344*(9), 1085–1094.

Nsor-Atindana, J., Chen, M., Goff, H.D., Zhong, F., Sharif, H.R. and Li, Y. (2017). Functionality and nutritional aspects of microcrystalline cellulose in food. *Carbohydrate Polymers*. *172*, 159–174.

Ougiya, H., Watanabe, K., Morinaga, Y. and Yoshinaga, F. (1997). Emulsion-stabilizing Effect of Bacterial Cellulose. *Bioscience, Biotechnology and Biochemistry*. *61*(9), 1541–1545.

Oza, K.P. and Frank, S.G. (1986). Microcrystalline cellulose stabilized emulsions. *Journal of Dispersion Science and Technology*. *7*(5), 543–561.

Oza, K.P. and Frank, S.G. (1989). Multiple emulsions stabilized by colloidal microcrystalline cellulose. *Journal of Dispersion Science and Technology*. *10*(2), 163–185.

Rein, D.M., Khalfin, R. and Cohen, Y. (2012). Cellulose as a novel amphiphilic coating for oil-in-water and water-in-oil dispersions. *Journal of Colloid and Interface Science*. *386*(1), 456–463.

Ries, M.E., Radhi, A., Green, S.M., Moffat, J. and Budtova, T. (2018). Microscopic and Macroscopic Properties of Carbohydrate Solutions in the Ionic Liquid 1-Ethyl-3-methyl-imidazolium Acetate. *Journal of Physical Chemistry B*. *122*(37), 8763–8771.

Sanchez-Salvador, J.L., Balea, A., Monte, M.C., Blanco, A. and Negro, C. (2019). Pickering emulsions containing cellulose microfibers produced by mechanical treatments as stabilizer in the food industry. *Applied Sciences*. *9*, 359.

Sarkar, A., Murray, B., Holmes, M., Ettelaie, R., Abdalla, A. and Yang, X. (2016). In vitro digestion of Pickering emulsions stabilized by soft whey protein microgel particles: Influence of thermal treatment. *Soft Matter*. *12*(15), 3558–3569.

Sescousse, R., Le, K.A., Ries, M.E. and Budtova, T. (2010). Viscosity of cellulose-imidazolium-based ionic liquid solutions. *Journal of Physical Chemistry B*. *114*(21), 7222–7228.

Shen, W., Guo, L., Wu, T., Zhang, W. and Abid, M. (2016). Stabilizing beverage emulsions by regenerated celluloses. *LWT - Food Science and Technology*. *72*, 292–301.

Stubley, S.J., Cayre, O.J., Murray, B.S., Torres, I.C. and Farrés, I.F. (2021). Enzyme cross-linked pectin microgel particles for use in foods. *Food Hydrocolloids*. *121*, 107045.

Tan, X., Li, X., Chen, L. and Xie, F. (2016). Solubility of starch and microcrystalline cellulose in 1-ethyl-3-methylimidazolium acetate ionic liquid and solution rheological properties. *Physical Chemistry Chemical Physics*. *18*(39), 27584–27593.

Tanford, C. (1973). *The Hydrophobic Effect: Formation of Micelles and Biological Membranes* [Online] Illustrate. Wiley. Available from: https://books.google.co.uk/books/about/The_Hydrophobic_Effect_Formation_of_Mice.html?id=ndpqAAAAMAAJ&redir_esc=y.

De Vries, A., Hendriks, J., Van Der Linden, E. and Scholten, E. (2015). Protein Oleogels from Protein Hydrogels via a Stepwise Solvent Exchange Route. *Langmuir*. *31*(51), 13850–13859.

Winuprasith, T. and Suphantharika, M. (2013). Microfibrillated cellulose from mangosteen (Garcinia mangostana L.) rind: Preparation, characterization, and evaluation as an emulsion stabilizer. *Food Hydrocolloids*. *32*(2), 383–394.

Yamane, C., Aoyagi, T., Ago, M., Sato, K., Okajima, K. and Takahashi, T. (2006). Two different surface properties of regenerated cellulose due to structural anisotropy. *Polymer Journal*. *38*(8), 819–826.

Zembyla, M., Lazidis, A., Murray, B.S. and Sarkar, A. (2020). Stability of water-in-oil emulsions co-stabilized by polyphenol crystal-protein complexes as a function of shear rate and temperature. *Journal of Food Engineering*. *281*, 109991.

Zhang, H., Wu, J., Zhang, J. and He, J. (2005). 1-allyl-3-methylimidazolium chloride room temperature ionic liquid: A new and powerful nonderivatizing solvent for cellulose. *Macromolecules*. *38*(20), 8272–8277.

Zhang, S., Holmes, M., Ettelaie, R. and Sarkar, A. (2020). Pea protein microgel particles as Pickering stabilisers of oil-in-water emulsions: Responsiveness to pH and ionic strength. *Food Hydrocolloids*. *102*, 105583.

Appendix A
Supporting information for Chapter 3

Table A 1. Vitacel Powdered Cellulose L 00 (*V*-cell): information provided by the manufacturer (J. Rettenmaier & Söhne GmbH & Co. KG).

	Vitacel Powdered Cellulose L 00
Colour	White
Structure	Fibers
Dietary Fiber Content	~98%
Bulk Density	~165 g/L
Fiber length	120 µm
Water binding capacity	525 %
Oil absorption	410 %

FFC NMR Relaxometry Theory

Lower frequency NMR spectroscopy can give information on the intra and intermolecular interactions and therefore the rotational and diffusional motion in solutions respectively, as described in the introduction. The measured value of R_1 (= $1/T_1$) obtained from FFC NMR is a sum of these interactions and is defined as follows:

Equation A 1. $$\boldsymbol{R_1(\omega) = R_{1,intra}(\omega) + R_{1,inter}(\omega)}$$

where $\omega = \gamma_H B_0$ and represents the proton resonance (Larmor) angular frequency, for which γ_H and B_0 correspond to the proton gyromagnetic ratio and the relaxation field, respectively.

For diffusional motion, a universal low frequency behaviour is observed: translational spectra density is linear with respect to the square root of the frequency ($\sqrt{\nu}$). This is a result of the Fickian diffusion limit at long times (Kaszyńska et al., (2017)). At sufficiently low frequencies, the translational contribution to R_1 is dominant and therefore D can be determined in a model-independent way (Kruk et al., (2012)):

Equation A 2. $$\boldsymbol{R_1(\omega) = a - b\sqrt{\nu}}$$

where a describes the intramolecular contribution to relaxivity which is frequency independent in the linear range of the intermolecular contribution:

Equation A 3. $$a = R_1(0)$$

and *b* is a constant, given by:

Equation A 4. $$b = N\left(\frac{\mu_0}{4\pi}\gamma^2\hbar\right)^2\left(\frac{\sqrt{2}+8}{30}\right)\left(\frac{\pi}{D}\right)^{3/2}$$

where *N* = number of spins per unit volume and can be calculated as using the number of protons per IL molecule (n_H = 18); density (ρ = 1.05 g mol^{-1}) and the molecular weight (*MW* = 198.26 g mol^{-1}), as:

Equation A 5. $$N = \frac{n_H N_A \rho}{MW}$$

Using this approach, *D* can be extracted by determining *b*, which does not require the model specific parameters (distance of closest approach between molecules and a translational correlation time) from the spectral density function, (J_{trans}). The value of *b* is therefore model-independent and can be determined by fitting Equation A 5 to low frequency relaxation dispersion data from FFC NMR (Freed, (1978); Kruk et al., (2012); Kaszyńska et al., (2017)).

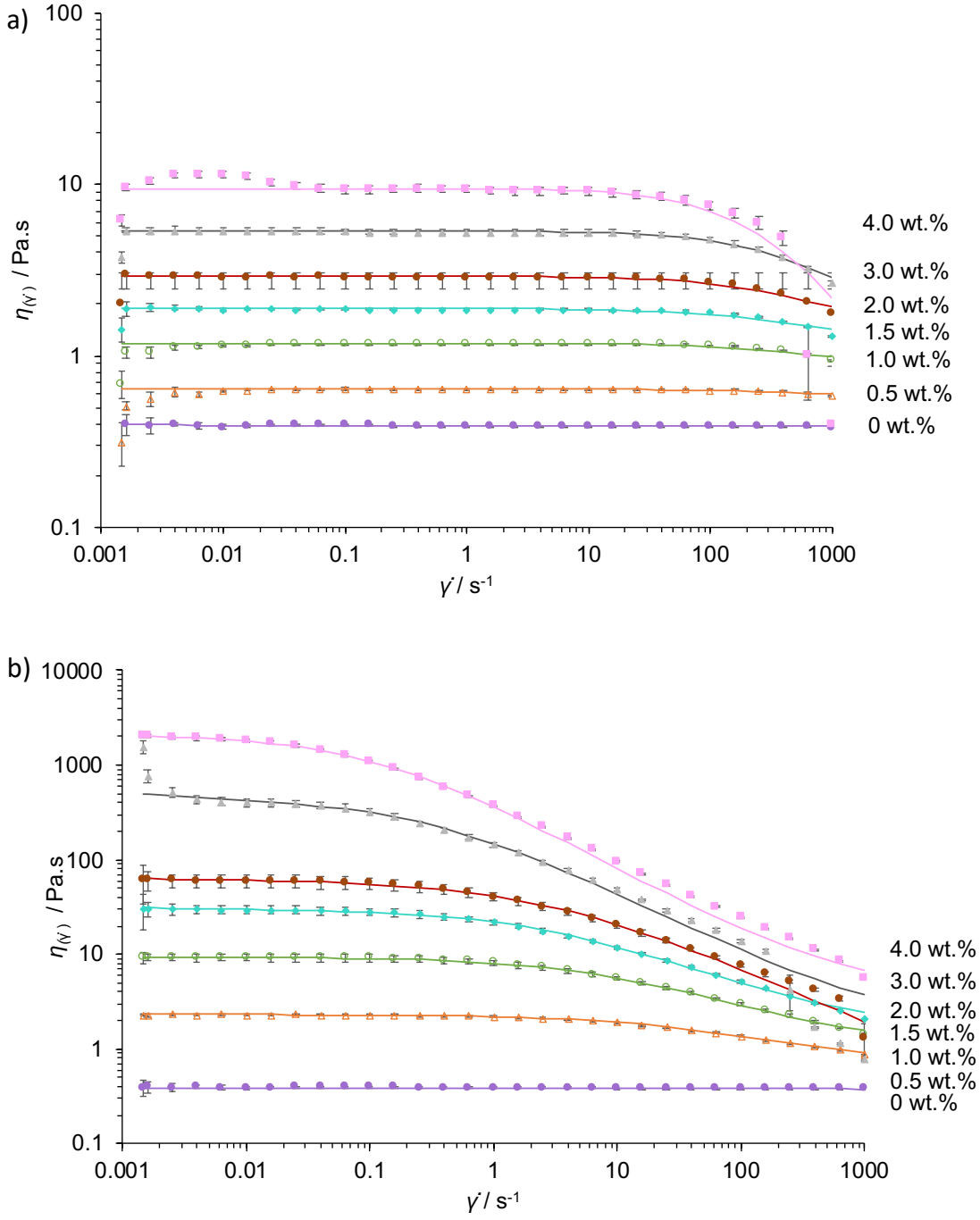

Figure A 1. Flow curves for 0-4 wt% *A*-cell/BmimAc (a), and 0-4 wt% *V*-cell/BmimAc (b), showing the logarithmic plot of viscosity vs shear rate at 25 °C (purple closed circle = 0 wt%; orange open triangle = 0.5 wt%; green open circle = 1.0 wt%; cyan closed diamond = 1.5 wt%; red closed circle = 2.0 wt%; grey closed triangle = 3.0 wt%; pink closed square = 4.0 wt%). Fits to the Cross-Model (Equation 3.1) are given by the solid lines in the corresponding colours. Error bars are all shown but some may be hidden by the symbol.

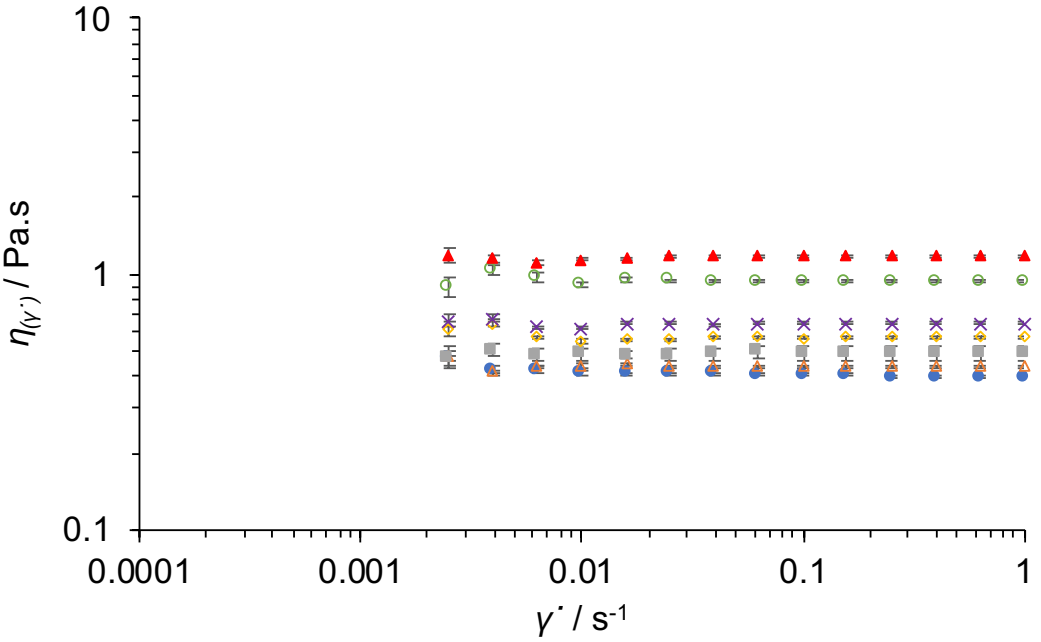

Figure A 2. Low frequency shear rate region for dilute solutions of *A*-cell/BmimAc (0-1 wt%), showing the logarithmic plot of viscosity vs shear rate at 25 °C (blue closed circle = 0 wt%; open orange triangle = 0.1 wt%; grey closed square = 0.2 wt%; yellow open diamond = 0.3 wt%; purple cross = 0.5 wt%; green open circle = 0.75 wt%; red closed triangle = 1.0 wt%).

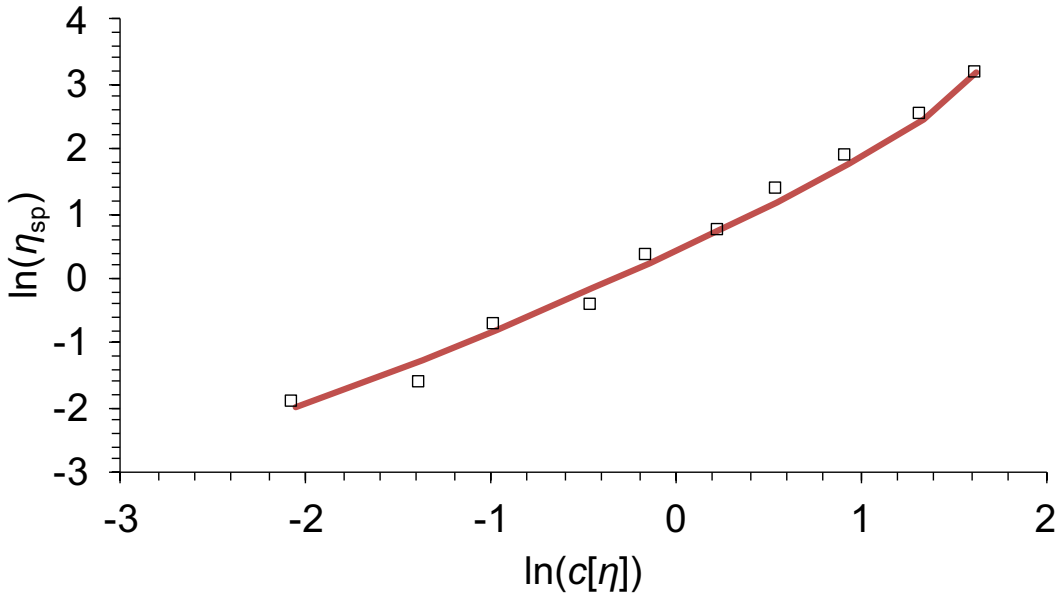

Figure A 3. Plot of log(η_{sp}) versus log($C[\eta]$) for *A*-cell/BmimAc solutions at 25 °C, where B = 6.4 x 10^{-5}, $[\eta]$ = 116 mL g^{-1} and m = 7 as determined from Equation 3.4 (red line).

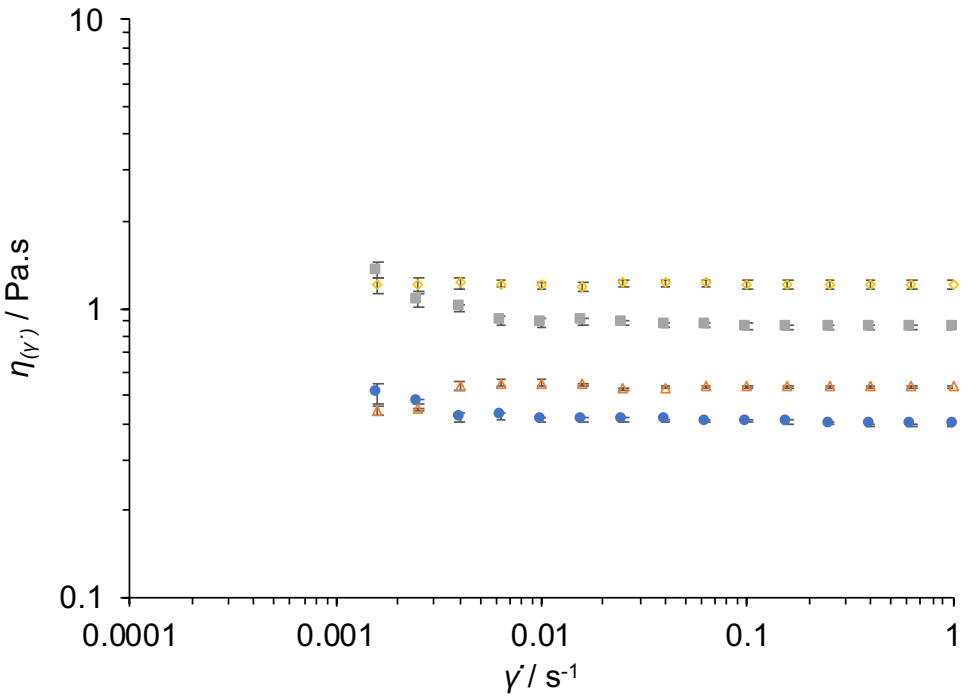

Figure A 4. Low frequency shear rate region for dilute solutions of *V*-cell/BmimAc (0-0.3 wt%), showing the logarithmic plot of viscosity vs shear rate at 25 °C (blue closed circle = 0 wt%; open orange triangle = 0.1 wt%; grey closed square = 0.2 wt%; yellow open diamond = 0.3 wt%).

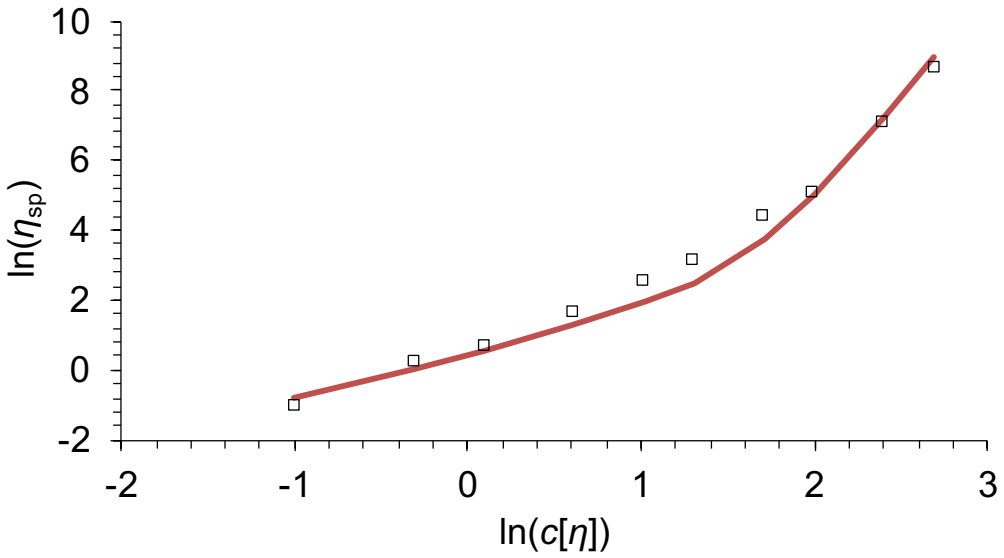

Figure A 5. Plot of log(η_{sp}) versus log($c[\eta]$) for *V*-cell/BmimAc solutions at 25 °C, where $B = 7.3 \times 10^{-4}$, $[\eta] = 350$ mL g^{-1} and $m = 6$ as determined from Equation 3.4 (red line).

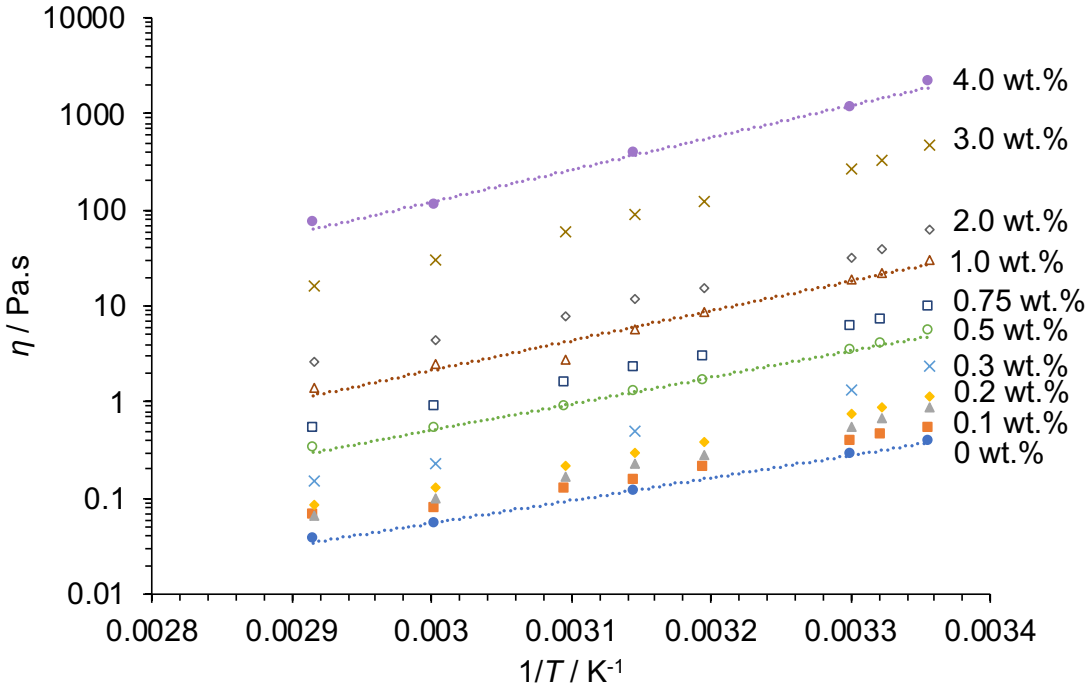

Figure A 6. Logarithmic plots of η as a function of 1/T (25-70 °C) for all concentrations 0-4 wt% of *V*-cell in BmimAc, obtained from Cross-Model (Equation 3.1, blue closed circle = 0 wt%; orange closed square = 0.2 wt%; grey closed triangle = 0.2 wt%; yellow closed diamond = 0.3 wt%; blue cross = 0.5 wt%; green open circle = 0.75 wt%; blue open square = 1.0 wt%; brown open triangle = 1.5 wt%; grey open diamond = 2.0 wt%; brown cross = 3.0 wt% and purple closed square = 4.0 wt%). The dashed lines give the Arrhenius analysis (Equation 3.6) and are given for *V*-cell concentrations of 4.0 wt% (purple); 1.0 wt% (brown); 0.5 wt% (green) and 0 wt% (blue).

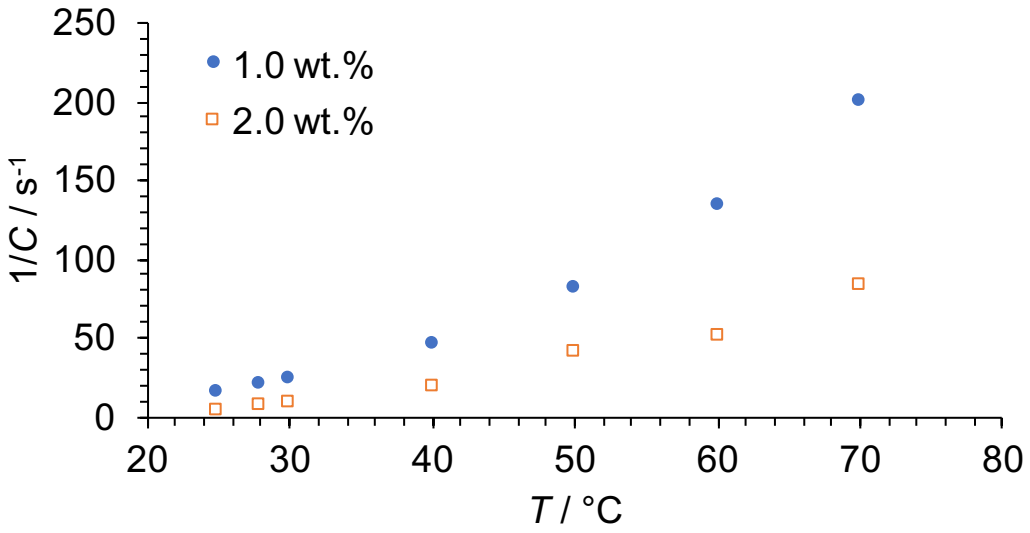

Figure A 7. Shear-thinning behavior (1/*C*) as a function of temperature, for 1.0 and 2.0 wt% *V*-cell in BmimAc, where *C* = Cross time constant (Equation 3.1).

Table A 2. c^*, c_e and exponents for *V*-cell/BmimAc solution (T = 25-70 °C).

T/°C	c^*/wt%	c_e/wt%	Exponent
25	0.20	2	2.53
28	0.20	2	2.49
30	0.20	2	2.47
40	0.26	2.1	2.45
45	0.21	2.1	2.40
50	0.26	2.2	2.37
60	0.22	2.2	2.28
70	0.28	2.3	2.24

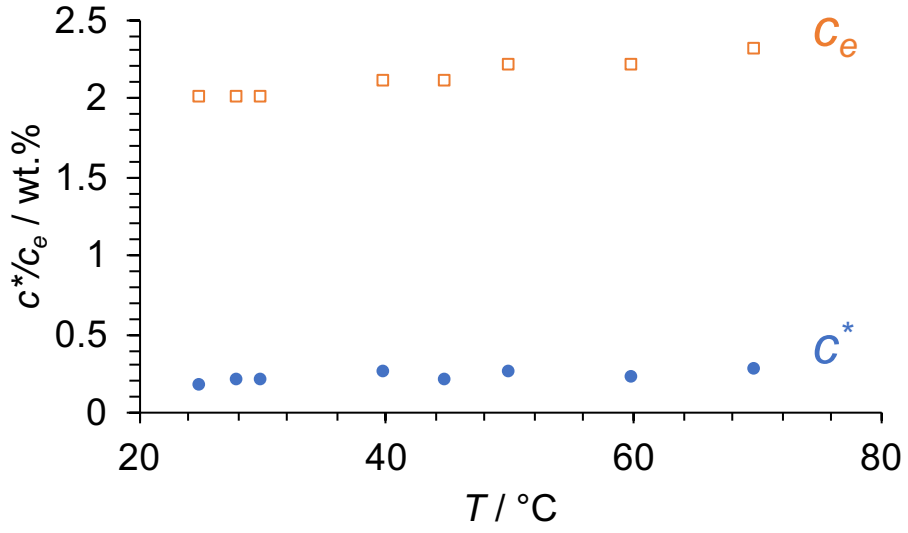

Figure A 8. Estimated overlap concentration (c^*, blue) and entanglement concentration (c_e, orange) as a function of temperature for *V*-cell/BmimAc solutions.

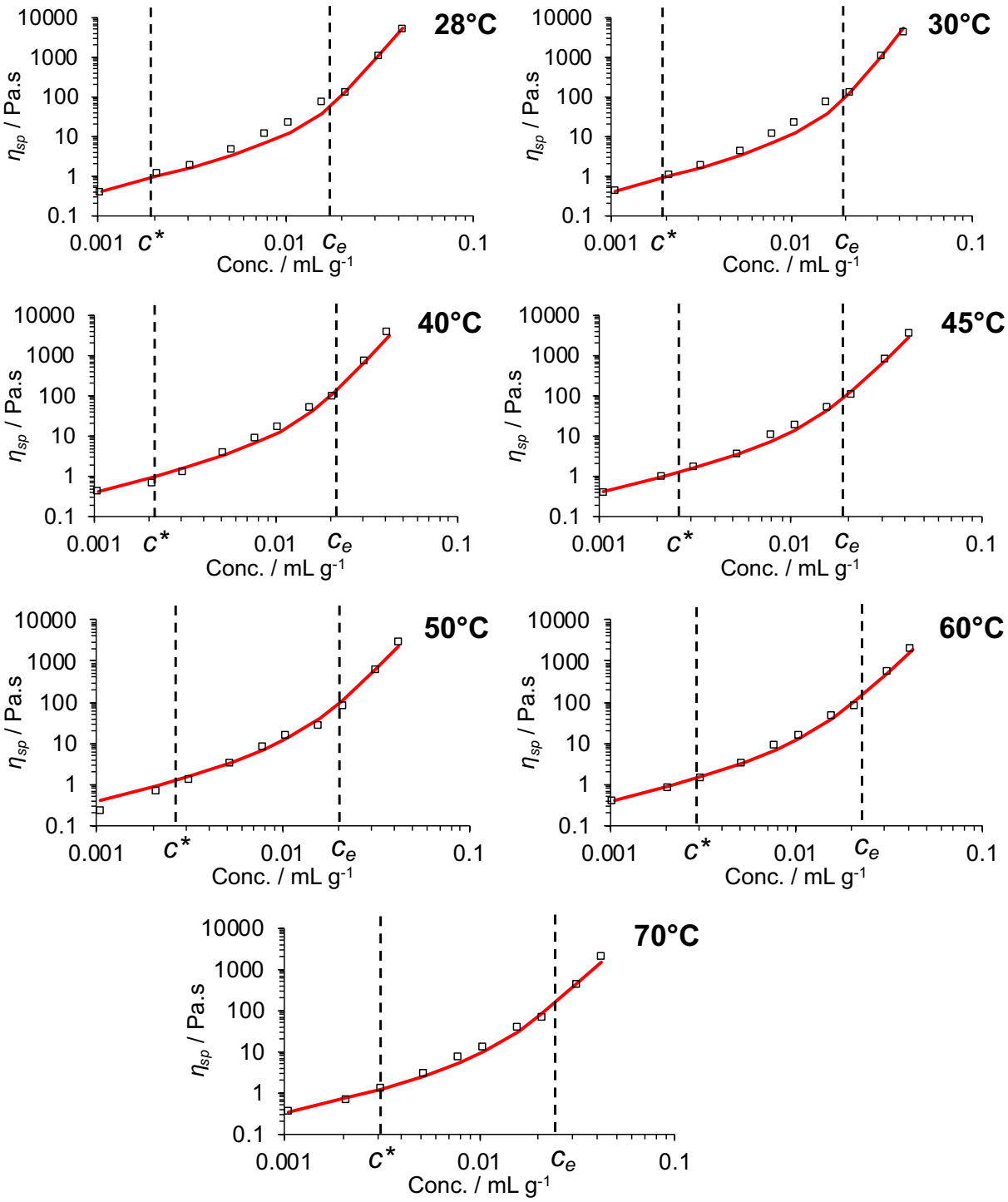

Figure A 9. η_{sp} as a function of *V*-cell concentration in BmimAc (28-70 °C), with c^* and c_e indicated by the dashed lines.

Table A 3. Activation energies for *V*-cell dissolved in BmimAc at various concentrations of cellulose (Conc. = 0 - 4.0 wt%). The uncertainty in determining $E_{a,\eta}$ from the gradient of the slope is given by the error margins (%).

Conc./wt%	$E_{a,\eta}$/kJ mol^{-1}	R^2
0	44.5±1.2	0.9956
0.1	49.1±4.0	0.9626
0.2	49.3±1.3	0.9956
0.3	49.2±1.2	0.9963
0.5	51.8±1.8	0.9931
0.75	52.5±1.2	0.9969
1	54.2±1.1	0.9974
1.5	59.4±4.1	0.9717
2	58.1±2.2	0.9916
3	62.8±0.9	0.9988
4	64.3±2.2	0.9928

Table A 4. Concentration of *V*-cell/BmimAc solutions with their respective water contents (wt%), as determined by high-field ^{1}H NMR (400 MHz).

Conc./wt%	Amount of Water/wt%
0	0.287
0.1	0.569
0.2	0.695
0.3	0.678
0.5	0.664
0.75	0.302
1	0.058
2	0.283
3	2.266
4	4.238

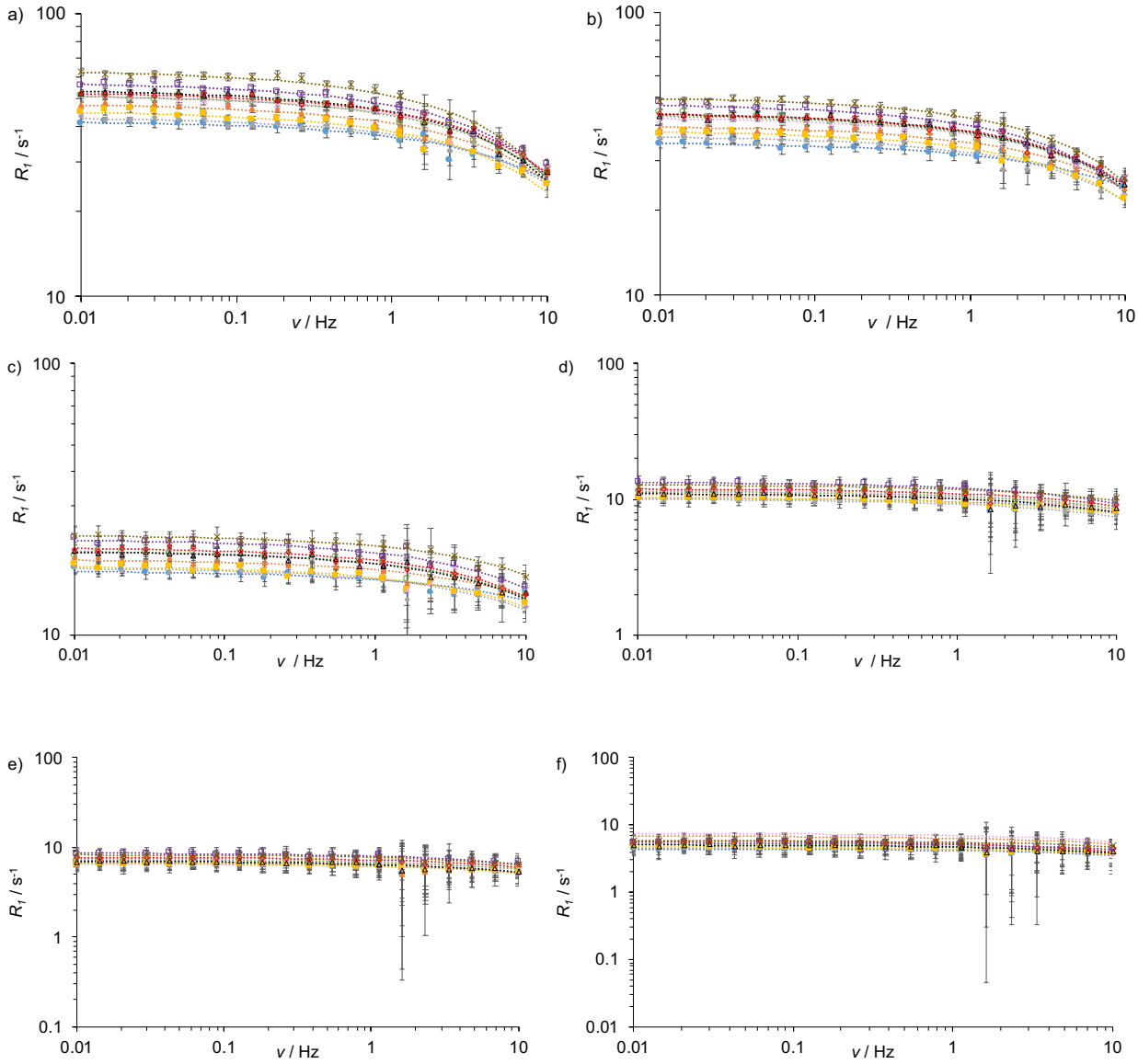

Figure A 10. NMRD profiles of 0-4 wt% *V*-cell/BmimAc at 28, 30, 40, 50, 60 and 70 ℃ (a, b, c, d, e and f), where relaxivities (R_1) are plotted as a function of frequency (v) and the dashed lines give the best fits to Equation A 2: 0 wt% (closed circle, blue); 0.1 wt% (closed triangle, orange); 0.2 wt% (closed diamond, grey); 0.3 wt% (closed square, yellow); 0.5 wt% (cross, pink); 0.75 wt% (open circle, grey); 1.0 wt% (open triangle, black); 2.0 wt% (open diamond, red); 3.0 wt% (open square, purple) and 4.0 wt% (cross, brown).

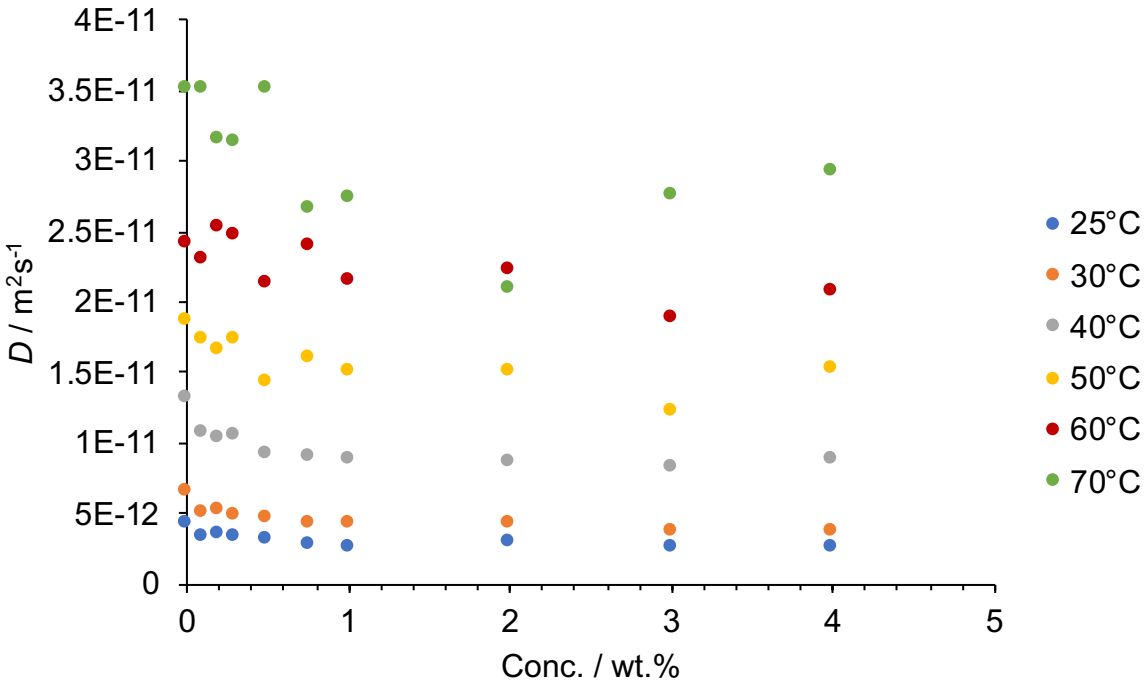

Figure A 11. Self-diffusion coefficients (*D*) of *V*-cell/BmimAc solutions obtained from NMRD profiles, as a function of cellulose concentration: 25 ℃ (blue); 30 ℃ (orange); 40 ℃ (grey); 50 ℃ (yellow); 60 ℃ (red) and 70 ℃ (green).

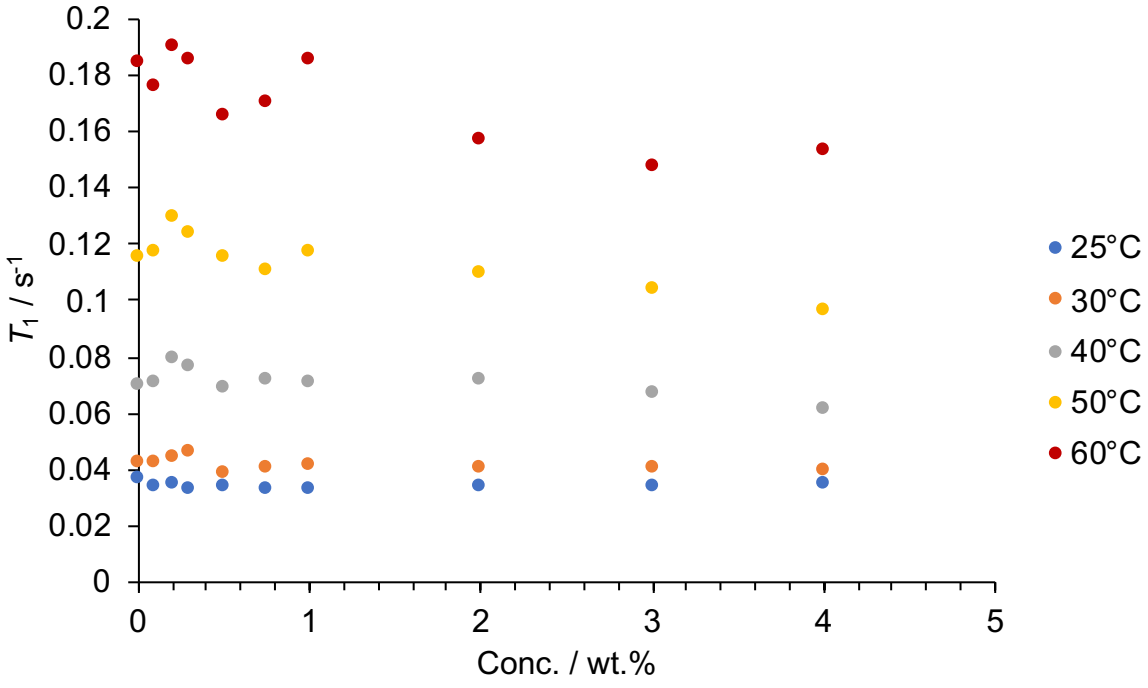

Figure A 12. Relaxation times (T_1) of *V*-cell/BmimAc solutions (ν = 10 MHz), as a function of cellulose concentration: 25 ℃ (blue); 30 ℃ (orange); 40 ℃ (grey); 50 ℃ (yellow) and 60 ℃ (red).

References

Kaszyńska, J., Rachocki, A., Bielejewski, M. and Tritt-Goc, J. (2017). Influence of cellulose gel matrix on BMIMCl ionic liquid dynamics and conductivity. *Cellulose*. *24*(4), 1641–1655.

Kruk, D., Meier, R. and Rössler, E.A. (2012). Nuclear magnetic resonance relaxometry as a method of measuring translational diffusion coefficients in liquids. *Physical Review E - Statistical, Nonlinear, and Soft Matter Physics*. *85*(2), 1–5.

Freed, J.H. (1978). Dynamic effects of pair correlation functions on spin relaxation by translational diffusion in liquids. II. Finite jumps and independent T 1 processes. *The Journal of Chemical Physics*. *68*(9), 4034–4037.

Appendix B
Supporting information for Chapter 4

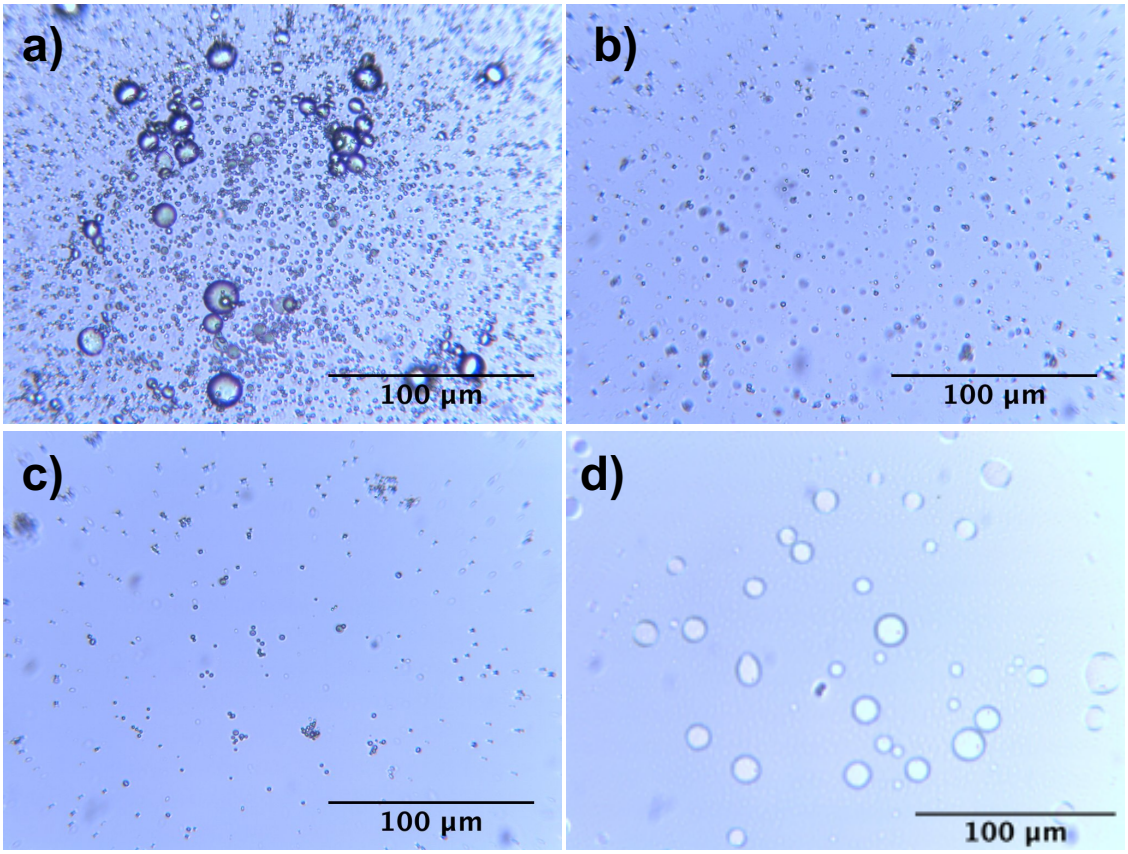

Figure B 1. Light micrographs of various O/W emulsions stabilised by a) 0.2 wt%; b) 0.5 wt%; c) 1.0 wt% and d) 1.5 wt% CMG.

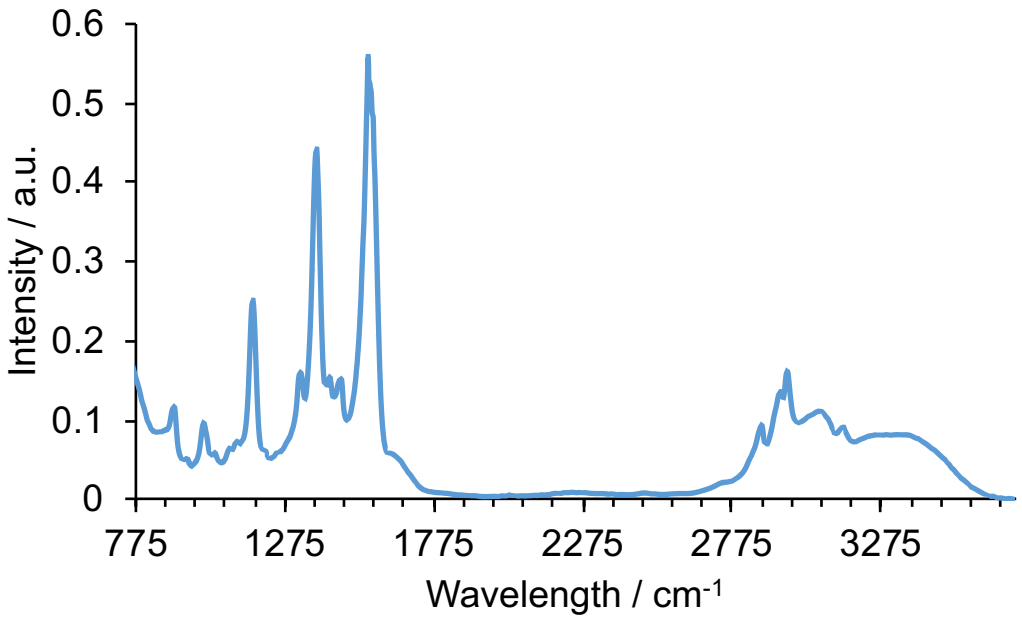

Figure B 2. ATR-FTIR spectrum of BmimAc, plotted as intensity of absorbance (a.u.) versus wavelength (cm^{-1}).

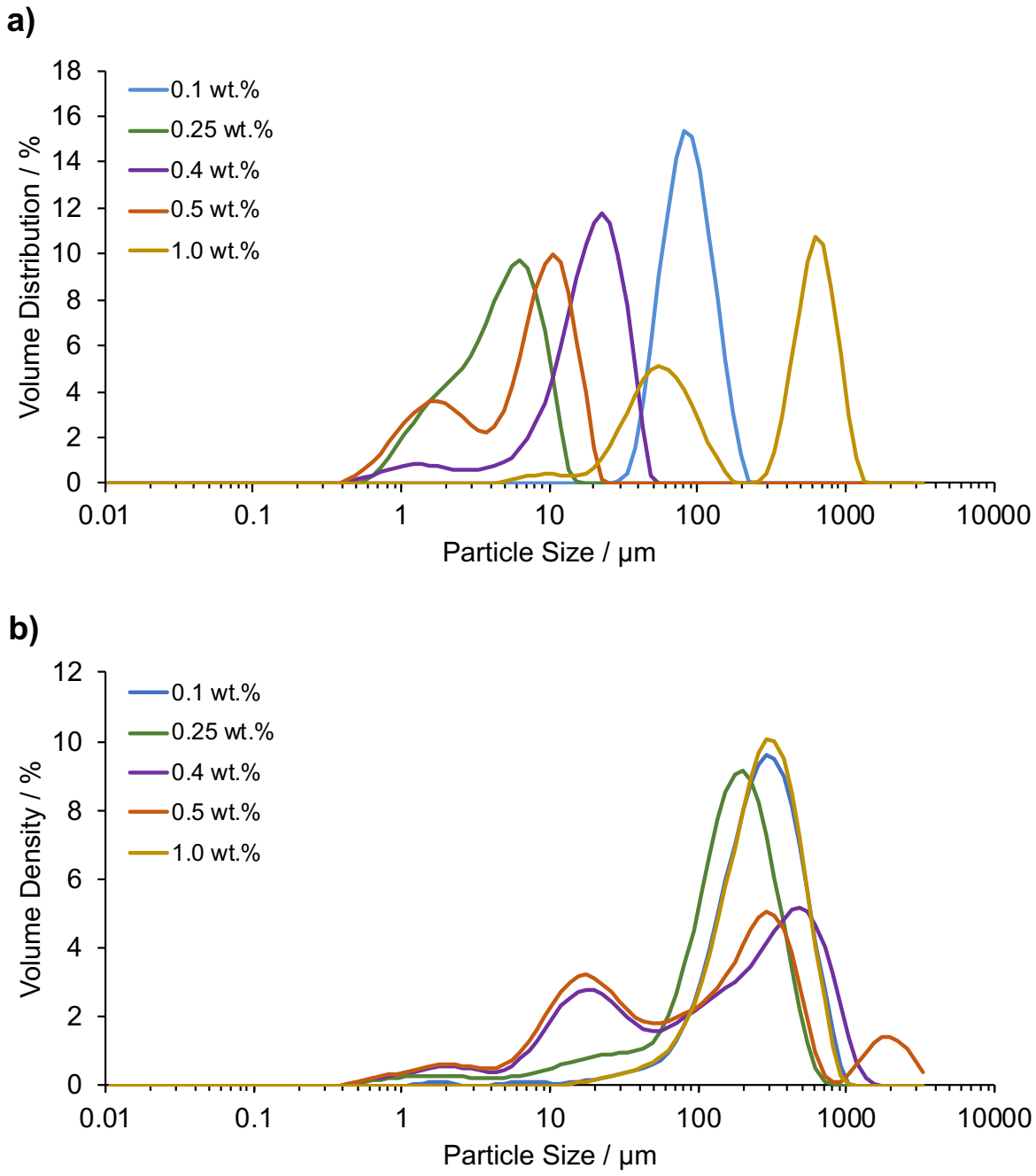

Figure B 3. Particle size distributions for 0.1 – 1.0 wt% CMG dispersions in a) HOSO b) water (0.1, 0.25, 0.4, 0.5 and 1.0 wt% cellulose, shown in blue, green, purple, orange and yellow respectively).

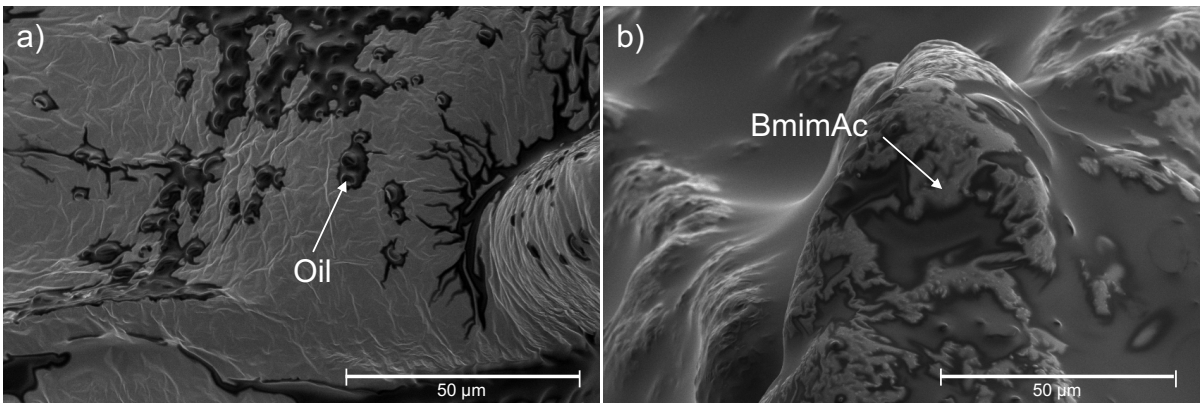

Figure B 4. SEM images of cellulose macrogels after freeze-drying, regenerated from a) 4.0 wt% cellulose dissolved in BmimAc and b) 2.0 wt% cellulose dissolved in BmimAc. Oil is seen as black 'droplets' and ionic liquid is seen as white. Scale bar reads 50 µm.

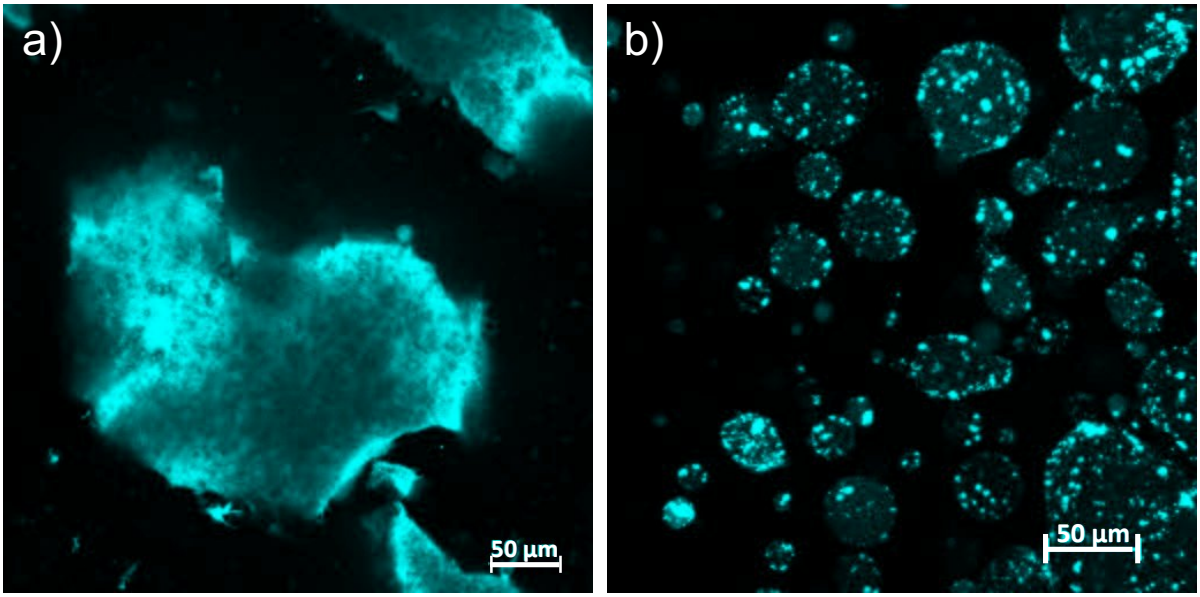

	1.0 wt% Water	1.0 wt% Oil
*(d*3,2*)* / µm	190	73.8
*(d*4,3*)* / µm	297	150

Figure B 5. Confocal image of 1.0 wt% CMG-water and CMG-HOSO dispersions (a and b respectively). Particle sizes are given in the table below, as surface-weighted and volume-weighted averages (*d*3,2 and *d*4,3 respectively).

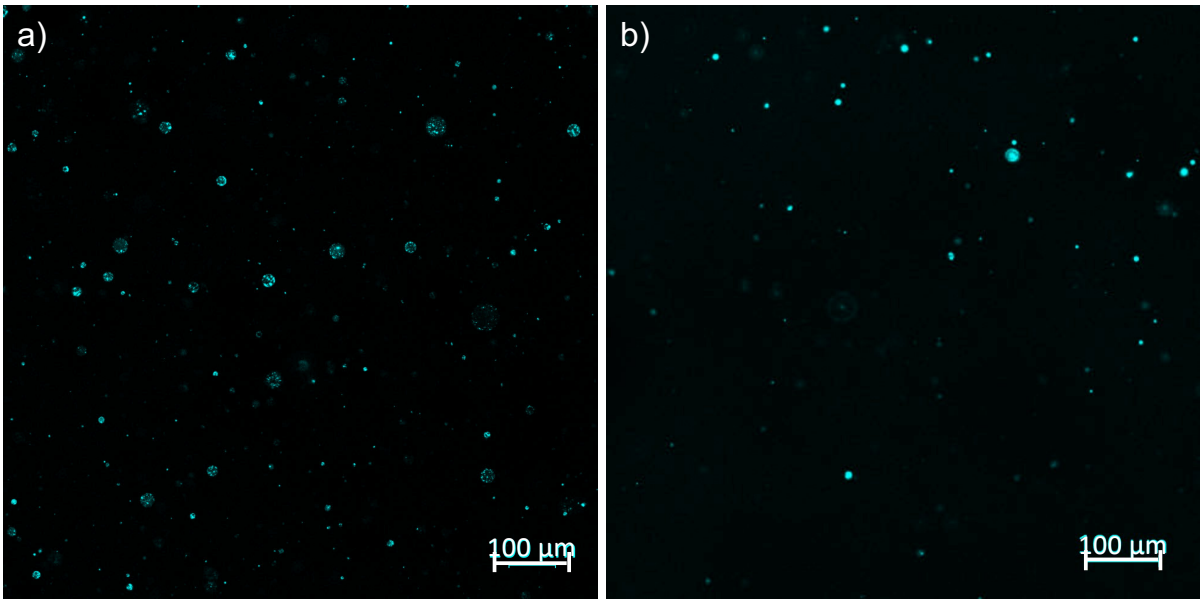

Figure B 6. Confocal images of 10 vol% W/O emulsions formed from 0.1 wt% CMG-HOSO a) CMG-HOSO oil dispersion; b) CMG-water dispersion. Scale bar reads 100 µm.

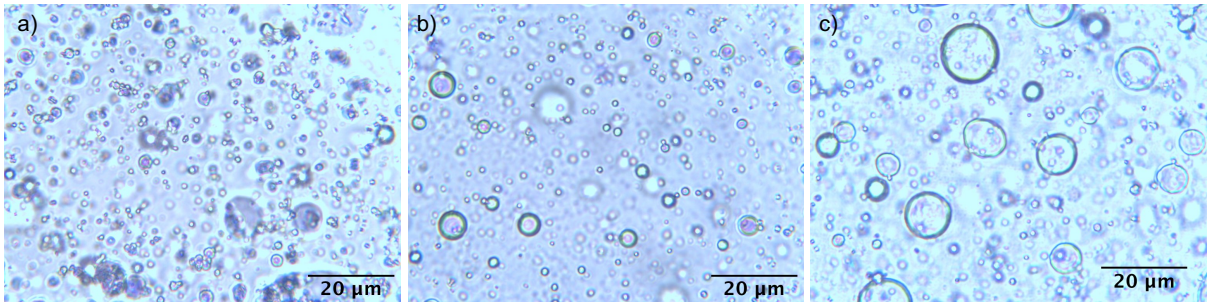

Average size / µm	0.05 wt% water	0.15 wt% water	0.2 wt% water	0.4 wt% water	1.0 wt% HOSO	1.0 wt% water	4.0 wt% HOSO	5.0 wt% HOSO
*(d*3,2*)*	0.285	8.39	5.43	3.75	3.74	3.9	0.0969	0.167
*(d*4,3*)*	10.3	18.1	28.8	15.3	6.1	6.28	29.2	11.9

Figure B 7. Light micrographs of various W/O emulsions stabilised by a) 0.05 wt% CMG (20 vol% water); b) 0.5 wt% CMG (20 vol% water); c) 7.5 wt% CMG (5 vol% water). Mean particle sizes of a range of W/O emulsions are given in the table below, where 'water' and 'HOSO' indicate that emulsions were formed from respective CMG-water and CMG-oil dispersions. Scale bar reads 20 µm.

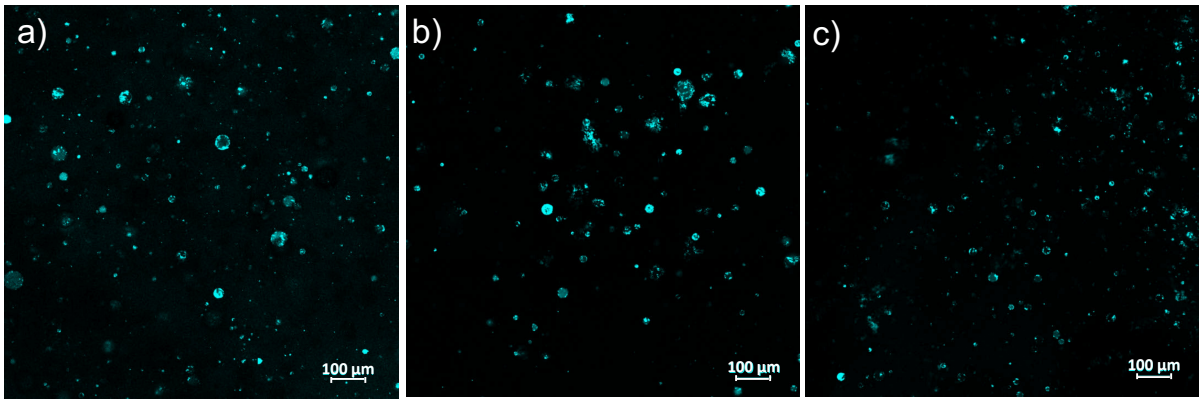

Average Size/µm	0.05 wt% CMG	0.18 wt% CMG	0.25 wt% CMG
*(d*3,2*)*	2.64	2.39	2.56
*(d*4,3*)*	11.9	9.05	11.5

Figure B 8. Confocal images of 20 vol% W/O emulsions formed from a) 0.05 wt%; b) 0.18 wt% and c) 0.25 wt% CMG-water dispersions. Mean particle sizes are given in the table below. Scale bar reads 100 µm.

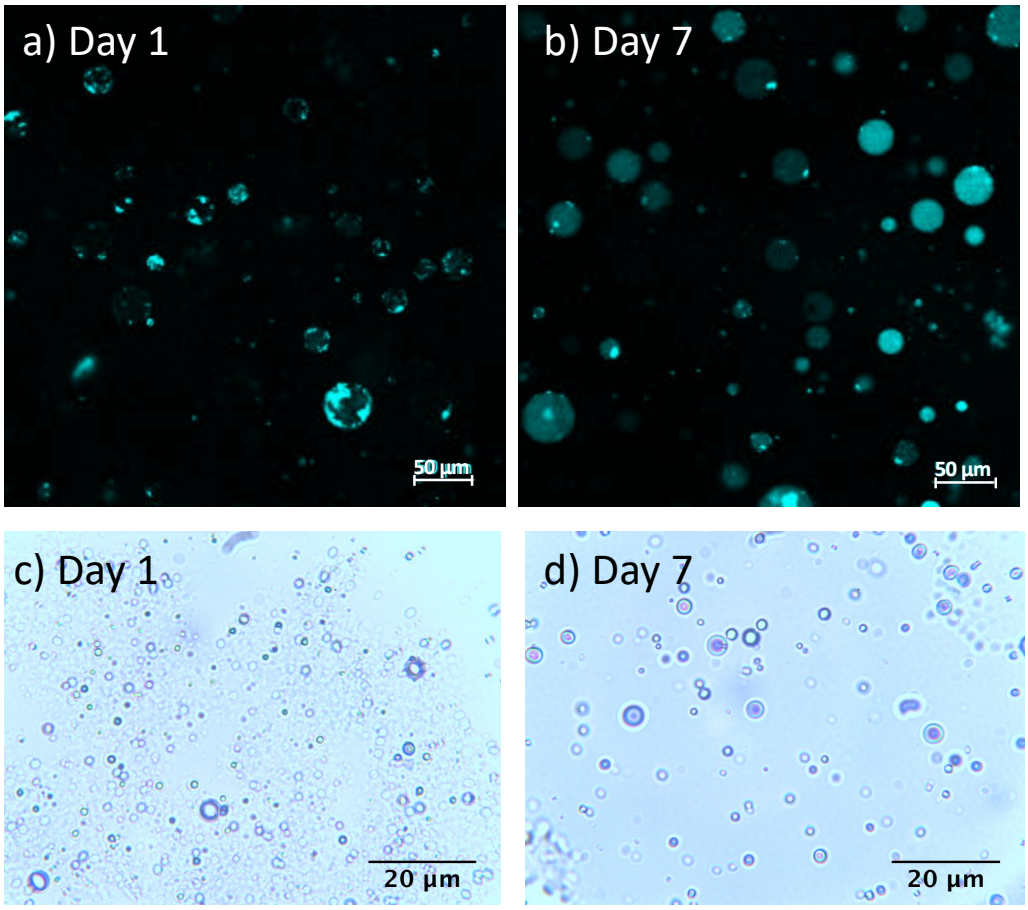

Figure B 9. Confocal microscopy images (a and b) and light microscopy images (c and d) of 20 vol% W/O emulsions formed from 0.25 wt% CMG-HOSO. Images on the left taken on day 1, images on the right taken on day 7, as labelled. Scale bar reads 50 µm (a and b) and 20 µm (c and d).

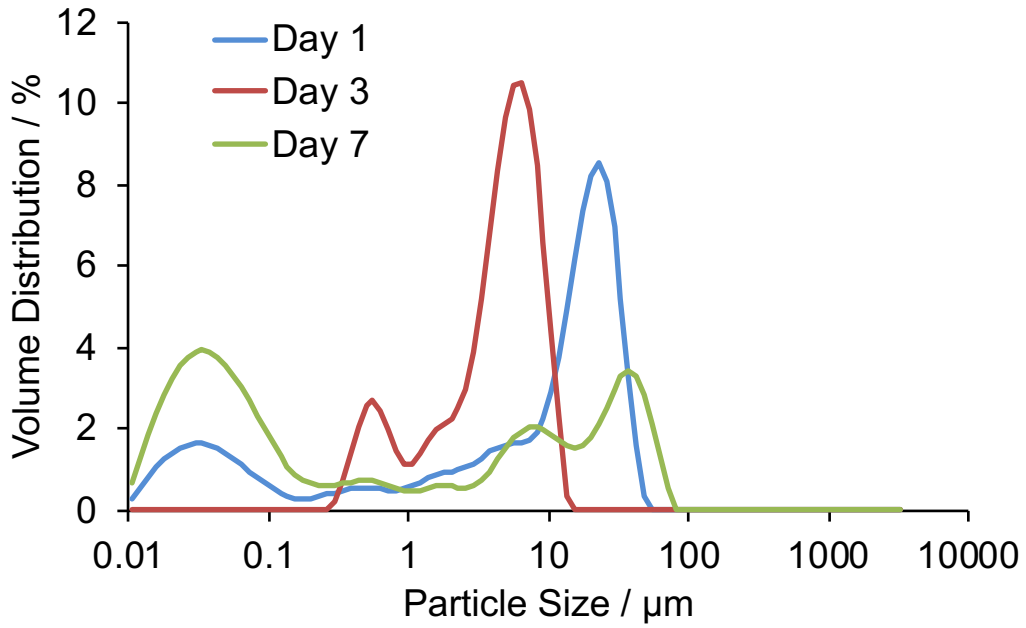

Figure B 10. Size distributions for 20 vol% W/O emulsion stabilised by 0.25 wt% CMG over time (day 1, day 3 and day 7, shown in blue, red and green respectively).

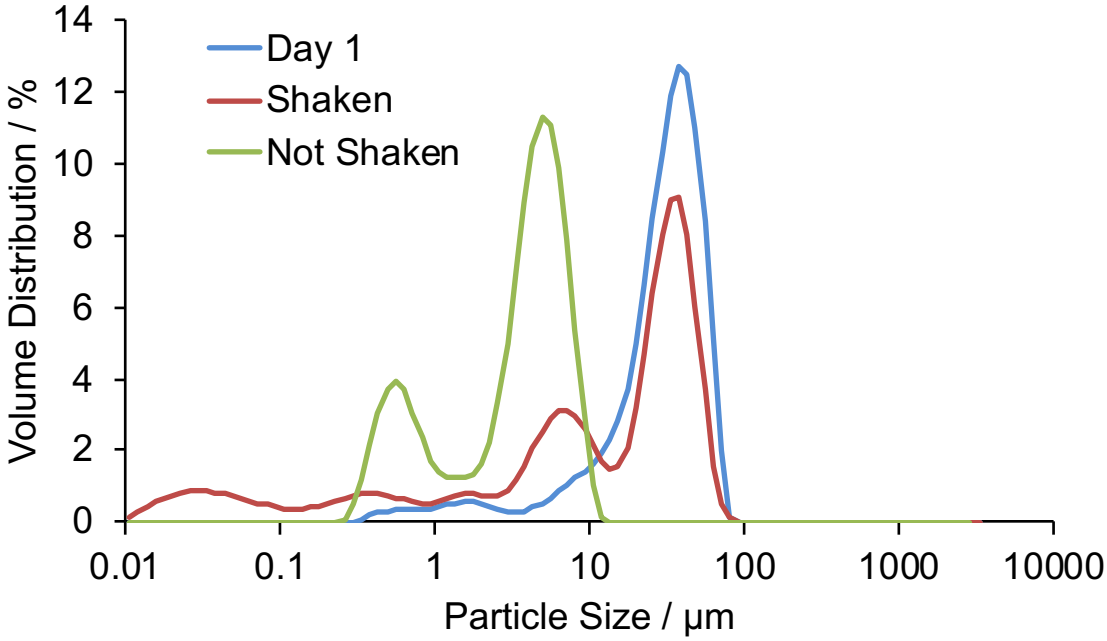

Figure B 11. Size distributions for 20 vol% W/O emulsion stabilised by 0.14 wt% CMG over time (day 1, day 2 shaken and day 2 not shaken, shown in blue, red and green respectively).

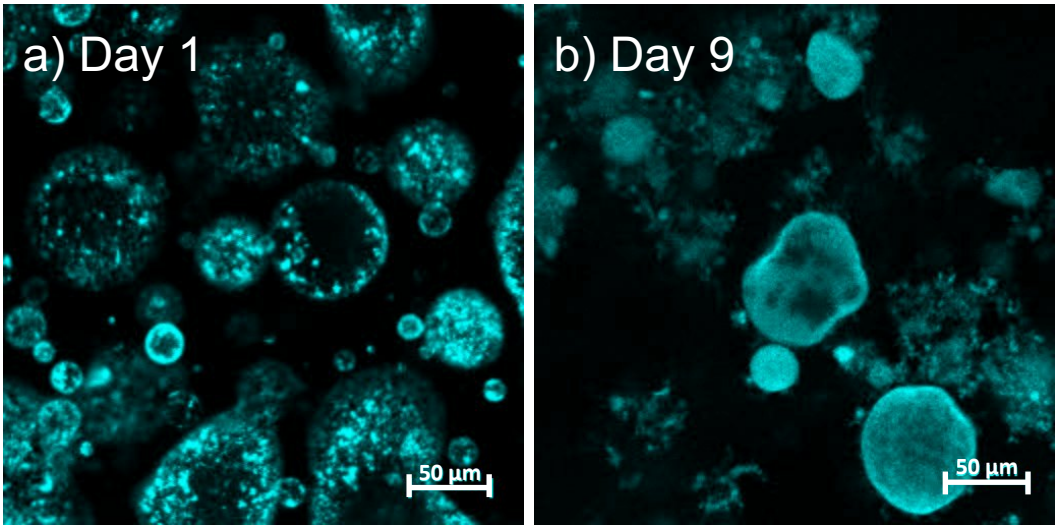

Figure B 12. 10 vol% W/O emulsions stabilised by 1.0 wt% CMGs over time, a and b correspond to day 1 and day 9 respectively.

Appendix C
Supporting information for Chapter 5

Table C 1. Vitacel Powdered Cellulose L 00 (*V*-cell): information provided by the manufacturer (J. Rettenmaier & Söhne GmbH & Co. KG).

	Vitacel Powdered Cellulose L 00
Colour	White
Structure	Fibers
Dietary Fiber Content	~98%
Bulk Density	~165 g/L
Fiber length	120 µm
Water binding capacity	525 %
Oil absorption	410 %

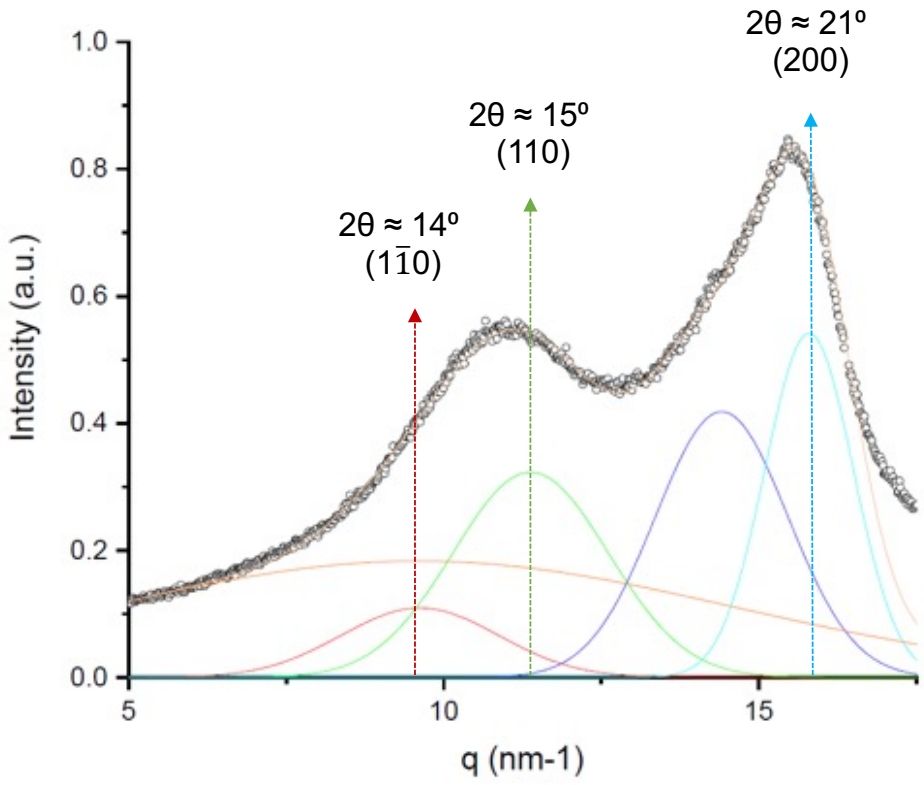

Figure C 1. Wide angle x-ray scattering (WAXS) spectrum (25 °C) for the L 00 cellulose powder, fitted to crystalline peaks corresponding to cellulose I (Sugiyama et al., (1991)) (red, green and light blue peaks).

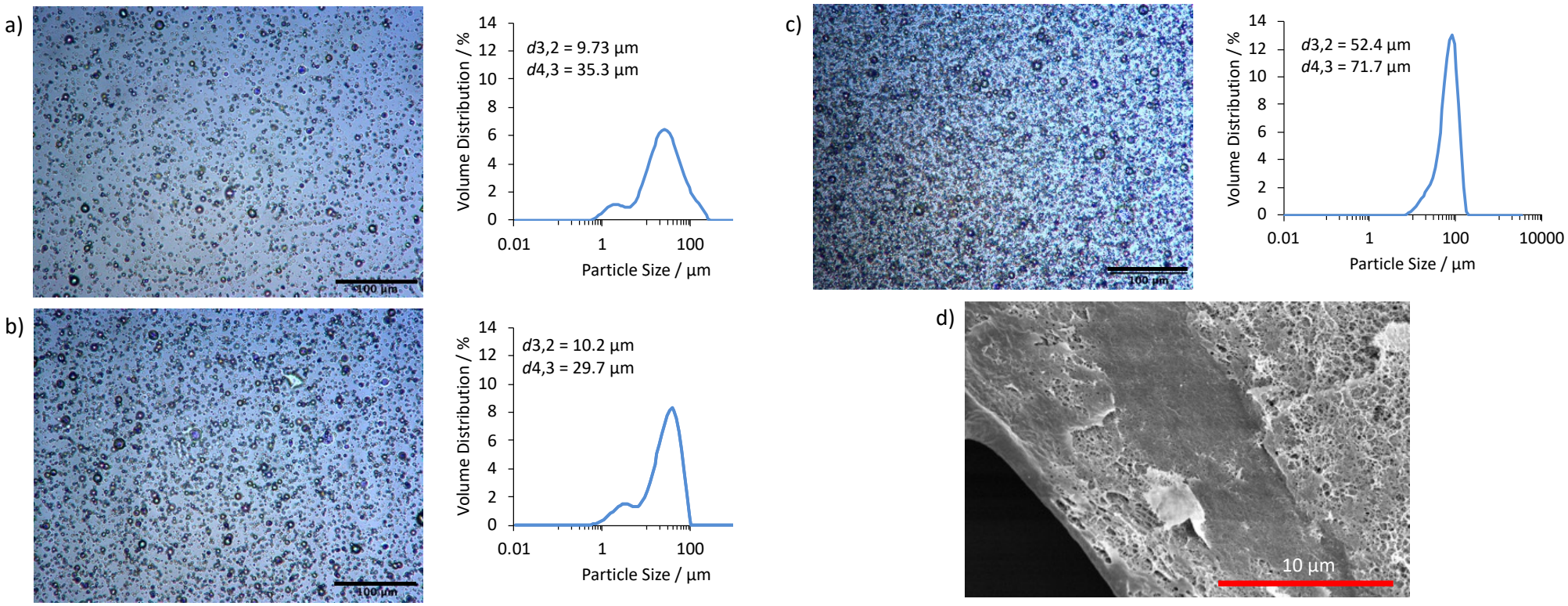

Figure C 2. Images and PSDs of CMG-in-oil dispersions (L-200): a) 2 wv%; b) 4 wv% and c) 6 wv%, with *d*3,2 and *d*4,3 values displayed on each graph. Scale bar = 100 µm, shown at bottom right in black; d) SEM image of the core structure of an L-200 cellulose macrogel (before dispersion in oil to form CMGs), showing the structural inhomogeneity. The cellulose gel was freeze-dried and then imaged using a FEI NanoSEM Nova 450 operating at 3 kV, using a TLD detector and a working distance of 3.7mm. The sample was mounted on an SEM stub with adhesive copper tape and sputter-coated with iridium (Cressington 208 HR). Scale bar = 10 µm, shown at the bottom right in red.

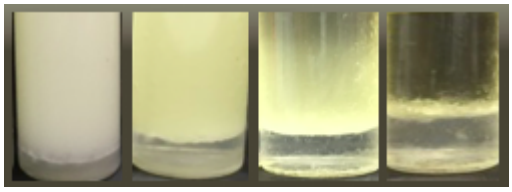

Figure C 3. Appearance of 20:80 W/O emulsions stabilized by 1 wv% L-200 over time (from left to right: 1-, 2-, 7- and 14-days storage).

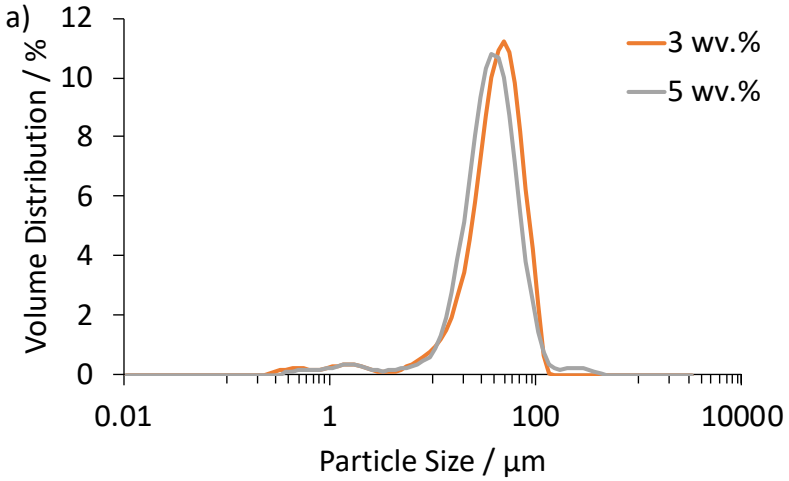

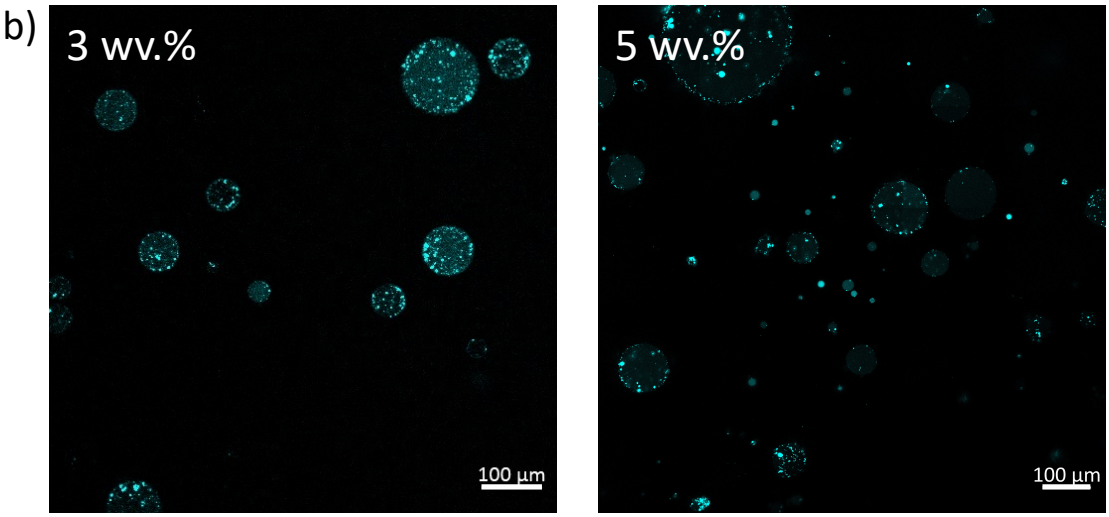

Figure C 4. a) PSDs for 'fresh' 20:80 W/O emulsions stabilized 3 and 5 wv% H-200 PSDs (orange and grey respectively); b) confocal micrographs of the emulsions. Scale bar = 100 µm, shown at bottom right in white.

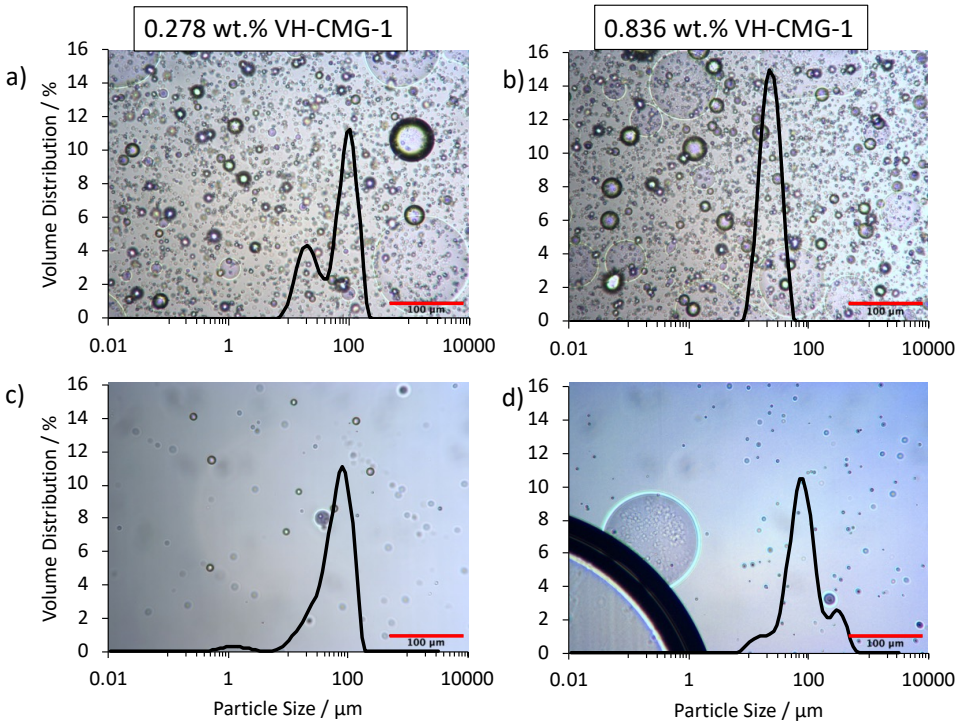

Figure C 5. Optical micrographs with PSDs overlaid and images in the top right for 20:80 emulsions stabilised by 0.278 wt% VH-1 (a and c) and 0.836 wt% VH-1 (b and d). Figures a) and b) give the 'fresh' emulsions; c) and d) give the emulsions after 7 days. Scale bar = 100 µm, shown at bottom right in red.

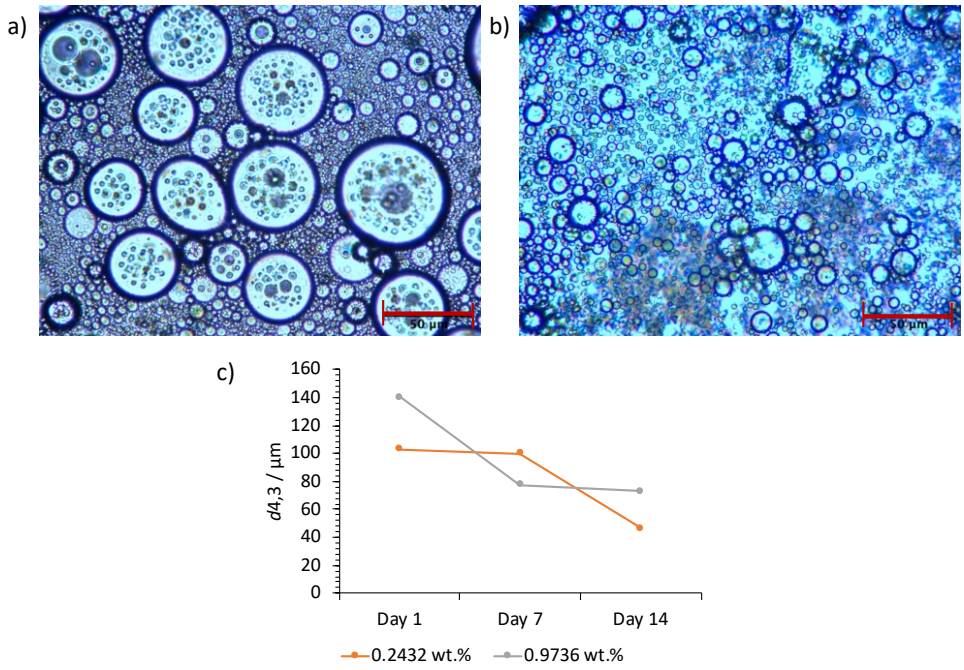

Figure C 6. Optical micrographs of 20:80 O/W emulsions stabilized by VH-1 (0.243 wt%) a) day 1; b) day 7. Scale bar = 50 µm, shown at bottom right in red. c) *d*4,3 values over time for 20:80 O/W emulsions stabilized by VH-1 (0.243 and 0.974 wt%). A reduction in *d*4,3 during storage was due to coalescence and creaming of larger, unstable droplets, which therefore disappeared from the PSDs on days 7 and 14.

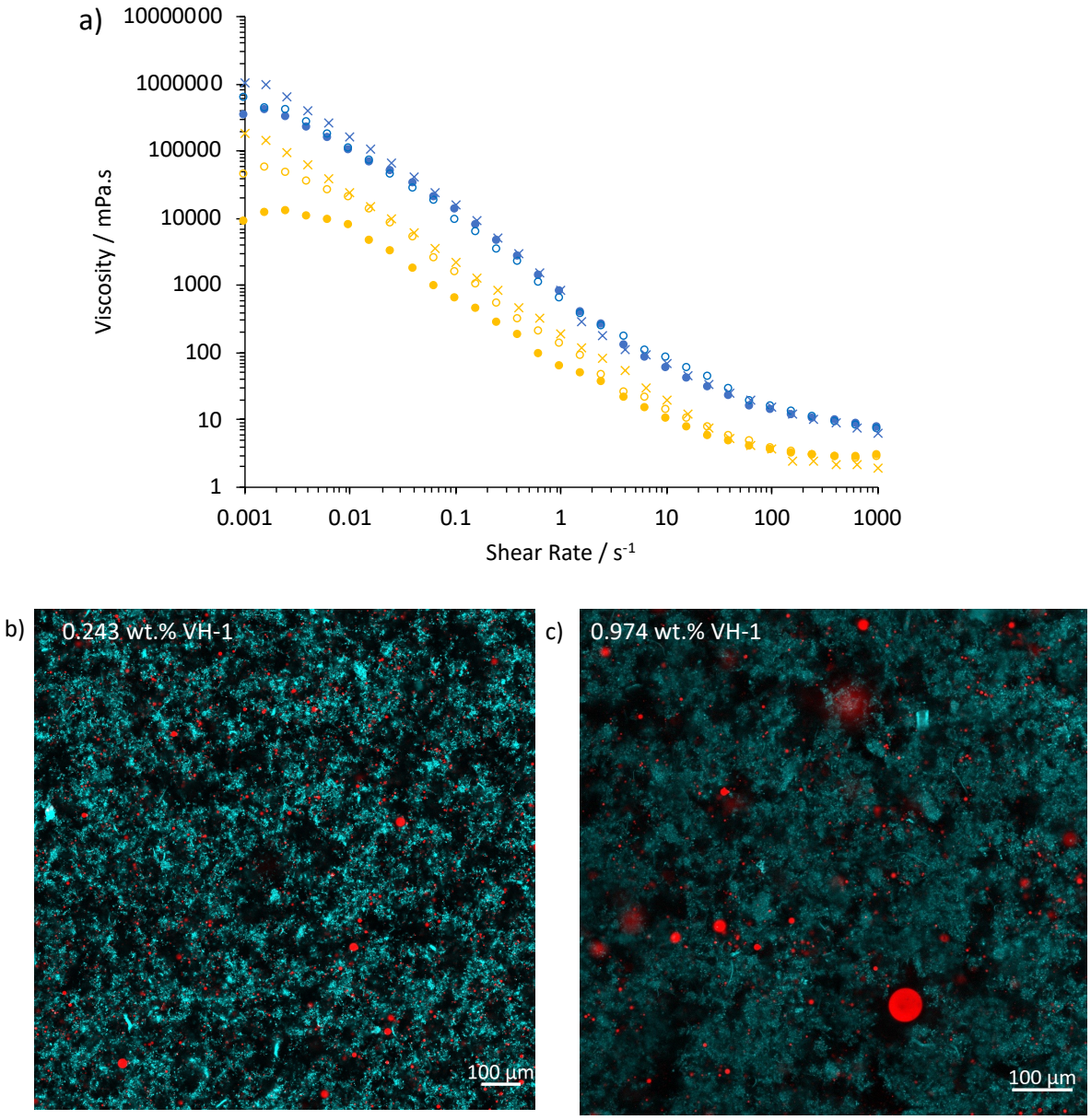

Figure C 7. 20:80 O/W emulsions stabilized by VH-1 (0.243 and 0.974 wt%) a) flow curves of day 1 (filled circle); day 7 (open circle) and day 14 (cross) for 0.243 wt% (yellow) and 0.974 wt% (blue). Error bars have not been included for clarity in the figure; confocal micrographs, day 14 with b) 0.243 wt% and c) 0.974 wt% VH-1. Oil was stained by Nile Red (0.4 mg mL^{-1} in DMSO), obtained from Sigma Aldrich. Scale bar = 100 µm, shown at bottom right in white.

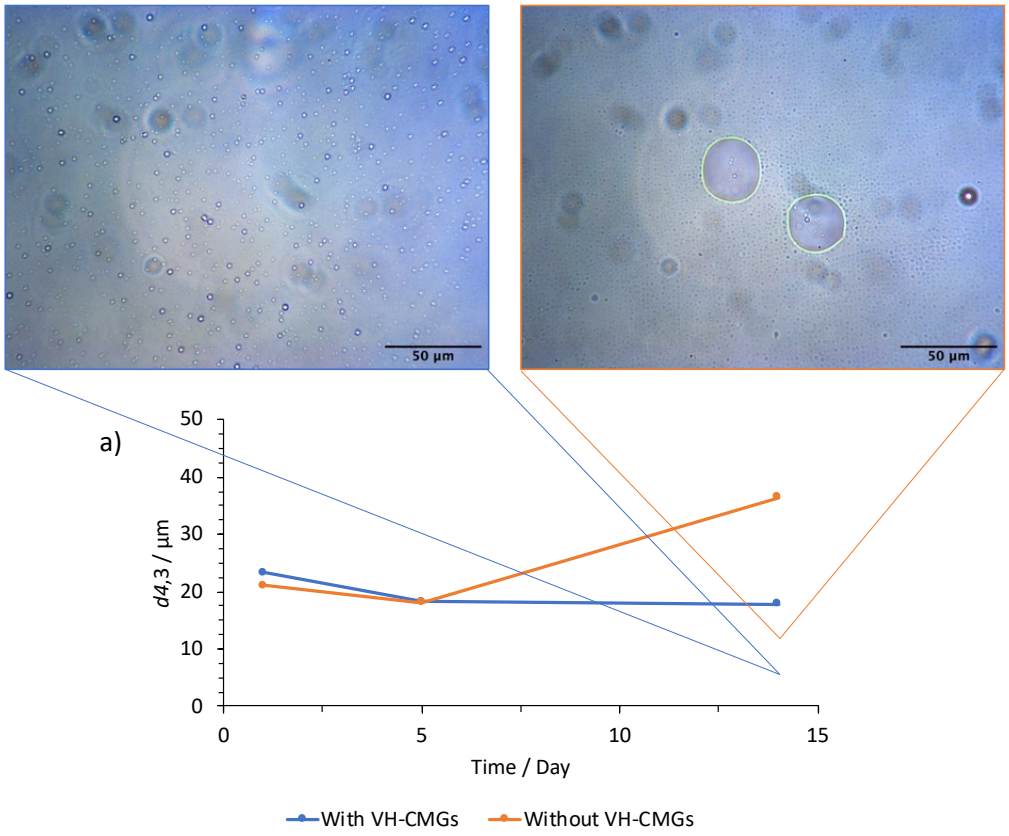

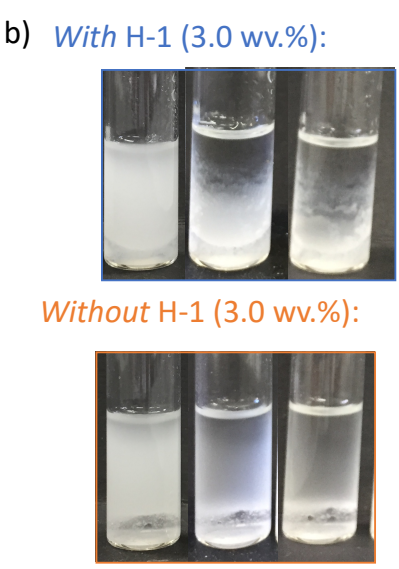

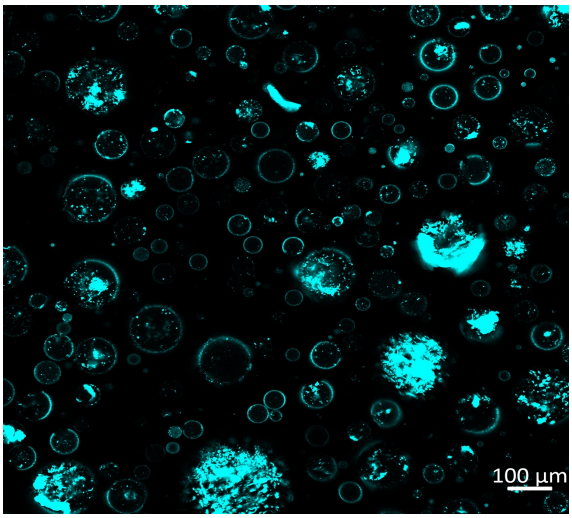

Figure C 8. a) *d*4,3 and appearance over time of 20:80 emulsion stabilised by H-1 (3 wv%) and with (blue) or without (orange) VH-1 (0.557 wt%). Optical micrographs show appearance of droplets after 14 days storage, with (blue border) and without (orange border) VH-1. Scale bar = 50 µm, shown at bottom right in black; b) images of emulsions with (blue border) and without (orange border) H-1 over time (from left to right: day 1, 5 and 14); c) confocal micrograph of 20:80 emulsion stabilized by H-200 (3 wv%) and VH-1 (0.398 wt%) after 2 months storage. Scale bar = 100 µm, shown at bottom right in black.

Method for subtracting the contribution from the excess CMGs to the PSDs of W/O emulsions

To separate the contributions of the excess CMGs and the water droplets to the PSDs of the emulsions, the fraction of the contribution of *free* CMGs was considered. PSDs for the CMG-in-oil dispersions were multiplied by a fraction, as determined by the volume of CMGs dispersed in the final emulsion and the volume of water in the final emulsion. For example, for 10 mL of a 20:80 W/O emulsion stabilised by '3 wv% L-200,' the fraction of CMGs is 3 wv% in 8 mL of oil (and therefore 2.4 wv% in 10 mL of emulsion), whilst the fraction of water is 2 mL in 10 mL. Therefore, the amount of CMGs and water in the emulsion is 0.24 g and 2 g respectively, and thus the contribution of excess CMGs to the PSD was taken to be 0.24/2 = 0.12. The volume distributions of the CMG-in-oil dispersions were multiplied by this fraction and then subtracted from the volume distributions of the W/O emulsions, to determine the PSDs for the emulsions without the excess CMGs. Comparison of the original PSDs and the modified PSDs are given in the figure below.

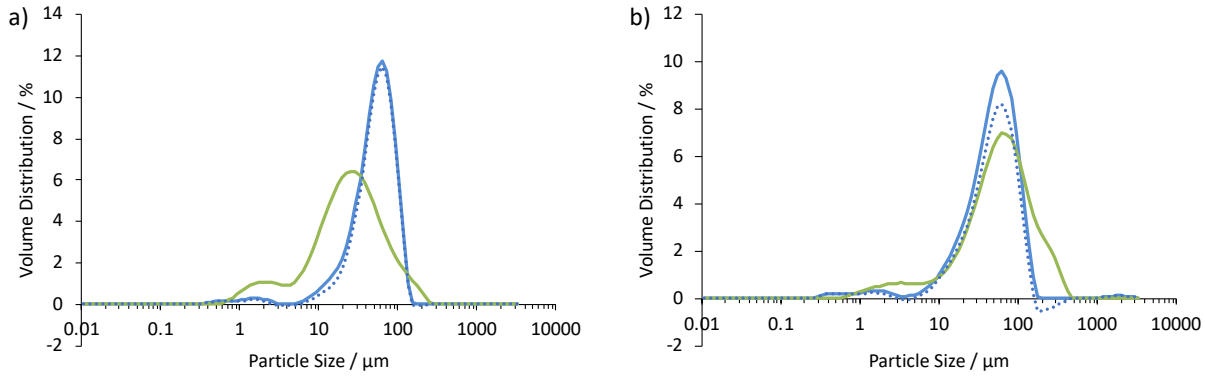

Figure C 9. PSDs for W/O emulsions stabilised by L-200 a) 2 wv%; b) 5 wv%. The original PSDs are given by the solid blue lines and the PSDs with the fraction of excess CMGs subtracted are given by the blue dashed lines. The original PSDs for the L-in-oil dispersions are also included for reference (green solid lines).

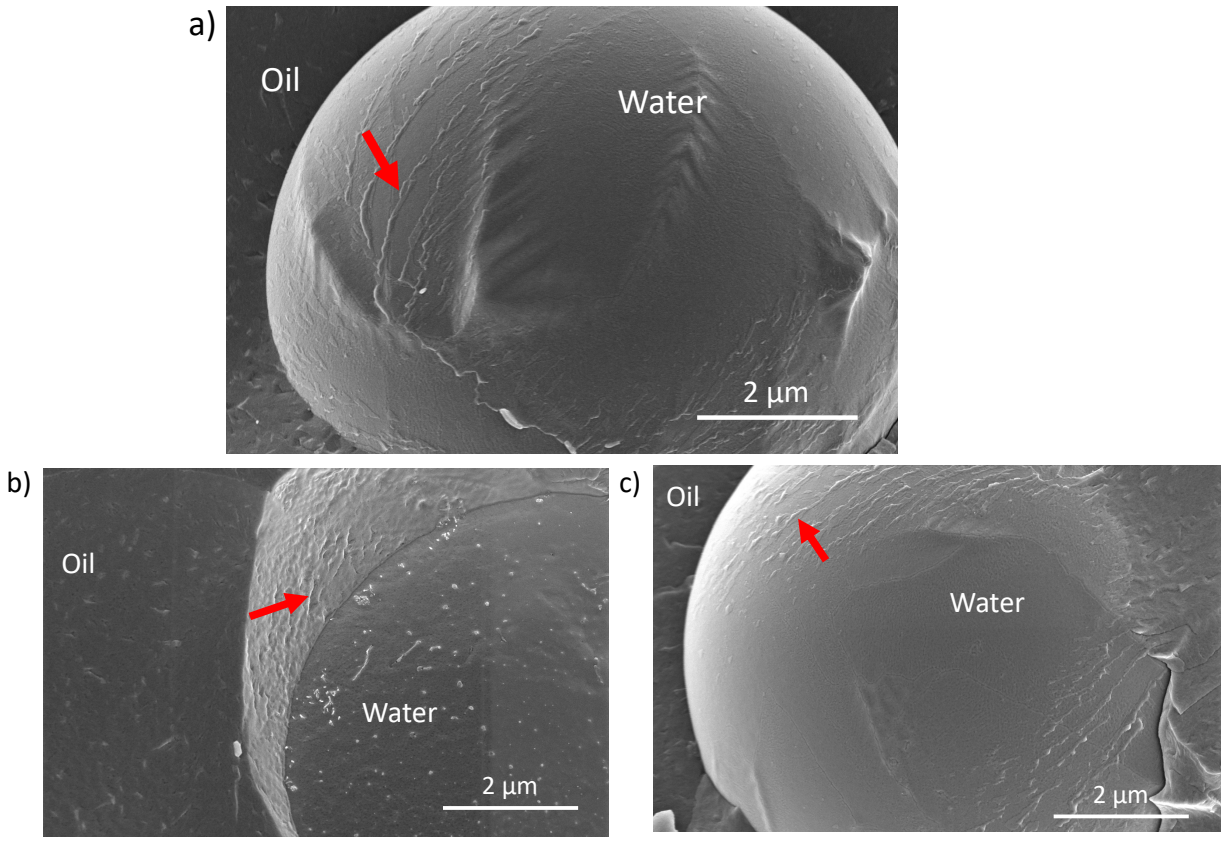

Figure C 10. Cryo-SEM of 20:80 emulsions stabilized by a) H-200 (5 wv%) and VH-0.25 (0.267 wt%); b and c) H-200 (3 wv%) and VH-0.25 (0.267 wt%), showing CMG coverage at the droplet interface (indicated by the red arrows). The continuous oil phase appears mainly in black, whilst the water is grey and the cellulose light grey/white. Scale bar = 2 µm, shown at bottom right in white.

Excitation and emission experiments of Calcofluor White (CW)-in-water and CW-in-oil (1:10 dye/solvent ratio, v/v%)

In order to determine whether a difference in emission and excitation is observed in the two solvents, oil and water, a 1 in 10 solution of Calcofluor White (CW) stain in MCT oil or water was prepared and gently shaken. CW mixed thoroughly with water, however it mixed with oil for a limited time and began to separate if left for a longer period. Therefore, excitation and emission measurements were performed immediately after preparation of the two solutions. The excitation and emission spectra for CW-in-water and CW-in-oil are given below (Figure C 10c and d, respectively). Droplet size analysis of optical micrographs was also conducted for the 20:80 emulsions using the 'threshold' plugin on ImageJ software. The average sizes of 50 stained droplets and 50 visible CMGs were 19.5±1.3 µm and 1.42±1.3 µm, respectively.

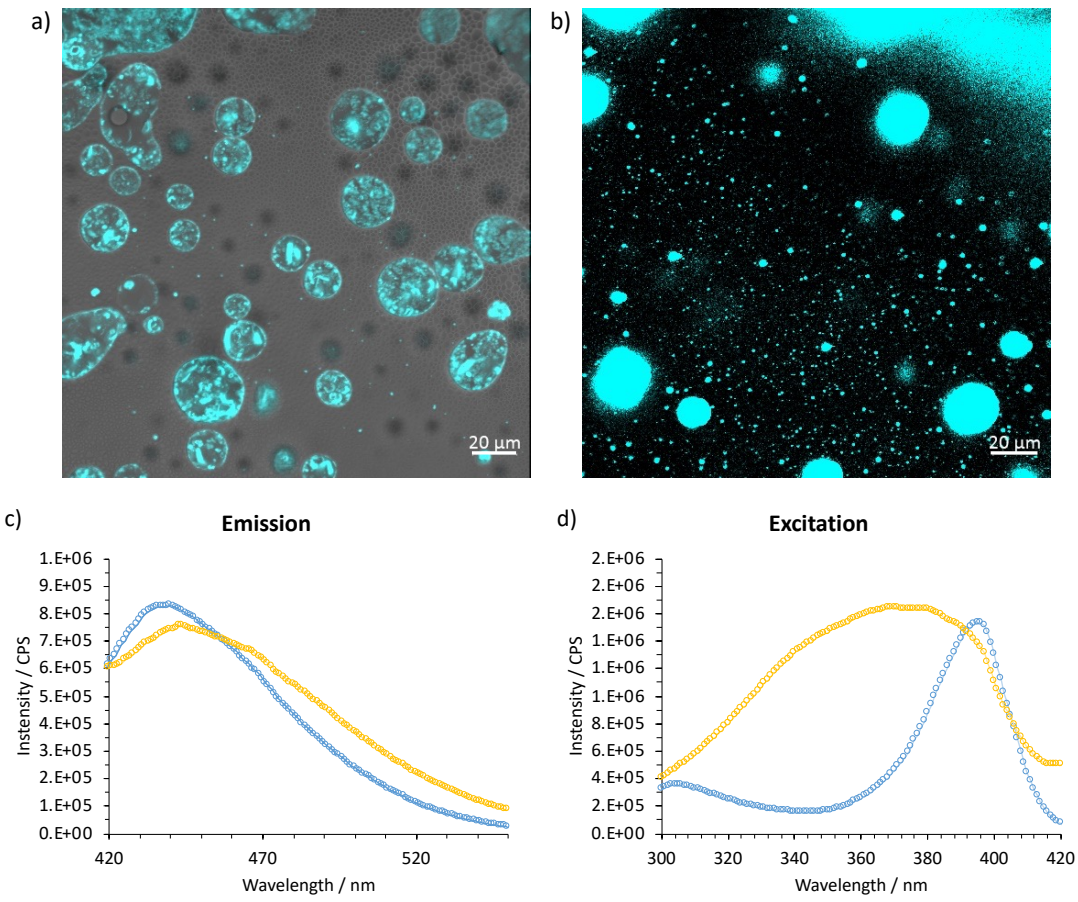

Figure C 11. H-0.25-in-oil dispersion a) confocal and optical micrographs overlaid; b) confocal micrograph with alternative emission filters (450-550 nm). Scale bar = 20 µm, shown at bottom right in white; c) excitation and d) emission spectra, for CW-in-water (blue) and CW-in-oil (yellow), both at 1:10 ratio (CW:water/oil, v/v %). For the emission spectra, λ_{ex} = 405 nm; for the excitation spectra, λ_{em} = 440 nm for CW-in-water and 443 nm for CW-in-oil.

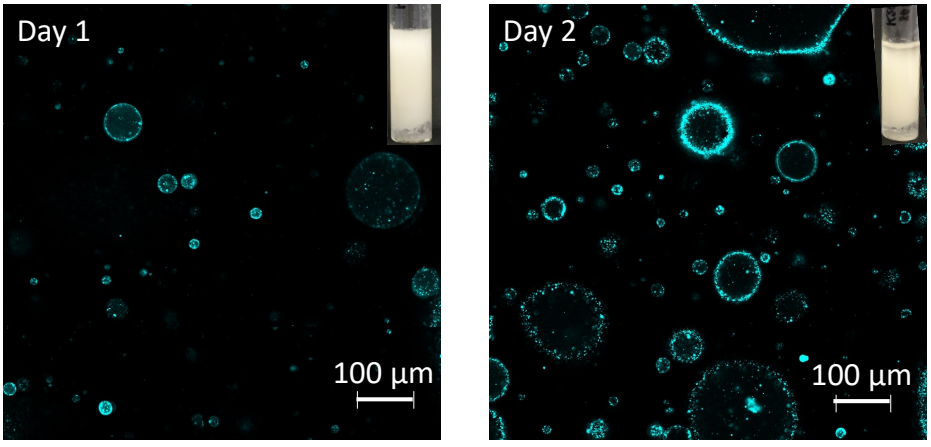

Figure C 12. Confocal micrographs for 20:80 emulsions stabilised by 3 wv% H-200 (day 1, left and day 2, right) with appearance of emulsions given on the top right. Each slide was prepared on the day of imaging and therefore the micrographs are from different emulsions samples in the image. Scale bar = 100 µm, shown at bottom right in white.

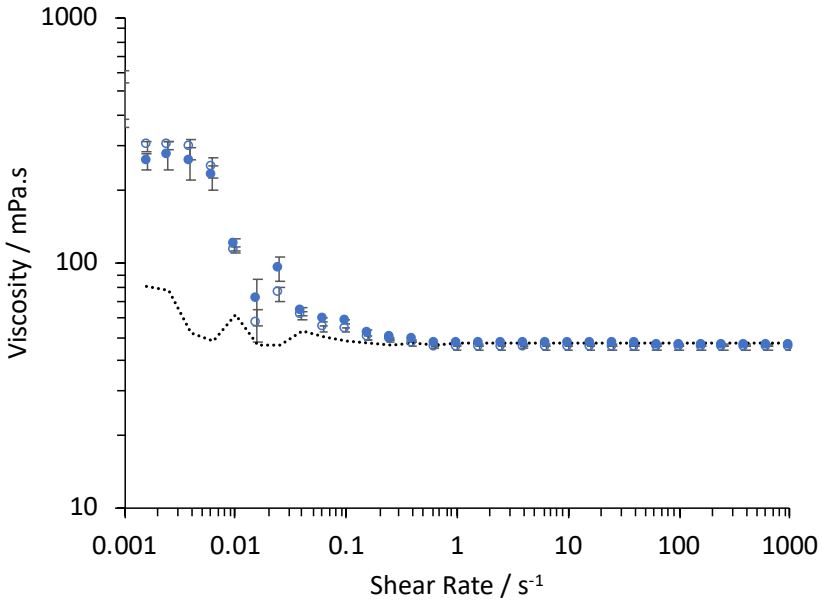

Figure C 13. Flow curves for 20:80 W/O emulsions (day 6), stabilized by 3 wv% H-200 and 0.267 wt% VH-0.25 (closed blue circle = original emulsion; open blue circle = 10x diluted emulsion), with pure sunflower oil (dashed black line). Error bars are all the same size/smaller than the symbols and are therefore not displayed.

References

Sugiyama, J., Vuong, R. and Chanzy, H. (1991). Electron Diffraction Study on the Two Crystalline Phases Occurring in Native Cellulose from an Algal Cell Wall. *Macromolecules*. *24*(14), 4168–4175.

Appendix D
Supporting information for Chapter 6

Table D 1. Vitacel Powdered Cellulose L 00 (V-cell): information provided by the manufacturer (J. Rettenmaier & Söhne GmbH & Co. KG).

	Vitacel Powdered Cellulose L 00
Colour	White
Structure	Fibres
Dietary Fiber Content	~98 %
Bulk Density	~165 g/L
Fiber length	120 µm
Water binding capacity	525 %
Oil absorption	410 %
Degree of polymerization (DP)	730-830 (Lefroy, Murray and Ries, (2021))

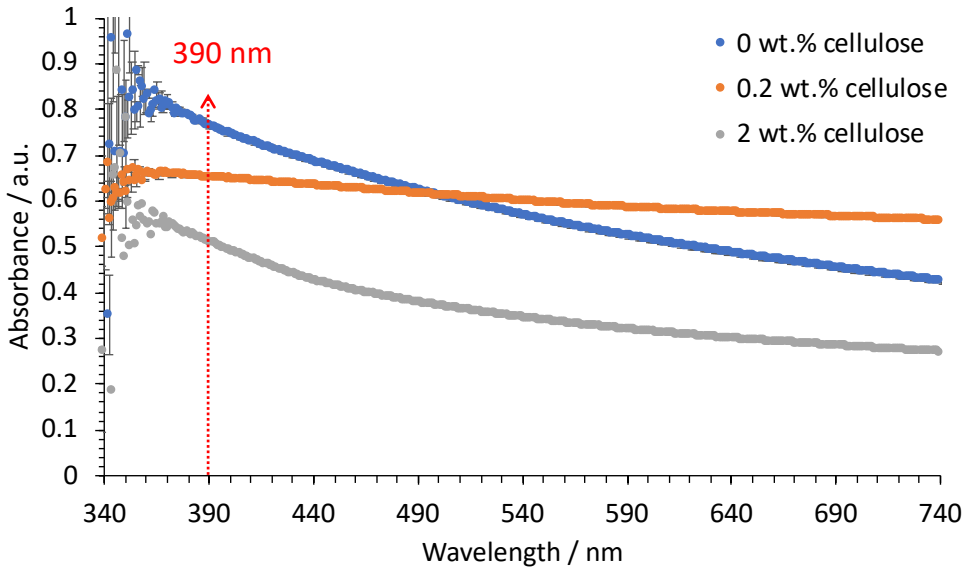

Figure D 1. UV-vis absorbance spectrum (measured from λ = 180-800 nm) of an oil-BmimAc solution (blue), 0.2 wt% cellulose-BmimAc-oil solution (orange) and 2 wt% cellulose-BmimAc-oil solution (grey), where in each case, [oil] = 0.25 wt%. Reference blanks of pure BmimAc, 0.2 wt% cellulose-BmimAc and 2 wt% cellulose-BmimAc solutions were used for each respective cellulose-BmimAc-oil solution. Error bars are shown but are covered by the symbols above λ ≃360 nm, absorbance data below λ = 340 nm is omitted due to the high level of noise.

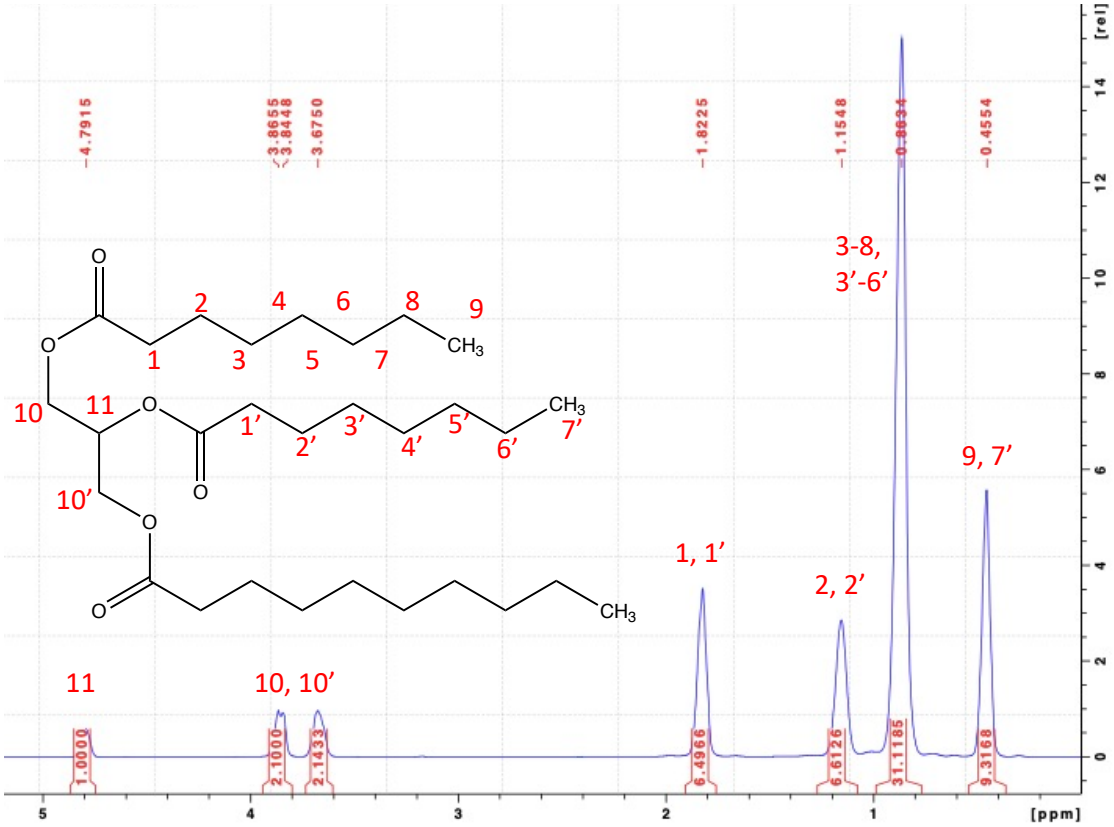

Figure D 2. ^{1}H NMR (400 MHz) spectrum of MCT-oil (Miglyol 812), with peak assignments to capric/caprylic acid shown in red in agreement with (Yan et al., (2017)).

Details on calculating Δδ for cellulose-BmimAc, cellulose-BmimAc-oil and cellobiose-BmimAc-oil solutions:

For pure BmimAc-oil solutions, the δ values of the peaks for the pure BmimAc were used as a reference. Therefore, the change in δ (Δδ) with [oil] is given as follows:

$$\boldsymbol{\Delta\delta = \delta_{[oil]} - \delta_{[BmimAc]}}$$

Where $\delta_{[oil]}$ represents δ of peaks in the BmimAc-oil samples and $\delta_{[BmimAc]}$ represents δ of the corresponding reference peak, in the pure IL.

For cellulose-BmimAc-oil solutions where [cellulose] = 2 wt%, the δ values of the peaks for the 'oil-free' 2 wt% cellulose-BmimAc solution were used as a reference. Therefore, the change in δ (Δδ) with [oil] is given as follows:

$$\boldsymbol{\Delta\delta = \delta_{[oil]} - \delta_{[C_{BmimAc}=2\ wt\%]}}$$

Where $\delta_{[oil]}$ represents δ of peaks in the BmimAc-oil samples and $\delta_{[BmimAc]}$ represents δ of the corresponding reference peak, in the 'oil-free' 2 wt% cellulose-BmimAc solution.

For cellobiose-BmimAc-oil solutions where [cellobiose] = 15 wt%, the δ values of the peaks for the 'oil-free' 15 wt% cellobiose-BmimAc solution were used as a reference. Therefore, the change in δ (Δδ) with [oil] is given as follows:

$$\boldsymbol{\Delta\delta = \delta_{[oil]} - \delta_{[C_{BmimAc}=15\ wt\%]}}$$

Where $\delta_{[oil]}$ represents δ of peaks in the BmimAc-oil samples and $\delta_{[BmimAc]}$ represents δ of the corresponding reference peak, in the 'oil-free' 15 wt% cellobiose-BmimAc solution.

For cellobiose-BmimAc-oil solutions where [cellobiose] = 2 wt%, the δ values of the peaks for the 'oil-free' 2 wt% cellobiose-BmimAc solution were used as a reference. Therefore, the change in δ (Δδ) with [oil] is given as follows:

$$\boldsymbol{\Delta\delta = \delta_{[oil]} - \delta_{[C_{BmimAc}=2\ wt\%]}}$$

Where $\delta_{[oil]}$ represents δ of peaks in the BmimAc-oil samples and $\delta_{[BmimAc]}$ represents δ of the corresponding reference peak, in the 'oil-free' 2 wt% cellobiose-BmimAc solution.

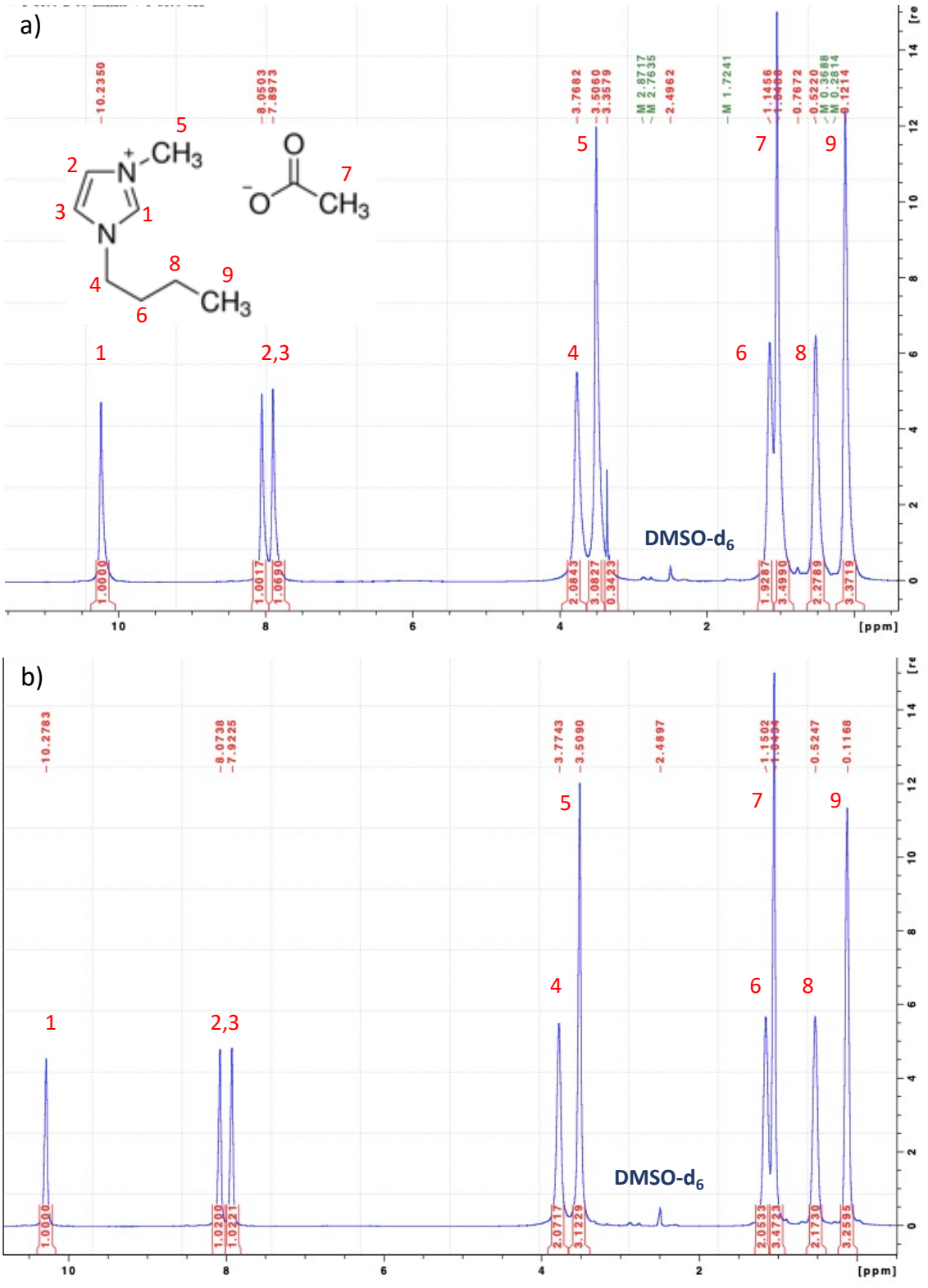

Figure D 3. ^{1}H NMR spectrum for a) cellulose-BmimAc-oil solution prepared via method B, ([cellulose] = 2 wt%; [oil] = 1 wt%) and b) pure BmimAc, highlighting the similarity between δ values (Δδ ≃ 0), suggesting that the addition of the oil 're-strengthens' the cation-anion H-bond and the proton resonances return to those of the pure BmimAc solution. The peak at Δδ ≃ 2.5 ppm corresponds to the external reference, DMSO.

Table D 2. Chemical shift values (δ) for cellulose-BmimAc-oil and pure BmimAc solutions, corresponding to Figure D 4a and b respectively.

Proton number	δ for Figure D 3a, ([cellulose] = 2 wt%; [oil] = 1 wt%)/ppm	δ for Figure D 3b, (pure BmimAc)/ppm
1	10.235	10.2783
2	8.0503	8.0738
3	7.8973	7.9225
4	3.7682	3.7743
5	3.5060	3.5090
6	1.1456	1.1502
7	1.0488	1.0434
8	0.5220	0.5247
9	0.1214	0.1168

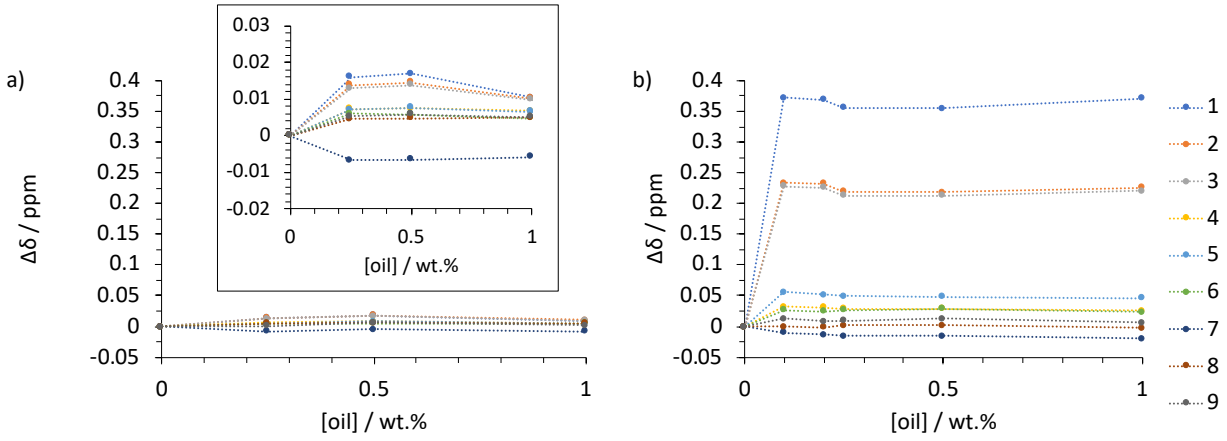

Figure D 4. Change in chemical shift values (Δδ) of protons 1-9 (BmimAc) after 1 month storage, as a function of oil concentration ([oil]), where a) cellulose was dissolved before the addition of oil (method A) and b) cellulose was dissolved after the addition of oil (method B). In both cases, [cellulose] = 2 wt%.

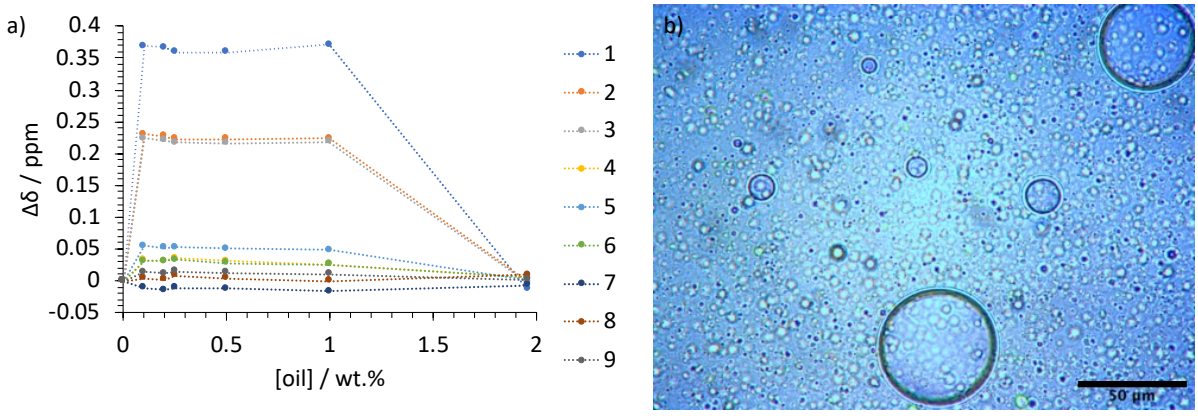

Figure D 5. a) Change in chemical shift values (Δδ) of protons 1-9 (BmimAc), as a function of oil concentration ([oil] = 0-2 wt%) for [cellulose] = 2 wt%, where cellulose was dissolved after the addition of oil (method B); b) optical micrograph of cellulose-BmimAc-oil solution, where [cellulose] = 2 wt% and [oil] = 2 wt%.

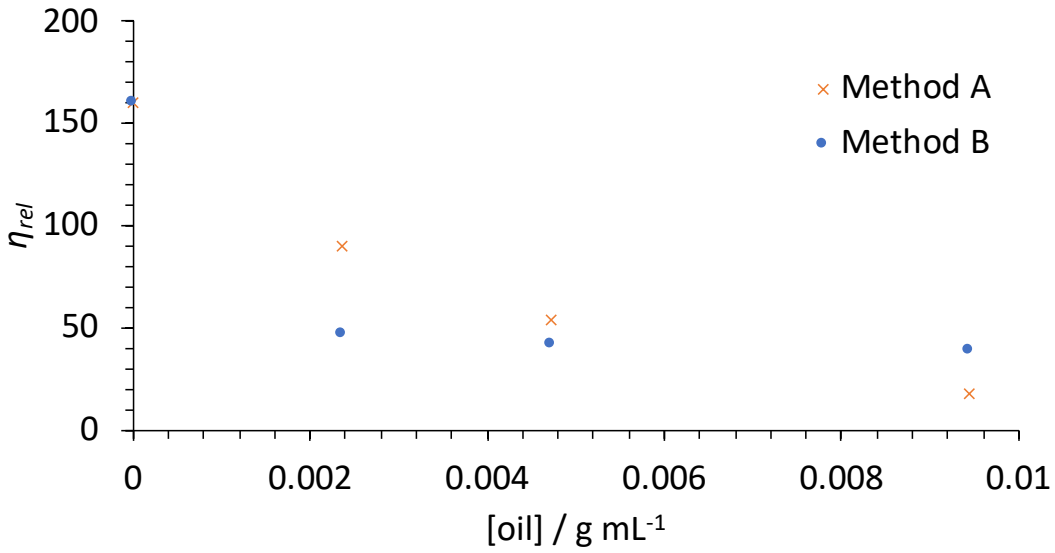

Figure D 6. Relative viscosity (η_{rel}) as a function of [oil], where the zero-shear rate viscosities (η_0) were determined by fitted the flow curves given in Figure 6.6 to the Cross-model equation:

Equation D 1. $$\eta_{\dot{\gamma}} = \eta_{\infty} + \frac{\eta_0 - \eta_{\infty}}{1+(C\dot{\gamma})^m}$$

Where η_0 = zero-shear rate viscosity; η_{∞} = infinite-shear rate viscosity; C = Cross time constant and m = (Cross) rate constant.

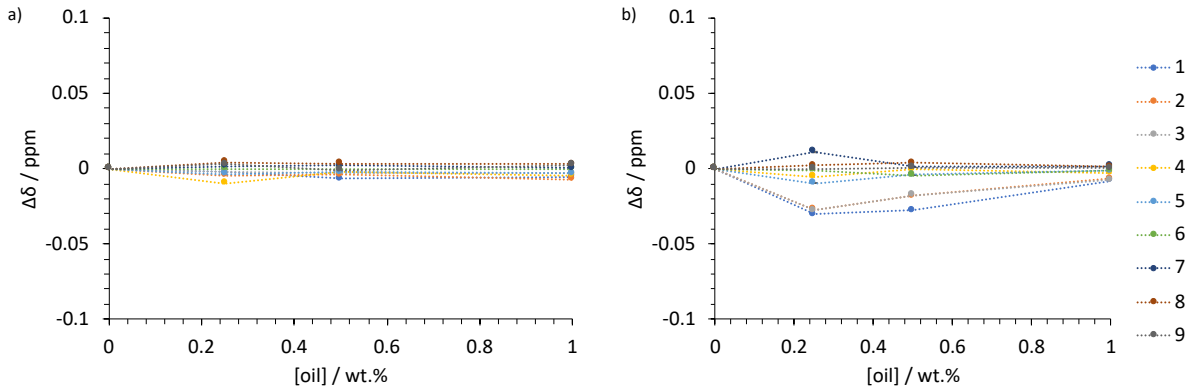

Figure D 7. Change in chemical shift values (Δδ) of protons 1-9 (BmimAc), as a function of oil concentration ([oil] = 0-1 wt%) for a) [cellobiose] = 15 wt%, and b) [cellobiose] = 2 wt%, where cellobiose was dissolved after the addition of oil (method B).

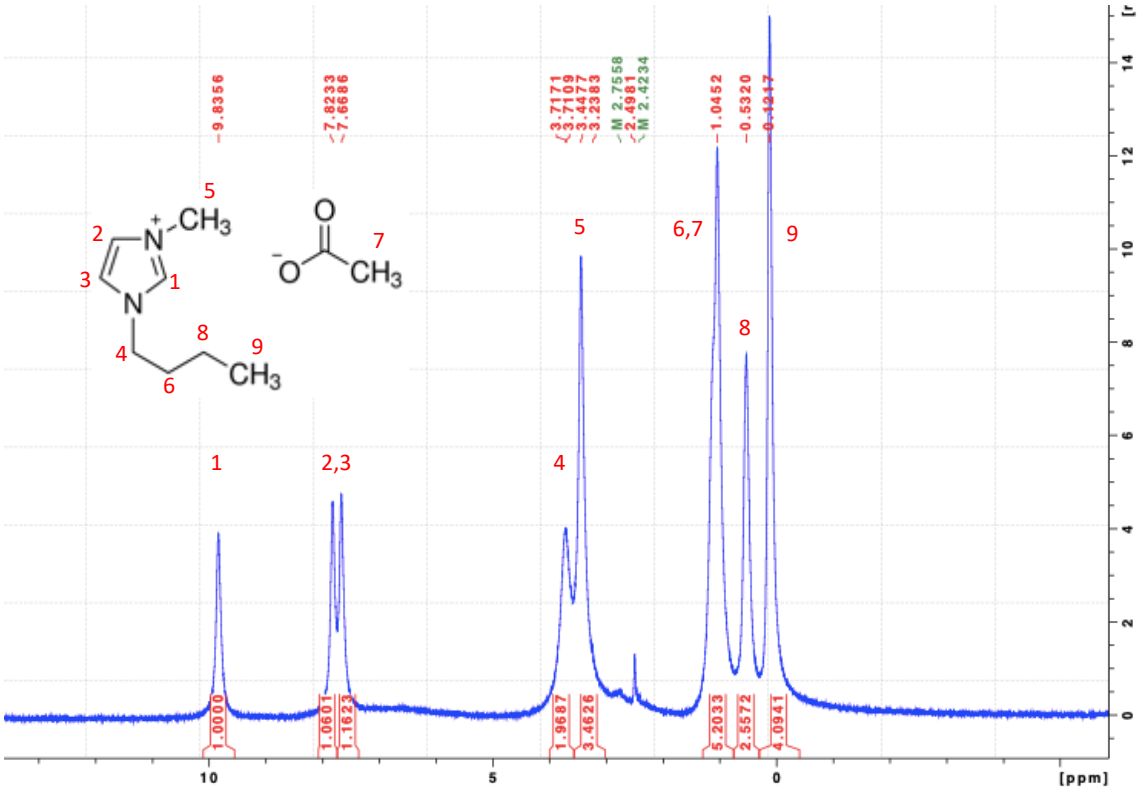

Figure D 8. ^{1}H NMR spectrum (400 MHz) for 15 wt% cellobiose dissolved in BmimAc, with peak assignments shown in red.

References

Lefroy, K.S., Murray, B.S. and Ries, M.E. (2021). Rheological and NMR Studies of Cellulose Dissolution in the Ionic Liquid BmimAc. *Journal of Physical Chemistry B*. *125*(29), 8205–8218.

Yan, X., Alcouffe, P., Sudre, G., David, L., Bernard, J. and Ganachaud, F. (2017). Modular construction of single-component polymer nanocapsules through a one-step surfactant-free microemulsion templated synthesis. *Chemical Communications*. *53*(8), 1401–1404.